NOTICE

The quality of this microform is heavily dependent upon the quality of the original thesis submitted for microfilming. Every effo t has been made to ensure the highest quality of reproduction possible.

If pages are missing, contact the university which granted the degree.

Some pages may have indistinct print especially if the original pages were typed with a poor typewriter ribbon or if the university sent us an inferior photocopy.

Reproduction in full or in part of this microform is governed by the Canadian Copyright Act, R.S.C. 1970, c. C-30, and subsequent amendments.

AVIS

La qualité de cette microforme dépend grandement de la qualité de la thèse soumise au microfilmage. Nous avons tout fait pour assurer une qualité supérieure de reproduction.

S'il manque des pages, veuillez communiquer avec l'université qui a conféré le grade.

La qualité d'impression de certaines pages peut laisser à désirer, surtout si les pages originales ont été dactylographiées à l'aide d'un ruban usé ou si l'université nous a fait parvenir une photocopie de qualité inférieure.

La reproduction, même partielle, de cette microforme est soumise à la Loi canadienne sur le droit d'auteur, SRC 1970, c. C-30, et ses amendements subséquents.

Canada

Photosynthetic characteristics of picoplankton and natural phytoplankton assemblages

By

Roderick E. Warnock

Submitted in partial fulfillment of the requirements for the degree

of Doctor of Philosophy

at

Dalhousie University

Department of Biology

February 1990

ISBN 0-315-64597-0

To

Susan

CONTENTS

PART I

LIST OF TABLES

LIST OF FIGURES

ABSTRACT

Photosynthetic rates of three marine picoplankton species were measured as a function of both photon flux density (P-I response) and photon wavelength (action spectra or P-S response). The picoplankton species examined included two prokaryotes, the marine cyanobacteria *Synechococcus* sp. WH 7803 and *Synechococcus* sp. WH 5701, and one eukaryote, the prymnesiophyte *Pavlova* sp. (clone NEP). The wavelength dependence of photosynthesis was also measured in natural phytoplankton assemblages, collected from latitudes ranging from the sub-tropical North Atlantic Ocean to the eastern Canadian Arctic.

The abilities of previous P-I formulations to provide a quantitative description of the P-I response of the picoplankton were compared. Three new P-I models are introduced that provide an improved overall fit (fidelity) to the P-I data. Two of these models, a simple geometrical description and a rational model based on target theory, accommodate the spectral dependence of photosynthesis by way of a simple spectral weighting function. The third model, a kinetic description involving two spectrally distinct photosystems, also includes the effects of Emerson enhancement at low PFDs.

The photosynthetic action spectra of both cyanobacterial species revealed the importance of the phycobiliproteins and Emerson enhancement. In contrast, the photosynthetic action spectra of natural phytoplankton assemblages closely resembled those of Chromophytic algae such as *Pavlova* sp., where chlorophyll is the dominant light-harvesting pigment and Emerson enhancement is minimal. For the natural phytoplankton assemblages the photosynthetic rate under polychromatic irradiance could be approximated using a suitable spectral weighting function. Absorption by detritus in natural phytoplankton assemblages eliminated the absorption spectrum as a suitable spectral weighting function. Using the photosynthetic action spectrum to predict rates of light-limited photosynthesis at depth shows that the ability of the phytoplankton to utilize underwater spectral distributions increases with depth. Furthermore, photosynthetic rates measured under artifical light significantly under-estimate the predicted photosynthetic rate at depth.

LIST OF SYMBOLS AND ABBREVIATIONS

Common units are included in square brackets [ ]. Greek symbols follow Roman symbols.

a	effective spectral absorption coefficient [m^{-1}]
a_λ	absorption cross-section at a specific wavelength λ [$m^2\ mg^{-1}$]
a^*_p	the diffuse volume absorption coefficient for particulates collected on GF/F filters [m^{-1}]
a^*_{chl}	the chlorophyll-specific diffuse volume absorption cross-section for particulates collected on GF/F filters [m^2 (mg Chl)$^{-1}$]
$a_{PSU\lambda}$	absorption cross-section of a photosynthetic unit at a specific wavelength λ [$m^2\ PSU^{-1}$]
$a_{PSU}(\lambda)$	absorption cross-section of a photosynthetic unit as a function of wavelength [$m^2\ PSU^{-1}\ nm^{-1}$]
$a(\lambda)$	absorption cross-section as a function of wavelength [$m^2\ mg^{-1}\ nm^{-1}$]
B	biomass
Chl	chlorophyll
E_1	Emerson enhancement function for Photosystem I
E_2	Emerson enhancement function for Photosystem II
E_{1max}	maximum Emerson enhancement for Photosystem I
E_{2max}	maximum Emerson enhancement for Photosystem II
g	acceleration due to gravity [$m\ s^{-2}$]
I^*	Dimensionless PFD (usually I/I_k or I/I_m)

Ia_λ the rate of photon absorption by volume of water [μmol m^{-3} s^{-1}]

Ia_λ' the rate of photon absorption by the viable phytoplankton component in a volume of water [μmol m^{-3} s^{-1}]

I_b the PFD where the photosynthetic rate is reduced to half the maximum potential rate due to photoinhibition (*PFD for* $P = P_s/2$) [μmol m^{-2} s^{-1}]

I_j the PFD used to scale photoinhibition. In the Poisson model $I_j = P_m^B/\sigma_{ic}$ [μmol m^{-2} s^{-1}]

I_k the PFD marking the intersection between the initial slope and the maximum photosynthetic rate ($= P_m/\alpha$) [μmol m^{-2} s^{-1}]

I_m the PFD where the photosynthetic rate is optimal [μmol m^{-2} s^{-1}]

I_O the PFD at the sea surface [μmol m^{-2} s^{-1}]

I_{RC} the rate of photon absorption by a reaction center [mol s^{-1}]

I_s the PFD marking the intersection of the initial slope and the maximum potential photosynthetic rate ($= P_s/\alpha$) [μmol m^{-2} s^{-1}]

I_Z the PFD at depth z [μmol m^{-2} s^{-1}]

I_1 *effective* rate of photon absorption by PS I [photons s^{-1}]

$I_{1\lambda}$ the rate of at which photons of wavelength λ are absorbed by PS I [photons s^{-1}]

I_2 *effective* rate of photon absorption by PS II [photons s^{-1}]

$I_{2\lambda}$ the rate of at which photons of wavelength λ are absorbed by PS II [photons s^{-1}]

I_3 the rate of exciton loss from PS II [excitons s^{-1}]

I_λ the PFD at a specific wavelength λ [μmol m^{-2} s^{-1}]

I_τ number of photons incident upon a reaction center within a time interval τ [mol]

$I(\lambda)$	the PFD as a function of wavelength [µmol m^{-2} s^{-1} nm^{-1}]
$I(\lambda_1)$	the PFD of the light beam that is absorbed predominantly by PS I (Light 1) [µmol m^{-2} s^{-1}]
$I(\lambda_2)$	the PFD of the light beam that is absorbed predominantly by PS II (Light 2) [µmol m^{-2} s^{-1}]
$I(\lambda)'$	the PFD within a specific 25 nm waveband as a fraction of the total PFD of PAR
k_c	the *effective* spectral chlorophyll-specific attenuation cross-section [m^2 (mg Chl)$^{-1}$]
$K_{c\lambda}$	vertical diffuse attenuation coefficient due to phytoplankton (chlorophyll) at a specific wavelength λ [m^{-1}]
$k_{c\lambda}$	chlorophyll-specific diffuse attenuation cross-section at a specific wavelength λ [m^2 (mg Chl)$^{-1}$]
$K_c(\lambda)$	vertical diffuse attenuation coefficient due to phytoplankton (chlorophyll) as a function of wavelength [m^{-1} nm^{-1}]
$k_c(\lambda)$	chlorophyll-specific diffuse attenuation cross-section as a function of wavelength [m^2 (mg Chl)$^{-1}$ nm^{-1}]
K_m	Michaelis Menten constant (rectangular hyperbola) [M]
K_m'	Generalized Michaelis-Menten constant (non-rectangular hyperbola) [M]
K_{PAR}	*effective* spectral attenuation coefficient for PAR [m^{-1}]
$K_{p\lambda}$	vertical diffuse attenuation coefficient due to detrital particles at a specific wavelength λ [m^{-1}]
$K_p(\lambda)$	vertical diffuse attenuation coefficient due to detrital particles as a function of wavelength [m^{-1} nm^{-1}]
K_S	diffuse attenuation coefficient [m^{-1}]

$K_{T\lambda}$	vertical diffuse attenuation coefficient at a specific wavelength λ [m^{-1}]
$K_T(\lambda)$	vertical diffuse attenuation coefficient as a function of wavelength [m^{-1} nm^{-1}]
$K_{w\lambda}$	vertical diffuse attenuation coefficient due to seawater itself at a specific wavelength λ [m^{-1}]
$K_w(\lambda)$	vertical diffuse attenuation coefficient due to seawater itself as a function of wavelength [m^{-1} nm^{-1}]
K_λ	absorption coefficient at a specific wavelength λ [m^{-1}]
LHA	light-harvesting antenna(e)
OD	optical density
p	probability [dimensionless]
P^*	dimensionless photosynthetic rate (usually P/P_m or P/P_s)
P'	integral photosynthesis beneath an area of ocean surface
P^B	photosynthetic rate normalized to biomass
P_g	gross photosynthetic rate
P_g^B	gross photosynthetic rate normalized to biomass
P_m^B	maximum realized photosynthetic rate normalized to biomass
P_n	net photosynthetic rate ($= P_g - R$)
P_n^B	net photosynthetic rate normalized to biomass ($= P_g^B - R^B$)
p_{RC}	the probability of photosynthesis occurring at a reaction center
P_s^B	maximum potential photosynthetic rate normalized to biomass in the absence of photoinhibition
P_1	the rate of Photoreaction I (molecules transformed s^{-1})
P_2	the rate of Photoreaction II (molecules transformed s^{-1})
$p(k)$	the probability of a single PSU absorbing k photons within a time interval Δt
$P(\lambda_1,\lambda_2)$	the rate of photosynthesis under two monochromatic light beams where one

	beam (λ_1) preferentially excites PS I and the second beam (λ_2) preferentially excites PS II
PAR	photosynthetically available radiation [μmol m^{-2} s^{-1}]
PC	phycocyanin
PCB	phycocyanobilin
PE	phycoerythrin
PEB	phycoerythrobilin
PFD	photon flux density [μmol m^{-2} s^{-1}]
PS I	photosystem I
PS II	photosystem II
PSR	photosynthetically stored radiation [μmol m^{-3} s^{-1}]
PSU	photosynthetic unit
PUB	phycourobilin
PUR	photosynthetically usuable radiation [μmol m^{-3} s^{-1}]
R^B	the respiration rate normalized to biomass
RC I	reaction center I
RC II	reaction center II
R_m^B	the maximum respiration rate normalized to biomass
S	dimensionless substrate concentration (= $[S]/K_m'$)
$[S]$	substrate concentration [M]
SS_{res}	sum of squared residuals
v	velocity of a reaction
V	dimensionless velocity of a reaction (= v/v_m)
v_m	maximum velocity of a reaction
z	depth [m]

α^B	the initial slope ($\partial P^B/\partial I$) of the P-I response as $I \rightarrow 0$ where the photosynthetic rate is normalized to biomass
α^B	the initial slope of the P-I response as $I \rightarrow 0$ at wavelength l where the photosynthetic rate is normalized to biomass ($\partial P^B_\lambda/\partial I_\lambda$)
$\alpha^{B'}$	the light utilization index, corresponding to the relative *effective* photosynthetic rate per photon
$\alpha^{B'}{}_O$	the light utilization index at the sea surface
$\alpha^{B'}{}_T$	the light utilization index in tungsten light
$\alpha^{B'}{}_Z$	the light utilization index at depth in the water column
$\alpha^B(\lambda)$	the initial slope of the P-I response as a function of wavelength ($\partial P^B(\lambda)/\partial I(\lambda)$)
$\alpha^B(\lambda)'$	the initial slope of the P-I response within a specific 25 nm waveband ($\partial P^B(\lambda)/\partial I(\lambda)$) as a fraction of the average initial slope over all the twelve 25 nm wavebands of PAR (each waveband weighted equally)
β^B	the negative slope ($\partial P^B/\partial I$) of the P-I response due to photinhibition where the photosynthetic rate is normalized to biomass (usually defined at some specific PFD)
$\beta(\lambda)$	the negative slope ($\partial P/\partial I$) of the P-I response due to photinhibition as a function of wavelength (usually defined at some specific wavelength)
γ	the fraction of the exciton flux diverted from PS II that is delivered to PS I by way of spillover
Δt	an infinitesimally short time interval
ε_λ	the molar absorption cross-section at a specific wavelength λ [$m^2\ mol^{-1}$]
z	the exciton flux that is diverted from PS II by way of spillover (I3) as a fraction of the photon flux absorbed by PS II (I2) (= I3/I2)
η	dynamic viscosity of seawater [$kg\ m^{-1}\ s^{-1}$]

Θ	parameter describing abruptness of curvature in a non-rectangular hyperbola
λ	wavelength [nm]
λ_1	wavelengths that excite PS I
λ_2	wavelengths that excite PS II
μm	micrometer
μ_1	the rate of exciton arrival at RC I [excitons s^{-1}]
μ_2	the rate of exciton arrival at RC II [excitons s^{-1}]
ν	frequency [Hz]
ξ	the absorption yield of the phytoplankton (= PUR/I_a) [dimensionless]
ξ'	the absorption efficiency of the phytoplankton (= PUR/I_a) [dimensionless]
ρ	density of phytoplankton cells [kg m^{-3}]
ρ'	density of seawater [kg m^{-3}]
Σ	sum
σ	the *effective* spectral action coefficient for photosynthesis [m^{-1}]
σ_c	the *effective* spectral chlorophyll-specific action
$\sigma_c(\lambda)$	chlorophyll-specific transformation cross-section as a function of wavelength [m^2 (mg Chl)$^{-1}$]
σ_{ic}	the *effective* chlorophyll-specific action cross-section for photoinhibition [m^2 (mg Chl)$^{-1}$]
σ_{pc}	the *effective* chlorophyll-specific action cross-section for carbon reduction [m^2 (mg Chl)$^{-1}$]
σ_λ	transformation cross-section at a specific wavelength λ [m^2 mol^{-1} or m^2 mg^{-1}]
$\sigma(\lambda)$	transformation cross-section as a function of wavelength [m^2 mol^{-1} nm^{-1} or m^2 mg^{-1} nm^{-1}]
τ	the turnover time of a reaction center [s]

ϕ	the *effective* quantum yield of phytoplankton photosynthesis (= *PSR/PUR*) [dimensionless]
ϕ'	the *effective* quantum efficiency of phytoplankton photosynthesis (= *PSR/PUR*) [dimensionless]
ϕ_a	the apparent quantum yield of phytoplankton photosynthesis [dimensionless]
ϕ_p	quantum yield for photosynthetic carbon reduction
ϕ_i	quantum yield for photodestruction of reaction centers
ϕ_1	the quantum yield of photoreaction I [dimensionless]
ϕ_2	the quantum yield of photoreaction II [dimensionless]
ϕ_λ	the quantum yield of photosynthesis at a specific wavelength λ [dimensionless]
$\Phi_E(\lambda)$	the enhanced quantum yield at wavelength λ, measured with a sufficiently strong background PFD of complementary wavelengths [dimensionless]
Φ_{max}	the maximum quantum yield of photosynthesis [dimensionless]
ψ	the light utilization yield of the phytoplankton (= PSR/I_a) [dimensionless]
ψ'	the light utilization efficiency of the phytoplankton (= PSR/I_a) [dimensionless]
ω_1	the fraction of absorbed photons that are absorbed by PS I
ω_2	the fraction of absorbed photons that are absorbed by PS II

ACKNOWLEDGEMENTS

I would like to thank Trevor Platt, my supervisor, for providing the opportunity to study oceanography in an environment as stimulating as the Bedford Institute of Oceanography. The privilege of participating on several oceanographic cruises is greatly appreciated. I should also like to thank my committee for allowing me the freedom to pursue my own research interests.

I am indebted to the many people comprising the Biological Oceanography Division at BIO for assistance, encouragement and *esprit de corps*. Brian Irwin was always helpful, particularly when preparing for a cruise. Jeff Anning answered a seemingly endless list of computer queries. Bill Li and Glen Harrison were always willing to discuss results and offer advice. I am also indebted to Marlon Lewis for introducing me to Dalhousie, and, of course, to the "photosynthetron". Marlon was a great help and was always enthusiastic about results and ideas.

Throughout the course of this work many people provided help, friendship and good company. They kept me sane (I think) and it is probably in their best interests to remain anonymous. I am grateful to the residents of Le Marchant Street who, upon my arrival in Halifax, ensured that I was familiarized with the drinking establishments of the City. My thanks also to the crew of the CSS Hudson for their willing assistance at sea and for ensuring that there was never a dull moment.

Most of all, thank you Sue for being so patient.

CHAPTER 1

INTRODUCTION.

1.1. STATEMENT OF THE PROBLEM.

The rate at which carbon and nitrogen are photosynthetically reduced in the ocean limits the magnitude of all subsequent biological transformations of energy and matter in the marine ecosystem. The magnitude of this process is central to our understanding of the trophodynamics of the marine ecosystem and the biogeochemical cycling of carbon and oxygen in the biosphere. Despite its importance, the absolute magnitude of global oceanic primary production is still uncertain to within a factor of ten (Eppley 1980; Shulenberger and Reid 1981; Jenkins 1982; Williams *et al.* 1983; Platt and Harrison 1985,1986; Reid and Shulenburger 1986; Platt *et al.* 1988a). The two principal reasons invoked for such uncertainty are i) the major disparities that exist among the estimates provided by different experimental methods and ii) the lack of a comprehensive set of production measurements from the open ocean with sufficient temporal and spatial resolution.

Differences in the measured rates of oceanic primary production obtained with alternative experimental techniques have aroused considerable debate (Kerr 1983). Primary production estimates based upon diel changes in oxygen, oxygen utilization rates in the aphotic zone or the sinking flux of particulate organic carbon (POC) are considerably higher than values obtained with the isotopic ^{14}C assimilation technique (Sheldon and Sutcliffe 1978; Eppley and Peterson 1979; Gieskes *et al.* 1979; Johnson *et al.* 1981; Shulenburger and Reid 1981; Jenkins 1982). This apparent disparity, and the

consequent uncertainty associated with any single primary production estimate, is most pronounced in the open oceans, particularly the oligotrophic tropical oceans. Initially such discrepancies were attributed to inconsistencies in the ^{14}C method (Peterson 1980; Williams 1981). However, recent comparisons of primary production rates based upon changes in dissolved oxygen, production of $^{18}O_2$ or the uptake of ^{14}C have all yielded comparable results (Williams *et al.* 1983; Platt 1984; Bender *et al.* 1987; Grande *et al.* 1989). Also, Davies and Williams (1984) found comparable photosynthetic rates using *in vitro* and *in vivo* techniques indicating that *in vitro* methods are satisfactory. The current consensus is that there is no experimental evidence to support the idea of persistent errors unique to the ^{14}C technique.

Measurements conducted at specific locations and depths throughout the world's oceans using various incubation techniques form the basis of current global estimates of oceanic primary production. Regrettably, the logistics of this approach impose severe constraints upon the spatial and temporal resolution that may be achieved. There is also a growing appreciation that the biogenic processes of ocean vary considerably from place to place and over time. This variability can lead to significant errors in estimates of the mean values of primary production for large ocean regions (Platt and Harrison 1985; Vezina and Platt 1987; Platt *et al.* 1988a). This has led to the hypothesis that the observed disparities in oceanic production estimates result directly from differences in the temporal and spatial scales associated with the various methods (Platt *et al.* 1988a). Conventional methods that rely upon measuring some chemical transformation (such as ^{14}C uptake or O_2 evolution) at a particular time and place may thus fail to provide suitable data for the computation of primary production on a global scale.

The only foreseeable means of achieving the synoptic coverage required is to use the capabilities of remote sensing (Revelle 1985). This approach requires that a

relationship be established between photosynthetic rate in the ocean and the ocean color as detected by the satellite. Since the absorption properties of the particulate material in the ocean affects the ocean color (Sathyendranath 1986) it is desirable that the photosynthetic rate be related to the absorption properties of the phytoplankton present. In the open ocean the principal phytoplanktonic organisms are minute cells less than 2 μm in diameter, termed the "picoplankton".

This thesis examines the photosynthetic characteristics of several oceanic picoplankton species and natural phytoplankton assemblages. The dependence of the photosynthetic rate upon both the photon flux density and the photon wavelength is quantified with a view to predicting primary production throughout the water column. The study examines various ways of incorporating the wavelength dependence of photosynthesis into the P-I response of phytoplankton. A comparison of the wavelength dependence of photosynthesis in picoplankton cultures with that of natural phytoplankton assemblages provides insight into the important phylogenetic phytoplankton groups in the open ocean. By comparing the the action spectrum of photosynthesis with the absorption spectrum of the different picoplankton groups, the validity of using photosynthetic action spectra as a means of predicting photosynthetic rates at depth is assessed.

1.2. THE UTILITY OF REMOTE SENSING FOR ESTIMATING PRIMARY PRODUCTION.

The oceans and smaller seas cover about 71% of the earth's surface, an area of about 3.611×10^8 square kilometers. The open oceans constitute over 90% of this area and account for greater than 80% of the marine primary production globally. The

uncertainties associated with the biogenic fluxes of carbon and oxygen in the open oceans limit current efforts to model the biogeochemical cycles of the ocean. This in turn confounds major climatological questions such as the importance of the present build-up of CO_2 in the atmosphere (Sarmiento and Togglweiler 1984).

Within the last decade the advent of remote sensing has provided the potential for continual synoptic measurements of the world's oceans with the required spatial and temporal resolution (Revelle 1985). This has encouraged the formulation of empirical primary production models, based upon the optical properties of the ocean, as a practical alternative for computing global oceanic production. Such models combine estimates of the surface irradiance and its attenuation with depth, the biomass of phytoplankton in the water column and a knowledge of the functional photosynthetic response of the phytoplankton to the available irradiance to derive an estimate of primary production throughout the water column.

The application of radiative transfer theory to satellite measurements of ocean reflectance has provided a means of estimating both the spectral irradiance arriving at the sea-surface and its subsequent attenuation throughout the water column (Gautier *et al.* 1980; Gautier 1982; Gordon and Morel 1983; Sathyendranath 1986). Similarly, phytoplankton biomass concentrations in the water column may be estimated from ocean color measurements (Morel and Prieur 1978; Pelevin 1978; Sathyendranath *et al.* 1982,1983; Gordon and Morel 1983; Sathyendranath and Morel 1983). The photosynthetic response of the phytoplankton to the incident irradiance provides the final link between the spectral reflectance of the ocean and the rate of primary production therein.

The photosynthetically available radiation (PAR) at any depth horizon in the ocean is the photon flux reaching the ocean surface less any attenuation by the overlying water column. The two most important depth-dependent properties of PAR relevant to both the surface reflectance and water column photosynthesis are i) the photon flux density and ii) the spectral composition of the radiation. The incident photon flux density (PFD) is the number of photons arriving in a unit area per unit time, a quantity often loosely called the "light intensity". The photon flux density is defined with respect to the geometry of the collecting surface. The *scalar* or 4π photon flux density (= quantum scalar irradiance) represents the number of photons per unit area per unit time arriving from all 4π directions. The *vectorial* or *cosine* photon flux density (= quantum flux density or quantum irradiance) represents the number of photons impinging on a horizontal unit area per unit time. Both measurements of PFD have the same dimensions (photons $L^{-2}\ T^{-1}$). The appropriate SI unit for PFD is mol $m^{-2}\ s^{-1}$ where a mole of photons (6.023×10^{23} photons) is often called an Einstein (E). Although "irradiance" is often used to denote PAR, the term strictly applies only to radiation measured in terms of energy units (1 Watt = 1 J s^{-1}) as opposed to photon units (photons s^{-1} or quanta s^{-1}) and is inappropriate for a quantum process such as photosynthesis. Differences between measured values of scalar and vectorial PFD may arise because of the geometrical distribution of the directionality of the arriving photons. For this reason it is necessary to state explicitly which geometry is employed (scalar or vectorial) to determine the PFD.

The energy content of a photon is spectrally dependent ($\varepsilon = h\nu = hc/\lambda$ where h is Planck's constant (6.62×10^{-34} J s^{-1}), ν is the frequency (s^{-1}), c is the velocity of light ($3 \cdot 10^8$ m s^{-1} *in vacuo*) and λ is the wavelength (m)). For polychromatic radiation such as PAR consisting of photons of many wavelengths, the energy content may be computed provided the spectral composition (distribution) of the photons is known.

The attenuation of photons by both absorption and scattering in the water column causes the PFD to decrease approximately exponentially with increasing depth. Attenuation of the different wavelengths is not uniform so that the spectral composition of PAR as well as the photon flux density changes with depth. Pure seawater acts as a monochromator for 475 nm with the longer wavelengths being attenuated most strongly. In the open ocean where the concentrations of dissolved and particulate material are low it is the blue wavelengths that penetrate to the greatest depths. The appreciable concentrations of organic particulates and dissolved "yellow substance" in coastal waters, which absorb strongly at blue wavelengths, shift the wavelength of maximum transmission toward the green. The spectral dependence of attenuation within the water column also affects the spectral characteristics of the oceans surface reflectance, which is the property detected by remote sensing.

The photon flux density and the spectral distribution of the photons uniquely defines the photosynthetically available radiation at each successive depth horizon. Both properties of PAR combine with the absorption properties of the phytoplankton to determine the rate of photon absorption (Kirk 1975a,b,1976,1986; Morel and Bricaud 1981,1986; Bricaud *et al.* 1983; Bricaud and Morel 1986), and the subsequent rate of photosynthetic transduction of the absorbed photons (Radmer and Kok 1977a,b; Govindjee and Whitmarsh 1982).

The phytoplankton include a diverse range of phylogenetic groups possessing a wide assortment of photosynthetic pigments with different spectral absorption characteristics. In addition, many phytoplankton assemblages are capable of altering their spectral absorption characteristics in response to irradiance conditions. Such variation may result from photoadaptive variations within a single species or changes in the species composition of the assemblage. It is therefore important when modelling

aquatic photosynthesis to establish the photosynthetic response that is appropriate for the phytoplankton groups present at the specific location, time and depth under consideration.

To estimate oceanic primary production by remote sensing on a global scale, Platt and Sathyendranath (1988) suggested partitioning the ocean into a set of regions or provinces based upon the physiological rate parameters of the phytoplankton and the biological structure of the water column. Within the different regions the physiological properties of the phytoplankton and the water column structure would be considered quasi-constant and could be established at a local scale. As both the boundaries of the regions and the magnitudes of the characteristic parameters may be expected to change with the season, the authors proposed the term "dynamic biogeography". The spatial extent and potential contribution of the oceanic basins to global primary production makes the open ocean the region of greatest interest. This is the reason that this study has focused upon the phytoplankton assemblages characteristic of the open ocean, particularly the assemblages of the tropical oligotrophic oceans and the "picoplankton".

1.3. THE DOMINANCE OF THE PICOPLANKTON IN THE OPEN OCEAN.

The discovery of the widespread existence of a population of minute, unicellular organisms collectively termed the "picoplankton" (Johnson and Sieburth 1979; Waterbury *et al.* 1979) coincided with the debate over the absolute magnitude of oceanic primary production. While the occurance of small cells in the plankton had been recognized for some time (Lohmann 1911; Gross 1937), they were not previously considered to be of any quantitative significance. The picoplanktonic component isolated by Johnson and Sieburth (1979) and Waterbury *et al.* (1979) comprised many cells

containing photosynthetic membranes and were, by inference, considered to be photoautotrophic. Of particular interest was the ubiquitous distribution of small marine, chroococcoid cyanobacteria of the order of 1 μm in diameter and assigned to the genus *Synechococcus*.

The "picoplankton" have been formally defined as those organisms within the size range 0.2-2.0 μm (Sieburth *et al.* 1978). However different authors have employed different operational definitions. Most commonly, definitions are in terms of the particulate material that passes through a membrane filter with a nominal pore diameter of 3 μm, 2 μm or 1 μm (Li *et al.* 1983; Glover *et al.* 1985; Joint 1986). In some cases, the term picoplankton has implicitly refered solely to the autotrophic or even cyanobacterial component, so that the term "picoplankton" is rather generic. In this study, the term picoplankton refers to cells passing a 3 μm Nuclepore® filter with a pressure differential of < 100 mm Hg. For cited references, the operational definition employed by each author should be noted.

Before their widespread discovery, material of bacterial size was traditionally considered to be responsible solely for heterotrophic processes (*ie.* Sverdrup *et al.* 1942, p.910). Since the discovery of the picoplankton, evidence has accumulated that this size fraction contains a significant, metabolically active, photoautotrophic component. This size fraction is now considered to contribute a significant proportion of the total primary production in a variety of water masses (Li *et al.* 1983; Platt *et al.* 1983; Glover *et al.* 1985,1986; Putt and Prezelin 1985; Gieskes and Kraay 1986; Prezelin *et al.* 1986; Magazzu *et al.* 1987; Furnas and Mitchell 1988; Gradinger and Lenz 1989). The photoautotrophic picoplankton are particularly abundant in the warmer oligotrophic oceans where they contribute substantially to primary production. The discovery of a photoautotrophic component of such small size, potentially overlooked or under-

represented in earlier experimental protocols, was considered a possible cause of the disparities surrounding primary production estimates.

1.4. CELL SIZE AND THE PRIMARY PRODUCTION POTENTIAL OF THE PICOPLANKTON.

From a photosynthetic perspective, the observation that the picoplanktonic component included a large number of prokaryotic cells corresponding to populations of unicellular, chroococcoid cyanobacteria was of particular interest. Cyanobacteria contain a distinctive photosynthetic pigment system based upon phycobiliproteins that contrasts sharply with the chlorophyll *a*-carotenoid system typical of the larger phytoplankton fractions. The ubiquitous presence of these prokaryotic cells introduced the possibility that there existed an assemblage of very small cells in the oceanic phytoplankton with potentially high biomass-specific rates of primary production. The expectation that picoplanktonic cells might exhibit high biomass-specific rates of primary production compared with the larger phytoplankton component was based upon several *a priori* physiological arguments.

Throughout the biological world there is a widely recognized tendency of intrinsic rate variables to increase with decreasing cell size (Fenchel 1974; Banse 1976; Blum 1977; Peters 1983; Calder 1985). The relationship is an allometric one and Platt and Silvert (1981) have suggested that this is because of the fundamental dimensionality of physiological processes. Higher biomass-specific physiological rates and cell division rates generally accompany reduction in size in a broad spectrum of taxonomic groups including both microalgae (Banse 1976; Blasco *et al.* 1982; Geider *et al.* 1986) and phytoplankton assemblages (Taguchi and Laws 1987).

Similar trends in the rate of photosynthesis are expected from first principles. The absorption of irradiance is strongly dependent upon the physical and geometrical properties of the absorbing cells, in particular the size of the cells. The occurence of the photosynthetic pigments in discrete packages within the thylakoids of the cell, rather than being uniformly distributed, causes a reduction in the pigment-specific absorption cross-section in the spectral wavebands where absorption is strongest. The implications of this discrete packaging with regard to the potential for light absorption have been investigated theoretically for homogeneous, spherical cells by the application of Mie theory (Kirk 1975a,b,1976; Morel and Bricaud 1981; Bricaud and Morel 1986). A major conclusion is that for a given intracellular concentration of pigment, the *in vivo* pigment-specific absorption cross-section of a suspension of cells increases with diminishing cell size and approaches that of a true solution. Geider *et al.* (1986) and Geider and Osborne (1987) found that the chlorophyll *a*-specific absorption cross-section increases exponentially with decreasing cell size in several diatom species in agreement with the predictions of Mie theory. Picoplankton cells, by virtue of their small size, are expected to exhibit higher pigment-specific absorption than larger phytoplankton cells.

Increased pigment-specific absorption should lead to higher pigment-specific rates of photosynthesis under low irradiance. The quantum efficiency of photosynthesis is not considered to be size dependent since the basic photochemistry appears universal in all O_2-evolving organisms (Staehelin and Arntzen 1986). Both the "leakage" (the H^+ flux by lipid solution across the photosynthetic membrane) and "slippage" (the short-circuiting of the "S-states" in O_2 evolution) reactions that tend to reduce the quantum efficiency at low rates of photon absorption are independent of size *per se* (Raven and Beardall 1981,1982).

The small size of picoplankton cells also influences their potential ability to acquire nutrients both actively and passively. Irrespective of cell shape there is an allometric relationship between surface area and volume. The surface area increases by a function of the second power of the linear dimension while volume increases as a function of the third power. Based solely upon geometrical considerations, smaller cells have proportionately larger surface area:volume ratios than larger cells. As an example, the expression for the surface area:volume ratio of a sphere as a function of the radius R is $(4\pi R^2)/(4/3\pi R^3)$ or $3R^{2/3}$. The increased surface area:volume ratio of small cells will enhance the diffusive entry of a nutrient (such as CO_2 or NO_3^-) or the effusive exit of a metabolite (O_2, nitrogenous waste). Likewise, where nutrient acquisition is mediated by a membrane porter, the relative area of plasmalemma available for such porters is greater in small cells.

Eppley *et al.* (1969) provided the first experimental support for the notion that small cells have an enhanced ability to acquire nutrients such as nitrate or phosphate when these nutrients are present at low concentrations. In several species of marine phytoplankton the half-saturation constants (k_m, the concentration supporting an uptake rate one-half the maximum rate) were approximately proportional to the cell size and inversely proportional to the specific growth rate. Similarly, Suttle and Harrison (1988) report that the < 3 μm size fraction in an oligotrophic freshwater lake, consisting largely of unicellular *Synechococcus*-like cyanobacteria, accounted for 43-88% of the total saturated uptake of NH_4^+ and exhibited lower k_m values than the > 3 μm size fraction. In reviewing the subsistence cell quotas for both phosphorus and nitrogen, Shuter (1978) found a strong dependence on cell size in a wide variety of bacteria, cyanobacteria and eukaryotic unicellular algae. The minimum nutrient content per cell increased allometrically with cell size as measured by cell volume or carbon content. These results

emphasize the potential advantage of small cell size for nutrient acquisition in the nutrient-poor oligotrophic oceans.

An additional advantage of small size for photoautotrophs in the pelagic environment concerns the rate of sinking through the euphotic zone. Setting aside any possible physiological or morphological adaptations to reduce cell density that might prolong the residence time within the euphotic zone, the sinking rate of a sphere is:

$$v = \frac{2 r^2 g (\rho' - \rho)}{9 \eta}$$

where v is the velocity of downward movement (m s^{-1}), r is the radius of a spherical cell (m), g is the acceleration due to gravity (= 9.807 m s^{-2}), ρ' is the density of the cell (kg m^{-3}), ρ is the density of the medium (kg m^{-3}) and η is the dynamic viscosity of the medium (kg m^{-1} s^{-1}). For a given cell in a given medium, the sinking rate is directly proportional to the square of the radius. For seawater $\rho \geq 1026$ kg m^{-3} and $\eta \geq 9.1 \times 10^{-4}$ kg m^{-1} s^{-1} while the density of cells (ρ') is typically ≥ 1075 kg m^{-3}. Application of these typical values implies that a 100 µm diameter cell will sink 26 m d^{-1}, a 10 µm diameter cell will sink 0.26 m d^{-1} while a 1 µm diameter cell will sink 2.6 mm d^{-1}. This means the latter would take 50 years to sink through a 50 m euphotic zone (Raven 1986). This simple analysis implies that the rate of sinking attained by picoplanktonic cells is negligible by virtue of their diminutive size. The actual residence times of picoplankton cells within the mixed layer of the ocean is thus governed primarily by the convective movement of water within the surface mixed layer and may result in extended residence times in the euphotic zone.

Raven (1986) has explored several additional biochemical and physiological consequences arising solely from a consideration of size. The general conclusion is that small cells have an increased capacity to utilize resources particularly when resources are limiting. The observed decrease in cell size in many phytoplankton cells in response to resource limitation (photons or nutrients) tends to increase the cells' capacity to acquire those resources in a low-resource environment (Raven 1986). This must be regarded as an important feature because of the prevalence of oligotrophic conditions throughout the euphotic zone of the world's oceans.

Finally, theoretical arguments based upon the relative abundance of organisms of different size in the marine ecosystem suggest that the smaller size fractions are of greatest importance (Platt and Denman 1977,1978; Silvert and Platt 1978,1980; Platt and Silvert 1981; Platt 1985). The general tenet is that the magnitudes of the physiological rates of the component organisms control the flux of energy through an ecosystem. As biomass and energy flows through the pelagic ecosystem migrating from particles of small size to those of larger size, the biomass-specific rates of growth, reproduction and respiration of the organisms control the turnover of material within each size class. Because biomass-specific rates may be described by a decreasing power function of size, the biomass size spectrum (the relative abundance of different sized organisms per volume of water) is also allometric in form (Platt and Denman 1977,1978). This biomass size spectrum, plotted on logarithmic co-ordinates, has a negative slope reflecting the decreased concentrations of biomass in the successively larger size classes.

Actual biomass size spectra of the organisms in pelagic ecosystems are accumulating. For oceanic waters the data of Beers *et al.* (1975,1982) extended by Rodriguez and Mullin (1986a,b) from the central gyre of the North Pacific, which covers the range from 2 μm - 7 mm, is considered applicable (Platt *et al.* 1984; Platt 1985). The

slope (-0.22) of the theoretical function relating the abundance of various biomass size classes to their size, predicted by Platt and Denman (1977,1978) from physiological grounds, agrees closely with that computed for the microplankton (-0.20 to -0.23) from the North Pacific Central Gyre (Platt *et al.* 1984). Unfortunately the end of this spectrum representing the smaller size classes is unreliable. This arises from the fragility of small forms and the absence of any data for size classes < 2 μm, thereby excluding the picoplanktonic component (0.2 - 2 μm). Extrapolation of the slope of the biomass spectrum below 2 μm may not be justified since the data shows a decrease in biomass over the three smallest size classes (10 μm to 2 μm).

This caveat to the extension of the slope of the biomass spectrum to even smaller size classes may result from the existence of a "microbial loop". This hypothesis suggests that a significant proportion of the net primary production is channelled initially through a pool of dissolved organic matter that is utilized by small heterotrophic bacteria prior to being available to the larger phagotrophic microzooplankton (Azam *et al.* 1983; Fenchel 1988). In the likely event of high rates of metabolite excretion by microzooplankton, which consist mainly of heterotrophic flagellates and ciliates, the microzooplankton become a major determinant in the remineralisation of nutrients in the ocean. This role was traditionally assigned to bacteria. This process would represent a flow of material through the biomass continuum in the opposite direction from that of small to large and would result in a reduction of the biomass concentrations in the smaller size classes.

The ensemble of physiological properties associated with small size, and the likely dominance of the small size classes in the biomass spectrum of the pelagic ecosystem, suggests that the picoplankton play a crucial role as the principal primary producers in the food web of the open ocean. As such, establishing upper limits to

primary production in the open oceans requires a quantitative assessment of the photosynthetic capacity of the picoplankton throughout the water column. A quantitative estimate of the photosynthetic contribution of the picoplanktonic component is also central to the way we perceive the structure and function of the pelagic ecosystem, particularly in the oligotrophic open ocean.

1.5. THE LOCAL ABUNDANCE AND CONTRIBUTION OF PICO-PLANKTON TO OCEANIC PRIMARY PRODUCTION.

The initial reports of Johnson and Sieburth (1979) and Waterbury *et al.* (1979) emphasized the presence of cyanobacteria in the picoplankton fraction. The orange fluorescence emitted by the photosynthetic pigment phycoerythrin clearly distinguished the cyanobacteria. Cyanobacterial abundances have been determined in waters from the tropics, subtropics, temperate oceanic and shelf seas, and polar waters. Concentrations range from 10^5 to 10^8 cells per liter (Johnson and Sieburth 1979,1982; Waterbury *et al.* 1979,1980; Krempin and Sullivan 1981; Li *et al.* 1983; Platt *et al.* 1983; Douglas 1984; Caron *et al.* 1985,1986; Davis *et al.* 1985; Moriarty *et al.* 1985; Murphy and Haugen 1985; Nelson *et al.* 1985; Smith *et al.* 1985; Glover *et al.* 1985,1986a,b; Putt and Prezelin 1985; Takahashi *et al.* 1985; Craig 1986; El Hag and Fogg 1986; Fahrenstiel *et al.* 1986; Hardy *et al.* 1986; Iturriaga and Mitchell 1986; Krogmann *et al.* 1986; Joint 1986; Prezelin *et al.* 1986; Wheeler and Kirchman 1986; Zaika 1986; Zevenboom 1986; Flik *et al.* 1987; Marchant *et al.* 1987; Campbell and Carpenter 1988; Carpenter and Campbell 1988; Glover *et al.* 1988; Iturriaga and Marra 1988; Jochem *et al.* 1988; Legendre *et al.* 1988; Lochte and Turley 1988; Olsen *et al.* 1988; Shapiro and Haugen 1988; Stockner 1988).

Eukaryotic cells are also recognized as a substantial component of the picoplankton. Eukaryotes may account for as much as 90% of the total number of chlorophyll-containing organisms in the picoplankton (Murphy and Haugen 1985; Glover *et al.* 1985). For the North Atlantic the numbers of eukaryotic cells are generally an order of magnitude less than the numbers of cyanobacteria. Considerably less information is available regarding the abundance of the eukaryotic component of the picoplankton. This results from the lack of a characteristic spectral fluorescence signature that would permit their discrimination from the larger phytoplankton components in unfiltered seawater. At present, the only way of estimating their abundance is by measuring the red fluorescence signal of chlorophyll *a* following filtration through a membrane filter of appropriate pore size. This approach is unsatisfactory as many eukaryotes are fragile and filtration can result in either their complete destruction or deformation such that larger cells successfully pass through the membrane. Thomsen (1986) has recently published a taxonomic survey of the eukaryotic components of the picoplankton.

In the warm oligotrophic regions of the oceans there is a strong permanent pycnocline with an associated deep subsurface chlorophyll maximum. Chlorophyll concentrations in the subsurface maximum are often an order of magnitude greater than in the overlying surface mixed layer. Bienfang and Szyper (1981) have reported that > 80% of the subsurface chlorophyll maximum off Hawaii consisted of small phytoplankton (< 5 μm). Takahashi and Bienfang (1983) found that a similar percentage (80%) of the chlorophyll maximum was < 3 μm, and Bienfang and Takahashi (1983) report that small cells were also present in the surface layer. The current evidence suggests that the picoplankton (*sensu latu*) are the most abundant in the subsurface chlorophyll maximum, at least in oligotrophic waters (Bienfang and Szyper 1981; Furuya and Marumo 1983; Takahashi and Hori 1984).

Vertical profiles of cyanobacterial abundance from a large number of stations taken along a longitudinal transect from Woods Hole, Massachusetts, USA (42°N) to Punta Arenas, Chile (53°S) reveal cyanobacterial numbers to be very constant throughout the euphotic zone. Occasionally a distinct subsurface maximum was observed (Waterbury *et al.* 1986). In the surface mixed layer of the Celtic Sea the numbers of cyanobacteria varied little with depth, although this homogeneity may have resulted from wind-generated mixing of the surface layer (Joint 1986). Whether the picoplankton are responsible for the actual formation of the subsurface chlorophyll maximum, particularly in tropical oceans, remains an open question.

In temperate waters where the development of a thermocline is seasonal, the development of a subsurface chlorophyll maximum occurs on a much shorter time scale. Nano- and micro-plankton dominate these chlorophyll maxima with little significant contribution by picoplankton (Krempin and Sullivan 1981 (< 2 μm); Glover *et al.* 1986a (< 1 μm); Joint 1986 (review)). Both the abundance and photosynthetic contribution of picoplankton vary considerably in temperate regions and depend upon the physical properties of the water mass. In particular the seasonal temperature strongly influences abundance and photosynthetic activity.

Glover *et al.* (1985) found that the picoplankton (< 3 μm) of Georges Bank in the Gulf of Maine contained both eukaryotes and cyanobacteria. Cyanobacterial numbers were lowest in well-mixed surface waters accounting for 66% of the picoplanktonic fraction while their contribution was greatest (91%) at the least productive stations. A more extensive analysis found the abundance of picoplankton (< 5 μm, <1 μm and < 0.6 μm) to differ significantly in three diverse water masses in the Northwest Atlantic Ocean (Glover *et al.* 1986a). Larger phytoplankton dominated a coastal front in the Gulf of

Maine while the 0.2 - 0.6 μm size fraction made a major contribution to the standing crop of chlorophyll in the modified Sargasso water of a warm-core eddy in the same vicinity. Surprisingly, *Synechococcus* spp. dominated the 0.6 - 1.0 μm size fraction at an inshore station at Wilkinson's Basin in the Gulf of Maine. Largest numbers occurred at the 18% isolume co-incident with the chlorophyll maximum with concentrations equal to those recorded in tropical waters.

The mere numerical abundance of picoplanktonic cells in the euphotic zone cannot be automatically equated with a significant contribution to photosynthesis throughout the water column. However preliminary evidence suggests that picoplankton contribute significantly to primary production in several ocean regions. In the North Equatorial Current of the North Atlantic Gieskes *et al.* (1979) found that 20-30% of the carbon fixed in primary production experiments passed a 1 μm Unipore® filter, with a further 16% passing a 3 μm filter. In the tropical North Pacific Li *et al.* (1983) found that the percentage of the total primary production attributable to cells passing a 1 μm Nuclepore® filter increased from 20% in surface waters to over 80% at a depth of 70 m. Platt *et al.* (1983) reported similar results for an open ocean site west of the Azores in the subtropical Atlantic. About 60% of the total primary production at the subsurface chlorophyll maximum could be attributed to cells passing a 1 μm Nuclepore® filter. Comparable contributions by picoplankton have been reported for other tropical and sub-tropical waters. Takahashi and Bienfang (1983) found cells < 3 μm in diameter contributed 77-82% of the total ^{14}C fixation in oceanic waters off Hawaii. Magazzu *et al.* (1987) found that material passing a 1 μm Nuclepore® filter accounted for 56-63% of the biomass and 24-43% of the total primary production in the Strait of Messina. Similarly, Waterbury *et al.* (1986) found that 11% of the primary production in the upper 80 m could be assigned to *Synechococcus* spp. at a station in the Sargasso Sea.

Picoplankton production is also significant in temperate waters. Picoplankton (< 1 μm) accounted for 20-30% of the primary production in the summer months in waters over the European continental shelf (Joint and Pomeroy 1983). Extending their analysis to all seasons, Joint *et al.* (1986) estimated that the picoplankton (< 1 μm) contributed 22.4% to total annual primary production. Cells < 5 μm contributed a further 40.7%. The upwelling region of the Benguala current off southern Africa yielded comparable results. The picoplankton contributed an estimated 27% of the primary production based upon ^{15}N uptake experiments (Probyn 1985). This contribution dropped to 10% in coastal stations. Using methods designed to measure the contribution of marine cyanobacteria to total production in the waters of Woods Hole during the summer months, Waterbury *et al.* (1986) found that *Synechococcus* spp. contributed between 10 and 24% of the total photosynthetic incorporation of ^{14}C throughout the euphotic zone.

As with cell numbers, the picoplanktonic contribution to total primary production also depends greatly upon water type. In waters from a coastal front in the Gulf of Maine, the major contributors to both chlorophyll concentration and primary production were cells > 5 μm (Glover *et al.* 1986a). *Synechococcus* spp. accounted for only 6% of the *in situ* primary production. In contrast, *Synechococcus* spp. contributed 25% of the integrated primary production in the modified Sargasso water of a warm-core eddy (84-E), a site where the 0.2 - 0.6 μm size fraction equalled or exceeded the contribution made by larger size fractions to both chlorophyll and primary production. Similarly, at an inshore station at Wilkinson's Basin, *Synechococcus* spp. dominated the 0.6 - 1.0 μm size fraction and contributed 46% of the *in situ* integrated primary production.

Local oceanic anomalies may also increase the abundance and the relative photosynthetic contribution of the picoplankton in temperate waters over short time scales. Putt and Prezelin (1985) found chroococcalean cyanobacteria dominated the

chlorophyll maximum in the Santa Barbara Channel during the Californian "el Nino" event in the summer of 1983, accounting for over 80% of the biomass. Numbers of cyanobacteria were twice those previously described (Krempin and Sullivan 1981) and matched those reported from other coastal waters. Concomitantly, the picoplankton contribution to chlorophyll-based primary production increased such that 75% could be associated with cells < 5 μm in diameter, a size fraction dominated by cyanobacteria. The overwhelming presence of cyanobacteria in Californian coastal waters, normally dominated by diatoms and dinoflagellates, was attributed to the weakening of the southerly flow of the California Current System coincident with the enhanced inflow of warmer offshore waters.

The only Arctic information is that provided by Smith *et al.* (1985) for the eastern Canadian Arctic and by Gradinger and Lenz (1989) for the East Greenland current at 80°N. Smith *et al.* (1985) report that the picoplanktonic component was responsible for 10-25% of the primary production in late summer. Gradinger and Lenz (1989) found the number of cyanobacteria decreased from warm Atlantic intermediate water to the cold Polar water where they were practically absent. In Antarctic waters Marchant *et al.* (1987) found the numbers of cyanobacteria decreased exponentially with decrease in temperature in the surface waters along a transect between Australia and Antarctica. Similarly the absence of *Synechococcus* cells from the waters of McMurdo Sound on the Ross Ice Shelf (Waterbury *et al.* 1986) suggests that picoplankton may also be of little significance in Antarctic waters. It would appear that picoplanktonic cyanobacteria are of little quantitative significance in polar waters.

There is a clear relation between latitude and cyanobacterial abundance with a strong trend toward decreasing numbers at higher latitudes (Murphy and Haugen 1985). Interestingly the only samples not to yield marine cyanobacteria were collected from the

Ross Ice Shelf in Antarctica (Waterbury *et al.* 1986). Temperature is considered the determining factor (although possibly indirectly) as there is a strong correspondence between increasing temperature and the upper limit of cyanobacterial abundance (Joint 1986). A similar relation between cyanobacterial numbers and temperature occurs in the freshwater system of Lake Ontario (Caron *et al.* 1985).

Several recent reviews provide further details of the physiology and ecology of marine *Synechococcus* spp. and the geographical distribution of picoplankton (Glover 1985; Fogg 1986; Stockner and Antia 1986; Platt and Li 1986).

1.6. PHOTOSYNTHETIC CHARACTERISTICS OF THE PICOPLANKTON.

Preliminary studies of the P-I response of marine cyanobacteria (Morris and Glover 1981; Glover and Morris 1981; Barlow and Alberte 1985; Kana and Glibert 1987a,b) and field populations of picoplankton (Li *et al.* 1983; Platt *et al.* 1983; Glover *et al.* 1985,1986a; Putt and Prezelin 1985; Iturriaga and Mitchell 1986; Prezelin *et al.* 1986; Magazzu *et al.* 1987; Furnas and Mitchell 1988) suggest that the assimilation numbers (P_m^B) and photosynthetic efficiencies at low light (α^B) of picoplanktonic cells are significantly greater than those of larger phytoplankton. PFDs corresponding to the light-adaptation parameter ($I_k = P_m^B/\alpha^B$), the optimal photosynthetic PFD (I_m) and the PFD marking the onset of photoinhibition (I_b), are all lower in the picoplankton. The increased photosynthetic efficiences observed under low light conditions (higher α^B) would permit the picoplankton to exploit low light environments. This would extend the lower depth limit of photosynthesis in the ocean.

There is not much information on the spectral characteristics of picoplankton photosynthesis. The phylogenetic identities of the major picoplankton components are still preliminary and undergoing rapid revision as new and different isolates are continually being identified (*ie.* Chisholm *et al.* 1988). Indeed the relative importance of prokaryotes and eukaryotes remains contentious. The early consensus suggested the dominance of the cyanobacteria together with several eukaryotic algae. Among the cyanobacteria, those containing phycoerythrin appear dominant in the open ocean (Waterbury *et al.* 1986; Olsen *et al.* 1988), cyanobacteria with phycocyanin as their principal light-harvesting pigment are only of importance in coastal or estuarine environments (Waterbury *et al.* 1986).

Experiments conducted in the open ocean at depths corresponding to the depth of collection show that cyanobacterial clones containing phycoerythrin (*Synechococcus* spp. WH 7803 and WH 8018) have higher photosynthetic rates at depth in clear ocean water than clones that utilize phycocyanin (*Synechococcus* sp. WH 5701) (Wood 1985). The rank order of cyanobacterial clones in terms of their relative ability to photosynthesize at depth correlated with the capacity of their light-harvesting pigments to absorb the wavelengths that successfully penetrated to depth. Under artifical light the two eukaryotic species (*Thalassiosira oceanica* Hasle and Heimdal (clone 13-1) and *Pavlova* sp. (clone NEP)) and the cyanobacterium *Synechococcus* sp. WH 7803 had similar P-I relationships. At depth however, the two eukaryotic species had higher photosynthetic rates at low light levels than *Synechococcus* sp. WH 7803. This difference was interpreted in terms of the organization of the photosynthetic apparatus in both groups. Specifically, that the Soret absorption band of chlorophyll *a* can "drive photosynthesis to a greater extent in eukaryotes than [in] the marine *Synechococcus*" (Wood 1985). Glover *et al.* (1986b) obtained similar results, showing that picoplanktonic eukaryotes had

greater photosynthetic efficiencies at low light levels (α^B) in blue light than the cyanobacteria, even when photosynthetic rates were normalized to chlorophyll.

The existence of both cyanobacteria, with a photosynthetic apparatus based upon phycobiliproteins and chlorophyll *a*, and eukaryotes whose photosynthetic pigmentation was similar to the chlorophyll *a*-chlorophyll *c*-carotenoid system present in the larger phytoplankton groups, suggested that the picoplankton potentially represented a spectrally diverse group. Furthermore, as a phylogenetic group the cyanobacteria can modulate their spectral absorption characteristics in response to the photon flux density (intensity adaptation: Raps *et al.* 1983; Barlow and Alberte 1985; Wyman and Fay 1986a), the spectral distribution of the incident photons (chromatic adaptation: Fujita *et al.* 1985; Manodori and Melis 1986a,b; Fujita *et al.* 1987), temperature (Anderson *et al.* 1983) and the external supply of a wide selection of nutrients (Bryant 1986).

1.7. MODELLING GLOBAL PICOPLANKTON PHOTOSYNTHESIS.

Since the picoplankton constitute a significant component of the photosynthetic biomass in the pelagic ecosystem, any serious effort to model oceanic primary production must take their photosynthetic characteristics into account. Initial analyses suggest that the optical properties of the ocean may be related to both the biomass concentration and the rate of primary production within the water column (Platt 1986; Lewis *et al.* 1986; Sathyendranath 1986; Platt and Lewis 1987; Platt *et al.* 1988b). Additionally, the unique spectral signature of the phycobiliprotein pigments comprising the photosynthetic apparatus of cyanobacteria permits the discrimination of this picoplanktonic component from the remainder of the phytoplankton. Fluorescent signals from the phycobiliprotein phycoerythrin in the ocean have already been remotely detected by satellite (Exton *et al.*

1983; Hoge and Swift 1983). Remote sensing therefore provides the potential for providing estimates of both the total primary production and the relative contribution by the phycobiliprotein-containing picoplankton (Sathyendranath 1986; Platt 1986).

Establishing a quantitative relationship between photosynthesis and available irradiance represents a point of departure for developing algorithms for computing oceanic production (Vollenweider 1965; Patten 1968; Straskraba 1974; Bannister 1974; Platt *et al.* 1977; Platt and Gallegos 1980; Baumert and Uhlmann 1983). Estimation of the integral primary production beneath an area of ocean requires a mathematical model that describes the rate at which photosynthesis will occur at the different depth horizons throughout the water column. Since irradiance is considered the limiting environmental variable, estimates of depth-integrated photosynthesis rely upon quantitative descriptions of the attenuation of irradiance with depth and the dependence of photosynthesis upon irradiance. Considerable attention has been devoted to the nature of the underwater irradiance field in the open ocean (Preisendorfer 1961; Jerlov 1976; Tyler and Smith 1970; Kirk 1983). The photosynthetic response of oceanic phytoplankton to different irradiance fields has received much less attention.

In general, the importance of the photon flux density or the spectral distribution of the photons in governing the photosynthetic response have been assessed independently. Experimental data regarding the photosynthetic response of phytoplankton have focused exclusively upon the relationship between photosynthetic rate and photon flux density, the so-called photosynthesis-irradiance (P-I) relationship (Jassby and Platt 1976; Platt and Jassby 1976; Platt *et al.* 1977; Bannister 1979; Platt and Gallegos 1980; Platt *et al.* 1980; Gallegos and Platt 1981). These studies gave little regard to the spectral composition of the incident photons. Analysis of the photosynthetic response to the wavelength of the incident photons (the action spectrum of photosynthesis or P-S

relationship) has been restricted to laboratory cultures of selected species and has been limited to low photon flux densities, where the photosynthetic rate is a linear function of the photon flux density (Myers and French 1960; Bannister and Vrooman 1964; Myers and Graham 1963; Jones and Myers 1964; Eley and Myers 1967; Malkin 1967; Myers 1971; Wang and Myers 1976a,b; Wang *et al.* 1977; Ried *et al.* 1977; Ried and Reinhart 1977).

A complete description of the photosynthetic response to submarine irradiance requires a mathematical model that incorporates the effects of spectral composition of the incident photons together with the response to increasing photon flux density (what might be termed a P-S-I response). As will become apparent in the later discussion, incorporation of the spectral nature of the incident photons into the P-I response is particularly important in any model of the photosynthetic response of phytoplankton aimed at including the picoplanktonic component.

Chapter 2 reviews the previous mathematical formulations employed to describe the photosynthetic response of phytoplankton in terms of the incident photon flux density (the P-I response). The form of the P-I response is discussed in terms of calculating the integral primary production beneath an area of ocean surface.

Chapter 3 provides a theoretical framework for including the spectral dependence of photosynthesis. The general approach adopted is the independent decomposition of the photosynthetic response in terms of both the photon flux density (P-I response) and the photon wavelength (P-S response). The results are then combined to yield the photosynthetic rate attainable under any specific photon flux density and spectral distribution (the P-S-I response). Several successively more complex approaches to combining P-I and P-S responses are examined. Each is discussed in terms of providing

a sufficiently quantitative description of the photosynthetic response under polychromatic irradiance.

The first solution constitutes a straightforward spectral weighting of the P-I response based upon the spectral absorption characteristics of the phytoplankton. The second approach, based upon the principles embodied in classical action spectroscopy, provides a spectral correction for the absorbance characteristics of the photosynthetically active pigments. This simple approach assumes that photosynthesis can be modelled as a single photoreaction whose spectral dependence may be determined from the P-I response determined in monochromatic irradiance. In this case the action brought about by photons of one wavelength are independent of that brought about by another such that their sum is simply additive. Two photosynthetic models are then introduced that may be scaled according to the deduced monochromatic action spectra. The first represents a simple empirical function designed to describe the observed P-S-I response from a geometrical perspective. The second is a simple rational model based upon Poissonian statistics that attempts to explain both photosynthesis and photoinhibition in terms of target theory.

Finally, the inter-dependent effects of photons of different wavelengths in determining the rate of photosynthesis are discussed. Such effects cause the combining of photons of different wavelengths to act in a non-additive fashion. This requires the introduction of analytical models to describe the photosynthetic process under polychromatic irradiance. This approach models photosynthesis in terms of two serially-linked photoreactions with independent spectral responses. In this model the quantum yield of photosynthesis is variable and is a function of the spectral distribution of the incident irradiance, the action spectra of both photoreactions and interaction the two photoreactions.

Chapter 4 describes the materials and procedures employed to determine the absorption and photosynthetic response as a function of photon flux density and wavelength.

Chapter 5 describes the P-I relationships obtained for laboratory cultures of selected picoplanktonic species determined under "white", "blue" and "green" polychromatic irradiance. The relative abilities of various empirical mathematical formulations for describing this relationship are compared.

Chapter 6 describes the absorption spectra of both laboratory cultures of picoplankton and natural seawater samples collected from several oceanographic regimes. These spectra are critically examined with the view to using the absorption spectra for spectrally weighting the P-I response.

Chapter 7 discusses the photosynthetic action spectra and quantum yield spectra determined for both picoplankton cultures and natural water samples under monochromatic irradiance. Action spectra and quantum yield spectra are evaluated as means of incorporating the spectral dependence of photosynthesis into a comprehensive P-S-I model.

Finally, Chapter 8 provides a general discussion of these results. The various spectral photosynthesis models are examined in relation to i) modelling primary production throughout the water column and ii) estimating the importance of the picoplanktonic contribution to global primary production.

CHAPTER 2

NON-SPECTRAL PHOTOSYNTHESIS-IRRADIANCE MODELS - A REVIEW.

2.1. THE PHOTOSYNTHETIC RESPONSE TO PHOTON FLUX DENSITY.

The photosynthetic response of autotrophic cells to increasing photon flux density (PFD) is very uniform, despite the phylogenetic diversity of photoautotrophs. The response may be described by a curve that may be partitioned into three or sometimes four regions. At very low PFDs, below the compensation point (~2-20 μmol m^{-2} s^{-1}), where the magnitude of the photosynthetic and respiratory rates are similar, the rate of photosynthetic oxygen evolution is a non-linear function of PFD (Kok 1949). This non-linearity is considered to arise from increased suppression of the respiratory reactions with increasing PFD. Measurement of the photosynthetic rate by isotopic (^{14}C) incorporation at these PFDs is also complicated by the fact that it is unclear whether the method measures net or gross photosynthesis (Bidwell 1977; Harris 1980; Peterson 1980; Dring and Jewson 1982; Smith and Platt 1984; Sondergaard 1988).

Above the compensation point at a PFD of between 2-20 to 50-100 μmol m^{-2} s^{-1}, photosynthesis is directly proportional to irradiance and photosynthesis is considered to be light-limited. Depending upon the organism and the method by which photosynthesis is measured (*ie.* ^{14}C or O_2) extrapolation of the linear portion of the curve to zero PFD results in the response intersecting the ordinate at some negative value. For reasons of pragmatism the point where the curve intersects the vertical axis has been interpreted as the magnitude of dark respiration, although this interpretation is oversimplified (Jassby

and Platt 1976). In many cases such extrapolation passes sufficiently close to the origin that any offset can be ignored.

At higher PFDs (typically 100-200 μmol m^{-2} s^{-1}) the rate of photosynthesis reaches a maximum at which point photosynthesis is no longer considered light-limited but rather is light-saturated. Above this threshold the photosynthetic response may or may not exhibit photoinhibitory decreases in photosynthetic rate. Where there is no photoinhibition the photosynthetic rate remains maximal up to 2000-3000 μmol m^{-2} s^{-1}, the PFD characteristic of full sunlight.

In many cells photoinhibition occurs and is evidenced by a decrease in the photosynthetic rate above a threshold PFD. Where the onset of photoinhibition occurs at low PFD (at or below the transition from light-limited to light-saturated photosynthesis) a pronounced peak in the P-I response is defined yielding a maximal photosynthetic rate at a specific PFD. If photoinhibition does not occur until higher PFDs then the P-I response a is characterized by a broad plateau where the photosynthetic rate is maximal over a range of PFDs.

A wide variety of analytical expressions have been employed to describe the photosynthetic response of cells to increasing PFD. To date, no single expression has been accepted as the "best" or most appropriate choice. The expression chosen is generally based upon characteristics of the data set (*ie.* whether photoinhibition is present) and the ultimate purpose for which the photosynthetic measurements were made. Alternative formulations reflect differences in the rationale employed to justify their particular choice.

2.2. TYPES OF P-I MODELS.

Models of the photosynthesis-irradiance response may be classified according to the rationale behind their formulation. Platt *et al.* (1977), following the principles described by Lucas (1964), have distinguished between empirical and rational models according to the models internal structure.

Empirical models are constructed with little or no regard for the underlying mechanism of the system. They are mathematical models which have the sole objective of describing the essential features of the available data with adequate precision *as simply as possible*. As such, they reduce to an exercise in curve-fitting. Two opposing criteria govern the choice of the appropriate mathematical expression: i) precision, which may be increased by the addition of extra parameters and ii) the principle of parsimony which dictates that the number of parameters employed should be the minimum required to adequately describe the data. The degree of "adequacy" is arbitrary although some objective criterion is usually used. Such empirical representations describe a family of curves according to a certain equation with particular members of the family being specified by particular sets of parameter values.

The actual mathematical expression chosen is often based solely upon mathematical intuition as to what function is likely to match the data set based upon visual inspection. A major detraction to empirical models of this sort is that the parameters are often uninterpretable due to the arbitrariness and lack of structure of the model. Most of the mathematical models that have been applied to the relationship between photosynthesis and PFD were formulated with some regard to the possible underlying biology. While this basis is undoubtedly overly-simplistic, it does mean that

such models are not strictly empirical and are more accurately described as semi-empirical.

In contrast, *rational models* are more highly structured and admit a minimum of arbitrariness. They are based upon the way in which the system is perceived to function and only admit assumptions concerning the less-well understood aspects of the system that may be considered reasonable. Rational models have the advantage that the parameters are interpretable with respect to the real system and their derived values provide insight into the underlying mechanism of the system. Mechanistic or reductionist models are a subset of rational models wherein the behavior of one level of the system is described in terms of the organization at a lower level of the system.

Application of such reductionist models to the relationship between photosynthesis and irradiance have been very rudimentary despite the potential of this approach. This stems in part from two historical perceptions of photosynthesis. Firstly, that the underlying mechanisms of photosynthesis are so poorly understood that a realistic model cannot be constructed. And secondly, that the process is so complex that an adequately realistic model would contain such a large number of interrelated parameters that their values could not be ascertained unequivocally because of the lack of information in the P-I curve. In mathematical terms, a single P-I curve could represent an infinite number of solutions to the model parameters.

2.3. EMPIRICAL MODELS.

At one end of the spectrum of possible models are those that are strictly mathematical formulations. For a mathematical formulation to be considered acceptable the parameters should be mutually independent. For reasons of parsimony the number of

independent parameters should be kept to a minimum consistent with providing an adequate description of the data.

2.3.1. Empirical Models excluding Photoinhibition.

The relationship between photosynthesis and irradiance up to a PFD where photoinhibition begins is most simply described as a saturation-type response. As such, a *minimum* of two independent parameters are required for its complete description. The early descriptions of light saturation curves of photosynthesis were formulated with a variety of different parameters, each possessing a unique geometrical interpretation according to the mathematical formulation employed. By analogy with the saturation constant K_m in Michaelis-Menten enzyme kinetics, these equations were most frequently formulated in terms of a parameter that represented the PFD where the photosynthetic rate switched from being light-limited to light-saturated.

Various symbols were employed for this parameter, often referred to as the "light adaptation" parameter, the most common being "I_k". In several cases the same symbol was employed for this parameter despite the fact that parameter's definition differed in the different formulations. Consequently the term I_k is somewhat "generic" in that its definition is not constant across the different mathematical formulations (see below). Furthermore, the parameter I_k is dependent upon the parameter describing the maximum light-saturated rate of photosynthesis (P_m^B) and so is not strictly an independent parameter. The precise form of this dependency varies according to the mathematical formulation employed (see Table 2.1).

Mathematical representations of several light-saturation curves which exclude photoinhibition have been discussed by Jassby and Platt (1976), Platt and Jassby (1976),

Platt *et al.* (1977), and Lederman and Tett (1981). For the purpose of comparison, Jassby and Platt (1976) and Platt *et al.* (1977) recast a number of these early formulations in terms of two common parameters: α^B, the slope of the light-saturation curve as the PFD tends to zero, and P_m^B, the maximum photosynthetic rate as the PFD tends to infinity. The initial slope of the photosynthesis-irradiance curve when photosynthetic rate is normalized to biomass, α^B, is defined as:

$$\alpha^B = \left. \frac{\partial P^B}{\partial I} \right|_{I \to 0} \qquad ...(2.1)$$

The maximum rate of photosynthesis normalized to biomass, P_m^B, is also frequently referred to as the assimilation number. These two parameters, α^B and P_m^B, are all that are required in all two-parameter formulations. While they are geometrically independent, in practice they are often found to be correlated. Use of these two parameters also permits a specific definition of the light adaptation parameter I_k where:

$$I_k = P_m^B / \alpha^B \qquad ...(2.2)$$

that is consistent for all of the different mathematical formulations.

Following the postulate of Liebig (1840,1843) known as the "law of the minimum" which suggested that crop yields were determined by the single nutrient element present in lowest concentration, Blackman (1905) suggested that the rate of any physiological process is proportional to a single rate-limiting factor. As the availability of one factor increases it reaches a point where it is no longer limiting and the process becomes limited by another factor. Extending this principal to the light-saturation curve of photosynthesis, Blackman (1905) proposed that the relationship could be described by the function:

$$P^B = \alpha^B I \quad \text{for} \quad I \leq \frac{P_m^B}{\alpha^B}$$

$$= P_m^B \quad \text{for} \quad I > \frac{P_m^B}{\alpha^B} \qquad \ldots(2.3)$$

This expression was subsequently been employed by Riley (1946) and Sverdrup (1953) in their analyses of aquatic primary production.

Since most experimental P-I data exhibited a gradual transition from the initial light-limited portion where photosynthesis increases linearly with increasing light ($P^B = \alpha^B I$) to the region where photosynthesis remains maximal and constant ($P^B = P_m^B$), an analytical description of this curvature was desirable. Baule (1917) appears to be the first to employ an exponential expression to describe the photosynthesis-irradiance relationship. As a purely empirical expression this form has since been applied by several authors (*ie.* Webb *et al.* (1974):

$$P^B = P_m^B \left[1 - exp^{-\alpha^B I / P_m^B} \right] \qquad \ldots(2.4)$$

This formulation approaches saturation more rapidly than the rectangular hyperbola (see below) and is characterized by an extended linear portion at low light intensities. As a result this expression generally provides a good fit to experimental data. As a certain rationale may be employed to justify its choice this formulation is discussed further under rational models below.

A minor modification of this exponential relation aimed at providing a steeper early response and more gradual final approach to the asymptote was suggested by Thornley (1976):

$$P^B = \alpha^B \left[1 - exp^{- P_m^B / \alpha^B I} \right] \quad ...(2.5)$$

This formulation has not been employed with respect to phytoplankton.

By analogy with the Michaelis-Menten curve of enzyme kinetics, several authors including Baly (1935), Arnold (1935) and Burk and Lineweaver (1935) employed the simple rectangular hyperbola to describe the relationship between photosynthesis and irradiance:

$$P^B = \frac{P_m^B \ \alpha^B \ I}{P_m^B + \alpha^B \ I} \quad ...(2.6)$$

The subsequent use of this curve has been extensive largely because of the analogy to enzyme kinetics. In the context of modelling aquatic photosynthesis it has been employed by Tamiya (1951) and Eppley and Sloan (1966) among others.

A major disadvantage of the rectangular hyperbola in describing light-saturation curve of photosynthesis is that the rate of change in the gradient is greatest as the light intensity tends to zero. The result is that as the PFD increases the rate of photosynthesis predicted by the curve decreases too rapidly compared to the experimental data, that is, the gradient of the curve ($\partial P/\partial I$) decreases too quickly. Experimental curves tend to exhibit an extended linear portion with more abrupt curvature in the region where light becomes saturating than predicted by the rectangular hyperbola. Consequently fitting a rectangular hyperbola to P-I data causes both α^B and P_m^B to be overestimated while the photosynthetic rate around the shoulder is underestimated.

To provide better correspondence with the data, Smith (1936) suggested a modification to the formulation of Baly (1935) whereby the individual terms in the denominator are squared and the square root is then taken of their sum:

$$P^B = \frac{P_m^B \, \alpha^B \, I}{\left[(P_m^B)^2 + (\alpha^B I)^2 \right]^{1/2}} \qquad ...(2.7)$$

This formulation has been employed by Winokur (1948) and Talling (1957) to describe algal photosynthesis.

Steele (1962) proposed a 2-parameter equation which attempted to include photoinhibition (see below). It was modified by Jassby and Platt (1976) to exclude the possibility of photoinhibition and may be rewritten in terms of the two biomass-normalized parameters α^B and P_m^B as:

$$P^B = \alpha^B I \exp^{-\alpha^B I / P_m^B e} \quad \text{for} \quad I \leq P_m^B \cdot e / \alpha^B$$

$$= P_m^B \quad \text{for} \quad I > P_m^B \cdot e / \alpha^B \qquad ...(2.8)$$

This modification was found to provide a superior fit to data lacking photoinhibition than the original formulation (Jassby and Platt 1976).

Another analytical expression suggested by Platt *et al.* (1977) was a modified formulation of an expression originally proposed by Vollenweider (1965) that included photoinhibition (see below). Their modification was such that the original form of the curve was retained up to the point where photosynthesis reached a maximum. Decreases in P^B above this threshold that were inherent in the original expression were replaced by

the maximum photosynthetic rate for all further increases in PFD. Stated formally, this formulation is:

$$P^B = \alpha^B - \left[(\alpha^B I)^2 / 4P_m^B\right] \quad \text{for} \quad I \leq 2P_m^B / \alpha^B$$

$$= P_m^B \quad \text{for} \quad I > 2P_m^B / \alpha^B \qquad ...(2.9)$$

Jassby and Platt (1976) also introduced the use of the hyperbolic tangent function:

$$P^B = P_m^B \tanh(\alpha^B / P_m^B) \qquad ...(2.10)$$

This formulation is a combination of exponentials and may be written:

$$P^B = P_m^B \left[\frac{e^{\alpha^B I/P_m^B} - e^{-\alpha^B I/P_m^B}}{e^{\alpha^B I/P_m^B} + e^{-\alpha^B I/P_m^B}} \right] \qquad ...(2.10a)$$

This function was found to provide a superior fit to a wide selection of saturation-type P-I curves from natural populations of marine phytoplankton (Jassby and Platt 1976; Platt and Jassby 1976).

As an alternative means of providing an extended linear portion at low PFDs, and thereby a sharper transition to light-saturation consistent with the experimental data, Thornley (1976) proposed the use of a three-parameter non-rectangular hyperbola:

$$\Theta(P^B)^2 - (\alpha^B I + P_m^B)(P^B) + \alpha^B P_m^B I = 0 \qquad ...(2.11)$$

where P^B is given by the lower root of the quadratic equation. The motivation for this formulation arises from a variety of rational models all of which reduce to this form (see below). However when applied in the absence of any underlying model the use of the non-rectangular hyperbola may be considered empirical.

Geometrically, the parameter Θ describes the abruptness of the transition from light-limitation to light-saturation. When $\Theta = 0$ the equation reduces to a rectangular hyperbola [Eq. 2.6] and where $\Theta = 1$ the response reduces to a Blackman-type curve [Eq. 2.3]. This curve provides a good fit to all saturation-type P-I data but at the expense of a third parameter.

Finally, Bannister (1979) also suggests a three-parameter formulation with geometric properties similar to that of the non-rectangular hyperbola:

$$P^B = \frac{P_m^B \, I}{\left[(I_k)^m + I^m \right]^{1/m}} \qquad ...(2.12)$$

This form is a generalization of the equation proposed by Smith (1936) [Eq. 2.7] where the parameter m describes the abruptness with which the curve makes the transition from the light-limited to light-saturated region. This more general form reduces to the rectangular hyperbola of Baly (1935) [Eq. 2.6] where $m = 1$ and to the equation of Blackman (1905) [Eq. 2.3] where $m = \infty$. Bannister (1979) notes that inspection of prior P-I responses suggest that m be greater than 2 and often closer to 3. He also pointed out that this formulation most closely matches the successful hyperbolic tangent function [Eq. 2.10] of Jassby and Platt (1976) when $m \approx 2.5$. Like the non-rectangular hyperbola this formulation provides a good fit to most P-I curves.

2.3.2. Empirical Models including Photoinhibition.

In the P-I responses of many cells, the photosynthetic rate is seen to decrease progressively at high irradiances indicative of a photoinhibitory process. For phytoplankton this inhibitory effect of high light intensity has been known for some time (Ryther 1956). Accordingly, many of the models of aquatic productivity employed mathematical formulations of the P-I response that had photoinhibition built into them (Steele 1962,1965; Vollenweider 1965,1970; Fee 1973; and see Patten 1968). The various mathematical models that include photoinhibition have been discussed by Platt *et al.* (1980) and Platt and Gallegos (1980). Empirical formulations that include photoinhibition fall into two categories - those that contain a separate photoinhibition function and those that do not.

The early model of Steele (1962) has photoinhibition built into it despite the fact that it is only a 2-parameter model:

$$P^B = P_m^B \left[(I / I_m) \exp (1 - I / I_m) \right] \qquad ...(2.13)$$

where I_m is the irradiance at which maximum photosynthesis occurs. In re-parameterised form (Platt *et al.* 1977) it may be expressed:

$$P^B = \alpha^B I \exp (- \alpha^B I / P_m^B e) \qquad ...(2.13a)$$

Because there is no independent parameter describing photoinhibition, the same parameter (α^B) governs the initial slope as governs the decrease in photosynthesis at high light intensities. This means that the shape of the curve is essentially fixed with a direct dependency between the light-limited and light-inhibited regions of the response. This

was intentional in the original formulation, however experimental data suggest that the photosynthetic response above the onset of photoinhibition can vary independently of the response below the photoinhibition threshold. The direct dependency that is inherent to this formulation causes it to provide a poor fit to most experimental data.

In an effort to improve the ability of Steele's (1962) equation to fit P-I data and obtain an expression that was flexible enough to describe a variety of metabolic responses Parker (1973) suggested that the entire expression be raised to a power:

$$P^B = P_m^B \left[(I/I_m) \exp(1 - I/I_m) \right]^m \quad \ldots(2.14)$$

In this formulation the initial slope is discrete, *ie.* either 0 or ∞, as the light intensity approaches zero. This feature is generally irreconcilable with observation and so Eq. 2.14 is considered to be of little value for the purposes of describing the P-I response.

The absence of any simple correlation between the processes of light-limited and light-inhibited photosynthesis in experimental data makes it preferable to introduce a separate function with independent parameters to describe photoinhibition. One approach to including photoinhibition is to segregate the P-I response into two discrete regions with separate formulations for each. Since for practical curve-fitting reasons it is preferable to describe the entire P-I response with a single analytical function, an alternative method originally proposed by Vollenweider (1965) is to simply multiply the empirical function describing light saturation by a second empirical function that describes the decrease in photosynthetic rate at high irradiances. If $f(I)$ denotes the function describing the photosynthetic rate at low light intensities and $g(I)$ denotes the function that describes increase in photoinhibition at high light intensities then the multiplicative expression for the entire P-I response may be written:

$$P^B = f(I) \cdot g(I) \quad \text{...(2.15)}$$

In order to provide the best fit to experimental data the function chosen to describe photoinhibition should have a value of 1.0 at zero light intensity where no photoinhibition occurs and should approach 0 asymptotically at high intensities. The form of *g(I)* at intermediate intensities controls the shape of the P-I response. Since *g(I)* is less than unity at all light intensities greater than zero, the multiplicative relationship between *g(I)* and *f(I)* means that the maximum photosynthetic rate attainable (P_m^B) will necessarily always be less than the asymptotic value of P_m^B predicted by *f(I)* alone. Consequently, Platt and Gallegos (1980) suggest the use of P_m^B to denote the maximum *realized* photosynthetic rate and P_s^B to denote the *potential* maximum photosynthetic rate predicted in the absence of *g(I)*. The exact relationship between P_m^B and P_s^B will depend upon the empirical functions chosen for *f(I)* and *g(I)*.

Platt and Gallegos (1980) have also suggested that it is preferable that the functional forms of *f(I)* and *g(I)* be algebraically similar so as to provide analogous parameters. In this case the observed photosynthetic rate may be expressed:

$$P^B = f(I) \cdot (1 - g(I)) \quad \text{...(2.16)}$$

since *f(I)* represents a photoenhanced reaction and *g(I)* is a photoinhibitory reaction.

As noted above the minimum number of independent parameters required to adequately describe P-I responses that exhibit photoinhibition is three. To date the only three-parameter model routinely employed to characterize P-I responses which include photoinhibition is that introduced by Platt *et al.* (1980):

$$P^B = P_s^B \left[1 - exp^{-\alpha^B I / P_s^B} \right] \left[exp^{-\beta^B I / P_s^B} \right] \quad ...(2.17)$$

In this formulation the photoinhibition parameter β^B characterizes the negative slope of the P-I response at high intensities and is analogous to (and has the same units as) α^B. Both α^B and β^B are scaled to P_s^B. By analogy to the derived parameter I_s describing the irradiance to which cells are adapted for photosynthesis in the absence of photoinhibition ($I_s = P_s^B/\alpha^B$), an irradiance index I_b may be similarly constructed that describes the susceptibility of photosynthesis to photoinhibition ($I_b = P_s^B/\beta^B$). The lower the value of I_b, the stronger is photoinhibition. Eq. 2.17 may be rewritten in terms of the parameter I_s:

$$P^B = P_s^B \left[1 - exp^{-I / I_s} \right] \left[exp^{-bI / I_s} \right] \quad ...(2.17a)$$

where the parameter b describes the negative slope of photoinhibition scaled to the initial slope at low irradiances.

A drawback to Eq. 2.17 is that the negative slope of the photoinhibition function $g(I)$ is constant throughout the entire range of I for all I greater than zero. When combined multiplicatively with the photochemical function $f(I)$ the result is a P-I response that exhibits a sharp peak at an optimum irradiance. This expression is thus suited to P-I responses with this characteristic form but is inadequate for responses characterized by an extended plateau.

The first model attempting to describe P-I responses that included photoinhibition by way of independent parameters was that of Vollenweider (1965):

$$P^B = P_s^B \left[\frac{I/I_s}{\left[1 + (I/I_s)^2 \right]^{1/2} \left[1 + (aI/I_s)^2 \right]^{n/2}} \right] \quad ...(2.18)$$

Re-parameterised by Platt *et al.* (1977) it may be written:

$$P^B = \left[\frac{P_s^B \alpha^B I}{\left[(P_s^B)^2 + (\alpha^B I)^2 \right]^{1/2}} \right] \left[\frac{(P_s^B)^2}{(P_s^B)^2 + (a\alpha^B I)^2} \right]^{n/2} \quad ...(2.18a)$$

This formulation is based upon Smith's (1936) function for $f(I)$ and an algebraically similar form for $g(I)$ that retains the hyperbolic properties of the original form. It has been applied to aquatic photosynthesis by Fee (1969).

This expression generates a family of curves whose shape depends upon the parameters a and n. Its flexibility means that it fits a variety of P-I responses. Increasing the parameter a reduces the amplitude of the curve at all intensities while an increase in n results in the curve to slope more sharply about the point of maximum curvature (Fee 1973). Despite its flexibility a number of factors make this formulation a poor choice. Like the 3-parameter equation of Platt *et al.* (1980) it yields a maximum photosynthetic rate at a specific optimal light-intensity and does not admit the possibility of an extended plateau prior to photoinhibitory decreases in P^B despite the addition of a fourth parameter. The two parameters of the photoinhibitory function $g(I)$ are not independent so that different combinations of a and n can result in the same curve. Both are difficult to interpret and in practice have been found difficult to estimate by non-linear fitting procedures due to lack of convergence (Williams 1978; Hameedi 1978). Furthermore the expression is difficult to integrate over depth and time and in only a few special cases could his general model be solved.

Several modifications to the equation of Vollenweider (1965) have been proposed in order to simplify the expression by reducing the number of parameters and to facilitate fitting the equation to data for purposes of calculating depth-integrated primary production. Steel (1973) suggested setting $a = 1/2I_k$, $n = 2$ and $P_m^B = P_s^B/2$ thereby reducing Eq. 2.18 to:

$$P^B = 2\,P_m^B \left[\frac{I/2I_k}{1 + (I/2I_k)^2} \right] \qquad ...(2.19)$$

This formulation has been used by Straskraba (1974) to model the P-I relationships of a number of phytoplankton groups.

In arriving at a numerical solution to Vollenweider's equation, Fee (1969) noted that an increase in the parameter a resulted in a general lowering of the curve at all light intensities while an increase in n caused the curve to slope more sharply about the point of maximum curvature. By fitting Eq. 2.18 to sets of P-I data Fee (1973) found the value of a to be almost invariably 1.0, and consequently suggested that the parameter a could be arbitrarily fixed at unity to yield the simplified expression:

$$P^B = P_s^B \left[\frac{I/I_s}{\left[1 + (I/I_s)^2\right]^{(n+1)/2}} \right] \qquad ...(2.20)$$

An alternate simplification, pointed out by Williams (1978), is if the parameter n in Eq. 2.18 is set equal to unity, then the Vollenweider equation may be re-parameterised in terms of the same parameters used by Steele (1962) in Eq. 2.13. Where $n = 1$, Eq. 2.18 simplifies to:

$$P^B = P_s^B \left[\frac{I/I_s}{\left[1 + (I/I_s)^2\right]^{1/2} \left[1 + (aI/I_s)^2\right]^{1/2}} \right] \quad ...(2.21)$$

More recently, a generalized hyperbolic inhibition equation based upon the Bannister's saturation function (Eq. 2.12) has been proposed by Iwakuma and Yasuno (1983). This expression contains four parameters:

$$P^B = P_s^B \left[\frac{I/I_s}{\left[1 + (I/I_s)^m\right]^{(1+n)/m}} \right] \quad ...(2.22)$$

where m is the parameter describing the shape of the curve in the low-light region and n is the parameter describing photoinhibition. This generalized equation reduces to that of Bannister (1979) [Eq. 2.12] when $n = 0$, and to that of Fee (1973) [Eq. 2.20] where $m = 2$. Iwakuma and Yasuno (1983) found Eq. 2.22 provided a superior description of photoinhibiting P-I curves than that of Vollenweider (1965) [Eq. 2.18] but noted that a total of four parameters yielded an expression that was often unnecessarily complicated. Because the geometric mean of the parameter m in their analyses was 1.76, they suggested that the equation of Fee (1973) [Eq. 2.20 = Eq. 2.22 where $m = 2$] might often prove more satisfactory. For all values of $n \neq 0$, Eq. 2.29 predicts a single optimal irradiance and so suffers the same restrictions as Eqs. 2.17 to 2.22.

The most versatile empirical model in terms of shape so far applied to P-I responses of phytoplankton is that proposed by Platt and Gallegos (1980) which provides for an extended plateau prior to the onset of photoinhibition. These authors modified the light-saturation function proposed by Bannister (1979) to yield a photoinhibition function $g(I)$ that maintains a value of 1.0 as the light intensity increases up to a threshold intensity I_t. The subsequent rate of decrease in photosynthetic rate is described by the

term I_b' which is defined as the irradiance where photoinhibition has reduced the photosynthetic rate to half of its maximum. The smaller the difference between I_b' and I_t the greater is the photoinhibitory decrease in photosynthetic rate. The precise form of $g(I)$ suggested is:

$$g(I) = \frac{1}{2} \cdot \left[1 - \frac{I - I_b'}{[(I - I_b')^m + (I_t - I_b')^m]^{1/m}} \right] \quad ...(2.23)$$

where m is a positive integer which may be considered a "shape parameter" analogous to that in Bannister's (1979) saturation function. Because this expression is cast in terms of parameters with dimensions of irradiance, Platt and Gallegos (1980) suggest that the formulation employed for $f(I)$ be recast using the parameter I_k (= P_m^B / α^B) which also has dimensions of irradiance. If, for algebraic consistency, the formulation of Bannister (1979) [Eq. 2.12] is used for $f(I)$ then the same parameter m defines the "shape" of both $f(I)$ and $g(I)$.

If the equation of Bannister (1979) [Eq. 2.12] is used for the photoenhanced function $f(I)$ and the photoinhibition function $g(I)$ is given by its analogue [Eq. 2.23], the final photosynthetic expression contains 5 parameters (P_s^B, I_k, m, I_b' and I_t). If the shape parameter of the photoinhibition function [m in Eq. 2.22] were to be made independent of the shape parameter of the photoenhanced function [m in Eq. 2.12], the final photosynthetic function would contain a total of 6 parameters.

The 5-parameter curve proposed by Platt and Gallegos (1980) has an extended plateau at irradiances between I_k and I_t, irradiances which may be considered optimal for photosynthesis. Where I_t is less than or equal to I_k this formulation reduces to a curve with a single optimal light intensity. Furthermore, since a value of $m = 6$ is required to

suppress curvature in the plateau region and variations in $m \geq 6$ have little effect upon the remaining parameters, Platt and Gallegos (1980) suggest that for practical reasons m may be fixed at a value of 6 thereby reducing the total number of parameters to four (P_s^B, I_b, I_b' and I_t). An alternative simplification tested in this study is to retain m as a parameter but set I_b' equal to I_t' (*ie.* set $I_t = 0$). This also yields a 4-parameter description that is capable of describing a wide variety of P-I forms.

The 4-parameter formulation suggested by Platt and Gallegos (1980) may be recast in terms of the initial slope α^B and an equivalent parameter that describes the sensitivity to photoinhibition, β'^B, which is defined as the negative slope of the P-I curve at $I = I_b'$. In the case where Bannister's equation [Eq. 2.12] is chosen for $f(I)$ then:

$$\alpha^B = \left.\frac{\partial P}{\partial I}\right|_{I \to 0} = P_s^B / I_s \qquad \text{...(2.24)}$$

and

$$\beta'^B = \left.\frac{\partial P}{\partial I}\right|_{I = I_{b'}} = \frac{P_s^B}{2\,(I_{b'} - I_t)} \qquad \text{...(2.25)}$$

The geometric flexibility of these formulations is such as to provide a successful representation of the wide variety of P-I curves that are encountered (Figure 2.1). Despite the capacity of such a formulation (*ie.* P^B = *[Eq.2.12]·[Eq.2.23]*) to describe a wide variety of P-I response curves it has only been employed in the original publication (Platt and Gallegos 1980). This is probably a result of the large number of parameters (four to six) and consequently the computational difficulties in fitting it to empirical data.

2.4. RATIONAL MODELS.

The first attempts at providing a rational basis for the form of the P-I curve stemmed from work with terrestrial plants. Mechanistic models for leaf photosynthesis were sought which integrated the photosynthetic-irradiance response with that of CO_2 assimilation. In addition to irradiance, CO_2 concentration was seen as a major rate-limiting factor due to its low concentration in air (~ 0.035%). Such models generally combine a biochemical kinetic stage, usually in the form of the Michaelis-Menten rectangular hyperbolic equation, with Fick's Law of Diffusion (often referred to as the Gaastra model) to provide a more complete description.

Rabinowitch (1951) first introduced a mechanistic biochemical-diffusion model where photosynthesis that incorporated both light-intensity and the CO_2 concentration. The basic tenets of the model have subsequently been developed by a number of authors and remain central to current efforts to interpret P-I responses of higher plants (Chartier 1970; Chartier and Prioul 1976; Thornley 1976; Prioul and Chartier 1977; Tenhunen *et al.* 1980; Marshall and Biscoe 1980; Farquhar and von Caemmerer 1983).

In these models, the biochemical stage describes the dependency of gross photosynthesis upon both irradiance (I) and CO_2 concentration (C_i) at the site of photosynthesis. This relation is generally described according to the classic Michaelis-Menten form:

$$P^B = \frac{\alpha^B I (C_i / r_c)}{\alpha^B I + C_i / r_c} \qquad ...(2.26)$$

where α^B is the photochemical efficiency and r_c is the carboxylation resistance. Choice of the rectangular hyperbola follows from the assumption that carboxylation of CO_2 in the Calvin Cycle occurs via a series of enzymic reactions one of which is considered to be the rate-limiting step. Gross photosynthesis may be distinguished from net photosynthesis by the relation:

$$P_g^B = P_n^B + R^B \qquad ...(2.27)$$

As irradiance tends to infinity, P_g^B tends to C_i / r_c, and so the ratio C_i / r_c may be considered the maximum rate of gross photosynthesis P_{gm}^B.

Combined with the biochemical reactions of photosynthesis is the physical diffusion of CO_2 from the environment to the site of photosynthesis. The flux of CO_2 from the environment to the site of photochemistry is by diffusion such that:

$$P_g^B = \frac{C_o - C_i}{r_d} \qquad ...(2.28)$$

where C_o is the CO_2 concentration in the environment and r_d is the diffusion resistance.

Substituting for C_i in Eq. 2.26 based upon the relation in Eq. 2.28 and replacing P_g^B by $P_n^B + R^B$ and re-arranging yields (Marshall and Biscoe 1980):

$$P_n^B + R^B = \frac{\alpha^B I (C_o / r_c - P_n^B r_d / r_c)}{\alpha^B I + (C_o / r_c - P_n^B r_d / r_c)} \qquad ...(2.29)$$

which describes a non-rectangular hyperbola for both the P_n^B-I and P_n^B-C_o responses.

Dividing both denominator and numerator in Eq. 2.29 by $r_c / (r_c + r_d)$ yields:

$$P_n^B + R^B = \frac{\alpha^B I (P_m^B - \Theta P_n^B)}{(1 - \Theta)\alpha^B + (P_m^B - \Theta P_n^B)} \quad ...(2.30)$$

where $P_m^B = C_o / (r_c + r_d)$ and $\Theta = r_c / (r_c + r_d)$. On expansion this gives:

$$\Theta(P_n^B)^2 - (P_m^B + \alpha^B I - \Theta R^B)P_n^B + \alpha^B(P_m^B - (1 - \Theta)R^B) - R^B P_m^B = 0 \quad ..(2.31)$$

where α^B is the initial slope as I tends to zero and Θ represents the ratio of the diffusion resistance to the total resistance. The maximum rate of net photosynthesis is given by the asymptote:

$$P_{nm}^B = P_m^B - (1 - \Theta)R^B \quad ...(2.32)$$

In cases where R^B is neglible, Eq. 2.31 reduces to:

$$\Theta(P^B)^2 - (P_m^B + \alpha^B I) P^B + \alpha^B I P_m^B = 0 \quad ...(2.33)$$

which constitutes a non-rectangular hyperbola of the form:

$$a(P^B)^2 + b(P^B) + c = 0 \quad ...(2.34)$$

Equation 2.33 is that suggested by Thornley (1976) based upon the original model of Rabinowitch (1951). The parameter Θ describes convexity of the hyperbola by changing the degree of curvature at the transition from the initial slope to the maximum photosynthetic rate (Marshall and Biscoe 1980). Values of Θ between zero and unity delimit two relevant extremes. When Θ equals 0 implying that r_c is much greater than r_d,

the curve reduces to a rectangular hyperbola [Eq. 2.6]. Where Θ equals 1 and r_d dominates, the curve becomes a hyperbola reduced to its two asymptotes equivalent to a "Blackman-type" response [Eq. 2.3].

Initial interest in the application of this model focused upon the relative importance of the chemical and physical resistances of carboxylation (Chartier 1970; Jones and Slayter 1972; Prioul and Chartier 1977). Since the model assumes that the photochemical response to irradiance at the biochemical level is adequately described by a rectangular hyperbola the more the response curve deviates from that of a rectangular hyperbola and tends toward that of a Blackman-type curve the greater is the importance of diffusion resistance. The sharp curvature of most P-I curves that result in values of Θ close to unity implies that the carboxylation resistance is only 2-3% of the total leaf resistance to CO_2 fixation.

Prioul and Chartier (1977) have correctly pointed out that this interpretation is only valid if the biochemical reactions are indeed faithfully described by a rectangular hyperbola. If photochemistry was described more accurately by a non-rectangular hyperbola of similar Θ then it would be impossible to distinguish between physical or biochemical resistance.

For descriptions of the photosynthetic response in environments other than air, a number of models have been presented which focus upon the light reactions of photosynthesis. Crill (1977) formulated a mechanistic model designed as a crude analog of photosynthesis. The model is composed of two distinct stages representing the light dependent and dark enzymic stages of the photosynthetic machinery respectively. A light dependent stage assumes that the cell contains a number of photosynthetic factories that are activated by a given amount of light energy to generate photoproduct.

Photosynthetic factories are deactivated if further light is absorbed before the initial photoreaction is completed. One "unit" of light is required to generate one "unit" of photoproduct. If the probability that a particular factory is hit by a particular light unit is p, the probability that at a given light intensity any factory is hit by any one unit of light to generate a unit of photoproduct ($prob.(I,1,p)$) is given by the binomial theorem:

$$prob.(I,1,p) = \frac{I!}{(I-1)!} p^1 q^{I-1} = I p q^{I-1} \quad ...(2.35)$$

where $q = 1 - p$. With N independent factories the average photosynthetic output (P) is:

$$P = N I p q^{I-1} \quad ...(2.36)$$

Crill (1977) also shows that this expression is identical to the empirical formulation of Steele (1962,1965) if expressed in terms of P_m (the rate of maximal photosynthesis) and I_m (the optimal light intensity) rather than N and p respectively. This identity permits changes in the parameters P_m and I_m in Steele's model to be interpreted in terms of the hypothetical number of factories (N) and their hit probability (p).

The second stage of the model, comprising the photosynthetic dark reactions, is approximated by the familiar rectangular formulation of first-order enzymic reactions:

$$Q = \frac{V_m S}{K_m + S} \quad ...(2.37)$$

The model considers that a factory, having processed a unit of light, is then occupied processing the photoproduct and may be considered removed from the system thereby modifying Eq. 2.36 so that:

$$P = (N - S)\, I\, p\, q^{I-1} \qquad ...(2.38)$$

At steady state $P = Q$ and the combined light- and dark-stage model is:

$$P = 1/2 \left\{ V_m + \gamma N + \gamma K_m - \left[(V_m + \gamma N + \gamma K_m)^2 - 4 V_m \gamma N \right] \right\}^{1/2} \qquad ...(2.39)$$

where $\gamma = I\, p\, q^{I-1}$.

The final formulation is a four-parameter equation with parameters N, p, V_m and K_m. The initial slope α^B may be computed as Np / q. The relative rate of the dark stage to that of the light stage at optimal intensity is given by:

$$T_m = Q_m / P_m \qquad ...(2.40)$$

where Q_m is the maximum *realized* photosynthetic rate given by Eq. 2.39 at $I = I_m$ and P_m is the maximum *potential* photosynthetic rate given by Eq. 2.36 at $I = I_m$.

The family of curves described by this model vary from a saturation type response to a distinctly peaked curve equivalent to the curves generated by Steele's (1962, 1965) equation. The model yields a saturation-type response where the potential output of the light reactions are limited by the speed of the dark reactions. Alternatively, a distinctly peaked curve exhibiting maximal photosynthesis at an optimal wavelength results where light is the limiting factor throughout the entire range of light intensities. Sensitivity analysis suggests that there are a large number of combinations of V_m and K_m which closely approximate the same curve. Consequently only the relative speed of the dark reactions may be extracted from an experimental curve with the relative contribution

of V_m and K_m remaining undetermined (Crill 1977). The success of the model in describing the wide variety of possible P-I response curves has not been adequately tested.

Peeters and Eilers (1978) and Eilers and Peeters (1988) introduced a simple black box model that assumes the photosynthetic "unit" responsible for photosynthesis can be in any one of three states (Figure 2.1(a)). The first state (X_1) may be thought of as a resting state where the photosystem is ready to perform photochemistry. Following the absorption of light the photosystem is transformed to an excited state (X_2) and which is then incapable of any further photochemistry. The probability of this transition is considered proportional to the light intensity. Reversion to the resting state is considered to occur at a constant rate that is independent of light intensity. This constant is the turnover rate of the photosystem. A transition from the excited state to an inactivated state (X_3) occurs if further light is absorbed. Again this transition is proportional to the light intensity. Reversion from the inactivated state to the resting state occurs at a constant rate that is independent of light intensity and may be considered as a recovery or repair rate.

This model yields a steady state expression that may be simplified to an inverse quadratic described by three parameters:

$$P^B = \frac{I}{aI^2 + bI + c} \qquad ...(2.41)$$

From these parameters a number of familiar characteristics of the curve may be derived including the initial slope α^B, the maximum photosynthetic rate $P_m{}^B$, the optimal irradiance I_m and a dimensionless parameter β which describes the sharpness of the peak. In a recent analysis of this formulation, Eilers and Peeters (1988) suggest plotting the P-I

response on logarithmic axes which results in a symmetrically peaked curve with asymptotes above and below the optimal irradiance represented by straight lines. Logarithmic axes facilitate the comparison of this model with other photoinhibition models (such as Platt *et al.* 1980) whose formulation does not exhibit such symmetry (Eilers and Peeters 1988).

A similar kinetic model proposed by Megard *et al.* (1984) [originally derived by Senft 1977] contains the same three states for the photosynthetic unit but with a slightly different transition structure (Figure 2.1(b)). In this scheme the reversion of the excited state (X_2) to the resting state (X_1) is characterized by two alternative pathways, one corresponding to photochemistry and a second representing de-excitation by fluorescence and radiationless transitions. Furthermore the inactivated state (X_3) reverts to the excited state (X_2) rather than the resting state (X_1). The resultant steady-state solution is identical to that of Peeters and Eilers (1978) although expressed in different form:

$$P^B = P_s^B \frac{I}{K_1 + I^2 + I/K_2} \qquad ...(2.42)$$

The parameter K_2 is inversely related to the extent of photoinhibition. When K_2 is infinite the curve becomes a rectangular hyperbola [Eq. 2.6].

The shape of the family of the inverse quadratic curves produced by both of the above models has been found to provide a reasonable fit to data where the P-I relationship exhibits photoinhibition resulting in a pronounced peak in photosynthesis at an optimal light intensity. Where photoinhibition is absent the curve becomes a rectangular hyperbola which in most cases provides an inferior fit to data for the reasons outlined in Section 2.3.1. Furthermore, this formulation does not provide a good

description in those cases that exhibit an extended plateau where the photosynthetic rate remains maximal over a range of light intensities.

Another model that focuses attention on the light reactions of photosynthesis has been proposed by Fasham and Platt (1983) which attempts to provide an adequate description of P-I responses that exhibit an extended plateau prior to the onset of photoinhibition. This model is based upon a kinetic description of electron flow around Photosystem II (PS II). The details of the models structure and the set of differential equations describing the reaction scheme are outlined in Figure 2.2.

The solution to this system of equations leads to a four-parameter equation that is a quadratic in P, the photosynthetic rate. When appropriately scaled to biomass the photosynthetic rate may be expressed:

$$(P^B)^2 - \mu^B P^B + (\chi^B exp(\beta I) + \alpha^B) I P^B + \alpha^B \mu^B I = 0 \quad ..(2.43)$$

The four derived parameters, α^B, μ^B, χ^B and β combine to describe the attributes of the final curve. In the case where photoinhibition is zero the term $\beta = 0$ and Eq. 2.43 reduces to a three-parameter form:

$$(P^B)^2 - \mu^B P^B + (\chi^B + \alpha^B) I P^B + \alpha^B \mu^B I = 0 \quad ...(2.44)$$

which is the equation of a non-rectangular hyperbola.

In Appendix A I show that this formulation may be rewritten in the more general form of a non-rectangular hyperbola as proposed by Thornley (1976) [Eq. 2.11] by substituting for $\mu^B = P_m^B / \Theta$ where $\Theta = \alpha^B / (\alpha^B + \chi^B)$. This provides further insight into the interpretation of the parameter χ^B. In the model of Fasham and Platt (1983), χ^B

is scaled to α^B and reflects the extent of the linear portion of the curve and the sharpness of the curvature where light becomes saturating. The lower the value of χ^B the more the curve tends toward a Blackman type response, larger values of χ^B yield a curve which tends to a rectangular hyperbola. In cases where photoinhibition occurs, the term χ^B is modified by the parameter $exp(\beta I)$ (see Eq. 2.43) such that greater photoinhibition (higher β) increases the value of $\chi^B\ exp(\beta I)$ resulting in a less extensive linear portion and increased photoinhibition at higher intensities. The lower the value of χ^B the greater is the extended plateau.

This model provides a useful description for the form of the P-I curve in that it is sufficiently flexible geometrically to accommodate a wide variety of data sets using a minimal number of parameters. As pointed out by the authors, provided the initial system of equations are maintained the final mathematical expression is not specific to electron flow around PS II and could be applicable to any biochemical scheme comprising two serial reactions. The expression is, however, highly non-linear and difficult to fit to data (Fasham and Platt 1983).

The form of the non-rectangular hyperbola has also been suggested as the appropriate description of the P-I response by Zvalinskii and Litvin (1982, 1983, 1984a,b, 1986). Their analysis is based upon a mathematical description of the steady-state kinetics of a series of coupled cyclic reactions representing the primary reversible photoconversions surrounding one (Zvalinskii and Litvin 1982,1983) or two (Zvalinskii and Litvin 1984a,b,1986) photosynthetic units.

The first photosynthetic model proposed (Zvalinskii and Litvin 1982) was a mathematical description of the migration of excitons within the photosynthetic unit and the trapping of excitons by reaction centers. The photosynthetic unit was considered an

aggregate of many identical unicenter or multicenter light-harvesting antennas within which energy transfer was possible. Exciton migration and trapping was described by a series of coupled cyclic reactions involving the pigment molecules of the antenna and the reaction centers (Zvalinskii and Litvin 1982,1983). The steady-state solution yielded a relation between the relative rate of photosynthesis and irradiance that could be approximated by a non-rectangular hyperbola.

Subsequent development of this model incorporated the potential non-linearity of the dark reactions (Zvalinskii and Litvin 1983) and revealed that increasing the number of reaction centers in a photosynthetic unit, increasing the efficiency of energy migration between unicenter photosynthetic units or changing the extent to which the dark reactions limit photosynthesis all resulted in analogous changes in the form of the P-I response. This suggested that the photosynthetic process could be modelled as an unbranched chain of cyclic reactions in which each component undergoes reversible conversions. This permitted the addition of a second photochemical reaction into one of the subsequent cycles which yielded an expression describing the dependence of the rate of photosynthesis upon irradiance (Zvalinskii and Litvin 1984a,b). The final model consisted of eleven independent differential equations (five for each photosystem and one for their interaction) and six equations of conservation for the energy traps (Zvalinskii and Litvin 1984b). The steady-state solution of this model was a quadratic expression relative to the irradiance and the sixth power of the dimensionless rate of the process. Again this expression could be adequately approximated by a non-rectangular hyperbola.

Zvalinskii and Litvin (1986) have further generalized their results by demonstrating that the rate of *any* sequence of coupled cyclic reactions involving linear chains, loops and networks, can be represented in the form of a continued fraction reflecting the structure of the network of reactions. The dependence of the steady-state

reaction rate upon substrate concentration can be approximated by a linear sequence of two cycles which can be approximated by a non-rectangular hyperbola.

For a linear sequence of coupled reactions where each component in the chain can only interact with the two neighboring components, the relative (dimensionless) reaction rate at steady state $V = v/v^m$ where v^m is the maximum reaction rate as the substrate concentration tends to infinity may be given by:

$$V = Se_1 = \frac{(1 - e_1)\, e_2}{r_{12}} = \ldots = \frac{(1 - e_{n-1})\, e_n}{r_{n-1,n}} = \frac{1 - e_n}{r_{n0}} \qquad \ldots(2.45)$$

where S is the dimensionless substrate concentration $([S]/K'_m)$, e_i is the relative dimensionless concentration of each of the two states (*ie.* oxidized and reduced) for each couple in the chain, and $r_{i,i+1}$ is the maximum relative resistance of the specified reaction couple which at steady state is equal to the resistance of the chain as a whole ($r_{i,i+1} = (1/v^m_{i,i+1})/(1/v^m) = v^m/v^m_{i,i+1}$). By successively excluding the values of e_i the relationship between V and S can be expressed as a continued fraction representing the structure of the sequence of reactions (Zvalinskii and Litvin 1986):

$$1 - \frac{V}{S} = \cfrac{r_{12}}{1 - \cfrac{r_{23}V}{\ldots \cfrac{}{1 - \cfrac{r_{n-1,n}V}{1 - r_{n0}V}}}} \qquad \text{or} \qquad 1 - R_s = \cfrac{R_{12}}{1 - \cfrac{R_{23}}{\ldots \cfrac{}{1 - \cfrac{R_{n-1,n}}{1 - R_{n0}}}}} \qquad \ldots(2.46)$$

where $R_s = V \cdot K'_m/[S] = V/S$ is the input resistance of the reaction sequence and $R_{ij} = r_{ij}V$ is the relative resistance of each coupled reaction within the sequence.

At high substrate concentrations ($[S] \rightarrow \infty$) the reaction rate approaches the maximum value ($v \rightarrow v^m$, $V \rightarrow 1$), the value of the input resistance approaches zero ($R_s \rightarrow$

0) and the resistances of the individual coupled reactions approach their maximum values ($R_{ij} \rightarrow r_{ij}$). Under these conditions Eq. 2.46 gives the relationship between the maximum rates of the individual reactions (v^m_{ij}) and the maximum rate of the entire sequence (v^m):

$$1 = \cfrac{v^m/v^m_{12}}{1 - \cfrac{v^m/v^m_{23}}{\cdots \; 1 - \cfrac{v^m/v^m_{n-1,n}}{1 - v^m/v^m_{n0}}}} \qquad \ldots(2.47)$$

Zvalinski and Litvin (1986) show that sequences of coupled cyclic reactions may be approximated by the equation for a dicyclic reaction in which the second cycle is equivalent to all of the additional cycles of the chain excluding the first. For a chain of sequential coupled reactions consisting of two cycles, the maximum rate of the reaction sequence as a whole relative to the maximum rate of each photoreaction is given by:

$$1 = \frac{v^m/v^m_{12}}{1 - v^m/v^m_{20}} = \frac{R_{12}}{1 - R_{20}} \qquad \ldots(2.48)$$

or

$$v^m = \frac{v^m_{12} \, , \, v^m_{20}}{v^m_{12} + v^m_{20}} \qquad \ldots(2.49)$$

In terms of the reaction rate of the reaction sequence as a whole relative to the reaction rates of the individual photoreactions, from Eq. 2.46 we find that for a 2 cycle system:

$$v = \frac{v^m[S]}{K'_m} \cdot \frac{1 - v/v^m}{1 - r_{20} \, v/v^m} \qquad \ldots(2.50)$$

where v is the rate of the reaction sequence, v^m is the maximum rate of the reaction sequence, K'_m is the generalized constant analogous to the Michaelis-Menten constant K_m ($K'_m = r_{12} K_m = (1 - r_{20})K_m$). r_{12} is the relative resistance of the first cycle ($(1/v^m_{12})/(1/v^m)$) and r_{20} is the relative resistance of the second cycle ($(1/v^m_{20})/(1/v^m)$). Where the resistance of the second cycle is greater than that of the first ($r_{12} < r_{20}$; $v^m_{12} > v^m_{20}$), the dependence between the reaction rate and the substrate concentration is described by a non-rectangular hyperbola which was found to provide a good description of the P-I response (Zvalinskii and Litvin 1986). The result that any sequence of coupled cyclic reactions may be represented by a non-rectangular hyperbola provides an explanation for the recurrence of this geometrical form in a number of different rational models (Rabinowitch 1951; Marshall and Briscoe 1980; Fasham and Platt 1983).

Finally, Peterson *et al.* (1987) have suggested using the exponential relation derived from the Poisson probabilities of photon capture:

$$P_g^B = P_{gm}^B \left[1 - exp^{-\alpha^B I}\right] \qquad ...(2.51)$$

or since $P_g^B = P_n^B - R^B$:

$$P_n^B = P_{nm}^B - P_{gm}^B exp^{-\alpha^B I} \qquad ...(2.52)$$

This exponential form has previously been employed on an empirical basis (Webb *et al.* 1974; Chalker 1981). It is also the same as the empirical exponential formulation introduced by Platt *et al.* (1980) where the parameter describing photoinhibition (β) is set to zero. In addition, it has been widely used to describe photosynthesis as a function of irradiance when the latter is delivered as short saturating flashes of sufficiently short duration that the photochemical apparatus can only turn over once (Emerson and Arnold

1932, 1933; Arnold and Kohn 1934; Gaffron and Wohl 1934; Briggs 1941; Herron and Mauzerall 1972; Ley and Mauzerall 1985; Mauzerall 1986). It arises as the solution to a simple Poissonian system in which the photosynthetic response is described by a cumulative one-hit Poisson distribution. The basis of such an interpretation, together with an extended formalism to include photoinhibition and the integration of spectral dependence, is developed in Section 3.3. In practice, this exponential formulation has proved to be very successful in providing an accurate fit to P-I data.

2.5. NORMALIZATION OF P-I MODELS TO BIOMASS.

While photosynthetic rates are usually measured on a volumetric basis they are generally normalized to some index of plant biomass to facilitate intercomparison between samples. Numerous indices have been employed including cell number, cell volume, particulate organic carbon (POC), optical density, various photosynthetic pigments and ATP. Where photosynthesis is measured as a reduction of inorganic carbon to organic carbon, as is the case when ^{14}C methodologies are employed, the most appropriate biomass index is often the organic carbon concentration of the sample. In this case, the photosynthetic rate is described by a dimensionless number representing the increase in biomass ($P^B = \partial C/\partial t \cdot 1/C$). Because contamination by heterotrophic material is significant in natural waters, photosynthetic rates are rarely scaled to carbon and the most common index of active biomass employed is chlorophyll *a* ($P^B = \partial C/\partial t \cdot 1/[Chl\ a]$).

Normalization of the photosynthetic rate to biomass alters the dimensions of the ordinate axis of the photosynthetic response. This can lead to erroneous interpretations of the relative photosynthetic capability of two different organisms or samples taken from

different environments when the two photosynthetic response curves are compared. For example, if the photosynthetic response is scaled to chlorophyll *a* in two different organisms, one of which has chlorophyll *a* as the major light-harvesting pigment while in the second chlorophyll *a* represents only a minor component of the light-harvesting apparatus, the apparent photosynthetic capacity of the latter organism will be greatly exaggerated relative to the former when P^B is expressed on a chlorophyll basis. For this reason comparisons of the biomass-normalized photosynthetic response between two samples which differ greatly in the stoichiometry of the chosen biomass index to carbon (*chl:C*, *N:C*, etc.) can lead to erroneous conclusions about the relative photosynthetic abilities.

The necessity of choosing an appropriate biomass index is particularly important when describing the photosynthetic responses of the picoplankton for the purpose of comparison to other phytoplankton groups. Differences in the photosynthetic pigment composition of the cyanobacteria compared to the larger eukaryotic algae complicates any comparison where chlorophyll *a* is employed for biomass normalization as is the general custom.

2.6. DIMENSIONALITY AND SCALING OF THE P-I RESPONSE.

The dimensions of the ordinate axis of a P-I curve determined on a volumetric basis are $M \cdot L^{-3} \cdot T^{-1}$; when normalized to biomass the dimensions become $M \cdot M^{-1} \cdot T^{-1}$. The scale is determined by the maximum biomass-specific photosynthetic rate (P_m^B) which, as noted above, is a function of the maximum photosynthetic rate of the sample (P_m) and the biomass index to which photosynthesis is normalized (B). The most commonly employed units are $mgC \cdot mgChl^{-1} \cdot hr^{-1}$. The relative rate of photosynthesis

(P or P^B) at any irradiance can be equated to the maximum photosynthetic rate attained (P_m or P_m^B respectively) to yield a *dimensionless* photosynthetic rate (P^*). In those formulations which include the possibility of photoinhibition it is often preferable to describe the relative rate of photosynthesis in terms of the maximum *potential* rate of photosynthesis, P_s^B, the rate of photosynthesis that would be achieved in the absence of photoinhibition. For each formulation there is a simple analytical relationship between P_s^B and P_m^B and so both dimensionless rates ($P^* = P/P_m^B$ or P/P_s^B) are interchangeable.

Similarly, the dimensions of the abscissa when irradiance is expressed on a quantum basis are photons $\cdot$ $L^{-2} \cdot T^{-1}$. The relevant scale is established by the maximum quantum irradiance experienced at the earths surface and the units commonly employed are $\mu mol\ m^{-2}\ s^{-1}$ ($= \mu E\ m^{-2}\ s^{-1}$). A dimensionless relative irradiance (I^*) may be defined by equating the measured irradiance to some chosen irradiance. The most appropriate irradiance value to choose in order to simplify the final dimensionless expression varies according to the formulation. The most frequently employed and that which is appropriate to all of the 2-parameter formulations (including Steele's formulation with photoinhibition) is the irradiance I_k, where I_k is defined as P_m^B / α^B. The relative irradiance is thus given by the dimensionless ratio I / I_k which may be denoted I^*. For those P-I responses that include the possibility of photoinhibition and define a single optimal irradiance value, I_m, it may be more convenient to employ this value to scale the response with respect to irradiance. The dimensionless irradiance I^* would then be I / I_m. For any particular formulation there is a direct analytical relationship between I_k and I_m so that the two dimensionless rates ($I^* = I/I_k$ or I/I_m) are of course interchangeable.

Accordingly, all of the mathematical formulations of the P-I response can be recast in dimensionless form in terms of P^* and I^*. All the dimensionless curves have the properties:

$$0 \leq P^*(I^*) \leq 1 \quad . \qquad \text{...(2.53)}$$

$$P^*(0) = 0 \qquad \text{...(2.54)}$$

$$\left.\frac{\partial P^*}{\partial I^*}\right|_{I^* \to 0} = 1 \qquad \text{...(2.55)}$$

The dependence of the dimensionless photosynthetic rate (P^*) upon the dimensionless irradiance (I^*) for a number of the 2-parameter saturation-type P-I responses is illustrated in Figure 2.3(a).

In the formulations of the P-I response that include photoinhibition two further properties are required:

$$\left.\frac{\partial P^*}{\partial I^*}\right|_{I^* = I^*_m} = 0 \qquad \text{...(2.56)}$$

$$P^*(I^*_m) = 1 \qquad \text{...(2.57)}$$

where I^*_m represents the dimensionless irradiance corresponding to the maximum photosynthetic rate (*ie.* I_m / I_k). Those mathematical expressions which include photoinhibition thus have a total of five conditions to fulfill. A function with less than five parameters cannot satisfy all five conditions and in P-I formulations it is generally the range of possible I^*_m values that is compromised (Baumert and Uhlmann 1983). For example, in all of the existing 3-parameter photoinhibition formulations only a single I^*_m value is permitted. This is also true for the original 4-parameter formulation of

Vollenweider (1965). Baumert and Uhlmann (1983) suggest a possible modification to Vollenweider's equation to yield an expression where I^*_m is governed by the parameter n:

$$P^B = P_m^B \left[\frac{I / I_k}{\left[1 + (1/n)(I/I_m)^2 \right]^{(n+1)/2}} \right] \quad ...(2.58)$$

In Eq. 2.58 the dimensionless irradiance corresponding to maximal photosynthesis ($I^*_m = I_m / I_k$) is given by:

$$I^*_m = \left[1 + (1/n) \right]^{(n+1)/2} \quad ...(2.59)$$

A comparison of the dependence of P^* upon I^* in several formulations that include photoinhibition is shown in Figure 2.3(b). Values of additional parameters have been chosen to emphasize similarities in the general shape.

2.7. INTERPRETATION OF MODEL PARAMETERS.

2.7.1. Empirical models.

Empirical functions are chosen on the sole basis of their ability to describe the photosynthetic response to irradiance as simply as possible. The resultant mathematical expression can then be used in further computations (such as the calculation of depth-integrated primary production). While such P-I expressions contain parameters that are purely geometrical there is a general tendency to attempt to interpret the parameters in some sort of physiological context. Jassby and Platt (1976) and Platt *et al.* (1977) have shown that all the two-parameter models describing the saturation-type photosynthetic

response to PFD may be recast in terms of two parameters, α^B and P_m^B. In all of the these formulations these two parameters are interpreted similarly.

The initial slope of the P-I response at low PFDs (α^B) is interpreted as the efficiency of transformation of photons into reduced carbon (or oxidized water, oxygen). As such it may be thought of as the product of the absorption cross-section (normalized to whatever biomass index is used for P^B) and the quantum yield.

The maximum photosynthetic rate normalized to biomass (P_m^B) represents the maximum rate of turnover of the photosynthetic apparatus. Because of its temperature dependency, it is often implicitly considered to represent the maximum rate attainable by the dark enzymic carboxylation reaction sequence. However, in many cases, the rate limiting step (and there may be more than one) is unknown and P_m^B could equally be limited by the maximum turnover of the non-cyclic electron transport chain, in which case, the entire P-I response could be considered to be governed by the light reactions.

In those formulations that describe the decrease in the photosynthetic rate at high PFDs by an independent parameter, the decrease is usually attributed to a physiological process termed photoinhibition. The parameter describing the rate with which photosynthesis decreases with increasing PFD, usually termed β^B and measuring the negative slope, is interpreted as an index of the sensitivity of the cell to photoinhibition and is given the same units as α^B.

2.7.2. Rational models.

In a rational model the parameters reflect the structure and the underlying tenets of the model. Interpretation is governed solely by the structure of the model. It is worth

noting however that goodness-of-fit alone does not confirm that the parameter truly represents the property that it purports to represent.

2.8. COMPARING P-I MODELS.

2.8.1. Empirical models.

For empirical models of the P-I response the single criterion that is accepted as a valid means of assessing the applicability of any particular mathematical formulation is the model's ability to fit a set of data. The fidelity of a particular formulation is generally ascertained by means of non-linear curve fitting where the parameters of the equation are evaluated so as to minimize some index of the residuals (Platt *et al.* 1977; Gallegos and Platt 1980). Where the errors are independent and normally distributed with a constant variance the optimal fit is obtained when the parameters are such as to minimize the sum of the squared residuals SS_{res} (Bard 1974; Smith 1979):

$$SS_{res} = \Sigma_i \left[P^B_i - f(I_i; P_m^B, \alpha^B \ldots.)^2 \right] \qquad \ldots(2.60)$$

Where the errors are normally distributed but not of constant variance, a weighted sum of squares is the appropriate quantity to minimize (Bevington 1969). Discussion of the most appropriate quantity to minimize in the fitting of light-saturation models can be found in several papers (Platt *et al.* 1977; Smith 1979; Silvert 1979; Gallegos and Platt 1980; Platt *et al.* 1980; Platt and Gallegos 1981; Lederman and Tett 1981). At this time quantitative efforts to compare the relative ability of various formulations to adequately describe the P-I response have largely focused upon formulations excluding photoinhibition (Jassby and Platt 1976; Lederman and Tett 1981; Chalker 1981; Nelson

and Siegrist 1987). Iwakuma and Yasuno (1983) provide the only attempt to evaluate the comparative ability of formulations incorporating photoinhibition.

Jassby and Platt (1976) recast eight 2-parameter models and compared their abilities based upon goodness-of-fit to describe a large number (188) of experimental P-I data sets. Models were then ranked according to the number of data sets for which the model yielded the best fit. In this analysis, a direct fitting method was chosen but parameters were estimated sequentially. Initially, α^B was estimated by simple linear regression of the data points in the light-limited range. The parameter $P_m{}^B$ was then estimated by non-linear least-squares employing a grid-search method. As Lederman and Tett (1981) have pointed out, the implication of estimating α^B first and holding it fixed when estimating $P_m{}^B$ for each of the subsequent models is that α^B is transcendental across all eight P-I formulations. If a non-linear parameterization method is employed in which both parameters are estimated simultaneously and independently using data points from the entire range of intensities, then the estimates derived for both α^B and $P_m{}^B$ can be (and will probably be) different in each of the different formulations. Under these circumstances it may not be possible to differentiate between the different formulations solely on the basis of goodness-of-fit because of the inherent error in the P-I measurements.

The important point is that when mathematical expressions are fitted to data whereby the parameters are estimated simultaneously and independently (such as by Marquart's algorithm (Conway *et al.* 1970)), the resultant parameter estimates may be different in each of the different mathematical formulations. For any single P-I response curve, the parameter values obtained using one formulation will not necessarily be identical to those obtained using a different formulation.

In their analysis, Jassby and Platt (1976) found that their hyperbolic tangent model was the most successful by providing the "best" fit more frequently than any of the other models. Lederman and Tett (1981) found that by employing Marquart's algorithm to the same data set, the models of Baule (1917; Eq. 2.4), Smith (1936; Eq. 2.7), Steele (1962 (modified); Eq. 2.8), Platt *et al.* (1977; Eq. 2.9), and Jassby and Platt (1976; Eq. 2.10) were statistically indistinguishable.

Furthermore, by the analysis of simulated data sets constructed by noise-corrupting data generated from the hyperbolic tangent (Eq. 2.10) and the rectangular hyperbola (Eq. 2.6) functions, Lederman and Tett (1981) found that several alternate formulations fitted the data almost as well as the generating model provided different values for the parameters α^B and P_m^B were used. In the case of the corrupted hyperbolic tangent data, the equation of Smith (1936; Eq. 2.7) actually provided a better fit than the generating model (Eq. 2.10) and only the formulation of Blackman (1905; Eq. 2.3) produced a markedly inferior fit. With the corrupted data set generated from the rectangular hyperbola, the generating function did provide the best fit but only the formulations of Blackman (1905; Eq. 2.3) and Platt *et al.* (1977; Eq. 2.9) were significantly inferior.

In a comparison of the ability of several 2-parameter expressions to describe the light-saturation curves of photosynthesis in natural water samples and tropical marine algae, both Iwakuma and Yasuno (1983) and Nelson and Siegrist (1987) found that different formulations yielded considerable differences in the parameter values ascribed to α^B and P_m^B. Estimates of P_m^B were found to be most sensitive to the model chosen where two-fold differences could exist between models fitted to the same data set. Some formulations consistently yielded higher or lower parameter estimates than others. In general, the formulation of Blackman (1905; Eq. 2.3) and the rectangular hyperbola (Eq.

2.6) produced the highest values of α^B and $P_m{}^B$ and consequently the lowest value of I_k. Similarly, the (modified) equation of Steele (1962; Eq. 2.8) and Jassby and Platt (1976; Eq. 2.10) produced the lowest estimates.

From these results it may be concluded that provided the values ascribed to both parameters α^B and $P_m{}^B$ are allowed to vary in different formulations, it may not be possible to distinguish a single "best" model if the only criterion employed is the goodness-of-fit. Furthermore, each different model has a tendency to either underestimate or overestimate the individual model parameters. In terms of using the P-I response to calculate integral production, the importance of such an error depends upon the relative sensitivity of the depth integral to the model parameters (see Section 2.9.2).

2.8.2. Rational Models.

Comparing the validity and usefulness of the various rational models is not as straightforward as with empirical formulations. In addition to correctly describing the data, rational models promise insight into the proposed mechanism underlying the response through the derived values and behavior of the parameters in the model. For a rational model to be considered of potential value, the derived values of the parameters must therefore provide a logically consistent explanation for the working of the model.

Furthermore, the fulfillment of these two criteria alone do not prove that the model is a true representation of the underlying mechanism. An independent measurement is required to confirm that the parameter values generated by the model do indeed describe what they purport to represent. This confirmation has been rarely carried out in the context of P-I models. Consequently, where several different models predict a similar form to the P-I response, it is not possible to distinguish which of these models

represents the more realistic description. An example of this is the non-rectangular hyperbolic form which arises as the solution to any series of coupled reactions (Rabinowitch 1951; Prioul and Chartier 1977; Fasham and Platt 1984). In this case the parameter Θ that describes the degree of curvature from the light-limited to the light-saturated portions of the P-I curve has a different interpretation in each model (relative importance of diffusion and carboxylation resistance, relative rate of the second coupled reaction to the first, *etc.*). Currently there are insufficient data to decide which interpretation (if either) has the greatest correspondence to reality.

2.9. INTEGRATING THE P-I RESPONSE OVER DEPTH.

2.9.1. Mathematical considerations.

Many of the empirical forms of the photosynthesis-irradiance relationship were derived with the principal aim of estimating integral production (*ie.*. Steele 1962,1965; Vollenweider 1965,1970). The parameters of these models are defined solely on a geometric basis and have no biological definition and consequently make no assumptions about the underlying physiological mechanisms. In this case, the existence of an analytical solution to the depth integral is a major advantage.

The rational models of Peeters and Eilers (1978) and Megard *et al.* (1984) permit integration of P throughout the water column (assuming a constant attenuation coefficient) to be accomplished analytically such that a simple equation containing the surface light intensity, the attenuation coefficient and P-I response parameters provides the desired integral.

In contrast, a major limitation of the successful hyperbolic tangent model proposed by Jassby and Platt (1976) is that when integrating over depth no analytic solution exists for situations where $\alpha^B I_o / P_m^B \geq \pi/2$ (*ie.* $I_o/I_k \geq \pi/2$) where I_o is the surface irradiance just below the sea surface. Since typical values of I_o and I_k are 2000 and 200 μmol m^{-2} s^{-1} respectively, this requires that numerical integration be employed under most circumstances.

2.9.2. Relative importance of model parameters to the computation of integral production.

Since in many cases the ultimate goal of establishing the P-I response is to permit calculation of the depth integral of the photosynthetic rate, it is important to choose a model that determines the most important parameters of the P-I response with the greatest accuracy and precision. A first-order estimate of the relative importance of the different parameters of the P-I response to the computed depth integral of primary production throughout the water column can be made by way of a simple sensitivity analysis. The irradiance profile may be considered to decrease exponentially with depth so that:

$$I(z) = I_o \exp\left(-\int_o^z K_s \, dz \right) \qquad \ldots(2.61)$$

where K_s is the diffuse attenuation coefficient for scalar irradiance and I_o is the scalar irradiance just below the sea surface. Substitution of Eq. 2.61 into any of the P-I response equations, yields the photosynthetic profile. If a 2-parameter formulation is employed the photosynthetic profile is a function of three dimensionless numbers:

$$P^B / P_m^B \ (= P^*), \qquad \text{...(2.62)}$$

$$I_o / I_k \ (= I^*), \qquad \text{...(2.63)}$$

$$\int_o^z K_s \, dz \qquad \text{...(2.64)}$$

(Platt *et al.* 1984; Lewis *et al.* 1985).

Under the simplifying assumptions of uniform attenuance, biomass and photosynthetic parameters throughout the water column, the integral photosynthetic rate beneath an area of ocean surface is given by (Vollenweider 1965; Platt *et al.* 1977; Lewis *et al.* 1986):

$$P' = \int_0^\infty P(z) \, dz$$

$$= \frac{P_m^B \, B}{K_s} \cdot f(I_o/I_k) \qquad \text{...(2.65)}$$

The function $f(I_o/I_k)$ has been tabulated for a number of P-I expressions by Vollenweider (1965) and Platt *et al.* (1977) and these are given in Table 2.3. In the specific case where the formulation for the P-I response is the exponential expression of Baule (1917) then the integral photosynthetic rate is given by (Lewis *et al.* 1985):

$$P' = \frac{P_m^B \, B}{K_s} \cdot \sum_{n=1}^{\infty} \left[\frac{(-I_o \cdot \tau_k)^n}{n \cdot n!} \right] \qquad \text{...(2.66)}$$

Although the limits to the integration are set from the sea surface to an infinite depth, the only significant contribution to the integral comes from the upper 200 m.

Differentiation of Eq. 2.66 with respect to the various parameters yields the relative sensitivity of the estimate of integral production to variation in the value ascribed to each of the parameters (Lewis *et al.* 1985):

$$\frac{\partial P'}{\partial P_m} = \frac{-1}{K_s} \sum_{n=1}^{\infty} \left[\frac{(-I_o / I_k)(1-n)^n}{n \cdot n!} \right] \qquad ...(2.67)$$

$$\frac{\partial P'}{\partial \alpha} = \frac{I_o}{K_s} \sum_{n=1}^{\infty} \left[\frac{(-I_o / I_k)^{n-1}}{n!} \right] \qquad ...(2.68)$$

$$\frac{\partial P'}{\partial K_s} = \frac{P_m}{K_s^2} \sum_{n=1}^{\infty} \left[\frac{(-I_o / I_k)^n}{n \cdot n!} \right] \qquad ...(2.69)$$

Equations 2.67 to 2.69 indicate that the sensitivities of the integral photosynthetic rate to the different parameters are all inverse functions of the diffuse attenuation coefficient (K_s). This means that errors in the computation of the integral photosynthetic rate arising from errors in the P-I response and irradiance profile parameters will be greatest in optically clear oceans. This is of significance when estimating the contribution of the picoplankton to integral production because the optically clear oligotrophic oceans are the regions where the picoplanktonic component appears to be the most abundant.

To assess the relative importance of an error in one parameter compared to that in another (say P_m^B compared to α^B) upon the estimate of integral production, the

conditions under which relative errors of both parameters are equal to one another may be determined from the condition:

$$\frac{\partial P_m}{P_m} = \frac{\partial \alpha}{\alpha} \qquad \ldots(2.70)$$

which leads to (Lewis *et al.* 1985):

$$\frac{\sum_{n=1}^{\infty} \left[(I_o / I_k)^n \cdot (n!)^{-1} \right]}{\sum_{n=1}^{\infty} \left[(-I_0 / I_k)^n \cdot (1-n) \cdot (n \cdot n!)^{-1} \right]} = 1 \qquad \ldots(2.71)$$

The result shows that the point where both errors are equal is a function of I_o / I_k and occurs when $I_o / I_k \approx 4$. Under circumstances where $I_o / I_k > 4$, a relative error in P_m leads to a greater error in the estimate of integral production than an equivalent relative error in α. Conversely, whenever $I_o / I_k < 4$, a relative error in α leads to a larger error in the integral production rate than a similar relative error in P_m.

The maximum daily average PAR (direct and diffuse) at the earth's surface (I_o) is 150 W m^{-2} ($\approx$ 690 µmol m^{-2} s^{-1}), a value taken from Reed (1977) for a latitude of 30° N in June. An average value of I_k based upon 722 P-I curves from the world's oceans is 52 W m-2 ($\approx$ 240 µmol m^{-2} s^{-1}) (Harrison (pers. comm.)). These values imply that under most oceanographic conditions the dimensionless ratio I_o / I_k is frequently < 4 and so errors in α rather than P_m are likely to dominate errors in estimates of integral production (Lewis *et al.* 1985). The precision of estimating α is also less than P_m, since the analytical errors

involved in estimating a from P-I data are considered about twice that associated with the estimation of P_m (Platt and Jassby 1976; Lewis and Smith 1983).

In conclusion, it can be stated that from simple dimensional arguments the most important factors in the calculation of integral photosynthetic rates are the values ascribed to the diffuse attenuation coefficient (K_s) and the light-limited rate of photosynthesis (α^B) determined from the P-I response. Since both K_s and α^B are known to be spectrally dependent, the accurate determination of integral photosynthesis requires a quantitative description of this spectral dependency. The spectral dependency of K_s has been measured *in situ* at many locations providing boundaries on its variability. Determination of K_s from satellite observations of ocean color (Gordon and Morel 1983; Sathyendranath 1986) should provide synoptic coverage of $K_s(\lambda)$ and provide information regarding the temporal and spatial variability of $K_s(\lambda)$.

With respect to phytoplankton photosynthesis, the spectral dependency of light-limited rate of photosynthesis (α^B) results from the spectral properties of the photosynthetic pigments involved in light absorption. In this respect, it is important to note that the cyanobacteria, which are considered to constitute a significant component of the picoplanktonic size fraction, differ from most of the larger eukaryotic phytoplankton in terms of their photosynthetic pigment complement and consequently their spectral response. Unlike the larger phytoplankton, cyanobacteria contain only one form of chlorophyll (chlorophyll *a*) and possess phycobiliproteins as accessory light-harvesting pigments rather than the carotenoids, fucoxanthin and peridinin, found in most marine phytoplanktonic algae (Stanier and Cohen-Bazire 1977; Glazer 1982,1983,1984,1985; Bryant 1986). Furthermore, the organization of the cyanobacterial apparatus in which the phycobiliproteins are exclusively associated with Photosystem 2 and chlorophyll *a* is predominantly associated with Photosystem 1 has profound implications for the serial

operation of both photosystems that is required for photosynthesis (Oquist 1974; Wang *et al.* 1977; Myers *et al.* 1980). These characteristics of cyanobacterial photosynthesis demand that special attention be paid to the determination of the spectral nature of α^B in both phytoplankton in general and picoplankton in particular.

CHAPTER 3

SPECTRAL PHOTOSYNTHESIS-IRRADIANCE (P-S-I) MODELS - A THEORETICAL FRAMEWORK.

3.1. INTRODUCTION.

The objective in modelling the photosynthetic response with respect to irradiance is to derive a useful quantitative description of transformation of the incident irradiance (the input) into photosynthetic product (the output) throughout the water column. The transformation rate is generally normalized to either water volume or some biomass index considered to represent the phytoplankton concentration. Because the spectral characteristics of the incident irradiance change with depth, any complete P-I model must consider both the photon flux density and the spectral distribution of the incident photons. As a point of departure it is useful to describe the spectral attenuation of underwater irradiance and in particular to consider the fraction of the incident photon flux that is absorbed by the phytoplankton component. Various P-I models can then be formulated in terms of the photon flux absorbed by the phytoplankton and the transduction of this absorbed flux into photosynthetic product.

3.1.1. Absorption by solutions.

Absorption is generally defined in terms of incident monochromatic beam (of wavelength λ) of collimated light of photon flux density Io_λ passing perpendicularly through an infinitely thin layer (dz) of a homogenous medium such as a solution of light-absorbing molecules. The solution must be sufficiently dilute so that incident photons do

not encounter more than one light-absorbing molecule while traversing the layer. The fraction of photons absorbed from the beam ($-dIo_\lambda/Io_\lambda$) is proportional to the amount of light absorbing molecules intercepted by the beam (Beer's Law) such that:

$$\begin{aligned} -dIo_\lambda / Io_\lambda &= K_\lambda\, dz \\ &= a_\lambda S\, dz \end{aligned} \qquad \ldots(3.1)$$

where the proportionality constant K_λ is the absorption coefficient at that wavelength (dimension: L^{-1}), dz is the thickness (dimension: L), S is the concentration of light absorbing molecules (dimension: $M\,L^{-3}$), and a_λ is a constant that specifies the absorption cross-section of the light-absorbing molecule at that wavelength (dimension: L^2) (Clayton 1980).

Integrating Eq. 3.1 over a finite thickness z, the photon flux density of the beam at depth z is:

$$Iz_\lambda = Io_\lambda \exp^{-a_\lambda S z} \qquad \ldots(3.2)$$

Since the exponent is dimensionless, the units of a_λ are the reciprocal of Sz: where S is measured in mg m^{-3}, and z is in m, then the absorption cross-section a_λ has units m^2 (mg S)$^{-1}$. The virtue of measuring light absorption in terms of the exponent $a_\lambda S z$ is that *it is linear with respect to concentration and additive for a mixture of light absorbers.* For a mixture of substances present at concentrations $S_1, S_2, S_3 \ldots S_n$ with absorption cross-sections $a_{1\lambda}, a_{2\lambda}, a_{3\lambda} \ldots a_{n\lambda}$ the PFD at depth z is:

$$Iz_\lambda = Io_\lambda \exp^{-[\,a_{1\lambda} S_1 + a_{2\lambda} S_2 + a_{3\lambda} S_3 + \ldots + a_{n\lambda} S_n\,] z} \qquad \ldots(3.3)$$

Because of this additivity property, it is not possible to distinguish between a single pigment and a mixture of pigments purely on the basis of absorption *at a single wavelength* λ. A mixture of pigment behave as a single *effective* pigment and the measured absorption cross-section is understood to represent a single *effective* absorption cross-section.

3.1.2. Partitioning the attenuation of underwater irradiance.

The attenuation of irradiance in the ocean differs from that of a true solution in a number of respects. Firstly, the solar radiation incident upon the ocean surface (I_O) is polychromatic rather than monochromatic. Of the total radiation striking the ocean surface less than half is of wavelengths utilizable for photosynthesis. The portion that may be utilized, termed the *Photosynthetically Available Radiation (PAR)*, is defined as the total photon flux density (I_O *(PAR)*) within the spectral range between 350 and 700 nm so that:

$$Io\ (PAR) \quad = \quad \int_{350}^{700} Io(\lambda)\, d\lambda \qquad \ldots(3.4)$$

The incident photon flux density, whether cosine or scalar, has units of mol m^{-2} s^{-1}.

In addition, the attenuation of irradiance in the ocean is dependent upon the scattering as well as the absorption properties of the water and the incident irradiance is diffuse rather than collimated. Where absorption rather than scattering is the dominant contributor to attenuation in the water column, the additivity principle of absorbance [Eq. 3.3] permits the total vertical diffuse attenuation coefficient at any wavelength λ ($K_{T\lambda}$) to

be partitioned into fractions corresponding to the attenuation coefficient due to seawater itself ($K_{w\lambda}$), that due to the phytoplankton biomass present ($K_{c\lambda}$) and the contribution of detrital particles ($K_{p\lambda}$). At any wavelength λ:

$$K_{T\lambda} = K_{w\lambda} + K_{p\lambda} + K_{c\lambda} \qquad ...(3.5)$$

where all coefficients have units of m^{-1} (Platt 1969; Verduin 1982). Because the diffuse attenuation coefficient $K_{T\lambda}$ depends upon scattering as well as absorption it will always be greater than the volume absorption coefficient a_λ. If chlorophyll is employed as a phytoplankton biomass index then:

$$K_{T\lambda} = K_{w\lambda} + K_{p\lambda} + k_{c\lambda}\,[Chl] \qquad ...(3.6)$$

where $k_{c\lambda}$ is the chlorophyll-specific attenuation cross-section at wavelength λ and [Chl] is the chlorophyll concentration. When the latter is expressed in units of mg Chl m^{-3} then the attenuation cross-section for chlorophyll $k_{c\lambda}$ has units of m^2 (mg Chl)$^{-1}$.

From Eq. 3.2 the photon flux density at depth for any wavelength (Iz_λ) is simply:

$$Iz_\lambda = Io_\lambda \exp^{-K_{T\lambda} z}$$

$$= Io_\lambda \exp^{-(K_{w\lambda} + K_{p\lambda} + k_{c\lambda} Chl)\, z} \qquad ...(3.7)$$

assuming attenuation is uniform throughout the depth interval. At any depth the rate of absorption of photons of wavelength λ (Ia_λ) is simply the product of the diffuse attenuation coefficient $K_{T\lambda}$ and the incident photon flux density at that depth (Iz_λ):

$$Ia_\lambda = K_{T\lambda} Iz_\lambda \qquad ...(3.8)$$

Since Iz_λ has units of mol m^{-2} s^{-1} and $K_{T\lambda}$ has units of m^{-1} the rate of photon absorption Ia_λ has units of mol m^{-3} s^{-1}. Similarly, the rate of photon absorption by the viable phytoplankton component at any wavelength λ (Ia_λ': mol m^{-3} s^{-1}) is:

$$Ia_\lambda' = k_{c\lambda} [Chl] Iz_\lambda$$

$$= Ia_\lambda [(k_{c\lambda} [Chl]) / K_{T\lambda}] \qquad ...(3.9)$$

In cases where attenuation is not uniform throughout the entire water column the total attenuation coefficient $K_{T\lambda}$ for any discrete depth interval is given by:

$$K_{T\lambda} = \frac{- ln [Iz_{1\lambda} / Iz_{2\lambda}]}{z_2 - z_1} \qquad ...(3.10)$$

Similarly, the rate at which photons of wavelength λ are absorbed by a water layer ($\Delta I_\lambda/\Delta z$) may be calculated by subtracting the photon flux density at the bottom of the layer from that incident on the top and dividing by the depth interval:

$$\frac{\Delta I_\lambda}{\Delta z} = \frac{I_{z1\lambda} - I_{z2\lambda}}{z_2 - z_1} \qquad ...(3.11)$$

As before rate of photon absorption $\Delta I_\lambda/\Delta z$ has units of mol m^{-3} s^{-1}. The rate of photon absorption by the viable phytoplankton component is then the product of the rate of photon absorption ($\Delta I_\lambda/\Delta z$) and a dimensionless factor (F) representing the fractional absorption of the phytoplankton pigments:

$$F = (k_{c\lambda}\,[Chl]) / K_{T\lambda} \qquad ...(3.12)$$

The attenuation coefficients K_w, K_p and k_c are all spectrally dependent and may be described by the spectral attenuation functions $K_w(\lambda)$, $K_p(\lambda)$ and $k_c(\lambda)$ for the wavelength region of interest. The spectral dependency of total attenuation $K_{PAR}(\lambda)$ for the wavelength interval corresponding to PAR (350 to 700 nm) is given by the sum of $K_w(\lambda)$, $K_p(\lambda)$ and $k_c(\lambda)\,[Chl]$. The *effective* spectral attenuation coefficient for PAR (K_{PAR}) depends also upon the spectral quantum irradiance $I(\lambda)$ and is defined as the integral of the product of $I(\lambda)$ and $K_{PAR}(\lambda)$ divided by the integral of $I(\lambda)$:

$$K_{PAR} = \int_{350}^{700} I(\lambda)\; K_{PAR}(\lambda)\, d\lambda \;\Big/\; \int_{350}^{700} I(\lambda)\, d\lambda \qquad ...(3.13)$$

Similarly, the *effective* spectral chlorophyll-specific attenuation cross-section (k_c) is defined by:

$$k_c = \int_{350}^{700} I(\lambda)\; k_c(\lambda)\, d\lambda \;\Big/\; \int_{350}^{700} I(\lambda)\, d\lambda \qquad ...(3.14)$$

The *effective* rate of photon absorption (I_a: mol m^{-3} s^{-1}) by all components at any depth is simply:

$$I_a = \int_{350}^{700} Iz(\lambda)\; K_{PAR}(\lambda)\, d\lambda \qquad ...(3.15)$$

The *effective* rate of photon absorption by the phytoplankton component, refered to as the *Photosynthetically Usable Radiation (PUR)*, corresponds to the fraction of PAR absorbed

by the phytoplankton. Expressed on a volumetric basis (Dubinsky 1980; Spitzer 1980; Priscu 1984; Tilzer 1984):

$$PUR = \int_{350}^{700} Iz(\lambda)\ K_c(\lambda)\ d\lambda$$

$$= [Chl] \int_{350}^{700} Iz(\lambda)\ k_c(\lambda)\ d\lambda \qquad \text{...(3.16)}$$

where PUR has units of mol m^{-3} s^{-1}. The term PUR has also been defined in chlorophyll-specific terms in which case it is simply the integral of the product of $I_z(\lambda)$ and $k_c(\lambda)$ with units of mol s^{-1} (mg Chl)$^{-1}$ (Morel 1978; Kishino *et al.* 1986).

A fraction of the PUR is transduced into chemical energy in the form of photosynthetic product. This quantity is refered to as the *Photosynthetically Stored Radiation (PSR)* (Morel 1978; Dubinsky 1980; Dubinsky and Berman 1981). The term PSR corresponds to the photosynthetic rate and is traditionally defined in terms of molecules of O_2 evolved or molecules of CO_2 reduced. When expressed on a volumetric basis PSR has units of mol m^{-3} s^{-1}.

3.1.3. The efficiency of phytoplankton absorption and photosynthetic transduction.

Comparisons of PAR, PUR and PSR throughout the water column lead to several dimensionless indices describing the efficiency of absorption and of photosynthetic transduction. Indices computed on a quantum/molecule basis will be termed *yields* in order to distinquish them from the analogous indices based upon energy units termed *efficiencies*. Efficiences may be calculated from yields provided both the spectral

distribution of the irradiance (1 quantum = $(1987/\lambda(nm)) \cdot 10^{-19}$ J) and the energy content of the photosynthetic product (J mol^{-1}) are known.

Obtaining dimensionless ratios from PAR, PUR and PSR has been complicated by differences in the dimensions of the three quantities; PAR has units of mol m^{-2} s^{-1} while PUR and PSR typically have units of mol m^{-3} s^{-1} (Platt 1969; Dubinsky 1980). In order for ratios of PAR, PUR and PSR to be dimensionless, it is necessary that PAR be expressed on a volumetric basis (mol m^{-3} s^{-1}). The solution most frequently used is to multiply the measured PAR (mol m^{-2} s^{-1}) by K_{PAR} (m^{-1}) to obtain the rate of photon absorption by a volume of water (*Ia*: mol m^{-3} s^{-1}).

The rate of photon absorption by the phytoplankton (PUR) relative to the rate of photon absorption by all the components (*Ia*), provides a measure of the absorption yield (ξ) of the phytoplankton. In this case, the absorption yield reduces to the ratio K_c/K_{PAR} representing the fraction of the absorbed irradiance that is absorbed by the chlorophyll (= phytoplankton) component.

$$\xi = \frac{PUR}{I_a} = \frac{\int_{350}^{700} I(\lambda)\ K_c(\lambda)\ d\lambda}{\int_{350}^{700} I(\lambda)\ K_{PAR}(\lambda)\ d\lambda} \qquad ...(3.17)$$

Alternatively, if PUR is integrated throughout the entire water column then both PUR and PAR will both have units of mol m^{-2} s^{-1} and the absorption yield (ξ) will be dimensionless as required (Platt 1969; Dubinsky 1980).

The light utilization yield (ψ), and its energy analogue the light utilization efficiency (ψ'), is the ratio PSR/PAR. Once again when calculated for discrete depths as opposed to integrating over the entire water column PAR must be expressed on a volumetric basis (*ie. Ia*) for the ratio to be dimensionless. The light utilization yield represents the efficiency with which incident quanta are transduced into photosynthetic product.

$$\psi = \frac{PSR}{I_a} = \frac{\phi \int_{350}^{700} I(\lambda)\, K_c(\lambda)\, d\lambda}{\int_{350}^{700} I(\lambda)\, K_{PAR}(\lambda)\, d\lambda} \qquad ...(3.18)$$

Finally the quantum yield (ϕ), and its energy analogue the quantum efficiency (ϕ'), is defined as the ratio PSR/PUR. The quantum efficiency describes the efficiency with which absorbed quanta are transduced into photosynthetic product. The quantum yield represents the molar ratio of molecules photosynthetically reduced or oxidised to the number of photons absorbed.

$$\phi = \frac{PSR}{PUR} = \frac{\phi \int_{350}^{700} I(\lambda)\, K_c(\lambda)\, d\lambda}{\int_{350}^{700} I(\lambda)\, K_c(\lambda)\, d\lambda} \qquad ...(3.19)$$

3.2. SCALING THE P-I RESPONSE TO SPECTRAL ABSORPTION.

All of the semi-empirical and rational models of the P-I response discussed in Chapter 2 describe photosynthesis as a function of the *incident* irradiance (*PAR*). As

Grotthus-Draper Law states that only absorbed photons can cause photochemical reactions and therefore bring about photobiological responses the photosynthetic rate is a function of the irradiance *absorbed* by the phytoplankton (PUR).

3.2.1. Recasting P-I models in terms of absorbed irradiance.

Where the rate of photosynthesis (P) is considered proportional to the rate that photons are absorbed (PUR) then:

$$P = \phi_a \int_{350}^{700} I(\lambda)\, a(\lambda)\, d\lambda \qquad \ldots(3.20)$$

where P is the (volumetric) photosynthetic rate (mol C m^{-3} s^{-1}), ϕ_a is the constant of proportionality (dimensionless), $a(\lambda)$ is the absorption coefficient (m^{-1}) and $I(\lambda)$ is the incident photon flux density (mol m^{-2} s^{-1}). Such a formulation implicitly assumes that the constant of proportionality ϕ_a, termed the *apparent* quantum yield, is *both constant and wavelength independent.* Under these circumstances any differences in the P-I relationship determined under different spectral distributions are considered to arise simply as a consequence of differences in the integral of the product of $I(\lambda)$ and $a(\lambda)$ such that all P-I curves will be proportional to one another with respect to the irradiance axis.

This proportionality between P-I responses determined under different spectral distributions means that if the photosynthetic rate is plotted as a function of *ln I* rather than *I*, all of the resultant P-I curves will be parallel to one another. Furthermore, the horizontal separation of P-I curves determined under different spectral distributions will correspond to the natural logarithm of the ratio of absorbed irradiances (*ie. ln* $[PUR_1/PUR_2]$). This graphical relationship for P-I curves determined in different

polychromatic irradiance fields and plotted as a function of both I and $ln\ I$ is illustrated in Figure 3.2.

Stating the photosynthetic rate (PSR: mol m^{-3} s^{-1}) in terms of the rate of photon absorption (PUR: mol m^{-3} s^{-1}) rather than the rate of photon incidence (PAR: mol m^{-2} s^{-1}) thus requires a simple re-scaling of the abscissa by a spectral weighting factor corresponding to the *effective* spectral absorption coefficient (a: units m^{-1}).

$$a = \int_{350}^{700} I(\lambda)\ a(\lambda)\ d\lambda \ \Big/ \int_{350}^{700} i(\lambda)\ d\lambda \qquad ...(3.21)$$

In the case of natural waters where photosynthetic rates are expressed on a chlorophyll basis (PSR: mol C (mg Chl)$^{-1}$ s^{-1}) the spectral weighting factor corresponds to the mean spectral chlorophyll-specific attenuation cross-section k_c (m^2 (mg Chl)$^{-1}$) as described in Eq. 3.14. Consequently, all of the various P-I models discussed in Chapter 2 may be restated in terms of *absorbed* PFD as opposed to *incident* PFD.

3.2.2. Advantages and Disadvantages of Scaling to the Absorption Spectrum.

Re-scaling the P-I response according to the spectral dependency of absorption constitutes a simple attempt to incorporate the spectral nature of irradiance into the photosynthesis-irradiance relationship. The principle advantage of using the absorption spectrum to spectrally weight the P-I response is the ease with which the spectral dependence of absorption can be measured. The absorption spectra of both laboratory cultures and oceanic particulate material is simply determined spectrophotometrically in the laboratory, in the latter case by collecting the particulate material on filters. The possibility also exists for estimating the spectral absorption properties of the

phytoplankton by remote sensing measurements of the spectral reflectance of the ocean (Gautier *et al.* 1980; Gautier 1982; Gordon and Morel 1983; Sathyendranath 1986).

Several major disadvantages are associated with the application of the absorption spectrum as an appropriate spectral weighting function for describing the spectral dependency of photosynthesis. Firstly, it is implicitly assumed that all photons absorbed by the sample have the potential to be photosynthetically utilized and that the apparent quantum yield is constant and wavelength independent. This assumes that photosynthetic pigments constitute the only (or at least predominant) absorbing substances present. The presence of any absorbing materials in the phytoplankton or oceanic particulates which do not participate in the photosynthetic process will lead to an inappropriate spectral weighting function for the P-I response.

Because of the additivity of absorption cross-sections in a mixture [Eq. 3.4] it is not possible to extract the absorption spectrum of the photosynthetic component based upon a single sample. In the case of oceanic particulates it is impossible to partition K_{PAR} into its components, specifically to extract an accurate estimate for k_c, based upon a single absorption spectrum. Consequently the spectral weighting function used to re-scale the P-I response corresponds to the mean spectral attenuation coefficient of *all* the particulate material present ($K_p + K_c$) and not just that portion corresponding to the viable phytoplankton component (K_c). The spectral characteristics of the dissolved and particulate material responsible for light absorption may be radically different from those of the photosynthetically active pigments within the phytoplankton. Where the latter is only a minor component their spectral absorption properties will be masked by absorption of the more abundant material.

Another disadvantage is the application of a single spectral weighting function to the entire P-I response. By suggesting that P-I curves obtained under different spectral distributions are proportional to one another with the proportionality constant depending upon absorption, it is implicitly assumed that the spectral dependency of photoinhibition is identical to that of photochemistry. The application of a single proportionality constant to both the photosynthetic and photoinhibitory portions of the P-I curve may not be valid.

In summary, modelling photosynthesis in terms of the absorbed irradiance rather than the incident irradiance provides a first-order approximation of the spectral dependency of photosynthesis. It is achieved in practice by simply re-scaling the irradiance axis by the the attenuation coefficient of the sample. To be valid it is required that the photosynthetic pigments constitute the sole source of absorption, the quantum yield be constant and wavelength independent and that photoinhibition (if present) exhibits an identical spectral response to that of photosynthesis. These constraints severely restict the usefulness of this approach in the oceanographic context where the photosynthetic component may represent only a small fraction of the absorbing component.

3.3. SCALING THE P-I RESPONSE TO THE MONOCHROMATIC ACTION SPECTRUM.

3.3.1. Introduction.

Because of interference by pigments that are not associated with photosynthetic photon harvesting, it is more appropriate to directly model the photosynthetic process itself as a function of photon wavelength. The study of how the photon wavelength

affects the rate of a chemical, biochemical or physiological response is referred to as action spectroscopy. An action spectrum is defined as a plot of the *relative response* of a biological system to irradiance of different wavelengths. In the case of a very simple system where the response is a function of absorption by a single stable pigment, the response in polychromatic irradiance may be obtained by way of "classical action spectroscopy".

3.3.2. Principles of Classical Action Spectroscopy.

Classical action spectroscopy provides the second basic approach to integrating the spectral distribution of incident irradiance into the P-I response. Classical action spectroscopy requires that the many reactions comprising photosynthesis be represented by a single ideal primary photoreaction. An ideal primary reaction is considered to be a photoreaction that corresponds directly to the first molecular change promoted by the absorbed photon. Under this assumption the rate of the primary reaction is proportional to the number of photons absorbed. Transduction of the incident irradiance is simply represented by a constant of proportionality linking the input (photons absorbed) to the output (molecules photosynthetically transformed). This proportionality constant is generally referred to as the quantum yield of the photoreaction.

Where absorption may be attributed to a single photosynthetic pigment, or a mixture of pigments *acting additively*, the photosynthetic response may be determined by similar reasoning to that employed to determine absorption. Under monochromatic radiation (wavelength λ) and photon flux density (I_λ: mol m^{-2} s^{-1}), the number of molecules transformed per second (*ie.* the rate of phototransformation v: mol s^{-1}) is:

$$v = c \cdot I_\lambda \cdot \varepsilon_\lambda \cdot \phi_\lambda \qquad ...(3.22)$$

where c is the concentration of pigment in the ground state and so capable of photon absorption (units: mol m^{-3}), ε_λ is the effective molar absorption cross-section of the pigment at wavelength λ (units: m^2 mol^{-1}) and ϕ_λ is the quantum yield of transformation (*ie.* the probability that an absorbed photon gives rise to a transformation) at that wavelength (units: dimensionless). The product $\varepsilon_\lambda \cdot \phi_\lambda$ is referred to as the transformation cross-section σ_λ (units: m^2 molecule):

$$\varepsilon_\lambda \cdot \phi_\lambda \quad = \quad \sigma_\lambda \qquad \text{...(3.23)}$$

As in the case of absorption, it is not possible to distinguish between a single pigment or many pigments each with unknown fractional concentrations and partial cross-sections but which act additively to bring about the response. Consequently Eq. 3.13 refers to a single *effective* pigment characterized by a single *effective* cross-section which *in vivo* may represent one or more real pigments such that σ_λ in Eq. 3.13 refers to the *effective* cross-section for transformation.

Under monochromatic irradiance the pigment-specific rate of the phototransformation r (where $r = v/c$: mol transformed (mol pigment)$^{-1}$ s^{-1}) is given by:

$$r \quad = \quad I_\lambda \cdot \varepsilon_\lambda \cdot \phi_\lambda \quad = \quad I_\lambda \cdot \sigma_\lambda \qquad \text{...(3.24)}$$

where I_λ is the incident photon flux density (mol m^{-2} s^{-1}), ε_λ is the absorption cross-section of the pigment (m^2 mol pigment $^{-1}$), ϕ_λ is the quantum yield (mol pigment transformed · mol photons $^{-1}$ = dimensionless) and σ_λ is the action cross-section of the pigment (m^2 mol pigment $^{-1}$).

Like absorption, this formulation may be extended to polychromatic irradiation where the discrete numbers ε_λ and ϕ_λ are replaced by the continuous spectral functions $\varepsilon(\lambda)$ and $\phi(\lambda)$. The PFD I_λ (mol m^{-2} s^{-1}) is replaced by the function $I(\lambda)$ (mol m^{-2} s^{-1} nm^{-1}). The *effective* pigment-specific rate of the phototransformation (r: mol transformed (mol pigment)$^{-1}$ s^{-1}) in polychromatic irradiation (PAR) is then:

$$r = \int_{350}^{700} I(\lambda)\, \varepsilon(\lambda)\, \phi(\lambda)\, d\lambda \qquad ...(3.25)$$

If photosynthesis is considered to be an ideal primary photoreaction where the rate of photosynthesis is considered to be equal to the rate of phototransformation of the primary photoreceptor, then k corresponds directly to the pigment specific rate of photosynthesis (P^B) so that:

$$P^B = \int_{350}^{700} I(\lambda)\, \varepsilon(\lambda)\, \phi(\lambda)\, d\lambda$$

$$= \int_{350}^{700} I(\lambda)\, \sigma(\lambda)\, d\lambda \qquad ...(3.26)$$

A basic assumption of classical action spectroscopy is the *principle of equivalent light action* which states that the response resulting from the absorption of a photon of one wavelength is identical to that brought about by the absorption of a photon of different wavelength. This assumption enables the direct comparison of the effectiveness of photons of different wavelengths in bringing about a certain level of response. In any two experiments where there are equal rates of *primary reactions* ($r_{\lambda 1} = r_{\lambda 2}$) then there will be equal *photosynthetic responses* ($R_{\lambda 1} = R_{\lambda 2}$).

The principle of equivalent light action requires two conditions be fulfilled. The first is that the concentration of photosynthetic pigment in the ground state remains constant over time (*ie. c(t) = constant*). This ensures *v(t)* will also be constant over time and may be replaced by the pigment-specific rate *r(t)* so that if $r_{\lambda 1} = r_{\lambda 2}$ then $R_{\lambda 1} = R_{\lambda 2}$. The second condition required is that *the response is always limited by the light action.* This condition ensures that the inverse is also true, such that if $R_{\lambda 1} = R_{\lambda 2}$ then $r_{\lambda 1} = r_{\lambda 2}$.

Provided these conditions are fulfilled Eqs. 3.22 and 3.23 predict that if the response observed under two different wavelengths are equal ($R_{\lambda 1} = R_{\lambda 2}$) then:

$$I_{\lambda 1}\sigma_{\lambda 1} = I_{\lambda 2}\sigma_{\lambda 2} \qquad ...(3.27)$$

and so

$$\frac{\sigma_{\lambda 1}}{\sigma_{\lambda 2}} = \frac{I_{\lambda 2}}{I_{\lambda 1}} \qquad ...(3.28)$$

Eqs. 3.27 and 3.28 state the basic equation of classical action spectroscopy: that if monochromatic irradiances of different wavelengths bring about an equal level of response then the effective cross-sections of the photoreceptor (with respect to the primary reaction) are related as the reciprocals of the PFDs (Schafer *et al.* 1983).

An action spectrum is obtained when the reciprocals of the monochromatic PFDs ($1 / I_\lambda$) required to bring about a fixed level of response (R_λ) is plotted as a function of wavelength. The response R_λ is usually normalized to some biomass index such as pigment. The action spectrum reflects the relative spectrum of cross-sections of the photoreceptor with respect to the primary reaction. Where the quantum yield is

wavelength-independent the action spectrum also provides the relative absorption spectrum of the photoreceptor and if the quantum yield is known then the absolute absorption cross-section of the photoreceptor can be estimated. Conversely, if an independent measure of the absorption cross-section of the photoreceptor is available then the quantum yield may be estimated.

At this point it is important to distinguish between the *actual* quantum yield (ϕ) of the photoreaction and the *apparent* quantum yield (ϕ_a). Division of the action spectrum of the photoreaction by the absorption cross-section of the material *as a whole* yields the *apparent* quantum yield. The apparent quantum yield is less than the *actual* quantum yield because of the presence of photosynthetically inactive pigments which contribute to absorption but not to the photoreaction. The presence of photosynthetically inactive pigments reduces the apparent quantum yield relative to the actual quantum yield at those wavelengths where the inactive pigments absorb most strongly.

The P-I response curves determined under different monochromatic wavelengths (I_λ) are proportional to one another, with the constant of proportionality equal to the ratio of the effective action cross-sections under the different wavelengths ($I_{\lambda 1}\sigma_{\lambda 1} / I_{\lambda 2}\sigma_{\lambda 2}$). If the response is plotted against $ln\ I_\lambda$ rather than I_λ, the response curves for each wavelength become parallel and may be super-imposed by shifting them horizontally along the x-axis ($ln\ I_\lambda$). The logarithmic transformation of I_λ to $ln\ I_\lambda$ converts proportionality to additivity, when $I_{\lambda 1}\sigma_{\lambda 1} = I_{\lambda 2}\sigma_{\lambda 2}$ it follows that:

$$ln\ (I_{\lambda 1}) - ln\ (I_{\lambda 2}) = ln\ \frac{\sigma_{\lambda 1}}{\sigma_{\lambda 2}} \qquad ...(3.29)$$

Eq. 3.29 states that for two response curves plotted as a function of $ln\ I_\lambda$, the value of $ln\ I_\lambda$ which brings about any fixed level of response on one curve is shifted with respect to a corresponding $ln\ I_\lambda$ value (that gives rise to an equal response) for another curve by the interval $ln\ [\sigma_{\lambda 1}/\sigma_{\lambda 2}]$.

This result is analogous to that found when re-scaling the P-I response to absorbed irradiance (PUR). In that case the horizontal translation factor was the natural logarithm of the ratio of absorbed irradiances (*ie.* $ln\ [PUR_1/PUR_2]$) rather than the ratio of the action cross-sections ($ln\ [\sigma_1/\sigma_2]$).

The relationship between the proportionality of response curves plotted against I_λ and the additivity of response curves when plotted against $ln\ I_\lambda$ is illustrated in Figure 3.1. The parallelism of "response versus $ln\ I_\lambda$" curves is a *minimal* requirement for the application of classical action spectroscopy. However it should be emphasized that proportionality between P-I curves does not in itself demonstrate that *all* of the requirements of classical action spectroscopy are fulfilled.

3.3.3. Recasting P-I models in terms of stored irradiance (PSR).

Under the restrictions of classical action spectroscopy Eq. 3.26 may be accepted as an accurate definition of the pigment-specific photosynthetic rate (mol (mol pigment)$^{-1}$ s^{-1}). Where the photosynthetic rate is normalized to chlorophyll (P^B = mol (mol Chl)$^{-1}$ s^{-1}), multiplication by the chlorophyll concentration (mg m^{-3}) yields the volumetric photosynthetic rate (mol m^{-3} s^{-1}) corresponding to the Photosynthetically Stored Radiation (PSR):

$$PSR = [Chl] \int_{350}^{700} I(\lambda)\ k_c(\lambda)\ \phi(\lambda)\ d\lambda$$

$$= [Chl] \int_{350}^{700} I(\lambda)\ \sigma_c(\lambda)\ d\lambda \qquad \text{...(3.30)}$$

where $k_c(\lambda)$ is the chlorophyll-specific absorption cross-section (m^2 (mg Chl)$^{-1}$), $\phi(\lambda)$ is the quantum yield (dimensionless) and $\sigma_c(\lambda)$ is the chlorophyll-specific action cross-section (m^2 (mg Chl)$^{-1}$).

All of the empirical and rational P-I expressions outlined in Chapter 2 may be recast in terms of PSR rather than PAR. Where photosynthetic rates are expressed on a volumetric basis (P: mol C m^{-3} s^{-1}), the P-I response may be re-defined in terms of PSR by multiplying the incident irradiance (PAR) by a spectral weighting factor corresponding to the *effective* spectral action coefficient for photosynthesis (σ, units m^{-1}):

$$\sigma = [Chl] \int_{350}^{700} I(\lambda)\ \sigma_c(\lambda)\ d\lambda \ / \int_{350}^{700} I(\lambda)\ d\lambda \qquad \text{...(3.31)}$$

Where the photosynthetic rate is expressed on a chlorophyll basis (P^B: mol C (mg Chl)$^{-1}$ s^{-1}) then the spectral weighting factor corresponds simply to the *effective* spectral chlorophyll-specific action cross-section σ_c (m^2 (mg Chl) ^{1}):

$$\sigma_c = \int_{350}^{700} I(\lambda)\ \sigma_c(\lambda)\ d\lambda \ / \int_{350}^{700} I(\lambda)\ d\lambda \qquad \text{...(3.31)}$$

3.3.4. Separate Spectral Scaling of Photosynthesis *f(I)* and Photoinhibition *g(I)*.

As was the case when scaling the P-I curve to absorption, spectrally weighting the entire P-I response to a *single* weighting function based upon the action spectrum for photosynthesis implicitly assumes that the spectral dependency of photoinhibition $g(I(\lambda))$ is identical to that of photosynthesis $f(I(\lambda))$. From a theoretical perspective this assumption would seem unlikely (although in practice it could prove to be a valid approximation).

In all of the P-I formulations in which the photoinhibition function ($g(I)$) is described independently of the photosynthetic response to irradiance ($f(I)$), the potential exists to independently apply a different spectral weighting function to each process in order to describe the overall P-I response. The determination of the spectral dependency of photoinhibition from a monochromatic action spectrum is identical in principle to the determination of the action spectrum of photosynthesis. As with photosynthesis, this approach assumes the principle of equivalent light action applies to the photoinhibition photoreaction. Despite the advances that have been made concerning the mechanism of photoinhibition, the spectral dependency of the process remains to be established.

3.3.5. Advantages and Disadvantages of Scaling to the Monochromatic Action Spectrum.

The principle advantage of using the monochromatic action spectrum to re-scale the irradiance axis of the P-I response rather than the absorption spectrum is that the former provides a spectral weighting factor appropriate to the response in question, namely photosynthesis or photoinhibition. Using the monochromatic action spectrum [Eq. 3.32] to scale photosynthesis is preferable to employing the absorption spectrum

[Eq. 3.14] in cases where the material in question contains a high proportion of photosynthetically inactive pigments (such as is frequently the case with oceanic phytoplankton assemblages).

The possibility that photoinhibition has a different spectral response to that of photosynthesis can also be accounted for if the action spectrum of photoinhibition is determined separately and a P-I model is chosen with a (mathematically) distinct photoinhibition component. The final model can spectrally-weight the P-I response at low irradiances according to the spectral dependency of photosynthesis (*ie.* $f(I(\lambda))$), and the response at high irradiances to the spectral dependency of photoinhibition (*ie.* $g(I(\lambda))$).

The central assumption underlying the use of a monochromatic action spectrum ($\sigma(\lambda)$) to calculate PSR under polychromatic irradiance [Eq. 3.26] is that the response to several photons of differing wavelength is *independent and strictly additive*. Under circumstances where the cumulative effects of photons are non-additive the principle of equivalent light action is violated and the use of the monochromatic action spectrum to scale the P-I response is invalid. As described later (Section 3.5.), the organization of the photosynthetic apparatus can result in photons of different wavelengths behaving in a non-additive manner. Consequently, the computation of PSR (P or P^B) under some hypothetical spectral distribution $I(\lambda)$ according to Eq. 3.26 based upon the photosynthetic response established under monochromatic irradiance ($\sigma(\lambda)$ or $\sigma_d(\lambda)$) is incorrect. Application of the resultant spectral weighting function [Eq. 3.31 or 3.32] to re-scale the irradiance axis will not yield an accurate estimate of the photosynthetic response under polychromatic irradiance.

In such cases scaling the P-I response to PSR based upon the monochromatic action spectrum [Eq. 3.32] may yield an inferior result to that obtained by scaling the response to the PUR based upon the absorption spectrum [Eq. 3.16]. Nevertheless, for many phytoplankton species the monochromatic action spectrum provides the best approximation for calculating the photosynthetic rate under polychromatic irradiance.

3.4. NEW P-I MODELS APPROPRIATE FOR SIMPLE SPECTRAL SCALING TO PUR AND PSR.

All of the P-I models discussed in Chapter 2 where the photosynthetic rate is expressed on a chlorophyll basis (P^B) may be restated in terms of PUR or PSR by simply re-scaling the irradiance axis by either the mean spectral chlorophyll-specific absorption cross-section k_c [Eq. 3.14] or the mean spectral chlorophyll-specific action cross-section σ_c [Eq. 3.32] respectively. Those formulations that contain independent descriptions of photoinhibition allow the separate spectral scaling of both processes according to the action spectra of photosynthesis ($f(I)$) and photoinhibition ($g(I)$) respectively. Examination of the P-I responses determined for cultures of picoplankton (see Chapter 5) suggested that none of the published empirical models provided a description that accorded with the geometric properties of the data. The empirical function proposed by Platt and Gallegos (1980) yielded the best solution but seemed inadequate at high irradiances. This model predicts a progressive decrease in the negative slope of the P-I curve at high irradiances, with the rate of photosynthesis approaching zero asymptotically. Such curvature was not observed, and photoinhibition decreased in a strictly linear fashion with increasing irradiance.

Consequently two new formulations were devised aimed at providing an accurate quantitative description of the picoplanktonic P-I response. Both models provide independent descriptions of photochemistry and photoinhibition to facilitate independent spectral scaling.

3.4.1. An Empirical Model.

This model was formulated strictly from a geometrical perspective. The results of curve-fitting the various models to experimental data (see Chapter 5) indicated that the three-parameter formulation of Bannister (1979) [Eq. 2.12] best described the curve up to the point of saturation. The photoinhibitory decrease in photosynthesis at high PFDs appeared to be a linear function of PFD above the threshold of its onset with no indication that this decrease lessened at higher irradiances. At its simplest, the entire response could be described by a function describing photosynthesis $f(I)$ and a function describing photodestructive processes $g(I)$ such that:

$$P^B = f(I) - g(I) \qquad \ldots(3.33)$$

where $f(I)$ is the equation of Bannister (1979) and $g(I)$ is a modified form of the classic Blackman (1905) equation. In terms of parameters based upon irradiance, $f(I)$ may be written:

$$f(I) = P_s^B \left[\frac{I/I_k}{\left[1 + (I/I_k)^m \right]^{1/m}} \right] \qquad \ldots(3.34)$$

and $g(I)$ may be written:

$$\begin{aligned} g(I) &= 0 && 0 < I < I_j \\ &= P_s^B (I - I_j) / (I_j - I_t) && I_j < I < I_t \\ &= P_s^B && I > I_t \end{aligned} \qquad ...(3.35)$$

where I_j is the irradiance marking the onset of photoinhibition and I_t is the irradiance at which photosynthesis is reduced to zero by photoinhibition. The negative slope of the linear decrease in photosynthesis ascribed to photoinhibition (β^B) is given by $P_s^B / (I_j - I_t)$.

To provide a gradual transition from the region of light saturation to the region where photosynthesis decreases linearly with increasing irradiance an alternative form of $g(I)$ was introduced. The form chosen was designed to be algebraically analogous to the equation of Bannister (1979), the function chosen for $f(I)$. By having analogous parameters, there is the potential that the final expression may be simplified considerably. Where fitted curves produce similar values for analogous parameters in the two components ($f(I)$ and $g(I)$) of the overall P-I function, they may be replaced by a single parameter.

Written in terms of irradiance parameters the expression for describing the photodestructive processes $g(I)$ is:

$$\begin{aligned} g(I) &= P_s^B \left[1 - \frac{(I_t - I) / (I_t - I_j)}{\left[1 + \left[\frac{I_t - I}{I_t - I_j} \right]^n \right]^{1/n}} \right] && I \le I_t \\ &= P_s^B && I > I_t \end{aligned} \qquad ...(3.36)$$

Eq. 3.36 corresponds to the equation of Bannister (1979) rotated about the y-axis and horizontally translated along the x-axis by the quantity I_t. The geometrical

properties of this function are illustrated in Figure 3.2. The parameter I_t is the irradiance where photosynthesis has been reduced to zero due to photoinhibition. The negative slope (β^B) of the *P-I* curve as *I* approaches I_t is given by $P_s^B / (I_j - I_t)$ where I_j represents the irradiance marking the onset of photoinhibition. The parameter I_j is analogous to I_k in Bannister's formulation and corresponds to the intersection of the negative photoinhibitory slope and the maximum photosynthetic rate. Extrapolating the negative slope of photoinhibition back to zero irradiance yields an intercept on the ordinate which we term the extrapolation number P_t^B. The extrapolation number $P_t^B = -\beta I_t$ and P_t^B / P_s^B is equal to $I_t / (I_t - I_j)$.

The parameter *n* is analogous to the parameter *m* in the equation of Bannister (1979) and describes the abruptness of the transition from the maximum photosynthetic rate (P_s^B) to the negative linear portion ascribed to photoinhibition (β^B). The more abrupt the transition, the more extended is the range for which the relationship between declining photosynthesis and irradiance is linear. In the extreme case where $n = \infty$, this formulation is identical to the Blackman-type response described in Eq. 3.25. In practice a value of $n > 3$ provides an abrupt transition from the light-saturated rate to a linear decrease in photosynthesis with increasing irradiance.

Both the photosynthetic and photodestructive functions *f(I)* and *g(I)* in the final expression share the same parameter P_s^B, the maximum *potential* rate of photosynthesis that could be attained where photosynthesis is not light-limited and in the absence of photoinhibition. With independent shape parameters for both photosynthesis and photoinhibition the overall formulation ($P^B = f(I) - g(I)$) constitutes a 6-parameter model (with parameters P_s^B, I_k, *m*, I_j, I_t, and *n*). This reduces to a 5-parameter formulation if *n* is set equal to *m* and may be further simplified to a 4-parameter formulation if both *n* and *m* are set at some arbitrary constant (usually > 3) so as to yield the required curvature.

The maximum photosynthetic rate P_s^B is the only parameter shared by photochemistry and photoinhibition and scales the ordinate. The parameter P_s^B is considered wavelength independent. Scaling of the curve with respect to the abscissa is by way of the remaining parameters, I_k and m scale the initial photochemical response while I_t , I_j and n scale the photoinhibitory decrease at higher irradiances. Because the processes of photochemistry and photoinhibition are described by independent parameters, both processes may be written independently in non-dimensional form. This permits independent spectral scaling of both photochemistry and photoinhibition according to their respective monochromatic action spectra.

3.4.2. A Rational Model.

This rational model provides a simple description of the photosynthetic process based upon the statistical behavior of a large number of identical photosynthetic units within the photosynthetic cell. It extends the models based upon target theory proposed by Herron and Mauzerall (1972), Ley and Mauzerall (1982) and Dubinsky *et al.* (1986) to include a Poissonian description of photoinhibition. An outline of this model is provided in Figure 3.3.

Model Structure: This model considers that the photosynthetic cell contains a large number (n) of identical yet independent photosynthetic units (PSUs). Each PSU comprises a reaction center capable of performing photochemistry connected to a light-harvesting antenna consisting of an assemblage of photosynthetic pigments. Any photons absorbed by the photosynthetic antenna are efficiently transferred to the reaction center where they may promote a photochemical transformation (Figure 3.3). The mechanism whereby absorbed photons are transferred to the reaction center is not

important other than the fact that it is considered to be 100% efficient. The radiationless, resonance mechanism proposed by Forster (1948,1959,1965) whereby energy transfer occurs by dipole-dipole interaction between donor and acceptor molecules (excitons) fulfils this criterion.

The PSU considered here is a statistical construction. *In vivo* a PSU may comprise a single photosystem with an antenna serving a single reaction center (the "puddle" arrangement). Alternatively a PSU may represent a collection of photosystems whose antennae are dynamically coupled to one another and to multiple reaction centers such that an absorbed photon has a probability of by-passing a closed reaction center and migrating within the antennae so as to find an open reaction center (the so-called "lake" model). Where the probability of by-passing an open reaction center equals that of by-passing a closed reaction center, the "lake" model is identical to the "puddle" model in which the effective PSU size equals the average antenna size per reaction center (Mauzerall 1986).

Absorption by the PSU: Absorption of photons by the PSU (a_{PSU}) is wavelength dependent and depends upon the mixture of pigments present in the PSU. Because of the addivity principle of absorption, the assemblage of pigments within a PSU behaves as a single *effective* pigment as far as the model is concerned. Transfer of the absorbed photons as excitons to the reaction center(s) is considered to be independent of wavelength and to be 100% efficient.

The average rate at which photons are absorbed by the PSU and subsequently arrive at a reaction center (I_{RC}: mol s^{-1}) is then simply the product of the incident photon flux density (mol m^{-2} s^{-1}) and the absorption cross-section of the PSU (m^2 PSU^{-1}). Under

monchromatic irradiance of wavelength λ the average exciton flux at a reaction center (mol s^{-1}) is:

$$I_{RC} = a_{PSU\lambda} \cdot I_{\lambda} \quad ...(3.37)$$

In a polychromatic light field $I(\lambda)$ consisting of wavelengths of PAR, the average exciton flux arriving at a reaction center (mol s^{-1}) is:

$$I_{RC} = \int_{350}^{700} I(\lambda)\, a_{PSU}(\lambda)\, d\lambda \quad ...(3.38)$$

Response of RC to exciton flux: The reaction center is considered to be either open or closed. Once a reaction center absorbs an exciton it is considered closed for a short interval of time (τ, the turnover time of the reaction center) during which it is incapable of performing any further photochemistry. Any exciton arriving during this time interval is ineffective from the standpoint of performing photochemistry and is considered lost from the PSU. After this interval the reaction center regains its capacity to perform photochemistry and is once again considered open.

While the average rate at which photons are absorbed by the PSU is a linear function of the incident PFD (Eq. 3.38), the probability that absorbed photons are *transduced* into photosynthetic product at the reaction centre is not a simple linear function of the PFD. This is because an exciton may arrive at a closed reaction center in which case it is not transduced into photosynthetic product. The likelihood of an arriving exciton encountering a closed reaction center is greater at higher PFDs.

In a cell where the number (n) of PSUs is very large and the likelihood that an individual PSU absorbs a photon (a_{PSU}) during an arbitrarily small interval (Δt) is very

small, the *average* rate of photon absorption by *any* PSU within the cell is given by Eq. 3.38. The *actual* number of photons absorbed by a *particular* PSU in the time interval Δt is given by the Poisson probability distribution. The probability $p(k)$ of a single PSU absorbing k photons in a time interval Δt when the average number of photons absorbed per PSU is μ is given by:

$$p(k) = \frac{(\mu\Delta t)^k}{k!} e^{-\mu\Delta t} \qquad ...(3.39)$$

Accordingly, the probability that *no photons are absorbed* by the cell (*ie.* by any of the PSUs within the cell) in a time interval Δt is:

$$p(0) = \frac{(\mu\Delta t)^0}{0!} e^{-\mu\Delta t} = e^{-\mu\Delta t} \qquad ...(3.40)$$

Since the sum of all the probabilities of the Poisson distribution is unity, the probability that any of the PSUs absorb *one or more photons* is:

$$p(\geq 1) = \sum_{k=0}^{\infty} [\, p(k) \,] - p(0)$$

$$= 1 - e^{-\mu\Delta t} \qquad ...(3.41)$$

If we assume that photosynthetic transduction at the reaction center requires the arrival of a minimum of x photons within the time interval Δt then the probability of photosynthesis occuring at a reaction center (p_{RC}) equals the probability that $\geq x$ photons arrive at the reaction center in the time interval Δt:

$$p_{RC} = p(\geq x) = \sum_{k=x}^{\infty} \frac{(\mu\Delta t)^k}{k!} e^{-\mu\Delta t} \quad \ldots(3.42)$$

This cumulative Poisson probability formulation provides a family of curves of the saturation type for different discrete values of k that may be employed to describe the P-I response (Figure 3.4(a)). Where the reaction center performs photosynthesis in response to the arrival of one or more excitons within an interval Δt, the probability of photosynthesis is described by a cumulative single hit Poisson distribution:

$$p_{RC} = p(\geq 1) = 1 - p(0) = 1 - e^{-\mu\Delta t} \quad \ldots(3.43)$$

Eq. 3.43 which describes photosynthesis under continuous irradiance differs from the analogous expression established for single saturating flashes (Ley and Mauzerall 1982) in that the exponential function includes the dimension of time. This may be rationalized by setting $\Delta t = \tau$, the turnover time of the reaction center. The arrival of more than one photon at the reaction center within the interval Δt results in the first photon performing photochemistry after which the reaction center is closed for the duration of τ. Further photochemistry is impossible and the additional photons are wasted. This function also satisfies the condition that at low PFD the rate of photosynthesis is a linear function of the PFD.

The Poissonian form of the model also provides a rational means of introducing photoinhibition at high PFDs. The photoinhibitory decrease in photosynthesis at high PFDs may be attributed to the arrival of greater than a specified number of photons (y) at the reaction center within the time interval Δt ($= \tau$) which inactivates the reaction center indefinitely. The photochemical effect generated by the arrival of the first photon is annulled and all of the arriving photons are effectively lost resulting in no

photochemistry. The exact mechanism of such photoinhibition is unknown but may result from singlet-singlet exciton annihilation at or near the reaction center (Wong *et al.* 1981; Doukas *et al.* 1981; Pellogrino *et al.* 1981).

As in Eq. 3.42, the probability that y or more photons are absorbed by a photosystem within an arbitrarily small time interval Δt is given by the cumulative Poisson expression:

$$p(\geq y) = \sum_{k=y}^{\infty} \frac{(\mu\Delta t)^k}{k!} e^{-\mu\Delta t} \qquad ...(3.44)$$

Again by setting $\Delta t = \tau$ Eq. 3.44 may be considered as the photoinhibition function $g(I)$ describing the probability that a reaction center will undergo photodestruction.

The probability that a PSU absorbs less than y photons within a time interval Δt and so survives photodestruction is:

$$p(<y) = 1 - p(\geq y) = 1 - \sum_{k=y}^{\infty} \frac{(\mu\Delta t)^k}{k!} e^{-\mu\Delta t} \qquad ...(3.45)$$

The form of this function is illustrated in Figure 3.4(b) for various discrete values of y. Eq. 3.45 may be rewritten:

$$1 - p(\geq y) = p(\leq (y-1)) = \sum_{k=0}^{y-1} \frac{(\mu\Delta t)^k}{k!} e^{-\mu\Delta t}$$

$$= e^{-\mu\Delta t} \left(1 + \frac{\mu\Delta t}{1!} + \frac{(\mu\Delta t)^2}{2!} + \ldots + \frac{(\mu\Delta t)^{y-1}}{(y-1)!}\right) \qquad ...(3.46)$$

which indicates that at high values of $\mu\Delta t$, the average rate of exciton arrival, the probability of a reaction center surviving photodestruction decreases exponentially as $\mu\Delta t$ increases.

The probability that a reaction center will perform photosynthesis (p_{RC}) during a short time interval Δt is then given by the cumulative Poisson probabilities of a PSU absorbing *x or greater* photons but *less than* y photons within a time interval Δt:

$$p_{RC} = p(\geq x, <y) = p(\geq x) - p(<y)$$

$$= \sum_{k=x}^{y} \frac{(\mu\Delta t)^k}{k!} e^{-\mu\Delta t} \qquad ...(3.47)$$

Where photosynthesis occurs in response to one or more hits (*ie.* cumulative single hit Poisson distribution) the probability of photosynthetic transduction at a reaction center (p_{RC}) simplifies to:

$$p_{RC} = p(\geq 1, <y) = 1 - p(0) - p(\geq y)$$

$$= 1 - e^{-\mu\Delta t} - \sum_{k=y}^{\infty} \frac{(\mu\Delta t)^k}{k!} e^{-\mu\Delta t} \qquad ...(3.48)$$

A series of such probability curves are illustrated in Figure 3.4(c) using various values for y, the number of excitons required within Δt to cause photoinhibition of photochemistry at the reaction center. As y increases relative to the number of photons required to drive photochemistry, the response changes from a peaked curve with a sharply defined optimum to a curve with a broad plateau where the response is optimal. The photoinhibitory decrease in photosynthesis, described by the cumulative Poissonian

term in Eq. 3.48, approaches an exponential decay at high irradiances. Re-scaling all the curves to the maximum probability of photosynthesis *attained* by a reaction center provides a family of P-I curves that illustrate the change in the shape of the response with varying degrees of photoinhibition (Figure 3.4(d)).

Scaling the P-I response: The ordinate in Figures 3.4 (a) - (c) corresponds to a probability value (dimensionless) ranging from zero to unity describing the probability of an individual reaction center performing photosynthesis. When the photosynthetic rate of many PSUs is considered (as is the case when the photosynthetic rate of a volume of water is determined), the maximum photosynthetic rate (P_m) is independent of the incident photon flux density and the rate of photon absorption and is determined only by the number of PSUs present (n) and their minimal turnover time τ ($P_m = n/\tau$) (Herron and Mauzerall 1971). Where the photosynthetic rate is normalized to chlorophyll, P_m^B is determined by the number of PSUs per unit chlorophyll ($n/[Chl]$) and the minimal turnover time τ of the PSU ($P_m^B = n/(\tau \cdot [Chl])$). If τ were constant and not dependent upon antenna size or other physiological parameters then P_m would be simply proportional to the chlorophyll concentration (Falkowski 1981).

The abscissa in Figure 3.4 represents the *average* number of photons absorbed by a PSU in a time interval corresponding to the turnover time of the reaction center τ. Assuming that the rate of photosynthesis (and photoinhibition) is proportional to this quantity then where P is the volumetric rate of photosynthesis (P: mol C m^{-3} s^{-1}) Eq. 3.48 may be rewritten:

$$P / P_m = 1 - e^{-n a_{PSU} \phi_p \tau I_\tau} - \sum_{k=y}^{\infty} \frac{(n a_{PSU} \phi_i \tau I_\tau)^k}{k!} e^{-n a_{PSU} \phi_i \tau I_\tau} \quad \ldots(3.49)$$

where n is the number of PSUs present (PSU m^{-3}), a_{PSU} is the average effective absorption cross-section of a PSU (m^2 PSU^{-1}), ϕ_p is the quantum yield for photosynthetic transduction (mol C mol photons^{-1}), ϕ_i is the quantum yield for photodestruction, τ is the turnover time of the reaction center and I_τ is the number of photons incident upon a PSU within the time interval τ. Where the photosynthetic rate is expressed in terms of the reduction of CO_2 normalized to chlorophyll (P^B: mol C (mg Chl)$^{-1}$ s^{-1}), Eq. 3.49 may be simplified to:

$$P^B / P_m^B = 1 - e^{-k_c \phi_p I} - \sum_{k=y}^{\infty} \frac{(k_c \phi_i I)^k}{k!} e^{-k_c \phi_i I}$$

$$= 1 - e^{-\sigma_{pc} I} - \sum_{k=y}^{\infty} \frac{(\sigma_{ic} I)^k}{k!} e^{-\sigma_{ic} I} \qquad \text{...(3.50)}$$

where k_c is the effective chlorophyll-specific absorption cross-section (m^2 (mg Chl)$^{-1}$), ϕ_p is the quantum yield for photosynthetic carbon reduction (mol C mol photons-1), ϕ_i is the quantum yield for photoinhibition, σ_{pc} is the effective chlorophyll-specific action cross-section for carbon reduction (m^2 (mg Chl)$^{-1}$), σ_{ic} is the effective chlorophyll-specific action cross-section for photoinhibition (m^2 (mg Chl)$^{-1}$) and I is the incident photon flux density (mol m^{-2} s^{-1}).

The initial portion of the P-I response which is dominated by the photosynthetic process is thus scaled by the action cross-section for photosynthesis σ_{pc} while the response at higher photon flux densities dominated by photoinhibition is scaled by the action cross-section for photoinhibition σ_{ic}. The entire P-I response may be expressed in dimensionless terms:

$$P^B/P_m^B = 1 - e^{-I/I_k} - \sum_{k=y}^{\infty} \frac{(I/I_j)^k}{k!} e^{-I/I_j} \quad ...(3.51)$$

where $I_k = P_m^B/\sigma_{pc}$ and $I_j = P_m^B/\sigma_{ic}$. The parameters I_k and I_j have units of photon flux density (mol m^{-2} s^{-1}) and serve to scale the photochemical and photoinhibitory portions of the curve respectively.

Where the spectral dependency of both photosynthesis and photoinhibition are identical, the exponent of the photoinhibitory decline in photosynthesis (*ie.* the negative slope (β) of the *ln P - I* curve) will be proportional to the initial slope (α) of the *P-I* response. The dimensionless proportionality constant $\sigma_{pc} / \sigma_{ic}$ ($= I_j / I_k$) determined under any spectral distribution equals the ratio of the number of absorbed photons required to cause photoinhibition compared to the number required to cause photochemistry (*ie.* ϕ_p / ϕ_i).

If the spectral dependency of photochemistry and photoinhibition are different, then both portions of Eq. 3.42 are independently spectrally scaled according to their respective effective action spectra σ_{pc} and σ_{ic}. In this case, the ratio I_j / I_k represents the ratio of the respective effective absorption cross-sections of photoinhibition and photochemistry, in addition to, the relative number of photons required for each process (*ie.* $I_j / I_k = \sigma_{pc} / \sigma_{ic} = k_c \phi_p / k_c \phi_p$).

3.5. INCORPORATION OF THE NON-ADDITIVE EFFECTS OF PHOTONS OF DIFFERENT WAVELENGTHS AT LOW PHOTON FLUX DENSITIES.

3.5.1. Introduction.

In more complex systems, where the response results from multiple pigments acting in a non-additive fashion or involving photochromic (photoreversible) photoreceptors, quantifying the response in polychromatic irradiance requires the use of mathematical models of the response, an approach referred to as analytical action spectroscopy (Hartmann and Unser 1972; Hartmann 1977).

Early analysis of the spectral dependence of the quantum yield of photosynthesis revealed that the quantum yield was not constant over the entire spectrum (Emerson and Lewis 1942; Haxo and Blinks 1950). In green algae a distinct decline in the quantum yield above 685 nm (the "red-drop" effect) was observed. A similar decrease at those wavelengths characteristic of chlorophyll *a* absorption (> 600 nm and < 650 nm) were noted in the phycobiliprotein-containing cyanobacteria and red algae yielding an additional "blue-drop". It was demonstrated that the decline in quantum yield could be overcome by supplementing the red photons absorbed predominantly by chlorophyll *a* with photons of a wavelength predominantly absorbed by the phycobiliproteins (Emerson *et al.* 1957). This effect, termed Emerson enhancement, was rationalized by the proposition that there are two separate photosystems involved in photosynthesis and that they act in series (Hill and Bendall 1960).

Further support for the serial operation of two separate photosystems was provided by Duysens and Amesz (1962) and Amesz and Duysens (1962) who determined

the action spectra of each photosystem in red algae and cyanobacteria by determining the rates of photosynthesis in weak monochromatic irradiance supplemented by a strong and constant background irradiance of wavelength selected to over-stimulate one or the other photosystem. This result and those of Jones and Myers (1964) suggested that photons absorbed by Photosystem II (PS II, the first photosystem in series) could "spillover" and contribute to Photosystem I (PS I, the second photosystem in series). The net result is that the action spectra for both PS I and PS II are corrupted by the contribution made by PS II to PS I. Other evidence confirming this serial arrangement of the two photosystems has been derived from the spectroscopic observation of electron carrier intermediates, fluorescence transients, and the physical separation of the two photosystems.

Because the two photoreactions of photosynthesis operate in series, the light-limited photosynthetic rate is optimized when both photoreactions are excited at equal rates. The spillover of energy excitation from PS II to PS I is considered a mechanism to ensure a balance of excitation and the optimal operation of both photosystems. Any model attempting to offer a complete description of the spectral nature of the photosynthetic response must incorporate the effects of Emerson enhancement and spillover.

The occurrence of the Emerson enhancement effect, which results in the quantum yield of a photon of a specific wavelength being dependent upon the spectral composition of the accompanying incident photons, violates the principle of equivalent light action which is a pre-requisite for the application of classical action spectroscopy. Consequently the computation of PSR by way of Eq. 3.26 becomes invalid. The only acceptable solution is an analytical model of the photosynthetic process.

3.5.2. A Two Photosystem Model.

Malkin (1967) provided a quantitative description of photosynthesis based upon the theoretical interaction of two spectrally-distinct photosystems. This formulation included the effects of spillover and Emerson enhancement in a single expression and allows the magnitude of spillover to be estimated from the relationship between unenhanced and enhanced quantum yields. While this model is confined to describing the rate of photosynthesis at low PFDs, its structure and the mathematical description of the partitioning of absorbed photons and subsequent interaction between the two photosystems provides a basis for the development of further models designed to include the entire range of PFDs.

Model structure: The photosynthetic apparatus is considered to consist of a large number of PSUs consisting of two types of photosystem - termed PS I and PS II. Both types of PSU (PSU I and PSU II) consist of a light-harvesting antenna (LHA I and LHA II) associated with a reaction center (RC I and RC II) where photochemistry can occur. As described previously, both types of PSU considered in this model are statistical constructions that may represent either a single PSU with a single reaction center or a collection of PSUs with multiple shared reaction centers *in vivo*. In the latter case the effective antenna size represents the average antenna size per reaction center. The structure of the model is outlined in Figure 3.5.

Absorption by Photosystems: The rate at which photons of wavelength λ are absorbed by a PS in an arbitrarily small time interval Δt (photons s^{-1}) is equal to the product of the effective absorption cross-section of that PS (σ_1 or σ_2) at that wavelength (units: m^2) and the incident PFD (units: photons m^{-2} s^{-1}). Under monochromatic radiation of wavelength λ the rate of photon absorption by the PS I and PS II (I_1 and I_2 respectively) are:

$$I_{1\lambda} = a_{1\lambda} \cdot I_{\lambda} \quad \text{and} \quad I_{2\lambda} = a_{2\lambda} \cdot I_{\lambda} \qquad ...(3.52)$$

The numeric subscripts *1* and *2* refer throughout the following to the appropriate PS (PS I or PS II respectively). In a polychromatic irradiance field with a spectral distribution $I(\lambda)$ bounded by the wavelengths characteristic of PAR (350 and 700 nm) the rates of photon absorption by both photosystems are:

$$I_1 = \int_{350}^{700} I(\lambda)\, a_1(\lambda)\, d\lambda \quad \text{and} \quad I_2 = \int_{350}^{700} I(\lambda)\, a_2(\lambda)\, d\lambda \qquad ...(3.53)$$

Where the combined light-harvesting antennae of the two photosystems constitute the sole absorbing components, the absorption cross-section of the cell at any wavelength $a(\lambda)$ equals the combined spectral absorption cross-section of both populations of photosystems at that wavelength such that $a(\lambda) = a_1(\lambda) + a_2(\lambda)$. Similarly, upon integration over the wavelength interval for PAR the effective absorption cross-section of the cell equals the sum of the effective absorption cross-sections of both populations of photosystems.

The rate of photon absorption can be partitioned into that absorbed by PS II and that absorbed by PS I. A fraction (ω_2) is absorbed by the PS II population and the remaining fraction (ω_1) is absorbed by the PS I population ($\omega_1 + \omega_2 = 1$). The relative values of ω_1 and ω_2 depend upon the spectral distribution of the incident irradiance and the spectral absorption characteristics of each photosystem. The rate of photon absorption by both populations of PS (I_2 and I_1 respectively) is then:

$$I_2 = \int_{350}^{700} I(\lambda)\, a_2(\lambda)\, d\lambda = \omega_2 \int_{350}^{700} I(\lambda)\, a(\lambda)\, d\lambda$$

$$I_1 = \int_{350}^{700} I(\lambda)\, a_1(\lambda)\, d\lambda = \omega_1 \int_{350}^{700} I(\lambda)\, a(\lambda)\, d\lambda \quad \ldots(3.53)$$

where $I_1 + I_2 = PUR$ if the photosynthetic pigments comprise the only light-absorbing components. The rate of photon absorption by each PS type (I_1 and I_2) is thus scaled according to the integral of the product of the spectral effective absorption cross-section of that PS and the spectral distribution of the incident irradiance.

Distribution of excitons to the reaction centers: The photons that are absorbed by either LHA II or LHA I are efficiently transferred as excitons toward their respective reaction centers (RC II or RC I). The two respective fluxes initially correspond to I_2 and I_1. Malkin (1967) introduced the phenomenon of spillover as a transfer of excitons from PS II to PS I under circumstances where PS II excitons arrive at a closed RC II. As the flux of excitons into RC II increases, producing an increase in the number of closed reaction centers in the RC II population, there is an increased probability that excitons absorbed by PS II are lost via spillover or some alternative dissipative pathway. This loss is represented by a exciton flux I_3. A fraction (γ) of this flux is transferred (by some unspecified spillover mechanism) to the reaction centers of PS I. The parameter γ reflects the efficiency of spillover and can take any value from 0 to 1. A zero value implies that no spillover takes place and both photosystems behave as separate packages. A value of unity implies that spillover efficiency is 100% and all excess excitons arriving at RC II are transferred to RC I.

Consequently the *effective* exciton flux driving the photochemical reaction rate at RC II (μ_2: excitons s^{-1}) is a function of the number of photons absorbed by LHA II less the number that are lost through dissipation or spillover to PS I ($\mu_2 = I_2 - I_3$). Similarly,

the effective flux at RC I driving the photochemical reaction rate at RC I (μ_1: excitons s^{-1}) is a function of the number of photons absorbed by LHA I plus the number contributed by PS II through spillover ($\mu_1 = I_1 + \gamma I_3$).

Response of reaction centers to exciton flux: Each of the photochemical reactions is driven by the rate of arrival of excitons at their respective reaction centers. Malkin (1967) considered the case where the rate of photochemistry at each reaction center was simply proportional to the flux of arriving photons. The proportionality constant of each photosystem is the quantum yield of the photoreaction, ϕ_1 for PS I and ϕ_2 and PS II:

$$P_1 = \phi_1 \mu_1 \quad \text{and} \quad P_2 = \phi_2 \mu_2 \qquad ...(3.54)$$

Dynamic Interaction of both Photoreactions: Under light-limiting PFDs the overall rate of photosynthesis (P) depends upon the distribution of excitons between the PS I and PS II (which determines μ_1 and μ_2) and the quantum yields of both photoreactions (ϕ_1 and ϕ_2 respectively). Photosynthesis requires the serial operation of both photoreactions so that the photosynthetic rate is governed by the slower of the two photoreactions.

Where the exciton flux at each reaction center is sufficiently low such that the rate of each photoreaction is linearly dependent upon the PFD, the overall quantum yield of photosynthesis (Φ) will be maximal where the rates of both photoreactions are exactly balanced ($P_1 = P_2$). If it is assumed that the quantum yields of both photoreactions are equal ($\phi_1 = \phi_2$) then the balanced operation of both photoreactions requires equal rates of exciton delivery to each type of reaction center ($\mu_1 = \mu_2$). Where there is an imbalance in the rate of exciton delivery such that the rate of exciton arrival is greater at one

photosystem type compared to the other ($\mu_1 \neq \mu_2$), there will be a drop in the overall photosynthetic quantum yield (Φ).

Initially, before any dynamic re-adjustments in exciton distribution by means of spillover take place, the average rates of exciton arrival driving both photoreactions (excitons s^{-1}) will be:

$$\mu_1 = I_1 \quad \text{and} \quad \mu_2 = I_2 \qquad ...(3.55)$$

Two situations can be readily identified corresponding to the cases where one photoreaction is overstimulated relative to the other:

$$(a) \quad \phi_1 I_1 > \phi_2 I_2 \qquad (b) \quad \phi_1 I_1 < \phi_2 I_2 \qquad ...(3.56)$$

In the first case where Photosystem I is overstimulated, the overall throughput of the two serial reactions will be limited by the rate of the first photoreaction (P_2) and the overall rate of photosynthesis (P) is:

$$P = \phi_2 I_2 \qquad ...(3.57)$$

In the second case, where $\phi_1 I_1 < \phi_2 I_2$, the photosynthetic rate will initially be limited by the rate of the second photoreaction (P_1). As the number of closed RC IIs increase there is the potential of achieving a more balanced excitation through spillover and a fraction of the excitons arriving at closed RC IIs are transferred to PS I. The rate of each photoreaction is given by:

$$P_2 = \phi_2 (I_2 - I_3) \qquad ...(3.58)$$

$$P_1 = \phi_1(I_1 + \gamma I_3) \quad ...(3.59)$$

Since photosynthesis (P) involves the two reactions operating serially, at steady-state the rates must be equal ($P_1 = P_2$) so that:

$$P = \phi_2(I_2 - I_3) = \phi_1(I_1 + \gamma I_3) \quad ...(3.60)$$

The exciton loss rate I_3 can be defined in terms of I_1 and I_2 as:

$$I_3 = \frac{\phi_2 I_2 - \phi_1 I_1}{\gamma\phi_1 + \phi_2} \quad ...(3.61)$$

Rewriting Eq. 3.60 in terms of I_1 and I_2 yields (Malkin 1967):

$$P = \frac{\phi_1\phi_2}{\gamma\phi_1 + \phi_2}(I_1 + \gamma I_2) \quad ...(3.62)$$

The two extreme cases for the efficiency of spillover can be considered. In the case where $\gamma = 0$ (*ie.* no spillover), then

$$I_3 = I_2 - (\phi_1/\phi_2)I_1 \quad ...(3.63)$$

and

$$P = \phi_1 I_1 \quad ...(3.64)$$

which is analogous to Eq. 3.57. Alternatively, when $\gamma = 1$ (complete spillover) then:

$$I_3 = (\phi_2 I_2 - \phi_1 I_1)/(\phi_1 + \phi_2) \quad ...(3.65)$$

and the photosynthetic rate (P) is equal to (Malkin 1967):

$$P = \phi_1\phi_2(I_1 + I_2)/(\phi_1 + \phi_2) \quad ...(3.66)$$

which for $\phi_1 = \phi_2$ yields a maximum theoretical quantum yield for photosynthesis (Φ) of 0.5 corresponding to a quantum requirement twice that of the individual photoreactions.

In the general case where γ is unknown Equations 3.57 and 3.62 may be used to analyze the rate of photosynthesis in the specific cases of irradiance fields consisting of a single monochromatic wavelength, a combination of two monochromatic wavelengths as described by Malkin (1967) and outlined below.

Where the irradiance field consists of a *single monochromatic wavelength*, the fluxes of excitons through the two photosystems (I_1 and I_2) are given by $\omega_1 I$ and $\omega_2 I$ (see Figure 3.6(a)). Within the range of wavelengths characterizing PAR (350 to 700 nm), two wavelength intervals may be defined according to which photoreaction dominates. Irradiance of a wavelength that preferentially excites Photoreaction 1 is termed Light 1 (λ_1) and irradiance that preferentially excites Photoreaction 2 is termed Light 2 (λ_2). As before numeric subscripts identify the photosystem under consideration or that which is preferentially affected. The symbols λ_1 and λ_2 identify the wavelength intervals for which the monochromatic photons preferentially excite PS I or PS II respectively. For example, $I(\lambda_1)$ is the PFD of monchromatic photons with a wavelength that preferentially excites PS I, $\omega_1(\lambda_2)$ is the fraction of monochromatic light, comprised of photons of a wavelength that are preferentially absorbed by PS II, that is absorbed by PS I.

Under Light 1 $\omega_1\phi_1 > \omega_2\phi_2$ while under Light 2 $\omega_1\phi_1 < \omega_2\phi_2$. Under Light 1 Eq. 3.57 is appropriate so the rate of photosynthesis (P) is (Malkin 1967):

$$P(\lambda_1) = \phi_2\, \omega_2(\lambda_1)\, I(\lambda_1) \qquad ...(3.67)$$

and the overall quantum yield of photosynthesis (Φ) is:

$$\Phi(\lambda_1) = \phi_2\, \omega_2\, (\lambda_1) \qquad ...(3.68)$$

Under Light 2, Eq. 3.62 is appropriate so the rate of photosynthesis (P) is (Malkin 1967):

$$P(\lambda_2) = \frac{\phi_1\phi_2}{\gamma\phi_1 + \phi_2}\, [\omega_1(\lambda_2) + \gamma\, \omega_2(\lambda_2)]\, I(\lambda_2) \qquad ...(3.69)$$

and the overall quantum yield of photosynthesis (Φ) is:

$$\Phi(\lambda_2) = \frac{\phi_1\phi_2}{\gamma\phi_1 + \phi_2}\, [\omega_1(\lambda_2) + \gamma\omega_2(\lambda_2)] \qquad ...(3.70)$$

The maximum quantum yield (Φ_{max}) is obtained when $\omega_1\phi_1 = \omega_2\phi_2$ which occurs at any wavelength that marks the border between the two wavelength regions. Since by definition $\omega_1 + \omega_2 = 1$ then the maximum quantum yield of photosynthesis (Φ_{max}) is given by:

$$\Phi_{max} = \frac{\phi_1\phi_2}{\phi_1 + \phi_2} \qquad ...(3.71)$$

The maximum quantum yield is thus independent of γ and depends solely upon the equal balance of the two photosystems. In the case where $\gamma = 1$ (perfect spillover), the quantum yield will be maximal throughout the entire wavelength 2 region.

Under conditions where the irradiance field is composed of *two monochromatic wavelengths* chosen such that each tends to preferentially excite different PS (λ_1 and λ_2) and where the relative photon flux densities are $I(\lambda_1)$ and $I(\lambda_2)$, the rate of photon absorption for both photosystems (see Figure 3.6(b)) is given by:

$$I_1 = \omega_1(\lambda_1)\, I(\lambda_1) + \omega_1(\lambda_2)\, I(\lambda_2) \qquad ...(3.72)$$

$$I_2 = \omega_2(\lambda_1)\, I(\lambda_1) + \omega_2(\lambda_2)\, I(\lambda_2) \qquad ...(3.73)$$

Once again two cases may be distinguished according to whether $\phi_1 I_1 > \phi_2 I_2$ or $\phi_1 I_1 < \phi_2 I_2$. In the case where $\phi_1 I_1 > \phi_2 I_2$, which occurs at a low ratio of $I(\lambda_2)/I(\lambda_1)$, the rate of photosynthesis will be (Malkin 1967):

$$P(\lambda_1,\lambda_2) = \phi_2\, \omega_2(\lambda_1)\, I(\lambda_1) + \phi_2\, \omega_2(\lambda_2)\, I(\lambda_2)$$

$$= \phi_2\, [\omega_2(\lambda_1)\, I(\lambda_1) + \omega_2(\lambda_2)\, I(\lambda_2)] \qquad ...(3.74)$$

which, because it is limited by the rate of reaction at RC II, is independent of γ, the degree of spillover.

In the case where $\phi_1 I_1 < \phi_2 I_2$, which occurs at a high ratio of $I(\lambda_2)/I(\lambda_1)$, the rate of photosynthesis is given by (Malkin 1967):

$$P(\lambda_1,\lambda_2) = \frac{\phi_1\phi_2}{\gamma\phi_1 + \phi_2}\{[\omega_1(\lambda_1) + \gamma\omega_2(\lambda_1)]\, I(\lambda_1) + [\omega_1(\lambda_2) + \gamma\omega_2(\lambda_2)]\, I(\lambda_2)\} \quad ...(3.75)$$

which clearly depends upon the degree to which excess excitation of PS II is transferred to PS I to balance excitation. In the case where there is no spillover ($\gamma = 0$) then Eq. 3.75 reduces to:

$$P(\lambda_1,\lambda_2) = \frac{\phi_1\phi_2}{\phi_2}[\omega_1(\lambda_1)\, I(\lambda_1) + \omega_1(\lambda_2)\, I(\lambda_2)] \quad ...(3.76)$$

which is analogous to Eq. 3.74. In the case where spillover is completely efficient ($\gamma = 1$) then Eq. 3.75 reduces to:

$$P(\lambda_1,\lambda_2) = \frac{\phi_1\phi_2}{\phi_1 + \phi_2}\{[\omega_1(\lambda_1) + \omega_2(\lambda_1)]\, I(\lambda_1) + [\omega_1(\lambda_2) + \omega_2(\lambda_2)]\, I(\lambda_2)\} \quad ...(3.77)$$

and the quantum yield is maximal throughout the λ_2 wavelength interval.

The above analysis may be simply extended to the case where the irradiance field consists of one or more polychromatic irradiance sources by replacing the absorbed fluxes under monochromatic wavelengths [I_1 and I_2 in Eqs. 3.64 and 3.66] by their polychromatic equivalents [Eq. 3.53].

As described by Malkin (1967) the Emerson enhancement functions, which describe the increase in the photosynthetic rate that occurs when the irradiance of one wavelength region is supplemented by irradiance of the other wavelength region, may be expressed in terms of the model parameters. The enhancement functions are classically

defined so as to yield the factor by which the photosynthetic rate is enhanced by the addition of supplemental background irradiance.

In the first case where PS I is overstimulated and PS II is understimulated (where $\phi_1 I_1 > \phi_2 I_2$ and which occurs at low $I(\lambda_2)/I(\lambda_1)$ ratios) the enhancement function for PS I (E_1) when additional Light 2 ($I(\lambda_2)$) is added is (Malkin 1967):

$$E_1 = \frac{P(\lambda_1,\lambda_2) - P(\lambda_2)}{P(\lambda_1)}$$

$$= 1 + \frac{\phi_2\,\omega_2(\lambda_2) - \phi_1\,\omega_1(\lambda_2)}{(\gamma\phi_1 + \phi_2)\,\omega_2(\lambda_1)} \cdot \frac{I(\lambda_2)}{I(\lambda_1)} \qquad ...(3.78)$$

As the ratio $I(\lambda_2)/I(\lambda_1)$ increases enhancement increases linearly up to the point where excitation of the two photosystems are balanced ($\phi_1 I_1 = \phi_2 I_2$) and maximum enhancement (E_{1max}) is reached. Further increase in $I(\lambda_2)$ brings about no further increase in the photosynthetic rate because photosynthesis is no longer limited by PS II ($\phi_1 I_1 < \phi_2 I_2$) and PS I enhancement (for large $I(\lambda_2)/I(\lambda_1)$ ratios) is (Malkin 1967):

$$E_1 = \frac{\phi_1}{\gamma\phi_1 + \phi_2} \cdot \frac{\gamma\omega_2(\lambda_1) + \omega_1(\lambda_1)}{\omega_2(\lambda_1)} = E_{1max} \qquad ...(3.79)$$

Enhancement of PS II may be similarly described. In the case where PS II is over-stimulated relative to PS I (where $\phi_1 I_1 < \phi_2 I_2$ and which occurs at low $I(\lambda_1)/I(\lambda_2)$ ratios), the enhancement function for PS II (E_2) when supplementary Light 2 ($I(\lambda_2)$) is added is (Malkin 1967):

$$E_2 = \frac{P(\lambda_1,\lambda_2) - P(\lambda_2)}{P(\lambda_2)}$$

$$= \quad 1 \quad + \quad \frac{\phi_1 \omega_1(\lambda_1) + \phi_2 \omega_2(\lambda_1)}{\phi_1 [\gamma\omega_2(\lambda_2) + \omega_1(\lambda_2)]} \cdot \frac{I(\lambda_1)}{I(\lambda_2)} \qquad ...(3.80)$$

As the ratio $I(\lambda_1)/I(\lambda_2)$ increases, enhancement increases linearly up to the point where both photoreactions are stimulated equally ($\phi_1 I_1 = \phi_2 I_2$) and maximum enhancement (E_{2max}) is reached. Further increase in $I(\lambda_1)$ causes no increase in photosynthesis as the process is no longer limited by PS I ($\phi_1 I_1 > \phi_2 I_2$) and PS II enhancement (for large $I(\lambda_1)/I(\lambda_2)$ ratios) is (Malkin 1967):

$$E_2 \quad = \quad \frac{\gamma\phi_1 + \phi_2}{\phi_1} \cdot \frac{\omega_2(\lambda_2)}{\gamma\omega_2(\lambda_2) + \omega_1(\lambda_2)} \quad = \quad E_{2max} \qquad ...(3.81)$$

Both E_{1max} and E_{2max} depend solely upon the wavelength of the supplementary irradiance ($I(\lambda_1)$ (Eq. 3.78) and $I(\lambda_2)$ (Eq. 3.80) respectively). Any wavelength is appropriate provided it is in the appropriate wavelength region (λ_1 or λ_2) and of sufficiently high PFD to over-excite the alternate photoreaction. The enhanced quantum yield at any wavelength ($\Phi_E(\lambda)$) is then defined as the quantum yield measured with a background of sufficiently strong complementary irradiance (Malkin 1967):

$$\Phi_E(\lambda_1) = \quad \frac{P(\lambda_1,\lambda_2) - P(\lambda_2)}{I(\lambda_1)} \quad = \quad E_{1max} \cdot \Phi(\lambda_1) \qquad ...(3.82)$$

and

$$\Phi_E(\lambda_2) = \quad \frac{P(\lambda_1,\lambda_2) - P(\lambda_1)}{I(\lambda_2)} \quad = \quad E_{2max} \cdot \Phi(\lambda_2) \qquad ...(3.83)$$

Malkin (1967) further suggested a method for the determination of γ based upon the relationships between the unenhanced ($\Phi(\lambda)$) and enhanced quantum yields ($\Phi_E(\lambda)$)

obtained under both wavelength region 1 and wavelength region 2. With $\omega_1 + \omega_2 = 1$, the relationship between the unenhanced and enhanced quantum yields were shown to be (Malkin 1967):

$$\Phi_E(\lambda_1) = \frac{\phi_1\phi_2}{\gamma\phi_1 + \phi_2} - \frac{\phi_1(1-\gamma)}{\gamma\phi_1 + \phi_2} \cdot \Phi(\lambda_1) \qquad ...(3.84)$$

and

$$\Phi(\lambda_2) = \frac{\phi_1\phi_2}{\gamma\phi_1 + \phi_2} - \frac{\phi_1(1-\gamma)}{\gamma\phi_1 + \phi_2} \cdot \Phi_E(\lambda_2) \qquad ...(3.85)$$

Equations 3.82 and 3.83 are identical except for the interchange of Φ and Φ_E and predict a linear dependence between Φ and Φ_E for both wavelength regions. If Φ_E is plotted against Φ on the same diagram two straight lines result corresponding to the two wavelength regions. Both branches intersect at the point $\Phi_E = \Phi = \Phi_{max}$ corresponding to the border of the two wavelength regions. The slope (S) of both lines, with respect to the $-\Phi$ and Φ_E axis respectively, are equal and are given by:

$$S = \frac{\phi_1(1-\gamma)}{\gamma\phi_1 + \phi_2} \qquad ...(3.86)$$

Where $\gamma = 1$ (complete spillover) $S = 0$ and both branches are parallel to their respective axes. Where $\gamma = 0$ (no spillover) $S = \phi_1/\phi_2$ and the two branches will have a slope ϕ_1/ϕ_2 with respect to the two axes. If the quantum requirements of both photoreactions are equal ($\phi_1/\phi_2 = 1$) then this slope will be 45° and both branches will merge together (Malkin 1967). The degree of spillover γ can then be solved in terms of S, ϕ_1 and ϕ_2:

$$\gamma = \frac{1}{1+S}\left[1 - S\frac{\phi_2}{\phi_1}\right] \qquad ...(3.87)$$

3.6. A NEW RATIONAL P-I MODEL TO INCLUDE NON-ADDITIVE SPECTRAL EFFECTS AT ALL PHOTON FLUX DENSITIES.

Clearly when differences in the spectral response of two photosystems result in Emerson enhancement effects an analytical model is required for the quantitative description of photosynthesis under polychromatic irradiance at low PFDs. A number of results also suggest that the two photosystems respond differently to high PFDs and these differences should be accounted for in any serious attempt to quantify photosynthesis in polychromatic irradiance at all PFDs.

Analysis of the mechanism of photoinhibition shows that the process appears to be exclusively associated with PS II, the most likely site of damage being either the reaction center itself or the associated 32 kDa Q_B-binding protein, the secondary electron acceptor on the reducing side of the PS II reaction center (Kyle *et al.* 1984,1985; Cleland *et al.* 1986; Kyle 1987). Photoinhibition of growth in the marine cyanobacteria *Synechococcus* spp. has been correlated with a decrease in the cellular concentration of PS II reaction centers and an increase in the RC I : RC II ratio suggesting preferential loss of PS II (Barlow and Alberte 1985). The spectral dependence of photoinhibition has not been established but would be expected to reflect the spectral characteristics of PS II, or a component of PS II, and possibly modified by any spillover to PS I which could act to reduce its magnitude. It may be considered to depend upon the dynamic linkage of the

two photosystems and may not be identical to the spectral dependency of the photosynthetic reaction.

The following section develops a kinetic model of photosynthesis based upon two independent photosystems which allows the description of partitioning the photon and exciton fluxes described by Malkin (1967) to be retained.

3.6.1. A Two-Photosystem Kinetic Model.

A simple kinetic model describing the serial interaction of two photosystems can also be developed with the aim of describing with a minimum of parameters the entire P-I response. This mechanistic model is based upon a kinetic description of a hypothetical two-link electron transport chain with each link representing a photosystem. The rate constants used to describe each of the two serial photoreactions may be re-stated in a such a way as to account for the initial partitioning of the absorbed irradiance between the two photosystems and any subsequent re-allocation of excitation by way of spillover. In mathematical structure the basic reaction scheme of the two linked cycles is similar to the model of electron flow around a single photosystem proposed by Fasham and Platt (1983).

Basic Reaction Scheme: The model consists of two photosystems PS II and PS I with reaction centers RC II and RC I respectively which operate in series. The primary electron acceptors of the two photosystems are arbitrarily designated Q and R. The photochemical reactions at the two reaction centers of the two photosystems are linked serially in the form of an electron transport chain (Figure 3.7). Arrival of an exciton at the reaction center of the first photosystem (RC II) raises the reaction center to an excited state with the subsequent donation of an electron to the primary acceptor Q leaving the

primary acceptor in a reduced state Q^-. The oxidized reaction center receives an electron from a proximate donor and is restored to the ground state. While the proximate donor is probably a tyrosine of the reaction center protein, the ultimate electron donor is water whose oxidation liberates O_2. The rate of Q reduction is a function of the rate of arrival of excitons at RC II and so depends upon the irradiance I. The rate constant for the reaction designated k_q:

$$Q + e^- \xrightarrow{k_q I} Q^- \qquad ...(3.88)$$

The reduced primary acceptor Q^- is incapable of accepting any further electrons until the electron is removed and Q^- is returned to its oxidized state (Q).

In a similar fashion, the arrival of an exciton at the reaction center of the second photosystem (RC I) raises this reaction center to an excited state that results in the donation of an electron to the primary acceptor R thereby reducing the primary acceptor to R^-. Oxidation of Q^- restores the electron to the oxidized reaction center of PS I ($R^- \rightarrow R$) and simultaneously restores the capacity of Q to accept another electron from PS II. The rate of this reaction depends upon the rate of arrival of excitons at RC I which in turn is a function of the irradiance, and the rate constant is designated k_p:

$$Q^- + R \xrightarrow{k_p I} Q + R^- \qquad ...(3.89)$$

The reduced primary acceptor (R^-) of PS I is incapable of accepting any further electrons until it is oxidized.

The electron on the reduced primary acceptor of PS I is ultimately removed and used for the reduction of inorganic carbon and nitrogen by way of a series of light-

independent reactions. Let the rate constant for this reaction sequence be k_r such that R^- is returned to the oxidized state:

$$R^- \xrightarrow{k_r} R + e^- \qquad ...(3.90)$$

This oxidation of R^- restores the capacity of the primary acceptor of PS I to accept further electrons from the reaction center and so ultimately from Q^-. The generation of reducing power in Eq. 3.90 may be taken as a measure of the rate of photosynthesis P.

The reaction scheme outlined by Eqs. 3.88 to 3.90 and illustrated in Figure 3.7 leads to the following set of differential equations:

$$\frac{\partial Q}{\partial t} = -k_q I Q + k_p I Q^- R \qquad ...(3.91)$$

$$\frac{\partial R}{\partial t} = -k_p I Q^- R + k_r R^- \qquad ...(3.92)$$

$$P = k_r R^- \qquad ...(3.93)$$

Note that for this reaction sequence $\partial Q^-/\partial t = -\partial Q/\partial t$ and that $\partial R^-/\partial t = -\partial R/\partial t$. The total concentration of primary acceptor associated with PS II, termed Q_O, remains constant at all times and is the sum of the oxidized (Q) and reduced (Q^-) forms. Similarly, R_O is the total concentration of the oxidized (R) and reduced (R^-) primary acceptors for PS I such that:

$$Q + Q^- = Q_O \qquad ...(3.94)$$

$$R + R^- = R_O \qquad ...(3.95)$$

Eqs. 3.91, 3.92 and 3.93 may be rewritten as:

$$\frac{\partial Q}{\partial t} = -k_q I Q + k_p I Q_O R - k_p I Q R \quad ...(3.96)$$

$$\frac{\partial R}{\partial t} = k_r R_O + (k_p I Q - k_r) R - k_p I Q_O R \quad ...(3.97)$$

$$P = k_r (R_O - R) \quad ...(3.98)$$

The system of equations 3.96, 3.97 and 3.98 can be solved for the equilibrium case where $\partial Q/\partial t = \partial R/\partial t = 0$. The solution is a quadratic in P:

$$P^2 - (k_r R_O + \frac{k_r k_q}{k_p}) P - k_q Q_O I P + k_r k_q R_O Q_O I = 0 \quad ...(3.99)$$

If we introduce the identities:

$$\alpha = k_q Q_O \quad ...(3.100)$$

$$\mu = k_r R_O \quad ...(3.101)$$

$$\chi = k_r k_q / k_p \quad ...(3.102)$$

then Eq. 3.99 becomes:

$$P^2 - ((\mu + \chi) + \alpha I) P + \alpha \mu I = 0 \quad ...(3.103)$$

Eq. 3.103 describes a curve defined by three parameters. It has two roots of which the required solution is the negative root such that when $I = 0$ the rate of photosynthesis $P = 0$. The solution is:

$$P = \frac{[(\mu + \chi) + \alpha I] - [((\mu + \chi) + \alpha I)^2 - 4\alpha\mu I]^{1/2}}{2} \quad ...(3.104)$$

Parameter Interpretation: Equation 3.103 is a non-rectangular hyperbola similar to that derived by Rabinowitch (1951, p.1307) and Fasham and Platt (1983), a geometric form requiring a minimum of three parameters to define it. The three derived parameters α, μ and χ are defined by a total of five independent variables k_q, k_p, k_r, Q_O and R_O and so there is a redundancy in the system. Different combinations of the five independent variables could yield identical P-I curves with the result that it is impossible to determine values for the five independent variables *from a single P-I response.*

The slope of the *P-I* response at low irradiances is given by the derivative of *P* with respect to *I* as the irradiance tends to zero. From Eq. 3.102 it follows that:

$$\left.\frac{\partial P}{\partial I}\right|_{I \to 0} = \alpha \left[\frac{\mu}{\mu + \chi}\right] \quad ...(3.105)$$

In the case where the parameter χ equals zero (see below) the initial slope is equal to α or $k_q Q_O$.

The value of *P* from Eq. 3.102 as the irradiance tends to infinity yields the maximum photosynthetic rate P_m. Evaluating Eq. 3.102 for $I \to \infty$ ($\partial P/\partial I \to 0$) yields:

$$P_m = \mu = k_r R_O \quad ...(3.106)$$

The maximum photosynthetic rate is thus related to the light-independent reactions and is unaffected by either of the photochemical rate constants k_q or k_p.

The parameter χ as defined as $k_r k_q / k_p$. As such it represents the rate of the first and third reactions *relative* to the second or intervening reaction. Where χ tends to zero ($k_p >> k_r k_q$) the maximum rate of the reaction sequence is governed by the maximum turnover of the first and third reactions ($k_q Q_O = k_r R_O$); the light-limited rate is governed solely by the rate constant of the intervening reaction (k_p). Where χ equals zero, the *P-I* response simplifies to a Blackman-type curve with photosynthesis increasing linearly ($P = k_p I$) up to the maximum rate ($P = k_r R_O$) and remains at this rate for all higher irradiances. Where χ equals 1 indicating that $k_r k_q = k_p$, the P-I response reduces to a rectangular hyperbola. The geometric influence of various values of χ upon the final P-I curve is illustrated in Figure 3.8.

It is worth noting that in practical terms this formulation turns out to be directly analogous to the expression suggested by Thornley (1976) [Eq. 2.11] and that derived by Fasham and Platt (1983) [Eq. 2.43]. Adopting equivalent identities to those of Fasham and Platt [*ie*. Eqs. 3.100, 3.101 and 3.102], the quadratic expression derived here [Eq. 3.103] differs from their Eq. (29) only in that the parameter χ is not multiplied by the irradiance. A consequence of this is that the initial slope ($\partial P/\partial I$ *as* $I \rightarrow 0$) in the present formulation is $\alpha\,(\mu/(\mu+\chi))$ [Eq. 3.105] rather than simply α [Fasham and Platt, Eq. (19)]. Conversely, the maximum photosynthetic rate is simply μ [Eq. 3.106] rather than $\mu\,(\alpha/(\alpha+\chi))$ [Fasham and Platt, Eq. (30)]. By multiplying Eq. 3.103 by $\Theta = \alpha/(\alpha+\chi)$ we can derive the expression proposed by Thornley (1976) [Eq. 2.11]. The analogous transformation may also be applied to the expression suggested by Fasham and Platt (1983) (see Appendix A).

Introducing Spectral Dependency: The purpose of developing a photosynthetic model comprising two serially interacting photosystems is to provide a mechanism for including

two independent spectral responses. In the above model, the reduction of the primary acceptor of PS II ($Q \rightarrow Q^-$) depends upon the exciton flux to RC II and similarly reduction of the primary receptor of PS I ($R \rightarrow R^-$) is dependent upon the exciton flux to RC I. Partitioning the absorbed irradiance, as described in Section 3.5.2., the fractions of the total irradiance directly absorbed by the PS II antenna (I_2) and by the PS I antenna (I_1) are:

$$I_2 = \omega_2 I \qquad \text{...(3.107)}$$

$$I_1 = \omega_1 I = (1 - \omega_2) I \qquad \text{...(3.108)}$$

In the absence of spillover, the reaction rate at each reaction center may be considered proportional to the exciton arrival rate and the constant of proportionality of each photosystem can be given by the quantum yield (ϕ_1 and ϕ_2) such that the rate constants k_q and k_p in Eq. 3.99 can be replaced by:

$$k_q = \phi_2 \omega_2 \qquad \text{...(3.109)}$$

$$k_p = \phi_1 (1 - \omega_2) \qquad \text{...(3.110)}$$

The occurrence of spillover modifies Eqs. 3.109 and 3.110. As the number of closed RC IIs increase a fraction (I_3) of the irradiance absorbed by PS II may be diverted from PS II to PS I to ensure balanced excitation. If the fraction of I_2 diverted in this way is ζ such that:

$$I_3 = \zeta I_2 = \zeta \omega_2 I \qquad \text{...(3.111)}$$

the actual exciton flux reaching RC II is given by:

$$I_2 - I_3 = \omega_2 I - \zeta \omega_2 I = [(1 - \zeta)\omega_2] I \qquad \text{...(3.112)}$$

Where a fraction (γ) of the exciton flux lost from PS II successfully arrives at PS I, the exciton flux reaching RC I becomes:

$$I_1 + \gamma I_3 \quad = \quad I_1 + \gamma\zeta I_2 \quad = \quad (1-\omega_2)I + (\omega_2\gamma\zeta)I \quad = \quad [1 - (1 + \zeta\gamma)\omega_2]\, I \qquad ...(3.113)$$

As in the case of no spillover if the rate of each photoreaction is proportional to the exciton flux where the proportionality constants of the two photoreactions are defined as the respective quantum yields ϕ_2 and ϕ_1, according to Eqs. 3.112 and 3.113 the rate constants k_q and k_p in Eqs. 3.88 and 3.89 may be expressed as:

$$k_q \quad = \quad \phi_2 [\, \omega_2 (\, 1 \, - \, \zeta \,) \,] \qquad ...(3.114)$$

$$k_p \quad = \quad \phi_1 [\, 1 \, - \, \omega_2 (\, 1 \, + \, \gamma\zeta) \,] \qquad ...(3.115)$$

The two parameters k_q and k_p in Eq. 3.99 may now be replaced by three new parameters (ϕ_1, ϕ_2 and ω_2 in Eqs. 3.109 and 3.110) in the case where we ignore the possibility of spillover, and by five new parameters (ϕ_1, ϕ_2, ω_2, ζ and γ in Eqs. 3.114 and 3.115) when we take spillover into account.

Introducing Photoinhibition: The simplest means of incorporating photoinhibition into the model as an inhibitory effect upon PS II is to consider the total concentration of the primary acceptor (Q_O) as a light-dependent variable. One solution is to replace Q_O with a light-dependent value such that the total concentration of *functional* PS II primary acceptors Q_i becomes:

$$Q_i \quad = \quad Q_O \exp^{-\beta I} \qquad ...(3.116)$$

where β represents the photoinhibitory coefficient governing the decrease in Q_O with increasing irradiance. Substituting this into Eq. 3.99 yields:

$$P^2 - (k_r R_O + \frac{k_r k_q}{k_p}) P - k_q Q_O \exp^{-\beta I} IP + k_r R_O k_q Q_O \exp^{-\beta I} I = 0 \quad ...(3.117)$$

Employing the same identities as before [Eqs. 3.100, 3.101 and 3.102] yields:

$$P^2 - (\mu + \chi + \alpha \exp^{-\beta I} I) P + (\mu \alpha \exp^{-\beta I}) I = 0 \quad ...(3.118)$$

Eq. 3.118 differs from the original expression lacking photoinhibition [Eq. 3.103] in that the parameter α is multiplied by the negative exponential term $exp(-\beta I)$. Eq. 3.118 is also a quadratic in P of which the desired solution is the negative root which yields $P = 0$ when $I = 0$:

$$P = \frac{[\mu + \chi + \alpha \exp^{-\beta I} I] - [(\mu + \chi + \alpha \exp^{-\beta I} I)^2 - 4 \alpha \exp^{-\beta I} \mu I]^{1/2}}{2} \quad ...(3.119)$$

In the special case where the reduction in Q_O is considered to be brought about by the exciton flux at RC II then the rate constant of photoinhibition (β) will have the same spectral dependency as the PS II photoreaction. In this case the term β may be replaced by $k_i k_q$ such that the photoinhibitory decrease in Q_O is given as a proportion of the rate constant for first photochemical reaction (k_q).

Taking the derivative of Eq. 3.119 with respect to the irradiance as I tends to zero yields the initial slope of the P-I response:

$$\left. \frac{\partial P}{\partial I} \right|_{I \to 0} = (1 - \beta) \alpha \left[\frac{\mu}{\mu + \chi} \right] \quad ...(3.120)$$

Eq. 3.118 differs from the case where there is no photoinhibition [Eq. 3.105] in that the initial slope is multiplied by the term $(1 - \beta)$. In the special case where $\chi = 0$ corresponding to a Blackman-type response prior to the onset of photoinhibition, Eq. 3.120 reduces to simply:

$$\left.\frac{\partial P}{\partial I}\right|_{I \to 0} = (1 - \beta)\,\alpha \qquad \ldots(3.121)$$

Setting $\partial P/\partial I$ equal to zero specifies the optimal irradiance I_m where photosynthesis is maximal. It can be shown that this occurs at an irradiance where the term $(1 - \beta I)$ equals zero such that:

$$I_m = 1/\beta \qquad \ldots(3.122)$$

Substituting the value of I_m into Eq. 3.119 yields the maximum rate of photosynthesis attained (P_m). In the limit of $\beta \to 0$ in which there is no photoinhibition, the optimal irradiance $I_m \to \infty$ and $P_m \to \mu$. For all $\beta > 0$ the maximum rate of photosynthesis attained (P_m) will be less than μ and is given by:

$$P(I_m) = \frac{[\mu + \chi + (\alpha/\beta e)] - \{[\mu + \chi (\alpha/\beta e)]^2 - 4\,\mu\,(\alpha/\beta e)\}^{1/2}}{2} \qquad \ldots(3.123)$$

3.7. EVIDENCE OF SPECTRAL PROPORTIONALITY IN P-I RESPONSES.

The principal attraction of a model in which the P-I response under polychromatic irradiance is scaled according to either the absorbed irradiance (PUR) [computed from the absorption spectrum $a(\lambda)$] or the active irradiance (PSR) [computed from the

monochromatic action spectrum of photosynthesis $\sigma(\lambda)$] is its simplicity. The entire P-I response is simply scaled according to the integral of the products of $a(\lambda)$ and $I(\lambda)$ [Eq. 3.16] or the integral of the product of $\sigma(\lambda)$ and $I(\lambda)$ [Eq. 3.26]. Where the photosynthetic rate is normalized to chlorophyll, the appropriate spectral weighting function is simply the effective absorption cross-section [Eq. 3.14] or the effective action cross-section for photosynthesis [Eq. 3.32] respectively.

In both cases the photosynthetic responses determined under different polychromatic irradiances are expected to be proportional to one another. Absence of proportionality indicates that attempts at simple spectral scaling of the P-I response to either PUR or PSR is inappropriate. Proportionality of response thus constitutes a minimal validation of this approach. Conversely, the existence of proportionality does not mean that scaling the P-I response to some arbitrary spectrum (such as $a(\lambda)$ or $\sigma(\lambda)$ or some alternate) is valid. Both the analytical model of Malkin (1967) and its extension by way of my kinetic model yield P-I curves in polychromatic irradiance that exhibit proportionality. In these two cases however no simple action spectrum exists that, when multiplied by the incident irradiance spectrum and integrated throughout the appropriate wavelength interval, provides an accurate estimate of the photosynthetic rate under polychromatic irradiance.

3.7.1. Proportionality in *Chlorella*.

The data of Pickett and Myers (1966) provide some preliminary evidence that P-I curves determined under different wavelengths exhibit proportionality in the green alga *Chlorella*. In this case the description of the photosynthetic response to increasing PFD in terms of Poissonian statistics (with or without photoinhibition) provides a simple

rational *P-I* model. In the case where photoinhibition is absent the *P-I* response simplifies to the cumulative one hit Poisson distribution:

$$P^B / P_m^B = 1 - exp^{-\sigma I} \quad ...(3.124)$$

where σ represents the transformation cross-section that may be spectrally scaled.

A priori support for this geometric form and for proportionality between the P-I responses determined under different monochromatic wavelengths is provided by light-saturation curves for *Chlorella* (Pickett and Myers 1966). These P-I curves are well described by Eq. 3.124 for all wavelengths. Re-plotting these response curves in both arithmetic and semi-logarithmic co-ordinates with respect to the PFD reveals the proportionality of the response curves (Figure 3.9). The parallelism of the curves when plotted semi-logarithmically indicates that up to the point of light-saturation the photosynthetic response may be considered light-limited.

This result provides some *a priori* evidence of the spectral proportionality of the P-I response. It remains to be established whether the P-I responses of oceanic phytoplankton assemblages, and in particular the picoplankton component, exhibit such proportionality. Furthermore, it is necessary to establish whether use of the absorption spectra or photosynthetic action spectra of these organisms can provide an accurate means of predicting their P-I response under polychromatic light.

CHAPTER 4

EXPERIMENTAL MATERIALS AND METHODOLOGY.

4.1. MONOSPECIFIC PICOPLANKTON CULTURES.

4.1.1. Origins of Culture Material.

A number of axenic cultures of representative picoplanktonic autotrophs were obtained from the Culture Collection of Marine Phytoplankton, Bigelow Laboratory for Ocean Sciences, West Boothbay Harbor, Maine, USA. Three species were selected based upon their phylogenetic affinities (and consequently their photosynthetic pigment content), their occurrence in different oceanic regimes and their ability to grow in culture. Two of the species are prokaryotic cyanobacteria representative of the genus *Synechococcus* (Rippka *et al.* 1979), a heterogeneous assemblage of small unicellular cyanobacteria with ovoid to cylindrical cells that reproduce by binary transverse fission in a single plane and that lack sheaths. The third species is a eukaryotic alga belonging to the genus *Pavlova* in the class Prymnesiophyceae (formerly Haptophyceae). In terms of photosynthetic pigment composition, this species may be considered typical of the few eukaryotic algal classes represented within the picoplanktonic size fraction (Thomsen 1986; Stauber and Jeffrey 1988).

Synechococcus sp. (clone synonym WH 5701; previously "Syn") is a phycocyanin-containing unicellular chroococcoid cyanobacteria that lacks phycoerythrin. Phycocyanin and chlorophyll *a* thus constitute the major light-harvesting pigments. This species was originally isolated by R.R.L. Guillard in 1957 from Long Island Sound (off

Milford, Conneticut, USA) and is typical of many strains isolated from coastal waters within the continental shelf margin and which constitute a major subgroup among the marine cyanobacteria. Like the other members of this subgroup, WH 5701 does not have elevated salt requirements for growth. This haloindependence, together with the fact that this strain has never been observed in or isolated from the open ocean, is suggestive of a terrestrial origin (Waterbury 1986).

Synechococcus sp. (clone synonym WH 7803; previously "DC-2") is representative of the second subgroup of marine chroococcoid cyanobacteria and contains phycoerythrin as its primary light-harvesting photosynthetic pigment along with chlorophyll *a*. Phycocyanin is present as a minor component. In common with this subgroup, strain WH 7803 has elevated salt requirements for growth. WH 7803 was originally isolated by L. Brand in 1978 from waters west of Bermuda (33°44.9′ N, 67°29.8′ W). Strains in this subgroup are abundant and have been isolated from both coastal and oceanic waters at both tropical and temperate latitudes (Waterbury 1986).

Pavlova sp. (clone synonym NEP) belongs to the class Prymnesiophyceae, a morphologically diverse assemblage of algae that includes the coccolith-bearing forms and which are frequently both qualitatively and quantitatively dominant in both coastal and oceanic waters (Thomsen 1986). While the Prymnesiophyceae primarily occur in salt water, representatives of the order Pavlovales are found in oceanic, coastal, brackish and freshwater habitats (Thomsen 1986). This strain was originally isolated from the Gulf Stream (37°10′ N, 68°30′ W) by R.R.L. Guillard in 1958. *Pavlova* sp. (clone NEP) possesses a suite of photosynthetic pigments similar to other chromophytic algal classes and which includes chlorophyll *a*, chlorophylls c_1 and c_2 and the xanthophyll fucoxanthin (Jeffrey 1980; Hiller *et al.* 1988).

4.1.2. Maintenance and Growth of Picoplankton Cultures.

All three picoplanktonic cultures were maintained in Guillard's *f*/2 medium less the silicate (Guillard and Ryther 1962). Cultures of approximately 500 mls were grown in batch mode in 1 l Ehrlenmeyer flasks in a controlled environment incubator (New Brunswick Scientific Co., Edison, New Jersey, USA, Model R-27). Illumination was provided by a horizontal bank of fluorescent lights (Sylvania Cool-White) situated underneath the culture flasks. Separate cultures of each of the three species were grown at 4 different PFDs. The different PFDs were achieved by attenuating the irradiance from the fluorescent lights with neutral density screening in the form of cheesecloth. Intensities of PAR measured with a Licor Quantum Meter (Model 190SB) and sensor (Model 190S) ranged from 7 to 70 $\mu E\ m^{-2}\ s^{-1}$. Growth of the cultures was monitored daily by the estimation of the cultures optical density at 676 nm, a primary absorbance peak of chlorophyll *a*. Cells were harvested in exponential growth judged from the linear increase in *ln* (OD_{675}) over time.

4.2. NATURAL SEAWATER SAMPLES.

4.2.1. Sites of Collection and Sampling Methodology.

Natural water samples were collected during a number of cruises aboard the CSS Hudson between 1983 and 1987 representative of a number of different oceanic regimes. Tropical open ocean samples were collected from the Eastern Caribbean. Sub-tropical samples were obtained from the Sargasso Sea and in the vicinity of several of the New England seamounts to the north and east of Bermuda. Samples from temperate latitudes were collected from the Western North Atlantic including stations in the Gulf Stream.

Finally, a large data set was obtained from oceanographic stations throughout the Eastern Canadian Arctic from the Labrador Sea and Baffin Bay as far north as Jones Sound (76°N).

The first photosynthetic action spectra measurements of natural phytoplankton assemblages were made at a single station in the Northern Sargasso Sea (35°20′ N, 62°30′ W) during the "Closure 83" cruise of the CSS Hudson. This station is located 220 nautical miles NE of Bermuda (Figure 4.1). Water samples were collected with a modified continuous pump sampler (Herman *et al.* 1984). The pressure-temperature probe was replaced with a Guideline® CTD (Model 8709) and an Aquatracka® submersible fluorometer. Water samples were collected from individual depths ranging from 10 to 100 m on separate days with sampling always taking place at approximately 0700 hours local time.

Samples of Arctic waters were collected in the Eastern Canadian Arctic during the "Arctic 83" cruise of the CSS Hudson from July to September 1983. The locations of the sampling stations are shown in Figure 4.2. As previously, water samples were collected from depths of 5 to 100 metres by means of a submersible pump equipped with CTD, attenuance and fluorescence sensors. These sensors attached to the pump housing permitted the selection of sampling depths based upon the vertical structure of the water column. All samples were collected in the morning (approximately 0700 hours local time) and stored in 8 l nalgene carboys in the dark at ambient temperatures (-1°C) until analysed.

A series of samples were also collected along a transect from the eastern Caribbean north through the Mona Passage through the Sargasso Sea and Gulf stream to a point off the eastern United States during the "Barbados 84" cruise of the *CSS Hudson*

(see Figure 4.3). As with all other natural seawater samples material was collected by means of a submersible pump.

Finally, a series of experiments were conducted using natural seawater samples collected from a number of stations in the mid-Atlantic during the "Plasma-87" cruise of the *CSᶜ Hudson* in July 1987. Stations sampled included waters directly over several of the New England Seamounts as well as an oligotrophic open-ocean station considered representative of the open ocean in general (see Figure 4.4).

4.3. BIOMASS ESTIMATION.

For natural seawater samples the chlorophyll concentration was based upon acetone extracts of particulate material collected on filters. For total particulates three replicate seawater samples of 100 mls were filtered onto separate GF/F filters which were then extracted in 90% acetone at -20°C overnight. The chlorophyll concentration was determined fluorimetrically according to the procedures of Holm-Hansen *et al.* (1965). The chlorophyll concentration of the smaller planktonic size fractions were determined in a similar manner from GF/F extracts of seawater that had been previously filtered through 3 μm and 1 μm Nucleopore filters.

For cultures of picoplankton strains it was discovered that the efficiency of chlorophyll extraction varied greatly between the different clones. Even within a single species extraction proved highly variable and a satisfactory technique yielding complete extraction with good replicatibility proved elusive. Consequently biomass was estimated in terms of the magnitude of the cells *in vivo* absorbance peak at 676 nm (units: $m^2\ m^{-3} = m^{-1}$). This peak is attributable solely to chlorophyll *a* and is present in all picoplankton

clones providing a common point of reference. Examination of the in vivo absorption spectra also provides an index of the relative contribution chlorophyll *a* makes to the total cellular absorbance. Similarily, this index may be related to the analogous absorbance peak always present in the *in vivo* particulate spectra of natural phytoplankton assemblages irrespective of phylogenetic composition.

4.4. DETERMINATION OF MONOCHROMATIC PHOTOSYNTHETIC ACTION SPECTRA.

The wavelength dependence of the rate of carbon fixation (measured as uptake of $H^{14}CO_3^-$) at light-limiting irradiances was determined from the initial slopes $\alpha^B(\lambda)$ of the photosynthesis-irradiance relationship obtained using 12 separate wavebands centred every 25 nm from 400 nm to 675 nm inclusively. Each waveband had a half-bandwidth of ~25 nm. Slopes were determined by least-squares linear regression of carbon fixation upon irradiance and were based upon 8 intensities per waveband. Incubations were carried out in a purpose-built incubator consisting of two temperature controlled (± 0.2°C) aluminum blocks, each bored to accommodate 48 glass mini-scintillation vials (7 mls) as incubation vessels (see Appendix B for a complete description of the incubation system employed for all photosynthetic rate measurements).

Irradiance, supplied from below by two 2000 W tungsten-halogen lamps (Atlas Model OHD 2000), first passed through a 5 cm glass cuvette of flowing seawater and then through the custom-built bandpass interference filters (PTR Optics) positioned below the incubation wells. In later experiments designed to increase the PFD in the six shorter wavebands (400 nm to 525 nm) irradiance was supplied by six 250 W tungsten halogen projector lamps (Sylvania model ENH). No significant spectral differences were

found betw. en the two sources. Eight separate intensities within each waveband were obtained by further attenuation using nickel neutral density screen (Perforated Products). Initially the spectral composition of the irradiance striking each vial was calculated from the spectral characteristics of the tungsten-halogen source and the transmission characteristics of the bandpass interference filters. Subsequently, the spectral distribution was determined directly using a prototype spectroradiometer custom-built by Focal Marine Ltd. This instrument (model OS-1) is a solid state spectrometer based upon a holographic grating and a linear photodiode array. It is sensitive in the spectral range 350-700 nm with a resolution of < 1 nm and is calibrated against an NBS traceable standard (Optikon lamp model 220A, SN M-553, operated at 6.5 A). The incident irradiance is acquired with a cosine collector probe and transmitted to the sensing array via fiber optic cable. Spectral correction for the response of the instrument including spectral attenuation by the fiber optic cable is carried out during post-processing of the acquired data. The resultant spectral composition of the irradiance incident on the base of the incubation vials within each waveband is shown in Figure 4.5. To allow a straightforward comparison between different wavebands the spectral composition of each waveband has been normalised to the maximum PFD determined for each sample. The spectral curves thus represent a relative spectral photon fluence rate distribution for each waveband. The absolute PFD emerging through the base of each incubation vial was measured with a Licor Quantum meter (Model 190SB) and sensor (Model 190S). A correction factor of 2.0 was applied to the readings obtained for the 400 nm waveband to compensate for the sharp cut-off of the quantum sensor at this wavelength.

Rates of carbon fixation were determined by the addition of $H^{14}CO_3^-$ (New England Nuclear, sp. act. 37 MBq ml^{-1}) to the sample and subsequent incubation in scintillation vials placed in the purpose-built temperature controlled incubator block. Scintillation vials were placed in the incubation block and allowed to come to thermal

equilibrium with the block (usually achieved in under 30 minutes) before addition of the sample. The procedure was modified according to the biomass of the sample with respect to the amount of $H^{14}CO_3^-$ added, the volume of sample added to each vial and the means whereby surplus inorganic ^{14}C was removed at the end of the incubation period (acidification or filtration).

Laboratory cultures of the various picoplanktonic species provided samples with the greatest biomass concentration. In these samples, ~2.75 MBq $H^{14}CO_3^-$ was added to ~120 mls of culture in the dark (yielding an added activity of ~0.025 MBq ml^{-1}). The sample was gently mixed in the dark for 5 minutes to ensure a homogeneous distribution of both cells and ^{14}C throughout the 120 ml sample volume. Three replicate aliquots of 5 µl were withdrawn and each added to three scintillation vials containing 10 µl of 6 N NaOH and 5 mls of scintillation cocktail. These three vials (the "totals") were used to compute the total added activity present in the sample. Replicate aliquots of 0.5 mls of the sample were then dispensed into each of the 96 experimental vials in the incubator block (the "light" vials), three vials that were maintained in darkness and at the experimental temperature throughout the incubation period (the "dark" vials) and three vials that were immediately acidified with 0.25 ml of 6 N HCl to provide a measure of activity at time zero (the "T-zeros"). In the laboratory experiments a further three vials were innoculated with 0.5 ml aliquots from a 10 ml subsample of the original 120 ml radioactive culture sample to which 10 µl of 10^{-3} M solution of DCMU had been added (yielding a final concentration of 10^{-6} M DCMU). As DCMU is considered a potent inhibitor of photosynthetic electron transport these three vials were considered to provide an alternative measure of "background" heterotrophic ^{14}C fixation to that provided by the vials incubated in the dark. These three vials were incubated at three different "white" light intensities.

At the end of the incubation period the sample was acidified with 0.25 ml of 6N HCl and shaken for 1 hour to remove excess inorganic carbon. The samples were then neutralized by adding 0.25 ml of 6N NaOH and 5 ml of scintillation fluid (BDH) was finally added. Samples were counted with a Beckman 7800 liquid scintillation counter and corrected for quenching using the H-number method. A third-order polynomial was found to provide a good description of the quench curve (% efficiency as a function of H-number) and was fitted using a non-linear regression routine (Marquart algorithm). Because of the biomass present in the laboratory cultures this procedure provided a very strong photosynthetic signal.

For natural seawater samples collected in the Sargasso Sea ("Closure 83" cruise) and in Arctic waters ("Arctic 83" cruise), 74 - 185 MBq $H^{14}CO_3^-$ were added to ~120 mls of sample (yielding 0.74 - 1.85 MBq ml^{-1}) and mixed in the dark. Aliquots 1 ml was then dispensed into each incubation vial (0.74 - 1.85 MBq $vial^{-1}$) and incubated for 1 hour. Upon completion of the incubation the samples were acidified, shaken, neutralised and scintillation cocktail was added as described for laboratory cultures. For Arctic waters this experimental procedure provided a strong photosynthetic signal yielding satisfactory results down to biomass concentrations of 0.5 mg Chl *a* m^{-3}.

Subsequent experiments during the "Barbados 84" cruise demonstrated that this procedure was totally inadequate in oligotrophic waters where the compounding effects of low biomass and low biomass-specific photosynthetic rates resulted in the failure to detect a significant photosynthetic signal in the samples. Consequently, on a subsequent cruise ("Plasma 87"), during which the action spectra of the picoplanktonic size fraction were determined, the procedure was substantially modified to increase its sensitivity. The concentration of isotope was increased such that 740 MBq of $H^{14}CO_3^-$ was added to ~500 ml of sample (yielding an added activity of ~1.48 MBq ml^{-1}) in the dark and 5 ml

was then dispensed into each incubation vial (~7.4 MBq vial^{-1}). PFDs in the shorter wavelength wavebands (400-525 nm) were increased by switching to different lamps (Sylvania ENH) and the incubation period was also increased from 1 to 6 hou This combination of modifications provided a theoretical increase in overall sensitivity of approximately 30-fold. At the end of the incubation period each 5 ml sample was filtered through a 3 µm Nuclepore filter. Filters were rinsed twice with 5 ml aliquots of GF/F filtered seawater. The combined filtrate (15 mls) was then filtered through a 0.2 µm Nuclepore filter and again rinsed twice with two 5 ml aliquots of GF/F filtered seawater. Filtration of the samples rather than simply acidifying them increased the photosynthetic signal to background noise ratio by removing any dissolved organic ^{14}C. Radioactive dissolved organic carbon is a nautural contaminant of commercial preparations of $H^{14}CO_3^-$ which although present in small amounts is sufficient to yield significant background counts when high specific activities are used. The 3 µm and 0.2 µm Nuclepore filters were then placed in separate scintillation vials and acidified with 0.25 ml of 6 N HCl. The vials were shaken for 1 hour and neutralised with 0.25 ml of 6 N NaOH and 5 mls of scintillation cocktail added and the samples counted as described.

4.5. DETERINATION OF THE POLYCHROMATIC P-I RESPONSE.

4.5.1. Incubation procedures.

Determination of the rate of photosynthetic carbon fixation in polychromatic irradiance was essentially identical to that outlined above for determination of photosynthetic action spectra. The principal difference between the two experiments was the sample illumination. The higher photon fluence rates in P-I incubations allowed the incubation period to be reduced to 30 minutes. Subsequent processing of the sample

(acidification, shaking, neutralisation, the addition of scintillation cocktail and counting procedure) was as previously described.

"White" irradiance was again supplied by 2000 W tungsten halogen lamps (Atlas OHD 2000) which was first filtered through a 5 cm glass cuvette of flowing water and then through nickel neutral density screen to provide a range of intensities. PFDs incident emerging through the base of the incubation vials ranged up to 2500 $\mu E\ m^{-2}\ s^{-1}$. The spectral composition of the "white" light derived from tungsten halogen sources is heavily weighted toward the red end of the spectrum. Figure 8.2(b) shows the relative spectral composition of this irradiance as determined with the solid state spectrometer (model OS-1). Considering the disproportionately greater contribution of the longer wavelengths to the total photosynthetically active irradiance in this source it is perhaps inappropriate to term it "white".

Both "Green" and "Blue" polychromatic irradiances were generated by the addition of acetate filters (Roscolene # 871 and # 856 filters respectively, Rosco Laboratories, Port Chester, New York) below the incubation vessels in the path of light from the 2000 W tungsten halogen lamps. The spectral composition of the irradiance emerging through the base of the incubation vessels with either filter in place are shown in Figure 8.2(b). The spectral distribution was determined with the Focal Marine solid state spectrometer model OS-1. The spectral composition of the "Blue" irradiance reveals a significant red component which arises because the "white" tungsten-halogen light source is so heavily weighted toward the red wavelengths. For all polychromatic irradiance fields the absolute PFD emerging through the base of each vial were determined using a Licor Quantum Meter (Model 190SB) and Sensor (Model 190S). All spectral irradiance data collected by the OS-1 spectrometer were transfered in the form of ASCII files to an IBM compatible computer for processing.

4.5.2. Non-linear curve-fitting of P-I models.

The various empirical and rational P-I models were fitted to the P-I data by non-linear regression analyses. The program employed was based upon the least-squares, gradient-expansion algorithm developed by Marquart (1963). Derivatives are calculated numerically and the step size over which the derivative (slope) is incremented is set by the program. All data points were weighted equally and the convergence test applied was that $\Delta\chi^2/\chi^2$ be less than 0.00001. In the models based upon Poissonian statistics, the cumulative Poisson distribution was computed according to the algorithms for the incomplete Gamma function provided by Press *et al.* (1986). This algorithm employs a series development of $g(a,x)$ and a continued fraction development for $G(a,x)$ providing evaluation of the function for all positive a and x.

For most of the functions the initial estimates were made by inspection of the data. Initial parameter estimates in the 4-parameter models of Vollenweider (1965) and Iwakuma and Yasuno (1983) were based upon a comparison of the shape of the experimental P-I curve with the published hypothetical curves generated from various parameter combinations (in Fee (1969) and Iwakuma and Yasuno (1983) respectively).

4.6. MEASUREMENT OF THE ABSORPTION SPECTRA.

The absorption spectra of the particulate phase in both cultures and natural seawater samples were determined according to the method described by Yentsch (1957,1962) and Truper and Yentsch (1967) as modified by Kiefer and SooHoo (1982), Mitchell and Kiefer (1984) and Mitchell *et al.* (1984). For natural water samples, known

volumes of seawater ranging from 250 ml to 3 litres were filtered through Whatman GF/F glass fibre filters (vacuum pressure < 5 cm Hg). In the case of culture samples, smaller volumes of generally 3 to 10 mls were sufficient. The filters were then frozen and stored (-20°C) in darkness until scanned. With the exception of the initial absorbance data collected from the Arctic and Sargasso Sea samples, a graded series of volumes were filtered and the absorption coefficients then determined by regression of absorbance versus volume. When determining the absorption spectra of the smaller planktonic size fractions (< 3 μm and < 1 μm) of natural seawater samples, seawater was first prefiltered through 3 μm and 1 μm Nuclepore filters prior to the filtration through GF/F filters. The volume-normalised absorption spectra of these size fractions were then used to determine the contribution of particles < 3 μm and < 1 μm (nominal diameter) to total particulate absorption.

Absorption spectra of particulate material collected on GF/F filters were determined using a Pye-Unicam single beam spectrophotometer (Model 8600) interfaced with a Hewlett Packard HP 85 microcomputer. Filters were thawed, moistened with filtered seawater and scanned from 380 nm to 750 nm, and the absorbance read every 1 or 2 nm and stored digitally on tape after subtraction of a blank filter. The ratio (V/S) of the clearance area of the filter (m^2) to the volume of seawater or culture filtered (m^3) represents the reciprocal pathlength (m^{-1}) permitting calculation of the semi-integral attenuance coefficient which, when measured by the above methods, approximates the absorptance of the sample (Shibata 1958; Kiefer and SooHoo 1982).

The diffuse volume absorption coefficient $a^*_p(\lambda)$ [units: m^{-1}] may be estimated from the absorptance measured in this way if the pathlength amplification factor $\beta(\lambda)$ of the filter is known (where $\beta(\lambda)$ is the ratio of the optical thickness of the diffusing

material to its geometric thickness (Butler 1962)) as described by Mitchell and Kiefer (1984) and Mitchell *et al.* (1984):

$$a^*_p(\lambda) = \frac{2.3 \cdot OD(\lambda)}{(V/S) \cdot \beta(\lambda)} \qquad ...(4.1)$$

(where $OD(\lambda)$ is equal to $-\log_{10}$[sample transmittance/blank transmittance]). A value of 2.45 was initially ascribed to $\beta(\lambda)$ based upon the particulate material of a natural seawater sample collected on a Whatman GF/F glass fibre filter (Kishino *et al.* 1985). Where the chlorophyll concentration was determined, the chlorophyll-specific attenuation coefficient ($a^*_{chl}(\lambda)$) [units: $m^2 \cdot mg\ Chl^{-1}$] was calculated by dividing $a^*_p(\lambda)$ [units: m^{-1}] by the chlorophyll concentration [units: $mg \cdot m^{-3}$] of the sample. Results indicated that $\beta(\lambda)$ was not a constant and varied with the optical density of the sample. Consequently latter samples were analysed by way of a graded series of particle concentrations as described in Chapter 6.1.

Because the method employing glass-fibre filters differs optically from that normally used to determine the chlorophyll-specific attenuation coefficient *in situ* I have retained the abbreviation a^*_{chl} rather than the more standard term k_c for the chlorophyll-specific attentuation coefficient.

4.7. COMPUTATION OF THE APPARENT QUANTUM YIELD ($\phi_a(\lambda)$).

The rate of photosynthetic carbon fixation as the irradiance tends to zero is the product of the rate of absorption of quanta and the efficiency with which absorbed quanta

bring about the reduction of inorganic carbon. The apparent quantum yield ($\phi_a(\lambda)$) [units: mol C fixed · mol photons $^{-1}$] was calculated as:

$$\phi_a(\lambda) = \frac{[\alpha^B(\lambda)]}{[a^*_{chl}(\lambda)]\cdot[43.2]} \quad \ldots(4.2)$$

where $\alpha^B(\lambda)$ is the initial slope of the photosynthesis-irradiance curve [units: $mgC \cdot mgChl^{-1} \cdot hr^{-1} \cdot (\mu E \cdot m^{-2} \cdot s^{-1})^{-1}$], $a^*_{chl}(\lambda)$ is the chlorophyll-normalized diffuse volume absorption coefficient [units: $m^2\ mgChl^{-1}$] and 43.2 is the proportionality constant required for conversion to common units.

CHAPTER 5

PHOTOSYNTHESIS-IRRADIANCE RESPONSE OF PICOPLANKTON CULTURES UNDER POLYCHROMATIC IRRADIANCE.

5.1. THE P-I RESPONSE TO WHITE IRRADIANCE.

The "white" light provided by the quartz-halogen light source provided the greatest dynamic range of PFDs (0 - 2000 $\mu E\ m^{-2}\ s^{-1}$) for establishing the P-I response of the representative picoplankton clones. The highest PFD approximates the maximum daylight irradiance experienced at the sea surface. However it should be remembered that the spectral distribution (and thus the potential for absorption) is significantly different (see Figure 8.2(b)).

The relationship between photosynthesis and PFD was different for each of the three picoplankton strains examined. For any particular clone the P-I response retained its characteristic shape irrespective of the PFD under which the culture was grown. Differences in the growth irradiance did have the effect of altering the magnitude of the various parameters describing the P-I response.

5.1.1. *Synechococcus* sp. WH 5701 (formerly "Syn").

The P-I response of *Synechococcus* sp. WH 5701, a cyanobacterial clone possessing phycocyanin as the major light-harvesting pigment, was unique among the picoplankton clones examined in that the P-I curve was always of the saturation type. No evidence of photoinhibition was present even when cells grown under extremely low

PFDs (< 10 μE m^{-2} s^{-1}) were exposed to PFDs as high as 2000 μE m^{-2} s^{-1}. The P-I response was proportional to PFD below 120-230 μE m^{-2} s^{-1}. Above this threshold the rate of photosynthesis quickly became saturated and remained at this maximal rate up to the highest incubation intensities (2000 μE m^{-2} s^{-1}).

Both the maximum photosynthetic rate (P_m^B) and the PFD marking the transition from light-limited to light-saturated photosynthesis (I_k) were related to the growth irradiance (see Section 5.4.). The P-I responses of the four cultures grown at 8 μE m^{-2} s^{-1} (*SY 9149*), 15 μE m^{-2} s^{-1} (*SY 9157*), 27 μE m^{-2} s^{-1} (*SY 9161*) and 70 μE m^{-2} s^{-1} (*SY 9153*) are shown in Figures 5.1, 5.2, 5.3 and 5.4 respectively. The resultant P-I curve obtained from fitting the new empirical model described in Chapter 3.4.1. to the data is also included together with a plot of the residuals (discussed below).

Empirical Models: A total of 7 saturation-type empirical P-I formulations were fitted to the P-I response data to ascertain which model provided the most precise description. The formulations were those proposed by Baule (1917) [Eq. 2.4], Baly (1935) [Eq. 2.6], Smith (1936) [Eq. 2.7], Rabinowitch (1951) [Eq. 2.11], Thornley (1976) [Eq. 2.5], Jassby and Platt (1976) [Eq. 2.10] and Bannister (1979) [Eq. 2.12]. The results of the non-linear regression analyses are given in Tables 5.1, 5.2, 5.3 and 5.4 corresponding to cultures of *Synechococcus* sp. WH 5701 grown under irradiances of 8 μE m^{-2} s^{-1} (*SY 9149*), 15 μE m^{-2} s^{-1} (*SY 9157*), 27 μE m^{-2} s^{-1} (*SY 9161*) and 70 μE m^{-2} s^{-1} (*SY 9153*) respectively. Goodness-of-fit was judged by both the standard deviation of the fit and an examination of the residuals plotted as a function of the PFD.

In all four cultures the 3-parameter formulation suggested by Bannister (1979) [Eq. 2.12] provided the "best" fit as judged by the selected criteria (Tables 5.1.-5.4.). In addition to providing the lowest standard deviation an examination of the residuals

indicates that this empirical formulation provides a good description of the P-I response throughout the entire range of PFDs from 0 to 2000 μE m^{-2} s^{-1}. Unlike many of the alternate formulations, deviations from the predicted curve appear random and do not display any systematic trend when plotted as a function of PFD (Figures 5.1.-5.4.).

With the exception of the culture grown under the lowest PFD (*SY 9149* grown under 8 μE m^{-2} s^{-1}), the 3-parameter non-rectangular hyperbola formulation originally proposed by Rabinowitch (1951) as recast by Thornley (1976) [Eq. 2.11] provided the second-best description of the P-I data. This is not surprising insofar as the non-rectangular hyperbola is very similar geometrically to equation proposed by Bannister (1979). In both formulations the third parameter (*m* or Θ) controls the convexity of the curve. The relative success of these two 3-parameter models compared to the remaining 2-parameter formulations indicates that the added geometrical flexibility produced by the introduction of an extra parameter clearly improves the ability of these two functions to describe the P-I response. Examination of the residuals of the Rabinowitch (1951) equation shows that this formulation also provides an adequate description of the entire P-I response with the residuals displaying a random scatter around the fitted curve at all PFDs.

The 2-parameter hyperbolic tangent function of Jassby and Platt (1976) was second-best for *SY 9149* and was ranked third for the other three cultures of *Synechococcus* sp. WH 5701. Examination of the residuals from the fitted curve of Jassby and Platt (1976) reveal that generally this function provides a good description of the P-I response, particularly in the case of *SY 9149*. For the remaining three cultures however, this function does tend to underestimate photosynthesis at PFDs corresponding to the point where photosynthesis switches from being light-limiting to being light-saturating.

The models of Rabinowitch (1951) [Eq. 2.11] and Bannister (1979) [Eq. 2.12] are both three-parameter models compared to the hyperbolic tangent model of Jassby and Platt (1976) which contains only 2 parameters. In both 3-parameter models the third parameter controls the convexity of the curve at the point of the transition from the linear light-limited region to the maximum light-saturated region. Bannister's (1979) model closely resembles the hyperbolic tangent when the parameter $m = 2.5$ to 3. For *Synechococcus* sp. WH 5701 the parameter m varies from 3.1 (*SY 9149*) to 5.3 (*SY 9153*) and like the other two parameters (P_m^B and α^B), m is dependent upon the growth irradiance (see Section 5.1.4.). Similarly, the parameter Θ in the model of Rabinowitch (1951), which also describes the abruptness of the transition from light-limited to light-saturated photosynthesis, varies from 0.93 to 0.98 and is correlated with the growth irradiance.

The success of the three-parameter models compared to the two-parameter models, judged by the reduction of the residual variance and the lack of any systematic deviation of the data from the predicted curve throughout the entire range of photon flux densities, provides a strong argument for the inclusion of a third parameter governing the convexity of the P-I response. Furthermore, the strong correlations between the estimates of both m and Θ and the growth irradiance, indicate that the convexity or "shape" of the P-I response is governed by the light-history of the cells. Taken together these results demonstrate that a third convexity parameter is required for a complete description of the P-I response of *Synechococcus* sp. WH 5701. Only in cells grown under the lowest PFD (8 $\mu E\ m^{-2}\ s^{-1}$) is the value of the shape parameter m of Eq. 2.12 sufficiently close to 3 that the 2-parameter hyperbolic tangent model of Jassby and Platt (1976) [Eq. 2.10] is capable of providing a comparable description of the P-I response of *Synechococcus* sp. WH 5701. That the convexity of the P-I response of this clone changes according to growth

irradiance is an important result, and one that may provide some insight into the photoadaptive mechanisms underlying the P-I response (see Sections 5.1.4. and 8.1.).

The new empirical model introduced in Chapter 3.4.1. also provided an excellent fit to the data (Tables 5.1, 5.2, 5.3 and 5.4). Where any trace of photoinhibition is absent the additional three parameters describing photoinhibition become redundant and may be arbitrarily set to zero in which case this formulation reduces to that of Bannister (1979). Consequently in cultures *SY 9149*, *SY 9157* and *SY 9161* the fewer parameters in Bannisters equation result in a better fit. In the case of *SY 9153* however there is an indication of a possible photoinhibitory decline at high irradiances due a single datum point (Figure 5.4). In this case, the new model provides a reduction in the residual variance providing a slightly superior fit although at the expense of three additional parameters (Table 5.4).

The remaining saturation-type empirical formulations all provided inferior descriptions of the P-I response of *Synechococcus* sp. WH 5701. In some cases the fit was so poor as to warrant the exclusion of a particular formulation as a potential P-I description. Many of these proposed functions yielded solutions with such a poor correspondence to the P-I data as to render their parameter estimates meaningless. The tendency of particular formulations to yield parameter values that were consistently either under- or over-estimates brought into focus the systematic inadequacies of several of the proposed empirical functions.

By far the worst expression was the rectangular hyperbola [Eq. 2.6] which consistently provided the worst correspondence with the P-I data from *Synechococcus* sp. WH 5701. Originally proposed by Baly (1935) by analogy to the Michaelis-Menten model of enzyme kinetics, the rectangular hyperbola does not provide an adequate

description of the P-I response. In all cases the fitted rectangular hyperbola was characterized by a high standard deviation with the residuals strongly correlated to the PFD. As a result this formulation consistently overestimated the maximum photosynthetic rate (P_m^B) by a factor of 1.2 and the initial slope (α^B) by factor of 2 when compared to the parameter estimates produced by the model of Bannister (1979). This leads to a consistent and pronounced under-estimation of the light-adaptation parameter I_k ($=P_m^B/\alpha^B$) by a factor of 0.5 (see Table 5.5). Examination of the residuals shows that the computed curve deviates from the data in a systematic manner related to the PFD. At PFDs below that required to half-saturate photosynthesis (*ie.* $< I_k/2$), the curve over-estimates the actual rate of photosynthesis. At PFDs between $I_k/2$ and $3\ I_k$, the model under-estimates the actual rate of photosynthesis by as much as 25%. Above PFDs ≥ 3 I_k, the model increasingly over-estimates the rate of photosynthesis yielding a value of P_m^B that is 10-20% too high. Clearly this model is totally inappropriate for the description of the P-I response.

Several alternate models frequently used to describe the P-I response also provided a very poor correspondence to the P-I data of *Synechococcus* sp. WH5701. The exponential function originally proposed by Baule (1917), and which has subsequently been suggested to provide a good description of photosynthesis in phytoplankton (Peterson *et al.* 1987), also appears a poor choice. While providing a substantial improvement over that of the rectangular hyperbola, the exponential function suffers from similar shortcomings. Although yielding a more realistic estimate of P_m^B (1 - 3% over-estimate) the exponential function consistently over-estimated α^B, in all cases by a factor of from 1.42 to 1.49 (Table 5.5). Once again the light adaptation parameter I_k is correspondingly under-estimated, in this instance by a factor of about 0.68 to 0.72 when compared to the value of I_k given by Bannister's equation.

The alternative exponential function [Eq. 2.5] proposed by Thornley (1976) and aimed at increasing the extent of the initial linear portion of the curve at light-limiting PFDs, consistently provided a worse fit than the original exponential function [Eq. 2.4]. Only the rectangular hyperbola yielded a poorer fit (Tables 5.1 - 5.4). Extending the linear region did reduce the factor by which α^B was over-estimated (1.29-1.31 versus 1.42-1.49) and I_k was under-estimated (0.83-0.88 versus 0.68-0.71) but at the expense of increasing the over-estimation of $P_m{}^B$ (1.10-1.15 versus 1.01-1.03). Consequently, neither exponential function can be considered to provide an adequate description of the P-I response of *Synechococcus* sp. WH 5701.

The modified rectangular hyperbola suggested by Smith (1936) [Eq. 2.7], a formulation frequently employed in phytoplankton studies because of the simplicity of its integration, does show a considerable improvement compared to both the rectangular hyperbola and exponential formulations. This equation is essentially that of Bannister (1979) in which the shape parameter m is fixed at a value of 2.0. For all four cultures of *Synechococcus* sp. WH 5701 this equation consistently ranked fourth based upon the standard deviation of the fit (Tables 5.1 - 5.4). The geometric effect of constraining $m = 2$ was that the fitted curve always approached saturation more rapidly than the data points. The sharper the transition from light-limited to light-saturated photosynthesis in the P-I data, the greater the deviation between the fitted curve and the experimental data. This is clear from a comparison of the residuals and the value of the parameter m derived from fitting Bannister's (1979) equation to the four cultures. The greater the value of m, the greater the deviation of the residuals (Tables 5.1 -5.4; Figures 5.1 - 5.4). In terms of the parameter estimates compared to those of Bannister (1979), the equation of Smith (1936) provides a reasonable estimate of the maximum photosynthetic rate, over-estimating $P_m{}^B$ by 2 - 5%. However the result of constraining the shape of the curve (compared to that of Bannister (1979)) results in α^B being over-estimated by 17 - 23%,

the difference being positively correlated with the value determined for m in Bannister's formulation. Again this leads to an under-estimation of I_k by a factor of 0.85 - 0.87 (Table 5.5).

Rational Models: Several of the rational models based upon the kinetics of a single photosystem provided a good quantitative description of the P-I response of *Synechococcus* sp. WH 5701. In particular, the two models that reduced to a non-rectangular hyperbolic form in the absence of photoinhibition, namely the models of Rabinowitch (1951) [Eq. 2.11], Fasham and Platt (1983) [Eq. 2.44] and my two-photosystem model [Eq. 3.101], yielded acceptable agreement to the data.

Both the 3-parameter formulation of Rabinowitch (1951) which does not include the possibility of photoinhibition and the 4-parameter model of Fasham and Platt (1983) provided good descriptions of the P-I data (Tables 5.1, 5.2, 5.3 and 5.4). The two-photosystem kinetic model introduced in Chapter 3.6.2. also provided a good description of the P-I response of *Synechococcus* sp. WH 5701. In the absence of significant photoinhibition both the model of Fasham and Platt (1983) and my two-photosystem kinetic model may be reduced to a 3-parameter form analogous to the non-rectangular expression of Rabinowitch (1951) (Appendix A). Consequently all three models provided good quantitative descriptions of the P-I response. Fitting my 4-parameter kinetic model or the 4-parameter version of the Fasham and Platt (1983) model invariably produced a very small value ($\approx 2 \cdot 10^{-4}$) for the parameter β describing photoinhibition. In my two-photosystem model this leads to very high optimal irradiances since I_m equals $1/\beta$ [Eq. 3.127] producing a P-I response that is indistinguishable from a simple non-rectangular hyperbola (where $I_m = \infty$).

The general conclusion is that the P-I response of *Synechococcus* sp. WH 5701 requires a minimum of three parameters to define it. Of the empirical models that of Bannister (1979) provides the best description. Among the rational models any of the models that reduce to a non-rectangular hyperbola in the absence of significant photoinhibition provide a good quantitative description. Hence the 3-parameter model of Rabinowitch (1951) suffices in all cases. The single photosystem model of Fasham and Platt (1983) and my two photosystem kinetic model introduced in Chapter 3.6.2. also provide excellent correspondence with the data. The flexibility of these latter two models in accommodating photoinhibition is largely redundant in the case of *Synechococcus* sp. WH 5701 and the value of the fourth parameter invariably tends to zero in both cases. From a statistical perspective there is little to chose between these four formulations.

The parameter which describes the convexity of the curve at the transition from light-limited to light-saturated photosynthesis (m in the empirical model of Bannister (1979), Θ in Rabinowitch (1951), and χ in Fasham and Platt (1983) and my two-photosystem kinetic model [Eq. 3.101]) varied according to the growth irradiance of the culture (see Section 5.4). The fact that the pattern of this variation was consistent in both formulations supports the contention that there is a consistent geometrical feature in the P-I response of WH 5701 that demands a third parameter for its description. Only in the case of *SY 9149* was this convexity such that the 2-parameter hyperbolic tangent model of Jassby and Platt (1976) provided a good description of the P-I data.

In contrast, the 3-parameter model proposed by Megard *et al.* (1984) provided an unacceptable description of the data. This formulation has devised for P-I responses with significant decreases in photosynthesis at high irradiances due to photoinhibition. When fitting this model to the saturation-type response of WH 5701 this constraint always led to a systematic deviation of the residuals where photosynthesis was underestimated at

irradiances corresponding to the transition from the light-limited to light-saturated region, overestimated at saturating irradiances and subsequently significantly underestimated at high irradiances. In general, the formulation of Megard *et al.* (1984) proved to be unsuitable for P-I responses characterized by little or no photoinhibition.

5.1.2. *Synechococcus* sp. WH 7803 (formerly "DC-2").

The P-I response of all cultures of *Synechococcus* sp. WH 7803, a cyanobacterial clone possessing phycoerythrin as its major light-harvesting pigment, exhibited significant photoinhibition at high PFDs. The rate of photosynthesis at low light (α^B), the maximum rate of photosynthesis attained (P_m^B) and the PFD marking the onset of photoinhibition differed in each of the cultures. These differences could be correlated to the growth irradiance. In all three cultures the rate of photosynthesis increased linearly with PFD up to 100-200 μE m^{-2} s^{-1} where the rate became saturated. Photosynthesis started to decline due to photoinhibition at PFDs between 100 and 800 μE m^{-2} s^{-1} depending upon the growth irradiance of the culture. Photoinhibition was a linear function of PFD. The P-I responses of *Synechococcus* sp. WH 7803 to "white" irradiance are given in Figures 5.5, 5.6 and 5.7 corresponding to cultures grown under 17 μE m^{-2} s^{-1} (*DC 9125*), 25 μE m^{-2} s^{-1} (*DC 9117*) and 35 μE m^{-2} s^{-1} (*DC 9121*). Also shown are the computed P-I curves computed for the empirical P-I formulation described in Chapter 3.4.1. and a plot of the residuals as a function of PFD.

Empirical Models: A total of ten discrete P-I formulations that included photoinhibition were fitted to the data in order to ascertain which provided the best description of the P-I response. The formulations chosen were representative of those previously employed for phytoplankton and discussed in Chapter 2.3.2. These equations included those proposed by Steele (1962) [Eq. 2.13], Vollenweider (1965) [Eq. 2.18],

Steel (1973) [Eq. 2.19], Fee (1973) [Eq. 2.20], Williams (1978) [Eq. 2.21], Platt *et al.* (1980) [Eq. 2.17], Platt and Gallegos (1980) [Eq. 2.23], Iwakuma and Yasuno (1983) [Eq. 2.22]. The rational model of Megard *et al.* (1984) was also included here as it is geometrically identical to the empirical model proposed by Peeters and Eilers (1978,1988) but with parameters that are more amenable to interpretation (see Chapter 2.4). In addition, a modified form of the original formulation proposed by Gallegos and Platt (1980) in which the number of parameters was reduced from 5 to 4 was also tested. Also included was the new empirical function described in Chapter 3.4.1.

The results of the non-linear regression analyses are given in Tables 5.6, 5.7 and 5.8 corresponding to cultures of *Synechococcus* sp. WH 7803 grown under PFDs of 17 μE m^{-2} s^{-1} (*DC 9125*), 25 μE m^{-2} s^{-1} (*DC 9117*) and 35 μE m^{-2} s^{-1} (*DC 9121*) respectively. In all three cases, the 5-parameter model of Platt and Gallegos (1980) provided the best fit in that this formulation yielded the lowest standard deviation of the fit with residuals that showed the least systematic correlation to the PFD. The empirical model described in Section 3.4.1. also provided a very satisfactory description of all three cultures of WH 7803 accommodating all the major geometrical features of the data (Figures 5.5, 5.6 and 5.7). Both models contain more parameters (5 and 6 respectively) than many of the alternative models, a feature that inevitably reduces the residual variance of the fit and at least partially explains the success of these two models.

Simplifying the Platt and Gallegos (1980) model by constraining I_t' to equal I_b', that is by setting irradiance marking the onset of photoinhibition (I_t) at zero as suggested in Section 2.3.2., yields a fit that is almost comparable to the original while reducing the number of parameters to four. The alternative means of reducing the number of parameters suggested by Platt and Gallegos (1980), namely setting the shape parameter m equal to 6, constrains the geometric shape of the curve in such a way as to artificially

depress the computed rate of photosynthesis at the optimal irradiance. The result is a considerably inferior fit as judged by the residual variance of the fit and the distribution of the residuals with respect to irradiance.

Numerical curve-fitting of the remaining published models incorporating photoinhibition yielded generally poor results. The model of Steele (1962), frequently employed in phytoplankton studies, consistently provided the worst fit to the P-I data of *Synechococcus* sp. WH 7803. This two-parameter formulation always over-estimated the maximum photosynthetic rate at optimal PFDs and subsequently under-estimated photosynthesis at high PFDs. Clearly the geometric restrictions imposed by only two parameters is too great a constraint and prohibits a quantitative description of the P-I response of this picoplankton species. The formulations of Vollenweider (1965), Steel (1973) and Fee (1973) also failed to adequately describe the P-I data of *Synechococcus* sp. WH 7803 despite the increased geometrical flexibility provided by an increased number of model parameters. Of these related formulations only the model of Williams (1978) showed any potential for describing the overall "shape" of the response. However even this formulation was found to significantly overestimate photosynthesis at high PFDs.

The simple exponential model of Platt *et al.* (1980) provided a reasonable description of the response but tended to overestimate photosynthesis at high irradiances. This results from the model being geometrically constrained to yield a well-defined photosynthetic maximum at some optimal irradiance above which point photosynthesis is defined as declining *exponentially*. The P-I responses of *DC 9125*, *DC 9117* and *DC 9121* all suggest that photosynthesis decreases *linearly* with respect to irradiance at photoinhibitory intensities (Figures 5.5, 5.6 and 5.7).

The general conclusion to be drawn is with the exception of the model of Platt and Gallegos (1980) none of these previously published formulations possess geometrical properties that make them suitable for accurately describing the P-I response of *Synechococcus* sp. WH 7803.

Rational Models: Both the single photosystem model of Fasham and Platt (1983) and the two-photosystem kinetic model described in Chapter 3.6.2. provide good descriptions of the P-I response of *Synechococcus* sp. WH 78C (Tables 5.6, 5.7 and 5.8). Both are 4-parameter formulations that are essentially a composite of a non-rectangular hyperbola with an exponential description of photoinhibition. The statistical superiority of these two 4-parameter models over all the empirical models, many of which have more parameters, provides additional support for their use.

The simple cumulative Poisson model introduced in Chapter 3.6.1. also provided an excellent fit. Where the number of hits required to bring about photochemistry is set at one ($a = 1$), this single-hit model also contains 4 independent parameters. When both the number of hits required to cause photoinhibition (b) and the action cross-section of photoinhibition (I_j) were independent of the analogous parameters defining photochemistry (a and I_k), the model successfully described the data (Tables 5.6, 5.7, and 5.8).

Reducing the number of parameters to three by setting the action cross-section for photoinhibition equal to that of photochemistry ($I_j = I_k$) resulted in the model's failure to describe the P-I response. With this restriction the large number of data points defining the gradient of the initial slope dominate the estimation of I_k (and hence I_j). The result is that the only parameter left to define the photoinhibitory decrease in photosynthesis at

nigh irradiances is *b*, the number of hits required to cause photoinhibition. The shape of the cumulative Poisson distribution constrained to provide a value of *b* large enough to yield realistic photosynthetic rates over *all* photoinhibitory irradiances produces a curve that systematically over-estimates photosynthesis throughout the first half and under-estimates photosynthesis throughout the second half of the photoinhibition range.

The 3-parameter model of Megard *et al.* (1984) failed to provide an accurate description of the P-I response of WH 7803. In all three cultures, this formulation over-estimated photosynthesis at high PFDs. The inability of this model to accommodate an extended plateau and at least quasi-linear photoinhibition resulted in a generally poor fit to all three cultures (*DC 9125*, *DC 9117* and *DC 9121*) (Appendix C).

In conclusion, the only empirical formulations providing a satisfactory description of the P-I response of *Synechococcus* sp. WH 7803 are the new empirical model (6-parameter) introduced in Chapter 3.4.1. and the model of Platt and Gallegos (1980), in either its general (five parameter) or modified (four parameter, $I_t = 0$) form. Among the rational models both the kinetic model of Fasham and Platt (1983) and my two-photosystem kinetic model yield good quantitative descriptions and with fewer parameters (4) than the empirical models. Also, the simple cumulative Poisson model yields an acceptable 4-parameter description provided the action cross-sections for photochemistry and photoinhibition are allowed to be independent of one another.

5.1.3. *Pavlova* sp. (clone NEP).

The form of the P-I response of *Pavlova* sp. (clone NEP) to "white" irradiance was strongly dependent upon the growth irradiance of the culture. The cells grown at 8 $\mu E\ m^{-2}\ s^{-1}$ (*PA 9141*) and to a lesser extent those grown at 12 $\mu E\ m^{-2}\ s^{-1}$ (*PA 9137*)

exhibited photoinhibitory decreases in photosynthetic rate at high PFDs. Photoinhibition was a linear function of PFD. Cells grown at the highest irradiance of 45 μE m^{-2} s^{-1} (*PA 9133*) showed no indication of any photoinhibitory decreases at high PFDs. In the two cultures grown under 8 and 12 μE m^{-2} s^{-1} that exhibited photoinhibition (*PA 9141* and *PA 9137*), the PFD marking the onset of photoinhibition were 400 and 800 μE m^{-2} s^{-1} respectively. The culture grown at intermediate PFD (*PA 9137*) possessed a broader plateau with a wider range of intensities over which photosynthesis was optimal.

The P-I responses of *Pavlova* sp. (clone NEP) grown under irradiances of 8 μE m^{-2} s^{-1} (*PA 9141*), 12 μE m^{-2} s^{-1} (*PA 9137*) and 45 μE m^{-2} s^{-1} (*PA 9133*) are given in Figures 5.8, 5.9 and 5.10 respectively. Also shown are the computed P-I curves for the empirical model described in Chapter 3.4.1. Results from numerical curve-fitting are given in Tables 5.9, 5.10 and 5.11.

Empirical Models: Various empirical P-I models incorporating photoinhibition were fitted to all three cultures of *Pavlova* sp. Six saturation type curves were also fitted to the high-light culture (*PA 9133*) which lacked photoinhibition. As with the other picoplankton species exhibiting photoinhibition (*Synechococcus* sp. WH 7803), the best fits were obtained for both *PA 9141* and *PA 9137* with the 6-parameter empirical model introduced in Chapter 3.4.1 and the 5-parameter model of Platt and Gallegos (1980). As before, simplification of the Platt and Gallegos model by setting $I_t' = I_b'$ yielded a comparable fit to that of the original expression but with a reduction to 4 parameters (Tables 5.9 and 5.10). Only in the case of PA 9133 where photoinhibition is essentially absent did this formulation fail to converge because I_b' tends to increase to infinity. The alternate simplification of setting $m = 6$ reduced the fidelity of the fit.

Most of the remaining formulations produced curves with very poor correspondence to the data. Only that of Williams (1978) could be conceived as providing a realistic description of the response. As with *Synechococcus* sp. WH 7803 the models of Steele (1962) and Steel (1973) were particularly poor descriptions. The residuals are systematically correlated to the PFD and the curves grossly over-estimate the maximum photosynthetic rate and under-estimate both the initial slope and the rate of photosynthesis at high PFDs.

For the high-light culture *PA 9133* lacking photoinhibition the models of Bannister (1979) and the non-rectangular hyperbola of Rabinowitch (1951) provided good approximations to the data. The value of the convexity parameter m in Bannister's model was 5.4. The degree of convexity implied by this value is greater than that accommodated in the hyperbolic tangent model of Jassby and Platt (1976) which explains the inadequacy of this expression.

Rational Models: The model of Fasham and Platt (1983) [Eq. 2.43] and my two-photosystem kinetic model [Eq. 3.101] both provide good descriptions of the P-I response of all cultures of *Pavlova* sp. (Tables 5.9, 5.10 and 5.11). The simple cumulative Poisson model also provides a good description of the P-I response provided the action cross-section of photoinhibition is kept independent of that for photochemistry ($\iota_J \neq I_k$). All three models are virtually indistinguishable in terms of the shape of the final curve.

As with *Synechococcus* sp. WH 7803, setting the action cross-section of photoinhibition equal to that of photochemistry constrained the final curve in a way as to render it useless as a description of the P-I response. Unlike *Synechococcus* sp. WH 7803 the model of Megard *et al.* (1984) provided a reasonable description in the two

cultures exhibiting photoinhibition (*PA 9141* and *PA 9137*). This model fails however to provide a realistic description in the absence of photoinhibition as with *PA 9133*.

5.2. THE COMPARATIVE P-I RESPONSE TO POLYCHROMATIC WHITE, GREEN AND BLUE IRRADIANCE.

Restricting the spectral distribution of the incident irradiance to predominantly blue or green wavelengths resulted in a substantial reduction in the incident PFD, yielding maximum PFDs of 200 and 120 $\mu E\ m^{-2}\ s^{-1}$ for blue and green polychromatic irradiance respectively. Regrettably, these PFDs were insufficient to cause photoinhibition thereby precluding any attempt to assess the spectral response of this process. Nevertheless the P-I responses of all three picoplankton clones exhibited significant differences in their P-I response up to the point of saturation, differences that could be correlated to the spectral distribution of the incident irradiance.

Two characteristics of the P-I response of *any single clone* were strongly dependent upon the spectral distribution of the incident irradiance. Firstly, the geometrical form of the P-I response at low PFDs (0 - 25 $\mu E\ m^{-2}\ s^{-1}$) was one of two types. In some cases, photosynthesis simply increased linearly such that the slope of the P-I curve remained constant from zero irradiance up to the onset of saturation, usually at a PFD around 80 - 200 $\mu E\ m^{-2}\ s^{-1}$. Alternatively, the P-I response assumed a sigmoid shape. The P-I response started out parallel to the abscissa at low PFDs, with the gradient gradually increasing to the point where the light-limited photosynthetic rate was attained, usually at a PFD of about 10 - 25 $\mu E\ m^{-2}\ s^{-1}$. Above this point the photosynthetic rate increased linearly as previously described up to the onset of saturation at PFDs of 80 - 200 $\mu E\ m^{-2}\ s^{-1}$.

Secondly, the rate of light-limited photosynthesis achieved (α^B) in the three different spectral distributions (white, green and blue) were always significantly different. Within any single clone the relative capacity to utilize photons of different wavelengths could be attributed to the photosynthetic pigment complement of that clone. The relative degree to which photons of different wavelengths (white, green or blue) promoted photosynthesis also differed *between the three different clones*. The utility of the different spectral distributions varied in accordance with the differences in their photosynthetic pigmentation. The spectral distribution yielding the greatest values of α^B was species-specific and was unaffected by growth PFD.

Although the maximum saturating rate of photosynthesis in either green or blue light was only achieved in few cultures, several blue and green P-I responses exhibited curvature at PFDs of 80 - 200 $\mu E\ m^{-2}\ s^{-1}$ indicative of the onset of saturation. In these cases the predicted maximum photosynthetic rate was similar to that of the white P-I response implying that P_m may be considered spectrally independent.

5.2.1. Modelling curvature at low PFDs.

The positive curvature observed in many of the P-I responses at PFDs below 25 $\mu E\ m^{-2}\ s^{-1}$ was empirically modelled in terms of a respiratory reduction in photosynthesis. The hypothetical "net" P-I response was envisaged as passing through the abscissa to intersect with the ordinate at some negative assimilation value corresponding to respiration. The observed positive curvature of the P-I response is interpreted simply as a consequence of the inability of the ^{14}C method to quantify negative assimilation.

In practice, the positive curvature of the P-I response at low PFDs was quantified by the subtraction of a saturating function from the function chosen to describe photosynthesis. This saturation function represents the fraction of the maximum respiration rate (R_m) that must be subtracted from the hypothetical "gross" photosynthetic rate to yield the assimilation rate measured by ^{14}C uptake. At PFDs above 25 $\mu E\ m^{-2}\ s^{-1}$ the ^{14}C method was assumed to measure "net" photosynthesis and the relevant quantity to be subtracted corresponds to the maximum respiration rate (R_m). Below this threshold the quantity subtracted is less than R_m. The specific formulation arbitrarily selected to represent this saturating function was the empirical 3-parameter formulation of Bannister (1979) [Eq. 2.12].

For P-I responses that lacked any tendency to saturate at high irradiances (80 - 200 $\mu E\ m^{-2}\ s^{-1}$), the overall P-I response could be described by the combination of a simple linear expression for photosynthesis and a negative saturation function for respiration:

$$P^B = \alpha^B I - \frac{R_m{}^B\, \alpha^B I}{\left[(R_m{}^B)^n + (\alpha^B I)^n \right]^{1/n}} + C \qquad ...(5.1)$$

In Eq. 5.1, a^B represents the light-limited rate of photosynthesis, $R_m{}^B$ is the maximum rate of photosynthesis and C is a constant (see Figure 5.11). By setting the initial slope of the respiration function Eq. 5.1 equal to the light-limited photosynthetic rate ($\partial R/\partial I = \alpha^B I$) ensures that the initial slope is zero when $I = 0$ and is always positive at $I > 0$. The parameter n describes the convexity of the curve and represents the abruptness with which the gradient of the P-I curve increases from zero ($I = 0$) to that describing the light-limited rate of photosynthesis (α^B). The constant C removes the constraint

requiring the curve to pass through the origin at zero PFD. Eq. 5.1 requires a total of 4 parameters to define it (α^B, R_m^B, n and C).

In several cases the P-I response was sigmoid in appearance as a result of both curvature at low PFDs (0 - 25 μE m^{-2} s^{-1}) due to respiratory effects and also at higher PFDs (80 - 200 μE m^{-2} s^{-1}) due to the onset of saturation of photosynthesis. P-I responses of this type were modelled as the sum of two saturating functions, one positive representing photosynthesis and the other negative representing respiration. Again the formulation of Bannister (1979) was chosen for both functions yielding the expression:

$$P^B = \frac{P_m^B \alpha^B I}{\left[(P_m^B)^m + (\alpha^B I)^m\right]^{1/m}} - \frac{R_m^B \alpha^B I}{\left[(R_m^B)^n + (\alpha^B I)^n\right]^{1/n}} + C \qquad ...(5.2)$$

As before, setting the initial slope of the negative respiration function equal to the initial slope of the photosynthesis function ($\partial R/\partial I = \alpha^B I$) ensures that the initial slope of the P-I response at $I = 0$ is zero and is always positive at $I > 0$. Eq. 5.2 requires a total of six parameters to define it (α^B, P_m^B, m, R_m^B, n and C).

In those P-I responses exhibiting no curvature at low PFDs (0 - 25 μE m^{-2} s^{-1}) the basic formulation of Bannister (1979) was applied with the addition of a constant to relax the constraint requiring the curve to exhibit zero assimilation when the PFD is zero. The final expression becomes simply:

$$P^B = \frac{P_m^B \alpha^B I}{\left[(P_m^B)^m + (\alpha^B I)^m\right]^{1/m}} + C \qquad ...(5.3)$$

Eq. 5.3 requires four parameters to define it (α^B, $P_m{}^B$, m and C).

Choice of the appropriate formulation from Equations 5.1 to 5.3 was made by inspection. Attempts to fit an inappropriate formulation to the data generally resulted in a lack of convergence in the non-linear fitting routine and thus a failure to provide a fit.

5.2.2. Comparative Rates of Light-limited Photosynthesis (α).

The P-I responses of *Synechococcus* sp. WH 5701 under polychromatic white, green and blue light are given in Figures 5.12, 5.13 and 5.14 corresponding to cultures grown at 8 μE m^{-2} s^{-1} (*SY 9149/9150/9151*), 15 μE m^{-2} s^{-1} (*SY 9157/9158/9159*) and 70 μE m^{-2} s^{-1} (*SY 9153/9154/9155*) respectively. The pattern of light utilization is similar in all three cultures; white light is utilized with the greatest efficiency, followed by green, with blue irradiance proving to be of the least utility. The initial slopes (α^B) for all three cultures under the three different spectral distributions are given in Table 5.12. In all cases the initial slope in white light is approximately twice that in green and five to six times that attained in blue light.

The P-I responses of *Synechococcus* sp. WH 7803 to polychromatic white, green and blue irradiance are given in Figures 5.15, 5.16 ,5.17 and 5.18 corresponding to cultures grown under 7 μE m^{-2} s^{-1} (*DC 9130/9131*), 17 μE m^{-2} s^{-1} (*DC 9125/9126/9127*), 25 μE m^{-2} s^{-1} (*DC 9117/9118/9119*) and 35 μE m^{-2} s^{-1} (*DC 9121/9122/9123*) respectively. In this cyanobacterial species green light is utilized most efficiently for photosynthesis, followed by white light and lastly blue light. The initial slopes (α^B) of all four cultures in each of the three spectral distributions are given in Table 5.13. In all cases the photosynthetic rate in green light is approximately twice that in white light and three to four times that observed in blue light.

The P-I responses of *Pavlova* sp. (clone NEP) to polychromatic white, green and blue irradiance are given in Figures 5.19, 5.20 and 5.21 corresponding to cultures grown under 8 μE m^{-2} s^{-1} (*PA 9141/9142/9143*), 12 μE m^{-2} s^{-1} (*PA 9137/9138/9139*) and 45 μE m^{-2} s^{-1} (*PA 9133/9134/9135*) respectively. As with both cyanobacterial clones the pattern of light utilization was identical in all three cultures. In all cases blue light promoted greater photosynthesis than white light which in turn is greater than under green light. The initial slopes of the P-I responses for all three cultures in the three different spectral distributions are given in Table 5.14. The differences were much less marked than in the case of the cyanobacterial clones. Photosynthetic rates in blue light were approximately 20% greater than in white light and 25 - 30% greater than that under green light.

These experiments demonstrate that the spectral ranking is different for each clone and relates to the spectral characteristics of the photosynthetic pigments present.

5.2.3. Spectral Nature of Respiratory Curvature at Low PFDs.

The presence and magnitude of the P-I response curvature at PFDs below 25 μE m^{-2} s^{-1} was also spectrally dependent. The occurrence of this curvature is evident from inspection of Figures 5.12 to 5.21 and from the success of the different formulations in describing the P-I responses to white, green and blue irradiance (Tables 5.12 to 5.14).

In *Synechococcus* sp. WH 5701 a slight curvature was evident in all cultures when the P-I response was determined under all three spectral distributions (Figures 5.12, 5.13 and 5.14). Curvature was greatest under green light, least under white light while the effect was intermediate in P-I responses determined under blue light. In *Synechococcus* sp. WH 7803 the presence of curvature was very marked in all cultures

incubated under green light. In contrast, those P-I responses determined under both blue and white irradiance showed no evidence whatsoever of any curvature at low PFDs (Figures 5.15, 5.16, 5.17 and 5.18). In *Pavlova* sp. (clone NEP) curvature was evident in all cultures and under all three spectral distributions. There appeared a distinct trend where the degree of curvature increased as the growth irradiance increased (Figures 5.19, 5.20 and 5.21).

5.3. SPECTRAL PROPORTIONALITY OF THE P-I RESPONSE

The fact that the P-I responses in green and blue polychromatic irradiance did not extend to include photoinhibition and in some cases not even to saturation severely constrains efforts to demonstrate proportionality. The data available thus only permits examination for proportionality up to the point of light saturation. For all P-I models the linear region of the P-I response, describing the rate of photosynthesis at light-limiting irradiances, guarantees that this region of the curve will exhibit proportionality under different spectral distributions. The remaining regions of the curve which determine whether proportionality exists throughout the entire measured P-I response are i) the convexity of the transition from light-limited to light-saturated photosynthesis and ii) the presence of respiratory-linked curvature at low PFDs.

Where a 2-parameter P-I formulation is applied to spectral P-I responses the responses are intrinsically proportional to one another because the curvature is an inherent geometric property of all such formulations. This was the case for the exponential model applied to the P-I curves of *Chlorella* described in Chapter 3.7.1. The general failure of 2-parameter models to quantitatively describe the P-I response of picoplankton (Chapter 5.1) requires that an independent third parameter be added (Tables

5.1 to 5.4 and 5.6 to 5.11). For proportionality to be retained this third parameter must remain constant in all spectral P-I responses.

Comparisons of the convexity of the P-I response under white light indicate that this parameter is certainly variable from one species to another and also within the same species if cultures are grown at different PFDs (Tables 5.1 to 5.4 and 5.6 to 5.11). Comparing the convexity of P-I responses determined for the *same clone* grown under the *same growth irradiance* but incubated in *different spectral distributions* is restricted by the number of P-I responses in green and blue light with sufficient data points to accurately quantify this curvature.

None of the green or blue P-I responses in *Synechococcus* sp. WH 5701 display any curvature indicative of light saturation so comparisons in this species are impossible (Figures 5.12 to 5.14; Table 5.12). For *Synechococcus* sp. WH 7803, a tendency toward saturation is evident in both green and blue P-I responses although the comparison is limited because complete saturation is never attained (thereby reducing the accuracy of the parameter estimates). Nevertheless the indication is that the convexity of the P-I response differs according to the spectral distribution of the irradiance field (Figures 5.15 to 5.18; Table 5.13). The parameter *m* describing the degree of curvature varies by up to a factor of 2 in P-I curves of the same culture determined under different spectral distributions. The differences are most pronounced in the two cultures grown at the highest PFDs, 25 and 35 $\mu E\ m^{-2}\ s^{-1}$, where the P-I response in green light exhibits a sharper transition from light-limited to light-saturated photosynthesis compared to that in both white and blue light (Figures 5.17 and 5.18). Variation in curvature is much less marked in *Pavlova* sp. (clone NEP). In the two cultures grown under the lowest PFD (8 and 12 $\mu E\ m^{-2}\ s^{-1}$), the P-I responses in both green and blue irradiance yield a sharper

transition from light-limited to light-saturated photosynthesis than the P-I response to white irradiance (Figures 5.19 to 5.21; Table 5.14).

The presence or absence and spectral dependency of curvature at low PFDs (described in Section 5.2.3) means that complete proportionality among different spectral P-I responses cannot occur. The need to choose different mathematical formulations to achieve a successful regression fit indicates that differences in the curves are significant and cannot be overlooked (Tables 5.12 to 5.14). Similarly, the spectral dependency of the convexity of the P-I response as it approaches light saturation is also significant. However, up to the point of saturation (at around 200 $\mu E\ m^{-2}\ s^{-1}$) the P-I response is dominated by an extended region where photosynthesis is a linear function of PFD. This significantly reduces the importance of spectral differences in curvature such that P-I responses determined under different spectral distributions are "macroscopically" proportional to one anotner. The macroscopic proportionality between P-I responses is evident when the rate of photosynthesis is plotted as a function of the logarithm of the PFD as discussed in Chapter 3.2.2 and 3.3.2 and illustrated in Figure 3.1.

The general proportionality in the P-I responses of *Synechococcus* sp. WH 5701 determined in white, green and blue polychromatic irradiance is evident from the semi-logarithmic plots given in Figures 5.22(a) - 5.22(d) for cultures grown under 8, 15, 27 and 70 $\mu E\ m^{-2}\ s^{-1}$. The horizontal displacement of the P-I response along the x-axis corresponds to the proportionality constant relating the response in each spectral distribution. The displacement between the extreme responses in white and blue polychromatic irradiance is approximately 0.67 $\log_{10}$ units corresponding to a blue/white ratio of approximately 0.215. This corresponds closely to the $\alpha^B_{blue} / \alpha^B_{white}$ ratio obtained by numerical curve-fitting procedures (Tables 5.12 and 5.19). Similarly, the horizontal displacement between the P-I response in green compared to white

polychromatic irradiance is approximately 0.35 $\log_{10}$ units corresponding to a factor of 0.45 in agreement with the $\alpha^B_{green} / \alpha^B_{white}$ ratio (0.51) obtained by curve fitting (Table 5.12 and 5.19).

The same correspondence occurs in the polychromatic spectral P-I responses *Synechococcus* sp. WH 7803 grown at different PFDs (Figure 5.23). In all four cultures the horizontal displacement of the P-I response in blue irradiance compared to that in green irradiance is approximately 0.53 $\log_{10}$ units corresponding to a proportionality factor of 0.3. This is virtually identical to the $\alpha^B_{blue} / \alpha^B_{green}$ ratio (0.28) determined from numerical curve-fitting analysis (Tables 5.13 and 5.19). Similarly, the P-I response in white light is horizontally displaced by 0.15 $\log_{10}$ units from that in blue light indicating a proportionality factor of 0.71 in close agreement to the $\alpha^B_{blue} / \alpha^B_{white}$ ratio (0.62) derived from curve-fitting (Table 5.13 and 5.19).

Overall proportionality between the spectral P-I responses was also evident in *Pavlova* sp. (clone NEP). The overall similarity of the P-I responses under all three different spectral distributions was particularly notable in this picoplanktonic clone resulting in a very reduced horizontal displacement between the various curves when plotted semi-logarithmically (Figure 5.24). The horizontal displacement between the P-I response in blue irradiance compared with that in white or green irradiances was only 0.17 $\log_{10}$ units, the equivalent of a proportionality factor of 1.5. As with both cyanobacteria this value is in general agreement with differences in the $\alpha^B_{blue} / \alpha^B_{white}$ (1.55) and $\alpha^B_{blue} / \alpha^B_{white}$ (1.72) ratios determined from the non-linear regression analyses (Tables 5.14 and 5.19).

The overall conclusion is that the P-I responses determined in polychromatic irradiances of different spectral composition may be considered to be generally

proportional to one another. The proportionality constant is essentially that which relates the light-limited rates of photosynthesis (α^B) in the different spectral distributions. Differences in the P-I responses in terms of the abruptness of the transition from light-limited to light-saturated photosynthesis (the basic convexity of the P-I response) and the presence or absence of (respiratory) curvature at low PFDs are largely negated by the extended linearity of the response at light-limiting PFDs. This extended linear region, which must be a feature of any P-I model attempting to accurately quantify the P-I response, dominates the geometry of the P-I response up to the point of saturation and is responsible for proportionality of P-I responses determined under different spectral distributions.

5.4. P-I PARAMETERS AND GROWTH IRRADIANCE.

Examination of the P-I responses of each of the three picoplankton clones reveals that the form of the entire P-I response up to PFDs of 2000 $\mu E\ m^{-2}\ s^{-1}$ is strongly influenced by the PFD under which the culture was grown. Interestingly, the observed pattern of the variation is not the same in each of the species examined. The most obvious differences in the P-I response are the maximum rate of photosynthesis attained, the extent of photoinhibition if present and the light-limited rate of photosynthesis. As discussed in Chapter 2, the maximum rate of photosynthesis (either potential P_s^B or realized P_m^B) and the light-limited rate of photosynthesis (α^B) combine to define what may be considered the optimal irradiance for growth ($I_k = P_m^B / \alpha^B$ or P_s^B / α^B). In comparing P-I model parameters in the various cultures it is important to remember that photosynthesis measurements were normalized to *in vivo* absorption at 675 nm corresponding to the red absorption peak of chlorophyll *a*.

The P-I response of the phycocyanin-containing cyanobacterium *Synechococcus* sp. WH 5701 in polychromatic white irradiance was distinct in that no indication of photoinhibition was present in any of the P-I responses. However, the maximum photosynthetic rate (P_m^B or P_s^B) did vary significantly with growth PFD (Figures 5.1, 5.2, 5.3 and 5.4). Table 5.15 lists the comparative P-I response parameters estimated from the best empirical and rational P-I models. The trend was toward greater maximum rates of photosynthesis with increasing growth PFD. Cells grown at 70 μE m^{-2} s^{-1} had maximum photosynthetic rates of 27 μmol C m^{-2} hr^{-1} compared to a P_m^B of 14 μmol C m^{-2} hr^{-1} in cells grown at 8 μE m^{-2} s^{-1}, a difference of almost a factor of 2.

In contrast to P_m^B, the initial slope of the P-I responses (α^B) describing the light-limited rates of photosynthesis remained virtually constant (≈ 0.1 μmol C m^{-2} hr^{-1} (μE m^{-2} s^{-1})$^{-1}$) despite the ten-fold differences in growth PFD. The combination of increasing P_m^B and constant α^B results in a progressive increase in the optimal PFD I_k from 120 to 230 μE m^{-2} s^{-1} with increase in growth PFD.

The abruptness of the transition from light-limited to light saturated photosynthesis (the convexity of the P-I curve) also increases with increasing growth irradiance as evidenced by the values of the parameters m and χ in both empirical and rational P-I models. The parameter m in my empirical model increased from 3.0 to 3.9 while in Bannister's (1979) model the change was even more pronounced, from 3.0 to 5.26 (Table 5.15). The suite of changes in P-I parameters in *Synechococcus* sp. WH 5701 is illustrated in Figure 5.25 and constitutes a uniform and systematic trend in relation to the growth PFD.

The relationship between the P-I response parameters and growth PFD were quite different in the phycoerythrin-containing cyanobacteria *Synechococcus* sp. WH 7803

(Figures 5.5, 5.6 and 5.7). Increases in growth PFD produced decreased values of both α^B and P_m^B. According to the empirical model described in Chapter 3.4.1, the maximum rate of photosynthesis dropped from 7.3 μmol C m^{-2} hr^{-1} to 2.5 μmol C m^{-2} hr^{-1} when the growth PFD was doubled from 17 to 35 μE m^{-2} s^{-1}. Similarly, the initial slope of the P-I response (α^B) decreased from 0.063 μmol C m^{-2} hr^{-1} (μE m^{-2} s^{-1})$^{-1}$ to 0.029 μmol C m^{-2} hr^{-1} (μE m^{-2} s^{-1})$^{-1}$ over the same range of growth PFDs (Table 5.16). The reduction in P_m^B is more pronounced than that in α^B resulting in a net *decrease* in the optimal PFD I_k from 120 μE m^{-2} s^{-1} to 85 μE m^{-2} s^{-1} as growth PFD *increased*, contrary to the expected photoadaptive trend.

Predictably, photoinhibition was most pronounced in cultures grown under low PFDs and diminished in effect as the growth PFD increased. The negative slope (β^B) declined from 3.53 x 10^{-3} μmol C m^{-2} hr^{-1} (μE m^{-2} s^{-1})$^{-1}$ in cells grown at 17 μE m^{-2} s^{-1} to 0.51 x 10^{-3} μmol C m^{-2} hr^{-1} (μE m^{-2} s^{-1})$^{-1}$ in cells grown at 35 μE m^{-2} s^{-1}. Despite this reduction in the negative slope of the P-I response, the PFD corresponding to the onset of photoinhibition (I_j in the new empirical model) systematically *decreased* with *increasing* growth PFD from 667 μE m^{-2} s^{-1} to 18 μE m^{-2} s^{-1} because of the steady reduction in P_m^B with increasing growth PFD. The value of P_t^B (= $-\beta I_t$), the expected potential photosynthetic capacity determined by extrapolating the photoinhibitory decrease in photosynthesis to zero PFD, systematically decreases from 9.65 μmol C m^{-2} hr^{-1} to 2.51 μmol C m^{-2} hr^{-1} as growth PFD increases from 17 to 35 μE m^{-2} s^{-1}.

While both α^B and β^B decrease with increasing growth PFD, the major decrease observed in P_m^B produces a decrease in both the optimal irradiance I_k and the PFD marking the onset of photoinhibition I_j. The abruptness of the transition from light-limited to light-saturated photosynthesis also increases with increasing growth PFD. The convexity parameter m in my empirical model increases from 1.7 to 3 over the range of

growth PFDs. The impression given by the three P-I responses (Figures 5.5, 5.6 and 5.7) is that this results from the progressive reduction in P_i^B which increases the linear fraction of the P-I response. The suite of changes in the P-I parameters as a function of growth PFD in *Synechococcus* sp. WH 7803 are illustrated in Figure 5.26.

Growth PFD also affected the P-I response of the prymnesiophyte *Pavlova* sp. (clone NEP). The culture grown at the highest PFD (45 μE m^{-2} s^{-1}) showed no signs of any photoinhibition (Figure 5.10) while cells grown at 8 and 12 μE m^{-2} s^{-1} did exhibit a photoinhibitory decrease in photosynthetic rate (Figures 5.8 and 5.9). The PFDs corresponding to the onset of photoinhibition (I_j) in the latter two cultures were 136 and 660 μE m^{-2} s^{-1} respectively (Table 5.18). The progressively lessening effects of photoinhibition with increasing growth PFD is similar to that in *Synechococcus* sp. WH 7803.

Confusing the pattern of P-I response parameters in relation to growth PFD was the absolute maximum rate of photosynthesis (P_m^B) attained. P_m^B was 15.8 μmol C m^{-2} hr^{-1} in cells grown at 8 μE m^{-2} s^{-1}, increasing to 36.6 μmol C m^{-2} hr^{-1} in cells cultured at 12 μE m^{-2} s^{-1} and decreasing once again to 21.7 μmol C m^{-2} hr^{-1} in cells grown under the highest PFD. The light-limited photosynthetic rate (α^B) and the negative slope of photoinhibition (β^B) also showed this pattern, with β^B decreasing to zero in cells cultured at the highest irradiance (Figure 5.27). It would appear that the maximum photosynthetic rate attained effectively scales both α^B and β^B. Comparing the cultures grown at 8 and 12 μE m^{-2} s^{-1}, the reduction in α^B with decreasing PFD parallels the reduction in P_m^B with the result that the optimal PFD I_k is virtually identical in both cultures (84 compared to 86 μE m^{-2} s^{-1}). The reduction in α^B in the culture from 45 μE m^{-2} s^{-1} is greater than the reduction in P_m^B which produces an increase in the optimal PFD (I_k = 220 μE m^{-2} s^{-1}) for

this culture. The absence of any photoinhibition in this culture means that all PFDs above this I_k value may be considered optimal for photosynthesis.

As with both cyanobacterial cultures, the abruptness of the transition from light-limited to light-saturated photosynthesis in the P-I responses of *Pavlova* sp. increase with growth PFD. The parameter m in my empirical model increases progressively from 1.996 (8 μE m^{-2} s^{-1}) to 2.247 (12 μE m^{-2} s^{-1}) and finally up to 4.134 in the culture from the highest growth PFD (45 μE m^{-2} s^{-1}); as with *Synechococcus* sp. WH 5701 if the model of Bannister (1979) is used m increases to over 5 (5.43).

In summary, the geometrical parameters of the P-I response of all three picoplankton species are influenced by the PFD during growth. The pattern of change brought about by the PFD during growth differed in all three species although several trends may be discerned.

5.5. CORRELATION BETWEEN MODEL PARAMETERS IN THE WHITE P-I RESPONSE.

From the foregoing results in Section 5.4., it is clear that there are strong correlations between many of the parameters used to describe the P-I response. In those P-I responses of *Synechococcus* sp. WH 7803 and *Pavlova* sp. (clone NEP) exhibiting photoinhibition there is a strong positive correlation between α^B and β^B (Figure 5.28). In both cases the relationship between the initial slope and the negative slope due to photoinhibition appears linear (however three data points is the minimal number and more replicates and a wider range of values are required to be certain). The data are most suggestive in the case of *Pavlova* sp. where the linearity is almost perfect.

CHAPTER 6

ABSORPTION SPECTRA OF PICOPLANKTON AND NATURAL PHYTOPLANKTON ASSEMBLAGES.

6.1. ABSORPTION SPECTRA USING GF/F FILTERS.

The absorption coefficient $a(\lambda)$ is normally calculated in terms of a monochromatic collimated beam crossing an infinitesimally thin layer of the medium normal to the beam. Specifically, $a(\lambda)$ is defined as $-dI_a/Idr$ where dr is the thickness of the layer, I is the incident flux, and dI_a is the flux lost by means of absorption. To obtain the diffuse attenuation coefficient ($a^*_p(\lambda)$), the optical density recorded by the spectrophotometer must be corrected according to Eq. 4.1. Absorption measurements are first multiplied by 2.303 to convert from base 10 to Naperian logarithms and secondly divided by the appropriate pathlength. This latter quantity is calculated from the volume of liquid filtered and the clearance area of the filter (V/S). A final and more complex correction involves the parameter $\beta(\lambda)$, which may be defined as the ratio of the optical pathlength to the geometric pathlength (Butler 1962). Inclusion of the parameter $\beta(\lambda)$ arbitrarily accounts for any increases in the mean optical path length of the light rays within the filter/particle combination relative to the shortest geometric pathlength.

Determination of absorption using glass-fibre filters measures absorption in a diffuse beam of light rather than a collimated beam perpendicular to the sample (in this case the filter). The diffuse absorption coefficient $a^*_p(\lambda)$ is consequently depends upon the radiance distribution function. For perfectly diffuse light $a^*_p(\lambda)$ is enhanced by a factor of $1/\mu$, where μ is the mean cosine for diffuse light. In order to obtain an

absorption coefficient equivalent to that obtained with a collimated beam of light ($a(\lambda)$), absorption measurements must be divided by $1/\mu$. For $0 < \theta < \pi$ the mean cosine of a perfectly diffuse beam is 0.5, yielding a value of 2 for $1/\mu$. Accounting for the diffuse nature of the light source thus yields a minimal value of 2 for the parameter $\beta(\lambda)$. Additional optical properties of the filter/particle composite together with the geometrical properties of the photodetector can yield values of $\beta(\lambda)$ greater than 2.

To further complicate the accurate estimate of $a^*_p(\lambda)$, there is some empirical evidence to suggest that the parameter $\beta(\lambda)$ is not a constant but is a function of the optical density of the filter/particle composite. Optical density measurements of serial dilutions of the same algal culture deposited on glass-fibre filters reveal that the measured absorption is not a linear function of cell concentration throughout the entire range of cell concentrations, a result inconsistent with Beer's Law. Above a critical cell concentration the relationship is linear but below this threshold the measured absorption is less than expected. This deviation from a linear relation between absorption and cell concentration increases monotonically with decreasing optical density below this threshold. Figure 6.1 shows a typical plot of $a^*_p(\lambda)$ as a function of particle concentration on GF/F filters based upon *in vivo* absorbance measurements of serial dilutions of the diatom *Chaetoceros gracilis*.

The deviation from linearity evident in Figure 6.1 may be explained by a monotonic increase in $\beta(\lambda)$ with decreasing optical density. The value of $\beta(\lambda)$ is initially high at low optical density and decreases rapidly with increasing optical density to approach value of 2 asymptotically. Independent determinations of $\beta(\lambda)$ under conditions where the optical configuration is such as to permit the unambiguous differentiation of the absorption coefficient $a(\lambda)$ and the scattering coefficient $b(\lambda)$

indicate that $\beta(\lambda)$ varies inversely with optical density (Mitchell and Kiefer 1984; Bricaud 1989).

In view of the variation in $\beta(\lambda)$ at low optical densities, it was necessary to determine $a^*_p(\lambda)$ with suitably high cell concentrations on the glass-fibre filters. In practice, a curve similar to that illustrated in Figure 6.1 was constructed and the volume- (or chlorophyll-) specific absorption coefficient was estimated from the slope of the linear region of the curve.

6.2. MONOSPECIFIC PICOPLANKTON CULTURES.

The three strains of picoplankton selected for study differ substantially in their photosynthetic pigment composition and consequently in their spectral absorbance characteristics. The two cyanobacterial species, *Synechococcus* sp WH 7803 and *Synechococcus* sp. WH 5701, both represent the chlorophyll *a*-phycobiliprotein light-harvesting system. They differ in that *Synechococcus* sp. WH 7803 is a phycoerythrin-containing strain while *Synechococcus* sp. WH 5701 lacks phycoerythrin and possesses phycocyanin as the principal phycobiliprotein. The eukaryotic representative of the picoplankton, *Pavlova* sp. (clone NEP), is a prymnesiophyte and possesses a photosynthetic pigment system characteristic of the "Chromophytic" group which typically comprises chlorophylls *a*, c_1 and c_2 together with the carotenoid fucoxanthin (Jeffrey 1980).

6.2.1. Principal spectral characteristics of the *in vivo* absorption spectra.

The *in vivo* absorption spectra of *Synechococcus* sp. WH 7803 (formerly "DC-2") from all cultures exhibited maxima at 438, 498, 542 and 678 nm (Figure 6.2). Peaks at 438 and 678 nm are attributable to chlorophyll *a* while those at 498 and 542 nm are due to phycoerythrin. Phycoerythrin is the major light-harvesting phycobiliprotein in WH 7803. The 498 nm peak arises from the PUB chromophore while that at 542 nm is due to the PEB chromophore. The carotenoids zeaxanthin and β-carotene also contribute to absorption in the 470-490 nm region. A minor peak at 626 nm is also discernable and may represent phycocyanin. In all cultures of WH 7803 an absorption minimum occurred at 604 nm.

The absorption spectra of *Synechococcus* sp. WH 5701 (formerly "Syn") grown under all irradiance levels displayed absorption maxima at 438, 622 and 678 nm (Figure 6.3). The peaks at 438 and 678 nm are attributable to chlorophyll *a* while that at 622 is due to phycocyanin. Phycocyanin is the major light-harvesting phycobiliprotein in WH 5701. A distinct shoulder is evident in all cultures at 492 nm and may be assigned to the carotenoid pigments zeaxanthin and β-carotene. Absorption minima occurred at 534 and 654 nm.

The absorption spectra of *Pavlova* sp. (clone NEP) was that of a typical chromophyte (Figure 6.4). *In vivo* absorption maxima occurred at 436 and 672 nm corresponding to the absorption peaks of chlorophyll *a*. The amplitude of the Soret band (438 nm) was slightly less than twice that at 672 nm. A minor peak was evident at 632 nm and is usually attributed to chlorophyll *c*. A narrow shoulder between 475 and 550 nm may be attributed to absorption by the light-harvesting carotenoid fucoxanthin. An absorption minimum occurred at 598 nm.

All three *in vivo* absorption spectra typified the characteristic absorption spectra of their respective taxonomic groups.

6.2.2. Absolute values of a_p - Dependence upon volume filtered.

Computation of absolute values of $a^*_p(\lambda)$ for each culture was based upon application of Eq. 4.1 to a series of glass-fibre filters. Each series represented a concentration gradient of particles generated by filtering increasing volumes of culture onto separate GF/F filters. The term (V/S) in the denominator of Eq. 4.1 accounts for the difference in volume filtered and so identical estimates of $a^*_p(\lambda)$ are expected from each filter if the parameter $\beta(\lambda)$ is a constant. Estimates of $a^*_p(\lambda)$ were initially computed with $\beta(\lambda)$ assigned a value of 2 (to provide a correction for the diffuse nature of the incident light beam). The estimates of $a^*_p(\lambda)$ derived from the concentration series of each culture were inversely correlated with the actual volume of culture filtered. For all wavelengths the estimated value of $a^*_p(\lambda)$ decreased asymptotically to some minimum value as the concentration of particles on the filter increased.

Figure 6.5 illustrates this decline in the estimated value of $a^*_p(\lambda)$ with increasing filtration volume in *Synechococcus* sp. WH 7803 for the culture grown at 17 $\mu E\ m^{-2}\ s^{-1}$ (culture DC 24). Similar results were found for all four cultures of WH 7803. Diffuse absorption coefficients for six wavelengths were selected - 438, 498, 542, 604, 626 and 678 nm - corresponding to the principal absorption maxima and minima in the spectrum. The effect is most pronounced for those wavelengths where absorption is greatest such as at 438, 498, 524 and 678 nm. At absorption minima (604 and 626 nm) the effect is still present but is much reduced in absolute terms. Estimates of $a^*_p(\lambda)$ varied by a factor of

1.5 depending upon the volume of culture filtered (= optical density of the particle/filter combination).

Similar results were found for *Synechococcus* sp. WH 5701. Figure 6.6 plots the data for culture SY 52 grown at 70 μE m^{-2} s^{-1} for the selected wavelengths 438, 492, 534, 622, 654 and 678 nm. The effect is most pronounced for wavelengths corresponding to greatest absorption. In the case of WH 5701 estimates of $a^*_p(\lambda)$ decreased by a factor of 2 depending upon the volume of culture filtered.

The pattern of decreasing estimates of $a^*_p(\lambda)$ with increasing quantities of material on the glass fibre filter was also repeated for all cultures of the prymnesiophyte *Pavlova* sp. (clone NEP). Figure 6.7 shows the data for the culture PA 36 grown at 12 μE m^{-2} s^{-1} which is typical. The wavelengths selected are 436, 598, 632 and 672 nm corresponding to the principal absorption maxima and minima in the absorption spectrum of this strain. Estimates of $a^*_p(\lambda)$ decreased by a factor of 2 with increasing volumes of culture filtered.

The consistent trend with all picoplankton cultures is one of decreasing estimates of volume-specific absorption $a^*_p(\lambda)$ with increasing quantities of material on the glass-fibre filter, that is, with increasing optical density. Such a decrease is consistent with the idea that the parameter $\beta(\lambda)$ is dependent upon the optical density of the sample.

6.2.3. Dependence of *in vivo* absorption spectra upon growth PFD.

No variation in the specific wavelengths marking maximum and minimum absorption was evident when any single picoplankton species was examined. All cultures exhibited identical absorption peaks irrespective of the intensity of the growth

PFD. Within each species there was some variation in the relative amplitude of the principal absorption peaks. This spectral variation among different cultures of the same species was correlated directly to the growth PFD. Differences in the ratios of absorption peaks attributable to the principal light-harvesting pigments were most evident in the two cyanobacterial clones while differences were much less marked in the prymnesiophyte.

In *Synechococcus* sp. WH 7803 several changes in the spectral shape of the absorption spectrum occurred with increasing growth PFD (Figure 6.8). The ratio of absorbance by the Soret band of chlorophyll *a* at 438 nm to that at 678 nm increased from 1.93 in cells grown at 17 $\mu E\ m^{-2}\ s^{-1}$ to 2.21 in cells grown at 35 $\mu E\ m^{-2}\ s^{-1}$. Such an increase in absorption in the blue region of the spectrum relative to that at 678 nm may result from increases in carotenoid content relative to chlorophyll *a* with increasing growth PFD. The ratio of absorption at 542 nm relative to that at 678 nm declined from 1.68 to 1.61 over the same range of growth PFDs. Similarly, the 542/438 nm ratio decreases from 0.85 to 0.73 (Figure 6.8). The decrease in the absorption at 542 nm, which evident even in the original spectra (Figure 6.2), implies a drop in the relative amount of phycoerythrin (PE) relative to chlorophyll *a* as the growth PFD increases. The ratio of absorption at 498 nm relative to that at 678 nm showed a consistent increase (1.52 to 1.68) for the same range of PFDs. Although in apparent conflict with the change in absorption observed at 542 nm, the increase at 498 nm may be explained by the absorption of the additional pigments other than PE. Absorption at 542 nm relative to that at 498 nm (the two peaks associated with PE absorption) decreased from 1.1 to 0.96 (Figure 6.8). Under the three lowest growth PFDs (7, 17 and 25 $\mu E\ m^{-2}\ s^{-1}$), absorption at 542 nm considerably exceeded that at 498 nm. At the highest growth PFD (35 $\mu E\ m^{-2}\ s^{-1}$) this pattern was reversed and absorption at 498 nm exceeded that at 542 nm. Absorption at 542 nm is largely due to the PEB chromophore of PE while absorption at 498 nm is due to both absorption by the PUB chromophore of PE together with

absorption by chlorophyll *a* and the carotenoids zeaxanthin and β-carotene. The change in the relative importance of absorption at 542 nm and 498 nm can be seen as a consequence of the reduction in PE relative to other pigments. Other pigments that absorb at 498 nm and whose relative contribution might increase at higher PFDs include the carotenoids zeaxanthin and β-carotene.

Similar spectral changes were observed in *Synechococcus* sp. WH 5701 (Figure 6.9). The ratio of absorbance at 438 nm relative to that at 678 nm increased from 1.61 to 1.80 as the growth PFD increased from 8 to 70 μE m^{-2} s^{-1}. Absorbance by the blue shoulder at 492 nm also increased relative to the absorbance at 678 nm with increasing growth PFD such that the 492/678 ratio increased from 0.90 to 1.04. Both of these changes suggest an increase in the amount of carotenoid absorption relative to that of chlorophyll *a* with increasing PFD. The relative absorption of the phycobiliprotein phycocyanin relative to chlorophyll *a* also showed a monotonic change with increasing growth PFD (Figure 6.3). Absorption at 622 nm relative to that at 678 nm progressively decreased from 1.04 to 0.87. Similarly, the ratio of absorption at 622 nm relative to that at 435 nm decreases from 0.65 in cells grown at 8 μE m^{-2} s^{-1} to 0.48 in cells grown at 70 μE m^{-2} s^{-1} (Figure 6.9). This decrease in absorption at 622 nm relative to that at both 678 and 438 nm indicates that the relative absorption of phycocyanin decreases as growth PFD increases.

The form of the absorption spectrum in *Pavlova* sp. (clone NEP) was generally conservative over the range of growth PFDs examined (8 to 45 μE m^{-2} s^{-1}), and exhibited only minor changes in spectral character (Figure 6.4). The ratio of absorption at the two principal peaks (436 nm relative to 672 nm) was identical (1.70) at both growth PFD extremes while the culture grown at 12 μE m^{-2} s^{-1} had a 436/672 nm ratio of 1.5 (Figure 6.10). In contrast, the ratio of absorption at the minimum at 598 nm relative to the 672

nm absorption maximum were almost identical (0.32 and 0.34) in the cultures grown at 12 and 45 $\mu E\ m^{-2}\ s^{-1}$, while that of the culture grown at 8 $\mu E\ m^{-2}\ s^{-1}$ was significantly higher (0.43) (Figure 6.10). This suggests that the culture grown at the lowest PFD possesses pigments in addition to chlorophyll *a* that are responsible for providing the additional absorption at 592 nm. These pigments may also have contributed to the 436 nm absorption peak in this culture thereby elevating the 436/672 nm ratio to that observed in the culture grown at the highest PFD.

In general, all three picoplankton cultures exhibited spectral changes in their respective absorption spectra that could be correlated to growth PFD. This plasticity in the spectral form of absorption in response to the growth PFD has important implications for the modelling of photosynthesis in terms of both photon wavelength and flux density.

6.3. NATURAL PHYTOPLANKTON ASSEMBLAGES.

The *in vivo* absorption spectra of oceanic particulate material collected from diverse locations and depths were remarkably uniform in spectral form. Quantitative estimates of absolute diffuse absorption coefficients from the particulate material retained upon GF/F filters were complicated by optical effects linked to the particle concentration on the filter.

6.3.1. Principal spectral characteristics of the *in vivo* absorption spectra.

The *in vivo* absorption spectra of particulate material collected from locations as diverse as the Eastern Canadian Arctic and the subtropical Sargasso Sea were all very uniform in their spectral form. In general, a distinct absorption maximum was present at

676 nm in all water samples in which there was fluorimetrically-detectable concentration of chlorophyll. This absorption peak may be assigned to absorption by chlorophyll *a*. The wavelength region between 550 and 650 nm was consistently low in absorption. Particulates of all samples absorbed strongly between the wavelengths of 400 and 520 nm, with absorption increasing progressively toward the shorter wavelengths. In waters containing significant quantities of chlorophyll (generally > ≈ 2-3 mg Chl m^{-3}), a distinct absorption maximum was evident around 435 nm, the wavelength corresponding to the Soret band of chlorophyll *a*. In waters containing less than ≈ 2-3 mg Chl m^{-3} no distinct absorbance peak was present although the rise in absorbance with decreasing wavelength frequently displayed a shoulder between 475 and 500 nm. Clear regional differences in the proportion of the particulate material attributable to phytoplanktonic cells and the taxonomic and size composition of this fraction were notable and such differences could be correlated to several general features of the absorption spectrum.

In the eastern Canadian Arctic microscopic examination revealed the particulate material to be dominated by phytoplankton and organic detrital particles that were retained by Nuclepore® filters of 3 μm porosity. The Arctic phytoplankton assemblages examined were dominated by large diatoms such as *Chaetoceros* spp., *Thalassiosira* spp., *Fragilaria* spp. and *Nitschia* spp. and coccolithophorids (J. Trotte pers. comm.). The particulate material retained from whole water samples exhibited a distinct absorbance maximum at 676 nm and in some cases a second peak was evident at 435 nm. Absorbance at 435 nm was generally 2-3 times that at 676 nm. An absorption shoulder was frequently present between 475 nm and 500 nm and absorption at these wavelengths may be attributed to carotenoid accessory pigments such as fucoxanthin. Figure 6.11 shows the *in vivo* absorption spectra of six phytoplankton assemblages collected from different Arctic oceanographic stations characterized by varying chlorophyll concentrations. The location of these stations is indicated in Figure 4.2. The presence of

a distinct chlorophyll *a* maximum at 435 nm in whole water samples is only evident in cases where the chlorophyll *a* concentration exceeds ≈ 2-3 mg Chl m^{-3}.

In contrast, the absorption spectra of particles passing a 3 μm or 1 μm porosity Nuclepore® filter showed insignificant absorbance at 676 nm. This small size fraction absorbs most strongly in the blue region of the spectrum, with absorbance increasing exponentially with decreasing wavelength and no indication of a shoulder around 435 nm that could be ascribed to chlorophyll *a*. The lack of any significant absorption at either 676 nm or 435 nm implies that chlorophyll makes a very small contribution to absorbance in the < 1 μm size fraction. The absorption properties of the < 1 μm size fraction closely resembles that attributed to tripton (Bricaud *et al.* 1981; Kirk 1980, 1983). The absorption spectra of particulates <3 μm were very similar to that of the < 1 μm fraction but contained traces of chlorophyll as indicated by a minor peak at 676 nm.

In most cases the absorption spectrum of the particulates of diameter > 1 μm, determined by subtraction of <1 μm absorption from that of the total particulates, was typical of chlorophyll-containing particulates (Figure 6.11). Removal of the absorption component attributable to particles < 1 μm in diameter left a spectrum with an increasingly discernable absorption peak at 435 nm, with a significant reduction in the rate of increasing absorption at shorter wavelengths, with in some cases even a reduction in absorbance below 435 nm. Microscopic examination of the > 1 μm size fraction showed that this fraction was dominated by phytoplanktonic biomass with little organic debris.

The increasing contribution of non-chlorophyllous particulates to total absorption in waters with low concentrations of chlorophyll is apparent from comparisons of the spectral curves in Figure 6.11. In water samples with high chlorophyll concentrations

such as # 4053 (Stn. 116, 30 m) and # 8730 (Stn. 73, 10 m), the contribution of < 1 μm particulates to total absorption is minimal with the only significant contribution occurring at the shorter blue wavelengths. As the chlorophyll concentration of the sample decreases the proportion of the total absorption attributable to the < 1 μm fraction steadily increases and the shape of the total particulate spectrum becomes more like that of tripton as in # 4059 (Stn. 116, 40 m) and # 4052 (Stn. 116, 10 m) in Figure 6.11.

Similar absorption spectra were obtained from more southerly stations in the eastern North Atlantic including the Sargasso Sea. These stations are more typical of the open ocean and characteristically contain < 1 mg Chl m^{-3}. In many cases chlorophyll concentrations decrease to less than 0.1 mg Chl m^{-3}. Figure 6.12 shows the particulate absorption spectra determined from the chlorophyll maximum at two representative stations in the eastern North Atlantic (Stns. 17 and 23 in Figure 4.3). Chlorophyll concentrations at Station 17 (29° 50.0′ N, 77° 18.9′ W) and Station 23 (35° 37.2′ N, 75° 13.6′ W) were 0.26 and 0.57 mg Chl m^{-3} respectively. Station 17 is typical of the oligotrophic eastern Sargasso Sea and Station 23 is representative of continental slope waters. Uniform chlorophyll concentrations were present throughout the mixed layer and sample depths (100 m and 60 m respectively) correspond to the base of the mixed layer in both cases.

Both spectra are similar to those described for Arctic waters of comparably low chlorophyll concentration. There is a distinct peak at 676 nm, a region of low absorption between 550 nm and 650 nm and an exponential increase in absorption at wavelengths shorter than 550 nm. For all water samples containing chlorophyll concentrations of this order of magnitude, the absorption spectrum was consistently dominated by the shortwave absorption, absorbance values at 400 nm were frequently ten times that at 676 nm. The relative magnitude of the absorption peak at 676 nm was directly related to the

chlorophyll concentration of the water sample; the lower the chlorophyll concentration the greater the relative magnitude of absorption at the shorter wavelengths and the greater the estimate of the chlorophyll-specific absorption cross-section. As with low chlorophyll samples from Arctic waters, the exponential increase in absorption at shorter wavelengths revealed no sign of any peaks or shoulders that could be unambiguously ascribed to the Soret band of chlorophyll *a*.

Absorption spectra of particulates were very uniform in spectral shape in samples collected from different depths throughout the mixed layer at many stations. This consistency is exemplified by the *in vivo* absorption spectrum of total particulates from depths of 5 and 80 m from Station 21 (Figure 6.13). Judging from vertical profiles of temperature and σ_θ these depths correspond to the top and bottom of the mixed layer. Chlorophyll concentrations were virtually identical in both samples (0.39 and 0.46 mg Chl m^{-3} respectively) as was the magnitude of the *in vivo* absorption spectra (0.0223 and 0.0189 m^2 mg Chl^{-1}) at 676 nm.

Differences in the *in vivo* absorption spectrum between total particulates and the particulates passing a 3 μm Nuclepore filter were also minimal at all oligotrophic stations characterized by low biomass. This emphasizes the importance of the small size fraction in contributing to the absorption spectrum of the whole water sample. An example is particulate material collected from the chlorophyll maximum at the base of the mixed layer (100 m) at Station 15 (26° 41.7′ N, 73° 39.4′ W) in the Sargasso Sea (Figure 6.14). The chlorophyll concentration at this biomass peak was 0.37 mg Chl m^{-3}, typical of values for the oligotrophic open ocean. In terms of spectral shape the absorption spectra of material passing a 3 μm Nuclepore filter is virtually identical to that of the total particulates. The only distinction is relative importance of absorption at the shorter wavelengths. Both the total particulates and particulates < 3 μm exhibit identical

chlorophyll-specific absorption cross-sections at the principal absorption peak of 676 nm (0.0255 compared to 0.0260 m^2 mg Chl^{-1}). Chlorophyll-specific absorption at wavelengths less than 550 nm relative to that at 676 nm is slightly greater in the < 3 μm particulates than the total particulates, probably attributable to increased contributions of tripton.

Microscopic examination of particulates from the oligotrophic oceans revealed the dominance of the smaller size fractions and tripton with few large cells. Material collected on 0.2 μm Nuclepore filters consisted of minute picoplankton cells with typical chlorophyll-type red fluorescence (blue excitation) in addition to cyanobacterial cells with typical yellow phycobilipigment fluorescence (green excitation). Chlorophyll-containing flagellates were also observed to be present together with much amorphous debris.

In general the oligotrophic waters with low chlorophyll biomass could be characterized by *in vivo* absorption spectra with increasingly strong absorption at shorter wavelengths. A small peak was usually detectable at 676 nm corresponding to chlorophyll *a* which constituted the sole spectral feature that could be unambiguously associated with photosynthetic pigments. Only in the dense bloom conditions found in the phytoplankton assemblages of the eastern Canadian Arctic were additional spectral characteristics evident. In these cases a second peak or shoulder was present at 435 nm corresponding to the Soret band of chlorophyll *a* and in some cases an additional shoulder at 475 nm to 500 nm was discernible which could be attributed to accessory carotenoid pigments such as fucoxanthin or peridinin.

6.3.2. Absolute values of a_p - Dependence upon particle concentration.

Estimation of diffuse attenuation coefficient $a^*_p(\lambda)$ was initially computed from Eq. 4.1 using a constant value for $\beta(\lambda)$, specifically 2.45 as suggested by Kishino *et al.* (1985). Consequently, values of a^*_p (and also a^*_{chl}) for the eastern Canadian Arctic are based upon the filtration of a constant volume of seawater through a GF/F filter. The high degree of correlation between the diffuse attenuation coefficient of particulates ($a^*_p(\lambda)$ spectrally averaged from 387.5 nm to 687.5 nm) and the chlorophyll content of the water confirms that chlorophyll-containing particulates are a major contributor to the attenuation of submarine irradiance in the eastern Canadian Arctic (Figure 6.15).

At chlorophyll concentrations greater than 1 - 2 mg Chl m^{-3} the relationship between diffuse attenuation and the chlorophyll content becomes linear as would be expected if Beer's Law applied. However at lower chlorophyll concentrations the relationship is distinctly non-linear (Figure 6.15(a)). Comparison of the absorption spectra (Figure 6.11) indicates that the contribution of non-chlorophyllous particles to total particulate attenuation increases as the chlorophyll concentration decreases. In samples where the chlorophyll concentration is < 1 mg Chl m^{-3} the spectral form implies both size fractions are dominated by non-chlorophyllous material. From this, it is unclear whether the non-linearity between diffuse absorption and chlorophyll concentration arises as a result of the decreasing *relative* contribution of chlorophyllous material at low chlorophyll concentrations or represents an increase in the parameter $\beta(\lambda)$ at low concentrations of particulate material on the filter.

The non-linearity between $a^*_p(\lambda)$ and chlorophyll concentration at low chlorophyll concentrations causes estimates of the chlorophyll-specific attenuation coefficient ($a^*_{chl}(\lambda)$) to be inversely related to the chlorophyll concentration of the water

sample (Figure 6.15(b)).. Estimates of $a^*_{chl}(\lambda)$ where the chlorophyll concentration of the sample is < 2 mg Chl·m^{-3} are particularly exaggerated. To overcome this effect an empirical equation was fitted to all the absorption data in Figure 6.15(a) in order to derive a generalized relationship between chlorophyll and attenuation for Arctic stations. The relationship was found to be well-described by the generalized hyperbolic equation:

$$a^*_p = a / [\text{Chl}] + b \cdot [\text{Chl}] + c \qquad ...(6.1)$$

where the parameter b may be interpreted as the chlorophyll-specific attenuation coefficient $a^*_{chl}(\lambda)$. The parameters a and c define the degree of curvature at low chlorophyll concentrations and the interpolated intercept (from the linear portion) on the ordinate axis respectively. Parameter a is always negative reflecting the direction of the curvature. In this formulation the parameters a and b are inherently related and all curves were fitted by non-linear regression using the algorithm of Marquardt (1963). Because the distribution of points is such that most fall in the region of the curve dominated by the linear component, the fit is weighted toward the optimum estimation of b.

Substituting a value of 2.0 rather than 2.45 for $\beta(\lambda)$ and fitting Eq. 6.1 to these corrected values of $a^*_p(\lambda)$ in Figure 6.15(a) yields a value of b of 0.0114 m^2·mg Chl^{-1} for the visible waveband spectrally averaged between 387.5 and 687.5 nm (all wavelengths equally weighted). This value is almost identical to that suggested for the mean spectral extinction coefficient k_c of PAR (0.014 ± 0.002 m^2 mg Chl^{-1}) suggested by Atlas and Bannister (1980).

Eq. 6.1 may be applied to the values of $a^*_p(\lambda)$ determined for any single wavelength or waveband to yield spectral estimates of the diffuse absorption coefficient $a^*_{chl}(\lambda)$ based upon all the samples. Figure 6.16 plots the resultant values of $a^*_{chl}(\lambda)$ for

the twelve 25 nm half-bandwidth wavebands centered from 400 nm to 675 nm (corresponding to the 12 wavebands used to determine the monochromatic photosynthetic action spectra described in Section 7.3.2.). The value determined for 675 nm waveband (0.0109 m^2 mg Chl^{-1}) is approximately half the value of k_c evaluated by Bannister (1979) for the 675 nm peak in *Chlorella pyrenoidosa* (0.020 m^2 mg Chl^{-1}) using opal glass cuvettes.

Estimating $a^*_{chl}(\lambda)$ (or $k_c(\lambda)$) by this approach poses a number of problems because each data point represents a different time and water mass (Bannister and Weideman 1984). Since the concentration of algae and non-algal absorbers and scatterers vary independently in time and space, $a^*_p(\lambda)$ need not vary linearily with chlorophyll. Consequently the assumption that the linear component of Eq. 6.1 represents the chlorophyll-specific attenuation may not be valid. Alternatively, where non-algal absorbers and scatterers do covary with chlorophyll, $\partial\, a^*_p(\lambda) / \partial\, Chl$ will over-estimate $a^*_{chl}(\lambda)$ (Kopelevich and Burenkov 1977; Bannister and Weidemann 1984). Under these circumstances the chlorophyll-specific attenuation coefficient ($a^*_{chl}(\lambda)$) derived from Eq. 6.1 will include the attenuation contribution of the non-algal absorbers and scatterers.

Results from the Arctic samples indicated several potential problems would apply to estimates of $a^*_p(\lambda)$ in open ocean samples where chlorophyll concentrations are typically < 1 mg Chl m^{-3}. At these concentrations non-chlorophyllous material represents a significant component of the absorbing material. This is borne out by the spectral nature of the *in vivo* absorption spectra (Figures 6.12, 6.13 and 6.14). Accurate estimates of $a^*_p(\lambda)$ (and consequently $a^*_{chl}(\lambda)$) necessitate that any non-linear optical effects arising from differences in the optical density of the sample be removed such that the

remaining inter-sample differences would be due solely to the relative contribution of non-chlorophyllous material.

Consequently, measurements of the particulate *in vivo* absorption spectra made in the eastern North Atlantic were performed on a graded series of sample volumes. For each water sample five to ten volumes of seawater were filtered unto separate GF/F filters. For practical reasons the graded series of volumes ranged from 250 ml to 2.5 liters. A lower limit of 250 ml was established by the requirement that the sample exhibit measurable absorption, the upper limit of 2.5 l was set by the clearance capacity of the filter. This upper limit generally corresponded to a maximum of 3 mg Chl deposited on a filter. For all open ocean stations the rate of filtration of sample through the glass-fibre filters decreased with time presumably due to progressive clogging of the filters and 2.5 l proved an empirical upper limit to the volume of seawater that could be passed through a 25 mm diameter GF/F filter. Estimates of $a^*_p(\lambda)$ and $a^*_{chl}(\lambda)$ based upon the volume of seawater filtered were then computed for each filter in the series.

Estimates of $a^*_p(\lambda)$ and $a^*_{chl}(\lambda)$ of natural seawater samples were found to depend upon the volume of seawater filtered but the relationship was not that expected from experiments with cultures (Section 6.1). For most samples the value of $a^*_p(\lambda)$ and $a^*_{chl}(\lambda)$ *increased* with increasing volume filtered approaching a final value asymptotically. In some cases a minor decrease in $a^*_p(\lambda)$ and $a^*_{chl}(\lambda)$ was detected in samples in which greater than 1.5 l had been filtered. To illustrate this effect two wavelengths were chosen, the absorption peak of chlorophyll *a* at 676 nm and the absorption shoulder at 476 nm which presumably represents both chlorophyll-carotenoid absorption together with absorption arising from tripton. The results from the chlorophyll maxima at Stations 17 (100 m) and 23 (60 m) are typical (absorption spectra given in Figure 6.12). At Station 17 (# 8563) the values of $a^*_p(\lambda)$ and $a^*_{chl}(\lambda)$ measured

at both 676 nm and 476 nm increase asymptotically (Figure 6.17). At Station 23 the increase is less marked at both wavelengths and there is some indication of a small decrease in the estimates based upon the highest volume. In both cases, the asymptotic value of $a^*_{chl}(676)$ is 0.022 m^2 mg Chl^{-1} in good agreement with the estimate of Bannister (1979).

Similar results were obtained from both the top and bottom of the mixed layer as exemplified by results from Station 21 at 5 m (# 8566) and 80 m (# 8565) in Figure 6.18. Estimates of $a^*_p(\lambda)$ and $a^*_{chl}(\lambda)$ increase with filtration volume to a little over a liter beyond which there is a gradual but definite decrease. As with all samples the estimate of $a^*_{chl}(676)$ for high volumes approaches a typical value of 0.020 m^2 mg Chl^{-1}. This pattern is also repeated when the seawater has been pre-filtered through a 3 μm Nuclepore filter to ascertain the absorption characteristics of both size fractions. Figure 6.19 illustrates the results for both total particulates and < 3 μm particulates. Estimates of both $a^*_p(\lambda)$ and $a^*_{chl}(\lambda)$ initially increase with filtration volume to some maximum and subsequently decrease asymptotically. The asymptote for $a^*_{chl}(676)$ was consistently 0.020 m^2 mg Chl^{-1} in excellent agreement with estimates of the chlorophyll-specific attenuation coefficient derived for *Chlorella* at this wavelength. Asymptotic values for $a^*_{chl}(476)$ were between 0.06 and 0.1 m^2 mg Chl^{-1} the magnitude of which will depend upon the relative contribution of non-chlorophyllous material.

The decrease in estimates of $a^*_{chl}(\lambda)$ observed in some samples at high filter volumes is analogous to the concentration effect observed with serial dilutions of culture material (Chapter 6.2.2.). As such it may be ascribed to changes in the value of $\beta(\lambda)$ with increasing optical density of the filter. In contrast, the under-estimates of $a^*_p(\lambda)$ and $a^*_{chl}(\lambda)$ obtained with low filter volumes are the inverse of that observed with culture

material. It is possible that the relationship between $\beta(\lambda)$ with optical density for ocean particulates is different than that for monospecific cultures.

An alternative explanation is that the filtration properties of the filter progressively change with increasing filtration volume such that the *effective* porosity decreases as more material becomes trapped on it. The nominal pore size of a GF/F glass-fibre filter is 0.7 μm. GF/F filters retain *Synechococcus* sp. cells which are coccoid and approximately 1.0 μm in diameter with an efficiency approaching 100%. Any particulate material initially passing through the filter would therefore have to be smaller than 1 μm. Because much of the particulate material of oligotrophic waters is small it is conceivable that a significant portion is less than 1 μm and may initially pass through the larger pores of a fresh filter. As material clogs up these pores the effective pore size decreases and a higher proportion of the total particulate fraction is successfully trapped.

CHAPTER 7

PHOTOSYNTHETIC ACTION SPECTRA AND APPARENT QUANTUM YIELDS.

7.1. LINEARITY OF LIGHT-LIMITED PHOTOSYNTHESIS.

For the purposes of computing action spectra, it is a pre-requisite that the relationship between photosynthesis and PFD be linear and that this linearity be demonstrated (see Chapter 3.3.2.). Furthermore, the range of experimental photon flux densities should be sufficient to include the entire P-I response up to the point of saturation. In practice, restricting the spectral distribution to 25 nm wavebands substantially reduced the maximum PFD attainable, particularly at blue wavelengths where the output from the tungsten-halogen light source is lowest. This restriction to low PFDs meant that the P-I relationship was not linear throughout the *entire* range of experimental PFDs in many experiments because of the presence of curvature at PFDs below 25 $\mu E\ m^{-2}\ s^{-1}$.

In many of the experiments the P-I response exhibited significant positive curvature at extremely low PFDs, with the slope of the P-I response increasing progressively with increasing PFD. At a PFD between 5 and 25 $\mu E\ m^{-2}\ s^{-1}$ the slope of the P-I response became constant and the photosynthetic rate became a linear function of PFD. This positive curvature at low PFDs was similar to that observed in white, blue and green polychromatic irradiance (Chapter 5.2) and may be interpreted as an respiratory effect upon the assimilation rate as measured by the incorporation of isotopic ^{14}C. Despite this curvature there were always a sufficient number of data points at PFDs

corresponding to the linear portion of the P-I response thereby permitting the computation of $\alpha^B(\lambda)$.

Both the light-limited rate of photosynthesis ($\alpha^B(\lambda)$) and the magnitude of curvature at low PFDs were wavelength dependent. The spectral dependency differed in each of the three picoplankton clones and in natural seawater assemblages. As described in Chapter 5.2.1. the curvature at low PFDs could be successfully modelled as a respiratory reduction in photosynthesis. In practice the P-I data obtained from incubations in monochromatic irradiance was well described by the function:

$$P^B(\lambda) = \alpha^B(\lambda)\, I(\lambda) - \frac{R_m^B(\lambda)\, \alpha^B(\lambda)\, I(\lambda)}{\left[(R_m^B(\lambda))^n + (\alpha^B(\lambda) I(\lambda))^n \right]^{1/n}} + C \qquad \ldots(7.1)$$

where $\alpha^B(\lambda)$ represents the light-limited rate of photosynthesis at wavelength λ and the second term describes the magnitude of curvature at low PFDs (see Figure 5.11).

The initial slope of the P-I response was wavelength dependent in both picoplankton cultures and natural phytoplankton assemblages. The absolute value of $\alpha^B(\lambda)$ varied by an order of magnitude across the spectrum. The spectral dependency of $\alpha^B(\lambda)$ was different in each of the three picoplankton cultures reflecting basic differences in photosynthetic pigmentation. Only in one of the picoplankton cultures, *Pavlova* sp., did the spectral dependency of $\alpha^B(\lambda)$ resemble that determined for natural seawater assemblages.

7.2. $\alpha(\lambda)$ OF MONOSPECIFIC PICOPLANKTON CULTURES.

7.2.1. *Synechococcus* sp. WH 5701 (formerly "Syn").

The action spectra of cultures of *Synechococcus* sp. WH 5701, the cyanobacterial clone containing phycocyanin as the major light-harvesting photosynthetic pigment, were all uniform in spectral shape irrespective of the growth PFD. Light-limited rates of photosynthesis were greatest at wavelengths greater than 550 nm, with maximal values of $\alpha^B(\lambda)$ occurring at 625 nm to 650 nm (Figure 7.1). At wavelengths between 425 nm and 550 nm the initial slopes of the P-I response were minimal, frequently less than 10% of the maximum value. At wavelengths above 550 nm $\alpha^B(\lambda)$ increased progressively to the maximum at 625 nm. A minor increase in $\alpha^B(\lambda)$ was evident at 425 nm and 400 nm in all four cultures.

The action spectra of *Synechococcus* sp. WH 5701 clearly demonstrate the photosynthetic participation of the phycobiliprotein phycocyanin. The major peak of the monochromatic action spectrum at 625 nm closely matches that at 622 nm of the *in vivo* absorption spectrum of phycocyanin (Figure 6.3). Also conspicuously absent from the monochromatic action spectra of *Synechococcus* sp. WH 5701 is any photosynthetic contribution attributable to absorption by chlorophyll. This is despite the fact that chlorophyll contributes significantly to absorption in this species with absorption maxima at 438 nm and 675 nm (Figure 6.3). The notable absence of chlorophyll participation in *Synechococcus* sp. WH 5701 is consistent with previous studies on cyanobacteria and results from the partitioning of the photosynthetic pigments between the two photosystems (see Chapter 8 for discussion).

When normalized to *in vivo* absorption at 675 nm, the absolute magnitude of $\alpha^B(\lambda)$ was found to be remarkably similar in all cultures irrespective of the growth PFD. Maximum light-limited photosynthetic rates were ~ 0.16 μmol C m^{-2} hr^{-1} (μE m^{-2} s^{-1})$^{-1}$ at 625 nm in all four cultures (Figure 7.1). This accords with the fact that cultures of *Synechococcus* sp. WH 5701 grown under different photon flux densities exhibited similar values of α^B in polychromatic irradiance when the same colors were compared (Chapter 5.2.2.).

The magnitude of $\alpha^B(\lambda)$ determined in monochromatic irradiance is also similar to that obtained under polychromatic irradiance when comparisons are made between the appropriate wavelengths. For example, the value of α^B determined under white irradiance is ~ 0.11 μmol C m^{-2} hr^{-1} (μE m^{-2} s^{-1})$^{-1}$ in all three cultures (SY 9149, SY 9157 and SY 9153 in Table 5.13). This value agrees closely with the value of $\alpha^B(\lambda)$ at wavelengths corresponding to the composition of white irradiance, that is a spectral average that is heavily weighted toward the red end of the spectrum. Similarly, values of α^B under green (SY 9150 and SY 9158 in Table 5.13) and blue (SY 9151, SY 9159 and SY 9155 in Table 5.13) polychromatic irradiance are also of similar magnitude to those values of $\alpha^B(\lambda)$ determined at the comparable monochromatic wavelengths (Figure 7.1).

7.2.2. *Synechococcus* sp. WH 7803 (formerly "DC-2").

The monochromatic action spectra of *Synechococcus* sp. WH 7803 reflects the photosynthetic contribution of the phycobiliprotein phycoerythrin. The wavelength dependence of $\alpha^B(\lambda)$ consisted of a single dominant maximum centered at 550 nm (Figure 7.2). Rates of light-limited photosynthesis were substantially greater between 500 nm and 600 nm compared to those above and below these wavelengths, where $\alpha^B(\lambda)$ decreased to less than 10% of the peak value at 550 nm. Like *Synechococcus* sp. WH

5701, there was a minor increase in the magnitude of $\alpha^B(\lambda)$ at wavelengths shorter than 425 nm. The major peak in $\alpha^B(\lambda)$ at 550 nm corresponds with the major absorbance peak of phycoerythrin at 542 nm (Figure 6.2).

When normalized to the *in vivo* absorption at 675 nm, maximum values of $\alpha^B(\lambda)$ attained were ~ 0.16 μmol C m^2 hr^{-1} (μE m^2 $s^{-1})^{-1}$ in cultures grown under the lowest growth PFDs (DC 9124 and DC 9116 grown under 17 and 25 μE m^{-2} s^{-1} respectively). This is of similar magnitude to that obtained for the corresponding phycocyanin maximum in *Synechococcus* sp. WH 5701 (~ 0.11 μmol C m^{-2} hr^{-1} (μE m^{-2} $s^{-1})^{-1}$). Peak values for $\alpha^B(\lambda)$ in DC 9120 grown at 35 μE m^{-2} s^{-1} were somewhat lower (~ 0.08 μmol C m^{-2} hr^{-1} (μE m^{-2} $s^{-1})^{-1}$). This difference accords with a similar reduction observed in the values of α^B determined under white, green and blue polychromatic irradiance (Chapter 5.2.2.).

Values of $\alpha^B(\lambda)$ established under monochromatic wavelengths also correspond to those determined under the different polychromatic irradiances of appropriate wavelength (Table 5.14). For example, taking the culture of WH 7803 grown under 25 μE m^{-2} s^{-1} (DC 9116/9117/9118/9119) the estimate of α^B under green polychromatic irradiance is 0.1324 (Table 5.14; DC 9118) compared to a value of 0.152 for $\alpha^B(\lambda)$ under monochromatic irradiance at 550 nm. Similarly, light-limited rates of photosynthesis in polychromatic white and blue irradiance correspond to that observed under monochromatic irradiance of appropriate wavelength, namely average $\alpha^B(\lambda)$ values obtained with strong spectral weighting toward the red and blue wavelengths respectively.

Like the cyanobacterium *Synechococcus* sp. WH 5701, the photosynthetic action spectrum of *Synechococcus* sp. WH 7803 determined under a single source of

monochromatic irradiance demonstrates the photosynthetic participation of the phycobiliprotein component (in this case phycoerythrin) with no sign of any photosynthetic contribution by photons absorbed by chlorophyll *a*. This absence is conspicuous in view of the significant *in vivo* absorption by chlorophyll in both the blue and red regions of the spectrum in *Synechococcus* sp. WH 7803 (Figure 6.2). *In vivo* absorption at the peak wavelengths of 438 nm and 678 nm is greater than or comparable to absorption by phycoerythrin at 542 nm. Like *Synechococcus* sp. WH 5701 the apparent lack of chlorophyll participation in the action spectrum of *Synechococcus* sp. WH 7803 results from the distribution of chlorophyll and phycobiliproteins between the two photosystems (see Chapter 8).

7.2.3. *Pavlova* sp. (clone NEP).

The action spectrum $\alpha^B(\lambda)$ of the prymnesiophyte *Pavlova* sp. differed significantly from those of the two cyanobacterial species. Light-limited rates of photosynthesis were maximal over a broad range of wavelengths from 400 nm to 550 nm (Figure 7.3) with a peak in $\alpha^B(\lambda)$ at 425 nm to 450 nm. A distinct shoulder is evident between 475 nm and 550 nm. A secondary peak at 675 nm is also present. Rates of light-limited photosynthesis between 575 nm and 650 nm were ~10% of peak value at 425-450 nm.

The values for $\alpha^B(\lambda)$ normalized to *in vivo* absorption at 675 nm correspond closely to those obtained in polychromatic irradiance. Peak values of $\alpha^B(\lambda)$ at 425-450 nm were generally greater than equivalent values at phycobilipigment maxima in the two cyanobacterial strains. In the culture grown at 8 $\mu E\ m^{-2}\ s^{-1}$ (PA 9140/9141/9142/9143) the maximum $\alpha^B(\lambda)$ attained was 0.20 $\mu mol\ C\ m^{-2}\ hr^{-1}\ (\mu E\ m^{-2}\ s^{-1})^{-1}$, only slightly greater than the maximum 0.15 $\mu mol\ C\ m^{-2}\ hr^{-1}\ (\mu E\ m^{-2}\ s^{-1})^{-1}$ attained by either cyanobacterium.

Cells grown at 12 μE m^{-2} s^{-1} had substantially greater light-limited rates of photosynthesis than either cyanobacteria, with $\alpha^B(\lambda)$ reaching a maximum of 1.0 μmol C m^{-2} hr^{-1} (μE m^{-2} s^{-1})$^{-1}$ at 425-450 nm. Substantially lower values of $\alpha^B(\lambda)$ characterized the culture grown at 45 μE m^{-2} s^{-1}, which had a peak $\alpha^B(\lambda)$ at 450 nm of 0.3 μmol C m^{-2} hr^{-1} (μE m^{-2} s^{-1})$^{-1}$. This pattern in the absolute values of $\alpha^B(\lambda)$ in cultures grown under different irradiances concurs with estimates of α^B determined for the separate cultures under polychromatic irradiance.

There was a clear trend in the spectral shape of the monochromatic action spectrum of *Pavlova* sp. related to the growth PFD. The magnitude of the shoulder between 450 nm and 550 nm decreased substantially with increasing growth PFD (Figure 7.3). The $\alpha^B(550) / \alpha^B(425)$ ratio is ~0.65 in cells grown at 8 μE m^{-2} s^{-1} (PA 9140) compared with 0.4 in cells grown under 12 μE m^{-2} s^{-1} and 0.3 in cells grown at the highest PFD (45 μE m^{-2} s^{-1}). Concurrently, the $\alpha^B(675) / \alpha^B(425)$ ratio increases from ~0.3 to ~0.5 over the same range of growth PFDs. Similarly, $\alpha^B(450) / \alpha^B(425)$ decreases with progressive increase in growth PFD. This suggests that the pigment(s) contributing to the photosynthetic action in the shoulder between 475 nm and 550 nm also contribute to both $\alpha^B(425)$ and $\alpha^B(450)$ with the greater contribution being to $\alpha^B(450)$.

7.3. $\alpha(\lambda)$ OF NATURAL PHYTOPLANKTON ASSEMBLAGES.

7.3.1. Sargasso Sea.

Monochromatic action spectra were obtained from a number of samples collected from different depths during early spring bloom conditions at a single station (35° 20′ N,

62° 30′ W) in the Sargasso Sea (Figure 4.1). The water column was well mixed with relatively uniform chlorophyll concentrations (~0.4 mg Chl m^{-3}) to a depth of 80 m. Detectable levels of nitrate were present in the mixed layer and concentrations increased considerably below 40 m (Figure 7.4). PAR decreased exponentially with depth.

The photosynthetic response to increasing PFD was generally linear for all wavelengths. Photosynthetic action spectra were all of similar shape with a broad maximum between 425 nm and 525 nm, low values of $\alpha^B(\lambda)$ between 550 nm and 650 nm and a second peak at 675 nm (Figure 7.5). The magnitude of $\alpha^B(\lambda)$ determined at different depths were fairly uniform. Peak values of $\alpha^B(\lambda)$ at 425 nm and 450 nm were 15 μmol C μmol Chl^{-1} hr^{-1} $(\mu E\ m^{-2}\ s^{-1})^{-1}$ in samples from the mixed upper 50 m. Below 60 m spectra became difficult to resolve as chlorophyll concentrations dropped below ~0.3 mg m^{-3}. For this reason the peak at 600 nm in the 70 m sample cannot be unambiguously assigned to phycocyanin, particularly in view of the low $\alpha^B(\lambda)$ value at 625 nm. Similarly, the $\alpha^B(525)$ peak in the 100 m sample should not be interpreted as definitive evidence of a phycoerythrin peak.

The monochromatic action spectra from the Sargasso Sea closely resemble the absorption spectra of the particulate material present and indicate the photosynthetic participation of chlorophyll which may be considered responsible for the peaks at 425-450 nm and at 675 nm. The shoulder in the action spectrum between 475 nm and 550 nm (very evident in the 10 m sample) may be attributed to the carotenoid accessory pigments fucoxanthin and/or peridinin. Microscopic examination of the samples showed that significant numbers of diatoms were present, a feature not considered "typical" of oligotrophic waters. The monochromatic action spectra obtained are consistent with the domination of photosynthetic carbon fixation by diatoms in which case the 475-550 nm shoulder may be attributed to fucoxanthin.

7.3.2. Eastern Canadian Arctic.

The monochromatic action spectra of all samples collected at different stations and different depths in the eastern Canadian Arctic were very similar in their spectral shape. Samples did exhibit some variation in the magnitude of $\alpha^B(\lambda)$ and these differences could be correlated to the prevailing oceanographic conditions.

Action spectra had a primary maximum at 425-450 nm, a secondary maximum at 675 nm, a shoulder which sometimes constituted a third peak between 475 and 550 nm and a trough between 575 and 650 nm. Values for $\alpha^B(\lambda)$ ranged from 0.05 to 1.7 nmol C·mg Chl^{-1}·s^{-1}·(μE·m^{-2}·s^{-1})$^{-1}$ depending upon the wavelength, sample location and depth of origin (Figures 7.6 to 7.10). Within any single sample the value of $\alpha^B(\lambda)$ varied by up to a factor of 3.5 depending upon the wavelength. A similar degree of variation was found for spectrally-averaged $\alpha^B(\lambda)$ between samples collected from different locations and different depths.

Among natural phytoplankton assemblages collected from the chlorophyll maximum at a series of stations along a latitudinal transect from the Labrador Sea through Baffin Bay to Jones Sound, chlorophyll-specific values of $\alpha^B(\lambda)$ were inversely related to the depth in the water column at which the maximum occurred (Figure 7.6). Comparison of action spectra measured at virtually identical locations (Stns. 53/54 and 73/75) but six days apart under conditions of progressive stratification indicates the spatial and temporal variability in $\alpha^B(\lambda)$. Chlorophyll-specific values for $\alpha^B(\lambda)$ increased two-fold over this period during which chlorophyll concentrations increased from 5-6 mg Chl·m^{-3} to 8-13 mg Chl·m^{-3} (Figures 7.6(d) and 7.7).

Depth profiles of $\alpha^B(\lambda)$ from two spatially separated stations in Baffin Bay (Stns. 113 and 116) and three temporally distinct stations (with virtually identical locations) in Jones Sound (Stns. 94/95, 98 and 124) yielded different results. $\alpha^B(\lambda)$ from coastal Baffin Bay (Stn. 116) and Jones Sound III (Stns. 94/95 and 98) generally increased with depth (Figures 7.8(b) and 7.9) whereas in central Baffin Bay (Stn. 113) and in Jones Sound IV (Stn. 124) $\alpha^B(\lambda)$ showed little variation with depth (Figures 7.8(a) and 7.10). These differing results may be explained in terms of the physical conditions present at the different locations.

The depth profiles in coastal Baffin Bay (Stn. 116) and Jones Sound III (Stns. 94, 95 and 98) that showed a consistent increase in $\alpha^B(\lambda)$ with increasing depth represented stations with a well-developed chlorophyll maximum containing 10-12 mg Chl m^{-3}. The 30 m chlorophyll maximum at the coastal Baffin Bay station coincided with a broad oxygen maximum that extended from below the pycnocline at 15 m to a depth of 40 m (Figure 7.8(b)). Similarly, the three stations representing the first depth profile in Jones Sound were also highly stratified, the virtually identical depth profiles being marked by a pronounced chlorophyll maximum at a depth of 30 m (Figure 7.9). Those stations with depth-related differences in the chlorophyll-specific value of $\alpha^B(\lambda)$ were thus all characterized by a stable, stratified water column with a well-developed chlorophyll maximum.

In two cases, the depth profiles showed little variability in the magnitude of $\alpha^B(\lambda)$ in relation to depth. In both cases vertical stratification was less intense and the biomass present was more homogeneously distributed throughout the water column. In central Baffin Bay (Stn. 113) the pycnocline was not as steep as other stations (as indicated by the gradient in σ_θ) and a broad chlorophyll maximum occurred between 15 and 30 m (Figure 7.8(a)). The reduced stratification and generally lower chlorophyll

concentrations present at the chlorophyll maximum (~4 mg Chl m^{-3}) at this station suggest that vertical stratification may have been at an early stage of development. Similarly, the second depth profile determined in Jones Sound (Stn. 124) followed a major wind-generated mixing event and much of the vertical structure previously evident had been dissipated (Figure 7.10). The depth profile revealed the breakdown of both the chlorophyll and oxygen maxima with concurrent mixing of the upper 20 m. No significant differences in the magnitude of $\alpha^B(\lambda)$ was evident in samples from different depths except for the sample from 20 m which, occurring at the base of the new mixed layer, had higher values of $\alpha^B(\lambda)$ compared to the rest of the water column. The new depth-independent value of $\alpha^B(\lambda)$ in the upper 20 m had diminished and was equivalent to the depth-averaged value of $\alpha^B(\lambda)$ found in the previously stratified condition.

In contrast to the variations observed in the amplitude of $\alpha^B(\lambda)$, the spectral shape of all the action spectra was remarkably uniform (Figures 7.6 to 7.10). All monochromatic action spectra consisted of two maxima at 450 nm and 675 nm and a wavelength region between 550 nm and 650 nm where $\alpha^B(\lambda)$ was minimal. To compare the spectral shapes of different samples, the action in each waveband was normalized to the average wavelength-independent action (yielding *relative* action) and to the total action (yielding *fractional* action) throughout the 400-675 nm range. Computation of the mean and 95% confidence intervals of these relative action spectra reveal the constancy in their spectral form (Figure 7.11). The conservative spectral form of the monochromatic action spectra determined for Arctic phytoplankton is an important result that greatly simplifies determination of the systematic error arising from differences in spectral irradiance as a function of depth.

7.3.3. Eastern North Atlantic.

Of the many attempts to measure monochromatic action spectra from samples collected from open ocean locations in the Caribbean Sea and eastern North Atlantic, interpretable results were obtained from only three stations. The failure of many experiments to detect a photosynthetic signal in ^{14}C uptake resulted from a number of compounding factors. These included the low biomass present, low biomass-specific photosynthetic rates and high dark ^{14}C fixation (high relative to fixation in the light). These factors necessitated the use of high concentrations of radioisotope (≈1.5 MBq ml^{-1}), concentrations where the contribution of ^{14}C-labelled organic contaminants dissolved in the $H^{14}CO_3^-$ tracer became significant.

A clear dependence between the rate of carbon uptake and the PFD was evident only in those experiments where the isotope addition was increased to ≈7.4 MBq vial^{-1}, the incubation period was extended to six hours and the particulate material was collected on Nuclepore® filters. Collection of material on Nuclepore® filters allowed the partitioning of carbon fixation between particulates greater than 3 μm compared to those that passed through a 3 μm filter but were retained on a 0.2 μm filter. Modifications in the incubation apparatus to increase the available PFD, particularly at the blue end of the spectrum, provided a range of intensities that frequently were sufficient to cause saturation (and in some wavebands even photoinhibition). Because the light-limited portion of the P-I response was established by a only a few data points, estimates of $\alpha^B(\lambda)$ in these samples were made by inspection rather than the usual linear regression procedure.

The three stations for which size-fractionated action spectra were successfully measured were located in the subtropical eastern North Atlantic. Two stations were

located adjacent to submarine seamounts, Station 27709 (34° 34.91′ N, 51° 02.48′ W) was over the Yakutat seamount and Station 27870 (34° 22′ N, 57° 10.4′ W) was over the Nashville seamount. The third station, Station 27805 (31° 57.96′ N, 55° 38.89′ W, also refered to as Station Purple (Li and Wood 1988)), was representative of the extreme oligotrophic ocean.

The water column above the Yakutat seamount (Stn. 27709) was well stratified with a strong pycnocline. Depth profiles of temperature and σ_t were essentially mirror images of one another. Temperature decreased exponentially from 23°C at the surface to 18°C at a depth of 100 m. A chlorophyll maximum ([Chl] = 0.55 mg m^{-3}; [Phaeo] = 0.58 mg m^{-3}) occurred between 70 and 80 m. A broad oxygen maximum was present immediately above the chlorophyll maximum which extended between 20 and 80 m (see Figure 7.12). Pigment concentrations of the < 3 μm size fraction were 0.49 and 0.48 mg m^{-3} for chlorophyll and phaeopigment respectively. By subtraction, the chlorophyll and phaeopigment concentrations of the > 3 μm size fraction were 0.06 and 0.1 mg m^{-3} respectively. Clearly, the majority of the biomass is less than 3 μm as this size fraction accounts for 88% of the total chlorophyll.

Despite the fact that the material collected on a 3 μm Nuclepore® filter only accounted for 12% of the chlorophyll biomass, photosynthetic rates were of sufficient magnitude as to yield a discernible action spectrum. The action spectra of this > 3 μm size fraction was similar in spectral shape to that determined for other unfractionated natural assemblages. A broad maximum was present between 400 nm and 525 nm with a second maximum occurring at 675 nm. Photosynthetic action was minimal between 550 nm and 650 nm (Figure 7.12). Only two data points establish the value of $\alpha^B(425)$ and so the significance of the apparent decrease in $\alpha^B(\lambda)$ at this wavelength should not be considered definitive. The magnitude of $\alpha^B(675)$ is roughly half that at the blue peak

which is similar to results of action spectra obtained from other unfractionated natural samples.

The monochromatic action spectrum of the < 3 μm size fraction differed from that of the large size fraction. Although broadly similar in spectral shape with pronounced peaks in the blue and the red, the red peak in $\alpha^B(\lambda)$ was at 650 nm rather than the usual 675 nm and the major shoulder usually present between 450 nm and 525 nm was considerably diminished. Higher $\alpha^B(550)$ were evident in the < 3 μm size fraction compared to the larger size class. This was the only photosynthetic action spectrum in which $\alpha^B(650)$ exceeded $\alpha^B(675)$.

A major difference between the photosynthetic response of the two size fractions was the absolute rate of photosynthesis. When normalized to chlorophyll, rates of carbon fixation were lower by more than an order of magnitude in the < 3 μm size fraction. Peak values of $\alpha^B(\lambda)$ were 0.0005 μmol C μmol Chl^{-1} hr^{-1} (μE m^{-2} $s^{-1})^{-1}$ compared to 0.008 μmol C μmol Chl^{-1} hr^{-1} (μE m^{-2} $s^{-1})^{-1}$ for the > 3 μm size fraction. Chlorophyll-specific values of $\alpha^B(\lambda)$ for the larger size fraction were comparable to those measured for diatom- and coccolithophorid-dominated natural assemblages in Arctic waters. The exceptionally low chlorophyll-specific photosynthetic rates measured in the < 3 μm size fraction provide an explanation for the difficulty in measuring photosynthetic action spectra in previous experiments with open ocean samples.

Analysis by epifluorescence microscopy and flow cytometry (Li and Wood 1988) indicated that this sample comprised of the order of 4200 cyanobacterial cells ml^{-1} compared with about 5800 "ultraplankton" cells ml^{-1} (Li, pers. comm.). The cyanobacteria always contained phycoerythrin with both PUB and PEB chromophores, and passed through a 3 μm filter. The "ultraplankton" comprised two groups designated

as "large eukaryotes" and "small eukaryotes" both characterized by significant fluorescence at > 630 nm. The "large eukaryotes" was a heterogeneous assemblage that tended to be trapped on a 3 μm filter (although many passed through) and displayed strong > 630 nm fluorescence. The "small eukaryotes" all passed a 3 μm Nuclepore® filter and displayed moderate > 630 nm fluorescence.

This phylogenetic composition accords with the action spectra determined for both size fractions. The blue and red peaks in both size fractions may be ascribed to chlorophyll. Differences in the wavelengths of maximum action between the two size fractions correlate with the differences in the intensity of > 630 nm fluorescence between the "small" and "large" eukaryotes (Li and Wood 1988). The high value of $\alpha^B(650)$ in the < 3 μm size fraction may reflect the photosynthetic participation of chlorophyll *b* which absorbs maximally at 650 nm in the red region of the spectrum. Chlorophyll *b* also absorbs strongly at 440-460 nm which could account for the broad shoulder between 450 nm and 500 nm in the < 3 μm fraction (see Chapter 8.5.3.). The low shoulder at 550 nm may be attributed to the photosynthetic participation of the PEB chromophore of cyanobacterial phycoerythrin in the < 3 mm size fraction.

The second seamount station (27870) over the Nashville seamount was also vertically stratified (Figure 7.13). In this instance there was a well-defined chlorophyll maximum at 70 m ([Chl] = 0.73 mg m^{-3}, [Phaeo] = 0.44 mg m^{-3}) overlaid by a broad oxygen maximum extending from this depth to the surface. Like the chlorophyll maximum at the Yakutut seamount the majority (72%) of the chlorophyll biomass at the Nashville chlorophyll maximum passed a 3 μm filter. Pigment concentrations for the < 3 μm size fraction were 0.52 and 0.33 mg m^{-3} for chlorophyll and phaeophytin respectively, which yield values of 0.21 and 0.11 mg m^{-3} for the concentrations of chlorophyll and phaeophytin in the > 3 μm size fraction.

The action spectra of both size fractions from the Nashville seamount displayed similar features to those at the Yakutat seamount (Figure 7.13). The > 3 μm size fraction provided a clear photosynthetic signal despite the low chlorophyll concentration and the action spectrum was characterized by a prominent maximum between 450 nm and 475 nm, a region of little photosynthetic activity between 500 nm and 625 nm with a minor increase in $\alpha^B(\lambda)$ at 675 nm. While broadly similar to many action spectra determined for other natural assemblages this spectrum was distinct in two respects. Firstly, there was no evidence of a carotenoid shoulder between 500 nm and 550 nm, a feature of many oceanic action spectra including the > 3 μm size fraction at the Yakutat seamount. Secondly, the photosynthetic efficacy of 675 nm irradiance was notably weak. The magnitude of $\alpha^B(675)$ is typically half that of the blue peak while in this case $\alpha^B(675)$ is less than 20% of this value.

As in the case of the sample from Yakutat, the < 3 μm size fraction at the Nashville seamount was characterized by extremely low chlorophyll-specific rates of photosynthesis compared to the > 3 μm size fraction. Maximum values of $\alpha^B(\lambda)$ were lower by almost an order of magnitude. In common with the larger size fraction the action spectra of the < 3 μm material was also characterized by prominent peaks at 450 nm to 475 nm and 675 nm. In addition, $\alpha^B(500)$ and $\alpha^B(550)$ were notably enhanced as was $\alpha^B(650)$ (Figure 7.13).

Epifluorescence microscopic and flow cytometric analyses of this sample contained approximately $5 \cdot 10^4$ cyanobacterial cells ml^{-1} compared to $1.3 \cdot 10^4$ "ultraplankton" cells ml^{-1} (Li, pers comm.). The dominance of the cyanobacte sample suggests that the prominent peak at 550 nm and the enhanced value of $\alpha^B(500)$ may be ascribed to the PEB and PUB chromophores of phycoerythrin res ly. As

before the major peaks in the $\alpha^B(\lambda)$ spectrum in the blue and red can be attributed to chlorophyll corresponding to the small and large eukaryotes comprising the "ultraplankton". The high value of $\alpha^B(475)$ and $\alpha^B(650)$ suggest that chlorophyll *b* as a potential photosynthetic participant in the < 3 μm size fraction action spectrum. It is interesting to note that despite the numerical dominance of the cyanobacteria in this sample (by almost factor of 4) the action spectrum is still dominated by the twin peaks of chlorophyll at the red and blue wavelengths.

Finally, experimental data collected the open ocean station (# 27805 at Station Purple) revealed a coherent irradiance-dependent signal for the > 3 μm size fraction only. Like both seamount locations this station was also vertically stratified with a broad but weak chlorophyll distribution extending from the surface to a depth of 180 m, the deepest of the three stations (Figure 7.14). Maximum chlorophyll values occurred at 110 m where the chlorophyll concentration was 0.39 mg m^{-3} and phaeophytin was 0.25 mg m^{-3}. Concentrations of chlorophyll and phaeophytin passing a 3 μm filter were 0.30 and 0.21 mg m^{-3} respectively indicating that approximately 75% of the chlorophyll biomass was in the small size fraction.

Despite the predominance of chlorophyll in the < 3 μm size fraction no discernible P-I signal was detectable. A reliable action spectrum was obtained for the > 3 μm size fraction however (Figure 7.14). This spectrum was dominated by a blue an a red peak in $\alpha^B(\lambda)$ presumably due to chlorophyll. The spectrum differed from others in that the magnitude of the red peak ($\alpha^B(675)$) matched that of the blue peak ($\alpha^B(475)$). Again the maximum value of $\alpha^B(\lambda)$ in the blue region was at 475 nm, a wavelength greater than that associated with the maximal absorption of chlorophyll *a* and closer to that marking the absorption maximum of chlorophyll *b*.

Microscopic and cytofluorimetric analyses indicated this sample consisted of some 250 cyanobacterial cells ml^{-1} and approximately 4200 "ultraplankton" cells ml^{-1} (Li, pers. comm.). The low number of cyanobacteria in this sample agrees with the low value of $\alpha^B(550)$ observed and the apparent dominance of a "chlorophyll-type" response. It is unknown what proportion of the "ultraplankton" pass a 3 μm filter however the low number of these cells combined with relative absence of cyanobacteria in the total sample would explain why a distinct photosynthetic signal was not forthcoming from the < 3 μm size fraction.

In summary, photosynthetic action spectra from the open ocean are not grossly dissimilar spectrally from those determined for diatom-dominated natural assemblages. All action spectra of natural assemblages appear to be dominated by the participation of chlorophyll, leading to major peaks in the blue and the red regions of the spectrum. The contribution of cyanobacterial phycoerythrin to the photosynthetic action spectrum appears minimal even where cyanobacteria are numerically dominant. Despite the fact that the majority of chlorophyll passes a 3 μm Nuclepore filter, chlorophyll-specific rates of photosynthesis in this < 3 μm size fraction were consistently an order of magnitude less than that of particulates trapped by a 3 μm filter. Consequently, the 10-20% of the chlorophyll retained on a 3 μm Nuclepore filter was responsible for 75-90% of the total photosynthesis. The contribution of cyanobacterial phycoerythrin was only discernable in action spectra of the < 3 μm size fraction in samples where the cyanobacterial numbers exceeded those of the chlorophyll-containing "ultraplankton" by a factor of 4. Since the photosynthetic contribution of the < 3 μm size fraction is ~10%, the influence of phycoerythrin to the $\alpha^B(\lambda)$ of the entire sample is neglible.

7.4. APPARENT QUANTUM YIELDS.

7.4.1. Monospecific picoplankton cultures.

The apparent quantum yields of photosynthesis was determined for each culture of the three picoplankton species grown in the laboratory using the absorption spectra described in Chapter 6.2. (Figures 6.2 to 6.4) and the monochromatic action spectra presented above in Section 7.2 (Figures 7.1 to 7.3). The apparent quantum yield of photosynthesis is dimensionless and corresponds to the number of CO_2 molecules reduced per photon absorbed. The quantum requirement is defined as the reciprocal of the quantum yield.

Comparison of the absorption spectrum (Figure 6.2) and monochromatic action spectrum (Figure 7.1) of the phycocyanin-dominated cyanobacterium *Synechococcus* sp. WH 5701 indicate that the apparent quantum yield of photosynthesis is maximal for those wavelengths where phycocyanin absorbs most strongly. In all four cultures of WH 5701 the quantum yield spectra consist of a single maximum located in the 650 nm waveband (Figure 7.15). This wavelength corresponds almost exactly to the mid point between the 622 nm absorption maximum of phycocyanin and the 675 nm absorption maximum of chlorophyll *a*. The apparent quantum yield diminishes either side of this peak with a pronounced shoulder on the shorter wavelength side corresponding to the region of predominantly phycocyanin absorption. The low values of $\alpha^B(\lambda)$ in the blue region of the spectrum where chlorophyll is the sole absorbing component lead to a very reduced apparent quantum yield at these wavelengths. The spectral form of the quantum yield, like the absorption spectrum, remains remarkably unchanged despite differences in the growth PFD.

The maximum apparent quantum yield attained at the optimal wavelength of 650 nm in all four cultures irrespective of growth PFD is approximately $6 \cdot 10^{-5}$. This value corresponds to a quantum requirement for photosynthesis of 16000 photons which is over three orders of magnitude greater than the minimal theoretical quantum requirement of about 10 photons for every molecule of CO_2 reduced.

Similar results were obtained for the cultures of the phycoerythrin-containing cyanobacterium *Synechococcus* sp. WH 7803 where a comparison of the absorption spectra (Figure 6.2) with the monochromatic action spectra (Figure 7.2) shows the importance of the phycobiliprotein phycoerythrin (Figure 7.16). The apparent quantum yield of photosynthesis was maximal at 550 nm corresponding to the wavelength of maximal absorption by phycoerythrin. The apparent quantum yield spectra of WH 7803 consisted of a single peak centered at 550 nm with a conspicuous shoulder on the longer wavelength side between 625 nm and 650 nm. As with the cyanobacterium WH 5701 the low values of $\alpha^B(\lambda)$ at the red and blue wavelengths where chlorophyll absorption is maximal result in greatly diminished values of $\phi_a(\lambda)$ at these wavelengths.

Apparent quantum yield spectra were broadly similar in spectral form for all cultures irrespective of their growth PFD. One spectral feature that did vary with growth PFD was the magnitude of the long wavelength shoulder at 625 nm to 650 nm. This shoulder was significantly more pronounced in the culture grown under the lowest PFD (DC 9124 grown at 17 $\mu E\ m^{-2}\ s^{-1}$). In this culture the apparent quantum yield at 625-650 nm was 60% of that attained at 550 nm. This compares to a relative value of about 30% for the two cultures grown at higher PFDs (DC 9116 and DC 9120 grown at 25 and 35 $\mu E\ m^{-2}\ s^{-1}$ respectively).

Maximum apparent quantum yields for *Synechococcus* sp. WH 7803 at 550 nm were between $2 \cdot 10^{-5}$ and $4 \cdot 10^{-5}$ molecules of CO_2 reduced per photon absorbed. This corresponds to a quantum requirement of 25000 to 50000 photons absorbed for every molecule of CO_2 reduced and is some 2500 to 5000 times the minimal theoretical quantum requirement of 10.

Comparison of the *in vivo* absorption spectra (Figure 6.4) and monochromatic action spectra (Figure 7.3) of the prymnesiophyte *Pavlova* sp. (clone NEP) indicates a much closer spectral correspondence than that of the two cyanobacterial clones. The principal absorption peaks attributable to chlorophyll in both the blue (425-450 nm) and the red (675 nm) regions of the spectrum along with the carotenoid shoulder in the green (450-550 nm) are clearly represented in the photosynthetic action spectrum. This produces an apparent quantum yield spectrum that is almost spectrally invariant (at least by comparison to that of the cyanobacterial clones) (Figure 7.17).

Apparent quantum yield spectra from cultures grown at all three PFDs possess a broad maximum between 450 and 550 nm. On the shorter wavelength side of this maximum $\phi_a(\lambda)$ falls slightly at 425 nm and then significantly at 400 nm. Above 550 nm the apparent quantum yield declines gradually to about 60% of its maximum value upon reaching 675 nm. Maximum apparent quantum yields of *Pavlova* occur in the wavelength region dominated by absorption by the accessory carotenoid pigment fucoxanthin.

Absolute quantum yields in the 450 nm to 550 nm region are $4 \cdot 10^{-5}$ to $2 \cdot 10^{-4}$ molecules CO_2 per photon absorbed corresponding to a quantum requirement of 5000 to 25000 photons for every molecule of CO_2 reduced.

7.4.2. Natural Phytoplankton Assemblages.

Calculations of the apparent quantum yields were determined for a number of natural assemblages from which quantitative estimates of both photosynthetic action spectra ($\alpha(\lambda)$) and absorption spectra ($a(\lambda)$) normalized to chlorophyll were available.

In natural assemblages from the eastern Canadian Arctic, calculations of the apparent quantum yield using a^*_{chl} values determined for individual samples according to Eq. 4.1 were all highly correlated with the chlorophyll concentration of the sample because of the inverse relationship between the chlorophyll-specific attenuation coefficient and the chlorophyll concentration (Figure 6.15(b)). Based upon these a^*_{chl} values, the spectrally-averaged apparent quantum yields ranged from 0.002 in samples containing little chlorophyll to 0.062 in samples high in chlorophyll where absorption was dominated by chlorophyll-containing cells. This corresponds to a quantum requirement of between 16 and 500 absorbed quanta per molecule CO_2 reduced.

To eliminate the effect of chlorophyll concentration upon $a^*_{chl}(\lambda)$, the generalized spectral attenuation coefficients computed from the hyperbolic model (Eq. 6.1 discussed in Chapter 6.3.2. and given in Figure 6.15) were used in conjunction with the action spectra data to determine a "sample-average" apparent quantum yield spectrum. This significantly reduced the variation in $\phi_a(\lambda)$ and produced spectrally-averaged apparent quantum yield (387.5 to 687.5 nm, all wavelengths weighted equally) ranging from 0.015 to 0.083 corresponding to an apparent quantum requirement of between 12 and 66 quanta per molecule CO_2 reduced.

For all natural assemblages from Arctic waters the similarity in spectral shape between the action spectra (Figure 7.11) and the absorption spectra (Figure 7.16) resulted

in a "sample-averaged" apparent quantum yield that was relatively constant across the spectrum except for a minor increase between 500 nm and 575 nm (Figure 7.18). A broad maximum occurred at 550 nm where the apparent quantum yield was about 40% greater than the baseline average between 425 nm and 675 nm. The spectral region over which this maximum occurred corresponds to that where the accessory carotenoid pigments such as fucoxanthin are the predominant absorbing species. Below 450 nm there was a significant decline in the apparent quantum yield such that at by 400 nm $\phi_a(\lambda)$ had dropped to about 50% of the baseline average between 425 nm and 675 nm. The decline in the $\phi_a(\lambda)$ at short wavelengths may be ascribed to absorption by non-chlorophyllous material in this spectral region.

Similar apparent quantum yield spectra result from a comparison of the action spectra determined for the > 3 μm and < 3 μm particulates collected from locations in the eastern North Atlantic (Figures 7.12 to 7.14) with *in vivo* absorption spectra typical for the region (Figures 6.11 to 6.13). The generally close correspondence between the spectral shape of $\alpha^B(\lambda)$ and $a^*_p(\lambda)$ results in an apparent quantum yield spectrum that is relatively invariant with respect to wavelength. A maximum usually occurs between 475 nm and 575 nm corresponding to the action of accessory photosynthetic pigments such as fucoxanthin. Absorption by photosynthetically-inactive chlorophyll and non-chlorophyllous material give rise to a decrease in the apparent quantum yield above and below this spectral region.

7.5. WAVELENGTH DEPENDENCY OF P-I CURVATURE AT LOW PFDs.

As mentioned in Section 7.1, many experimental action spectra exhibited a departure from linearity in the P-I response at monochromatic PFDs below 25 μE m^{-2} s^{-1}.

This curvature was particularly well-defined in the case of the monospecific picoplankton cultures and was present in all the P-I responses determined under polychromatic light. The degree of curvature in the different monochromatic wavebands may be quantified in terms of the parameter $R_m(\lambda)$ in Eq. 7.1 which constitutes a measure of the vertical displacement of the P-I response along the ordinate axis. Analysis of $R_m(\lambda)$ showed that the extent of such curvature was wavelength dependent and that the spectral dependence of the curvature were different in each of the three picoplankton species. Furthermore, the spectral dependency of this low PFD curvature could be correlated with the apparent quantum yield.

The spectral dependency of $R_m(\lambda)$ was most pronounced in the two cyanobacterial species. In *Synechococcus* sp. WH 5701 curvature was absent at wavelengths below 550 nm. The degree of curvature increased with increasing wavelength reaching a broad maximum between 600 nm and 650 nm. $R_m(\lambda)$ decreased once again at 675 nm (Figure 7.19). The spectral pattern of $R_m(\lambda)$ is thus virtually identical to that of $\alpha^B(\lambda)$ (Figure 7.1). The maximum value of $R_m(\lambda)$ attained at 600 nm is 1.61 μmol C m^{-2} hr^{-1} which is 9.5% of the maximum photosynthetic rate achieved by this culture (P_m^B = 16.96 μmol C m^{-2} hr^{-1} according to my geometric model; see Table 5.3 and Figure 5.3).

The spectral dependency of $R_m(\lambda)$ was also strongly correlated with $\alpha^B(\lambda)$ in *Synechococcus* sp. WH 7803. The spectrum of $R_m(\lambda)$ comprised a single peak with a maximum at 550 nm. The degree of curvature decreased at higher and lower wavelengths (Figure 7.19) yielding a $R_m(\lambda)$ spectrum similar to that for $\alpha^B(\lambda)$ (Figure 7.2). The maximum value of $R_m(\lambda)$ observed at 550 nm is 0.8 μmol C m^{-2} hr^{-1} corresponds to 12% of the maximum photosynthetic rate achieved by this culture (P_m^B = 6.6 μmol C m^{-2} hr^{-1} according to my geometric model; see Table 5.7 and Figure 5.6). The P-I response of this strain exhibits significant photoinhibition and so the maximum

potential photosynthetic rate (P_s^B) predicted in the absence of photoinhibition is somewhat greater (Table 5.7). Among those models found to yield a good fit to the P-I data of this culture P_s^B ranges from between 9.02 μmol C m^{-2} hr^{-1} (Platt and Gallegos 1980) and 9.2 μmol C m^{-2} hr^{-1} (Platt *et al.* 1980) to 11.9 μmol C m^{-2} hr^{-1} (Fasham and Platt 1983). Using these values the maximum value of $R_m(\lambda)$ is equivalent to between 6.7% and 8.9% of the maximum *potential* photosynthetic rate.

Curvature at low PFDs was evident at all wavelengths in *Pavlova* sp. NEP. No consistent spectral pattern in $R_m(\lambda)$ was evident among all three cultures. The magnitude of $R_m(\lambda)$ varied from between 4% and 9% of the maximum photosynthetic rate.

CHAPTER 8

GENERAL DISCUSSION.

8.1. QUANTIFYING THE P-I RESPONSE OF PICOPLANKTON.

8.1.1. Choice of Empirical Model.

The determination of the photosynthetic rate at a total of 96 separate PFDs ranging from 0 to 2000 $\mu E\ m^{-2}\ s^{-1}$ provided data sets with a resolution that was more than adequate for the purpose of describing the major features of the P-I response. This high resolution allowed discrimination between the different mathematical formulations which have been proposed by previous authors and also permitted testing the applicability of new models. The form of the P-I response was found to differ in each of the three picoplankton species examined.

The phycocyanin-containing cyanobacterium *Synechococcus* sp. WH 5701 was the only clone that showed no signs of photoinhibition at PFDs up to 2000 $\mu E\ m^{-2}\ s^{-1}$. The P-I response of all cultures of this species were of the saturation type despite the fact that cells were grown at PFDs as low as 7 $\mu E\ m^{-2}\ s^{-1}$. In the case of all cultures the 3-parameter formulation of Bannister (1979) yielded the best fit. The non-rectangular hyperbola suggested by Rabinowitch (1951), an alternate 3-parameter model, was also found to provide a satisfactory description of the P-I response. Of the various 2-parameter models only the hyperbolic tangent model of Jassby and Platt (1976) yielded an acceptable fit to the data and in many cases this model tended to under-estimate the degree of curvature at the point of transition from light-limited to light-saturated

photosynthesis. The remainder of the 2-parameter models showed very poor correspondence to the data. From this it may be concluded that even picoplanktonic P-I responses lacking photoinhibition require a minimum of three parameters for an accurate description.

The P-I responses of the phycoerythrin-containing cyanobacterium *Synechococcus* sp. WH 7803 and the eukaryotic prymnesiophyte *Pavlova* sp. (NEP) both displayed a photoinhibitory decrease in photosynthetic rate at high PFDs. In both cases the 5-parameter model of Platt and Gallegos (1980) provided the most satisfactory description of the P-I response based upon goodness-of-fit criteria. The new 6-parameter model introduced in Chapter 3.4.1. also showed excellent agreement with the data with residuals showing little systematic correlation to the PFD. Reducing the number of parameters in the formulation of Platt and Gallegos (1980) to 4 by setting $I_t = 0$ (so $I_t' = I_b'$) as described in Chapter 2.3.2. produced curve fits that were comparable to the original expression. This simplification was superior to the alternative of setting the shape parameter $m = 6$ as originally suggested by the authors. Alternative empirical models that are commonly employed to describe P-I curves with photoinhibition (*ie.* the 3-parameter model of Platt *et al.* 1980) were found to provide inadequate descriptions of the P-I response. This analysis suggests that the P-I responses of picoplankton species which include photoinhibition require an empirical model with a minimum of 4 parameters, and the model must possess sufficient geometrical flexibility to allow sharp transitions from one region of the curve to another.

The decline in photosynthesis observed at high PFDs depended upon the irradiance history of the cells. The extent to which photoinhibition is present in the water column where cells are photosynthetically adapted to high PFDs remains unclear. Photoinhibition is generally considered to result when cells that are adapted to lower

PFDs are exposed to excessively high PFDs causing damage to one or several components of the photosynthetic apparatus (Powles 1984). As such it is a short-term response and is generally not considered a feature of cells adapted to high PFDs (Harris 1978).

Several reports indicate that *Synechococcus* sp. cells in surface waters are not photoinhibited. Iturriaga and Mitchell (1986) found *Synechococcus* sp. cells from surface waters and from 75 m of the North Pacific had comparable growth rates and Landry *et al.* (1984) estimated growth rates of 1.4 - 2.0 d^{-1} for natural samples suspended at 5 m, a growth rate close to the maximum. Similarly, Campbell and Carpenter (1986) concluded that cells from the surface or depth generally grew faster when incubated at the surface based upon the frequency of dividing cells.

Synechococcus populations growing in the surface mixed layer also lack signs of photoinhibition (Glover *et al.* 1985; Joint and Pomroy 1986; Prezelin *et al.* 1986). Furthermore, by pre-conditioning low-PFD grown cells to higher PFDs by a step-wise exposure to intermediate PFDs, Kana and Glibert (1987) found that maximal growth rates of *Synechococcus* spp. WH 7803 and WH 8018 could be sustained up to 2000 μE m^{-2} s^{-1}. Photoinhibition of growth and photosynthesis only occurred in low-PFD adapted cells subjected to sudden increases in the PFD (Kana and Glibert 1987a). From the P-I responses of cells grown under different PFDs, a plot of the photosynthetic rates attained at PFDs corresponding to the growth PFD produced a saturation-type response (Kana and Glibert 1987b) indicating that through adaptation, the photoinhibitory effects of high PFDs could be removed. Barlow and Alberte (1987) have also shown that photoinhibitory losses are reversible and recovery is rapid and can occur within hours in both *Synechococcus* spp. WH 7803 and WH 8013.

It may be concluded that a P-I formulation must be geometrically capable of providing a quantitative description of photoinhibition if it is to provide a useful description of experimentally-derived P-I data from picoplanktonic species. However, it is likely that depth profiles of photosynthesis *in situ*, where cells are adapted to ambient PFDs, will not show signs of photoinhibition.

8.1.2. Choice of Kinetic Model.

Analyses showed that several kinetic models provided good quantitative descriptions of the picoplanktonic P-I response. In the case of the saturation-type P-I response of *Synechococcus* sp. WH 5701, the model of Rabinowitch (1951) which constitutes a non-rectangular hyperbola, or one of the rational models that reduce to a non-rectangular hyperbola in the absence of photoinhibition, showed close correspondence with the data. The latter include the models of Fasham and Platt (1983) and my two photosystem kinetic model described in Chapter 3.6.2. In the absence of photoinhibition both models reduce to a 3-parameter form analogous to that of Rabinowitch (1951).

For the P-I responses of *Synechococcus* sp. WH 7803 and *Pavlova* sp. (NEP) which exhibit photoinhibition, the only models to consistently provide good descriptions of the P-I response were the single photosystem model of Fasham and Platt (1983) and my two-photosystem model. Both are similar geometrically and consist of a non-rectangular hyperbola describing photochemistry combined with a negative exponential describing photoinhibition. The cumulative Poissonian model also provides a good description of picoplankton photosynthesis provided that the parameters describing the number of hits required to produce photoinhibition (b) and the action cross-section of

photoinhibition (I_j) are allowed to be independent of the analogous parameters describing photochemistry (a and I_k).

Several points favor the choice of my two-photosystem kinetic model in preference to the model of Fasham and Platt (1983). Firstly, in my two photosystem model the PFD where photosynthesis is optimal (I_m) is simply the reciprocal of the parameter describing photoinhibition (β), that is, $I_m = 1/\beta$. In contrast, Fasham and Platt (1983) could find no explicit solution for the optimal PFD in terms of their model parameters. This simple relation between I_m and β also provides a straightforward means of estimating an initial value of β for purposes of curve-fitting. An initial estimate of I_m can be easily derived from a plot of the P-I data by inspection and the reciprocal of I_m provides an initial estimate of β.

Secondly, the two-photosystem structure of the model allows the introduction of non-linear effects such as Emerson enhancement which result from the serial operation of two spectrally distinct photosystems (see Chapter 3.6.1). The two rate constants that determine the light-dependent photoreactions (k_q and k_p) can be further decomposed to account for both the initial partitioning of the absorbed photons between the two photosystems and any subsequent redistribution of excitation as may occur by way of spillover. The parameters k_q and k_p in Eqs. 3.104 and 3.105 are simply replaced by the parameters ϕ_1, ϕ_2, ω, ζ and γ which describe the distribution of photons within the light-harvesting antenna.

It is impossible to determine the original model parameters k_q and k_p directly *from a single P-I response* under monochromatic (or polychromatic) irradiance because of redundancy in the system of equations that comprise the model. Further decomposition of k_q and k_p to yield five new parameters only increases this redundancy making it

impossible to evaluate these model parameters from a single P-I response. However, given certain assumptions it is possible to determine several of the key parameters *if* the rates of light-limited photosynthesis are measured under different monochromatic beams both singly and in combination (see Chapter 3.5.2.).

Thirdly, the model of Fasham and Platt (1983) and my two-photosystem model both admit the introduction of a spectral dependency for photoinhibition. This is by an explicit definition of $\beta(\lambda)$. With the two-photosystem model the spectral dependency of $\beta(\lambda)$ can be easily made proportional to the spectral dependency of either photosystem. In accordance with current knowledge regarding the site of photoinhibitory action, the appropriate photosystem would be Photosystem II ($\sigma_2(\lambda)$). The spectral dependency of Photosystem II can be derived from photosynthetic rate measurements made under light-limited conditions as outlined in Chapter 3.5.2.

Fourthly, the photoadaptive mechanisms of algae in general, and cyanobacteria in particular, involve the dynamic modulation of both the pigment-protein composition of each photosystem and the relative stoichiometry of the two photosystems. Both processes have significant effects upon the spectral dependency of the P-S-I response. Such photoadaptive changes in the photosynthetic apparatus are induced by a wide range of environmental variables including temperature, PFD, photon spectral distribution and nutrient availability.

Among certain cyanobacteria, the phycobiliprotein content of the phycobilisomes serving Photosystem II are under direct chromatic control. The phycobiliprotein content is modulated by the wavelengths present in the ambient light field such that the pigmentation of the cell is adjusted to complement the spectral distribution of the incident irradiance. This form of photoadaptive response, referred to as

"complementary" chromatic adaptation, is unique to the cyanobacteria (Tandeau de Marsac 1977,1983), specifically to a subset of those species that utilize phycoerythrin as the principal light harvesting pigment.

An alternate type of photoadaptive response common to many algal groups involves the modulation of the relative cellular concentrations of the two photosystems, Photosystem I and Photosystem II. In cyanobacteria changes in the PS I:PS II ratio alters the spectral characteristics of the cell because of the spectral differences of the photosynthetic pigments associated with each photosystem. The spectral changes brought about by photoadaptive changes in photosystem stoichiometry were contrary to those expected (namely the production of pigment whose spectral properties complement the incident spectrum) and so such changes were termed "inverse" chromatic adaptation. First noted in red algae (Yocum and Blinks 1958; Brody and Emerson 1959a,b), similar changes have been noted in cyanobacteria containing phycocyanin such as *Anacystis nidulans* (Jones and Myers 1965; Myers *et al.* 1978,1980; Kawamura *et al.* 1979; Fujita *et al.* 1985; Matsuura and Fujita 1986). Dynamic adjustment of photosystem stoichiometry is also commonplace among organisms with a chlorophyll *a*-chlorophyll *b* light-harvesting antenna (see review by Melis (1989)).

Photosystem stoichiometry has been found to vary in the marine *Synechococcus* sp. WH 7803 and WH 8013 in response to growth PFD (Barlow and Alberte 1985). The cellular concentrations of both photosystems decreased exponentially with increasing growth irradiance. Cellular concentrations of reaction center (RC) I declined to a lesser extent than RC II resulting in a consistent increase in the RC I:RC II ratio. The ratio increased from 0.94 to 1.26 and from 1.10 to 1.62 in WH 7803 and WH 8013 respectively according to whether cells were grown at low (10 $\mu E\ m^{-2}\ s^{-1}$) or high (250 $\mu E\ m^{-2}\ s^{-1}$) PFDs (Barlow and Alberte 1985). Changes in photosystem stoichiometry

clearly affect the spectral characteristics of cyanobacteria under light-limiting conditions. In addition, Barlow and Alberte (1987) have suggested that the reduction in the maximum photosynthetic rate (P_m^B) observed in high-light cells results from a reduction in RC I (P700) activity. The kinetics of photoinhibition recovery match the recovery of P700 with a delay of 1-2 hours. From these results, it is clear that photosystem stoichiometry is a major determinant of the P-I response of cyanobacteria including *Synechococcus* spp.

In contrast, none of the *Synechococcus* sp. isolated to date have been shown to be capable of complementary chromatic adaptation (Waterbury *et al.* 1986) although as our perception of the taxonomic affinities of the marine *Synechococcus* component changes (see Section 8.5.2.), new isolates may be identified with this capability. The description of the P-I response in terms of the action of two photosystems operating in series whose spectral characteristics may be individually defined provides a P-I model suitable for describing the photoadaptive behavior of all phytoplanktonic algae.

Fifthly, by describing the P-I response in terms of two serially-interacting photosystems, it is possible to include the spectral dependency of the interaction of respiration and photosynthesis that is observed in cyanobacteria. Because components of respiratory and photosynthetic electron chain are shared, respiration is inhibited in the light under certain conditions. Because of spectral differences between the photosystems the inhibition of respiration shows a spectral dependency (see Section 8.4.3.).

Finally, the kinetic model of photosynthesis based upon the interaction of two photosystems has structural similarities to recent attempts to model the photosynthetic process from measurements of *in vivo* fluorescence (Falkowski *et al.* 1986a,b; Kolber *et*

al. 1988). This provides a potential avenue for directly comparing the analogous parameters in both photochemical and fluorescence models.

Cumulatively, these features set the two-photosystem kinetic model apart from other P-I formulations as the basis for a realistic and quantitative description of the photosynthetic response under different PFDs and spectral compositions.

8.1.3. The P-I Parameters of Picoplankton.

Difficulties arising in the determination of cell numbers and the carbon and chlorophyll content of laboratory picoplankton cultures meant that only *in vivo* absorbance was available as a reliable biomass index. The lack of a common biomass index makes comparisons of the determined photosynthetic rates to published values difficult in absolute terms. The PFD marking the transition from light-limited to light-saturated photosynthesis ($I_k = P_m^B/\alpha^B$) is biomass-independent and so most readily compared. From Tables 5.1 to 5.11 it is clear that the estimated value of I_k varies according to the P-I formulation selected.

Synechococcus sp. WH 5701 exhibited I_k values between 120 -140 μE m^{-2} s^{-1} (new geometric model) depending upon growth PFD (Tables 5.1 - 5.4) . This is in close agreement with the value of 130 μE m^{-2} s^{-1} given by Morris and Glover (1981) for the same clone. Values of I_k for *Synechococcus* sp. WH 7803 are somewhat lower, ranging from 86-120 μE m^{-2} s^{-1} (Tables 5.6 - 5.8) depending upon growth PFD, in close agreement with the value of 110 μE m^{-2} s^{-1} given by Morris and Glover (1981). Using cells grown between 10 and 100 μE m^{-2} s^{-1} Barlow and Alberte (1985) report values of I_k for WH 7803 between 23 and 87 μE m^{-2} s^{-1} based upon P-I responses determined using a tungsten lamp. I_k values were generally inversely related to growth PFD, and the value

of 23 μE m^{-2} s^{-1} was obtained from cells grown at 250 μE m^{-2} s^{-1} which had a growth rate of zero (Barlow and Alberte 1985). No P-I model was used, values of I_k were calculated from "the intersection of the regression line created by the initial slope ... extrapolated through zero, and the regression line generated by the P_{max} values". A maximum of four points were used in the regression and inspection of the data suggests that forcing the regression through zero was inappropriate. Direct non-linear modelling of the entire P-I response would probably yield lower initial slopes (α^B) and so higher values of I_k. Similar, although generally higher, values of I_k were obtained from another cyanobacterial clone *Synechococcus* sp. WH 8013, where I_k ranged from 69 - 112 μE m^{-2} s^{-1} (Barlow and Alberte 1985). The general conclusion from these low values of I_k has been that *Synechococcus* spp., and particularly WH 7803 which exhibited photoinhibition at high PFDs, were photosynthetically adapted to low PFDs (Glover 1986; Fogg 1986).

In contrast, Kana and Glibert (1987b) found that provided cells were pre-adapted to higher PFDs in a step-wise fashion, *Synechococcus* sp. WH 7803 was capable of maximal growth up to growth PFDs of 2000 μE m^{-2} s^{-1}. When the P-I response was normalized to either cell number, cell carbon or cell chlorophyll *a*, the initial slope decreased exponentially with increasing growth PFD while P_m^B remained relatively constant. This results in a steady increase in I_k with increasing growth PFD up to values of about 1000 μE m^{-2} s^{-1} for cells grown at 700 μE m^{-2} s^{-1}, above which point I_k remains relatively constant. Values of I_k for cultures grown at 30 and 50 μE m^{-2} s^{-1} are 60 and 130 μE m^{-2} s^{-1} respectively. These values agree closely with those obtained in this study.

Optimal PFD values for *Pavlova* sp. (NEP) range from 84 - 220 μE m^{-2} s^{-1} depending upon growth PFD (Tables 5.9 - 5.11). The value of 220 μE m^{-2} s^{-1} obtained for cells grown at the highest growth PFD (45 μE m^{-2} s^{-1}) closely matches the value of

232 μE m^{-2} s^{-1} provided for another clonal isolate of this genus *Pavlova* sp. (IIB3) grown at growth-saturating PFDs (> 141 μE m^{-2} s^{-1}) (Glover *et al.* 1987).

8.1.4. Photoadaptation and P-I Parameters.

Each of the picoplankton clones examined exhibited consistent changes in the values of the parameters describing the P-I response that could be correlated with the growth PFD. For *Synechococcus* sp. WH 5701, which lacked any sign of photoinhibition, the maximum rate of photosynthesis (P_m^B) increased with increasing growth PFD. In contrast, the photosynthetic efficiency at low PFDs (α^B) remained virtually constant for the range of growth PFDs examined (Table 5.15). This combination led to a progressive increase in the optimal photosynthetic PFD I_k with increasing growth PFD. The parameter describing the abruptness of the curvature from light-limited to light-saturated growth increased concomitantly (Figure 5.25) such that the P-I response of cells grown at higher PFDs tended to progressively approach a Blackman-type curve (Figures 5.1 - 5.4).

The photoadaptive changes in the P-I response of *Synechococcus* sp. WH 7803 grown under different PFDs were quite different from those of *Synechococcus* sp. WH 5701 (Table 5.16). Both P_m^B and α^B decreased as growth PFD increased from 17 to 35 μE m^{-2} s^{-1} (Figure 5.26). The reduction in P_m^B was the more pronounced leading to a decrease in the optimal photosynthetic PFD (I_k). The potential rate of photosynthesis when the negative slope of photoinhibition is extrapolated back to zero PFD, P_t^B, also decreased steadily with increasing growth PFD. The apparent reduction in P_m^B with increasing growth PFD contrasts with the results of Kana and Glibert (1987). These authors found a steady increase in P_m^B and a decrease in α^B (producing an increase in I_k) for this clone when photosynthetic rates were normalized to cell number or carbon

content. When normalized to chlorophyll *a*, the biomass index most closely related to *in vivo* absorbance at 678 nm, P_m^B was greatest in cells grown under high PFD.

In keeping with other algal studies, the magnitude of the photoinhibitory decrease in photosynthesis at high irradiances (β) was inversely related to growth PFD. However, because of the significant reduction in P_m^B, the PFD corresponding to the onset of photoinhibition (I_j) actually decreased with increasing growth PFD. In common with *Synechococcus* sp. WH 5701, the degree of convexity of the P-I response at the transition from light-limited to light-saturated photosynthesis in *Synechococcus* sp. WH 7803 increases with growth PFD. Inspection of the P-I responses (Figures 5.5 - 5.7) suggests that this results from the progressive reduction in P_t^B causing the curve describing photoinhibition to intersect the linear portion of the P-I response.

The pattern of photoadaptive change in P-I parameters in response to growth PFD was less consistent in the prymnesiophyte *Pavlova* sp. (NEP). In common with *Synechococcus* sp. WH 7803 there was a decrease in the extent of photoinhibition (β) as growth PFD increased with a concomitant increase in the PFD marking the onset of photoinhibition (I_j). The high value of P_m^B observed in the culture grown under intermediate PFD appears to scale the values obtained for the other parameters (α^B and β^B). These photoadaptive changes mean that the optimal photosynthetic PFD remains virtually unchanged in the two low-PFD cultures (I_k = 85 μE m^{-2} s^{-1}) and subsequent increases in the high PFD culture (220 μE m^{-2} s^{-1}). As with both cyanobacterial cultures there is an increase in the convexity of the P-I response with increasing growth PFD.

From analysis of the P-I responses of the three picoplankton clones examined, it is clear that the differences in the P-I parameters that occur are directly related to the growth PFD. In particular there is a consistent trend toward increasing the optimal

photosynthetic PFD (I_k) and the degree of convexity in the P-I response as growth PFD increases. The consistent pattern of photoadaptive adjustment in P-I parameter values require that such changes be incorporated into efforts to model depth profiles of photosynthesis in stable water columns. In particular, the consistent pattern of variability in the convexity of the P-I curve in relation to growth PFD emphasizes the importance of this parameter in P-I formulations.

8.2. RELATIVE PHOTOSYNTHETIC RATES IN BLUE, GREEN AND WHITE POLYCHROMATIC IRRADIANCE.

8.2.1. Relative Rates in Different Spectral Distributions.

Not surprisingly, the ranking of the rate of light-limited photosynthesis (α^B) achieved in each of the three spectral distributions (green, blue and white) was different for each of the three picoplankton clones. These differences man be explained on the basis of the spectral properties of the principal light-harvesting pigments and their distribution among the two serially-arranged photosystems. The ranking of α^B in the different polychromatic irradiances remained the same for each clone irrespective of growth PFD.

For the phycocyanin-containing cyanobacterium *Synechococcus* sp. WH 5701 photosynthetic efficiencies in white light were twice that in green and five times that in blue light (Table 5.12; Figures 5.12 to 5.14). The high photosynthetic efficiencies in white light result from the heavy spectral weighting of red wavelengths in the white light produced by tungsten-halogen bulbs (Figure 8.2(b)), and which overlap the strong orange absorption of phycocyanin between 550 and 650 nm (Figure 6.3). Phycocyanin is

associated with Photosystem II as indicated by action spectrum determined under monochromatic light (Figure 7.1). Most of the chlorophyll is associated with Photosystem I and absorbs strongly at 676 nm. Consequently, the spectral distribution of white light efficiently excites both photosystems ensuring balanced turnover and high throughput.

The low photosynthetic efficiency observed in blue light has considerable ecological significance for the potential ability of *Synechococcus* sp. WH 5701 to compete in the open ocean environment where the spectral distribution of the ambient irradiance field at depth in the water column is dominated by blue wavelengths (see Section 8.5.3). Clearly the photosynthetic apparatus of this clone is more suited to the irradiance environment of shallower waters, particularly those with a higher proportion of longer wavelengths. The absence of any trace of photoinhibition in the white light P-I response (Figures 5.1 to 5.4), a spectral composition that is most efficiently absorbed and utilized, also suggests that this picoplankton clone is adapted to the high PFDs expected at shallow depths.

The color ranking of *Synechococcus* sp. WH 7803 also follows that expected according to the spectral absorption properties of the photosynthetic pigments (Table 5.13; Figures 5.15 to 5.18). The high photosynthetic efficiency observed in green light results from absorption by phycoerythrin which absorbs maximally between 475 and 575 nm (Figure 6.2). Phycoerythrin is associated with Photosystem II and its photosynthetic participation is clear from the monochromatic action spectrum (Figure 7.2). The higher efficiency observed in white light compared to blue light reflects the relative amount of absorption by phycoerythrin under both spectral distributions.

Differences in the photosynthetic efficiency in the different polychromatic irradiance fields were less pronounced in the prymnesiophyte *Pavlova* sp. (NEP) (Table 5.14; Figures 5.19 to 5.21). In contrast to the two cyanobacterial clones blue wavelengths were the most effective for promoting photosynthesis, α^B measured in polychromatic blue light was 20% and 30% greater than that in white and green light respectively. This ranking may be explained by both the absorption spectrum (Figure 6.4) and the monochromatic action spectrum (Figure 7.3) of *Pavlova*. The close correspondence between the monochromatic action spectrum and the absorption spectrum demonstrates both the photosynthetic participation of both chlorophyll and fucoxanthin in this species and the similarity in the spectral response of both photosystems. The latter provides for a balanced excitation of both photoreactions irrespective of the spectral distribution of the incident irradiance. Consequently, differences in α^B simply reflect differences in the spectral overlap between the incident irradiance and the chlorophyll-fucoxanthin light-harvesting antenna. The superior photosynthetic performance in white light compared to green reflects absorption by the long wavelength peak of chlorophyll *a* (676 nm) of the red photons which dominate the white irradiance produced by tungsten bulbs.

A similar color ranking was obtained by Wood (1985) who examined the photosynthetic rates of two PE-containing cyanobacteria (WH 7803 and WH 8018), one PC-containing cyanobacterium (WH 5701) and the prymnesiophyte *Pavlova* sp. (NEP) in artificial white light compared to the same PFD but incubated *in situ* in clear ocean water. Clear ocean water is dominated by blue wavelengths. Light-limited photosynthetic rates in *Synechococcus* sp. WH 5701 were greater in artificial white light compared to that measured *in situ* by a factor of 4, a difference of similar magnitude to that of α^B in white and blue polychromatic irradiance determined herein (Table 5.12). Differences were less

pronounced for *Synechococcus* sp. WH 7803 and *Pavlova* sp. (NEP) where the rates were comparable in both light regimes (Wood 1985, Table 1).

Similar results were also reported by Glover *et al.* (1986b,1987) who determined the photosynthetic efficiencies of the cyanobacteria *Synechococcus* WH 7803 and *Synechococcus* WH 7805 and a prasinophyte clone Ω48-23 under blue-violet, blue, green and white irradiance. Since the irradiance source (used alone for the white light and in combination with plastic filters to produce the various polychromatic distributions) consisted of fluorescent bulbs the results are only broadly comparable to those in this study. Both *Synechococcus* spp. contain phycoerythrin as the major light-harvesting phycobiliprotein but WH 7803 contains both PEB and PUB chromophores whereas WH 7805 contains only the PEB chromophore. The PUB chromophore absorbs maximally at 498 nm compared to the PEB chromophore with an absorbance maximum at 542 nm (Chapter 6.2.1) thereby enhancing the ability of WH 7803 to utilize blue wavelengths. The rank order of photosynthetic efficiency in WH 7803 was green > blue > blue-violet > white (Glover *et al.* 1986b, Table 1), in accord with the results obtained for WH 7803 in Chapter 5 (Table 5.13). The difference in the rank of white light results from differences in the spectral distribution of "white" fluorescent bulbs compared to "white" tungsten bulbs.

The rank order for the prasinophyte Ω48-23 was blue-violet > blue > white > green which, again with the exception of "white", is identical to that determined for the prymnesiophyte *Pavlova* sp. (NEP) (Table 5.14). Prasinophytes are marine green algae with chlorophylls *a* and *b* as the major light-harvesting pigments (Jeffrey 1980). This pigment complement means that their absorption properties are broadly similar to the chlorophyll *a* - chlorophyll *c* - fucoxanthin system of the prymnesiophytes in that the

absorbance spectrum is dominated by the twin absorbance peaks of chlorophyll in the blue (Soret band) and in the red region of the spectrum.

The dramatic differences in the photosynthetic efficiency (α^B) in different spectral distributions, particularly in the case of the cyanobacterial clones, and the fact that the pattern differs significantly for the different species according to pigment composition, emphasizes the need to account for the spectral distribution of submarine irradiance in primary production models.

8.2.2. Spectral Proportionality of the P-I Response.

The dominance of the linear portion of the P-I response at PFDs up to the point of saturation results in a high degree of proportionality between the different polychromatic P-I response curves. Differences in the convexity of the curve at the point of transition from light-limited to light-saturated photosynthesis, or at extremely low PFDs, that are detected from numerical curve-fitting are important from the point of view of understanding the photosynthetic mechanism and the relative importance of different processes under different spectral conditions. However from the perspective of establishing the parameters that are of quantitative significance in defining the P-I response they are of minor importance as established by the degree of parallelism in the logarithmically-transformed P-I curves (Figures 5.22 - 5.24).

It is important to note that for the picoplankton species examined the horizontal displacement separating the different P-I responses under different wavelength distributions remains constant for all growth PFDs. In other words, the proportionality constants describing the rank order of the P-I responses remain unchanged irrespective of the growth PFD. This results from the fact that the spectral response of the cells ($\alpha^B(\lambda)$)

did not change appreciably with growth PFD *over the range of growth PFDs examined.* If growth PFDs caused photoadaptive changes in the spectral response of the cells ($\alpha^B(\lambda)$) then the proportionality between P-I curves determined under different spectral distributions would become dependent upon growth PFD. While this is not observed in this study, the range of PFDs under which cells were coerced to grow is not as great as in nature. Evidence from Kana and Glibert (1987) regarding the pigment content of *Synechococcus* spp. grown under PFDs from 10 - 2000 μE m^{-2} s^{-1} suggests that significant changes in the abundance of phycobiliproteins relative to chlorophyll *a* could lead to significant variation in the proportionality constants between curves.

It is also worth noting that the logarithmic transformation of the PFD axis, performed to demonstrate proportionality in the P-I response, may also be used as an index of depth in studies of aquatic photosynthesis. Rotated by 90° the plot becomes a depth profile. This is because the attenuation of the PFD with increasing depth is approximately exponential (assuming uniform attenuance with depth). Altering the spectral composition of the irradiance $I(\lambda)$, or the spectral response of the phytoplankton $\alpha^B(\lambda)$, results in a simple vertical displacement of the photosynthetic profile.

8.3. THE ABSORPTION SPECTRUM.

8.3.1. Spectral Characteristics of Absoption.

The principal features of the absorption spectra $a^*(\lambda)$ obtained from both laboratory picoplankton cultures and natural water samples are in close agreement with previously published spectra. In the case of the cyanobacterial clones *Synechococcus* spp. WH 5701 and WH 7803, the contribution of the phycobiliproteins phycocyanin and

phycoerythrin respectively to absorption is clearly evident as the appropriate maxima are of similar magnitude to the absorption by chlorophyll (Figures 6.2 and 6.3). In the prymnesiophyte *Pavlova* sp. (NEP) the contribution of the accessory pigments, namely the chlorophylls c_1 and c_2 and the carotenoid fucoxanthin, is also evident in the form of a broad shoulder on the Soret band of chlorophyll (Figure 6.4).

The absorption spectra of picoplankton cultures grown under varying growth PFDs also remained largely invariant. The wavelengths of peak absorption remained constant although there was some slight variation in the relative amplitude of the various peaks correlated to growth PFD indicating some change in the relative concentrations of the different photosynthetic pigments. This was most marked in the two cyanobacterial clones. In both *Synechococcus* sp. WH 5701 and *Synechococcus* sp. WH 7803 the ratio of the Soret band of chlorophyll *a* (438 nm) increased relative to the chlorophyll peak at 678 nm. At the same time absorption attributable to phycobiliprotein, the phycoerythrin peak (542 nm) in WH 7803 and the phycocyanin peak (622 nm) in WH 5701, decreased relative to chlorophyll absorption at 678 nm (Figures 6.2, 6.3, 6.8 and 6.9).

The changes in absorption in both species are consistent with a general decrease in phycobiliprotein (PC or PE) combined with an increase in carotenoids such as zeaxanthin with increasing growth PFD. A substantial decrease in cellular PE has been found to occur in *Synechococcus* sp. WH 7803 in response to increased growth irradiance (Kana and Glibert 1987b). Furthermore, cellular concentrations of the carotenoid zeaxanthin (β,β-carotene-3,3' diol) remain constant while the cellular concentration of β-carotene decreases exponentially (Kana *et al.* 1988). Normalized to the chlorophyll *a*, which also decreases exponentially with increasing growth PFD, the β-carotene : chlorophyll *a* ratio remains constant while the zeaxanthin : chlorophyll *a* ratio increased five-fold (Kana *et al.* 1988). These changes are consistent with the allocation of β-

carotene as a photosynthetic accessory pigment (Siefermann-Harms 1985) while zeaxanthin functions in the cytoplasmic or outer membrane and is uninvolved in photosynthetic energy transduction (Wasielewski *et al.* 1986; Siefermann-Harms 1987). These results suggest that the increase in absorption at blue wavelengths relative to absorption at 678 nm observed in this study results is caused by an increase in the amount of zeaxanthin relative to chlorophyll *a*. Spectral changes in the absorption spectrum of *Pavlova* sp. (NEP) were very minor over the range of growth irradiances examined (Figures 6.4 and 6.10).

In the case of natural phytoplankton assemblages, the most interesting result was the uniformity in spectral form displayed by absorption spectra obtained for particulate material collected from diverse locations and depths. An absorbance peak at 676 nm was ubiquitous and the magnitude of this peak correlated with the chlorophyll concentration. Strong absorption was also present in the blue region of the spectrum. For waters with chlorophyll concentrations exceeding 2-3 mg m^{-3}, represented by samples from the Eastern Canadian Arctic, a second maximum at 435 nm was generally present. For lower chlorophyll concentrations, particulate absorbance tended to increase monotonically toward shorter wavelengths (Figures 6.11). This monotonically increasing absorption spectrum is characteristic of inanimate particulate matter (tripton) (Kirk 1980,1983: Bricaud *et al.* 1981). Size-fractionated particulates show the < 1 μm and < 3 μm particulates are dominated by tripton while larger material exhibits a more typical chlorophyll spectrum (Figure 6.10).

Similarities in the spectral absorption of tripton and particulate chlorophyll *a* at the shorter wavelengths complicate estimation of the chlorophyll-specific absorption cross-section (a^*_{chl}). The case is most extreme in waters with low chlorophyll concentrations where contributions to total absorption by tripton is greatest (Figure 6.11).

Plotting the attenuation coefficient (a^*_p, units: m^{-1}) as a function of chlorophyll concentration indicates that relationship is linear only at concentrations above 1 - 2 mg Chl m^{-3}, where estimates of a^*_{chl} are valid (Figure 6.15(a)). Below this chlorophyll concentration, increases in the proportion of tripton (and possible increases in the value of pathlength factor $\beta(\lambda)$) result in overestimates of a^*_{chl} (Figure 6.15(b)).

Unfortunately from the perspective of remote sensing, this is the case for the open ocean where chlorophyll concentrations are typically less than 1 mg m^{-3}. Absorption spectra from open ocean stations in the North Atlantic, including the Sargasso Sea, were always dominated by shortwave absorption typical of tripton (Figures 6.12 - 6.14). This spectral signature was shared by both large (> 3 μm) and small (< 3 μm) particulates (Figure 6.14).

Aside from the uniformity of oceanic absorption spectra, a major feature was the conspicuous absence of any spectral features that could be directly attributed to absorption by phycobiliproteins. Even in cases where particulates were size-fractionated, the picoplanktonic size fraction (< 3 μm) showed no sign of phycobiliprotein absorption. The total absence of any absorption by phycoerythrin or phycocyanin is in agreement with the extensive collection of measurements made of the optical properties of the upper ocean (Jerlov 1976; Morel and Prieur 1977; Morel 1978; Smith and Baker 1978; Prieur and Sathyendranath 1981). Similarly, previous measurements of the optical properties of particulate material concentrated on filters failed to demonstrate any clear absorption peaks that could be identified with phycobilipigments (Yentsch 1957,1962,1980; Kiefer and SooHoo 1982; Mitchell *et al.* 1984; Kishino *et al.* 1985).

The absence of an absorption signal corresponding to phycobiliproteins in samples known to contain significant numbers of cyanobacteria is puzzling in view of the

intense *in vivo* fluorescence signal observed at 580 nm in natural waters by both submersible fluorometers (Glover *et al.* 1985) and by remote sensing (Hoge and Swift 1983; Exton *et al.* 1983). Enough phycobilipigment is present to permit the discrimination of these cells by epifluorescent microscopy and flow cytometry (Wood *et al.* 1985; Olson *et al.* 1988). Phycocyanin-containing cyanobacteria are generally rare in the open ocean. Recent indications are that the phycoerythrin-containing cyanobacteria present are rich in the chromophore phycourobilin (PUB) rather than the more common phycoerythrobilin (PEB) (see Section 8.5.2). This chromophore absorbs more strongly at shorter wavelengths (498 rather than 550 nm) corresponding more closely to that of chlorophyll or tripton. This may partially explain the apparent absence of phycobiliprotein absorbance. Also, the increased sensitivity offered by fluorescence compared with absorption methods may play some part. Absorption measurements of the picoplankton component are made against a large background signal due to the tripton which may simply overwhelm the phycobilipigment signal.

Clearly, the absorption properties of particulate material from the open ocean correspond most closely to the common chlorophyll *a*-chlorophyll *c*-carotenoid light harvesting system typical of chromophytes. However, on the basis of absorbance alone it is impossible to exclude the chlorophyll *a*-chlorophyll *b* system. The dominance of tripton, presumably containing chlorophyll degradation products and other possible "yellow substances", greatly biases the spectral shape of particulate absorption in the open ocean.

8.3.2. Complications with GF/F Filters.

While the method of filtering particulate material onto glass-fibre filters overcomes the dilute nature of seawater and permits evaluation of the attenuation

spectrum, the technique is not without problems. As discussed in Chapter 6.1, these largely relate to choosing a value for the path amplification factor $\beta(\lambda)$ which relates the optical pathlength to the geometric pathlength. By virtue of the complex optical geometry of the filter/particle combination and its geometric relationship to the detector, the exact geometrical distribution of the light field is unknown and an analytical solution impossible.

Empirical evidence suggests that $\beta(\lambda)$ is variable and a function of the optical density of the sample (Mitchell and Kiefer 1984; Bricaud 1989). This is corroborated by the dependence of the attenuation coefficient a^*_p upon particle concentration (Chapter 6.2.2.). The possibility that $\beta(\lambda)$ varies according to the optical density of the particle/filter combination introduces a bias into estimates of the attenuation coefficient a^*_p (and hence a^*_{chl}). Judging from the relationship between a^*_p (or a^*_{chl}) and the particle concentration (measured in terms of volume filtered for cultures, chlorophyll content for natural samples), estimates only converge on a consistent value at high optical densities. This agrees with independent determinations of $\beta(\lambda)$ made under conditions where the optical configuration permitted unambiguous differentiation of the absorption coefficient $a(\lambda)$ and the scattering coefficient $b(\lambda)$ where $\beta(\lambda)$ was found to increase exponentially at low optical densities (Bricaud 1989).

8.3.3. Validity of using $a(\lambda)$ to calculate PUR.

Estimates of attenuation throughout the water column, whether made directly *in situ* or by means of remote sensing, contain the attenuation contribution of seawater itself. While the sum of these components determine the spectral character of the underwater irradiance field, estimating the spectral absorption by particulates alone requires subtraction of the water component. The strict additivity of absorption

coefficients [Eq. 3.3] permit the simple subtraction of the spectral attenuance of seawater and furthermore allow the straightforward calculation of the rate of irradiance absorption by particulates [Eq. 3.16] (Chapter 3.2.1).

The absorption spectra of marine particulates determined from material collected on GF/F filters closely matches that obtained directly *in situ* and that inferred from the remote sensing of the oceans' optical properties. Absorption spectra of natural samples from stations rich in chlorophyll (*ie.* Figure 6.11) correspond to those derived by Morel and Prieur (1977) for phytoplankton from *in situ* studies. For locations with low chlorophyll concentrations the absorption spectrum of particulates corresponds in spectral shape to that of tripton (Kirk 1983), in which the absorption spectrum is dominated by short wavelength absorption. The general accord between estimates of the absorption properties of oceanic particulates derived by different techniques suggests that the spectral irradiance at depth may be computed unambigously.

The second question of importance for the purposes of computing depth-integrated P-I profiles, is whether the absorption spectrum of marine particulates so obtained constitutes a suitable spectral weighting function for the P-I response. To do so, a *minimal* condition is that the spectral absorption properties of marine particulates match those of the photosynthetically active pigments. Where chlorophyll concentrations exceed 1-2 mg Chl m^{-3} particulate absorption is generally dominated by phytoplankton cells and their photosynthetic pigments. In these cases absorption properties of the assemblage as a whole correspond to the photosynthetically active components. In the open ocean where chlorophyll concentrations are low and particulate absorption is dominated by tripton, the absorption spectrum of the whole assemblage does not correspond to that of the photosynthetic component. Consequently, for the open ocean it

is inappropriate to apply the absorption spectrum of the particulate material as a whole as a spectral-weighting function for photosynthesis.

8.4. THE PHOTOSYNTHETIC ACTION SPECTRUM.

8.4.1. Spectral Characteristics of Light-Limited Photosynthesis.

The photosynthetic action spectra $\alpha^B(\lambda)$ determined under monochromatic irradiance are all in close agreement with previous measurements on taxonomically similar species (*ie.* Haxo 1960). Action spectra correspond to that expected on the basis of the absorption properties of the photosynthetic pigments present in the case of both picoplankton cultures and natural phytoplankton assemblages.

The action spectrum of the prymnesiophyte *Pavlova* sp. (NEP) indicated that photosynthetic assimilation was maximal over all wavelengths corresponding to absorption (Figure 7.3). The high photosynthetic efficiencies found between 475 nm and 550 nm (Figure 7.17) confirm the photosynthetic participation of the carotenoid fucoxanthin in this species. Evidence of fucoxanthin participation in photosynthesis has been appreciated for some time in the case of other chromophytic algae particularly diatoms (Tanada 1951; Haxo 1960; Jeffrey 1984) and brown algae (Haxo and Blinks 1950; Haxo 1960). This study extends this observation to the prymnesiophytes. The photosynthetic action spectra obtained for members of this broad taxonomic group (the Chromophyta) indicate that photons absorbed by any of the photosynthetic pigments can be utilized in photosynthesis. Furthermore, the relative spectral invariance of the apparent quantum efficiency across the spectrum implies that absorption characteristics of both photosystems are effectively very similar. This means that the two antennae have

similar spectral absorption characteristics or that there exists an efficient mechanism of distributing absorbed photons to both photosystems.

The photosynthetic action spectra of the two cyanobacteria studied provide a sharp contrast in this regard. Monochromatic action spectra of both *Synechococcus* sp. WH 5701 and *Synechococcus* sp. WH 7803 reveal the photosynthetic participation of the accessory phycobiliproteins, phycocyanin and phycoerythrin respectively. Photosynthetic action spectra correlate with absorption spectra only at wavelengths marking phycobiliprotein absorption, they show no evidence of any photosynthetic involvement of chlorophyll *a*. In *Synechococcus* sp. WH 5701, the action spectrum constitutes a single peak centered at 625-650 nm with a half-bandwidth of almost 100 nm (Figure 7.1). This peak corresponds to absorption by phycocyanobilin (PCB), the sole chromophore of phycocyanin. Similarly, the photosynthetic action spectrum of *Synechococcus* sp. WH 7803 consists of a single peak centered at 550 nm corresponding to absorption by the chromophore phycoerythrobilin (PEB) (Figure 7.2). Absorption by phycourobilin (PUB), the second chromophore of phycoerythrin and which in WH 7803 is present in a molar ratio of 1:4 with PEB, produces a slight shoulder on the short wavelength side of the peak around 500 nm. The half-bandwidth of the overall action spectrum peak is around 80 nm.

The conspicuous depression in photosynthetic activity at wavelengths corresponding to chlorophyll *a* absorption was first noted in the action spectra of the phycocyanin-containing cyanobacterium *Chroococcus* sp. (Emerson and Lewis 1942) and subsequently in the red algae, the other major taxonomic group utilizing phycobiliproteins as the major light-harvesting pigments (Haxo and Blinks 1950; Duysens 1952; Yocum and Blinks 1954; Haxo 1960). As mentioned in Chapter 3.5.1. and discussed below (Section 8.4.3) this apparent paradox was resolved by Emerson's

discovery of photosynthetic enhancement (Emerson 1957) and the concept that photosynthesis requires the serial operation of two photosystems.

The fact that the photosynthetic action spectra of cyanobacteria determined under irradiance composed of a single wavelength correspond solely to phycobiliprotein absorption, with the result that chlorophyll participation is not represented, provides a sensitive diagnostic assay for cyanobacterial (or red algal) participation in the photosynthetic activity of natural assemblages. Monochromatic action spectra of the two major algal taxonomic lines, the Chromophyta (brown algal line) and the Chlorophyta (green algal line), are characterized by the twin peaks marking chlorophyll *a* absorption supplemented by a shoulder on the long-wavelength side of the Soret band due to participation of accessory pigments (carotenoids or chlorophylls *b* or *c*). Photosynthetic efficiencies are markedly reduced at green wavelengths which is in direct contrast to the action spectra of phycobiliprotein-containing algae.

Analysis of the photosynthetic action spectra obtained from natural phytoplankton assemblages collected from diverse locations and depths revealed an exceptional degree of uniformity in spectral form. All action spectra consisted of a primary maximum at 425 - 450 nm, a shoulder extending from 475 - 550 nm, a trough of low photosynthetic efficiencies between 575 nm and 650 nm and a final secondary maximum at 675 nm. This spectral shape is typical of light-harvesting systems where absorption is dominated by chlorophylls with accessory carotenoid pigments extending photosynthetic action into the "green window" where chlorophyll absorption is low. This invariance in spectral shape constitutes an important conservative feature of aquatic photosynthesis, one that is of considerable significance when attempting to model aquatic photosynthesis (Section 8.5.1).

Clear correlations between the wavelength dependency of photosynthesis and the taxonomic composition of the natural assemblage were only possible for Arctic waters where microscopic examination provided an unambiguous identification as to the major photosynthetic components. For these waters the phytoplankton assemblages were most frequently dominated by diatoms and coccolithophorids and the action spectrum obtained is that expected for such chromophytic algae where the light-harvesting system is based upon chlorophylls *a* and *c* together with a carotenoid such as fucoxanthin. Because the photosynthetically active component is such a minor component of the particulate material in open ocean water, microscopic examination yields a much less definitive result regarding the taxonomic affinities of the phytoplanktonic component responsible for the observed action spectrum (see Section 8.5.3.).

8.4.2. Spectral Variation in Apparent Quantum Yield.

Inspection of the apparent quantum yield spectra shows that the transduction of absorbed irradiance is not spectrally invariant in either picoplankton cultures or natural assemblages (Figures 7.15 - 7.18). Since the apparent quantum yield is obtained by dividing the action spectrum $\alpha(\lambda)$ by the absorption spectrum $a(\lambda)$, the presence of photosynthetically incompetent pigments in the sample will reduce the apparent quantum yield. The second cause of reduced quantum yields concerns the differences in the absorption characteristics of the two photosystems (see Section 8.4.3.).

Reductions in the apparent quantum yield arising from the presence of photosynthetically incompetent pigments is most pronounced in natural assemblages. In comparing samples from Arctic waters, it is clear that while the wavelength dependency of $\alpha^B(\lambda)$ remains virtually constant (Figure 7.11), the absorption spectrum varies in a systematic manner according to the amount of tripton in the sample (Figure 6.11). In

general, the relative importance of tripton is inversely related to the chlorophyll concentration; samples with low chlorophyll concentrations have absorption spectra that are dominated by the tripton component.

For samples with high chlorophyll concentrations in which the absorption properties of the natural assemblage are dominated by the phytoplankton component, the photosynthetic action spectrum corresponds closely with the absorption spectrum. Apparent quantum yields reached 0.062 corresponding to a quantum requirement of only 16 photons for every molecule of CO_2 reduced. Compared to a theoretical maximum quantum requirement of 10 photons this represents a very high figure and implies that approximately 60% of the photons absorbed by the particulate material were efficiently utilized in photosynthesis.

As the chlorophyll concentration decreases and the tripton component becomes more important, the absorption spectrum diverges from the action spectrum and the overall quantum yield decreases. In samples of low chlorophyll, quantum yields declined to 0.002 corresponding to a quantum requirement of over 500 photons for every molecule of CO_2 reduced. Because the absorption spectrum of tripton increases exponentially toward shorter wavelengths, the reductions in the quantum yield due to tripton absorption are most evident at these wavelengths.

One approach to eliminating the absorption contribution of tripton is to derive a "generalized" chlorophyll-specific absorption cross-section (a^*_{chl}) by regressing absorption within each 25 nm waveband against chlorophyll concentration according to Eq. 6.1. Despite the limitations of this approach (see Chapter 6.3.2.), this procedure produced a generalized chlorophyll-specific absorption coefficient for each waveband (Figure 6.16) that, when applied to the different action spectra, produced quantum yield

spectra that were relatively constant across the spectrum (Figure 7.18). A minor increase in the apparent quantum efficiency was evident between 500 and 575 nm corresponding to absorption by carotenoids, probably fucoxanthin. This spectral pattern corresponds closely to the apparent quantum efficiency spectra obtained for the prymnesiophyte *Pavlova* sp. (NEP) (Figure 7.17). The increased quantum efficiency probably relates to the distribution of fucoxanthin between the two photosystems (see Section 8.4.3.).

The extremely low quantum efficiencies for photosynthesis in all laboratory grown picoplankton cultures is noteworthy in view of the high quantum efficiencies obtained in some field samples. Such low quantum efficiencies could result from some systematic under-estimation of photosynthesis or over-estimation of *in vivo* absorption. While absorption measurements made using GF/F filters are problematical (Chapter 6.1), the values of a^*_{chl} obtained with natural samples concur with previous estimates.

An alternative explanation is that under the growth conditions of the picoplankton cultures, cells accumulated significant quantities of photosynthetic pigment that were not photosynthetically competent. Evidence that photosynthetic pigments might serve an alternative function to photosynthetic light-harvesting have been suggested for the picoplanktonic cyanobacteria (Wyman *et al.* 1985). That phycoerythrin (PE) might serve as a nitrogen reserve material was initially suggested by the high level of autofluorescence observed from phycoerythrin in marine *Synechococcus* spp. (Waterbury *et al.* 1979; Johnson and Sieburth 1979; Yentsch and Yentsch 1979; Glover *et al.* 1985). In addition, the common cyanobacterial nitrogen reserve, cyanophycin, has not been detected in *Synechococcus* sp. WH 7803 and PE:PC ratios (15 - 21.6) in *Synechococcus* sp. WH 7803 grown with excess nitrogen exceed that of other cyanobacteria (Wyman *et al.* 1985; Kana and Glibert 1987b).

Wyman *et al.* (1985) have hypothesized that nitrogen-sufficient cultures of *Synechococcus* sp. WH 7803 accumulate phycoerythrin in excess of that required for light-harvesting providing a pool of energetically uncoupled ("free") PE within the cell. Their hypothesis is based upon a comparison between nitrogen-limited and nitrogen-sufficient cells with respect to steady-state fluorescence characteristics and growth rate measurements. Autofluorescence measurements at 570 nm made in the presence and absence of glycerol yield a crude "coupling efficiency" index ($\eta = F_{570,g} / F_{570,ng}$) because glycerol uncouples PE from PC. Progressively higher levels of autofluorescence were noted in nitrogen-sufficient cultures at high growth rates while nitrogen-limited cultures showed no difference. It was concluded that high-nitrogen grown cells had higher levels of "free" PE. At the same time comparable delayed fluorescent yields were obtained from both nitrogen treatments which was interpreted as indicating turnover of a similar number of reaction centers. Nitrogen sufficient cells also maintained high growth rates following the removal of nitrogen while the growth rate of nitrogen-limited cells decreased immediately. In continuous culture, increasing available nitrogen enhanced phycoerythrin synthesis although the biomass (and hence growth rate) remained constant. The increase in phycoerythrin led to a decrease in quantum yield.

Yeh *et al.* (1986) subsequently questioned the interpretation that *Synechococcus* sp. WH 7803 accumulated "free" PE as a nitrogen reserve. Based upon time-resolved (nanosecond) measurements of PE fluorescence in nitrogen-sufficient cultures of five different marine cyanobacteria including *Synechococcus* sp. WH 7803 they concluded that > 90 % of the cellular PE was present in phycobilisomes with < 10 % due to "free" PE. These authors pointed out that while fluorescence in the presence of glycerol is proportional to total PE content, minor changes (3%) in the proportion of "free" PE to "bound" PE will produce significant changes in the "coupling efficiency" index. This arises from differences in the fluorescent lifetimes of the two PE species (0.1 nsec for

bound PE compared to 2 nsec for free PE) so that the *steady-state* fluorescence signal detects contributions from free PE 20 times more sensitively than contributions from bound PE.

Despite these objections, the fact that cultures grown under high nitrogen and high light contain more PE than low nitrogen cultures yet exhibit similar yields of delayed fluorescence must be reconciled before the hypothesis of PE functioning as a nitrogen reserve is discarded.

8.4.3. The Importance of Emerson Enhancement.

In the case of the two cyanobacteria, the low apparent quantum efficiency at wavelengths corresponding to chlorophyll *a* absorption may be explained by the serial operation of the two photosystems PS I and PS II and the association of the different pigments with each photosystem as discussed in Chapter 3. The phycobilipigments are associated exclusively with PS II, the photosystem first in series, while the majority of the chlorophyll (85%) is associated with PS I, the photosystem that is second in line (Jones and Myers 1964; Mimuro and Fujita 1977; Wang *et al.* 1977). Photons of blue and red wavelengths that are absorbed by chlorophyll *a* are delivered predominantly to PS I. The lack of absorption by the PS II antenna at these wavelengths results in the rapid exhaustion of reduced donors for PS I and consequently the impedance of the entire transduction chain.

In contrast, photons that are absorbed by phycocyanin or phycoerythrin are delivered initially to PS II. With accumulation of the reduced products from PS II (and hence reduced donors for PS I) excess photons spill over to PS I ensuring that both photoreactions proceed in a balanced manner. Photosynthetic transduction is most

efficient when excitation of both photosystems is balanced. In *Synechococcus* sp. WH 5701 this occurs at wavelengths between 625 and 650 nm where absorption by phycocyanin and chlorophyll *a* is equal. Photosynthesis occurs throughout the spectral region where phycocyanin absorbs presumably by virtue of spillover. In *Synechococcus* sp. WH 7803 monochromatic light that preferentially excites the phycoerythrin corresponds to wavelengths of minimal absorbance for chlorophyll *a*. Consequently, photosynthesis within this waveband occurs predominantly by means of spillover and is maximal at wavelength corresponding to maximal phycoerythrin absorption (550 nm). In both cyanobacteria, differences in the spectral characteristics of the two photosystems lead to significant drops in quantum efficiency at both blue and red wavelengths. The presence of significant Emerson enhancement effects in picoplanktonic cyanobacteria has important consequences for the computation of light-limited photosynthetic rates under polychromatic light (Section 8.5.1.).

The differences in the spectral characteristics of PS I and PS II are substantially less in the prymnesiophyte *Pavlova* sp. (NEP). The excitation pathway has not yet been firmly established for chromophytic algae and it is not yet known whether the spectral constancy in the apparent quantum efficiency arises from similarity between both photosystem antennas (a bipartite model) or whether both photosystems are served by a common antenna (a tripartite model). Previous photosynthetic oxygen action spectra of diatoms have shown that both chlorophyll *c* and fucoxanthin efficiently absorb and transfer excitation energy to reaction center chlorophyll *a* (Tanada 1951; Mann and Myers 1968). Mann and Myers (1968) demonstrated classical Emerson enhancement in the diatom *Phaeodactylum tricornutum*. Their enhancement spectra as well as fluorescence excitation spectra (Goedheer 1970) suggested that fucoxanthin and chlorophyll *c* were preferentially associated with PS II while chlorophyll *a* and β-carotene were preferentially associated with PS I. Chlorophyll *a* fluorescence emission

spectra are also similar regardless of whether chlorophyll *a* or fucoxanthin are stimulated confirming the efficient transfer of light energy absorbed by fucoxanthin to chlorophyll *a* (Shimura and Fujita 1973).

The increased apparent quantum efficiencies observed between 500 and 575 nm in both the prymnesiophyte *Pavlova* sp. (NEP) (Figure 7.17) and diatom- or prymnesiophyte (coccolithophorid)-dominated natural assemblages of Arctic waters (Figure 7.18) are consistent with the preferential association of fucoxanthin and chlorophyll *c* with PS II. The relative spectral invariance of the apparent quantum yield suggests that enhancement effects are of minor significance in both *Pavlova* sp. (NEP) and Arctic natural assemblages, a result with major repercussions for calculating light-limited rates of photosynthesis under polychromatic light (see Section 8.5.1.).

8.4.4. Spectral Variation in Respiration.

The presence of curvature in the P-I response at PFDs below 25 $\mu E\ m^{-2}\ s^{-1}$ was evident in all P-I responses determined under polychromatic irradiance (Figures 5.12 - 5.21). The magnitude of this curvature was also a function of wavelength and differed in each of the three picoplankton clones. Significant differences in the amount of curvature under white, green and blue polychromatic irradiance was evident in both *Synechococcus* species. Spectral differences in the magnitude of curvature were less striking in the prymnesiophyte *Pavlova* sp. (NEP).

Quantifying the curvature under monochromatic irradiance shows that the amount of curvature present (defined in terms of the parameter $R_m(\lambda)$ in Eq. 7.1) varies with wavelength. In the two cyanobacterial species the spectral dependency of $R_m(\lambda)$ corresponds closely to the monochromatic action spectrum ($\alpha^B(\lambda)$). In *Synechococcus*

sp. WH 5701 curvature is greatest at wavelengths corresponding to phycocyanin absorption while in *Synechococcus* sp. WH 7803 curvature is most pronounced in the spectral region dominated by phycoerythrin absorption (Figure 7.19). At wavelengths corresponding to chlorophyll absorption there is a complete absence of curvature and the P-I response extrapolates linearly through the origin. The maximum value of R_m in both cyanobacterial species amounts to about 7 - 9 % of the maximum potential photosynthetic rate. The spectral dependency of $R_m(\lambda)$ in *Pavlova* sp. was less pronounced with significant curvature present at all wavelengths with the magnitude of R_m corresponding to 4 - 9 % of the maximum photosynthetic rate.

The simplest explanation of this curvature at PFDs below 25 $\mu E\ m^{-2}\ s^{-1}$ is that it constitutes a respiratory effect that is manifest due to measuring photosynthesis by ^{14}C incorporation. The hypothetical net photosynthetic P-I curve would have no curvature and would pass through the abscissa to intersect the ordinate at some negative value corresponding to the magnitude of residual respiration in the light. The observed positive curvature is imposed by the inability of the ^{14}C method to measure net photosynthesis below the compensation point.

According to this hypothesis the magnitude of the parameter $R_m(\lambda)$ represents the amount of respiration occurring in the light. In *Pavlova* sp. (NEP) $R_m(\lambda)$ is significant and of similar magnitude in all monochromatic and polychromatic P-I curves and so the interpretation is that respiration occurs irrespective of the wavelength of incident irradiance. In sharp contrast, in both *Synechococcus* sp. WH 5701 and *Synechococcus* sp. WH 7803 the parameter $R_m(\lambda)$ drops to zero at wavelengths where phycobiliprotein absorption is negligible. This result may be rationalized according to the known interaction between photosynthesis and respiration in cyanobacteria regarding electron flow between the two photosystems.

In the prokaryotic cyanobacteria there is a direct link between photosynthesis and respiration in that several thylakoid membrane components, including plastoquinone and cytochrome b_6f, serve as electron carriers between the two photoreactions of photosynthesis and also in the respiratory pathway from NAD(P)H to cytochrome oxidase (Jones and Myers 1963; Hirano *et al.* 1980; Sandman and Malkin 1983; Scherer and Boger 1982; Myers 1986) (Figure 8.1(a)). Consequently, both cytochrome b_6f and P700 (the reaction center of PS I) become reduced in the dark due to electron flow (Figure 8.1(b)).

In the cyanobacterium *Agmenellum quadruplicatum*, the P-I curve measured under wavelengths absorbed predominantly by PS II (Light 2) extrapolated to zero *net* O_2 production at zero PFD (Myers 1986). In contrast, under wavelengths absorbed predominantly by PS I (Light 1) the P-I response for *net* O_2 production extrapolated to a positive intercept at zero PFD corresponding to a rate equal to that of dark respiration. This result was rationalized according to the possible pattern of electron flow under the assumption that photosynthetic O_2 production on the oxidizing side of PS II and O_2 consumption by the terminal respiratory oxidase are the only two significant exchange reactions (Myers 1986).

Under Light 2, PS II is overstimulated relative to PS I thereby maintaining all of the components of the photosynthetic electron transport chain up to and including P700, in a reduced condition. The result is that P700 *does not effectively compete* with cytochrome oxidase for electrons (Figure 8.1(c)). Under Light 1 however, PS I is overstimulated relative to PS II maintaining P700 and prior electron carriers in an oxidized state. The result is that P700 successfully competes with cytochrome oxidase for electrons from reduced cytochrome b_6f thereby increasing the total input to

Photoreaction I to electrons supplied by PS II turnover *plus* electrons derived from respiratory electron flow to cytochrome b_6f (Myers 1986) (Figure 8.1(d)).

Similar reasoning applies to the P-I responses observed for *Synechococcus* spp. WH 5701 and WH 7803 with the only difference being that the ^{14}C curves are displaced vertically by an amount corresponding to dark respiration. The inability of the ^{14}C method to measure net photosynthesis below the compensation point results in the curvature observed in P-I curves determined in Light 2.

The respiratory input of electrons to balance PS I excitation in Light 1 can be easily introduced to the two-photosystem kinetic model outlined in Chapter 3.6.1. Under Light 2 conditions where PS II is overstimulated relative to PS I the rate constants driving Photoreactions I and II are $k_q I$ and $k_p I$ respectively. As described, k_q and k_p may be adjusted by spillover to ensure balanced excitation. Under Light 1 conditions where PS II is understimulated relative to PS I, a more balanced excitation may be achieved by the reduction of cytochrome b_6f by respiratory electrons. This effectively increases the rate constant for PS II to $(k_q I + R)$ where R corresponds to the rate of supply of electrons by way of respiratory oxidation of organic substrates.

8.5. APPLICATION OF $\alpha(\lambda)$ FOR COMPUTING DEPTH-INTEGRATED PRIMARY PRODUCTION.

8.5.1. Validity of using $\alpha(\lambda)$ to calculate PSR.

The validity of using photosynthetic action spectra determined under monochromatic irradiance to compute the photosynthetic rate under polychromatic

irradiance by way of Eq. 3.26 requires that photosynthetic energy transduction *effectively* behaves as a single ideal photoreaction. From our current understanding of the photosynthetic mechanism it is clear that photosynthesis is not a single photoreaction but rather is a complex sequence of reactions involving the serial operation of two separate photosystems (Staehelin and Arntzen 1986). The presence of Emerson enhancement, with the resultant major drops in the quantum efficiency at wavelengths where Photosystem II is insufficiently excited to provide balanced excitation of both photosystems, means that *a priori* this assumption is invalid.

Nevertheless there are circumstances under which Emerson enhancement effects may be small and photosynthetic energy transduction *effectively* behaves as a single photoreaction. For Emerson enhancement to be of neglible significance it is necessary that under ambient irradiance conditions excitation of both photosystems be balanced (or almost so). This situation will arise where the absorption properties of the two photosystems are similar, or where any differential in absorption may be overcome by means of some spillover mechanism. In this regard it is important to note that such spillover is only likely to occur from PS II to PS I. Spillover from PS I to PS II is improbable because of the differences in the energy levels of the active pigments associated with both photosystems. Furthermore, from the point of view of calculating PSR *within the water column* it is only necessary that excitation of both photosystems be effectively balanced *under spectral conditions representative of the incident irradiance spectrum at depth* in the ocean.

In the simplest case in which both photosystems have similar spectral cross-sections the effects of enhancement are neglible and the monochromatic action spectrum may be convoluted with the *in situ* irradiance spectrum to yield a true estimate of the photosynthetic rate in polychromatic light [Eq. 3.16]. The action spectrum ($\alpha^B(\lambda)$) is

simply proportional to the absorption spectrum of the *photosynthetically active pigments* with the proportionality constant representing the quantum efficiency of photosynthesis. This is essentially the case for green algae where the differences in the two photosystems are only considered to be significant above 680 nm, wavelengths that are quickly absorbed in the ocean and so are not present to any extent in submarine light fields. Deviation from strict proportionality between the monochromatic action spectrum $\alpha^B(\lambda)$ and the absorption spectrum $a^*(\lambda)$ of oceanic phytoplankton will arise *solely* from the presence of material in the ocean that absorbs PAR but is not photosynthetically competent.

In cases where the spectral absorption properties of the two photosystems differ significantly, calculation of PSR by way of Eq. 3.26 is inappropriate. In the absence of spillover, photosynthesis would occur only at those wavelengths where photons are absorbed by both photosystems. The possibility of distributing photons absorbed by Photosystem II to Photosystem I by way of some spillover mechanism permits photosynthesis to operate over a wider range of wavelengtns. Where spillover is complete the monochromatic action spectrum determined under irradiance of a single wavelength describes the spectral characteristics of Photosystem II, the first photosystem in series. If the spillover mechanism is not 100% efficient then such a spectrum is not a true Photosystem II spectrum because the overall quantum yield of photosynthesis is reduced at those wavelengths where spillover is required to balance the excitation of both photosystems. Significant differences in photosystem absorption occur in the cyanobacteria where the phycobiliproteins are associated exclusively with Photosystem II and chlorophyll is predominantly (85%) associated with Photosystem I (Jones and Myers 1964; Mimuro and Fujita 1977; Wang *et al.* 1977). That this also true for the two marine cyanobacteria *Synechococcus* sp. WH 5701 and *Synechococcus* sp. WH 7803 is clearly

demonstrated by a comparison between their action and absorption spectra (compare Figure 6.2 with Figure 7.2 and Figure 6.3 with Figure 7.1).

The extent to which the spectral characteristics of the two photosystems differ, and consequently the magnitude of the error associated with Eq. 3.26 for computing photosynthetic rates under polychromatic irradiance, depends upon the taxonomic composition of the phytoplankton assemblage. The validity of using the monochromatic action spectrum ($\alpha^B(\lambda)$) determined for natural assemblages for computing the depth-integrated primary production therefore depends ultimately upon the types and relative abundances of the different taxanomic groups throughout the water column.

8.5.2. The Magnitude of Emerson Enhancement in Picoplankton Cultures.

The validity of calculating the photosynthetic rate by way of Eq. 3.26 may be directly tested by comparing the actual photosynthetic rates observed under polychromatic irradiance of different spectral distributions with that predicted by a simple model approximating Eq. 3.26. In common with Eq. 3.26, the model assumes *strict independence and additivity between wavelengths.*

The *fraction* of the available quanta in each 25 nm waveband ($I(\lambda)'$) was calculated for the white, blue and green irradiance sources (Figure 8.2(b)). A *relative* action spectrum ($\alpha^B(\lambda)'$) was computed for each culture (*i.e.* under each growth PFD) by dividing the rate of photosynthesis per quantum in each waveband ($\alpha^B(\lambda)$) by the *average* rate of photosynthesis per quantum for all twelve wavebands (α^B(387.5-687.5 nm)). A mean of the relative action spectra obtained for each culture was then calculated to yield a relative action spectrum for each species (Figure 8.2(a)).

The contribution of each 25 nm waveband to the total photosynthesis (between 387.5 and 687.5 nm) is calculated by multiplying the *fraction* of the total quanta in that waveband ($I(\lambda)'$) by the corresponding *relative* photosynthetic action per quantum in the same waveband ($\alpha^B(\lambda)'$). Because the integral of $I(\lambda)'$ for all wavebands is unity, summing these products for all wavebands yields the *effective* photosynthetic rate per quantum ($\alpha^{B'}$):

$$\alpha^{B'} = \sum_{400}^{675} \alpha^B(\lambda)' \cdot I(\lambda)' \qquad ...(8.1)$$

The effective rates of photosynthesis per quantum ($\alpha^{B'}$) are based upon the *relative* rates of photosynthesis in the different wavebands so that the mean of all wavebands is unity. Consequently $\alpha^{B'}$ depends only upon the covariance of the spectral distribution of the irradiance source ($I(\lambda)$) and the action spectrum of the phytoplankton ($\alpha(\lambda)$). Differences in the absolute rates of photosynthesis determined for the different species do not affect the calculation of $\alpha^{B'}$. The value of $\alpha^{B'}$ represents a light utilization index describing the rate of photosynthesis of a particular species under a particular spectral distribution relative to that another spectral distribution. Using Eq. 8.1 the effective rates of photosynthesis per quantum ($\alpha^{B'}$) were then calculated for each of the three picoplankton clones under each of the three experimental irradiance distributions (white, blue and green).

Two special cases aid interpretation of the light utilization index ($\alpha^{B'}$) obtained with this simple model (Dring 1981). A totally absorbing algae (*ie.* one that is optically "black") absorbs all wavelengths equally and will exhibit a completely flat action spectrum such that the relative action in each waveband will be 1.0. Such an action spectrum when multiplied by *any* irradiance spectral distribution and integrated over all

wavebands will have a light utilization index of 1.0. Thus an alga with a spectrally flat action spectrum will achieve the same total photosynthesis per photon ($\alpha^{B'} = 1.0$) regardless of the spectral composition of the light field. The corollary is where the spectral distribution of the light field is perfectly flat such that the relative photon flux density in each waveband is equal (*ie.* a perfect "white" light source). When such a spectral distribution is multiplied by *any* action spectrum and integrated over all wavebands the light utilization index obtained ($\alpha^{B'}$) will also be 1.0. In a light field in which all wavelengths are equally represented on a quantum basis, all algae will achieve the same light utilization index ($\alpha^{B'} = 1.0$) regardless of their action spectrum.

Where the spectral distribution of irradiance is not spectrally "flat" (*ie.* not perfectly "white") *or* the action spectrum that is not spectrally "flat" (*ie.* not perfectly "black"), the light utilization index will be either greater or less than 1.0. The deviation of the light utilization index from unity is a measure of the covariance between a specfic action spectrum and a specific spectral distribution. Values greater than unity imply that algae make more efficient use of the incident photons than the hypothetical "black" alga *under that specific spectral distribution.* Conversely, values of $\alpha^{B'}$ less than unity imply the alga utilizes photons less efficiently than the hypothetical "black" alga *under that specific spectral distribution.* Table 8.1(a) provides estimates of the light utilization indices of Arctic phytoplankton assemblage, the prymnesiophyte *Pavlova* sp. (NEP) and the two cyanobacterial species *Synechococcus* sp. WH 5701 and *Synechococcus* sp. WH 7803 calculated according to Eq. 8.1 using the spectral distributions of natural sunlight (sea surface), tungsten-halogen lamps and the polychromatic irradiances produced by tunsten-halogen lamps in combination with the "blue" and "green" acetate filters.

For any one species, the ratio between the light utilization indices obtained under two different spectral distributions ($\alpha^{B'}{}_1/\alpha^{B}{}_2$) equals the ratio between light-limited

photosynthetic rates expected under the two different light sources (α^B_1/α^B_2) provided the effects of different wavelengths are both independent and additive. Where Emerson enhancement is minimal, ratios of light utilization indices calculated in this manner should approximate ratios in light-limited photosynthetic rates determined experimentally in polychromatic light. Table 8.1(b) lists the ratios of light utilization indices ($\alpha^{B'}$) determined for each of the four spectral distributions. These values represent the ratios between the photosynthetic rates under the different polychromatic light sources *predicted* by the model on the basis of the measured action spectra of the algae and the spectral distribution of the light sources. For comparison, Table 8.1(c) lists the ratios of the *actual* photosynthetic rates per quantum (α^B) determined experimentally and calculated by fitting a P-I response formulation by non-linear regression (data from Tables 5.13, 5.14, 5.15 and 5.19).

For the prymnesiophyte *Pavlova* sp. the ratios of photosynthesis predicted by the model ($\alpha^{B'}_1/\alpha^{B'}_2$) compare reasonably with the experimentally determined ratios (α^B_1/α^B_2). Photosynthesis in blue irradiance is approximately 1.5 times that under white irradiance according to both calculation (1.53) and experiment (1.55). The ratio of photosynthesis under green irradiance compared to white irradiance differ slightly; according to the model the green/white ratio = 1.18 while the experimental value of the green/white ratio = 0.93. The greatest difference lies in the ratio between photosynthesis in blue irradiance compared to that in green irradiance, the model estimates this ratio to be 1.29 while the experimental value is 1.72. These results imply that the model either under-estimates the rate of photosynthesis in green irradiance and/or over-estimates the rate of photosynthesis in both blue and white irradiance.

Poor correspondence between model prediction and experiment was found with *Synechococcus* sp. WH 7803. Estimated rates of photosynthesis in blue compared to

white irradiance are 0.75 according to the model and 0.62 in practice. Similarly, the green/white ratios are 1.93 (model) and 2.20 (experiment) respectively. The ratio of photosynthesis predicted in blue irradiance compared to that in green irradiance (blue/green = 0.39) does differ considerably from that found experimentally (blue/green = 0.28).

Divergence between model estimates and experimental values were particularly apparent in *Synechococcus* sp. WH 5701. Model estimates of the relative rates of photosynthesis in the different spectral distributions showed little relation to the experimentally-derived values. Photosynthetic rates under blue irradiance was estimated to be 80% of that in white irradiance while in actuality the rate is only 20%. Similarly, the green/white ratio is estimated at 0.33 while in practice it is 0.51. The largest discrepancy arises in the estimated rates of photosynthesis in blue as compared to green irradiance. The model predicts that the photosynthetic rate in blue irradiance will be 2.4 times that in green irradiance while the experimentally-derived rates show that photosynthesis in blue irradiance is only 40% of that in green irradiance. Such large differences can only be explained by significant non-additive effects between the different wavelengths.

The overall conclusion is that the simple method of computing the photosynthetic rate in polychromatic irradiance according to Eq. 8.1 provides a reasonable approximation for the prymnesiophyte *Pavlova* sp. (NEP) but is inappropriate for the two cyanobacteria *Synechococcus* sp. WH 5701 and *Synechococcus* sp. WH 7803. This result is consistent with the extent of the wavelength ranges where the effects of Emerson enhancement are considered to be important. Differences in the absorption properties of the two photosystems are largely restricted to wavelengths > 680 nm in prymnesiophytes

but occur throughout a significant portion of the PAR spectrum in cyanobacteria, corresponding to those wavelengths where absorption is dominated by chlorophyll.

8.5.3. The Magnitude of Emerson Enhancement in the Open Ocean.

A direct test of the validity of Eq. 3.26 for computing the photosynthetic rate of natural assemblages of phytoplankton in different polychromatic irradiance fields has not yet been carried out. However, an analysis of both the presumed taxonomic composition and the experimentally-derived action spectra of natural assemblages from the open ocean provides some insight into the likely importance of Emerson enhancement with respect to computing photosynthesis *in situ*.

In the open ocean it is generally agreed that the picoplanktonic size fraction are the most abundant component. Microscopic examination reveals that this component consists of both prokaryotic and eukaryotic cells. In addition to the direct measurement of the action spectra of natural assemblages, an examination of the taxanomic composition of the picoplankton provides a basis for the acceptance or rejection of the validity of using $\alpha^B(\lambda)$ to spectrally-weight photosynthesis under the changing spectral distribution that accompanies increasing depth. The spectral signature of $\alpha^B(\lambda)$ from oceanic assemblages should concur with the those of the constituent taxonomic components.

As difficulties associated with the isolation, culturing and preservation of picoplanktonic cells are overcome, the importance of the eukaryotic component is becoming evident. This component is dominated by prymnesiophytes, chrysophytes, prasinophytes and cryptophytes (Johnson and Sieburth 1982; Furuya and Marumo 1983;

Hallegraeff 1983; Yentsch 1983; Foss *et al.* 1984; Estep *et al.* 1984; Takahashi and Hori 1984).

The occurrence of prymnesiophytes among the oceanic phytoplankton has been appreciated for some time as this group includes the coccolithophorids, a small sized oceanic group characterized by calcite depositions on their surface (coccoliths). The deposition of calcite by these cells is considerable and globally represents a substantial carbon sink. The photosynthetic apparatus of prymnesiophytes is typical of the Chromophyta or brown algal line and contains chlorophylls *a*, c_1 and c_2 together with the carotenoid fucoxanthin. An unusual fucoxanthin derivative, 19'-hexanoyloxy-fucoxanthin, has recently been identified as the major carotenoid of the coccolithophorid *Emiliania huxleyi* (Arpin *et al.* 1976; Hertzberg *et al.* 1977). The absorption spectra of prymnesiophytes reflects this pigment composition and is typified by that of the *Pavlova* sp. strain examined (Figure 6.4). Furthermore, the photosynthetic action spectra of *Pavlova* sp. (NEP) indicate the participation of all pigments (Figure 7.3). The conclusion is that enhancement is likely to be of only minor significance in this taxonomic group considering the spectral distribution of underwater irradiance.

The light-harvesting system of the chrysophytes and prymnesiophytes are superficially similar in that the thylakoids are arranged in groups of three and the photosynthetic pigments comprise chlorophyll *a*, chlorophyll c_1, chlorophyll c_2 and fucoxanthin. Chlorophyll *a*:*c* ratios range from 1.7-3.6 (Jeffrey 1976). Absorption spectra exhibit high absorption in the 400-550 nm region, little absorption between 550 and 650 nm with a major peak at 676 nm (Vesk and Jeffrey 1977; Jeffrey 1980; Figure 6.4). An unusual minute chrysophyte has been isolated from the North Pacific Ocean which has an atypical pigment composition with two fucoxanthin-like pigments, chlorophyll c_2 only and a very labile chlorophyll *a* system (Lewin *et al.* 1977). No action

spectra appear to be available for any chrysophyte species however they are implicitly considered to be similar to those of other chromophytic algae such as prymnesiophytes or diatoms.

The presence of prasinophytes in the ocean has been inferred from the existence of chlorophyll *b* in the water column (Jeffrey 1974; Hallegraeff 1981; Bidigare *et al.* 1985). Green flagellates belonging to the Chlorophyta, Prasinophyta and Euglenophyta constitute a significant component of the phytoplankton in the open ocean (Jeffrey 1976; Jeffrey and Hallegraeff 1980). The photosynthetic system of prasinophytes comprises chlorophylls *a* and *b* together with the carotenoid siphonaxanthin in some species (Jeffrey 1980, 1984). Action spectra for the prasinophyte *Micromonas pusilla* indicate the participation of both chlorophylls such that the monochromatic action spectrum closely resembles the absorption spectrum (Jeffrey 1984). Like terrestrial plants and the green algae *Chlorella* (Haxo 1960) and *Ulva* sp. (Neori *et al.* 1986,1988), enhancement is considered to be only of significance at wavelengths above 680 nm, and so of minor importance in the marine light field.

In contrast, the photosynthetic system of cryptophytes consists of chlorophyll *a*, phycobiliproteins and chlorophyll c_2 (but not chlorophyll c_1) (O'hEocha and Raftery 1959; Jeffrey 1976). The presence of both chlorophyll *c* and phycobiliproteins is unique to this group. Phycoerythrin contributes significantly to absorption in the 500-570 nm region (Ingraham and Hiller 1983) and absorption peaks at 436 and 676 nm are attributable to chlorophyll *a* while a shoulder at 454 nm is due to chlorophyll c_2. In general terms, the absorption spectrum of oceanic cryptophytes is not unlike that of phycobiliprotein-containing cyanobacteria. The photosynthetic action spectra (oxygen evolution) of the marine cryptophyte *Chroomonas* sp. show that the phycobiliproteins functions as an efficient light-harvesting component in photosynthesis (Haxo and Fork

1959; Haxo 1960; Jeffrey 1984; Neori *et al.* 1986,1988). The phycobiliproteins of cryptophytes are not assembled into phycobilisomes like cyanobacteria, and the path of excitation transfer is unknown with the role of chlorophyll c_2 remaining undefined. Monochromatic action spectra show that wavelengths corresponding to both chlorophyll and phycobiliprotein absorption are effective in photosynthesis (Haxo and Fork 1959; Haxo 1960; Lichtle *et al.* 1980; Harnischfeger and Herold 1981; Jeffrey 1984; Neori *et al.* 1986,1988). This is in sharp contrast to the cyanobacteria and red algae and is undoubtedly due to the presence of chlorophyll c. The clear participation of the chlorophylls in the action spectrum of cryptophytes suggests that the role of enhancement is not as important in the determination of α^B in polychromatic light in cryptophytes as it is in cyanobacteria.

From the initial reports of prokaryotic cells as a "ubiquitous and diverse" component of the phytoplankton, chroococcoid cyanobacterial cells assigned to the genus *Synechococcus* have been considered the major constituent of the picoplankton. Early isolates consisted of both phycoerythrin (PE) and phycocyanin (PC) containing clones however it was soon realized that PE-rich species dominated open ocean assemblages and that PC-containing forms were only prevalent in inshore neritic waters (Glover 1985,1986,1988; Murphy and Haugen 1985; Fogg 1986; Joint 1986; Li 1986; Shapiro and Guillard 1986; Waterbury *et al.* 1986; Li and Platt 1987). The spectral properties of phycoerythrin arise from the presence and relative abundance of two chromophores phycoerythrobilin (PEB) and phycourobilin (PUB), which give rise to absorption peaks at 545-560 nm and 490-500 nm respectively. The first PE-containing *Synechococcus* spp. clones isolated before 1980 either lacked PUB altogether or more frequently exhibited a high PEB:PUB ratio (see Table 3 in Waterbury *et al.* 1986). Wood *et al.* (1985) have shown that strains containing both PEB and PUB chromophores ("Type I") can be distinguished from those containing only PEB ("Type II") by their fluorescence emission

spectrum following excitation by blue light. *Synechococcus* sp. WH 7803 (formerly DC-2) examined in this study is typical of Type I with a PUB:PEB ratio of about 1:4 (Alberte *et al.* 1984).

Subsequent studies found marine cyanobacteria with novel spectral characteristics and such cells were found to contain phycoerythrins with much higher PUB content (Kursar *et al.* 1981; Ong *et al.* 1984; Alberte *et al.* 1984). For example, *Synechococcus* sp. WH 8103 has a PUB:PEB ratio of 2:1 (Ong *et al.* 1984). Olson *et al.* (1988) have shown that it is possible to quantify the relative PUB content of strains within the Type I group by flow cytometry. The ratio of fluorescence emission intensity produced by individual cells when excited by both blue (488 nm) and green (515 nm) light constitutes a two point fluorescence excitation spectrum and varies with PUB content. Using this technique, Olsen *et al.* (1988) quantitatively examined the distribution of *Synechococcus* cell types in natural seawater samples along transects between Puerto Rico and Woods Hole and between Woods Hole and Senegal. They found that all natural populations had fluorescence properties similar to PUB-containing strains of *Synechococcus* and concluded that *Synechococcus* cells containing only PEB were not present in significant numbers. Furthermore, the most abundant forms of *Synechococcus* had a very high PUB content, most samples had PUB:PEB ratios as high or higher than the cultured strains considered to possess unusually high PUB contents.

The fact that the most abundant forms of *Synechococcus* sp. in oceanic waters are PUB-rich has important consequences in terms of their action spectra. The action spectra of the two cyanobacteria *Synechococcus* sp. WH 5701 and *Synechococcus* sp. WH 7803 (Figures 7.1 and 7.2) clearly demonstrate the segregation of phycobiliproteins and chlorophylls to Photosystems II and I respectively. Monochromatic action spectra of both species indicate the photosynthetic participation of phycobiliproteins only. Indeed,

this feature constitutes a clear diagnostic feature of cyanobacterial (and red algal) photosynthesis. The action spectrum of the phycocyanin-containing WH 5701 accords closely with that of the *Synechococcus* sp. given by Jeffrey (1984), an action spectrum dominated by a single major peak centered around 620 nm (Figure 7.1). In the case of the phycoerythrin-containing clone *Synechococcus* sp. WH 7803, a strain with a high PEB content, this results in a monochromatic action spectrum with a single peak around 550 nm (Figure 7.2). Similarly, the fluorescence excitation spectrum of *Synechococcus* sp. WH 7803 consists of a single peak at 550 nm with only a minor shoulder at 500 nm due to PUB absorption (Olsen *et al.* 1988).

In contrast, the fluorescence excitation spectra of clones such as *Synechococcus* sp. WH 8103 with a high PUB content exhibit a second major shoulder at 498 nm which is equal or greater in magnitude than the peak at 550 nm (Olsen *et al.* 1988). A similar bimodal photosynthetic action spectrum would be expected for all PUB-rich *Synechococcus* sp. strains. A major peak at 498 nm in the action spectrum of marine *Synechococcus* sp. would greatly enhance the cells photosynthetic performance at depth in the open ocean where blue wavelengths predominate. The pigment segregation evident in cyanobacterial action spectra means that effects of enhancement will be important when computing rates of photosynthesis under polychromatic irradiance at depth. However, because the narrowing of the spectral distribution of underwater irradiance is centred in the blue-green, the errors resulting with strains of *Synechococcus* sp. with a high PUB content will be less than for strains with PEB-dominated phycoerythrins. The largest errors would be expected for the cyanobacterial strains containing phycocyanin. In practical terms, the computation of PSR by the convolution of such a monochromatic action spectrum with the *in situ* irradiance spectrum could produce results that are not grossly dissimilar from those of cells based upon a chlorophyll-carotenoid light-harvesting system.

Perhaps of greatest significance is the recent identification of a distinctive component of the picoplankton consisting of prokaryotic chlorophyll-fluorescing cells believed to contain chlorophylls *a* and *b* and which resemble the prokaryote *Prochloron* (Chisholm *et al.* 1988). The discovery of an oxygenic chlorophyll *a*-chlorophyll *b*-containing prokaryote in itself has had tremendous evolutionary implications. The original isolate, *Prochloron* sp., was a unicellular symbiont of marine ascidians (Lewin 1975; Schuster *et al.* 1984). A free-living filamentous organism containing chlorophylls *a* and *b*, *Prochlorothrix nollandica*, has also been isolated and cultured (Burger-Wiersma *et al.* 1986).

The prochlorophytes identified by Chisholm *et al.* (1988) were found to reach concentrations exceeding 10^5 cells ml^{-1} in the deep euphotic zone. Cells were consistently found in the southern Californian Bight, the Panama Basin, the Gulf of Mexico, the Caribbean and across the North Atlantic along a transect from Woods Hole to Dakar, Senegal. These cells were most abundant at the bottom of the euphotic zone, close to the nitrite maximum layer, and below the *Synechococcus* maximum which was always above the nitrite maximum layer. The cells fluoresce red and contain a divinyl chlorophyll *a*-like pigment in addition to chlorophyll *b*, α-carotene and zeaxanthin. The divinyl chlorophyll *a*-like pigment is characterized by a red-shift of the Soret peak by 8-10 nm compared to normal chlorophyll *a* and is similar to a pigment isolated by Gieskes and Kraay (1983) from the < 1 μm size fraction in surface waters of the tropical North Atlantic. The presence of α- rather than β-carotene and the divinyl chlorophyll *a*-like pigment set these cells apart from the other prochlorophytes. Also, the chlorophyll *a*/*b* ratio was approximately 1, which contrasts sharply with the value of 4-7 for *Prochloron* sp. (Withers *et al.* 1978) and 8-9 for *Prochlorothrix hollandica* (Burger-Wiersma *et al.* 1986) but is similar to the values of 1-3 reported for marine eukaryotic chlorophytes

(Wood 1979). The combination of a chlorophyll *a* pigment with a 8-10 nm red shift and chlorophyll *b* with absorption maxima at 457 and 646 nm optimizes the absorption of the *in situ* irradiance which is dominated by blue (460-480 nm) wavelengths.

Although these cells differ in several respects from other prochlorophytes, some characteristics concerning the organization of the photosynthetic apparatus may be conserved within the prochlorophyte group. Both *Prochloron* sp. and *Prochlorothrix hollandica* contain a chlorophyll *a/b* antenna composed of an apoprotein of similar molecular mass and which may be homologous (Schuster *et. al.* 1984; Hiller and Larkum 1985; Bullerjahn *et al.* 1987). Separation of the major chlorophyll-protein complexes indicate that chlorophyll *b* was associated with the PSI immediate antenna complex and also the remaining three complexes that constitute the major chlorophyll *a/b* accessory antenna of *P. hollandica* (Bullerjahn *et al.* 1987). With both chlorophylls in the major light-harvesting antenna it is likely that Emerson enhancement effects will only be pronounced at red wavelengths greater than 680 nm. If the light-harvesting apparatus of these new marine prochlorophytes are similar to those of *Prochloron* sp., *P. hollandica* and eukaryotic green algae, the quantum efficiency should be relatively constant across the spectrum. In this case errors in the simple calculation of PSR due to the effects of Emerson enhancement will be minimal under *in situ* irradiance conditions.

The photosynthetic action spectra actually obtained for natural phytoplankton assemblages provide a consistent pattern. Action spectra of whole water samples from the Eastern Canadian Arctic (Figures 7.6 - 7.11), the North Atlantic (Figures 7.12 - 7.14) and the Sargasso Sea (Figure 7.5) reveal a spectral shape that corresponds closely to the absorption spectrum. That is they are typical of chlorophyll *a*-chlorophyll *c*-carotenoid or chlorophyll *a*-chlorophyll *b* light-harvesting systems (Chapter 7.3). In all cases, whole

water samples indicate little evidence of any significant peaks at wavelengths corresponding to phycobiliprotein absorption.

In the case of Arctic waters this clearly reflects the dominance of large diatoms and coccolithophorids in the phytoplankton assemblages. All the action spectra obtained from Arctic waters closely resemble that obtained for the diatoms *Stephanopyxis turris* (Jeffrey 1984) and *Chaetoceros gracilis* (Neori *et al.* 1986,1988). In open ocean samples the taxonomic identity of the principal photosynthetic components is less obvious from microscopical examination. Nevertheless the spectral form of the action spectra is remarkably consistent and similar in overall spectral shape. The whole water samples from the Sargasso Sea are consistent with diatoms observed to be present. However the spectral shape is also consistent with the photosynthetic action spectra determined for other Chromophytes such as the dinoflagellates *Glenodinium* sp. (Prezelin *et al.* 1976; Neori *et al.* 1986,1988) and *Gymnodinium* sp. (Jeffrey 1984) or the prymnesiophyte *Pavlova* sp. (NEP) (Figure 7.3). At other stations in the sub-tropical North Atlantic the action spectra determined for the > 3 μm size fraction is also consistent with that of the chlorophyll *a* - chlorophyll *c* - polyoxy xanthophyll pigment system of the chromophytes or even the chlorophyll *a* - chlorophyll *b* pigment system of the Chlorophyte lineage (Chlorophyta, Euglenophyta and Prasinophyta).

The action spectra of the < 3 μm size fraction, although limited to two samples, was also consistent with this designation or possibly that of the recently discovered prochlorophyte population. Only at the Nashville station, where cyanobacteria greatly outnumbered eukaryotes, did the action spectra did show signs of phycoerythrin participation by the PEB chromophore (550 nm). Even in this case the overall spectrum was dominated by a broad peak at blue wavelengths. Although both samples showed increased photosynthetic efficiencies at 675 nm indicating the active participation of

chlorophyll, the possibility also exists that activity at blue wavelengths was supplemented by the participation of the PUB chromophore of marine *Synechococcus* sp. In general however, the single peaked spectrum characteristic of phycobiliprotein-rich cyanobacteria was not a feature of the action spectra of natural assemblages.

The overall conclusion is that action spectra measurements of natural assemblages provide a spectral signature in accord with that typical of chlorophyll *a*-chlorophyll *c*-carotenoid or chlorophyll *a*-chlorophyll *b* light-harvesting systems. The uniformity and spectral shape of action spectra determined for natural assemblages constitute an important result. Two important points must be emphasized:

1. The spectral uniformity of all monochromatic action spectra determined for natural assemblages of phytoplankton from diverse locations and depths means that a single action spectrum may be universally applied. The validity of a single spectral weighting function of photosynthesis for primary production calculations greatly simplifies algorithms for remote sensing applications.

2. The general spectral invariance of the apparent quantum efficiency (*ie.* Figure 7.18), which implies that multiple wavelength interactions such as Emerson enhancement are minimal, suggests that the application of a simple spectral photosynthetic weighting function to the calculation of photosynthesis under polychromatic irradiance provides a reasonable first approximation.

8.5.4. Light Utilization at Depth.

The spectral dependency of $\alpha^B(\lambda)$ means that for any given action spectrum, the effective α^B determined under polychromatic light will depend upon the spectral

distribution of the light $I(\lambda)$. Consequently, the effective value of α^B *in situ* will change with depth because $I(\lambda)$ changes with depth due to the wavelength dependent attenuation of PAR. Where attenuation causes enrichment of those wavelengths that are efficiently utilized in photosynthesis then there will be a progressive increase in the light utilization index with depth. Conversely, where attenuation causes enrichment of wavelengths not efficiently utilized in photosynthesis there will be a progressive decrease in the light utilization index with increasing depth. Increases in the light utilization index with depth may be interpreted as a measure of spectral adaptation of the specific action spectrum to the specific light field *in situ* (chromatic adaptation in the strict sense). Conversely, any reduction in the light utilization index with increasing depth indicates that the specific action spectrum is negatively adapted to the changing spectral composition of the incident irradiance.

The effect of changing spectral composition upon the light utilization index at depth in different water types was determined by means of a simple model based upon the spectral attenuation characteristics of different water types given by Jerlov (1976). Light utilization indices were calculated according to Eq. 8.1 for successive depths for each water type using the relative action spectra established for the different species.

In the computation of this model, the spectral distribution of the surface irradiance ($I_O(\lambda)$) was based upon data from Strickland (1958) assuming clear sky conditions (sun + sky) with a solar elevation of 35° (Figure 8.2). The PFD within each 25 nm waveband was expressed relative to the average PFD of PAR (387.5 - 687.5 nm). The decrease in the PFD within each waveband $I_z(\lambda)$ at increasing depths z in the different water types was computed from the exponential relation:

$$I_z(\lambda) = I_O(\lambda) \exp^{-k(\lambda) z} \qquad ...(8.4)$$

The spectral attenuation coefficients $k(\lambda)$ were calculated from percentage transmission per meter values given by Jerlov (1976) (Figure 8.3). The photon flux density within each waveband was then expressed as a fraction of the total PFD of PAR at each depth. Based upon these spectral attenuation coefficients, the total PFD ($PAR = \Sigma I(\lambda)$) decreases approximately exponentially with depth in all water types (Figure 8.4).

Relative action spectra ($\alpha^B(\lambda)$) were calculated for both natural assemblages and picoplankton cultures from action spectra given in Chapter 7. Photosynthetic action in each 25 nm waveband was computed relative to the average over all twelve wavebands. In the case of the phytoplankton assemblages from Arctic waters the averaged action spectra (Figure 7.11) was the basis of the relative action spectrum. For the picoplankton cultures, relative action spectra were calculated for each culture by expressing photosynthesis in each waveband as a proportion of the average photosynthesis of all wavebands. The average relative action at each wavelength then computed for each species by averaging the relative action spectra of the three or four cultures (Figure 8.2).

The results of the model calculations show that for an action spectrum equivalent to that of Arctic phytoplankton assemblages or the prymnesiophyte *Pavlova* sp. NEP the light utilization index at the sea surface is slightly greater than that of a hypothetical black alga ($\alpha^{B'} = 1.06$ and 1.08 respectively in Table 8.1(a)). Light utilization indices of the two cyanobacterial species are lower. *Synechococcus* sp. WH 7803 with phycoerythrin has a light utilization index of 1.02 while *Synechococcus* sp. WH 5701, the phycocyanin-containing clone, has a light utilization index of 0.85 at the surface (Table 8.1(a)).

The direction and magnitude of the change in the light utilization index with increasing depth is dependent upon both the optical water type and action spectrum (Figures 8.5, 8.6, 8.7 and 8.8). For action spectra typical of both Arctic phytoplankton assemblages and the prymnesiophyte *Pavlova* sp. NEP, the light utilization efficiency increases significantly with depth in the clearest ocean water (Type I). At 150 m, a depth corresponding to 2 % surface PAR irradiance, the light utilization index increased to 1.52 and 1.68 respectively (Figures 8.5 and 8.6). These high values result from the strong co-variance between the action spectrum ($\alpha^B(\lambda)$) and the spectral distribution of irradiance at depth ($I_z(\lambda)$) for this optical water type. A similar increase, but of lesser magnitude, occurs in water Types IA, IB and II. In Type III, the light utilization index increases to 1.2 at a depth of 10 m (20 % surface PAR) and subsequently declines with further increase in depth to reach 1.15 at 35 m (0.8 % surface PAR). In optical water types characteristic of coastal waters (Types 1 - 9), the light utilization index decreases with increasing turbidity as the wavelengths of maximal transmission increases from blue to green to coincide with the spectral region of minimal photosynthesis, the so-called "green window" typical of the chlorophylls. In the most turbid water type, Type 9, the light utilization index of both Arctic assemblages and *Pavlova* sp. (NEP) decreases appreciably (Figures 8.5 and 8.6).

As the depth corresponding to the base of the euphotic zone differs in each water type it is convenient to plot the change in the light utilization index as a function of the incident irradiance (I_z/I_0) rather than simply depth. The base of the euphotic zone may be taken as 0.1 % of surface irradiance (corresponding to a PFD of 2-3 μmol m^{-2} s^{-1} assuming a PFD at the surface of 2000 - 3000 μmol m^{-2} s^{-1}). For action spectra characteristic of Arctic assemblages and *Pavlova* sp. in oceanic waters (Types I - III), the light utilization index changes as a linear function of I_z/I_0 for all values of I_z/I_0 greater than 0.1 (Figures 8.5 and 8.6). The relationship between the light utilization index and

I_z/I_o is generally non-linear for values of I_z/I_o between 0.1 and 0.001 (the base of the euphotic zone). This is the range of PFDs for which photosynthesis is most likely to be light-limited.

Depth-related changes in the light utilization index of the two cyanobacterial species are significantly different. In *Synechococcus* sp. WH 7803 there is a decrease in the light utilization index in all the open ocean water types (Figure 8.7). In the clearest water type, Type I, $\alpha^{B'}$ decreases to 0.58 at a depth of 150 m (2 % surface PAR). Parallel decreases are seen in optical water Types IA, IB and II although the magnitude of the decrease lessens with increasing turbidity. In water Type III the light utilization efficiency actually increases with depth to reach almost 1.4 at 35 m (0.8 % surface PAR). The further increases in turbidity in water Types 1 - 9 produce substantial increases in the light utilization index at depth as the wavelengths of maximal transmission shift to coincide with the action maximum of phycoerythrin (Figure 8.7). When plotted as a function of the ratio I_z/I_o, the light utilization index is clearly a non-linear function of I_z/I_o for all values of I_z/I_o (Figure 8.7).

Depth-related changes in the light utilization index of the phycocyanin-dominated cyanobacteria *Synechococcus* sp. WH 5701 indicate that the action spectrum of this species is poorly suited to the prevalent wavelengths of submarine irradiance in all but the most turbid waters. The light utilization index decreases exponentially with depth in all but the two most turbid water types (Types 7 and 9). In optical water types I, IA and IB which are characteristic of the open ocean, the light utilization index decreases from 0.85 at the surface to between 0.16 and 0.28 at 150 m (Figure 8.8). The wavelengths of maximum photosynthetic action which correspond to phycocyanin absorption are rapidly attenuated in all these water types leaving an incident spectral distribution at depth ill-suited to drive photosynthesis in this species. In oceanic waters the relationship between

the light utilization index and the ratio I_z/I_o is also highly non-linear for all values of I_z/I_o (Figure 8.8). In the more turbid coastal waters the relationship is almost linear for values of I_z/I_o between 0.1 and 1.0 (Figure 8.8).

From this simple comparison it is clear that the action spectrum established for both Arctic phytoplankton and the prymnesiophyte *Pavlova* sp. constitute a spectral response that is well suited for efficient photosynthetic utilization of the incident irradiance at depth in the ocean. This is particularly true for the open ocean for which the optical water types I, IA, IB and II predominate (see Jerlov 1976, Figure 72). The high rate of photosynthetic action at wavelengths between 400 and 500 nm attributable to the photosynthetic participation of chlorophylls *a* and *c* and carotenoids such as fucoxanthin (and potentially peridinin) provides for high light utilization indices.

The ratio of the light utilization index at depth relative to that at the surface also suggests the magnitude of the correction required to adjust "*simulated in situ*" production measurements made using deck incubators, where the irradiance source is natural sunlight and the PFD within the deck incubators is adjusted by way of neutral density screen. From values of $\alpha^{B'}$ in Figures 8.5 and 8.6, the rates of light-limited photosynthesis measured in such deck incubators need to be increased by a factor of between 1.06 and 1.69 to yield the photosynthetic rate attained under equivalent PFD at depth. The value at depth depends upon the optical water type and for oceanic water types varies from 1.3 to 1.69 at depths marking the base of the euphotic zone. This value closely corresponds to correction estimates suggested by the use of color filters to simulate the spectral composition of underwater irradiance (Jerlov 1954; Jitts 1963; Kiefer and Strickland 1970; Shimura and Ichimura 1973; Brown 1982).

8.5.5. Light Utilization under Artificial Light.

A second principal means of simulating the *in situ* irradiance gradient on board ship is with the use of incubators employing a tungsten-halogen lamp as the irradiance source. The spectral distribution of this irradiance source differs significantly from that of natural sunlight at the sea surface (Figure 4.6). There is a much lower proportion of blue wavelengths and a higher proportion of red wavelengths compared to the solar spectrum. By virtue of the spectral dependency of $\alpha^{B}(\lambda)$, light utilization under artificial light conditions can be expected to differ markedly from that *in situ*, even at the surface. By applying the simple spectral model (Eq. 8.1), the light utilization index for a tungsten-halogen light source ($\alpha^{B'}{}_{T}$) may be compared with those expected at different depths *in situ* ($\alpha^{B'}{}_{Z}$) in different optical water types.

As expected from the similarity in their action spectra, both Arctic assemblages and the prymnesiophyte *Pavlova* sp. (NEP) yielded similar results. Light utilization indices in tungsten light were 0.75 and 0.73 times those expected under natural solar radiation *at the sea surface* based solely upon differences in the spectral distribution of the irradiance source (Table 8.1(b)). In contrast, the light utilization index of the phycoerythrin-containing cyanobacterium *Synechococcus* sp. WH 7803 were almost identical under both irradiance sources such that $\alpha^{B'}{}_{T}/\alpha^{B'}{}_{O} = 0.98$. The light utilization index of *Synechococcus* sp. WH 5701 was considerably greater in tungsten light compared to solar irradiance ($\alpha^{B'}{}_{T}/\alpha^{B'}{}_{O} = 1.75$) by virtue of the greater action at red wavelengths due to the photosynthetic participation of phycocyanin (Figure 8.10).

Differences between the light utilization index calculated for tungsten light compared to that calculated under natural irradiance *at depth* depended upon both species and optical water type. For optical water types characteristic of the open ocean (Types I

and III) the ratio $\alpha^{B'}{}_T/\alpha^{B'}{}_Z$ of both Arctic assemblages and *Pavlova* sp. decreased with increasing depth (Figures 8.9). The decrease was most pronounced in Type I waters where $\alpha^{B'}{}_T/\alpha^{B'}{}_Z$ decreased to 0.52 and 0.47 respectively. The decrease in Type III waters was less pronounced (to 0.72 and 0.63 respectively). With increasing turbidity, the light utilization under tungsten relative to that *in situ* increased with depth such that the ratio $\alpha^{B'}{}_T/\alpha^{B'}{}_Z$ approached unity in coastal water types 1 - 5 (Figure 8.9). For the most turbid water type (Type 9) the ratio increased to 1.5. These results indicate that for the open ocean, experimental values of α^B determined using tungsten-halogen lamps will be significantly less than that expected *in situ* at similar PFDs because of the differences in light utilization associated with the different spectral distributions.

The relationship between the light utilization under tungsten light and that *in situ* is very different in the two cyanobacteria. In the case of *Synechococcus* sp. WH 7803, the ratio $\alpha^{B'}{}_T/\alpha^{B'}{}_Z$ decreases with depth in all water types *except* Type I. For the clearest ocean water $\alpha^{B'}{}_T/\alpha^{B'}{}_Z$ increases to a value of 1.7 at a depth of 150 m (Figure 8.10). This implies that rates of light-limited photosynthesis at depth in the open ocean will be substantially less than estimates of α^B obtained at similar photon flux densities using tungsten lamps. This situation is reversed in the more turbid coastal water types (Types 1 - 5) where the ratio $\alpha^{B'}{}_T/\alpha^{B'}{}_Z$ decreases with increasing depth to a value of about 0.4. This implies that considerably higher rates of light-limited photosynthesis can be expected at depth compared to those measured under tungsten-halogen light source at equal photon flux densities.

The heavy spectral weighting of tungsten-halogen bulbs toward the red end of the spectrum means that the light utilization of the phycocyanin-containing cyanobacteria *Synechococcus* sp. WH 5701 is considerably greater under artificial light compared to *in situ* (Figure 8.10). The ratio $\alpha^{B'}{}_T/\alpha^{B'}{}_Z$ lies between 4 and 5 for water types I, 1 and 5 and

is maximal for Type III waters where it reaches 9. Only in the most turbid waters (Type 9) does the light utilization index *in situ* approach that determined under tungsten-halogen lights ($\alpha^{B'}{}_T/\alpha^{B'}{}_Z = 1.45$). This prediction agrees closely with the experimental value of 4 obtained by Wood (1985) where photosynthetic rates *in situ* were compared to those under artificial lights. The magnitude of the difference in light utilization under both light sources means that special caution must be exercised in interpreting P-I results obtained using tungsten lamps.

8.5.6. Light Utilization at Depth and Primary Production Models.

The task of estimating oceanic primary production at regional or basin scales by means of remote sensing consists of two parts: first, the development of an algorithm for the estimation of local water column production; and second, the extrapolation of such local results to larger horizontal and temporal scales (Platt and Sathyendranath 1988). Algorithms for estimating local water column primary production require as input information describing the incident flux of photons, the attenuation of irradiance within the water column, the depth distribution of photosynthetic pigments capable of utilizing the ambient light and finally a functional relationship relating the photosynthetic rate to ambient irradiance. The change in the utilization index of phytoplankton with depth resulting from the changing spectral distribution of the ambient light field represents an important part of this final local algorithm.

To extend estimates of primary production from a local scale to the larger horizontal scales typical of ocean basins Platt and Sathyendranath (1988) proposed the partitioning of the oceans into regions based upon consideration of the biological structure of the water column and the physiological characteristics of the phytoplankton. The regions are considered "dynamic" in that the boundaries of the regions and the

magnitudes of the parameters describing physiological characteristics of the phytoplankton can change with the season. Differences in the taxonomic composition of the phytoplankton assemblages, the spectral attenuation of underwater irradiance and biological structure of the water column in each region necessitate that mathematical descriptions of the depth-dependence of light utilization be specific to the region. The combination of action spectra determined for phytoplankton sampled from the different regions with the spectral attenuation coefficients for the different water types, as described in Section 8.5.4., comprises a preliminary attempt to provide a spectral correction to depth-integrated primary production.

CHAPTER 9

CONCLUSIONS.

1. This study examined the photosynthetic characteristics of several oceanic picoplankton species and natural assemblages. The dependence of the photosynthetic rate upon both the photon flux density (the P-I response) and the photon wavelength (the P-S response) was quantified with a view to predicting primary production throughout the water column.

2. The photosynthetic response of the three picoplankton clones to both photon flux density (the P-I response) and spectral distribution (the P-S response) were unique to each species.

3. The P-I response of the cyanobacterium *Synechococcus* sp. WH 5701 showed no sign of photoinhibition up to PFDs of 2000 μmol m^{-2} s^{-1}, despite the fact that growth PFDs were as low as 7 μmol m^{-2} s^{-1}. A quantitative description of the P-I response required a saturation function with a minimum of 3 parameters. Bannister's (1979) three-parameter empirical model provided the best fit to the data. All the rational models that reduced to the form of a non-rectangular hyperbola (Rabinowitch 1951; Fasham and Platt 1983; my two-photosystem model [Eq. 3.104]) also provided excellent descriptions of the P-I response.

4. A reduction in photosynthetic rate at high PFDs characterized the P-I responses of the cyanobacterium *Synechococcus* WH 7803 and the prymnesiophyte *Pavlova* sp. (NEP). The magnitude of this reduction depended upon the growth PFD. For both

species the five-parameter empirical model of Platt and Gallegos (1981) consistently provided the best fit. The new four-parameter version of this formulation, where $I_t = 0$, and the new six-parameter model [Eqs. 3.34 and 3.36] were also sufficiently flexible geometrically to provide a good quantitative description of all the P-I responses. The only kinetic models to provide good consistent results were the single-photosystem model of Fasham and Platt (1983) and my two-photosystem model [Eq. 3.119]. The new Poissonian model also yielded a reliable fit provided the parameters describing photoinhibition were kept independent of the parameters describing photochemistry. Setting the number of hits required for photochemistry to unity provides an alternative four-parameter formulation that includes photoinhibition.

5. The success of the new two-photosystem kinetic model introduced in Chapter 3.6.2. as a description of the P-I response of all picoplankton clones makes it the model of choice. Besides the ease of choosing initial estimates for all the parameters by simple inspection of the P-I curve, the model structure has the potential for including the effects of Emerson enhancement upon the photosynthetic rate at light-limiting PFDs.

6. Values of the parameters describing the P-I response of each of the picoplanktonic clones depended upon the growth PFD. In *Synechococcus* sp. WH 5701 the light-limited rate of photosynthesis (α^B) of different cultures were similar despite the cultures being grown at PFDs ranging from 7 to 70 μmol m^{-2} s^{-1}. The maximum rate of photosynthesis, P_m^B, increased by a factor of two with increasing PFD over the range of growth PFDs. The combined effect led to a progressive increase in the optimal PFD ($I_k = P_m^B/\alpha^B$) from 120 to 230 μmol m^{-2} s^{-1}.

7. In *Synechococcus* sp. WH 7803, both the light-limited (α^B) and light-saturated (P_m^B) rates of photosynthesis decreased as growth PFD increased from 17 to 35 μmol m^{-2}

s^{-1}. The relative decrease of P_m^B was greater than that of α^B, yielding a decrease in I_k from 130 to 85 μmol m^{-2} s^{-1}. The amount by which the photosynthetic rate was reduced at high PFDs was inversely related to growth PFD.

8. *Pavlova* sp. (NEP) exhibited similar photoadaptive trends. Despite indications that the culture grown at the lowest PFD (8 μmol m^{-2} s^{-1}) was light-stressed (*ie.* reduced α^B), the culture maintained an optimal irradiance (I_k) of 85 μmol m^{-2} s^{-1}. In the culture grown at 45 μmol m^{-2} s^{-1} the combination of increased maximal photosynthetic rates (P_m^B) and reduced photoinhibition led to a substantial increase in the optimal growth irradiance (I_k = 220 μmol m^{-2} s^{-1}).

9. The abruptness of the transition from light-limited to light-saturated photosynthesis in the P-I responses of all three picoplankton species increased with increasing growth PFD. This consistent photoadaptive trend emphasizes the importance of including a third parameter describing this curvature in both photoinhibition- and saturation-type P-I formulations.

10. In both *Synechococcus* sp. WH 7803 and *Pavlova* sp. (NEP), the slope describing the light-limited rate of photosynthesis (α^B) correlated positively with the slope describing light-inhibited photosynthesis at high PFDs (β^B).

11. The relative ranking of the light-limited rate of photosynthesis (α^B) in white (= red), blue and green polychromatic light differed in all species. The relative ranking of α^B in each species could be explained on the basis of the photosynthetic pigments present. For *Synechococcus* sp. WH 5701 the rank order was $\alpha_{white(=red)} > \alpha_{green} > \alpha_{blue}$, showing the photosynthetic importance of phycocyanin. The rank order in *Synechococcus* sp. WH 7803, $\alpha_{green} > \alpha_{white(=red)} > \alpha_{blue}$, showing the active

photosynthetic participation of phycoerythrin. Spectral differences in the light-limited rates of photosynthesis were less pronounced in *Pavlova* sp. where the ranking $\alpha_{blue} > \alpha_{white(=red)} > \alpha_{green}$ reflected the dominant light-harvesting role of chlorophyll.

12. The magnitude of differences in the light-limited rates of photosynthesis observed under different spectral distributions in any single clone (up to a factor of five), and the different color ranking within each species, serve to emphasize the importance of the spectral distribution of the incident irradiance when determining the P-I response of the picoplankton. The results show that spectral response of the prymnesiophyte *Pavlova* sp. (NEP) is particularly well-suited for photosynthesis at depth in the ocean where blue wavelengths predominate. In contrast, the phycocyanin-containing cyanobacterium *Synechococcus* sp. WH 5701 is poorly suited to the wavelengths found at depth.

13. In any single species, the P-I responses obtained under different spectral distributions were proportional to one another *over the range of PFDs measured.* Plotting the photosynthetic response as a function of the logarithm of the PFD produced response curves that appeared parallel. This general proportionality resulted from the domination of the extended linear region in the P-I response for the range of PFDs examined. For any single species, the ratio between the light-limited photosynthetic rates determined under the different spectral distributions (*ie.* $\alpha_{blue} : \alpha_{green} : \alpha_{white\ (=red)}$) was similar for all cultures and thus unaffected by growth PFD, *at least for the range of growth PFDs examined.*

14. The monochromatic action spectra ($\alpha^B(\lambda)$) based upon the incorporation of ^{14}C by each of the three picoplankton species were very different. The spectral characteristics of the action spectrum, which approximates the action spectrum of photosystem II, closely

resembled the action spectrum established for phylogenetically related species based upon oxygen production measurements.

15. The action spectrum of the prymnesiophyte *Pavlova* sp. (NEP) demonstrates the active photosynthetic participation of chlorophylls *a* and *c* and the carotenoid fucoxanthin. The spectra show a broad maximum in $\alpha^B(\lambda)$ between 475 nm and 550 nm, low values from 550 nm to 650 nm, and a second maximum at 675 nm. This spectral dependence corresponds to that established for other Chromophytes with similar pigmentation. The action spectrum established for *Pavlova* sp. (NEP) is the first for a prymnesiophyte. The close spectral correspondence between the action spectrum and the absorption spectrum also suggests that the spectral properties of both photosystems are very similar in this species.

16. In contrast, the action spectra obtained from the two cyanobacterial species consisted of a single maximum corresponding to the photosynthetic participation of the phycobilipigment present. In *Synechococcus* sp. WH 5701 this maximum is at 625-650 nm corresponding to the photosynthetic participation of phycocyanin; in *Synechococcus* sp. WH 7803 the peak occurs at 550 nm corresponding to the photosynthetic activity of phycoerythrin. In neither species is the photosynthetic involvement of chlorophyll *a* evident despite the unequivocal importance of this pigment based upon the absorption spectra. This result is consistent with previous studies on cyanobacteria that show the predominant association of chlorophyll *a* with photosystem I.

17. The absence of any photosynthetic signal due to chlorophyll *a* participation in the monochromatic action spectra of cyanobacteria constitutes a valuable diagnostic spectral signature. The single peak attributable to phycobiliproteins may be used to identify the presence and photosynthetic contribution of cyanobacteria to the light-limited

photosynthetic rates observed in natural assemblages. However, the significant difference in the spectral responses of the two photosystems in cyanobacteria suggests that Emerson enhancement is of potential importance when photosynthesis occurs under polychromatic irradiance. Such enhancement significantly complicates attempts to model photosynthetic rates at depth in the ocean.

18. Monochromatic action spectra of natural phytoplankton assemblages reveal the dominant role of chlorophyll *a*. The phytoplankton assemblages from the Eastern Canadian Arctic, dominated by Chromophytes such as diatoms and coccolithophorids, exhibited action spectra ($\alpha^B(\lambda)$) with a maximum between 425 and 475 nm, a shoulder from 475 to 550 nm, a distinct trough of low photosynthetic efficiency between 575 and 525 nm, and a second maximum at 675 nm. These spectra demonstrate the photosynthetic participation of chlorophylls *a* and *c* and the carotenoid fucoxanthin. As with the Chromophyte *Pavlova* sp., the close correspondence between the action spectrum and the absorption spectrum implies that both photosystems have similar spectral responses. The quantum yield spectrum is relatively uniform across the spectrum, the slight maximum between 500 and 575 nm suggests that fucoxanthin is associated preferentially with photosystem II.

19. In Arctic waters, depth-related differences in the action spectrum affected only the magnitude of light-limited photosynthetic rates, not the spectral dependence. Phytoplankton assemblages from deeper water in well-stratified water columns exhibited higher chlorophyll-specific rates of photosynthesis at all wavelengths. There was no evidence for any increase in the photosynthetic participation of accessory pigments in assemblages from deeper waters. Similar rates of light-limited photosynthesis were found in both deep and shallow samples from well-mixed water columns.

20. Monochromatic action spectra for natural phytoplankton assemblages from oligotrophic waters were more difficult to measure because of the low biomass present. A similar spectral dependence was discernible with increased photosynthetic efficiencies at wavelengths corresponding to chlorophyll absorption. The action spectrum of one sample dominated by cyanobacteria, collected from the chlorophyll maximum at the Yakutat seamount, had an additional minor peak at 550 nm which could be attributed to photosynthetic participation of PE.

21. In Arctic waters with high chlorophyll concentrations (> 2 mg Chl m^{-3}), the spectral similarity of the action spectrum and the absorption spectrum suggests that the spectral responses of both photosystems are similar. Given the spectral distribution of irradiance at depth in these waters, Emerson enhancement effects are likely to be little importance in determining the photosynthetic rate at depth. This feature of phytoplankton photosynthesis greatly simplifies attempts to model photosynthesis at depth in these waters.

22. Results suggest that the photosynthetic response of natural phytoplankton assemblages from the Sargasso Sea and Mid-North Atlantic show similar spectral dependence to that of less oligotrophic waters. If confirmed, the effects of Emerson enhancement may be considered minimal throughout the world's oceans and the monochromatic action spectra typical of Chromophytes (such as *Pavlova* sp. or the Arctic phytoplankton assemblage) may be considered an appropriate spectral weighting function for determining photosynthetic rates under polychromatic light. This simplifies modelling the photosynthetic rate at depth under the various spectral distributions characteristic of the different water types. The conservative nature of $\alpha^B(\lambda)$ also means that a single spectral weighting function could be universally applied.

23. Absorption spectra of the three picoplankton species identified the major photosynthetic pigments present. In the cyanobacteria *Synechococcus* spp. WH 5701 and WH 7803 the magnitude of the absorption peaks attributable to the phycobilipigments (PC and PE respectively) were comparable to those of chlorophyll *a*. In the prymnesiophyte *Pavlova* sp. (NEP), chlorophylls c_1 and c_2 and the carotenoid fucoxanthin gave rise to a broad shoulder on the Soret band of chlorophyll *a*.

24. In each species, minor differences in the relative magnitude of the absorbance peaks were related to growth PFD. These differences were most pronounced in the two cyanobacteria. In all species the ratio between the Soret peak of chlorophyll *a* (438 nm) and the long-wave peak (678 nm) *increased* as growth PFD increased. In both *Synechococcus* spp. the absorption peaks due to the phycobilipigment, PE (542 nm) in WH 7803 or PC (622 nm) in WH 5701, *decreased* relative to the 678 nm absorption peak of chlorophyll as the growth PFD increased.

25. The absorption spectra of natural particulate material contained fewer distinctive features. Absorption spectra from diverse locations and depths were very similar in spectral form, with a ubiquitous absorbance peak at 676 nm characteristic of chlorophyll and strong absorption at blue wavelengths. In samples where the chlorophyll concentration exceeded 2-3 mg Chl m^{-3} a distinct absorbance peak occurred at 435 nm. In samples with chlorophyll concentrations below this threshold, the absorbance increased monotonically with decreasing wavelength below 650 nm. No evidence of phycobilipigment absorption was found in any of the natural water samples.

26. The diffuse attenuation coefficient of particles (a^*_p) obtained using GF/F filters (units: m^{-1}) was dependent upon the optical density of the filter/particle combination. A significant under-estimation of a^*_p at low optical densities (= low pigment/particle

concentrations) leads to a systematic over-estimation of the chlorophyll-specific attenuation cross-section (a^*_{chl}). The dependence of a^*_p estimates upon the optical density of the sample introduces a systematic bias to the calculated ratio of absorption peaks (since in any sample each peak has a different optical density). This effect was minimized when chlorophyll concentrations on the filter exceeded 1 μg Chl cm^{-2}. In practice, such concentrations are difficult to achieve when sampling oligotrophic waters with a high content of detritus.

27. Detrital material contributes significantly to absorption at blue wavelengths in waters of low chlorophyll concentration. As a result the absorption spectrum of oceanic particulates deviates significantly from that of the photosynthetically active cells. Therefore the absorption spectrum of oceanic particulates does not provide a suitable spectral weighting function for the P-I response, particularly in oligotrophic waters where the contribution of detritus is high.

28. The photosynthetic action spectra of individual picoplankton species or natural assemblages can be used as a spectral weighting function in models to compute the light-limited photosynthetic rate under different spectral distributions of light. Results from a simple additive model show that the ability of Chromophytes (exemplified by *Pavlova* sp. (NEP) or Arctic phytoplankton assemblages) to utilize the ambient spectral distribution increases significantly with depth in all oceanic water types. This increase in the light utilization ability of the phytoplankton must be included in models of depth-integrated primary production.

29. The spectral dependence of photosynthesis also affects the rate of light-limited photosynthesis under artifical (tungsten) lights relative to that expected at depth under the ambient spectral distributions characteristic of different water types. The results suggest

that light-limited rates of photosynthetic determined under artificial (tungsten) light may under-estimate the photosynthetic rate expected at depth by up to a factor of two in oceanic waters. Primary production models that use photosynthetic parameters determined from P-I responses using deck incubators utilizing either natural surface sunlight or artificial light need to have a spectral correction applied.

30. The spectral uniformity of the photosynthetic action spectra ($\alpha^B(\lambda)$) determined for phytoplankton assemblages isolated from a such a broad range of latitudes and water types greatly simplifies the modelling of photosynthesis at depth. In addition, since the spectral response is similar to that of the Chromophyta or Chlorophyta, the effects of Emerson enhancement that arise from significant differences in the spectral properties of the two photosystems are considered minimal. The photosynthetic rate under polychromatic irradiance may consequently be approximated as the integral of the product of $I(\lambda)$ and $\alpha^B(\lambda)$. This approximation implicitly assumes that the effect of photons of different wavelength are independent and additive.

31. The conservative spectral form of the photosynthetic action spectrum also means that the biomass-normalized action spectra ($\alpha^B(\lambda)$) may be constructed from the relative action spectra ($\alpha(\lambda)_{rel}$) established in this study (Table 8.2) and the apparent quantum yield determined at any single wavelength ($\phi_a(\lambda) = \alpha^B(\lambda)/a^*_{chl}(\lambda)$). The chlorophyll absorption peak of 675 nm constitutes the most appropriate wavelength for determining $\phi_a(\lambda)$ since interference by detrital absorption is minimal at this wavelength. The relative action spectra ($\alpha(\lambda)_{rel}$) provided by this study could be combined with regional values of the apparent quantum yield at 675 nm $\phi_a(675)$, the spectral attenuation coefficients $k(\lambda)$ and the spectral irradiance at the sea surface $I_o(\lambda)$ to predict the photosynthetic rate throughout the water column at different locations.

32. The success of the new kinetic model as a quantitative description of the P-I response suggests that this P-I formulation be the basis of such depth-integrated production models. In addition to providing an excellent fit to the P-I response of the picoplankton species examined, the model provides a preliminary means of incorporating the effects of Emerson enhancement into a spectral description of photosynthesis in those phylogenetic groups possessing photosystems that differ significantly in their spectral response. Although the action spectra of natural assemblages determined in this study indicate that enhancement is of only minor importance, the potential exists that further studies may identify regions or depth horizons within the world's oceans that are dominated by phylogenetic groups where enhancement is quantitatively important.

Photosynthetic characteristics of picoplankton and natural phytoplankton assemblages

By

Roderick E. Warnock

Submitted in partial fulfillment of the requirements for the degree

of Doctor of Philosophy

at

Dalhousie University

Department of Biology

February 1990

PART II

Table 2.1.

Mathematical formulations of the P-I response. I. Saturation models.

Formulations are expressed in dimensionless form. P_m is the maximum photosynthetic rate and I_k is the *PFD* at which the initial slope intersects with the maximum photosynthetic rate. Parameters Θ and m govern the curvature at the point of transition from light-limited to light-saturated photosynthesis.

BLACKMAN (1905)	P / P_m	=	I / I_k	$0 \le I / I_k \le 1$
		=	1	$1 < I / I_k$
BALY (1935)	P / P_m	=	$\dfrac{I / I_k}{1 + I / I_k}$	
SMITH (1936)	P / P_m	=	$\dfrac{I / I_k}{[1 + (I / I_k)^2]^{1/2}}$	
BAULE (1917)	P / P_m	=	$1 - exp(-I / I_k)$	
THORNLEY (1976a)	P / P_m	=	$I / I_k [1 - exp(-I_k / I)]$	
JASSBY & PLATT (1976)	P / P_m	=	$tanh(I / I_k)$	
THORNLEY (1976b)	P / P_m	=	$\dfrac{(1 + I / I_k) - [(1 + I / I_k)^2 - 4\Theta(I / I_k)]^{1/2}}{2\Theta}$	
BANNISTER (1979)	P / P_m	=	$\dfrac{I / I_k}{[1 + (I / I_k)^m]^{1/m}}$	

Table 2.2.

Mathematical formulations of the P-I response. II. Inhibition models.

Formulations are expressed in dimensionless form. P_s is the maximum *potential* photosynthetic rate in the absence of photoinhibition, P_m is the maximum *realized* photosynthetic rate. I_s is the *PFD* at which the initial slope intersects with the maximum potential photosynthetic rate ($= P_s / \alpha$), I_k is the PFD at which the initial slope intersects with the maximum realized photosynthetic rate ($= P_m / \alpha$) and I_m is the PFD where photosynthesis is optimal. The parameters a, b and n control the magnitude of photoinhibition while m is a shape parameter. I_b is the PFD where the photosynthetic rate is half the maximal potential rate (I for $P = P_s / 2$) and I_t is the difference between the threshold PFD marking the onset of photoinhibition and I_b.

STEELE (1962)
$$P / P_s = (I / I_m) \exp(1 - I / I_m)$$

VOLLENWEIDER (1965)
$$P / P_s = \frac{I / I_s}{[1 + (I / I_s)^2]^{1/2} [1 + (a I / I_s)^2]^{n/2}}$$

FEE (1973)
$$P / P_s = \frac{I / I_s}{[1 + (I / I_s)^2]^{(n+1)/2}}$$

WILLIAMS (1978)
$$P / P_s = \frac{I / I_s}{[1 + (I / I_s)^2]^{1/2} [1 + (a I / I_s)^2]^{1/2}}$$

STEEL (1973)
$$P / P_s = \frac{I / I_s}{[1 + (I / 2 I_s)^2]}$$

PLATT *et al.* (1980)
$$P / P_s = [1 - \exp(-I / I_s)] [\exp(-b I / I_s)]$$

PLATT & GALLEGOS (1980)
$$P / P_s = \frac{1}{2} \left[\frac{I / I_s}{[1 + (I/I_s)^m]^{1/m}} \right] \left[\frac{I - I_b}{[(I - I_b)^m + (I_b - I_t)^m]^{1/m}} \right]$$

IWAKUMA & YASUNO (1983)
$$P / P_s = \frac{I / I_s}{[1 + (I / I_s)^m]^{(n+1)/m}}$$

Table 2.3.

Solutions for the calculation of integral photosynthesis throughout the water column for various P-I formulations. I_0 is the *PFD* at the ocean surface, I_k is the *PFD* at which the initial slope of the P-I response intersects with the maximum photosynthetic rate and I_m is the *PFD* yielding the optimal photosynthetic rate. The attenuation coefficient k is assumed to be uniform throughout the water column so that the PFD decays exponentially with depth (*ie.* $I_z = I_0 \exp(-k z)$).

	$f(I_0 / I_k)$	
	Analytical solution	Numerical solution
BLACKMAN (1905)	$I_0 / I_k \quad I_0 / I_k < 1$ $1 + \ln(I_0 / I_k) \quad I_0 / I_k \geq 1$	
BALY (1935)	$\ln(1 + I_0 / I_k)$	
SMITH (1936)	$\sinh^{-1}(I_0 / I_k)$	
BAULE (1917)	*no solution found*	$\sum_{n=1}^{\infty} \frac{-(I_0 / I_k)}{n \cdot n!}$
STEELE (1962)	$(I_m / I_k)[1 - \exp(-I_0 / I_m)]$	
VOLLENWEIDER (1965)	- *no general solution found* - *specific case solutions:*	
$n = 1$	$2[\arctan(I_0 / I_k)]$	
$n = 2$	$(I_0 / I_k) / [1 + (I_0 / 2.6 I_k)^2]^{1/2}$	
JASSBY & PLATT (1976)	- *no solution for* $I_0 / I_k > \pi / 2$	

Table 5.1.

Parameter estimates for the P-I response of *Synechococcus* sp. WH 5701 grown under a photon flux density of 8 μE m^{-2} s^{-1} (culture SY 9149). Parameter estimates in the different formulations were determined by non-linear regression.

Function	Std. Dev. of Fit	Parameter			± Std. Dev.
(i) Empirical models.					
BALY (1935)	1.08	P_m	=	14.0[b]	± 0.23
		I_k	=	66[a]	± 4.7
SMITH (1936)	0.661	P_m	=	12.8[b]	± 0.11
		I_k	=	104[a]	± 3.4
BAULE (1917)	0.687	P_m	=	12.8[b]	$\pm 8.8 \cdot 10^{-3}$
		I_k	=	86[a]	± 0.04
THORNLEY (1976)	0.894	P_m	=	13.7[b]	± 0.17
		I_k	=	101[a]	± 5.2
JASSBY & PLATT (1976)	0.587	P_m	=	12.5[b]	± 0 09
		I_k	=	112[a]	± 2.9
BANNISTER (1979)	0.586	P_m	=	12.5[b]	± 0.1
		I_k	=	119[a]	± 4.1
		m	=	3.1	± 0.32
NEW GEOMETRIC MODEL *[Eqs. 3.34 & 3.36]*	0.596	P_m	=	12.5[b]	± 0.36
		I_k	=	119[a]	± 6.6
		m	=	3.1	± 0.45
		I_j	=	4026[a]	$\pm 1.1 \cdot 10^{5}$
		I_t	=	$2.43 \cdot 10^{5}$[a]	$\pm 7.7 \cdot 10^{6}$
		n	=	115	$\pm 3.5 \cdot 10^{3}$
(ii) Rational models.					
RABINOWITCH (1951)	0.593	P_m	=	12.7[b]	± 0.1
		I_k	=	119[a]	± 4.0
		Θ	=	0.93	± 0.02

Table 5.1. (contd.)

FASHAM & PLATT (1983)	0.594	μ	=	13.9 [b]	$\pm$ 0.6
		α	=	0.107 [c]	$\pm$ 0.004
		χ	=	0.0088	$\pm$ 0.003
		β	=	$1.89 \cdot 10^{-4}$ [d]	$\pm 1.8 \cdot 10^{-4}$
MEGARD *et al.* (1984)	0.849	P_s	=	17.9 [b]	$\pm$ 0.76
		K_1	=	107 [a]	$\pm$ 10
		K_2	=	3315 [a]	$\pm$ 592
NEW TWO-PHOTOSYSTEM MODEL *[Eq. 3.119]*	0.596	μ	=	12.66 [b]	$\pm$ 0.19
		α	=	0.114 [c]	$\pm$ 0.007
		χ	=	0.897	$\pm$ 0.67
		β	=	$3.14 \cdot 10^{-5}$ [d]	$\pm 2.0 \cdot 10^{-3}$

Units:

[a] $\mu E\ m^{-2}\ s^{-1}$
[b] $\mu mol\ C\ m^{-2}\ hr^{-1}$
[c] $\mu mol\ C\ m^{-2}\ hr^{-1}\ [\mu E\ m^{-2}\ s^{-1}]^{-1}$
[d] $[\mu E\ m^{-2}\ s^{-1}]^{-1}$

Table 5.2.

Parameter estimates for the P-I response of *Synechococcus* sp. WH 5701 grown under a photon flux density of 15 μE m^{-2} s^{-1} (culture SY 9157). Parameter estimates in the different formulations were determined by non-linear regression.

Function	Std. Dev. of Fit	Parameter			± Std. Dev.
(i) Empirical models.					
BALY (1935)	1.24	P_m	=	15.8 [b]	± 0.28
		I_k	=	81 [a]	± 6.0
SMITH (1936)	0.754	P_m	=	14.3 [b]	± 0.07
		I_k	=	124 [a]	$\pm 3.2 \cdot 10^{-3}$
BAULE (1917)	0.795	P_m	=	14.1 [b]	± 0.13
		I_k	=	101 [a]	± 3.4
THORNLEY (1976)	1.01	P_m	=	15.4 [b]	± 0.2
		I_k	=	121 [a]	± 6.4
JASSBY & PLATT (1976)	0.646	P_m	=	13.9 [b]	± 0.10
		I_k	=	132 [a]	± 3.2
BANNISTER (1979)	0.633	P_m	=	13.9 [b]	± 0.11
		I_k	=	145 [a]	± 4.6
		m	=	3.46	± 0.38
NEW GEOMETRIC MODEL *[Eqs. 3.34 & 3.36]*	0.638	P_m	=	14.3 [b]	± 0.34
		I_k	=	140 [a]	± 6.7
		m	=	3.11	± 0.42
		I_j	=	2647 [a]	± 341
		I_t	=	2720 [a]	± 422
		n	=	1.14	± 0.91
(ii) Rational models.					
RABINOWITCH (1951)	0.645	P_m	=	14.1 [b]	± 0.13
		I_k	=	144 [a]	± 4.6
		Θ	=	0.947	± 0.01

Table 5.2. (contd.)

FASHAM & PLATT (1983)	0.640	μ	=	15.6 [b]	$\pm$ 0.63
		α	=	0.099 [c]	$\pm 3.6 \cdot 10^{-3}$
		χ	=	$8.85 \cdot 10^{-3}$	$\pm 2.4 \cdot 10^{-3}$
		β	=	$1.89 \cdot 10^{-4}$ [d]	$\pm 1.78 \cdot 10^{-4}$
MEGARD *et al.* (1984)	0.928	P_s	=	21.6 [b]	$\pm$ 1.09
		K_1	=	144 [a]	$\pm$ 14.3
		K_2	=	2624 [a]	$\pm$ 454
NEW TWO-PHOTOSYSTEM MODEL *[Eq. 3.119]*	0.642	μ	=	14.3 [b]	$\pm$ 0.20
		α	=	0.1066 [c]	$\pm$ 0.004
		χ	=	0.400	$\pm$ 0.18
		β	=	$1.21 \cdot 10^{-3}$ [d]	$\pm 1.65 \cdot 10^{-4}$

Units:

[a] $\mu E\ m^{-2}\ s^{-1}$
[b] $\mu mol\ C\ m^{-2}\ hr^{-1}$
[c] $\mu mol\ C\ m^{-2}\ hr^{-1}\ [\mu E\ m^{-2}\ s^{-1}]^{-1}$
[d] $[\mu E\ m^{-2}\ s^{-1}]^{-1}$

Table 5.3.

Parameter estimates for the P-I response of *Synechococcus* sp. WH 5701 grown under a photon flux density of 27 μE m^{-2} s^{-1} (culture SY 9161). Parameter estimates in the different formulations were determined by non-linear regression.

Function	Std. Dev. of Fit	Parameter			± Std. Dev.
(i) Empirical models.					
BALY (1935)	1.486	P_m	=	18.8 [b]	± 0.34
		I_k	=	80 [a]	± 6.0
SMITH (1936)	0.906	P_m	=	17.0 [b]	± 0.15
		I_k	=	122 [a]	± 4.0
BAULE (1917)	0.959	P_m	=	16.8 [b]	± 0.16
		I_k	=	100 [a]	± 3.4
THORNLEY (1976)	1.216	P_m	=	18.4 [b]	± 0.25
		I_k	=	120 [a]	± 6.4
JASSBY & PLATT (1976)	0.780	P_m	=	16.6 [b]	$\pm 3.3 \cdot 10^{-6}$
		I_k	=	131 [a]	$\pm 1.2 \cdot 10^{-6}$
BANNISTER (1979)	0.762	P_m	=	16.6 [b]	± 0.13
		I_k	=	143 [a]	± 4.58
		m	=	3.44	± 0.38
NEW GEOMETRIC MODEL *[Eqs. 3.34 & 3.36]*	0.770	P_m	=	17.0 [b]	± 0.44
		I_k	=	139 [a]	± 6.9
		m	=	3.15	± 0.45
		I_j	=	4373 [a]	± 3130
		I_t	=	6047 [a]	± 6946
		n	=	2.58	± 4.11
(ii) Rational models.					
RABINOWITCH (1951)	0.774	P_m	=	16.8 [b]	± 0.15
		I_k	=	142 [a]	± 4.6
		Θ	=	0.946	± 0.014

Table 5.3. (contd.)

FASHAM & PLATT (1983)	0.772	μ	=	18.4 [b]	$\pm$ 0.75
		α	=	0.119 [c]	$\pm 4.4 \cdot 10^{-3}$
		χ	=	$8.1 \cdot 10^{-3}$	$\pm 2.9 \cdot 10^{-3}$
		β	=	$2.9 \cdot 10^{-4}$ [d]	$\pm 1.8 \cdot 10^{-4}$
MEGARD *et al.* (1984)	1.13	P_s	=	25.5 [b]	$\pm$ 1.3
		K_1	=	141 [a]	$\pm$ 14
		K_2	=	2709 [a]	$\pm$ 485
NEW TWO-PHOTOSYSTEM MODEL *[Eq. 3.119]*	0.778	μ	=	17.0 [b]	$\pm$ 0.24
		α	=	0.1288 [c]	$\pm$ 0.0058
		χ	=	0.551	$\pm$ 0.24
		β	=	$1.1 \cdot 10^{-3}$ [d]	$\pm 2.8 \cdot 10^{-4}$

Units:

[a] $\mu E\ m^{-2}\ s^{-1}$
[b] $\mu mol\ C\ m^{-2}\ hr^{-1}$
[c] $\mu mol\ C\ m^{-2}\ hr^{-1}\ [\mu E\ m^{-2}\ s^{-1}]^{-1}$
[d] $[\mu E\ m^{-2}\ s^{-1}]^{-1}$

Table 5.4.

Parameter estimates for the P-I response of *Synechococcus* sp. WH 5701 grown under a photon flux density of 70 μE m^{-2} s^{-1} (culture SY 9153). Parameter estimates in the different formulations were determined by non-linear regression.

Function	Std. Dev. of Fit	Parameter			± Std. Dev.
(i) Empirical models.					
BALY (1935)	2.412	P_m	=	29.7[b]	± 0.7
		I_k	=	143[a]	± 12
SMITH (1936)	1.570	P_m	=	26.0[b]	± 0.3
		I_k	=	197[a]	± 7
BAULE (1917)	1.706	P_m	=	25.6[b]	± 0.31
		I_k	=	159[a]	± 6
THORNLEY (1976)	1.972	P_m	=	28.6[b]	± 0.48
		I_k	=	206[a]	± 12
JASSBY & PLATT (1976)	1.326	P_m	=	25.2[b]	± 0.23
		I_k	=	204[a]	± 5
BANNISTER (1979)	1.155	P_m	=	24.9[b]	± 0.20
		I_k	=	232[a]	± 5
		m	=	5.26	± 0.93
NEW GEOMETRIC MODEL *[Eqs. 3.34 & 3.36]*	1.078	P_m	=	26.5[b]	± 0.47
		I_k	=	221[a]	± 7
		m	=	3.91	± 0.56
		I_j	=	2116[a]	± 133
		I_t	=	2119[a]	± 140
		n	=	0.58	± 0.23
(ii) Rational models.					
RABINOWITCH (1951)	1.166	P_m	=	25.1[b]	± 0.23
		I_k	=	231[a]	± 5.28
		Θ	=	0.981	± $8.1 \cdot 10^{-3}$

Table 5.4. (contd.)

FASHAM & PLATT (1983)	1.152	μ	=	26.8 [b]	$\pm$ 0.90
		α	=	0.1094 [c]	$\pm 2.97 \cdot 10^{-3}$
		χ	=	2.88	$\pm 1.42 \cdot 10^{-3}$
		β	=	$7.53 \cdot 10^{-4}$ [d]	$\pm 2.1 \cdot 10^{-4}$
MEGARD *et al.* (1984)	1.660	P_s	=	54.2 [b]	$\pm$ 5.1
		K_1	=	364 [a]	$\pm$ 51
		K_2	=	1346 [a]	$\pm$ 270
NEW TWO-PHOTOSYSTEM MODEL *[Eq. 3.119]*	1.242	μ	=	25.3 [b]	$\pm$ 0.40
		α	=	0.1260 [c]	$\pm 3.2 \cdot 10^{-3}$
		χ	=	0.164	$\pm$ 0.147
		β	=	$1.19 \cdot 10^{-3}$ [d]	$\pm 6.1 \cdot 10^{-5}$

Units:

[a] $\mu E\ m^{-2}\ s^{-1}$
[b] $\mu mol\ C\ m^{-2}\ hr^{-1}$
[c] $\mu mol\ C\ m^{-2}\ hr^{-1}\ [\mu E\ m^{-2}\ s^{-1}]^{-1}$
[d] $[\mu E\ m^{-2}\ s^{-1}]^{-1}$

Table 5.5.

Function parameter estimates derived for different empirical formulations *relative* to the parameter values determined for the model of Bannister (1979) *[Eq. 2.12]* for the cyanobacteria *Synechococcus* sp. WH5701.

Function	Culture	Growth PFD	P_m^B	I_k	α^B
BALY (1935)	*SY 9149*	8	1.118	0.555	2.014
	SY 9157	15	1.133	0.559	2.027
	SY 9161	27	1.134	0.562	2.019
	SY 9153	70	1.193	0.617	1.932
SMITH (1936)	*SY 9149*	8	1.022	0.873	1.171
	SY 9157	15	1.028	0.859	1.197
	SY 9161	27	1.027	0.856	1.199
	SY 9153	70	1.045	0.848	1.232
BAULE (1917)	*SY 9149*	8	1.022	0.718	1.424
	SY 9157	15	1.014	0.698	1.452
	SY 9161	27	1.014	0.701	1.446
	SY 9153	70	1.026	0.686	1.495
THORNLEY (1976)	*SY 9149*	8	1.096	0.844	1.298
	SY 9157	15	1.106	0.838	1.320
	SY 9161	27	1.107	0.843	1.312
	SY 9153	70	1.150	0.886	1.298
JASSBY & PLATT (1976)	*SY 9149*	8	0.999	0.939	1.064
	SY 9157	15	1.002	0.912	1.099
	SY 9161	27	1.002	0.915	1.094
	SY 9153	70	1.012	0.880	1.151
RABINOWITCH (1951)	*SY 9149*	8	1.013	0.995	1.018
	SY 9157	15	1.012	0.999	1.014
	SY 9161	27	1.012	0.997	1.015
	SY 9153	70	1.006	0.995	1.012

Table 5.6.

Parameter estimates for the P-I response of *Synechococcus* sp. WH 7803 grown under a photon flux density of 17 μE m^{-2} s^{-1} (culture DC 9125). Parameter estimates in the different formulations were determined by non-linear regression.

Function	Std. Dev. of Fit	Parameter			± Std. Dev.
(i) Empirical models.					
STEELE (1962)	0.749	P_m	=	7.83 [b]	± 0.12
		I_s	=	494 [a]	± 11
VOLLENWEIDER (1965)	0.352	P_s	=	39.2 [b]	$\pm 2.8 \cdot 10^{-8}$
		I_s	=	663 [a]	$\pm 1.2 \cdot 10^{-6}$
		a	=	-7.15	$\pm 8.1 \cdot 10^{-9}$
		n	=	0.733	$\pm 4.3 \cdot 10^{-10}$
STEEL (1973)	0.669	P_s	=	7.76 [b]	± 0.11
		I_s	=	199 [a]	± 5
FEE (1973)	0.457	P_s	=	10.0 [b]	$+ 9.6 \cdot 10^{-7}$
		I_s	=	201 [a]	$\pm 5.0 \cdot 10^{-5}$
		n	=	0.348	$\pm 8.7 \cdot 10^{-8}$
WILLIAMS (1978)	0.358	P_s	=	7.51 [b]	± 0.15
		I_s	=	137 [a]	± 6
		a	=	0.115	± 0.01
PLATT *et al.* (1980)	0.357	P_s	=	8.66 [b]	± 0.02
		I_s	=	137 [a]	± 1
		b	=	0.058	$\pm 3.1 \cdot 10^{-6}$
PLATT & GALLEGOS (1980) *[m = 6]*	0.460	P_s	=	9.0 [b]	± 0.64
		I_k	=	160 [a]	± 5
		I_b'	=	2756 [a]	± 385
		I_t'	=	1504 [a]	± 115
PLATT & GALLEGOS (1980) *[$I_t' = I_b'$]*	0.299	P_s	=	9.77 [b]	± 0.33
		I_s	=	127 [a]	± 6
		m	=	1.54	± 0.12
		I_b'	=	1349 [a]	± 56
PLATT & GALLEGOS (1980)	0.298	P_s	=	8.8 [b]	± 0.02
		I_s	=	124 [a]	± 1
		m	=	1.65	$\pm 2.7 \cdot 10^{-4}$
		I_b'	=	1480 [a]	$\pm 4.4 \cdot 10^{-5}$
		I_t'	=	1116 [a]	± 11

Table 5.6. (contd.)

IWAKUMA & YASUNO (1983)	0.357	P_s	=	27.8 [b]	$\pm 20 \cdot 10^{-7}$
		I_s	=	417 [a]	$\pm 7.7 \cdot 10^{-6}$
		m	=	0.996	$\pm 6.0 \cdot 10^{-9}$
		n	=	1.01	$\pm 8.7 \cdot 10^{-9}$
NEW GEOMETRIC MODEL *[Eqs. 3.34 & 3.36]*	0.302	P_s	=	7.30 [b]	± 0.33
		I_k	=	116 [a]	± 5
		m	=	1.73	± 0.19
		I_j	=	667 [a]	± 89
		I_t	=	2730 [a]	± 136
		n	=	1.01	± 5.0
(ii) Rational models.					
FASHAM & PLATT (1983)	0.321	μ	=	29.9 [b]	± 22.4
		α	=	0.0666 [c]	$\pm 4.7 \cdot 10^{-3}$
		χ	=	0.126	± 0.137
		β	=	$7.06 \cdot 10^{-4}$ [d]	$\pm 9.3 \cdot 10^{-5}$
MEGARD *et al.* (1984)	0.356	P_s	=	13.6 [b]	± 0.88
		K_1	=	201 [a]	± 21
		K_2	=	833 [a]	± 102
NEW POISSONIAN MODEL $[I_j = I_k]$	0.379	P_s	=	6.49 [b]	± 0.07
		a	=	1.0	
		I_k	=	89 [a]	± 3
		b	=	18.7	± 0.8
NEW POISSONIAN MODEL $[I_j \neq I_k]$	0.297	P_s	=	6.83 [b]	± 0.10
		a	=	1.0	
		I_k	=	97 [a]	± 4
		b	=	5.04	± 0.83
		I_j	=	371 [a]	± 70
NEW TWO-PHOTOSYSTEM MODEL *[Eq. 3.119]*	0.300	μ	=	8.22 [b]	± 0.58
		α	=	0.0822 [c]	± 0.0118
		χ	=	2.0	± 1.15
		β	=	$1.98 \cdot 10^{-3}$ [d]	$\pm 2.6 \cdot 10^{-5}$

Units:

[a] $\mu E\ m^{-2}\ s^{-1}$
[b] $\mu mol\ C\ m^{-2}\ hr^{-1}$
[c] $\mu mol\ C\ m^{-2}\ hr^{-1}\ [\mu E\ m^{-2}\ s^{-1}]^{-1}$
[d] $[\mu E\ m^{-2}\ s^{-1}]^{-1}$

Table 5.7.

Parameter estimates for the P-I response of *Synechococcus* sp. WH 7803 grown under a photon flux density of 25 μE m^{-2} s^{-1} (culture DC 9117). Parameter estimates in the different formulations were determined by non-linear regression.

Function	Std. Dev. of Fit			Parameter	± Std. Dev.
(i) Empirical models.					
STEELE (1962)	0.545	P_m	=	6.91 [b]	± 0.09
		I_s	=	402 [a]	± 7
VOLLENWEIDER (1965)	0.283	P_s	=	32.8 [b]	$\pm 7.1 \cdot 10^{-8}$
		I_s	=	631 [a]	$\pm 2.8 \cdot 10^{6}$
		a	=	4.34	$\pm 1.2 \cdot 10^{-8}$
		n	=	0.98	$\pm 1.9 \cdot 10^{-9}$
STEEL (1973)	0.410	P_s	=	6.73 [b]	± 0.07
		I_s	=	157 [a]	± 3
FEE (1973)	0.356	P_s	=	11.32 [b]	$\pm 3.1 \cdot 10^{-8}$
		I_s	=	240 [a]	$\pm 1.3 \cdot 10^{-6}$)
		n	=	0.69	$\pm 1.7 \cdot 10^{-10}$)
WILLIAMS (1978)	0.281	P_s	=	7.55 [b]	± 0.18
		I_s	=	144 [a]	± 6
		a	=	0.217	± 0.018
PLATT *et al.* (1980)	0.240	P_s	=	9.2 [b]	$\pm 5.3 \cdot 10^{-8}$
		I_s	=	148 [a]	$\pm 1.6 \cdot 10^{-6}$
		b	=	0.118	$\pm 1.2 \cdot 10^{-9}$)
PLATT & GALLEGOS (1980) *[m = 6]*	0.292	P_s	=	6.0 [b]	± 0.09
		I_k	=	131 [a]	± 4
		I_b'	=	1379 [a]	± 25
		I_t'	=	857 [a]	± 53
PLATT & GALLEGOS (1980) *[$I_t' = I_b'$]*	0.219	P_s	=	8.09 [b]	± 0.18
		I_s	=	130 [a]	± 4
		m	=	2.21	± 0.15
		I_b'	=	1070 [a]	± 27
PLATT & GALLEGOS (1980)	0.218	P_s	=	9.03 [b]	± 0.71
		I_s	=	134 [a]	± 5
		m	=	2.02	± 0.17
		I_b'	=	938 [a]	± 98
		I_t'	=	1181 [a]	± 88

Table 5.7. (contd.)

IWAKUMA & YASUNO (1983)	0.259	P_s	=	28.0 [b]	$\pm 4 \cdot 10^{-8}$
		I_s	=	470 [a]	$\pm 1.8 \cdot 10^{-6}$
		m	=	1.13	$\pm 1.7 \cdot 10^{-9}$
		n	=	1.50	$\pm 3.2 \cdot 10^{-9}$
NEW GEOMETRIC MODEL *[Eqs. 3.34 & 3.36]*	0.219	P_s	=	6.60 [b]	± 0.5
		I_k	=	121 [a]	± 7
		m	=	2.16	± 0.37
		I_j	=	326 [a]	± 117
		I_t	=	2270 [a]	± 48
		n	=	36	± 56
(ii) Rational models.					
FASHAM & PLATT (1983)	0.215	μ	=	11.9 [b]	± 2.03
		α	=	0.0572 [c]	$\pm 2.2 \cdot 10^{-3}$
		χ	=	0.0222	$\pm 9.6 \cdot 10^{-3}$
		β	=	$1.46 \cdot 10^{-3}$ [d]	$\pm 1.26 \cdot 10^{-4}$
MEGARD *et al.* (1984)	0.289	P_s	=	20.37 [b]	± 1.99
		K_1	=	349 [a]	± 46
		K_2	=	277 [a]	± 36
NEW POISSONIAN MODEL $[I_j = I_k]$	0.496	P_s	=	5.90 [b]	± 0.12
		a	=	1.0	
		I_k	=	84 [a]	± 5
		b	=	15.5	± 1.1
NEW POISSONIAN MODEL $[I_j \neq I_k]$	0.224	P_s	=	6.89 [b]	± 0.21
		a	=	1.0	
		I_k	=	105 [a]	± 5
		b	=	2.37	± 0.33
		I_j	=	595 [a]	± 84
NEW TWO-PHOTOSYSTEM MODEL *[Eq. 3.119]*	0.285	μ	=	8.72 [b]	± 1.27
		α	=	0.0915 [c]	± 0.0228
		χ	=	3.13	± 2.82
		β	=	$2.5 \cdot 10^{-3}$ [d]	$\pm 2.8 \cdot 10^{-5}$

Units:

[a] $\mu E\ m^{-2}\ s^{-1}$
[b] $\mu mol\ C\ m^{-2}\ hr^{-1}$
[c] $\mu mol\ C\ m^{-2}\ hr^{-1}\ [\mu E\ m^{-2}\ s^{-1}]^{-1}$
[d] $[\mu E\ m^{-2}\ s^{-1}]^{-1}$

Table 5.8.

Parameter estimates for the P-I response of *Synechococcus* sp. WH 7803 grown under a photon flux density of 35 μE m^{-2} s^{-1} (culture DC 9121). Parameter estimates in the different formulations were determined by non-linear regression.

Function	Std. Dev. of Fit	Parameter			± Std. Dev.
(i) Empirical models.					
STEELE (1962)	0.492	P_m	=	2.92 [b]	± 0.09
		I_s	=	438 [a]	± 17
VOLLENWEIDER (1965)	0.140	P_s	=	3.49 [b]	$\pm 1.7 \cdot 10^{-9}$
		I_s	=	113 [a]	$\pm 1.7 \cdot 10^{-6}$
		a	=	1.625	$\pm 7.1 \cdot 10^{-8}$
		n	=	0.213	$\pm 4.3 \cdot 10^{-9}$
STEEL (1973)	0.385	P_s	=	2.95 [b]	± 0.07
		I_s	=	157 [a]	± 6
FEE (1973)	0.139	P_s	=	3.18 [b]	± 0.09
		I_s	=	104 [a]	± 5
		n	=	0.209	± 0.019
WILLIAMS (1978)	0.150	P_s	=	2.49 [b]	$\pm 6.7 \cdot 10^{-3}$
		I_s	=	75 [a]	$\pm 3 \cdot 10^{-3}$
		a	=	-0.054	$\pm 6.4 \cdot 10^{-4}$
PLATT *et al.* (1980)	0.146	P_s	=	2.63 [b]	± 0.06
		I_s	=	67 [a]	± 3
		b	=	0.0186	$\pm 2.5 \cdot 10^{-3}$
PLATT & GALLEGOS (1980) *[m = 6]*	0.146	P_s	=	2.51 [b]	± 0.20
		I_s	=	89 [a]	± 3
		I_b'	=	2492 [a]	± 187
		I_t'	=	2492 [a]	± 688
PLATT & GALLEGOS (1980) *[$I_t' = I_b'$]*	0.140	P_s	=	2.66 [b]	± 0.07
		I_s	=	84 [a]	± 3
		m	=	3.38	± 0.58
		I_b'	=	2162 [a]	± 178
PLATT & GALLEGOS (1980)	0.138	P_s	=	4.07 [b]	± 2.4
		I_s	=	86 [a]	± 4
		m	=	3.0	± 0.49
		I_b'	=	930 [a]	± 2372
		I_t'	=	4017 [a]	± 2406

Table 5.8. (contd.)

IWAKUMA & YASUNO (1983)	0.139	P_s	=	3.25 [b]	± 0.26
		I_s	=	105 [a]	± 6
		m	=	1.91	± 0.27
		n	=	0.22	± 0.04
NEW GEOMETRIC MODEL *[Eqs. 3.34 & 3.36]*	0.139	P_s	=	2.50 [b]	$\pm 6.5 \cdot 10^{-6}$
		I_k	=	86 [a]	$\pm 7.6 \cdot 10^{-4}$
		m	=	3.04	$\pm 8.1 \cdot 10^{-5}$
		I_j	=	18 [a]	± 0.01
		I_t	=	4951 [a]	± 712
		n	=	$1.8 \cdot 10^5$	$\pm 3.1 \cdot 10^7$
(ii) Rational models.					
FASHAM & PLATT (1983)	0.144	μ	=	2.68 [b]	± 0.20
		α	=	0.0303 [c]	$\pm 1.6 \cdot 10^{-3}$
		χ	=	$2.5 \cdot 10^{-3}$	$\pm 1.5 \cdot 10^{-3}$
		β	=	$1.25 \cdot 10^{-3}$ [d]	$\pm 1.2 \cdot 10^{-4}$
MEGARD *et al.* (1984)	0.166	P_s	=	3.67 [b]	± 0.17
		K_1	=	84 [a]	± 8
		K_2	=	1292 [a]	± 152
NEW POISSONIAN MODEL $[I_j = I_k]$	0.206	P_s	=	2.18 [b]	± 0.03
		a	=	1.0	
		I_k	=	51 [a]	± 3
		b	=	37.8	± 2.6
NEW POISSONIAN MODEL $[I_j \neq I_k]$	0.146	P_s	=	2.86 [b]	± 0.28
		a	=	1.0	
		I_k	=	73 [a]	± 7
		b	=	0.64	± 0.28
		I_j	=	6784 [a]	± 3829
NEW TWO-PHOTOSYSTEM MODEL *[Eq. 3.119]*	0.177	μ	=	2.26 [b]	± 0.06
		α	=	0.0336 [c]	$\pm 2.5 \cdot 10^{-3}$
		χ	=	0.088	± 0.062
		β	=	$2.08 \cdot 10^{-3}$ [d]	$\pm 5.4 \cdot 10^{-5}$

Units:

[a] $\mu E\ m^{-2}\ s^{-1}$
[b] $\mu mol\ C\ m^{-2}\ hr^{-1}$
[c] $\mu mol\ C\ m^{-2}\ hr^{-1}\ [\mu E\ m^{-2}\ s^{-1}]^{-1}$
[d] $[\mu E\ m^{-2}\ s^{-1}]^{-1}$

Table 5.9.

Parameter estimates for the P-I response of *Pavlova* sp. (NEP) grown under a photon flux density of 8 μE m^{-2} s^{-1} (culture PA 9141). Parameter estimates in the different formulations were determined by non-linear regression.

Function	Std. Dev. of Fit	Parameter			± Std. Dev.
(i) Empirical models.					
STEELE (1962)	2.64	P_m	=	18.05 [b]	± 0.46
		I_s	=	468 [a]	± 16
VOLLENWEIDER (1965)	0.822	P_s	=	16.06 [b]	± 0.01
		I_s	=	93 [a]	± 0.25
		a	=	-0.359	$\pm 2.5 \cdot 10^{-3}$
		n	=	0.165	$\pm 3.6 \cdot 10^{-5}$
STEEL (1973)	2.184	P_s	=	17.85 [b]	± 0.37
		I_s	=	176 [a]	± 6
FEE (1973)	0.826	P_s	=	18.4 [b]	± 0.5
		I_s	=	112 [a]	± 6
		n	=	0.169	± 0.02
WILLIAMS (1978)	0.761	P_s	=	15.27 [b]	± 0.21
		I_s	=	86 [a]	± 3
		a	=	0.054	$+ 4.8 \cdot 10^{-3}$
PLATT *et al.* (1980)	0.789	P_s	=	16.06 [b]	± 3.45
		I_s	=	78 [a]	± 4
		b	=	0.0182	$\pm 2.5 \cdot 10^{-3}$
PLATT & GALLEGOS (1980) *[m = 6]*	0.887	P_s	=	13.95 [b]	± 0.24
		I_s	=	95 [a]	± 3
		I_b'	=	2486 [a]	± 250
		I_t'	=	1590 [a]	± 388
PLATT & GALLEGOS (1980) *[$I_t' = I_b'$]*	0.766	P_s	=	17.51 [b]	± 0.5
		I_s	=	90 [a]	± 4
		m	=	2.28	± 0.24
		I_b'	=	2105 [a]	± 162
PLATT & GALLEGOS (1980)	0.768	P_s	=	21.51 [b]	± 9.18
		I_s	=	91 [a]	± 5
		m	=	2.09	± 0.32
		I_b'	=	1643 [a]	± 1322
		I_t'	=	3196 [a]	± 2129

Table 5.9. (contd.)

IWAKUMA & YASUNO (1983)	0.793	P_s	=	24.68 [b]	± 3.45
		I_s	=	130 [a]	± 13
		m	=	1.35	± 0.18
		n	=	0.3	± 0.06
NEW GEOMETRIC MODEL *[Eqs. 3.34 & 3.36]*	0.768	P_s	=	15.84 [b]	± 2.0
		I_k	=	84 [a]	± 8
		m	=	1.996	± 0.54
		I_j	=	136 [a]	± 668
		I_t	=	4822 [a]	± 600
		n	=	18.5	± 35

(ii) Rational models.

FASHAM & PLATT (1983)	0.764	μ	=	19.59 [b]	+ 2.04
		α	=	0.1764 [c]	$\pm 9.7 \cdot 10^{-3}$
		χ	=	0.037	± 0.017
		β	=	$8.2 \cdot 10^{-4}$ [d]	$\pm 1.2 \cdot 10^{-4}$
MEGARD *et al.* (1984)	0.843	P_s	=	22.48 [b]	± 0.88
		K_1	=	96 [a]	± 8
		K_2	=	1501 [a]	± 156
NEW POISSONIAN MODEL $[I_j = I_k]$	1.086	P_s	=	13.73 [b]	± 0.18
		a	=	1.0	
		I_k	=	60 [a]	± 3
		b	=	32.9	± 1.9
NEW POISSONIAN MODEL $[I_j \neq I_k]$	0.791	P_s	=	15.43 [b]	± 0.68
		a	=	1.0	
		I_k	=	74 [a]	± 5
		b	=	1.41	± 0.59
		I_j	=	2545 [a]	± 1603
NEW TWO-PHOTOSYSTEM MODEL *[Eq. 3.119]*	0.896	μ	=	14.90 [b]	± 0.48
		α	=	0.2074 [c]	± 0.0194
		χ	=	1.587	± 0.79
		β	=	$1.95 \cdot 10^{-3}$ [d]	$\pm 4.5 \cdot 10^{-5}$

Units:

[a] $\mu E\ m^{-2}\ s^{-1}$
[b] $\mu mol\ C\ m^{-2}\ hr^{-1}$
[c] $\mu mol\ C\ m^{-2}\ hr^{-1}\ [\mu E\ m^{-2}\ s^{-1}]^{-1}$
[d] $[\mu E\ m^{-2}\ s^{-1}]^{-1}$

Table 5. 10.

Parameter estimates for the P-I response of *Pavlova* sp. (NEP) grown under a photon flux density of 12 μE m^{-2} s^{-1} (culture PA 9137). Parameter estimates in the different formulations were determined by non-linear regression.

Function	Std. Dev. of Fit	Parameter			± Std. Dev.
(i) Empirical models.					
STEELE (1962)	6.117	P_m	=	41.75 [b]	± 1.01
		I_s	=	492 [a]	± 17
VOLLENWEIDER (1965)	1.802	P_s	=	36.0 [b]	± 0.68
		I_s	=	94 [a]	± 4
		a	=	-0.085	± 0.044
		n	=	0.487	± 0.214
STEEL (1973)	5.204	P_s	=	41.54 [b]	± 0.84
		I_s	=	187 [a]	± 6
FEE (1973)	1.865	P_s	=	42.02 [b]	± 0.09
		I_s	=	115 [a]	± 1
		n	=	0.145	$\pm 2.5 \cdot 10^{-5}$
WILLIAMS (1978)	1.800	P_s	=	35.39 [b]	$\pm 8 \cdot 10^{-8}$
		I_s	=	89 [a]	$\pm 7 \cdot 10^{-8}$
		a	=	-0.048	$\pm 7 \cdot 10^{-10}$
PLATT *et al.* (1980)	1.900	P_s	=	37.2 [b]	± 0.7
		I_s	=	82 [a]	± 4
		b	=	0.0156	$\pm 2.5 \cdot 10^{-3}$
PLATT & GALLEGOS (1980) *[m = 6]*	1.929	P_s	=	32.5 [b]	± 0.4
		I_s	=	100 [a]	± 3
		I_b'	=	2524 [a]	± 270
		I_t'	=	1386 [a]	± 376
PLATT & GALLEGOS (1980) *[$I_t' = I_b'$]*	1.754	P_s	=	40.3 [b]	± 1.1
		I_s	=	98 [a]	± 4
		m	=	2.47	± 0.27
		I_b'	=	2490 [a]	± 237
PLATT & GALLEGOS (1980)	1.758	P_s	=	36.6 [b]	± 2.9
		I_s	=	97 [a]	± 4
		m	=	2.65	± 0.38
		I_b'	=	2446 [a]	± 215
		I_t'	=	1703 [a]	± 678

Table 5.10 (contd.)

IWAKUMA & YASUNO (1983)	1.864	P_s	=	45.7 [b]	± 4.0
		I_s	=	120 [a]	± 8
		m	=	1.73	± 0.23
		n	=	0.182	± 0.041
NEW GEOMETRIC MODEL *[Eqs. 3.34 & 3.36]*	1.734	P_s	=	36.7 [b]	± 1.8
		I_k	=	87 [a]	± 7
		m	=	2.25	± 0.38
		I_j	=	659 [a]	± 747
		I_t	=	4430 [a]	± 1477
		n	=	6.51	± 5.07
(ii) Rational models.					
FASHAM & PLATT (1983)	1.751	μ	=	41.2 [b]	± 2.9
		α	=	0.3668 [c]	± 0.0176
		χ	=	0.0472	± 0.0202
		β	=	$8.5 \cdot 10^{-4}$ [d]	$\pm 1.2 \cdot 10^{-4}$
MEGARD *et al.* (1984)	2.105	P_s	=	51.9 [b]	± 2.1
		K_1	=	101 [a]	± 9
		K_2	=	1719 [a]	± 199
NEW POISSONIAN MODEL $[I_j = I_k]$	2.312	P_s	=	32.6 [b]	± 0.4
		a	=	1.0	
		I_k	=	66 [a]	± 3
		b	=	3.08	± 1.62
NEW POISSONIAN MODEL $[I_j \neq I_k]$	1.906	P_s	=	35.9 [b]	± 1.7
		a	=	1.0	
		I_k	=	79 [a]	± 6
		b	=	1.38	± 0.7
		I_j	=	3083 [a]	± 2507
NEW TWO-PHOTOSYSTEM MODEL *[Eq. 3.119]*	1.909	μ	=	34.1 [b]	± 0.8
		α	=	0.414 [c]	± 0.026
		χ	=	2.05	± 0.94
		β	=	$1.83 \cdot 10^{-3}$ [d]	$\pm 4.26 \cdot 10^{-5}$

Units:

[a] $\mu E\ m^{-2}\ s^{-1}$

[b] $\mu mol\ C\ m^{-2}\ hr^{-1}$

[c] $\mu mol\ C\ m^{-2}\ hr^{-1}\ [\mu E\ m^{-2}\ s^{-1}]^{-1}$

[d] $[\mu E\ m^{-2}\ s^{-1}]^{-1}$

Table 5.11.

Parameter estimates for the P-I response of *Pavlova* sp. (NEP) grown under a photon flux density of 45 μE m^{-2} s^{-1} (culture PA 9133). Parameter estimates in the different formulations were determined by non-linear regression.

Function	Std. Dev. of Fit	Parameter			± Std. Dev.
(i) Empirical models.					
BALY (1935)	1.972	P_m	=	24.73 [b]	± 0.58
		I_k	=	151 [a]	± 12
SMITH (1936)	1.312	P_m	=	21.52 [b]	± 0.25
		I_k	=	203 [a]	± 7
BAULE (1917)	1.441	P_m	=	21.09 [b]	± 0.26
		I_k	=	164 [a]	± 7
THORNLEY (1976)	1.608	P_m	=	23.76 [b]	± 0.40
		I_k	=	217 [a]	± 12
JASSBY & PLATT (1976)	1.13	P_m	=	20.79 [b]	± 0.19
		I_k	=	209 [a]	± 6
BANNISTER (1979)	0.9855	P_m	=	20.54 [b]	± 0.17
		I_k	=	238 [a]	± 6
		m	=	5.43	± 1.01
STEELE (1962)	2.362	P_m	=	23.42 [b]	± 0.38
		I_s	=	71 [a]	± 21
VOLLENWEIDER (1965)	1.183	P_s	=	26.41 [b]	$\pm 2.0 \cdot 10^{8}$
		I_s	=	265 [a]	$\pm 6.2 \cdot 10^{7}$
		a	=	1.008	$\pm 6.9 \cdot 10^{9}$
		n	=	0.149	$\pm 7.4 \cdot 10^{10}$
STEEL (1973)	2.142	P_s	=	23.57 [b]	± 0.34
		I_s	=	292 [a]	± 8
FEE (1973)	1.177	P_s	=	26.39 [b]	± 1.21
		I_s	=	264 [a]	± 18
		n	=	0.150	± 0.038

Table 5.11. (contd.)

WILLIAMS (1978)	1.253	P_s	=	22.7 [b]	± 0.5
		I_s	=	220 [a]	± 10
		a	=	0.0712	± 0.0154
PLATT *et al.* (1980)	1.394	P_s	=	23.3 [b]	± 1.0
		I_s	=	188 [a]	± 14
		b	=	0.0185	± 0.0088
PLATT & GALLEGOS (1980) *[m = 6]*	0.993	P_s	=	40.3 [b]	± 7.0
		I_s	=	240 [a]	± 5
		I_b'	=	$3.53 \cdot 10^5$ [a]	± $3.15 \cdot 10^6$
		I_t'	=	$2.1 \cdot 10^7$ [a]	± $1.73 \cdot 10^8$
PLATT & GALLEGOS (1980) *[$I_t' = I_b'$]*	*no convergence*	P_s	→	21.5 [b]	
		I_s	→	237 [a]	
		m	→	5.667	
		I_b'	→	∞ [a]	
PLATT & GALLEGOS (1980)	0.997	P_s	=	20.51 [b]	± 0.36
		I_s	=	238 [a]	± 5
		m	=	5.432	± 0.92
		I_b'	=	$1.3 \cdot 10^{12}$ [a]	± $3.81 \cdot 10^{13}$
		I_t'	=	$-2.0 \cdot 10^{10}$ [a]	± $5.78 \cdot 10^{11}$
IWAKUMA & YASUNO (1983)	0.990	P_s	=	20.30 [b]	± 0.63
		I_s	=	236 [a]	± 8
		m	=	5.76	± 1.53
		n	=	-0.0088	± 0.022
NEW GEOMETRIC MODEL *[Eqs. 3.34 & 3.36]*	0.911	P_s	=	21.70 [b]	± 0.35
		I_s	=	220 [a]	± 7
		m	=	4.13	± 0.61
		I_j	=	$3.57 \cdot 10^4$ [a]	± $1.43 \cdot 10^5$
		I_t	=	$1.14 \cdot 10^5$ [a]	± $4.66 \cdot 10^5$
		n	=	3.98	± 12.4
(ii) Rational models.					
RABINOWITCH (1951)	0.996	P_m	=	20.68 [b]	± 0.20
		I_k	=	238 [a]	± 6
		Θ	=	0.982	± $8.5 \cdot 10^{-3}$

Table 5.11. (contd.)

FASHAM & PLATT (1983)	0.998	μ	=	21.08 [b]	$\pm$ 0.83
		α	=	0.0872 [c]	$\pm 2.27 \cdot 10^{3}$
		χ	=	$1.7 \cdot 10^{-3}$	$\pm 8.1 \cdot 10^{-4}$
		β	=	$-2.3 \cdot 10^{-5}$ [d]	$\pm 1.38 \cdot 10^{-3}$
MEGARD *et al.* (1984)	1.506	P_s	=	41.56 [b]	$\pm$ 4.03
		K_1	=	337 [a]	$\pm$ 50
		K_2	=	1599 [a]	$\pm$ 363
NEW TWO-PHOTOSYSTEM MODEL *[Eq. 3.104]*	0.921	μ	=	21.0 [b]	$\pm$ 0.20
		α	=	0.089 [c]	$\pm 2.7 \cdot 10^{3}$
		χ	=	0.485	$\pm$ 0.192
NEW TWO-PHOTOSYSTEM MODEL *[Eq. 3.119]*	*no convergence*	β	$\rightarrow$	0 [d]	

Units:

[a] $\mu E\ m^{-2}\ s^{-1}$
[b] $\mu mol\ C\ m^{-2}\ s^{-1}$
[c] $\mu mol\ C\ m^{-2}\ hr^{-1}\ [\mu E\ m^{-2}\ s^{-1}]^{-1}$
[d] $[\mu E\ m^{-2}\ s^{-1}]^{-1}$

Table 5.12.

P-I response parameters of *Synechococcus* sp. WH 5701 determined under white, green and blue polychromatic irradiance.

Expt #	Growth *PFD* [a]	Color	Model Eq. #	α^B [c]	P_m^B [b]	m	R_m^B [b]	n	C [b]
SY 9149	8	white	5.3	0.112	12.91	3.295	*n/a*	*n/a*	- 0.43
SY 9150		green	5.1	0.054	*n/a*	*n/a*	1.056	1.253	0.075
SY 9151		blue	5.1	0.022	*n/a*	*n/a*	0.323	4.34	0.19
SY 9157	15	white	5.2	0.114	15.75	2.747	2.732	0.462	0.075
SY 9158		green	5.1	0.062	*n/a*	*n/a*	3.063	1.06	0.098
SY 9159		blue	5.1	0.024	*n/a*	*n/a*	0.70	2.29	0.234
SY 9153	70	white	5.1	0.117	*n/a*	*n/a*	1.722	9.36	0.506
SY 9154		green	-	-	-	-	-	-	-
SY 9155		blue	5.1	0.038	*n/a*	*n/a*	8.98	0.772	0.532

Units:

[a] $\mu E\ m^{-2}\ s^{-1}$

[b] $\mu mol\ C\ m^{-2}\ hr^{-1}$

[c] $\mu mol\ C\ m^{-2}\ hr^{-1}\ [\mu E\ m^{-2}\ s^{-1}]^{-1}$

Table 5.13.

P-I response parameters of *Synechococcus* sp. WH 7803 determined under white, green and blue polychromatic irradiance.

Expt #	Growth PFD [a]	Color	Model Eq. #	α^B [c]	P_m^B [b]	m	R_m^B [b]	n	C [b]
DC 9129	7	white	-	-	-	-	-	-	-
DC 9130		green	5.3	0.031	1.869	2.028	*n/a*	*n/a*	0.1656
DC 9131		blue	5.3	0.009	1.672	2.237	*n/a*	*n/a*	0.1408
DC 9125	17	white	5.3	0.050	7.569	1.972	*n/a*	*n/a*	0.069
DC 9126		green	5.2	0.116	6.791	3.225	0.504	2.966	0.175
DC 9127		blue	5.3	0.031	5.901	3.177	*n/a*	*n/a*	0.118
DC 9117	25	white	5.3	0.061	7.586	1.626	*n/a*	*n/a*	- 0.163
DC 9118		green	5.2	0.132	8.104	3.214	0.428	3.256	0.137
DC 9119		blue	5.3	0.039	9.163	1.810	*n/a*	*n/a*	0.052
DC 9121	35	white	5.3	0.032	2.778	2.043	*n/a*	*n/a*	- 0.113
DC 9122		green	5.2	0.070	2.500	4.002	0.289	4.908	0.135
DC 9123		blue	5.3	0.019	2.349	2.138	*n/a*	*n/a*	0.061

Units:

[a] $\mu E\ m^{-2}\ s^{-1}$

[b] $\mu mol\ C\ m^{-2}\ hr^{-1}$

[c] $\mu mol\ C\ m^{-2}\ hr^{-1}\ [\mu E\ m^{-2}\ s^{-1}]^{-1}$

Table 5.14.

P-I response parameters of *Pavlova* sp. (NEP) determined under white, green and blue polychromatic irradiance.

Expt #	Growth PFD [a]	Color	Model Eq. #	α^B [c]	P_m^B [b]	m	R_m^B [b]	n	C [b]
PA 9141	8	white	5.2	0.176	14.63	2.44	0.010	0.143	- 0.227
PA 9142		green	5.2	0.141	15.62	4.83	0.678	2.924	0.060
PA 9143		blue	5.2	0.208	16.15	4.52	0.762	8.158	0.261
PA 9137	12	white	5.2	0.548	40.63	2.31	7.078	1.862	0.547
PA 9138		green	5.2	0.473	50.68	3.35	3.814	4.064	0.156
PA 9139		blue	5.2	0.684	49.20	3.48	3.254	1.959	0.451
PA 9133	45	white	5.2	0.106	22.98	3.13	1.651	3.571	0.179
PA 9134		green	5.1	0.119	*n/a*	*n/a*	2.757	2.968	0.075
PA 9135		blue	5.2	0.236	28.05	2.90	5.029	2.055	0.116

Units:

[a] $\mu E\ m^{-2}\ s^{-1}$

[b] $\mu mol\ C\ m^{-2}\ hr^{-1}$

[c] $\mu mol\ C\ m^{-2}\ hr^{-1}\ [\mu E\ m^{-2}\ s^{-1}]^{-1}$

Table 5.15.

P-I response parameters of *Synechococcus* sp. WH 5701 determined under white polychromatic irradiance as a function of growth photon flux density. P-I parameters are for the four most successful formulations were determined by non-linear regression.

Culture #	Growth PFD [a]	Bannister (1979) Model	New Geometric Model	Fasham & Platt (1983) Model	New Two-photosystem Model
SY 9149	8	$P_m^B = 12.50$ [b] $I_k = 119$ [a] $m = 3.096$	$P_s^B = 12.53$ [b] $I_k = 119$ [a] $m = 3.076$ $I_j = 4026$ [a] $I_t = 2.43 \cdot 10^5$ [a] $n = 115$	$\mu^B = 13.94$ [b] $\alpha^B = 0.1074$ [c] $\chi^B = 0.0088$ $\beta^B = 1.89 \cdot 10^{-6}$ [d]	$\mu^B = 12.66$ [b] $\alpha^B = 0.1142$ [c] $\chi^B = 0.8973$ $\beta^B = 3.14 \cdot 10^{-5}$ [d]
SY 9157	15	$P_m^B = 13.92$ [b] $I_k = 145$ [a] $m = 3.457$	$P_s^B = 14.28$ [b] $I_k = 140$ [a] $m = 3.114$ $I_j = 2647$ [a] $I_t = 2720$ [a] $n = 1.14$	$\mu^B = 15.56$ [b] $\alpha^B = 0.0988$ [c] $\chi^B = 0.0088$ $\beta^B = 1.89 \cdot 10^{-5}$ [d]	$\mu^B = 14.26$ [b] $\alpha^B = 0.1066$ [c] $\chi^B = 0.3991$ $\beta^B = 1.21 \cdot 10^{-3}$ [d]
SY 9161	27	$P_m^B = 16.59$ [b] $I_k = 143$ [a] $m = 3.441$	$P_s^B = 16.96$ [b] $I_k = 139$ [a] $m = 3.154$ $I_j = 4373$ [a] $I_t = 6047$ [a] $n = 2.58$	$\mu^B = 18.38$ [b] $\alpha^B = 0.1190$ [c] $\chi^B = 0.0081$ $\beta^B = 2.91 \cdot 10^{-4}$ [d]	$\mu^B = 16.97$ [b] $\alpha^B = 0.1288$ [c] $\chi^B = 0.5509$ $\beta^B = 1.11 \cdot 10^{-3}$ [d]

Table 5. 15 (contd.)

SY 9153	70	P_m^B	= 24.91 [b]	P_s^B	= 26.5 [b]	μ^B	= 26.78 [b]	μ^B	= 25.35 [b]
		I_k	= 232 [a]	I_k	= 221 [a]	α^B	= 0.1094 [c]	α^B	= 0.126 [c]
		m	= 5.258	m	= 3.91	χ^B	= 2.876	χ^B	= 0.1645
				I_j	= 2116 [a]	β^B	= $7.53 \cdot 10^{-5}$ [d]	β^B	= $1.19 \cdot 10^{-3}$ [d]
				I_t	= 2119 [a]				
				n	= 0.581				

Units:

[a] $\mu E\ m^{-2}\ s^{-1}$
[b] $\mu mol\ C\ m^{-2}\ hr^{-1}$
[c] $\mu mol\ C\ m^{-2}\ hr^{-1}\ [\mu E\ m^{-2}\ s^{-1}]^{-1}$
[d] $[\mu E\ m^{-2}\ s^{-1}]^{-1}$

Table 5.16.

P-I response parameters of *Synechococcus* sp. WH 7803 determined under white polychromatic irradiance as a function of growth PFD. P-I parameters are for the four most successful formulations as determined by non-linear curve-fitting.

Culture #	Growth PFD (a)	New Poissonian Model	New Geometric Model	Fasham & Platt (1983) Model	New Two-photosystem Model
DC 9125	17	P_s^B = 6.83 [b] I_k = 97 [a] a = 1.0 I_j = 371 [a] b = 5.04	P_s^B = 7.29 [b] I_k = 116 [a] m = 1.73 I_j = 667 [a] I_t = 2730 [a] n = 1.01	μ^B = 29.88 [b] α^B = 0.0666 [c] χ^B = 0.1259 β^B = $7.06 \cdot 10^{-4}$ [d]	μ^B = 8.22 [b] α^B = 0.0822 [c] χ^B = 1.996 β^B = $1.97 \cdot 10^{-3}$ [d]
DC 9117	25	P_s^B = 6.89 [b] I_k = 105 [a] a = 1.0 I_j = 595 [a] b = 2.37	P_s^B = 6.60 [b] I_k = 121 [a] m = 2.16 I_j = 326 [a] I_t = 2270 [a] n = 35.6	μ^B = 11.87 [b] α^B = 0.0572 [c] χ^B = 0.0222 β^B = $1.46 \cdot 10^{-3}$ [d]	μ^B = 8.72 [b] α^B = 0.0915 [c] χ^B = 3.131 β^B = $2.5 \cdot 10^{-3}$ [d]
DC 9121	35	P_s^B = 2.86 [b] I_k = 73 [a] a = 1.0 I_j = 6784 [a] b = 0.64	P_s^B = 2.50 [b] I_k = 86 [a] m = 3.04 I_j = 18 [a] I_t = 4951 [a] n = $1.76 \cdot 10^5$	μ^B = 2.68 [b] α^B = 0.0303 [c] χ^B = 0.0025 β^B = $1.25 \cdot 10^{-3}$ [d]	μ^B = 2.26 [b] α^B = 0.0357 [c] χ^B = 0.0883 β^B = $2.08 \cdot 10^{-3}$ [d]

Units: [a] $\mu E\ m^{-2}\ s^{-1}$ [b] $\mu mol\ C\ m^{-2}\ hr^{-1}$ [c] $\mu mol\ C\ m^{-2}\ hr^{-1}\ [\mu E\ m^{-2}\ s^{-1}]^{-1}$ [d] $[\mu E\ m^{-2}\ s^{-1}]^{-1}$

Table 5.17.

P-I response parameters of *Pavlova* sp. (NEP) determined under white polychromatic irradiance as a function of growth PFD. P-I parameters are for the four most successful formulations as determined by non-linear regression. * denotes Eq. 3.104 used.

Culture #	Growth PFD [a]	New Poissonian Model	New Geometric Model	Fasham & Platt (1983) Model	New Two-photosystem Model
PA 9141	8	$P_s^B = 15.54$ [b] $I_k = 74$ [a] $a = 1.0$ $I_j = 2545$ [a] $b = 1.41$	$P_s^B = 15.84$ [b] $I_k = 84$ [a] $m = 1.996$ $I_j = 136$ [a] $I_t = 4822$ [a] $n = 18.5$	$\mu^B = 19.59$ [b] $\alpha^B = 0.1764$ [c] $\chi^B = 0.0371$ $\beta^B = 8.2 \cdot 10^{-4}$ [d]	$\mu^B = 14.9$ [b] $\alpha^B = 0.2074$ [c] $\chi^B = 1.587$ $\beta^B = 1.9 \cdot 10^{-3}$ [d]
PA 9137	12	$P_s^B = 35.93$ [b] $I_k = 79$ [a] $a = 1.0$ $I_j = 3083$ [a] $b = 1.385$	$P_s^B = 36.67$ [b] $I_k = 87$ [a] $m = 2.247$ $I_j = 659$ [a] $I_t = 4430$ [a] $n = 6.506$	$\mu^B = 41.24$ [b] $\alpha^B = 0.3668$ [c] $\chi^B = 0.0472$ $\beta^B = 8.5 \cdot 10^{-4}$ [d]	$\mu^B = 34.07$ [b] $\alpha^B = 0.4139$ [c] $\chi^B = 2.05$ $\beta^B = 1.83 \cdot 10^{-3}$ [d]
PA 9133	45	$P_s^B = n/a$ $I_k = n/a$ $a = n/a$ $I_j = n/a$ $b = n/a$	$P_s^B = 21.7$ [b] $I_k = 220$ [a] $m = 4.134$ $I_j = 3.57 \cdot 10^4$ [a] $I_t = 1.14 \cdot 10^5$ [a] $n = 3.98$	$\mu^B = 21.08$ [b] $\alpha^B = 0.0872$ [c] $\chi^B = 0.0017$ $\beta^B = 2.3 \cdot 10^{-5}$ [d]	$\mu^B = {}^*21.0$ [b] $\alpha^B = {}^*0.0894$ [c] $\chi^B = {}^*0.4849$ $\beta^B = n/a$

Units: [a] $\mu E\ m^{-2}\ s^{-1}$ [b] $\mu mol\ C\ m^{-2}\ hr^{-1}$ [c] $\mu mol\ C\ m^{-2}\ hr^{-1}\ [\mu E\ m^{-2}\ s^{-1}]^{-1}$ [d] $[\mu E\ m^{-2}\ s^{-1}]^{-1}$

Table 5.18

Ratios of light-limited photosynthetic rates (α^B) under different polychromatic irradiances as a function of growth photon flux density.

Expt. #	Growth PFD (a)	α^B_{blue} / α^B_{white}	α^B_{green} / α^B_{white}	α^B_{blue} / α^B_{green}
SY 9149/50/51	8	0.197	0.480	0.409
SY 9157/58/59	15	0.208	0.539	0.386
SY 9153/54/55	70	0.323	-	-
	Mean	0.243	0.510	0.398
DC 9129/30/31	7	-	-	0.306
DC 9125/26/27	17	0.610	2.303	0.265
DC 9117/18/19	25	0.642	2.153	0.298
DC 9121/22/23	35	0.599	2.161	0.277
	Mean	0.617	2.206	0.287
PA 9141/42/43	8	1.181	0.802	1.472
PA 9137/38/3	12	1.249	0.863	1.448
PA 9133/34/35	45	2.229	1.121	2.229
	Mean	1.553	0.929	1.716

Units: a $\mu E\ m^{-2}\ s^{-1}$

Table 8.1

(a) Light utilization indices (α') under different light sources according to Eq. 8.1. based upon the relative photosynthetic action spectra of Arctic phytoplankton assemblages, the prymnesiophyte *Pavlova* sp. (NEP) and the cyanobacteria *Synechococcus* sp. WH 5701 and *Synechococcus* sp. WH 7803 given in Figure 8.2(a).

	Arctic	Pavlova	WH 5701	WH 7803
$\alpha'_{tungsten}$	0.782	0.774	1.480	0.963
α'_{sun}	1.062	1.077	0.850	1.020
α'_{blue}	1.159	1.185	1.193	0.724
α'_{green}	0.852	0.916	0.495	1.861

(b) Light utilization indices *relative* to tungsten.

	Arctic	Pavlova	WH 5701	WH 7803
$\alpha'_{sun} / \alpha'_{tungsten}$	1.353	1.391	0.574	1.059
$\alpha'_{blue} / \alpha'_{tungsten}$	1.482	1.531	0.806	0.751
$\alpha'_{green} / \alpha'_{tungsten}$	1.090	1.182	0.334	1.932
$\alpha'_{blue} / \alpha'_{green}$	1.359	1.294	2.410	0.389

(c) Proportionality coefficients of P-I responses determined experimentally under polychromatic irradiance (from Table 5.12).

	Arctic	Pavlova	WH 5701	WH 7803
$\alpha^B_{blue} / \alpha^B_{white}$	no data	1.553	0.202	0.617
$\alpha^B_{green} / \alpha^B_{white}$	no data	0.929	0.510	2.206
$\alpha^B_{blue} / \alpha^B_{green}$	no data	1.716	0.398	0.280

Figure 2. 1. The structure and equations describing the P-I models of Peeters and Eilers (1978) [Hydrobiol. Bull. 12: 134-136] and Megard *et al.* (1984) [J. Plankton Res. 6: 325-337]. In both models P is the photosynthetic rate, α is the initial slope as the PFD tends to zero, P_m is the maximum photosynthetic rate and I_m is the PFD where the photosynthetic rate is maximal.

Peeters and Eilers (1978)

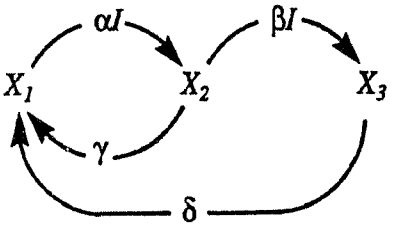

$$\frac{\partial X_1}{\partial t} = -\alpha I X_1 + \gamma X_2 + \delta X_3$$

$$\frac{\partial X_2}{\partial t} = \alpha I X_1 - (\beta I + \gamma) X_2$$

$$\frac{\partial X_3}{\partial t} = \beta I X_2 - \delta X_3$$

$$P = \gamma X_2$$

$$= \frac{\alpha \gamma \delta I}{\alpha \beta I^2 + \delta(\alpha + \beta) I + \gamma \delta}$$

$$= I / (a I^2 + b I + c)$$

where

$$a = \beta / \gamma \delta$$

$$b = (\alpha + \beta) / \alpha \gamma$$

$$c = 1 / \alpha$$

In this formulation:

$$\alpha = 1 / c$$

$$P_m = 1 / (b + 2(ac)^{1/2})$$

$$I_m = (c/a)^{1/2}$$

Megard *et al.* (1984)

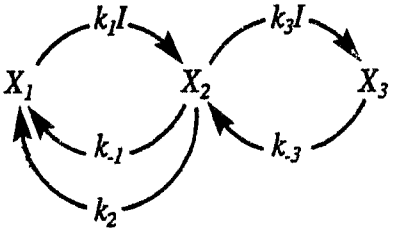

$$\frac{\partial X_1}{\partial t} = -k_1 I X_1 + (k_{-1} + k_2) X_2$$

$$\frac{\partial X_2}{\partial t} = k_1 I X_1 - (k_{-1} + k_2 + k_3 I) X_2 + k_{-3} X_3$$

$$\frac{\partial X_3}{\partial t} = k_3 I X_2 - k_{-3} X_3$$

$$P = k_2 X_2$$

$$= \left[\frac{\nu I}{K_1 + I + I_2 / K_2} \right]$$

where

$$K_1 = (k_{-1} + k_2) / k_1$$

$$K_2 = k_{-3} / k_3$$

$$\nu = k_2 (X_1 + X_2 + X_3)$$

In this formulation:

$$\alpha = \nu / K_1$$

$$P_m = P_s / (1 + 2 (K_1 / K_2)^{1/2})$$

$$I_m = (K_1 / K_2)^{1/2}$$

Figure 2. 1

Figure 2. 2. The structure and equations describing the P-I model of Fasham and Platt (1983) [Proc. Roy. Soc. Lond. B 219: 355-370]. The photosynthetic rate P is given by the negative root of the quadratic expression and the initial slope of the P-I response as the PFD tends to zero is α.

Fasham and Platt (1983)

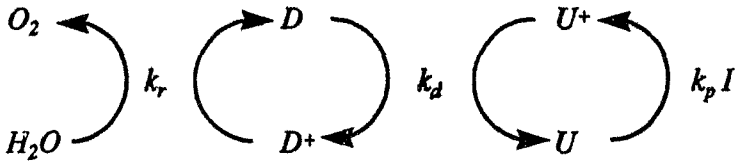

$$\frac{\partial D}{\partial t} = k_r D^+ - k_d D U^+ \qquad U + U^+ = U_o$$

$$\frac{\partial U^+}{\partial t} = k_p I U - k_d D U^+ \qquad D + D^+ = D_o$$

$$P = k_r D^+$$

Photoinhibition introduced as:

$$k_i = k_d e^{-\beta I}$$

Photosynthetic formulation:

$$P^2 - k_r D_o P \left[\frac{k_p k_r}{k_c} e^{-\beta I} + k_p U_o \right] I P + k_p k_r D_o U_o I = 0$$

or

$$P^2 - \mu P - \left[\chi e^{-\beta I} + \alpha \right] I P + \alpha \mu I = 0$$

where

$$\alpha = k_p U_o$$

$$\mu = k_r D_o$$

$$\chi = (k_p k_r)/k_d$$

Figure 2. 2

Figure 2.3. Mathematical formulations commonly employed to describe the P-I response of phytoplankton. The models are expressed in dimensionless form and assigned similar parameter values to provide a comparison of geometrical shapes.

(a) Saturation-type models: □ , Blackman (1905); + , Baule (1917); ◇ ,Baly (1935); △ , Smith (1936); × , Jassby and Platt (1976); ▽ , Bannister (1979).

(b) Photoinhibition models: □ , Steele (1962); ◇ , Vollenweider (1965) [$a = 1.5, n = 2.5$]; + , Steel (1973); × , Fee (1973) [$n = 2.5$]; △ , Platt *et al.* (1980) [$b = 0.1$]; ▽ , Iwakuma and Yasuno (1983) [$n = 2.5, m = 1.5$].

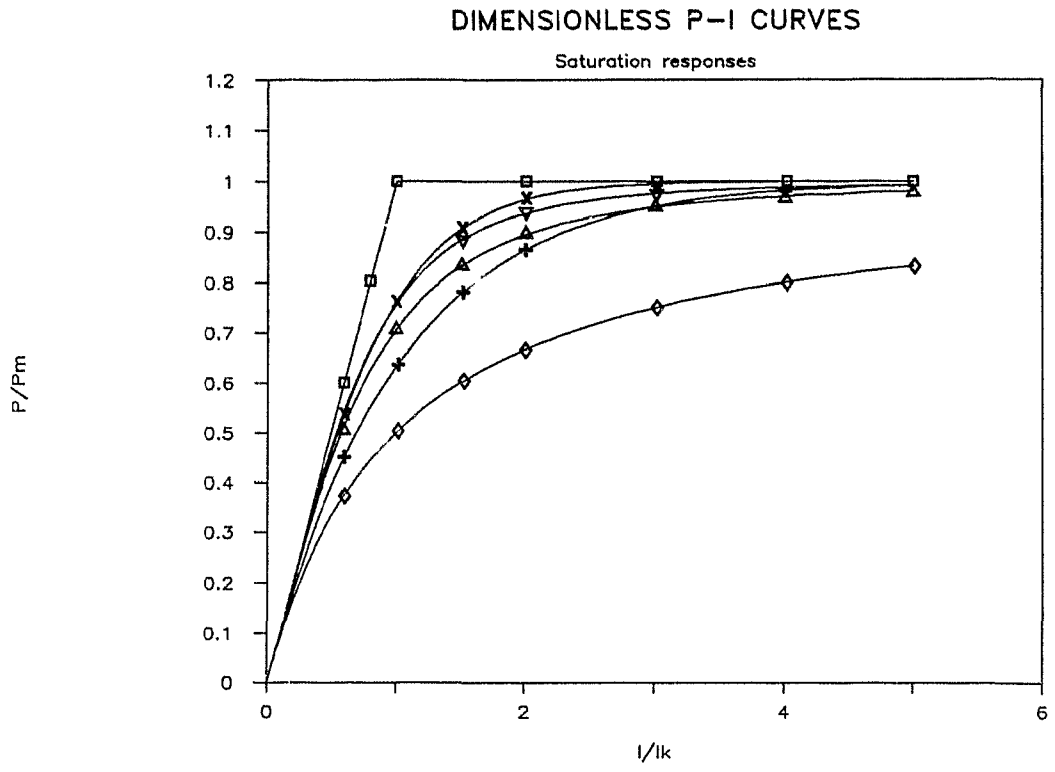
DIMENSIONLESS P–I CURVES
Saturation responses
P/Pm
1.2
1.1
1
0.9
0.8
0.7
0.6
0.5
0.4
0.3
0.2
0.1
0
0
2
4
6
I/Ik

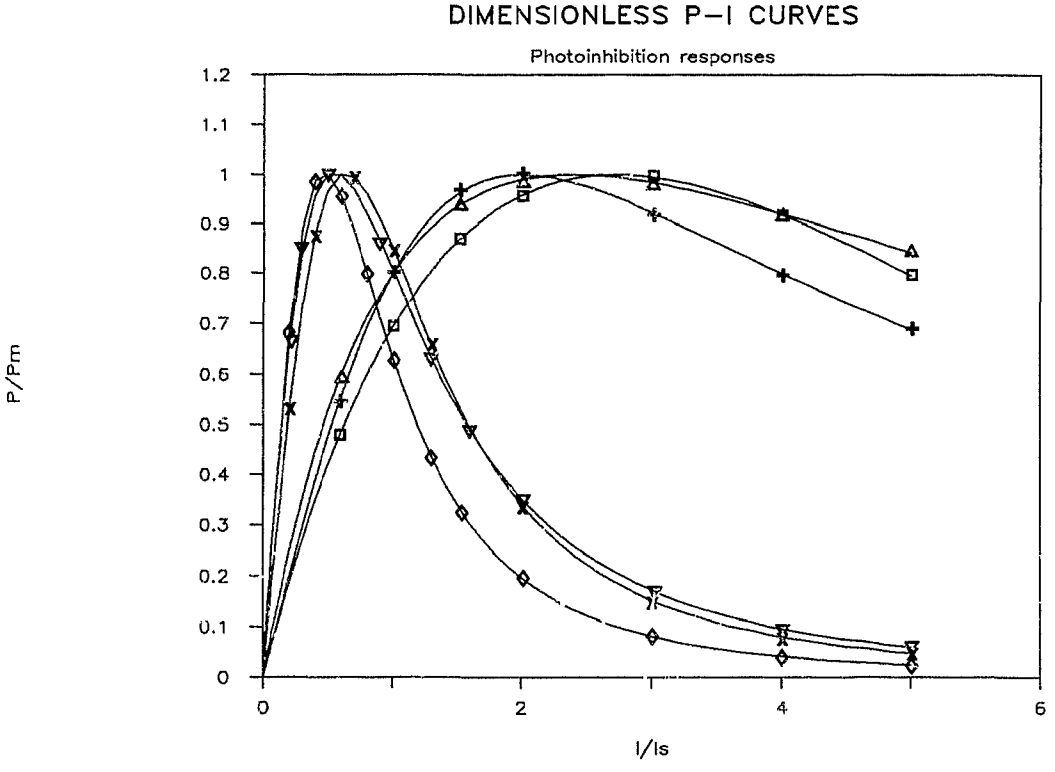
DIMENSIONLESS P–I CURVES
Photoinhibition responses
P/Pm
1.2
1.1
1
0.9
0.8
0.7
0.6
0.5
0.4
0.3
0.2
0.1
0
0
2
4
6
I/Is

Figure 2.3

Figure 3. 1. Spectral proportionality of the ideal photosynthetic response. Where a series of P-I responses are proportional to one another (upper panels (a) and (c)), replotting the curves as a function of the *logarithm* of the PFD produces a series of curves that are parallel to one another (lower panels (b) and (d)). The horizontal separation between any two curves corresponds to the logarithm of the proportionality constant. This transformation is illustrated for both saturation type (panels (a) and (b)) and photoinhibition-type (panels (c) and (d)) P-I responses.

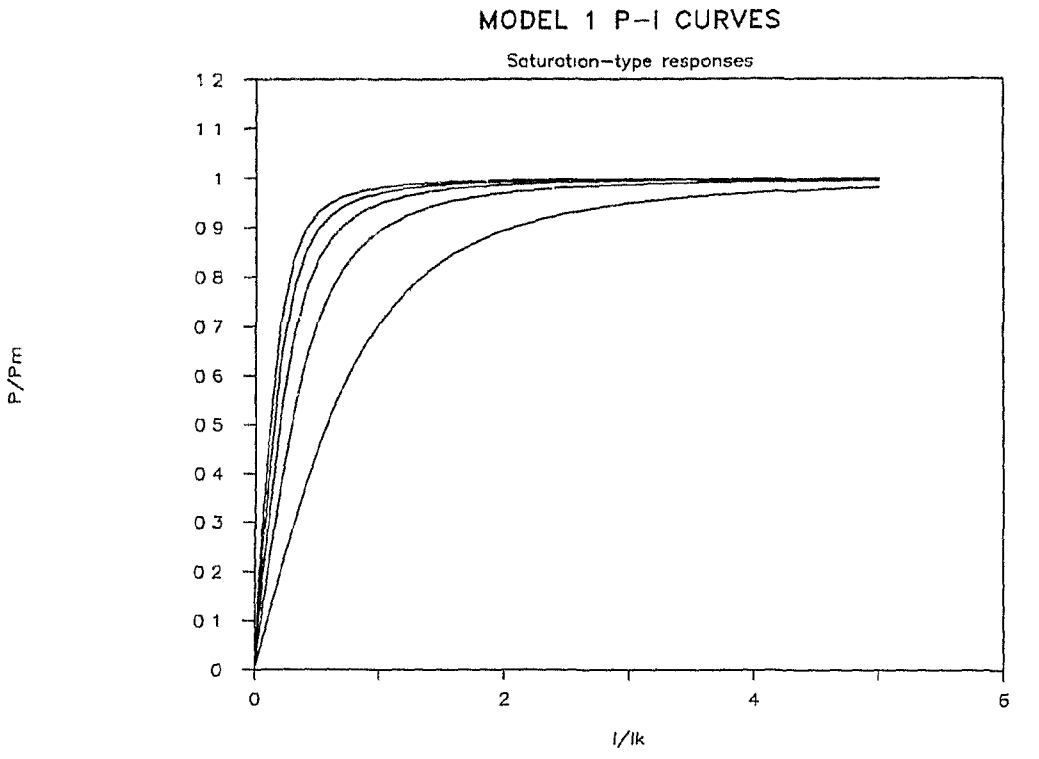
MODEL 1 P–I CURVES
Saturation–type responses
P/Pm
1 2
1 1
1
0 9
0 8
0 7
0 6
0 5
0 4
0 3
0 2
0 1
0
0
2
4
6
I/Ik

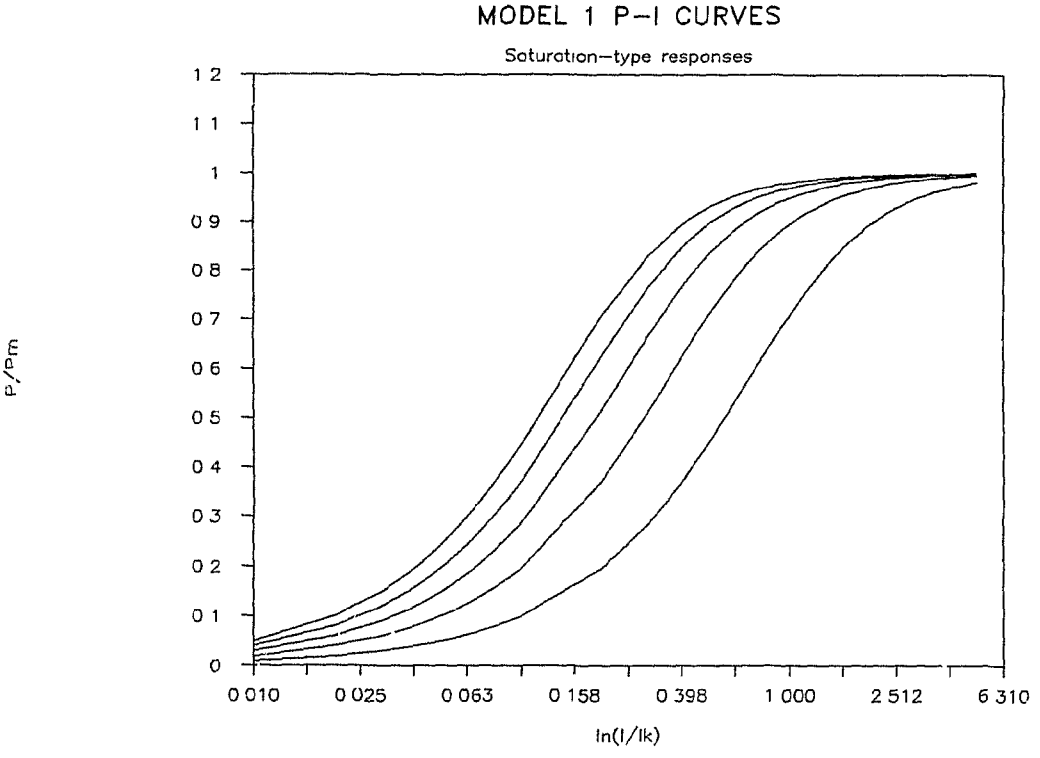
MODEL 1 P–I CURVES
Saturation–type responses
P/Pm
1 2
1 1
1
0 9
0 8
0 7
0 6
0 5
0 4
0 3
0 2
0 1
0
0 010
0 025
0 063
0 158
0 398
1 000
2 512
6 310
ln(I/Ik)

Figure 3. 1

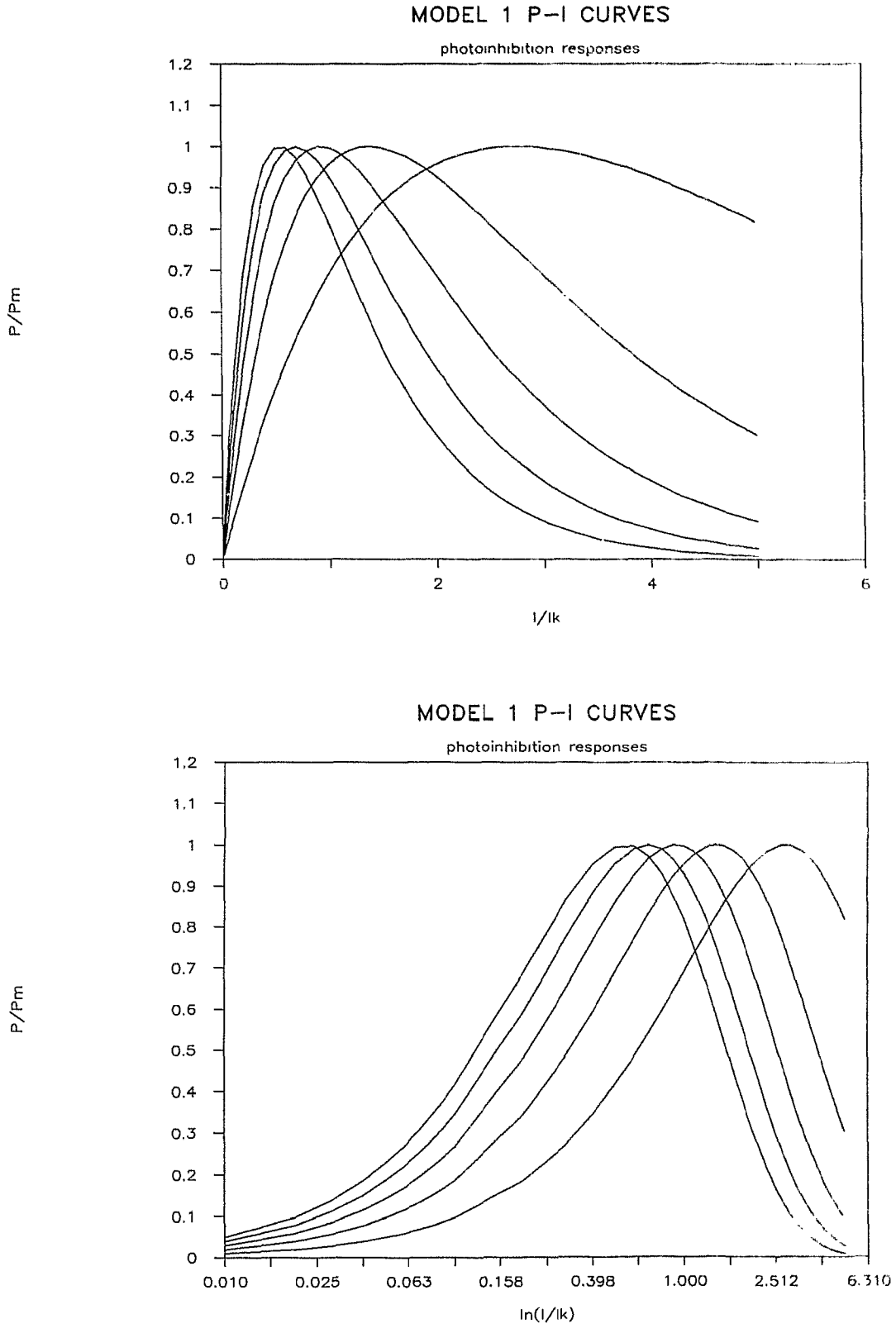

Figure 3. 1 (contd.)

Figure 3. 2. Geometrical properties of the empirical photoinhibition function $g(I)$ described in Eq. 3.36. This function is an analogue of the saturation function introduced by Bannister (1979). The upper panel illustrates the effect of varying the ratio I_t / I_j with the parameter n held constant ($n = 20$; $I_t / I_j = 5$ (∇), 10 ($\times$) and 20 (Δ)). The lower panel illustrates the effect of varying the parameter n while the ratio I_t / I_j is held constant ($I_t / I_j = 10$; $n = 5$ (∇), 10 ($\times$) and 50 (Δ)).

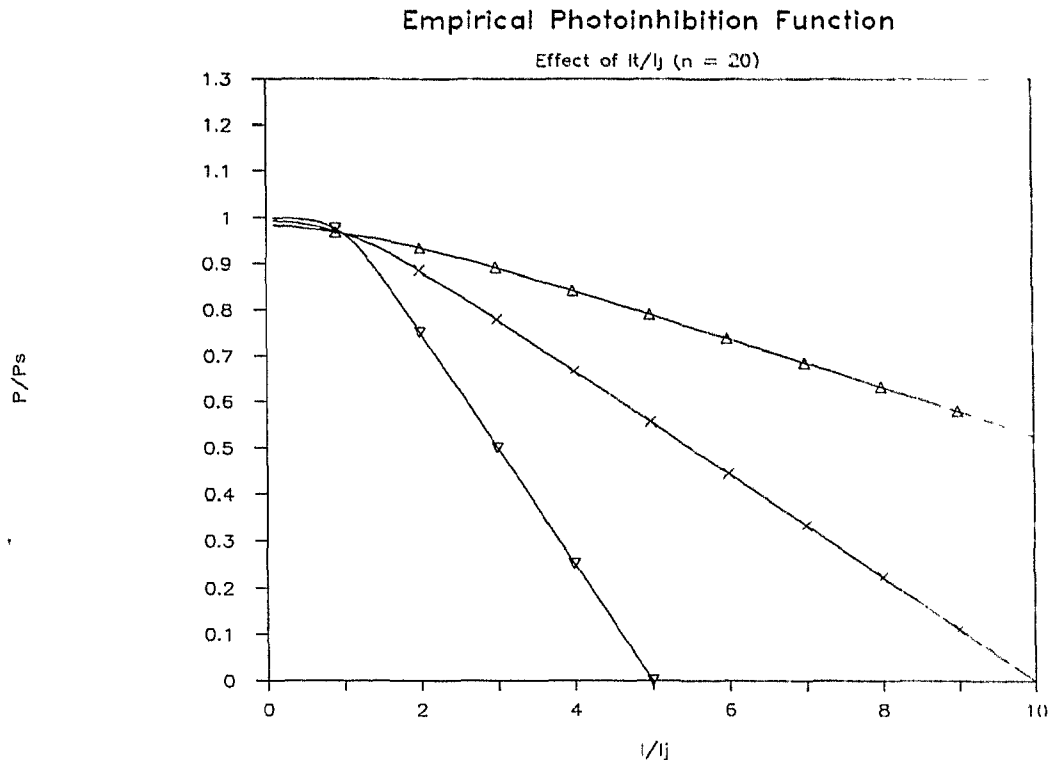
Empirical Photoinhibition Function
Effect of It/Ij (n = 20)
P/Ps
1.3
1.2
1.1
1
0.9
0.8
0.7
0.6
0.5
0.4
0.3
0.2
0.1
0
0
2
4
6
8
10
I/Ij

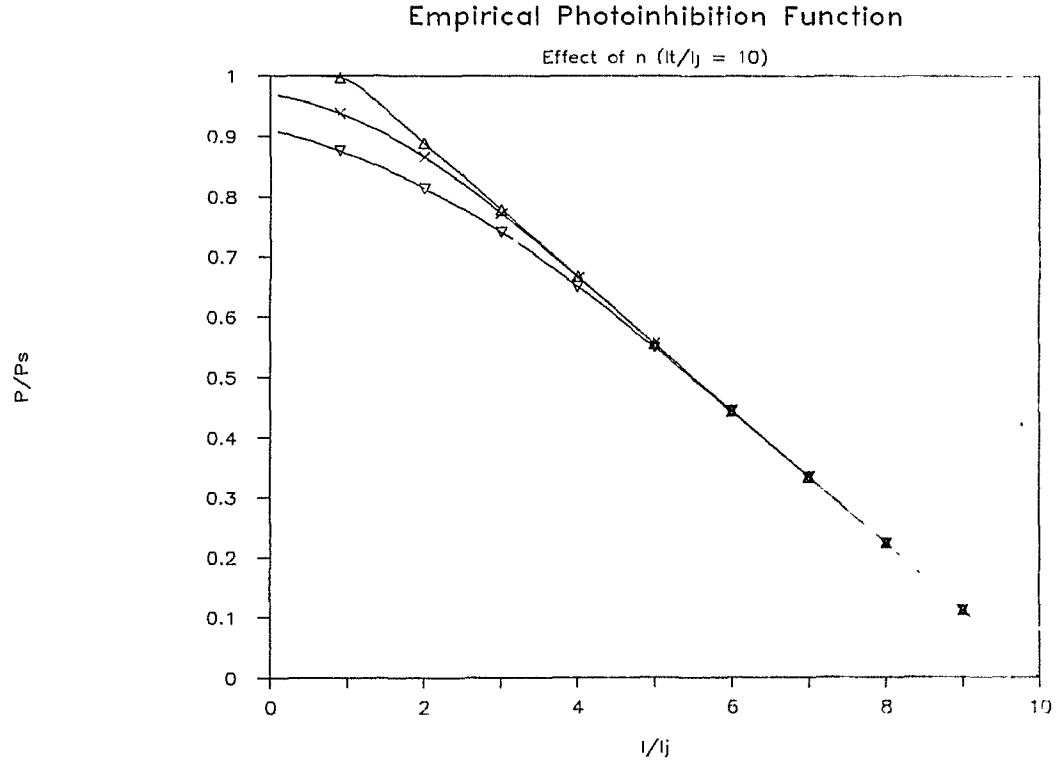
Empirical Photoinhibition Function
Effect of n (It/Ij = 10)
P/Ps
1
0.9
0.8
0.7
0.6
0.5
0.4
0.3
0.2
0.1
0
0
2
4
6
8
10
I/Ij

Figure 3.2

Figure 3. 3. Outline of photon absorption and photosynthesis in a single photosystem model. The yield of photosynthetic transduction at the reaction center may be described either by a constant (Linear model) or in terms of target theory (Poissonian model).

Single Photosystem Photosynthesis Model.

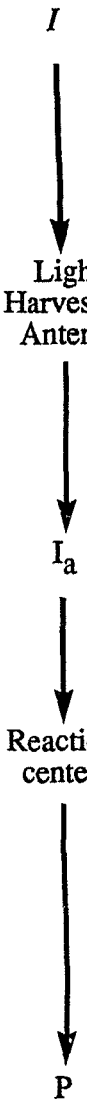

Incident PFD ($\mu mol\ m^{-2}\ s^{-1}$)

$$[= \int_{350}^{700} I(\lambda)\, d\lambda\ ]$$

Absorption cross-section (m^2)

$$[= \int_{350}^{700} a(\lambda)\, d\lambda\ ]$$

Absorbed photon flux ($\mu mol\ s^{-1}$)

$$[= \int_{350}^{700} I(\lambda)\, a(\lambda)\, d\lambda\ ]$$

Quantum efficiency

Linear model:
$= constant = P/I_a$

Poisson model:
$= f(n, I_a)$

Stored Irradiance ($\mu mol\ s^{-1}$)

Figure 3. 3

Figure 3. 4. Representative P-I curves derived from cumulative Poisson probabilities for photochemistry and photoinhibition based on target theory.

(a) The family of curves describing the probability of a reaction center performing photochemistry ($p(\geq x)$) as a function of the *average* number of excitons arriving at the reaction center (μ). Each curve corresponds to a different discrete value of x, the number of excitons required to arrive within the turnover time of the reaction center in order for photochemistry to occur ($x = 1, 2, 3 \ldots 18$).

(b) The family of curves describing the probability of a reaction center surviving photodestruction ($p(<y)$) as a function of the *average* number of excitons arriving at the reaction center (μ). Each curve corresponds to a different discrete value of y, the number of excitons required to arrive within the turnover time of the reaction center in order for photodestruction to occur ($y = 1, 2, 3 \ldots 18$).

(c) The family of curves describing the probability of photosynthesis ($p(\geq 1, <y)$) as a function of the average number of excitons arriving at a reaction center (μ). The number of excitons required bring about photochemistry is set to unity (single hit). Each curve corresponds to a different discrete value of y ($y = 2, 3, 4 \ldots 18$), the number of excitons required to cause photodestruction.

(d) The family of curves shown in (c), but normalized to the maximum probability of photosynthesis attained by a reaction center.

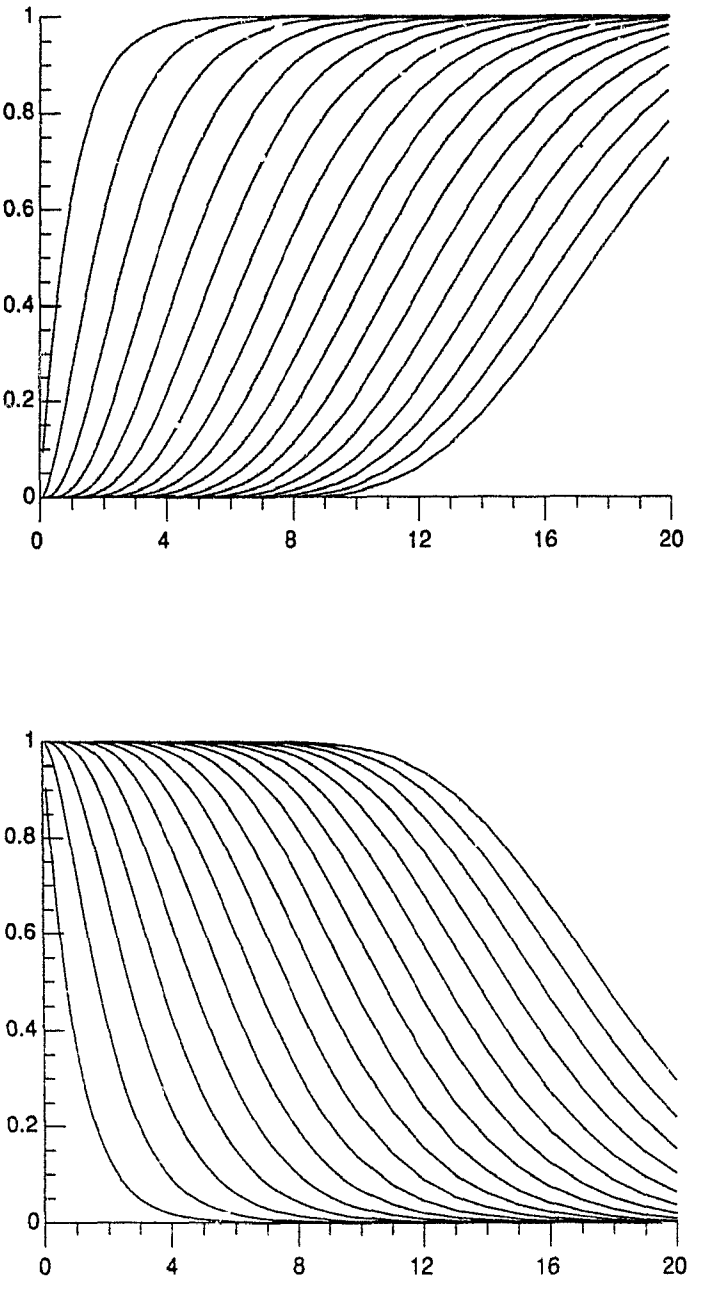

Figure 3.4

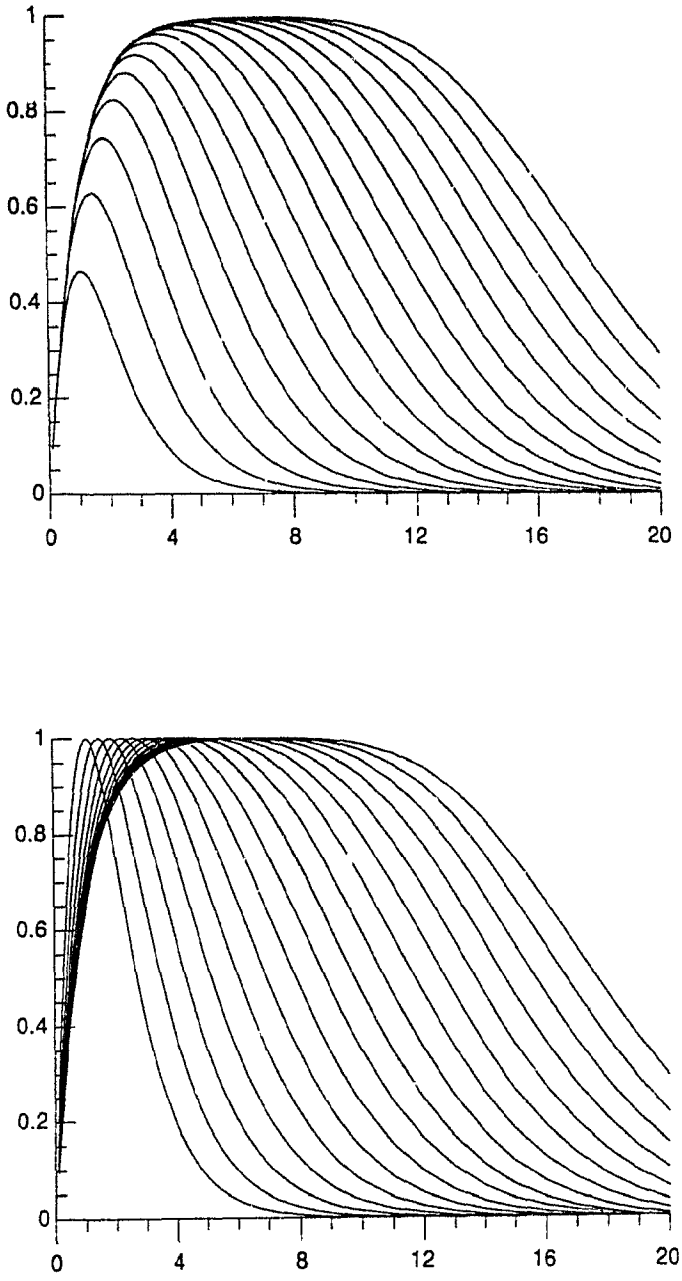

Figure 3.4 (contd.)

Figure 3. 5. Outline of photon absorption, distribution and photosynthesis in the two-photosystem model of Malkin (1967) [Biophys. J. 7: 629-649]. The photosynthetic quantum yields of photoreactions 1 and 2 are considered to be constants (ϕ_1 and ϕ_2 respectively).

Malkin (1967) model:

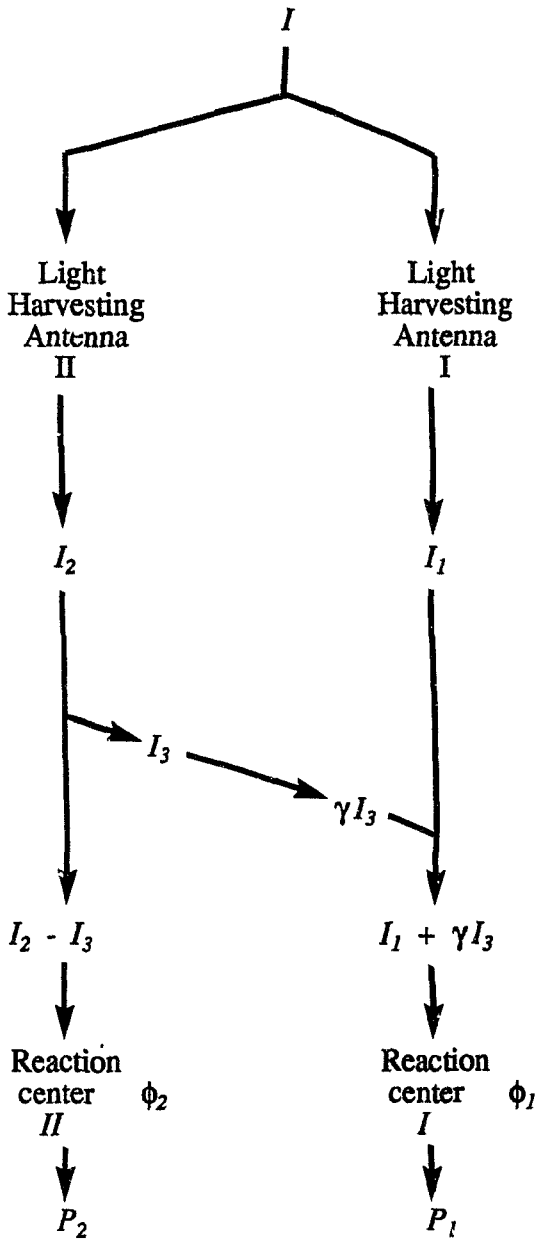

Incident Photon Flux Density

$$= \int_{350}^{700} I(\lambda)\, d\lambda$$

Absorption cross-section

$$= \int_{350}^{700} a_1(\lambda)\, d\lambda + \int_{350}^{700} a_2(\lambda)\, d\lambda$$

Absorbed flux

$$= I_1 + I_2$$

$$= \int_{350}^{700} I(\lambda)a_1(\lambda)d\lambda + \int_{350}^{700} I(\lambda)a_2(\lambda)d\lambda$$

Redistribution by way of spillover

Excitation flux arriving at each photosystem

Quantum efficiency of reaction centers (ϕ_1 and ϕ_2)

Photosynthetic flux through each reaction center

Photosynthetic rate is lesser of P_1 or P_2

Figure 3. 5

Figure 3. 6. Distribution of the exciton flux between the two photosystems in Malkin's (1967) model [Biophys. J. 7: 629-649].

(a) Under a single monochromatic beam $I(\lambda)$. Solutions are for the equilibrium case where $P_1 = P_2$. Two situations are considered corresponding to the cases where one photoreaction is overstimulated relative to the other.

(b) Under two monochromatic beams $I(\lambda_1)$ and $I(\lambda_2)$. The beam $I(\lambda_2)$ preferentially excites Photosystem 2 and the beam $I(\lambda_1)$ preferentially excites Photosystem 1. As in (a) solutions are for the equilibrium case where $P_1 = P_2$ and two situations are considered corresponding to the cases where one photoreaction is overstimulated relative to the other.

Single Monochromatic beam:

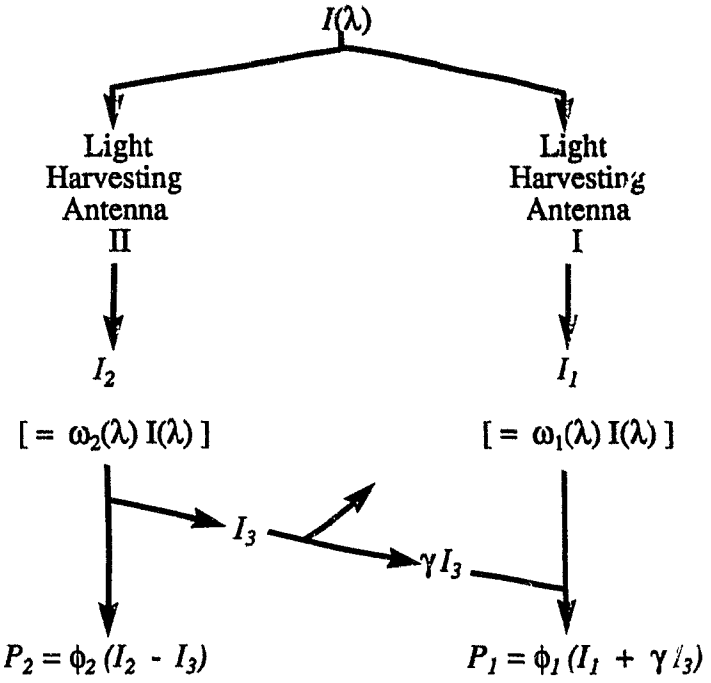

(i) $\phi_1 I_1 > \phi_2 I_2$ (*ie.* PS II limited):

$$P(\lambda) = \phi_2 I_2$$

$$= \phi_2 \omega_2(\lambda) I(\lambda)$$

$$\Phi(\lambda) = \phi_2 \omega_2(\lambda)$$

(ii) $\phi_1 I_1 < \phi_2 I_2$ (*ie.* PS I limited):

$$P(\lambda) = \frac{\phi_1 \phi_2}{\gamma \phi_1 + \phi_2} \left[\omega_1(\lambda) I(\lambda) + \gamma \omega_2(\lambda) I(\lambda) \right]$$

$$= \frac{\phi_1 \phi_2}{\gamma \phi_1 + \phi_2} \left[\omega_1(\lambda) + \gamma \omega_2(\lambda) \right] I(\lambda)$$

$$\Phi(\lambda) = \frac{\phi_1 \phi_2}{\gamma \phi_1 + \phi_2} \left[\omega_1(\lambda) + \gamma \omega_2(\lambda) \right]$$

Figure 3. 6 (a)

Dual Monochromatic beams:

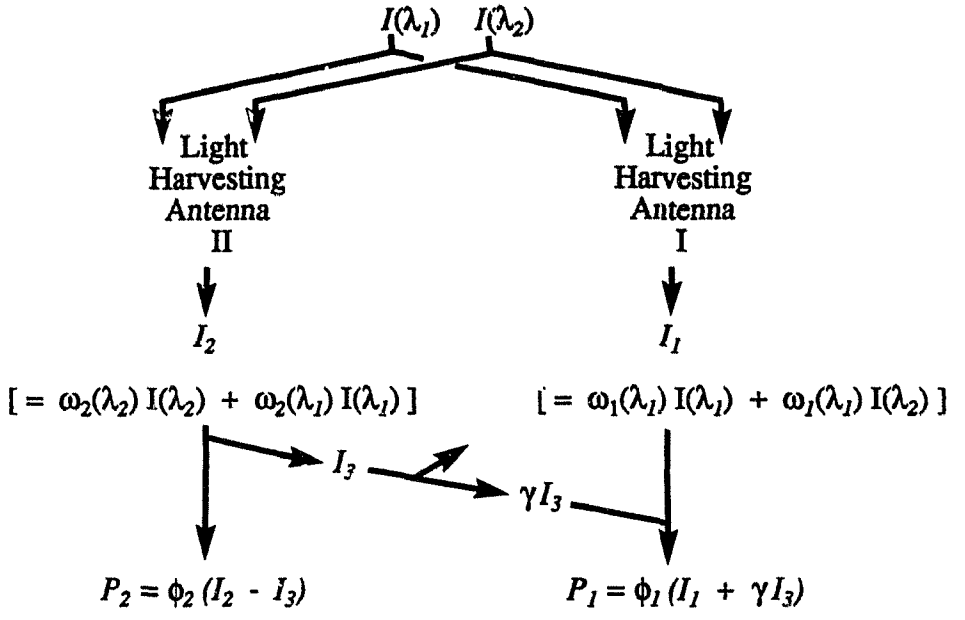

(i) $\phi_1 I_1 > \phi_2 I_2$ (*ie.* PS II limited):

$$P(11,12) = \phi_2 I_2$$

$$= \phi_2\, \omega_2(\lambda_1)\, I(\lambda_1) + \phi_2\, \omega_2(\lambda_2)\, I(\lambda_2)$$

$$= \phi_2\, [\, \omega_2(\lambda_1)\, I(\lambda_1) + \omega_2(\lambda_2)\, I(\lambda_2)\,]$$

(ii) $\phi_1 I_1 < \phi_2 I_2$ (*ie.* PS I limited):

$$P(\lambda_1,\lambda_2) = \frac{\phi_1 \phi_2}{\gamma \phi_1 + \phi_2} \left[[\omega_1(\lambda_1) + \gamma\, \omega_2(\lambda_1)]\, I(\lambda_1) + [\omega_1(\lambda_2) + \gamma\, \omega_2(\lambda_2)]\, I(\lambda_2) \right]$$

with no spillover ($\gamma = 0$) this simplifies to:

$$= \frac{\phi_1 \phi_2}{\phi_2} \left[\omega_1(\lambda_1)\, I(\lambda_1) + \omega_1(\lambda_2)\, I(\lambda_2) \right]$$

and with complete spillover ($\gamma = 1$) this simplifies to:

$$= \frac{\phi_1 \phi_2}{\phi_1 + \phi_2} \left[[\omega_1(\lambda_1) + \omega_2(\lambda_1)]\, I(\lambda_1) + [\omega_1(\lambda_2) + \omega_2(\lambda_2)]\, I(\lambda_2) \right]$$

Figure 3. 6 (b)

Figure 3. 7. Reaction scheme, set of equations and parameter interpretation of a new two-photosystem kinetic model.

(a) Reaction scheme and resultant equations. The rate of photosynthesis is given by the negative root of the quadratic expression. In this formulation α' is the initial slope of the P-I response as the PFD tends to zero, P_m is the maximum photosynthetic rate and I_m is the PFD corresponding to the maximum rate of photosynthesis. The following graphs illustrate the geometrical effects of different parameter values and show the flexibility of the model to describe a wide variety of P-I curves.

(b) P-I curves for three different values of χ ($\Delta = 0.01$, $\times = 0.2$ and $\nabla = 2.0$) assuming zero photoinhibition ($\beta = 0$). In the upper panel the parameter α is held constant. In the lower panel the initial slope of the P-I curve (α') is held constant.

(c) P-I curves for three different values of χ ($\Delta = 0.01$, $\times = 0.1$ and $\nabla = 1.0$) with constant photoinhibition ($\beta = 0.5$). In the upper panel the parameter α is held constant. In the lower panel the initial slope of the P-I curve (α') is held constant.

(d) P-I curves for three different values of β ($\Delta = 0.2$, $\times = 0.4$ and $\nabla = 0.8$) and constant value of χ ($\chi = 0.05$). In the upper panel the parameter α is held constant. In the lower panel the ratio between β and the initial slope (α') is held constant ($\beta/\alpha' = 0.25$).

Reaction scheme of new two-photosystem kinetic model:

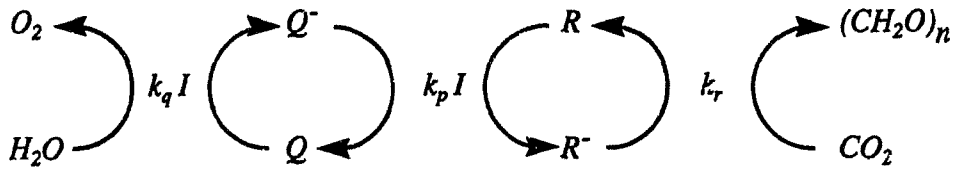

$$\frac{\partial Q}{\partial t} = -k_q I Q + k_p I Q^- R \qquad Q + Q^- = Q_o$$

$$\frac{\partial R}{\partial t} = -k_p I Q^- R + k_r R^- \qquad R + R^- = R_o$$

$$P = k_r R^-$$

Photoinhibition introduced as: $Q_o' = Q_o e^{-\beta I}$

Steady-state solution:

$$P^2 - \left[k_r R_o + \frac{k_q k_r}{k_p} \right] P - k_q Q_o e^{-\beta I} I P + k_r R_o k_q Q_o e^{-\beta I} I = 0$$

or

$$P^2 - \left[\mu + \chi + \alpha e^{-\beta I} I \right] P + \left[\mu \alpha e^{-\beta I} \right] I = 0$$

where $\alpha = k_q Q_o$, $\mu = k_r R_o$ and $\chi = (k_q k_r)/k_p$.

In this formulation:

$$\alpha' = \alpha [\mu / (\mu + \chi)] [1 - \beta]$$

$$P_m = 1/2 \left[[\mu + \chi + (\alpha/\beta e)] - [[\mu + \chi + (\alpha/\beta e)]^2 - 4\mu(\alpha/\beta e)]^{1/2} \right]$$

$$I_m = 1 / \beta$$

Figure 3.7

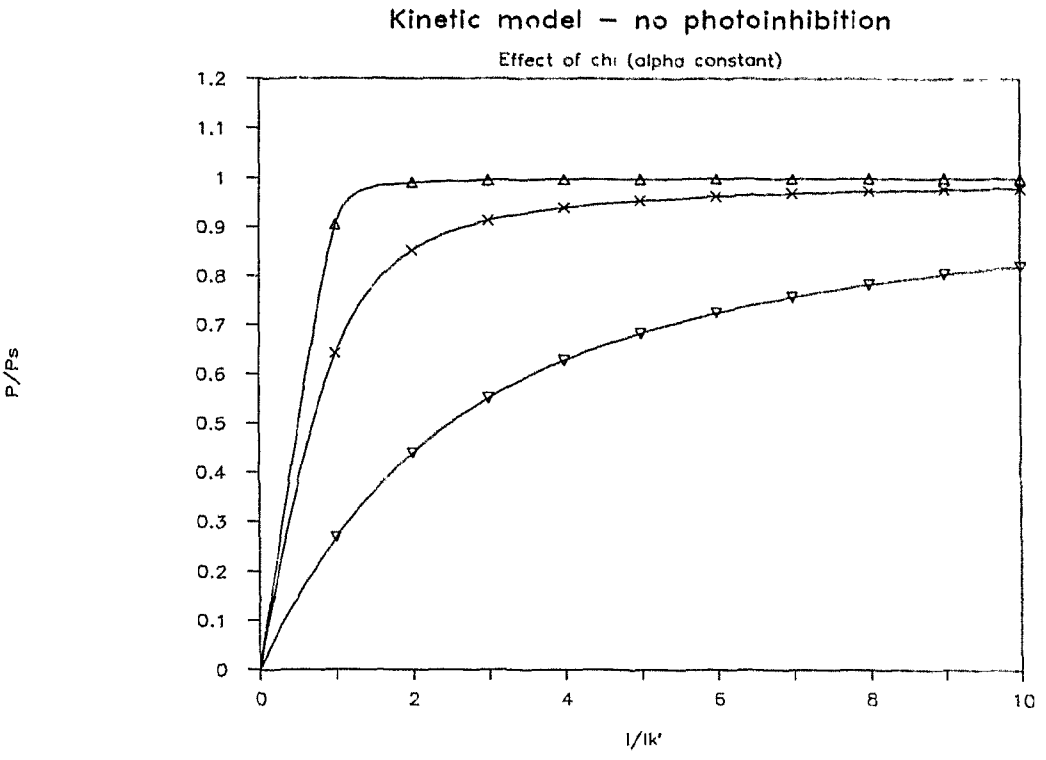

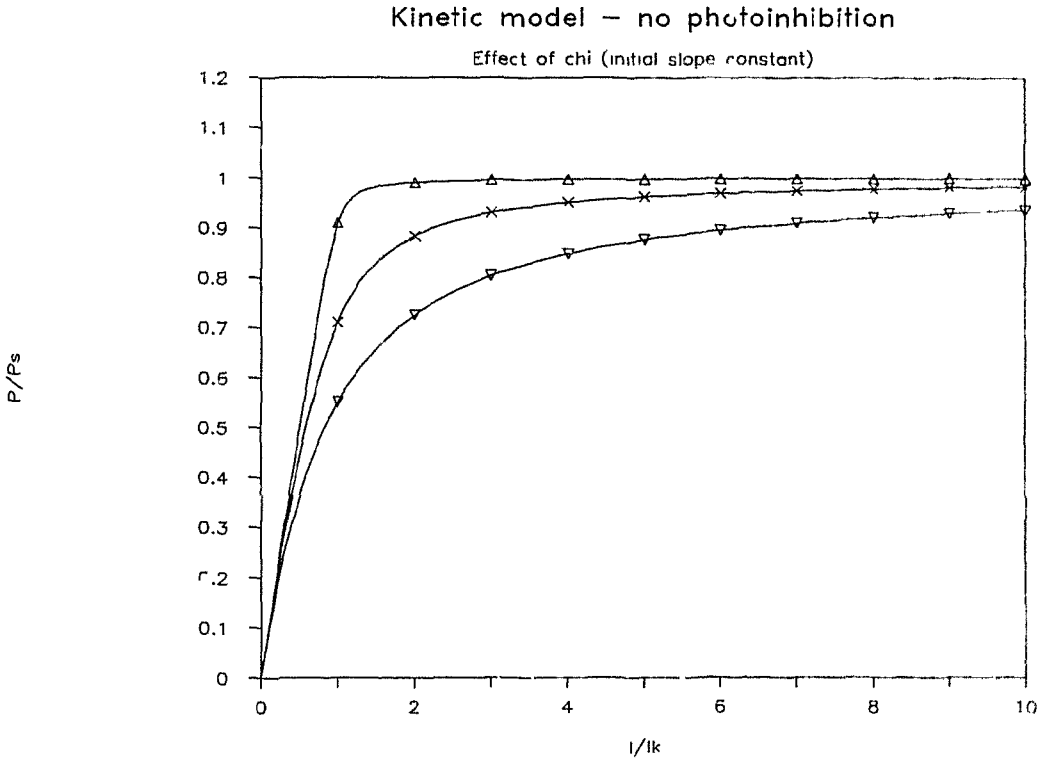

Figure 3. 7 (contd.)

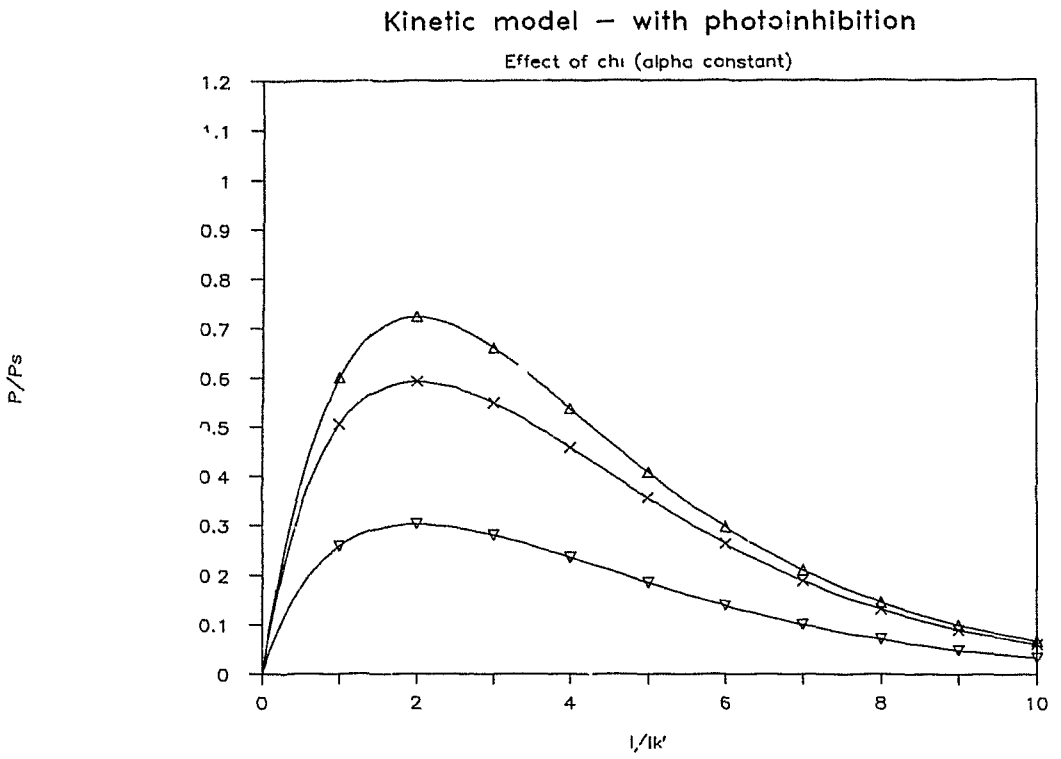

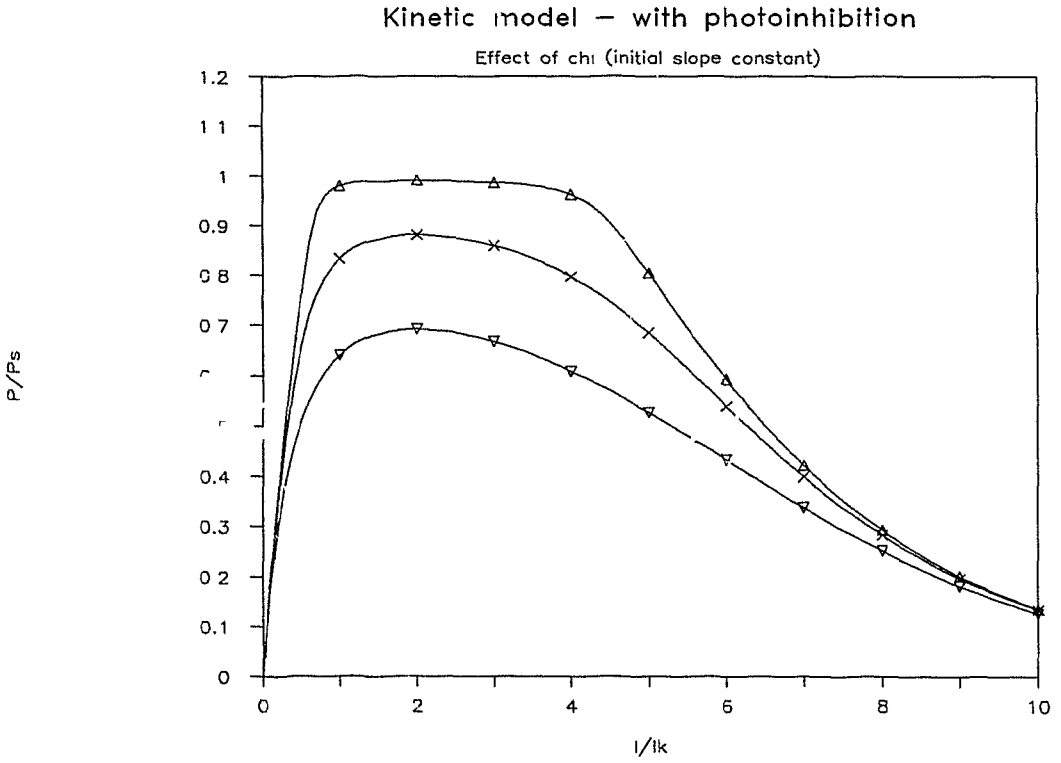

Figure 3. 7 (contd.)

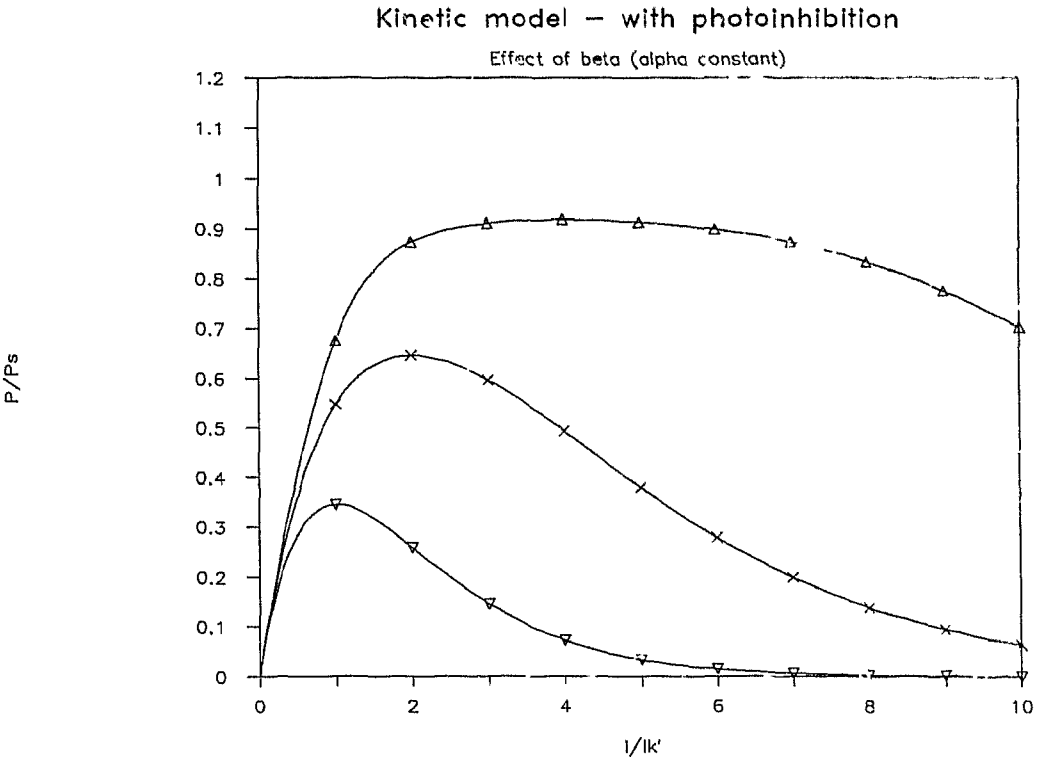

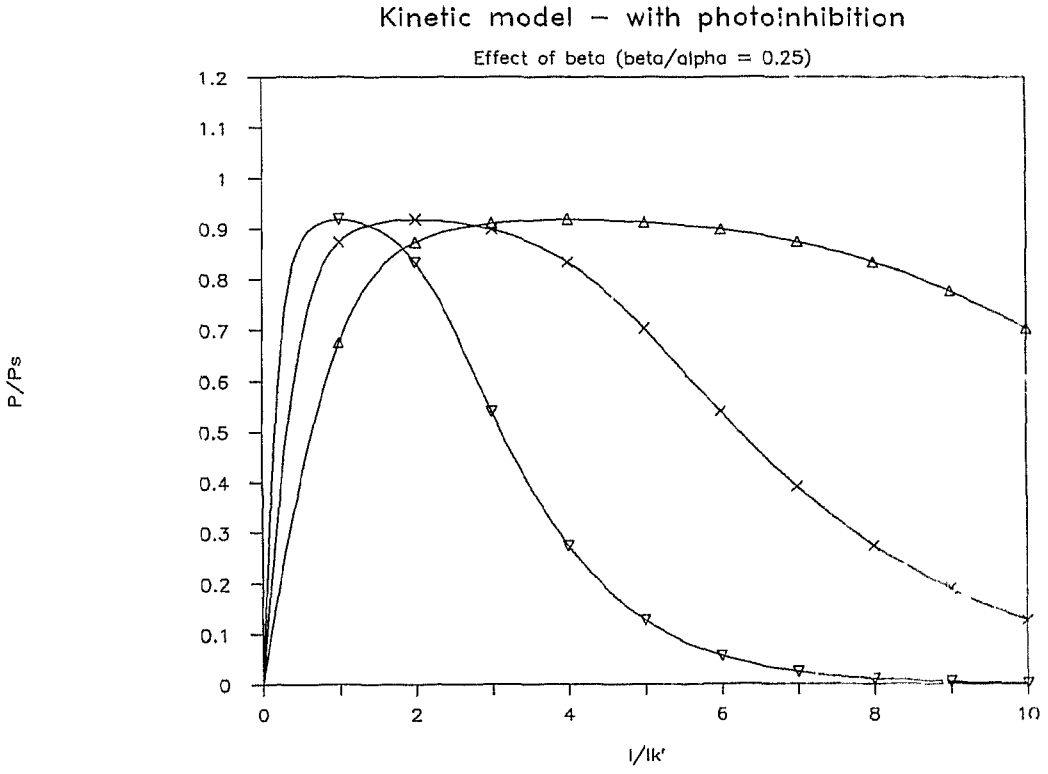

Figure 3.7 (contd.)

Figure 3. 8. Rectifying co-ordinates for a non-rectangular hyperbola. Parameterization of the non-rectangular hyperbola is that of Thornley (1976) [Eq. 2.11]. The upper panel contains five P-I curves with different values of Θ (Θ = 0 (∇), 0.5 ($\times$), 0.75 ($\triangle$), 0.9 ($\diamond$), 0.98 ($+$) and 1.0 ($\square$). The values of the maximum photosynthetic rate (P_m) and initial slope (α') are held constant. The lower panel plots the same five P-I curves in rectified co-ordinates. Note that the intercept on the abscissa in rectifying co-ordinates corresponds to $1/\Theta$.

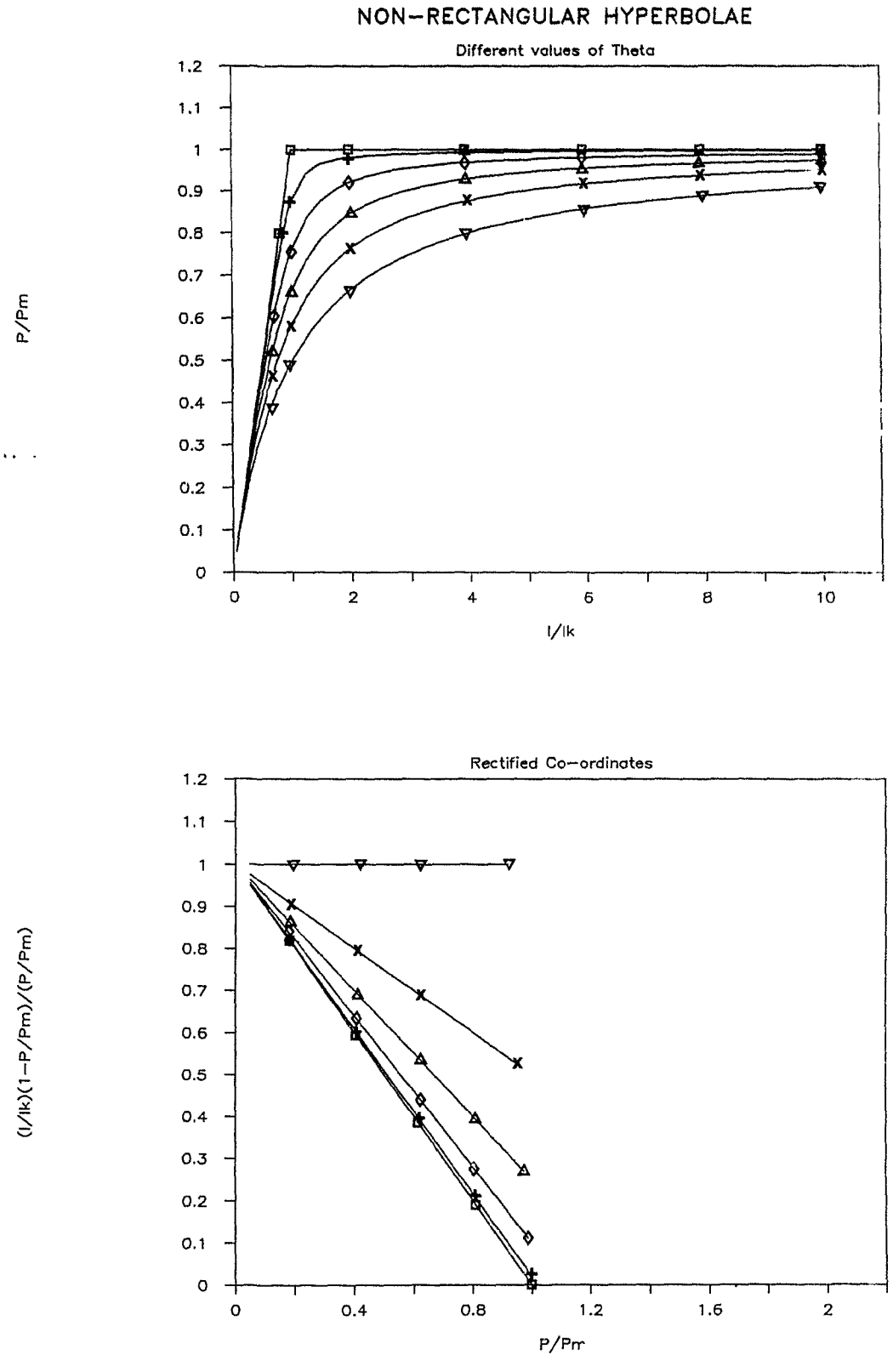
NON-RECTANGULAR HYPERBOLAE
Different values of Theta
P/Pm
I/Ik
Rectified Co-ordinates
(I/Ik)(1-P/Pm)/(P/Pm)
P/Pm

Figure 3.8

Figure 3. 9. Proportionality between the P-I responses of *Chlorella* sp. determined under different monochromatic wavelengths (data from Pickett and Myers (1966) [Plant Physiol. 41: 90-98]). Proportionality between the P-I curves requires that the responses determined under irradiance of different wavelengths be parallel when plotted as a function of the logarithm of the PFD. The upper panel shows the P-I response at wavelengths of 450 nm (□), 525 nm (+), 576 nm (◇), 630 nm (△) and 650 nm (×). The lower panel shows the P-I response at wavelengths of 680 nm (□), 700 nm (+), 705 nm (◇), 710 nm (△) and under "white" polychromatic light(×).

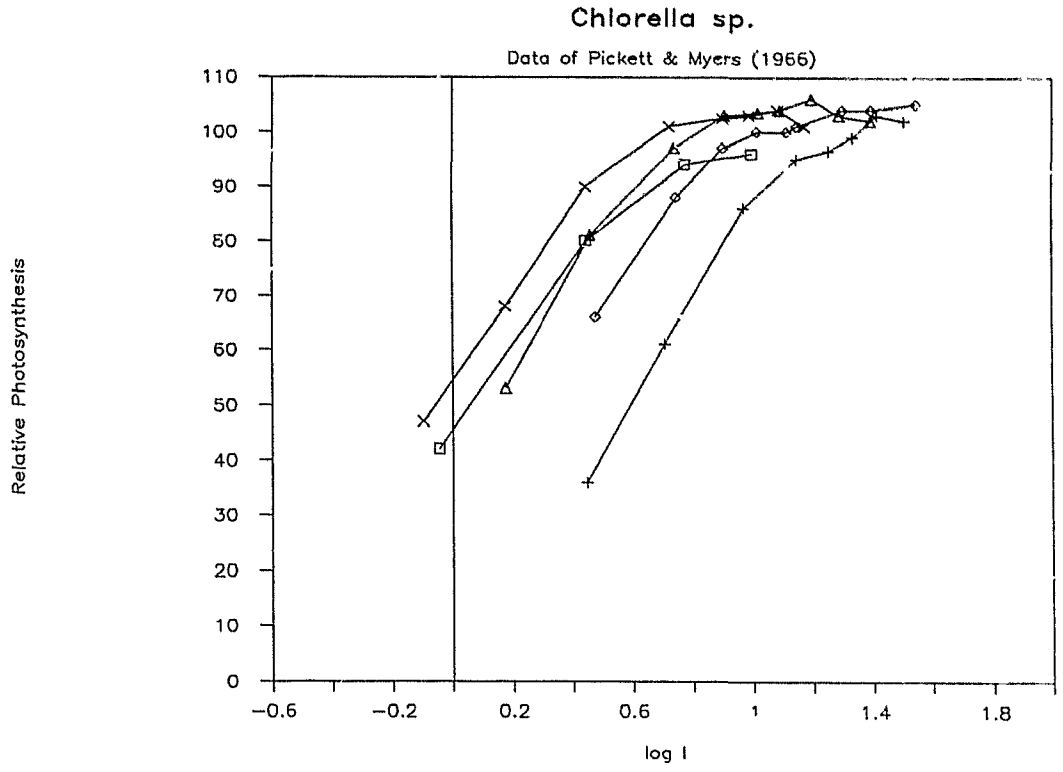
Chlorella sp.
Data of Pickett & Myers (1966)
Relative Photosynthesis
110
100
90
80
70
60
50
40
30
20
10
0
−0.6
−0.2
0.2
0.6
1
1.4
1.8
log I

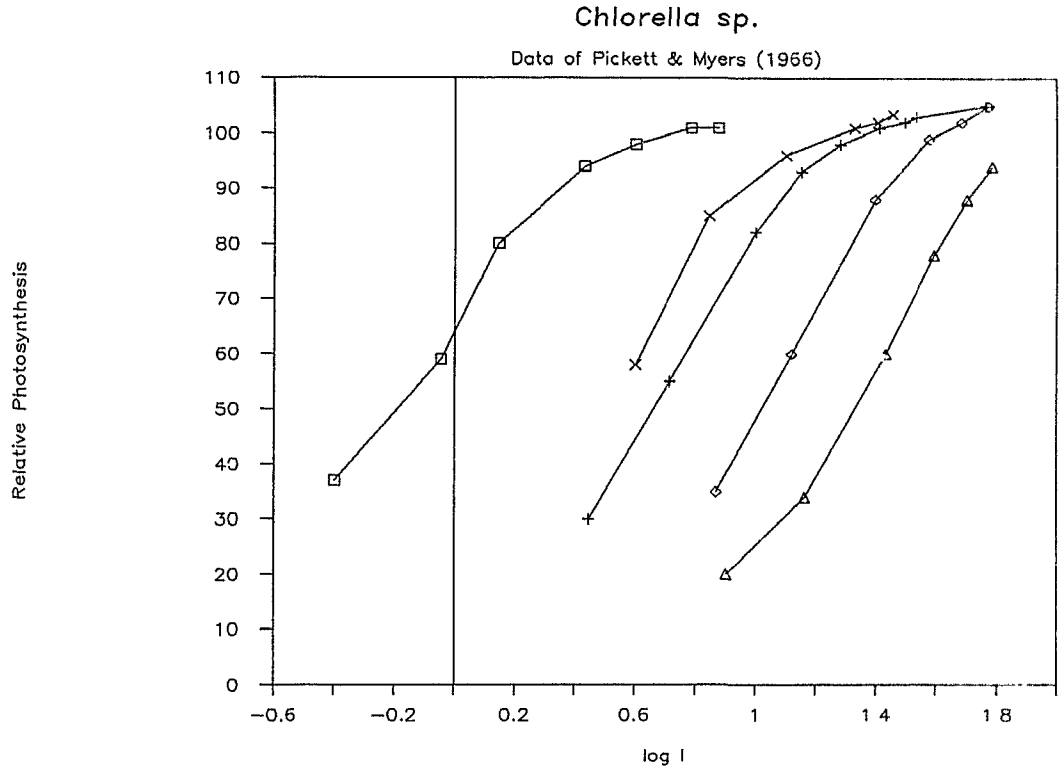
Chlorella sp.
Data of Pickett & Myers (1966)
Relative Photosynthesis
110
100
90
80
70
60
50
40
30
20
10
0
−0.6
−0.2
0.2
0.6
1
1.4
1.8
log I

Figure 3.9

Figure 4. 1. Geographical location of the sampling site in the northern Sargasso Sea (35°20′ N, 62°30′ S). The station is about 220 nautical miles NE of Bermuda.

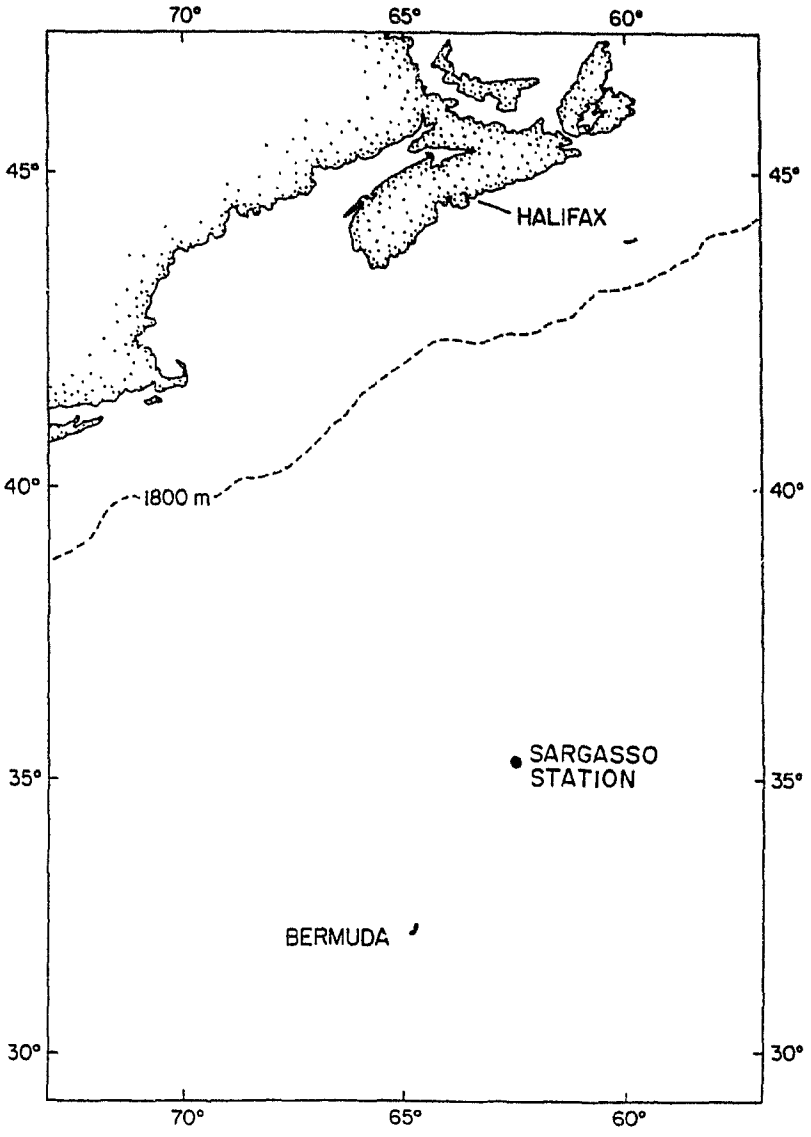

Figure 4.1

Figure 4. 2. Geographical locations of the sampling sites in the eastern Canadian Arctic. The inset shows the locations of the stations occupied in Jones Sound and Lancaster Sound.

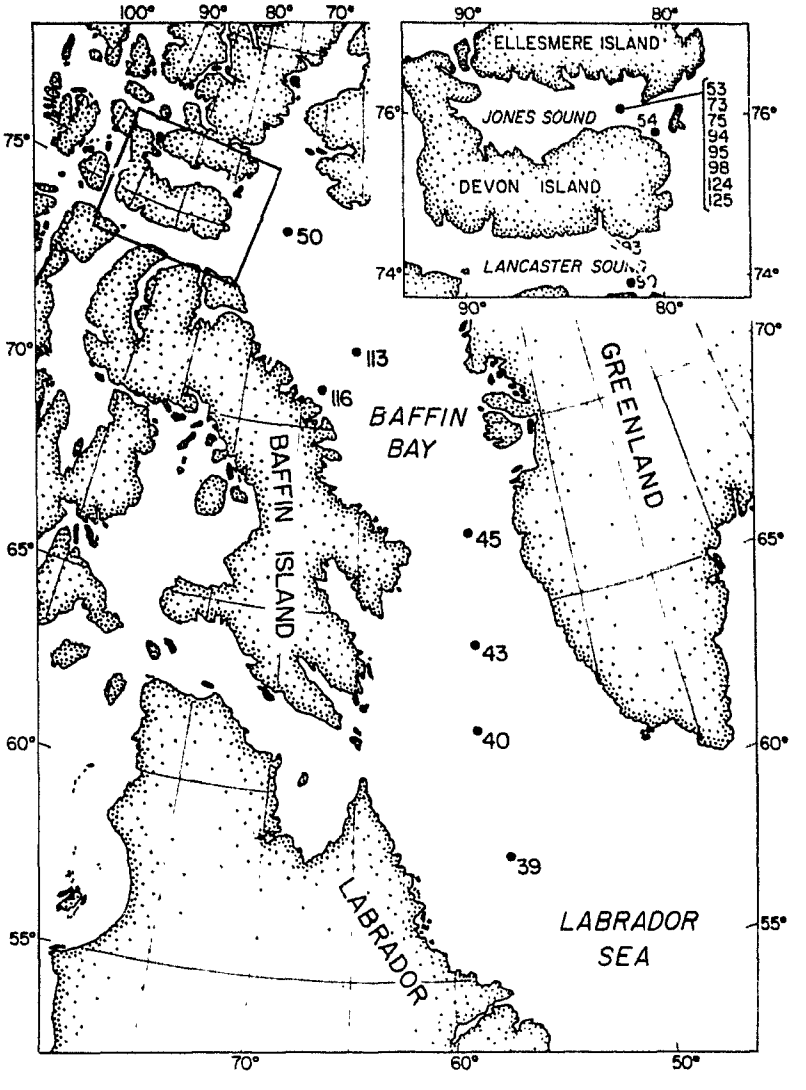
100°
90°
80°
70°
75°
70°
65°
60°
55°
50
113
116
45
43
40
39
BAFFIN BAY
BAFFIN ISLAND
GREENLAND
LABRADOR
LABRADOR SEA
70°
60°
50°
ELLESMERE ISLAND
JONES SOUND
DEVON ISLAND
LANCASTER SOUND
53
73
75
94
95
98
124
125
54
92
76°
74°

Figure 4.2

Figure 4. 3. Geographical locations of the sampling sites in the eastern Sargasso Sea and eastern North Atlantic Ocean.

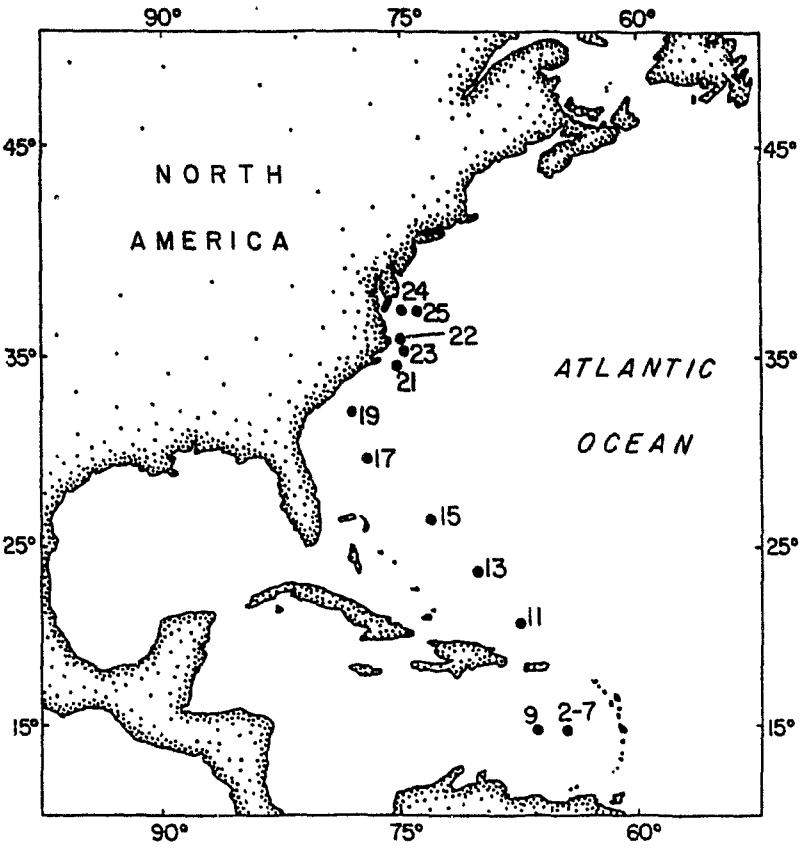
90°
75°
60°
45°
35°
25°
15°
NORTH
AMERICA
ATLANTIC
OCEAN
24
25
22
23
21
19
17
15
13
11
9
2-7

Figure 4.3

Figure 4. 4. Geographical locations of the sampling sites in the mid-North Atlantic Ocean east of Bermuda. Sampling stations correspond to the Nashville seamount (Stn. "N", 34°22′ N, 57°10.4′ W), the Yakutat seamount (Stn. "Y", 34°34.9′ N, 51°02.5′ W) and the oligotrophic Station Purple (Stn. "P", 31°58′ N, 55°38.9′ W.

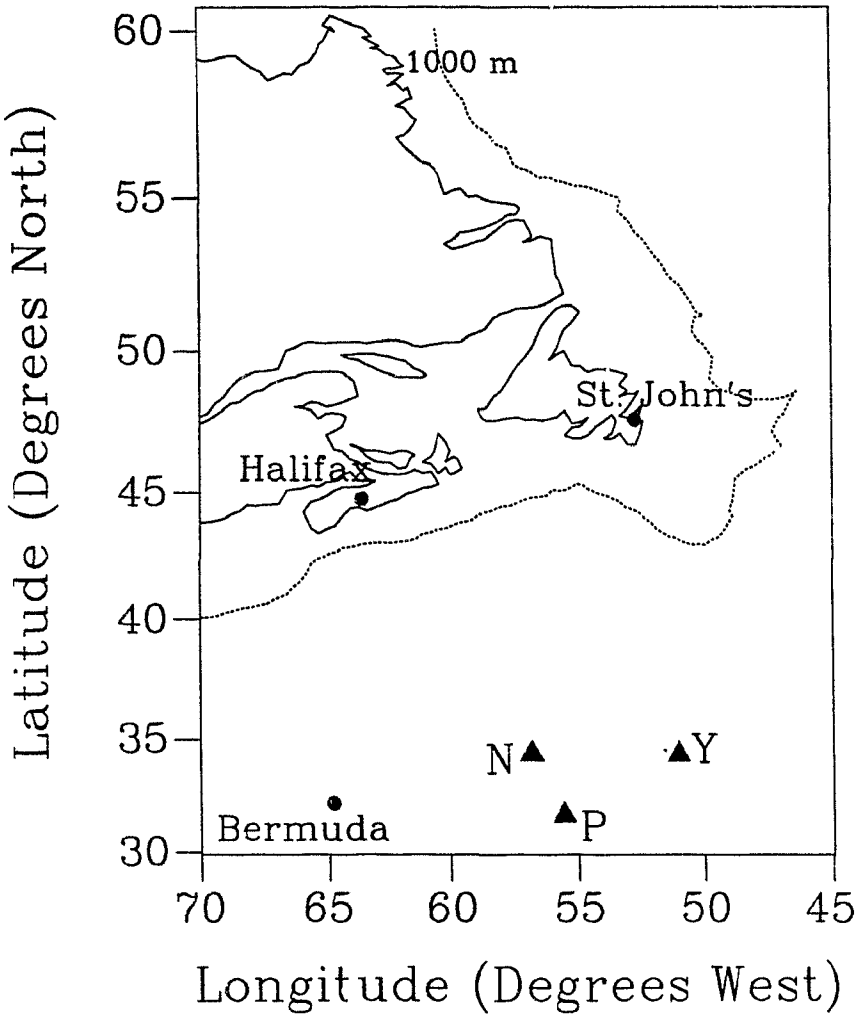
60
55
50
45
40
35
30
1000 m
St. John's
Halifax
N
Y
P
Bermuda
70
65
60
55
50
45
Latitude (Degrees North)
Longitude (Degrees West)

Figure 4.4

Figure 4. 5. Relative spectral composition of the irradiance within the twelve "monochromatic" wavebands employed to determine the spectral dependence of photosynthesis. Measurements were made at 1 nm intervals from 368 nm to 698 nm with a prototype spectroradiometer (Focal Marine Ltd., Dartmouth, Nova Scotia, model OS-1). PFDs emerging through the base of the incubation vials were measured with a cosine-corrected sensor (units: $\mu mol\ m^{-2}\ s^{-1}\ nm^{-1}$) and normalized to the maximum spectral PFD. The upper panel corresponds to interference filters with nominal maximum transmission peaks at 400 nm, 425 nm, 450 nm, 475 nm, 500 nm and 525 nm. The lower panel correponds to interference filters with nominal maximum transmission peaks at 550 nm, 575 nm, 600 nm, 625 nm, 650 nm and 675 nm.

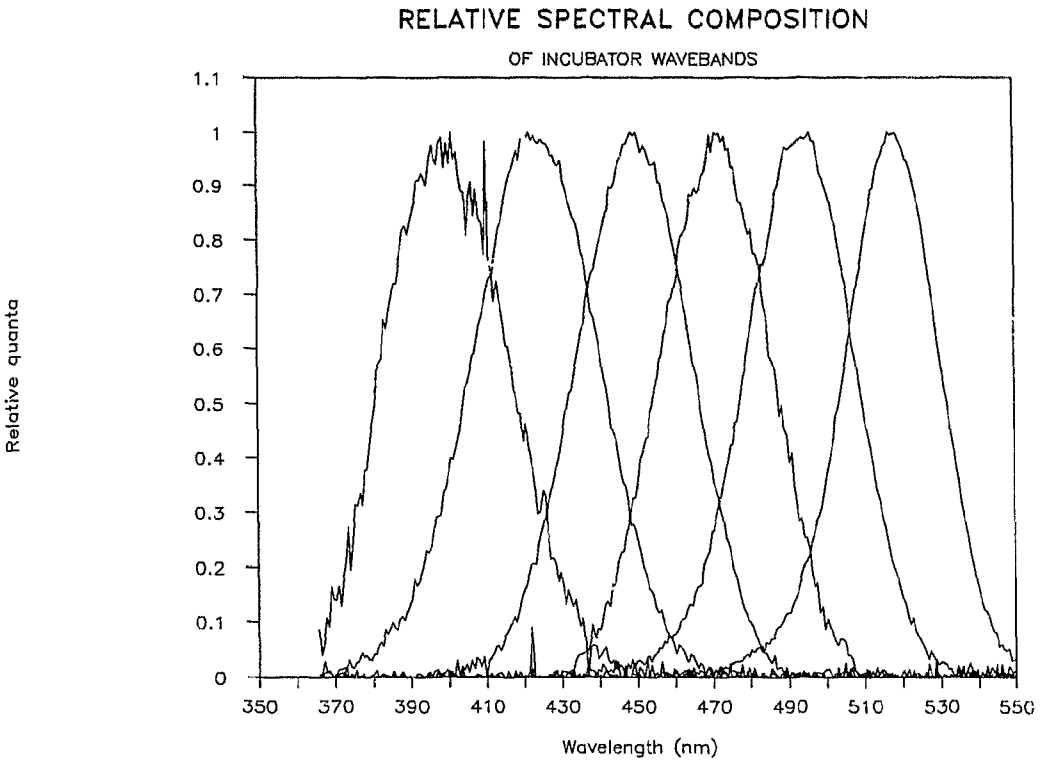
RELATIVE SPECTRAL COMPOSITION
OF INCUBATOR WAVEBANDS
Relative quanta
1.1
1
0.9
0.8
0.7
0.6
0.5
0.4
0.3
0.2
0.1
0
350 370 390 410 430 450 470 490 510 530 550
Wavelength (nm)

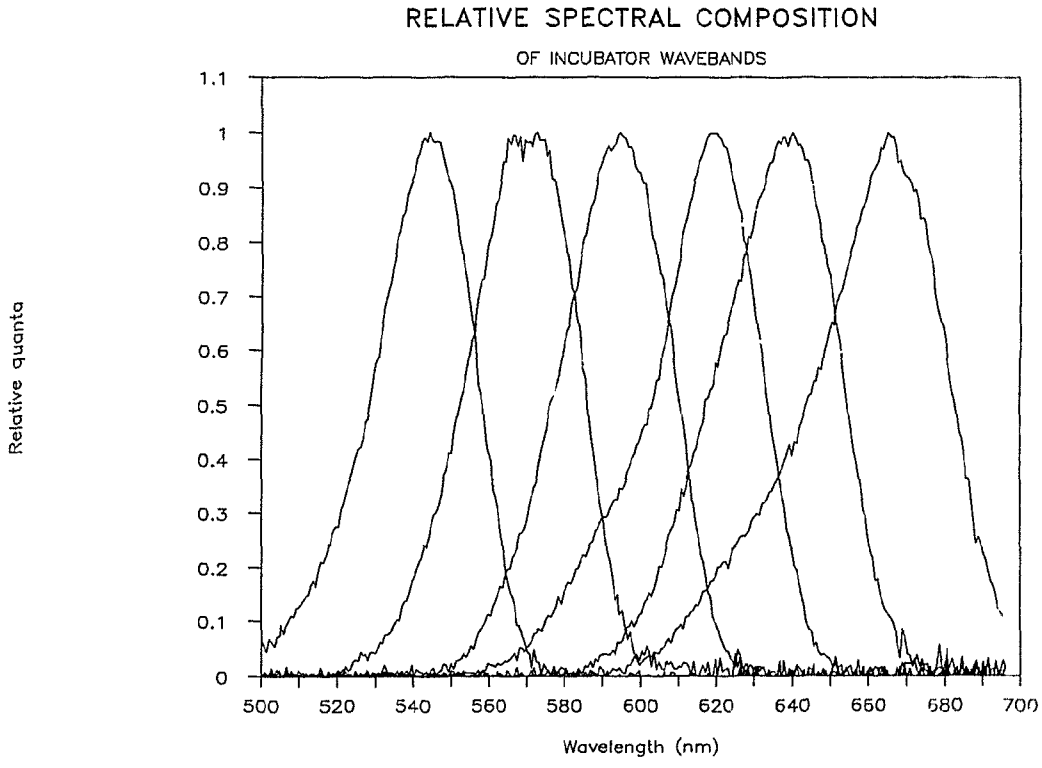
RELATIVE SPECTRAL COMPOSITION
OF INCUBATOR WAVEBANDS
Relative quanta
1.1
1
0.9
0.8
0.7
0.6
0.5
0.4
0.3
0.2
0.1
0
500 520 540 560 580 600 620 640 660 680 700
Wavelength (nm)

Figure 4.5

Figure 5. 1. The P-I response of *Synechococcus* sp. WH 5701 grown under a PFD of 8 μmol m^{-2} s^{-1}. The upper panel shows the P-I data and the fitted curve obtained with the new empirical model [Eqs. 3.34 and 3.36]. The lower panel is a plot of the residuals about the fitted curve as a function of PFD.

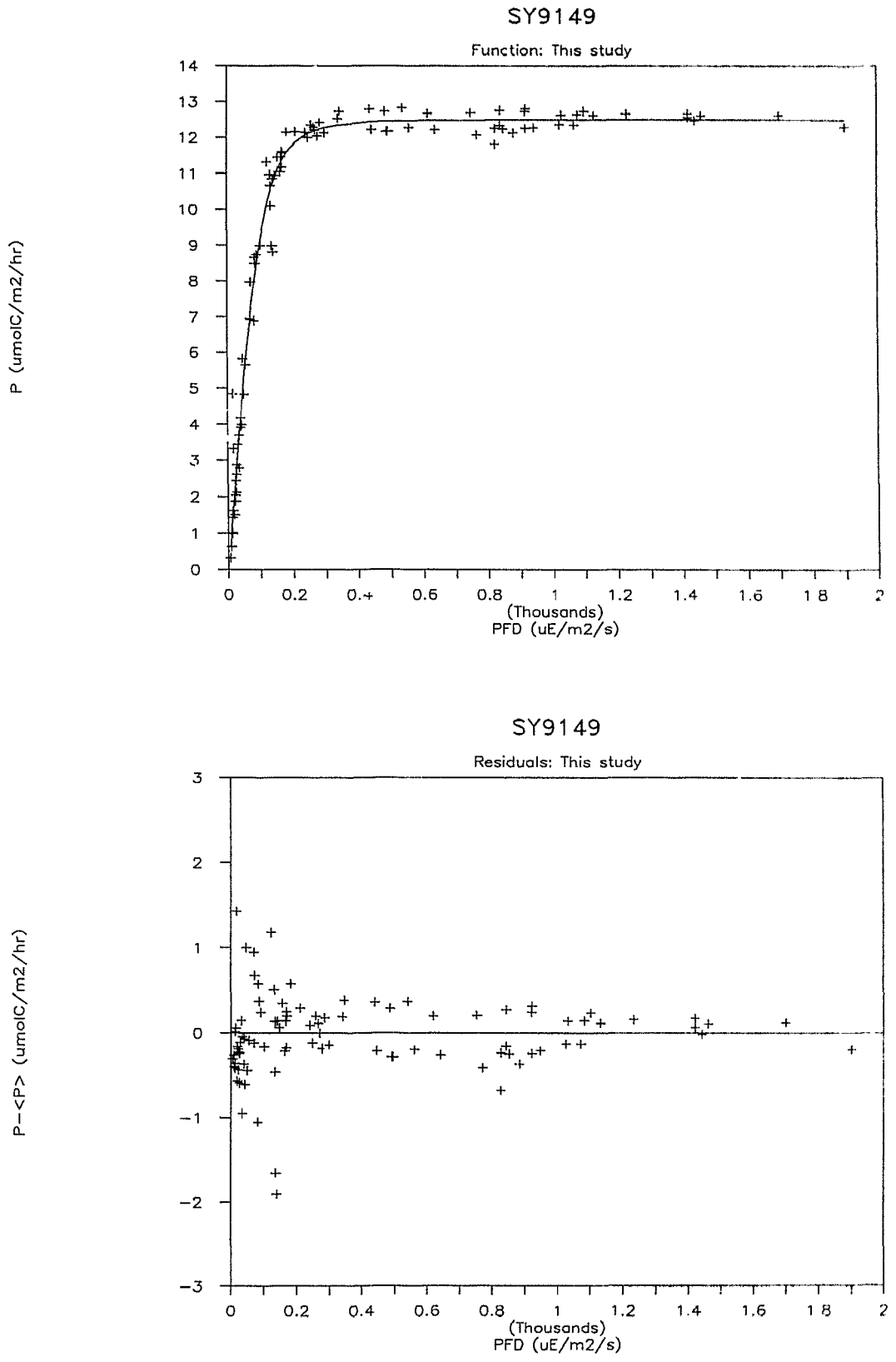
SY9149
Function: This study
P (umolC/m2/hr)
(Thousands)
PFD (uE/m2/s)
SY9149
Residuals: This study
P-<P> (umolC/m2/hr)
(Thousands)
PFD (uE/m2/s)

Figure 5. 1

Figure 5. 2. The P-I response of *Synechococcus* sp. WH 5701 grown under a PFD of 15 μmol m^{-2} s^{-1}. The upper panel shows the P-I data and the fitted curve obtained with the new empirical model [Eqs. 3.34 and 3.36]. The lower panel is a plot of the residuals about the fitted curve as a function of PFD.

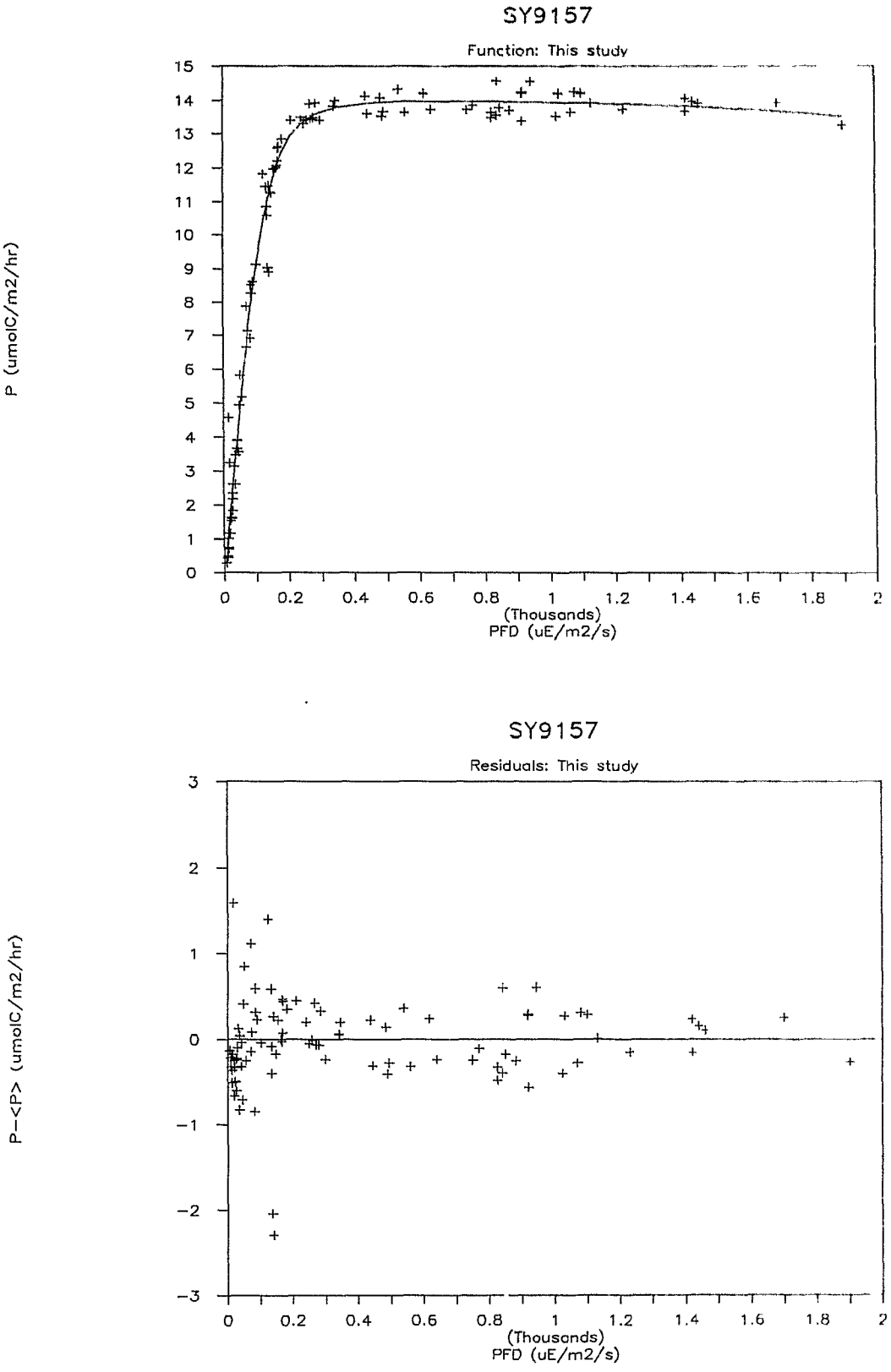
SY9157
Function: This study
P (umolC/m2/hr)
(Thousands)
PFD (uE/m2/s)
SY9157
Residuals: This study
P-<P> (umolC/m2/hr)
(Thousands)
PFD (uE/m2/s)

Figure 5.2

Figure 5. 3. The P-I response of *Synechococcus* sp. WH 5701 grown under a PFD of 27 μmol m^{-2} s^{-1}. The upper panel shows the P-I data and the fitted curve obtained with the new empirical model [Eqs. 3.34 and 3.36]. The lower panel is a plot of the residuals about the fitted curve as a function of PFD.

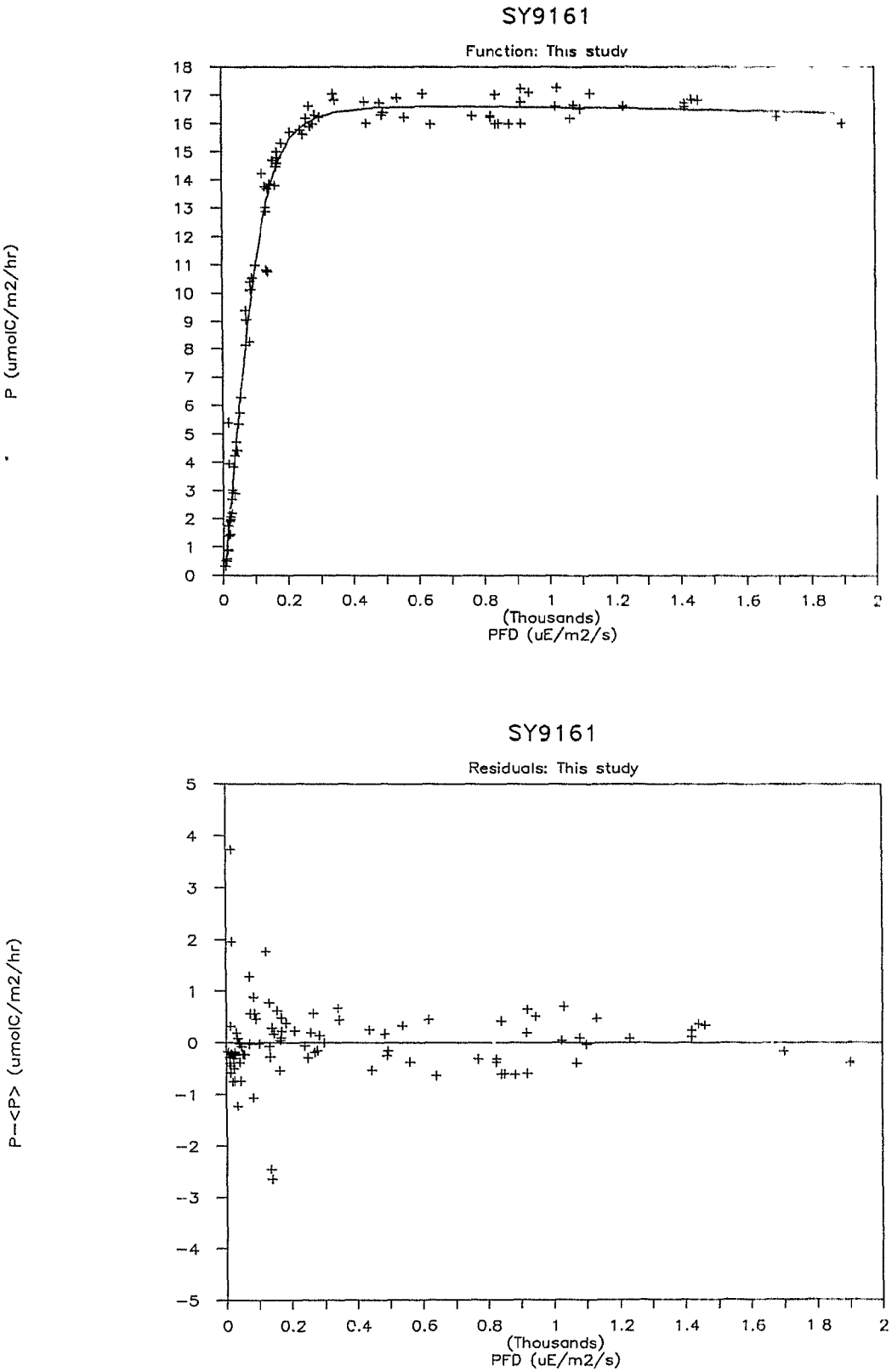
SY9161
Function: This study
P (umolC/m2/hr)
(Thousands)
PFD (uE/m2/s)
SY9161
Residuals: This study
P-<P> (umolC/m2/hr)
(Thousands)
PFD (uE/m2/s)

Figure 5.3

Figure 5. 4. The P-I response of *Synechococcus* sp. WH 5701 grown under a PFD of 70 μmol m^{-2} s^{-1}. The upper panel shows the P-I data and the fitted curve obtained with the new empirical model [Eqs. 3.34 and 3.36]. The lower panel is a plot of the residuals about the fitted curve as a function of PFD.

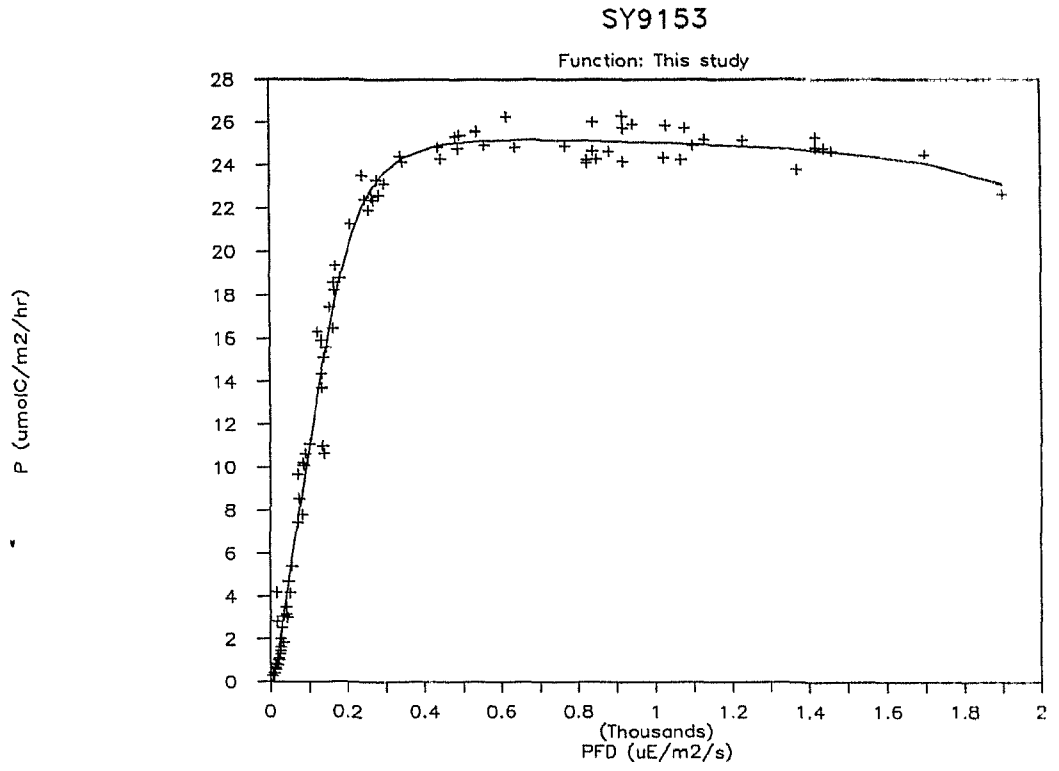
SY9153
Function: This study
P (umolC/m2/hr)
28
26
24
22
20
18
16
14
12
10
8
6
4
2
0
0
0.2
0.4
0.6
0.8
1
1.2
1.4
1.6
1.8
2
(Thousands)
PFD (uE/m2/s)

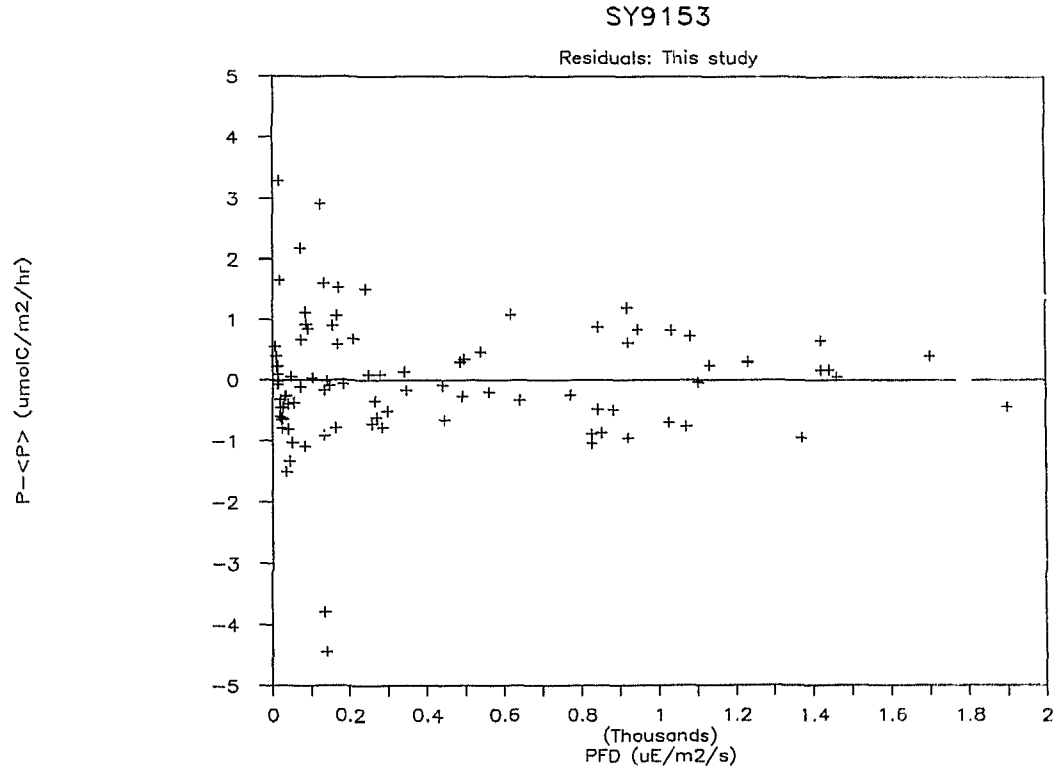
SY9153
Residuals: This study
P-<P> (umolC/m2/hr)
5
4
3
2
1
0
-1
-2
-3
-4
-5
0
0.2
0.4
0.6
0.8
1
1.2
1.4
1.6
1.8
2
(Thousands)
PFD (uE/m2/s)

Figure 5.4

Figure 5. 5. The P-I response of *Synechococcus* sp. WH 7803 grown under a PFD of 17 μmol m^{-2} s^{-1}. The upper panel shows the P-I data and the fitted curve obtained with the new empirical model [Eqs. 3.34 and 3.36]. The lower panel is a plot of the residuals about the fitted curve as a function of PFD.

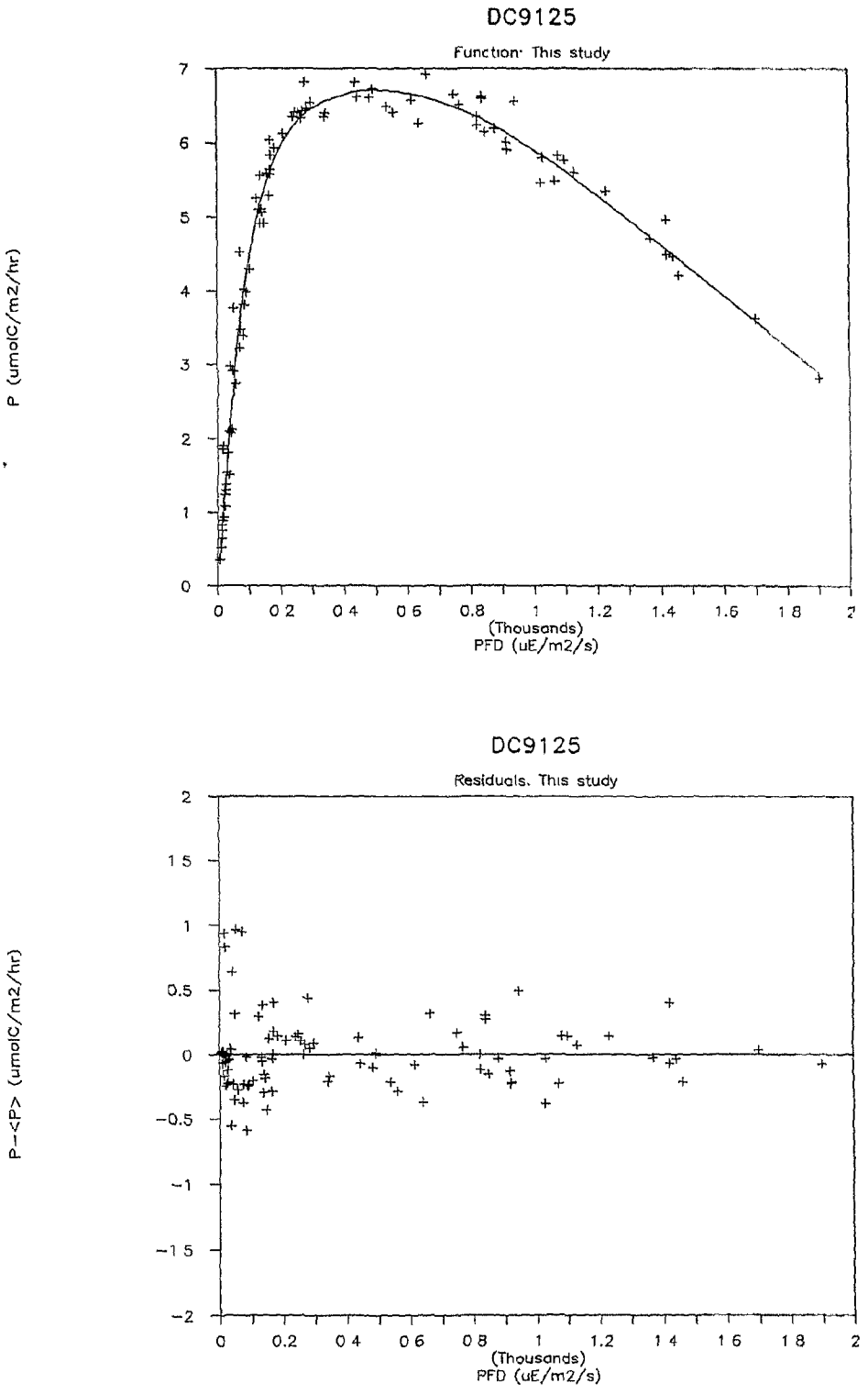
DC9125
Function: This study
P (umolC/m2/hr)
0
1
2
3
4
5
6
7
0
0.2
0.4
0.6
0.8
1
1.2
1.4
1.6
1.8
(Thousands)
PFD (uE/m2/s)
DC9125
Residuals. This study
P-<P> (umolC/m2/hr)
2
1.5
1
0.5
0
-0.5
-1
-1.5
-2
0
0.2
0.4
0.6
0.8
1
1.2
1.4
1.6
1.8
2
(Thousands)
PFD (uE/m2/s)

Figure 5.5

Figure 5. 6. The P-I response of *Synechococcus* sp. WH 7803 grown under a PFD of 25 μmol m^{-2} s^{-1}. The upper panel shows the P-I data and the fitted curve obtained with the new empirical model [Eqs. 3.34 and 3.36]. The lower panel is a plot of the residuals about the fitted curve as a function of PFD.

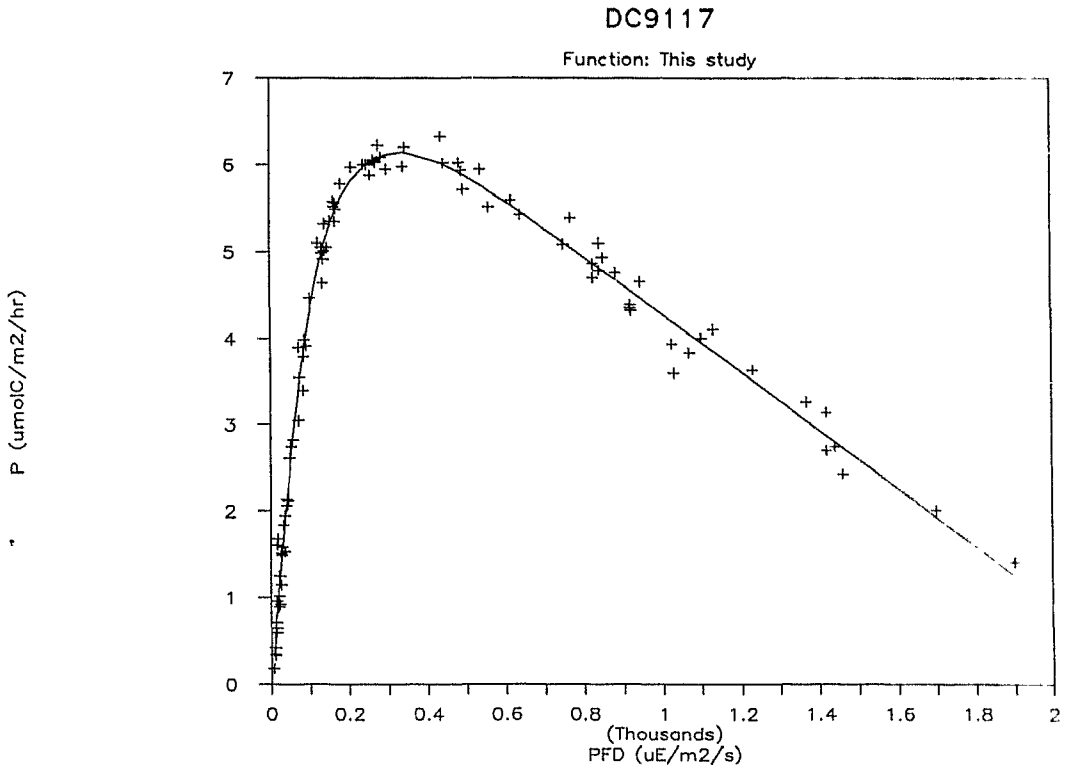
DC9117
Function: This study
P (umolC/m2/hr)
0
1
2
3
4
5
6
7
0
0.2
0.4
0.6
0.8
1
1.2
1.4
1.6
1.8
2
(Thousands)
PFD (uE/m2/s)

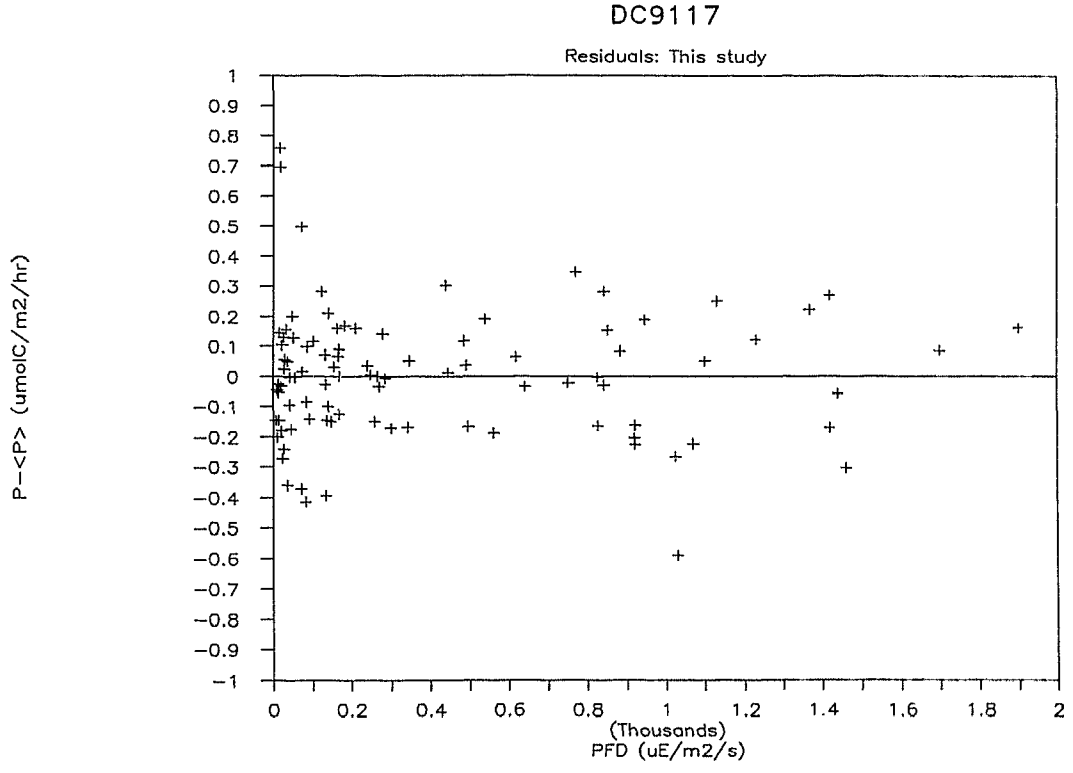
DC9117
Residuals: This study
P-<P> (umolC/m2/hr)
1
0.9
0.8
0.7
0.6
0.5
0.4
0.3
0.2
0.1
0
-0.1
-0.2
-0.3
-0.4
-0.5
-0.6
-0.7
-0.8
-0.9
-1
0
0.2
0.4
0.6
0.8
1
1.2
1.4
1.6
1.8
2
(Thousands)
PFD (uE/m2/s)

Figure 5.6

Figure 5. 7. The P-I response of *Synechococcus* sp. WH 7803 grown under a PFD of 35 μmol m^{-2} s^{-1}. The upper panel shows the P-I data and the fitted curve obtained with the new empirical model [Eqs. 3.34 and 3.36]. The lower panel is a plot of the residuals about the fitted curve as a function of PFD.

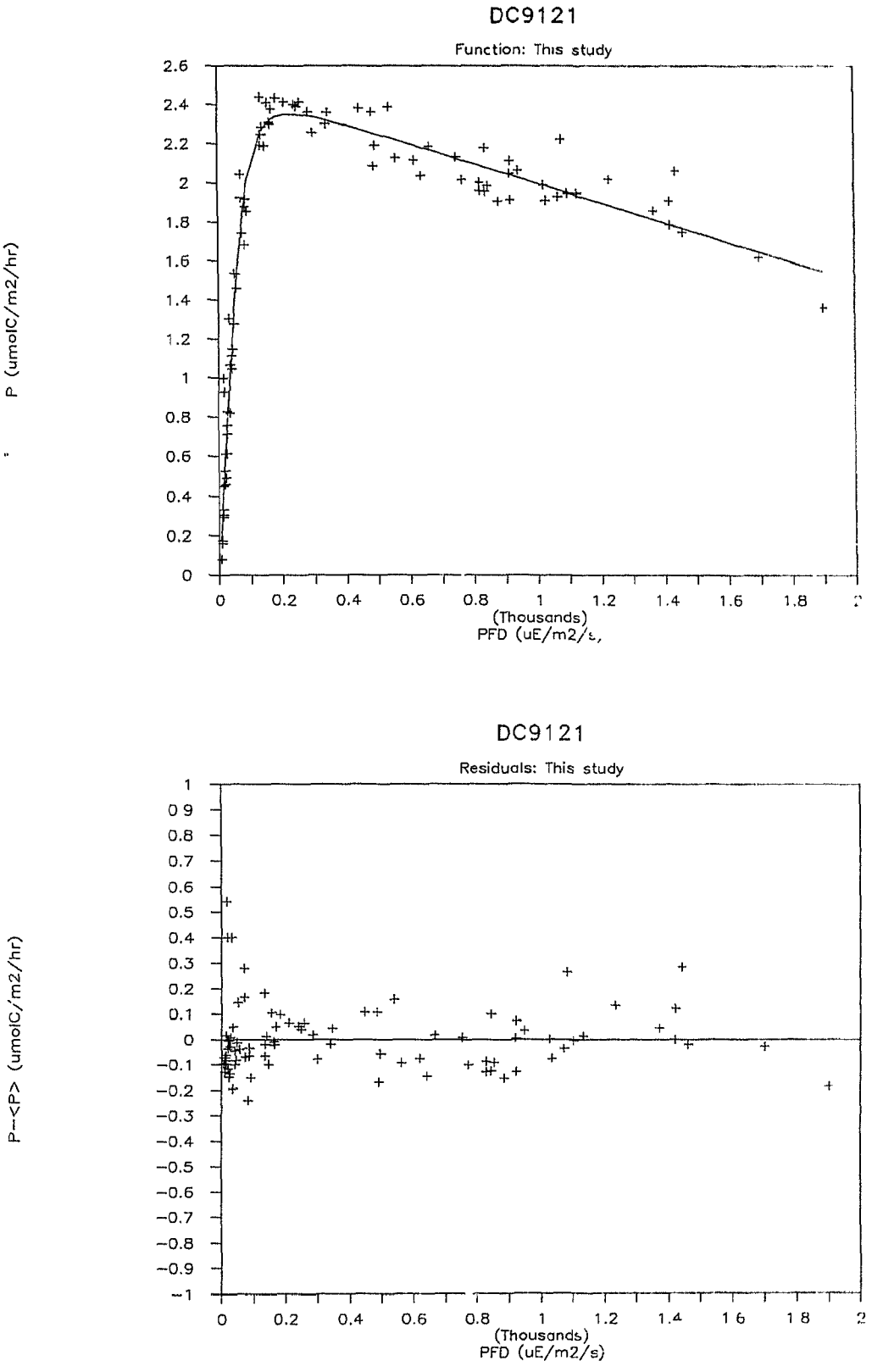
DC9121
Function: This study
P (umolC/m2/hr)
2.6
2.4
2.2
2
1.8
1.6
1.4
1.2
1
0.8
0.6
0.4
0.2
0
0
0.2
0.4
0.6
0.8
1
1.2
1.4
1.6
1.8
(Thousands)
PFD (uE/m2/s)
DC9121
Residuals: This study
P--<P> (umolC/m2/hr)
1
0.9
0.8
0.7
0.6
0.5
0.4
0.3
0.2
0.1
0
-0.1
-0.2
-0.3
-0.4
-0.5
-0.6
-0.7
-0.8
-0.9
-1
0
0.2
0.4
0.6
0.8
1
1.2
1.4
1.6
1.8
2
(Thousands)
PFD (uE/m2/s)

Figure 5.7

Figure 5. 8. The P-I response of *Pavlova* sp. (clone NEP) grown under a PFD of 8 μmol m^{-2} s^{-1}. The upper panel shows the P-I data and the fitted curve obtained with the new empirical model [Eqs. 3.34 and 3.36]. The lower panel is a plot of the residuals about the fitted curve as a function of PFD.

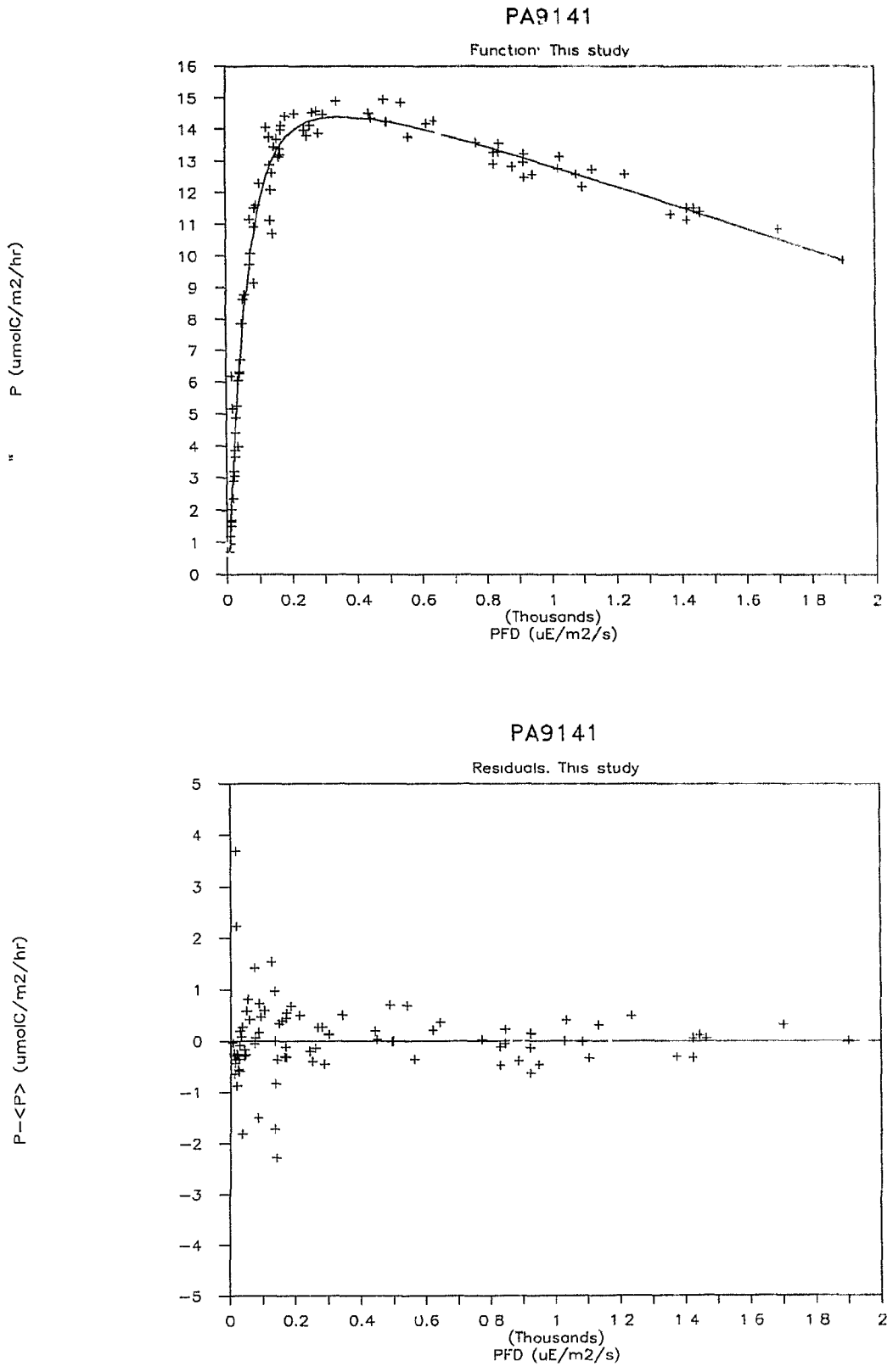
PA9141
Function: This study
P (umolC/m2/hr)
(Thousands)
PFD (uE/m2/s)
PA9141
Residuals. This study
P-<P> (umolC/m2/hr)
(Thousands)
PFD (uE/m2/s)

Figure 5.8

Figure 5. 9. The P-I response of *Pavlova* sp. (clone NEP) grown under a PFD of 12 μmol m^{-2} s^{-1}. The upper panel shows the P-I data and the fitted curve obtained with the new empirical model [Eqs. 3.34 and 3.36]. The lower panel is a plot of the residuals about the fitted curve as a function of PFD.

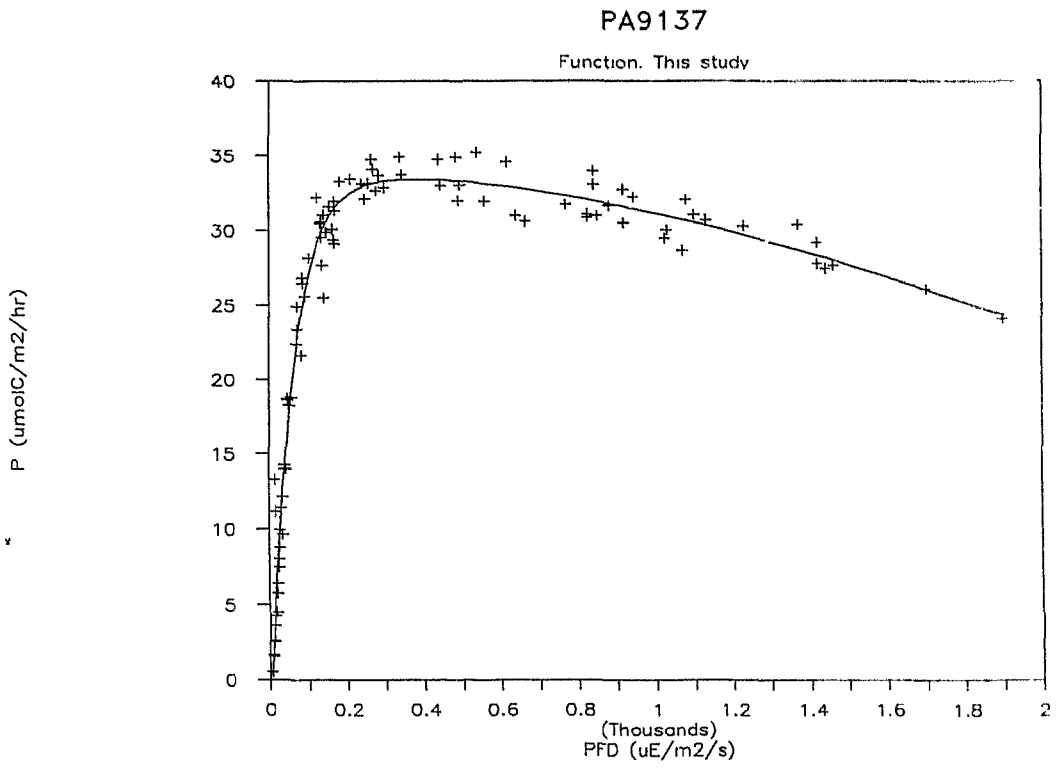
PA9137
Function. This study
P (umolC/m2/hr)
40
35
30
25
20
15
10
5
0
0
0.2
0.4
0.6
0.8
1
1.2
1.4
1.6
1.8
2
(Thousands)
PFD (uE/m2/s)

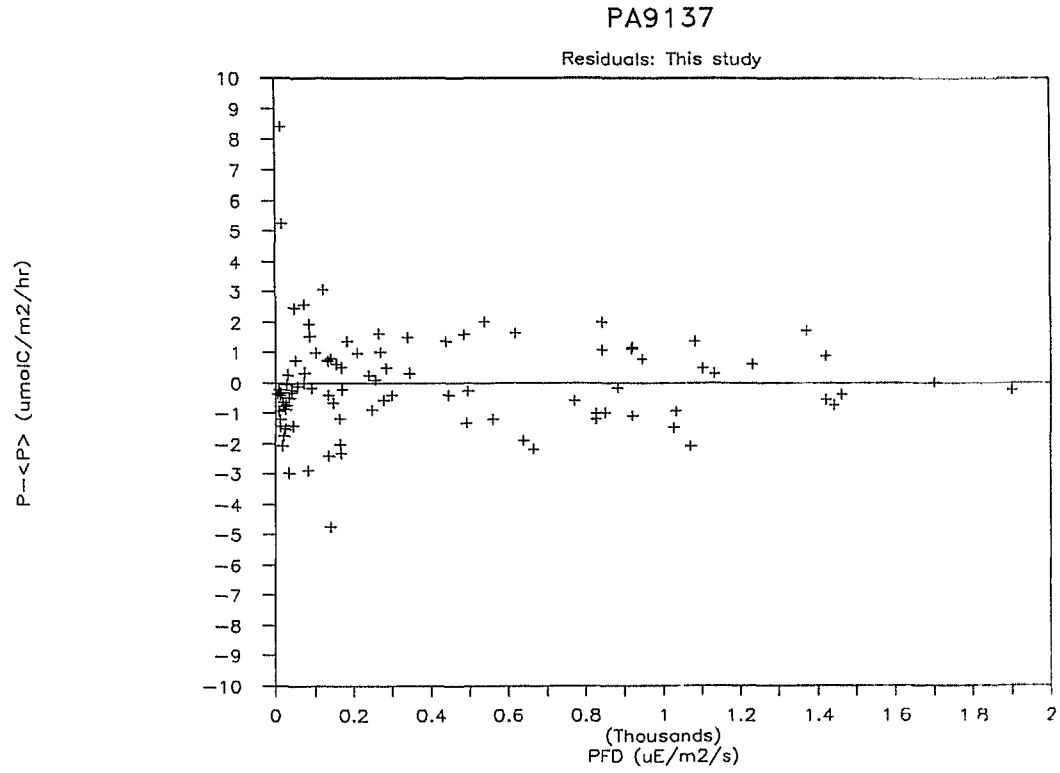
PA9137
Residuals: This study
P--<P> (umolC/m2/hr)
10
9
8
7
6
5
4
3
2
1
0
−1
−2
−3
−4
−5
−6
−7
−8
−9
−10
0
0.2
0.4
0.6
0.8
1
1.2
1.4
1.6
1.8
2
(Thousands)
PFD (uE/m2/s)

Figure 5.9

Figure 5. 10. The P-I response of *Pavlova* sp. (clone NEP) grown under a PFD of 45 μmol m^{-2} s^{-1}. The upper panel shows the P-I data and the fitted curve obtained with the new empirical model [Eqs. 3.34 and 3.36]. The lower panel is a plot of the residuals about the fitted curve as a function of PFD.

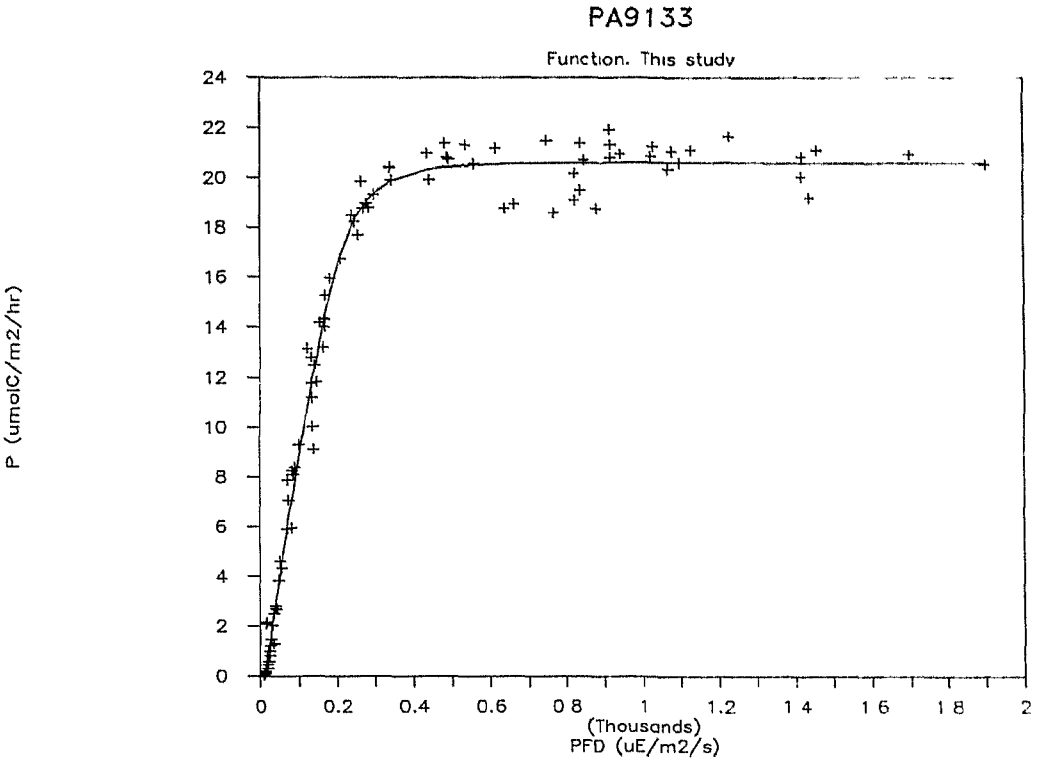
PA9133
Function. This study
P (umolC/m2/hr)
24
22
20
18
16
14
12
10
8
6
4
2
0
0
0.2
0.4
0.6
0.8
1
1.2
1.4
1.6
1.8
2
(Thousands)
PFD (uE/m2/s)

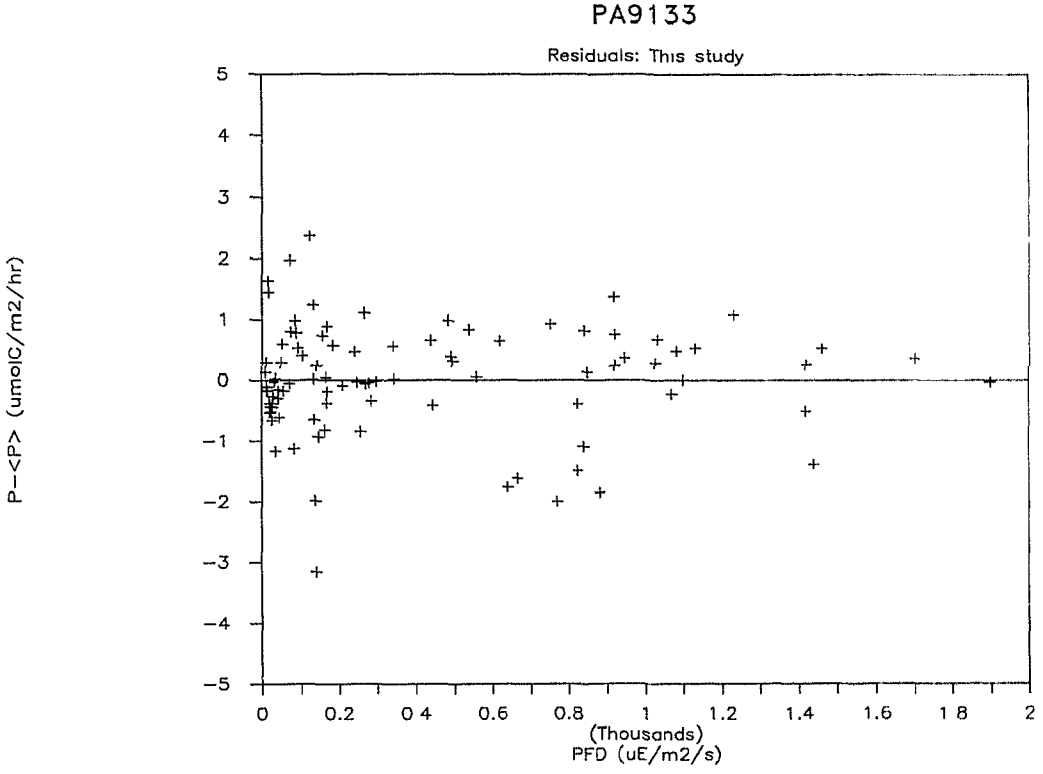
PA9133
Residuals: This study
P-<P> (umolC/m2/hr)
5
4
3
2
1
0
-1
-2
-3
-4
-5
0
0.2
0.4
0.6
0.8
1
1.2
1.4
1.6
1.8
2
(Thousands)
PFD (uE/m2/s)

Figure 5.10

Figure 5. 11. Theoretical P-I responses showing the effects of respiration upon the P-I response at low PFDs when photosynthesis is measured by ^{14}C incorporation. The upper panel illustrates the effect of respiration when photosynthesis is a simple linear function of PFD [Eq. 5.1], the lower panel illustrates the effect of respiration when the P-I response is a saturating function of PFD [Eq. 5.2]. In both panels the upper curve (—△—) represents gross photosynthesis (P), the lower curve (—X—) represents net photosynthesis ($P - R_m$) and the intermediate curve (—▽—) represents the photosynthetic rate estimated by ^{14}C incorporation.

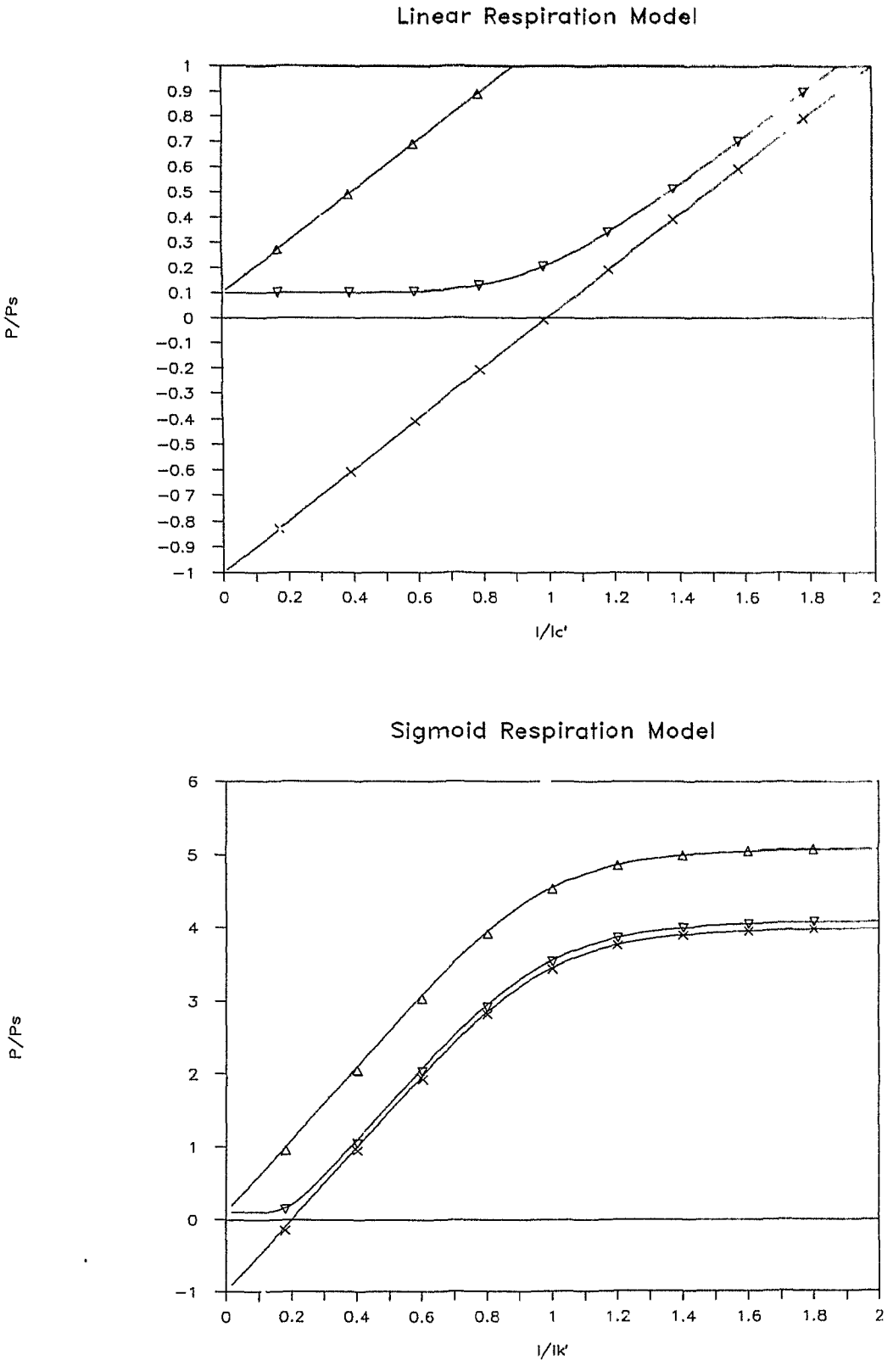
Linear Respiration Model
P/Ps
1
0.9
0.8
0.7
0.6
0.5
0.4
0.3
0.2
0.1
0
−0.1
−0.2
−0.3
−0.4
−0.5
−0.6
−0.7
−0.8
−0.9
−1
0
0.2
0.4
0.6
0.8
1
1.2
1.4
1.6
1.8
2
I/Ic'
Sigmoid Respiration Model
P/Ps
6
5
4
3
2
1
0
−1
0
0.2
0.4
0.6
0.8
1
1.2
1.4
1.6
1.8
2
I/Ik'

Figure 5. 11

Figure 5. 12. The P-I responses of *Synechococcus* sp. WH 5701 in green, blue and white polychromatic light for the culture grown at a PFD of 8 μmol m^{-2} s^{-1}.

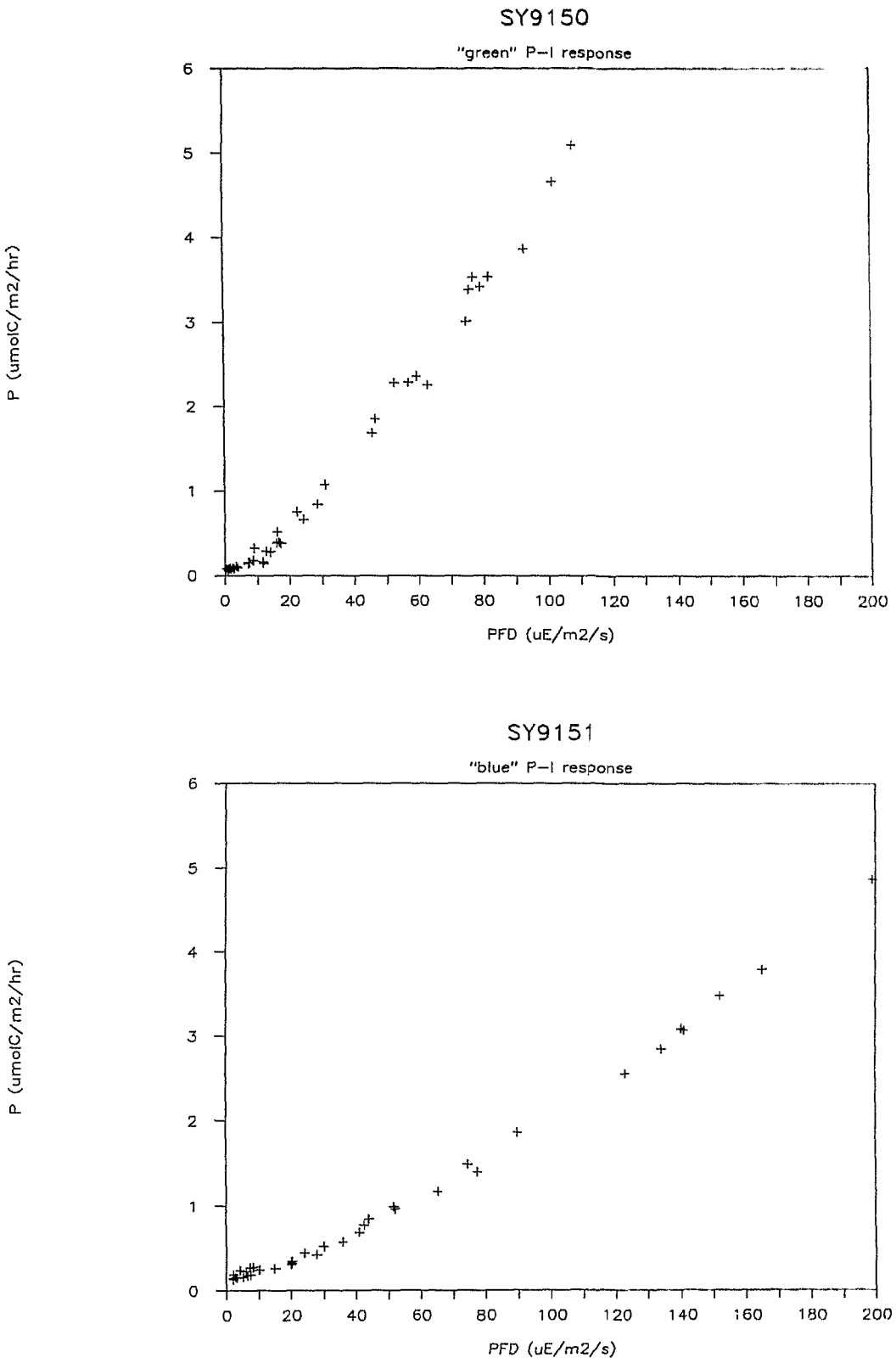
SY9150
"green" P–I response
P (umolC/m2/hr)
PFD (uE/m2/s)
0
1
2
3
4
5
6
0
20
40
60
80
100
120
140
160
180
200
SY9151
"blue" P–I response
P (umolC/m2/hr)
PFD (uE/m2/s)

Figure 5. 12

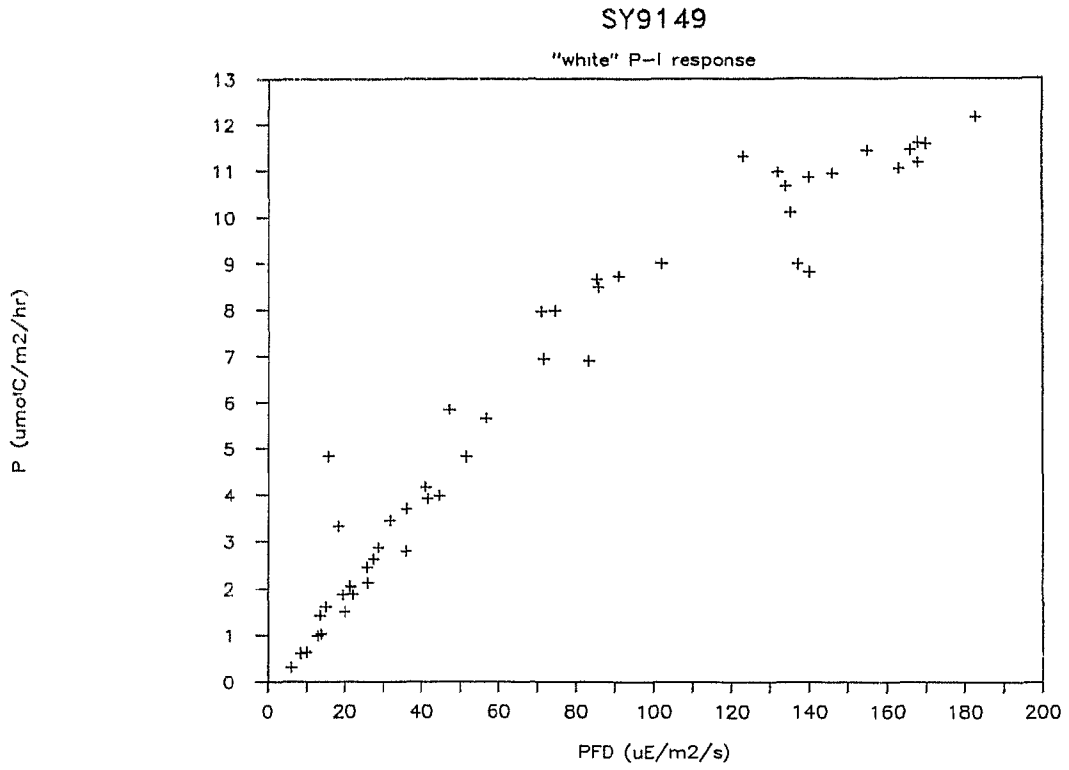

Figure 5. 12 (contd.)

Figure 5. 13. The P-I res$_p$onses of *Synechococcus* sp. WH 5701 in green, blue and white polychromatic light for the culture grown at a PFD of 15 μmol m^{-2} s^{-1}.

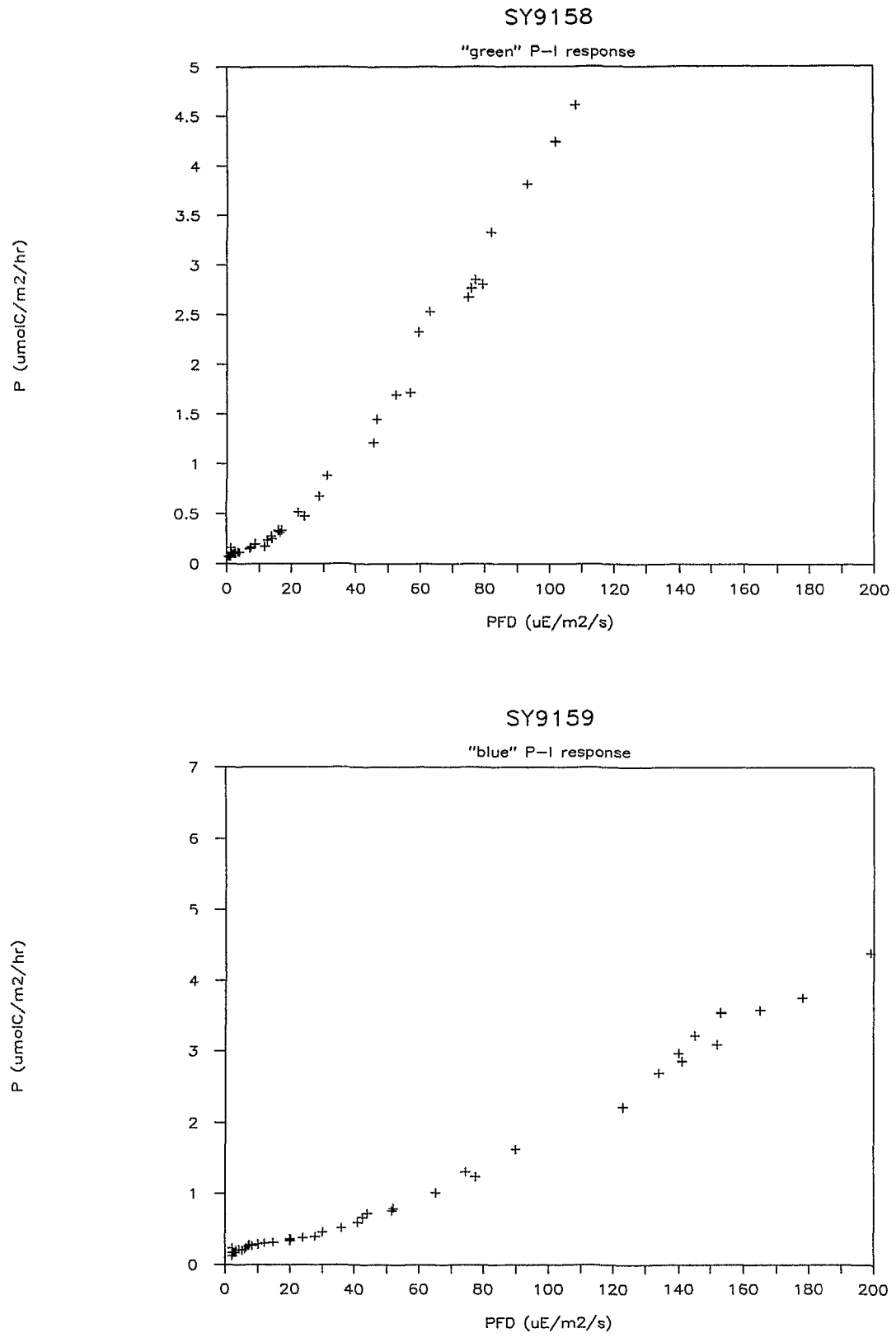
SY9158
"green" P–I response
P (umolC/m2/hr)
PFD (uE/m2/s)
0
0.5
1
1.5
2
2.5
3
3.5
4
4.5
5
0
20
40
60
80
100
120
140
160
180
200
SY9159
"blue" P–I response
P (umolC/m2/hr)
PFD (uE/m2/s)
0
1
2
3
4
5
6
7
0
20
40
60
80
100
120
140
160
180
200

Figure 5. 13

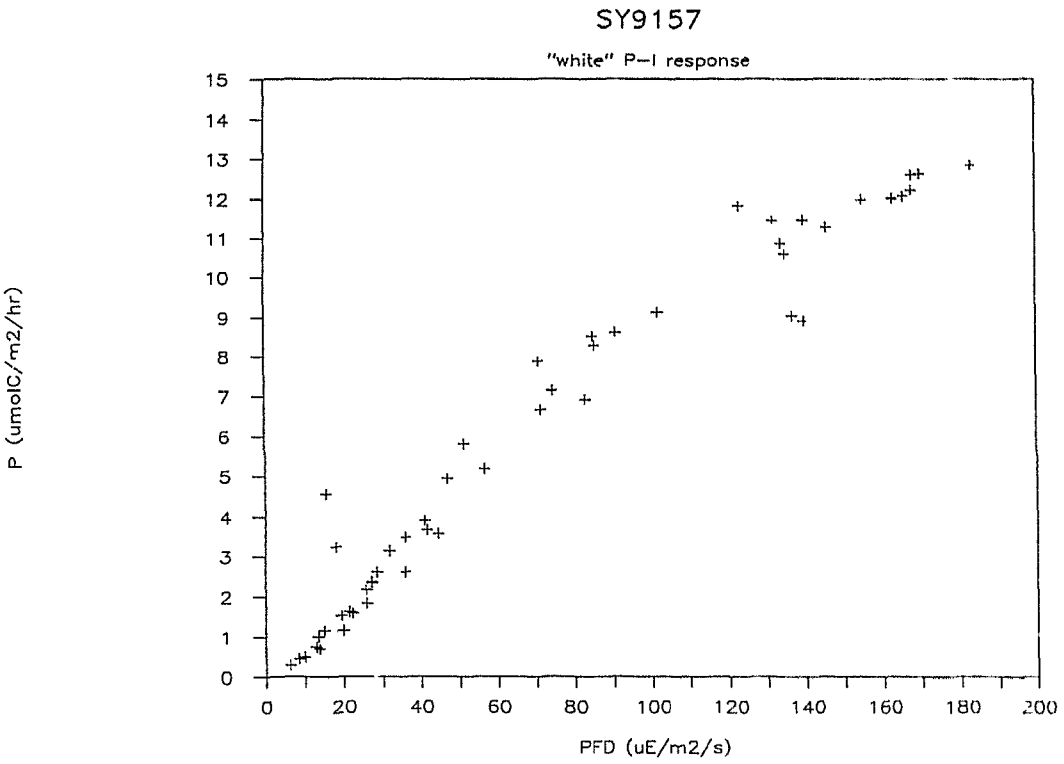

Figure 5. 13 (contd.)

Figure 5. 14. The P-I responses of *Synechococcus* sp. WH 5701 in green, blue and white polychromatic light for the culture grown at a PFD of 70 μmol m^{-2} s^{-1}.

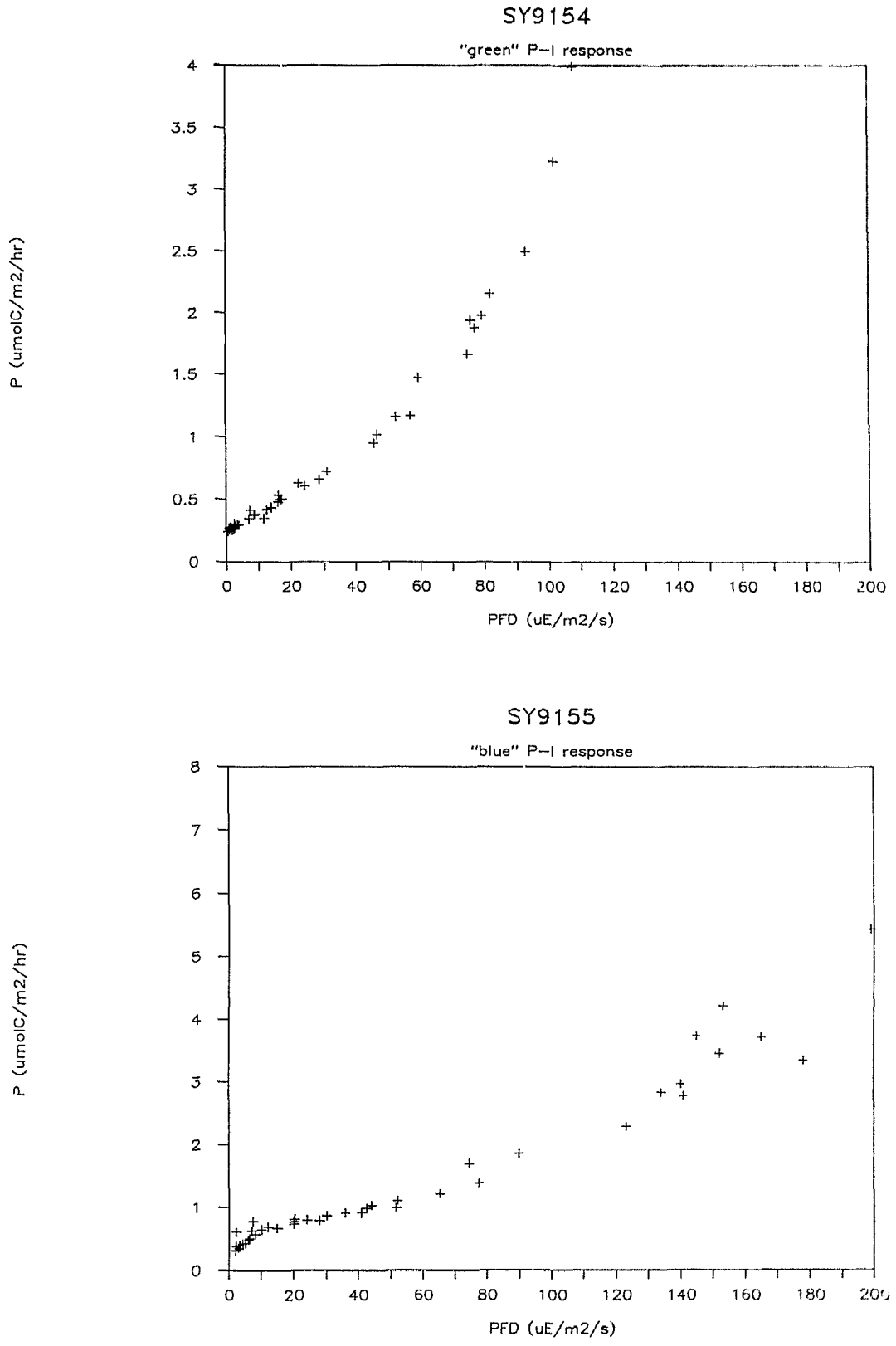
SY9154
"green" P-I response
P (umolC/m2/hr)
PFD (uE/m2/s)
0
0.5
1
1.5
2
2.5
3
3.5
4
0
20
40
60
80
100
120
140
160
180
200
SY9155
"blue" P-I response
P (umolC/m2/hr)
PFD (uE/m2/s)
0
1
2
3
4
5
6
7
8
0
20
40
60
80
100
120
140
160
180

Figure 5. 14

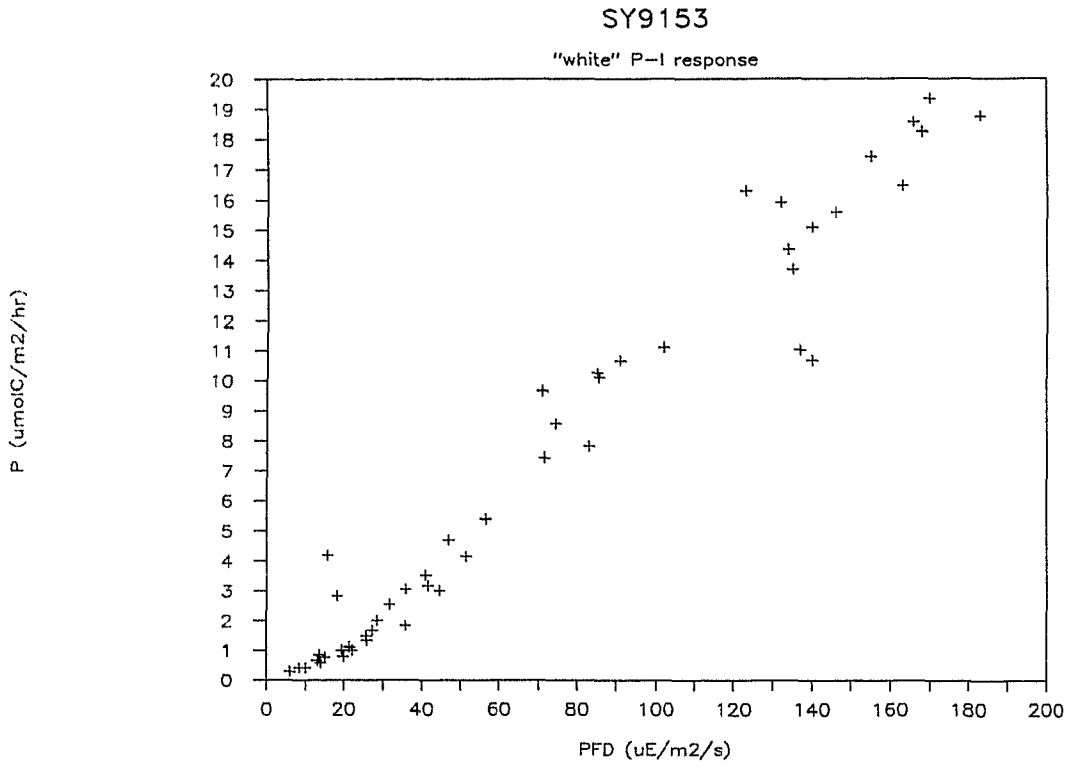

Figure 5. 14 (contd.)

Figure 5. 15. The P-I responses of *Synechococcus* sp. WH 7803 in green and blue polychromatic light for the culture grown at a PFD of 7 μmol m^{-2} s^{-1}.

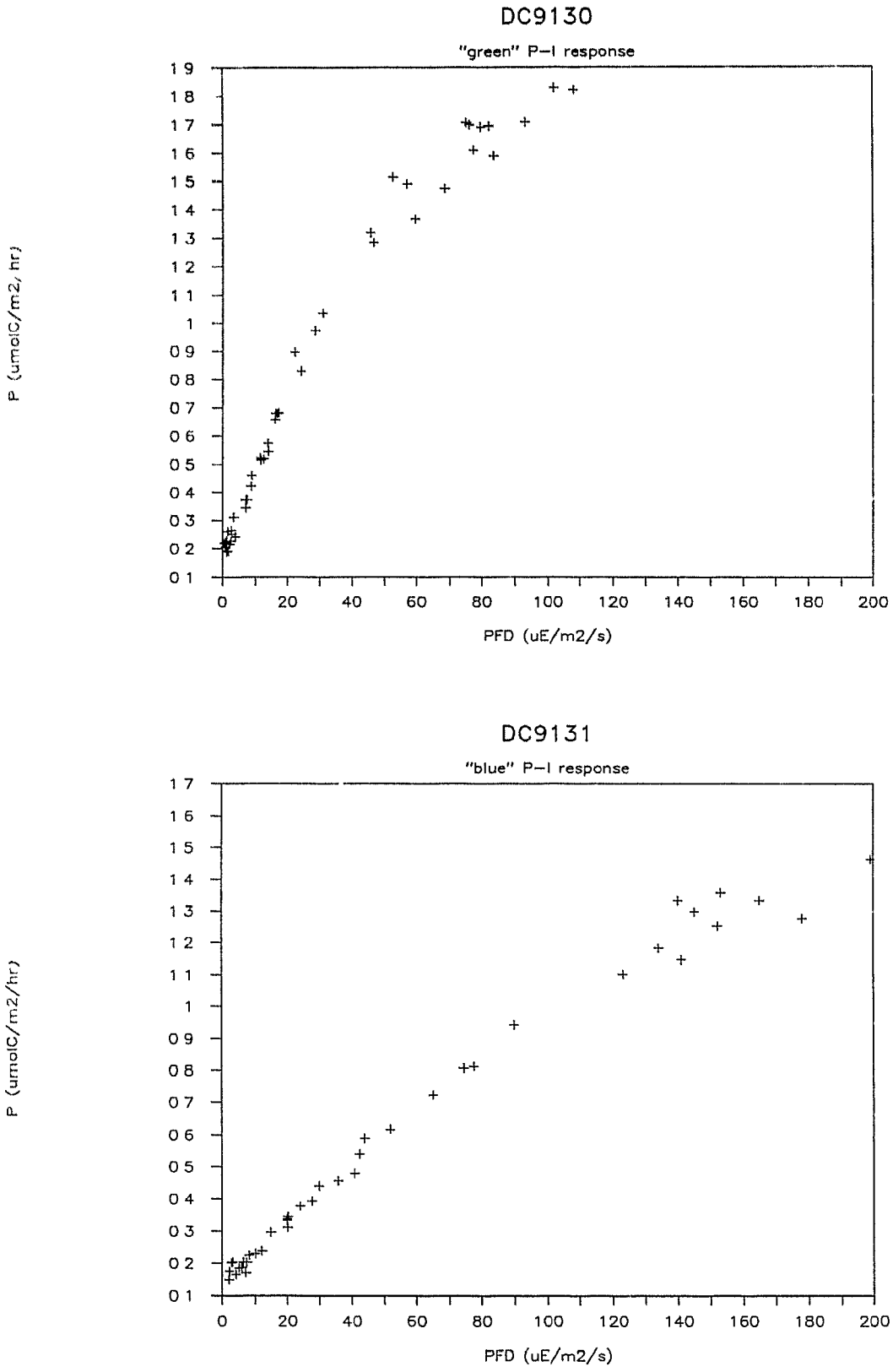
DC9130
"green" P–I response
P (umolC/m2/hr)
PFD (uE/m2/s)
DC9131
"blue" P–I response
P (umolC/m2/hr)
PFD (uE/m2/s)

Figure 5. 15

Figure 5. 16. The P-I responses of *Synechococcus* sp. WH 7803 in green, blue and white polychromatic light for the culture grown at a PFD of 17 μmol m^{-2} s^{-1}.

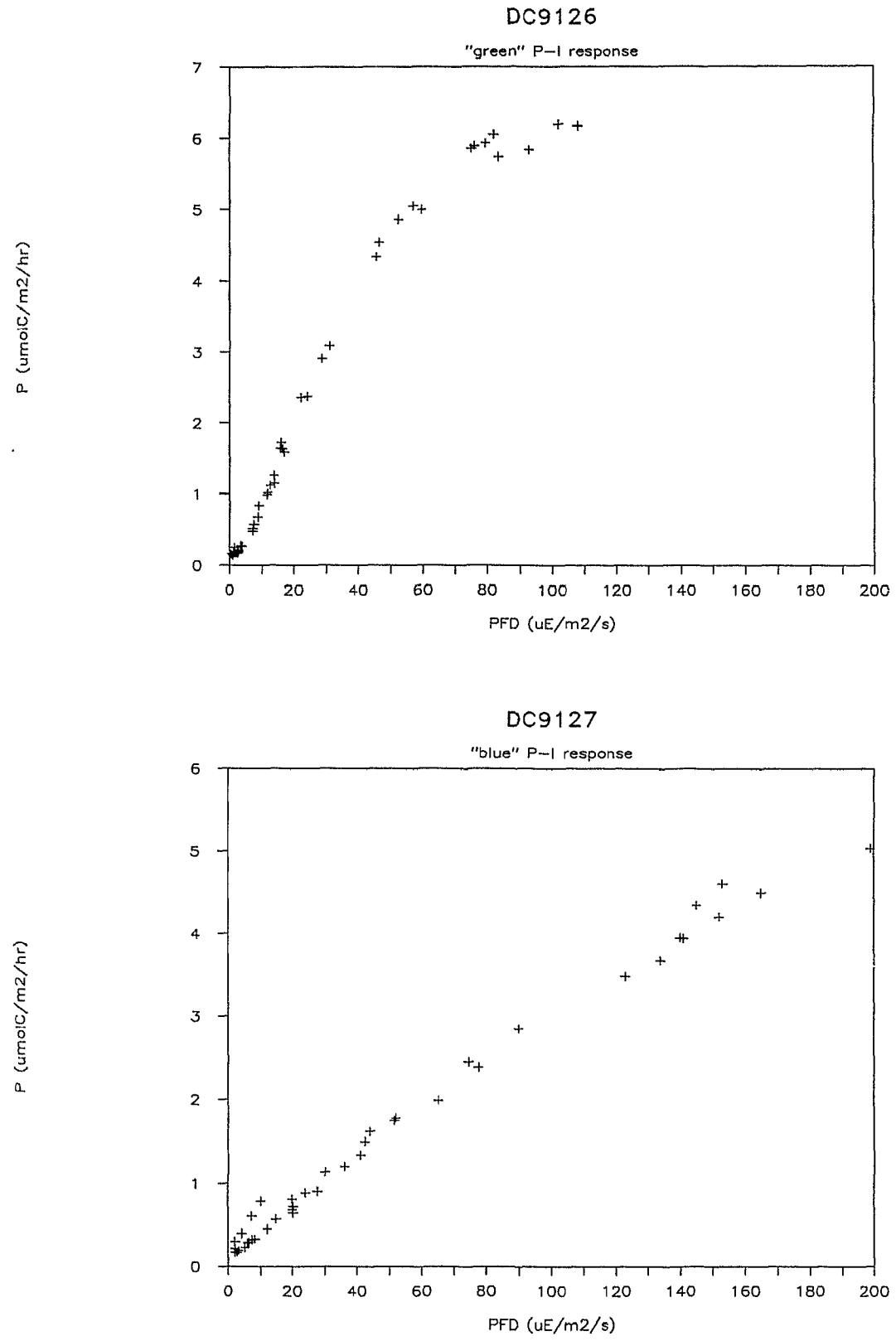
DC9126
"green" P–I response
P (umolC/m2/hr)
PFD (uE/m2/s)
0
1
2
3
4
5
6
7
0
20
40
60
80
100
120
140
160
180
200
DC9127
"blue" P–I response
P (umolC/m2/hr)
PFD (uE/m2/s)
0
1
2
3
4
5
6
0
20
40
60
80
100
120
140
160
180
200

Figure 5. 16

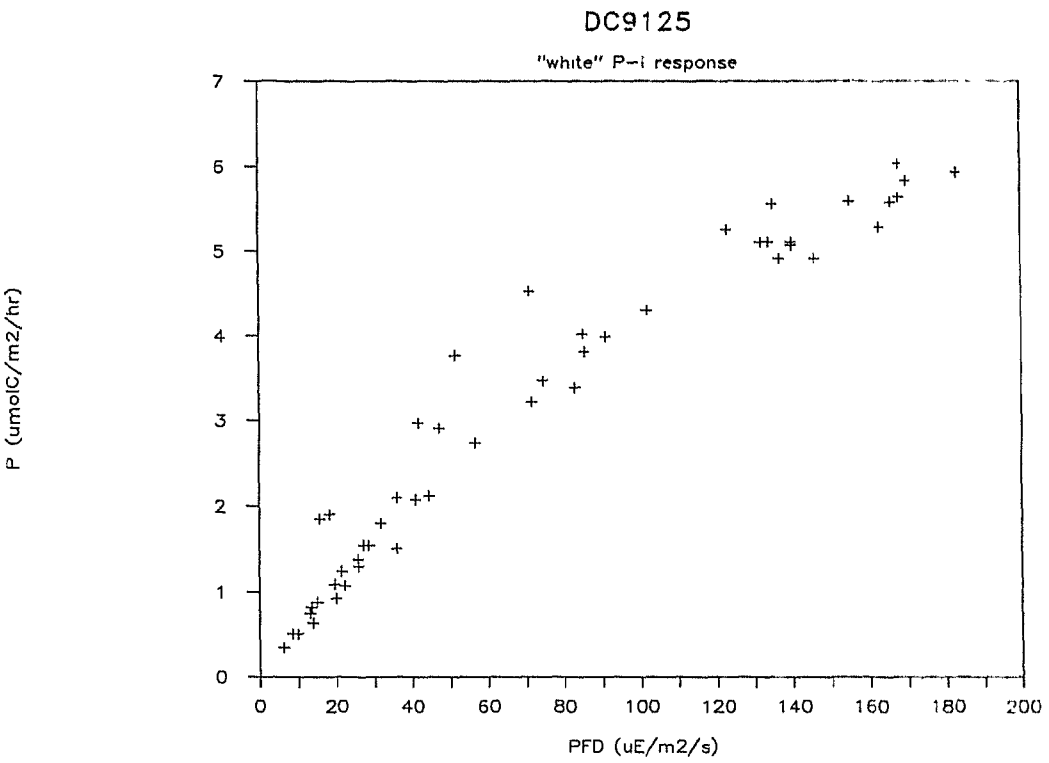

Figure 5. 16 (contd.)

Figure 5. 17. The P-I responses of *Synechococcus* sp. WH 7803 in green, blue and white polychromatic light for the culture grown at a PFD of 25 μmol m^{-2} s^{-1}.

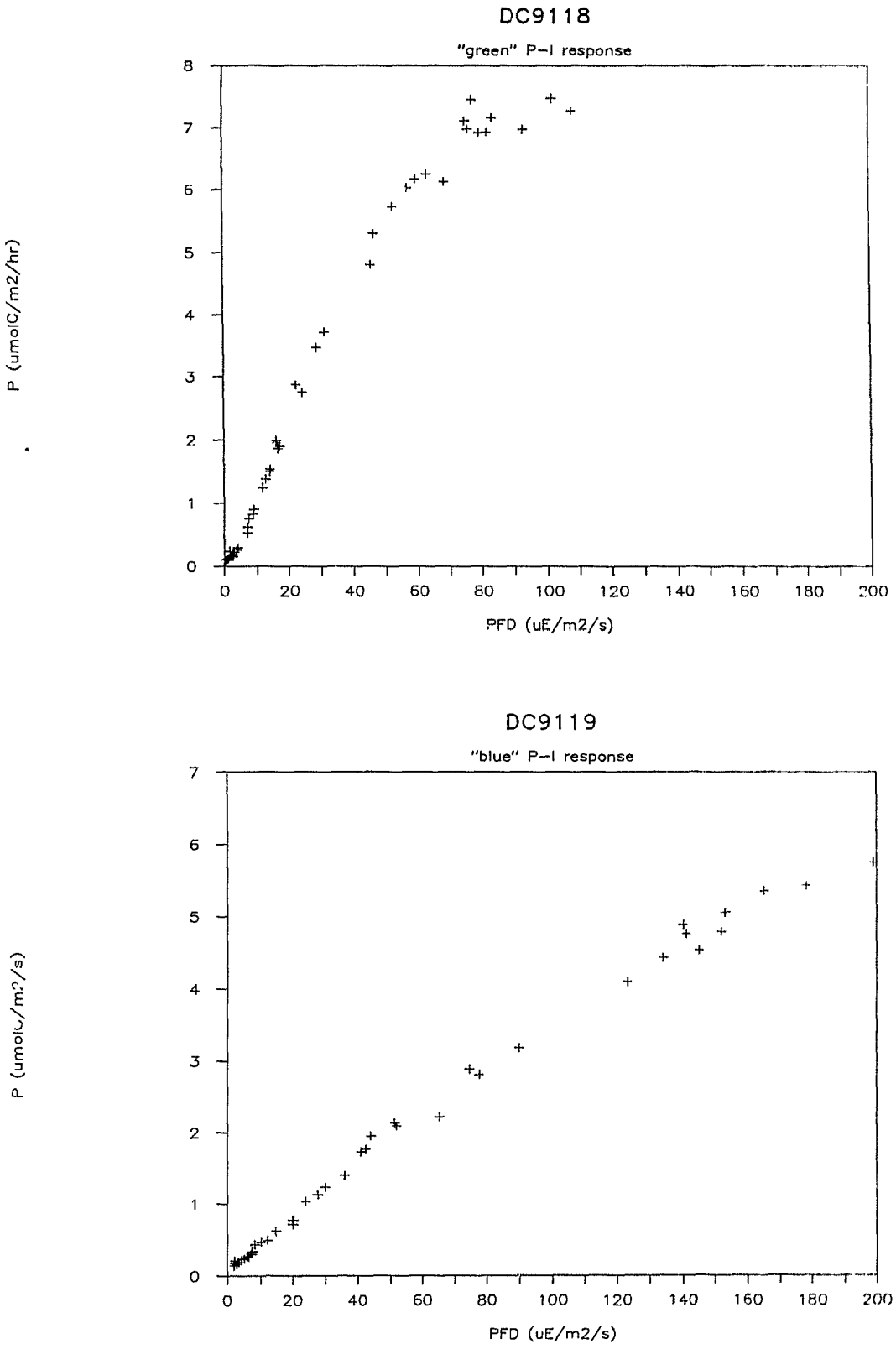
DC9118
"green" P-I response
P (umolC/m2/hr)
PFD (uE/m2/s)
0
1
2
3
4
5
6
7
8
0
20
40
60
80
100
120
140
160
180
200
DC9119
"blue" P-I response
P (umolC/m2/s)
PFD (uE/m2/s)
0
1
2
3
4
5
6
7
0
20
40
60
80
100
120
140
160
180
200

Figure 5. 17

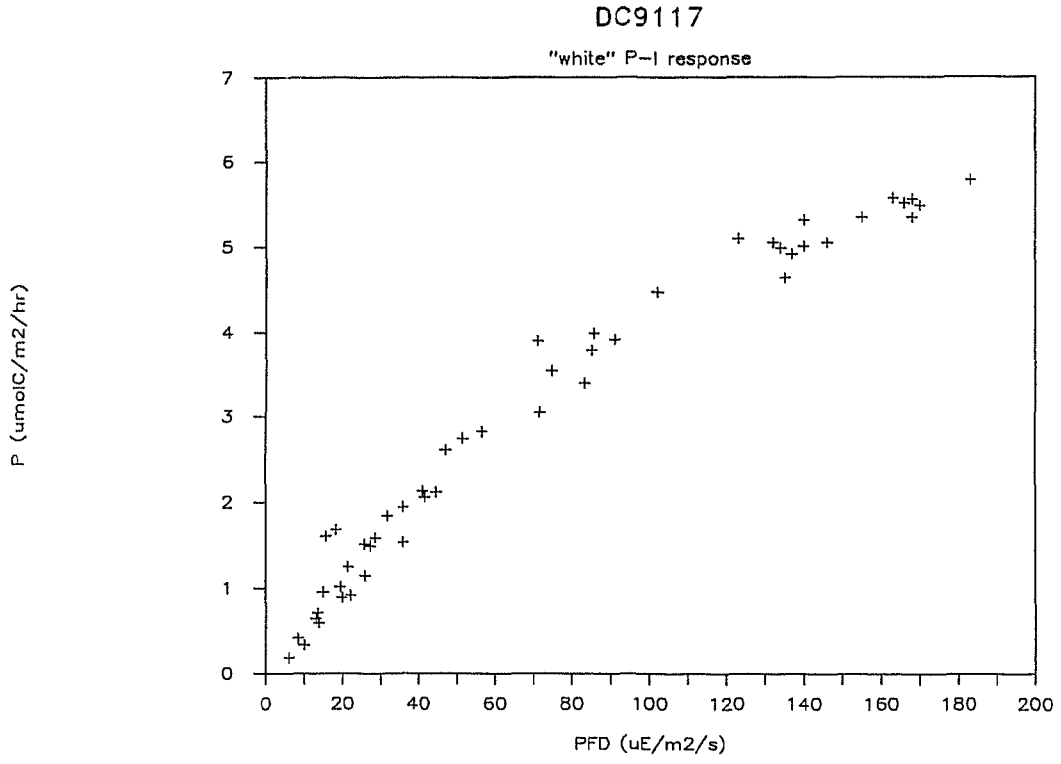

Figure 5. 17 (contd.)

Figure 5. 18. The P-I responses of *Synechococcus* sp. WH 7803 in green, blue and white polychromatic light for the culture grown at a PFD of 35 μmol m^{-2} s^{-1}.

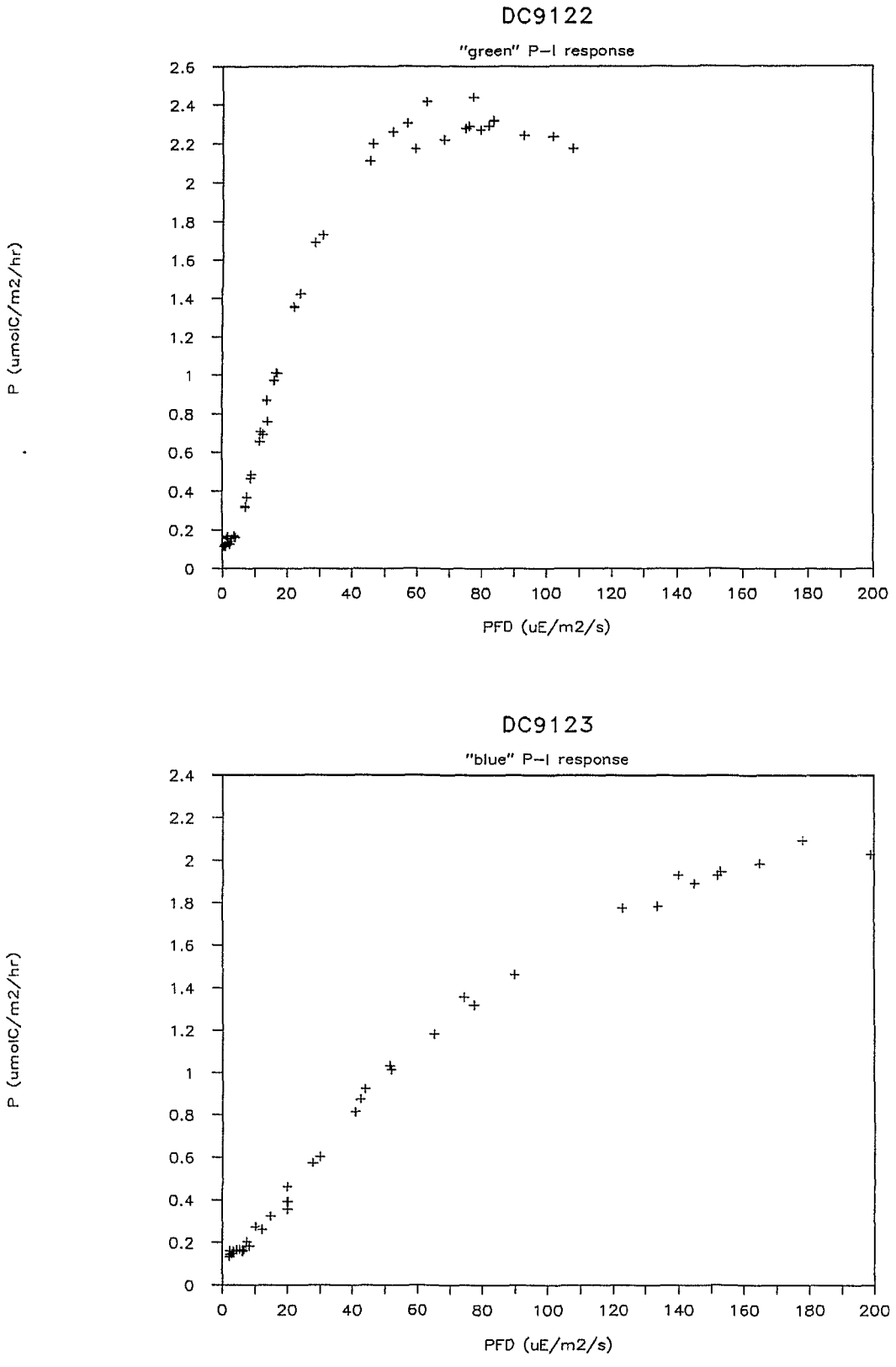
DC9122
"green" P–I response
P (umolC/m2/hr)
PFD (uE/m2/s)
DC9123
"blue" P–I response
P (umolC/m2/hr)
PFD (uE/m2/s)

Figure 5.18

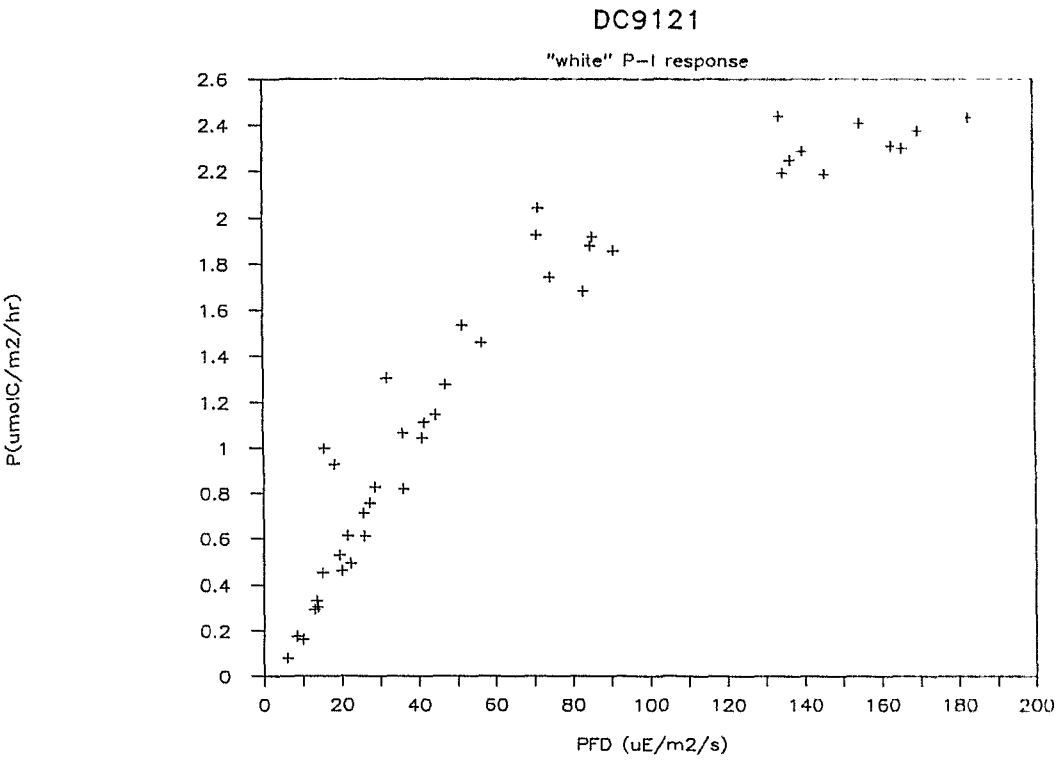

Figure 5. 18 (contd.)

Figure 5. 19. The P-I responses of *Pavlova* sp. (clone NEP) in green, blue and white polychromatic light for the culture grown at a PFD of 8 μmol m^{-2} s^{-1}.

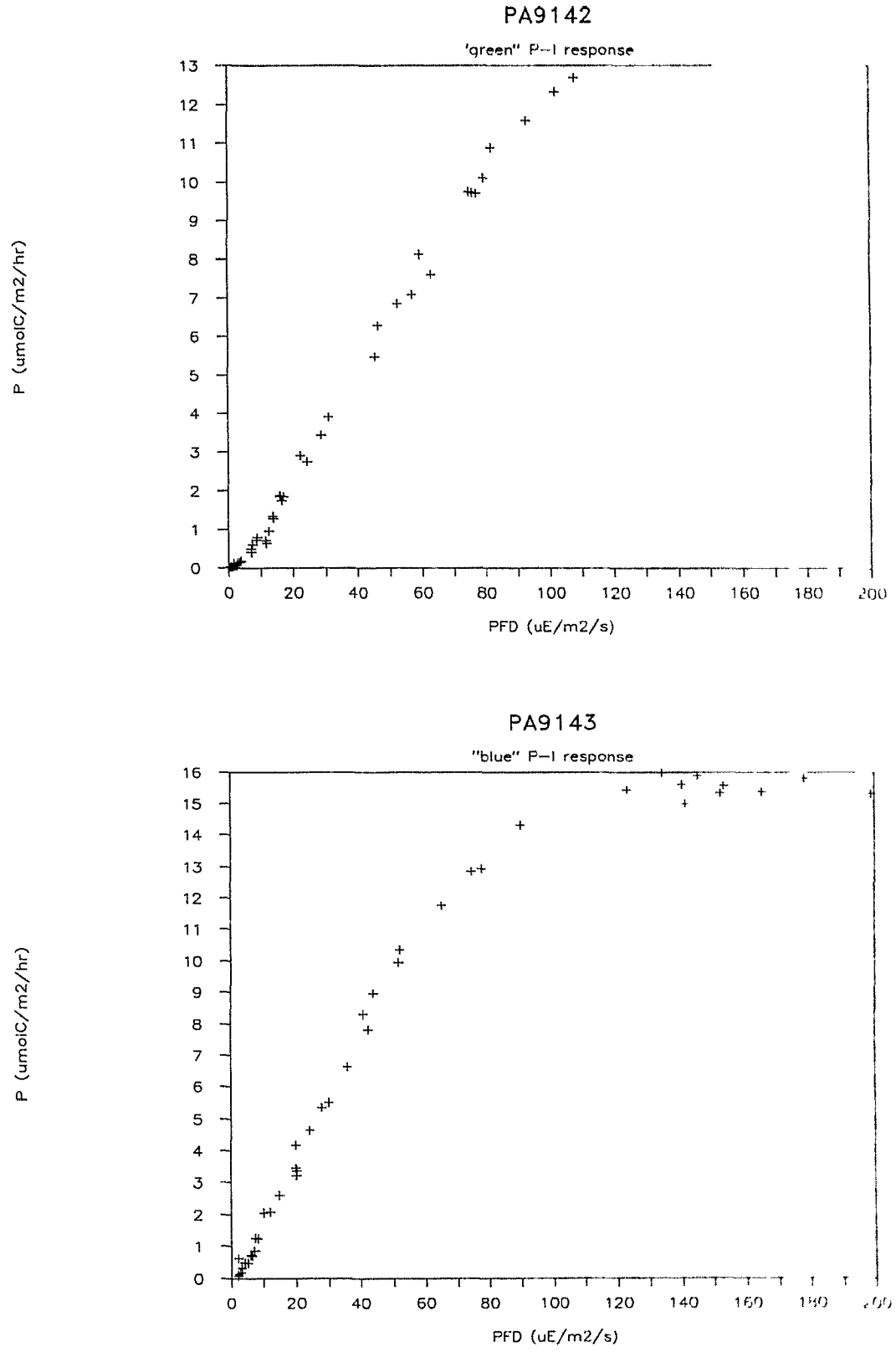
PA9142
'green" P–I response
P (umolC/m2/hr)
PFD (uE/m2/s)
PA9143
"blue" P–I response
P (umolC/m2/hr)
PFD (uE/m2/s)

Figure 5. 19

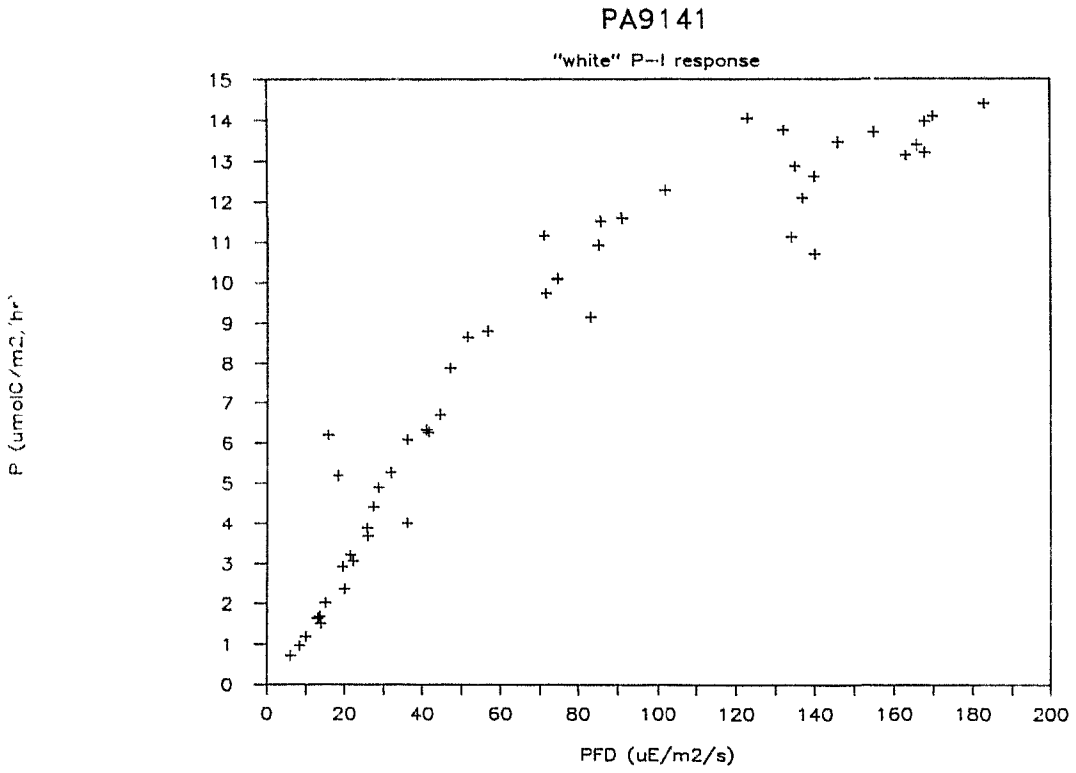

Figure 5. 19 (contd.)

Figure 5. 20. The P-I responses of *Pavlova* sp. (clone NEP) in green, blue and white polychromatic light for the culture grown at a PFD of 12 μmol m^{-2} s^{-1}.

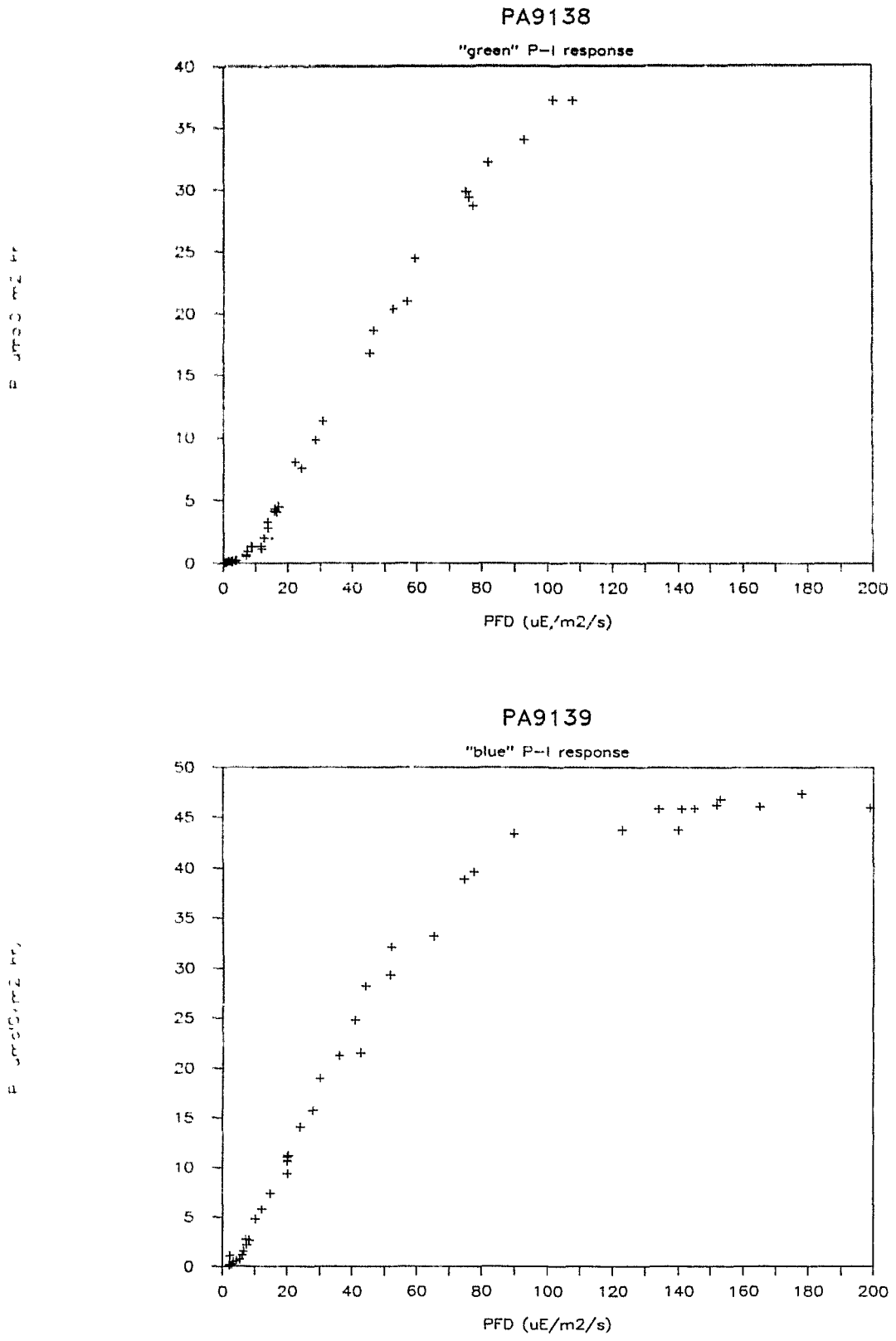
PA9138
"green" P-I response
40
35
30
25
20
15
10
5
0
0
20
40
60
80
100
120
140
160
180
200
PFD (uE,'m2/s)
PA9139
"blue" P-I response
50
45
40
35
30
25
20
15
10
5
0
0
20
40
60
80
100
120
140
160
180
200
PFD (uE/m2/s)

Figure 5. 20

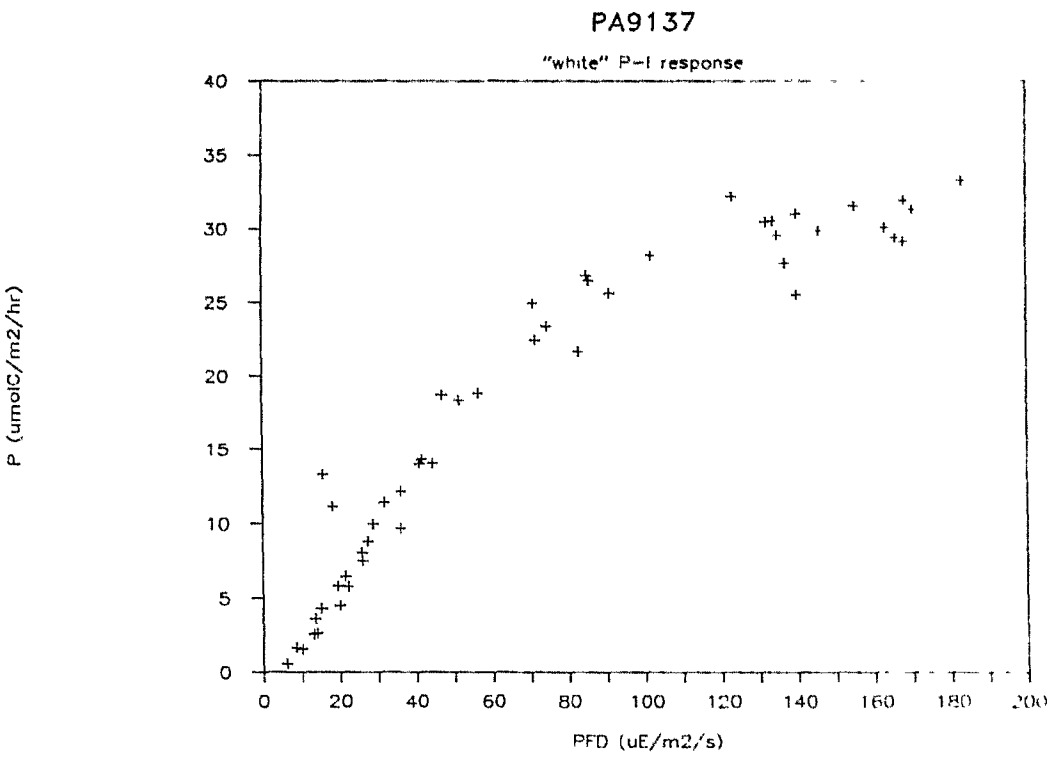

Figure 5. 20 (contd.)

Figure 5. 21. The P-I responses of *Pavlova* sp. (clone NEP) in green, blue and white polychromatic light for the culture grown at a PFD of 45 μmol m^{-2} s^{-1}.

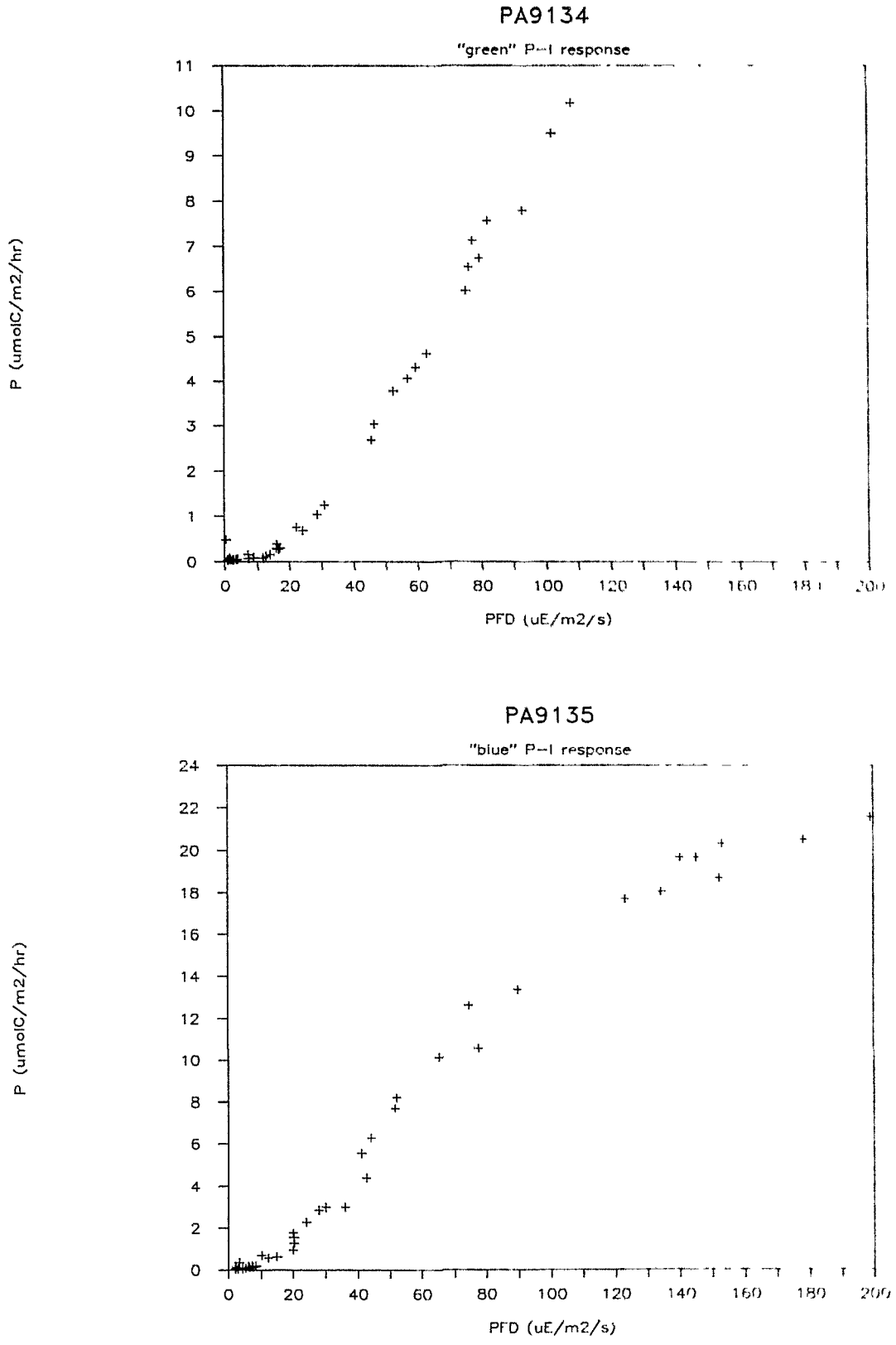
PA9134
"green" P-I response
P (umolC/m2/hr)
PFD (uE/m2/s)
PA9135
"blue" P-I response
P (umolC/m2/hr)
PFD (uE/m2/s)

Figure 5.21

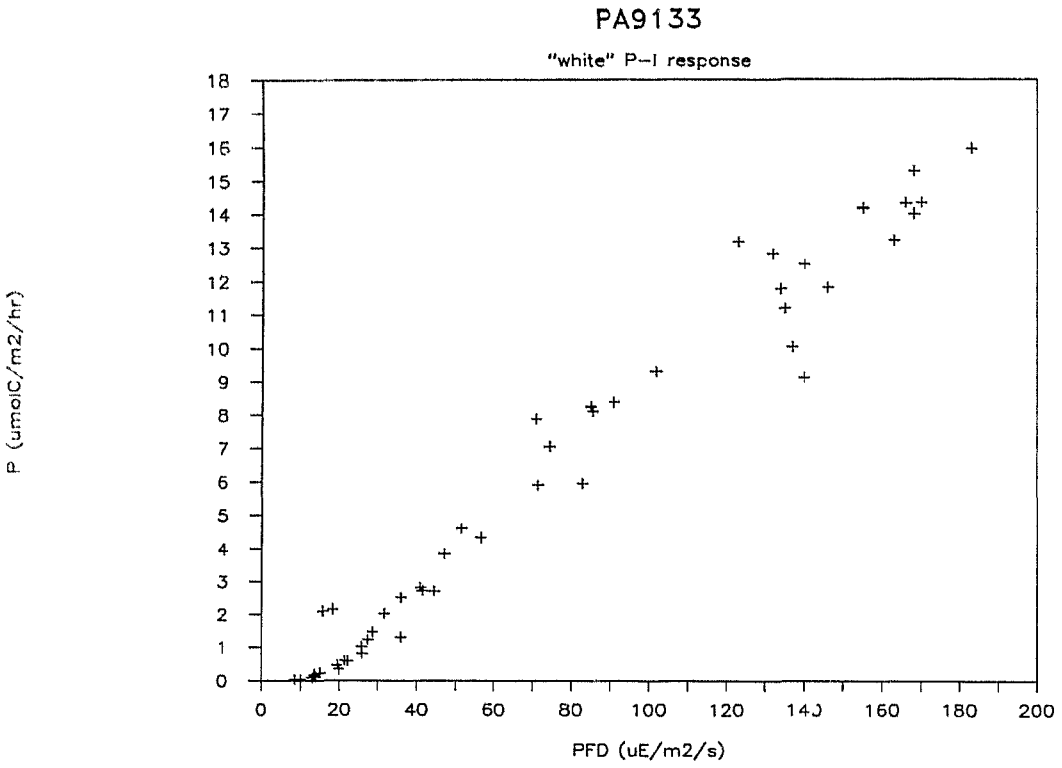

Figure 5. 21 (contd.)

Figure 5. 22. Proportionality between the P-I responses of *Synechococcus* sp. WH 5701 in green (□), blue (◇) and white (+) polychromatic light. Growth PFDs for the different cultures were 8 μmol m^{-2} s^{-1} (SY 9149/50), 15 μmol m^{-2} s^{-1} (SY 9157/8), 27 μmol m^{-2} s^{-1} (SY 9161) and 70 μmol m^{-2} s^{-1} (SY 9153/4).

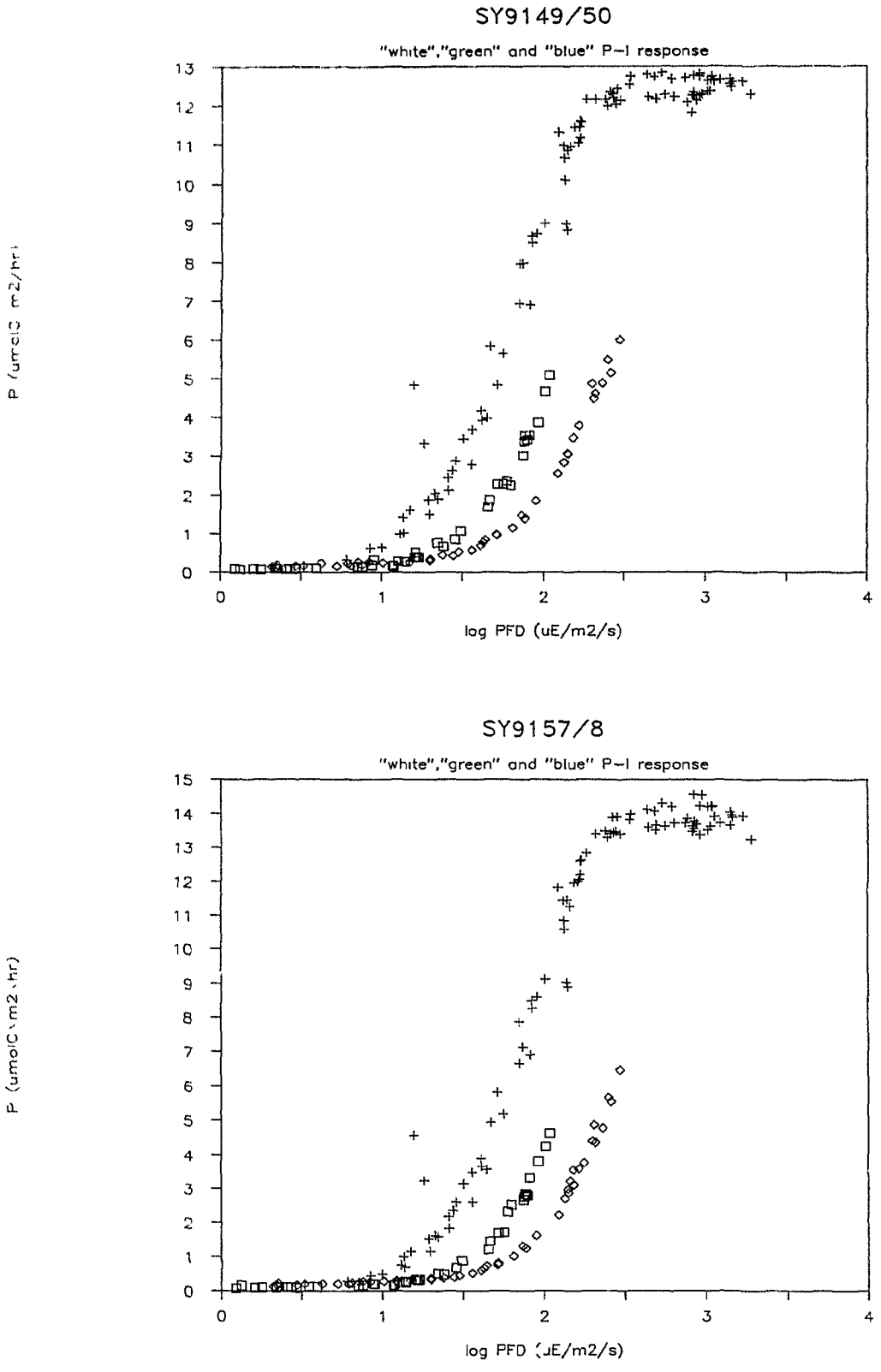
SY9149/50
"white","green" and "blue" P-I response
P (umolC/m2/hr)
log PFD (uE/m2/s)
SY9157/8
"white","green" and "blue" P-I response
P (umolC/m2/hr)
log PFD (uE/m2/s)

Figure 5.22

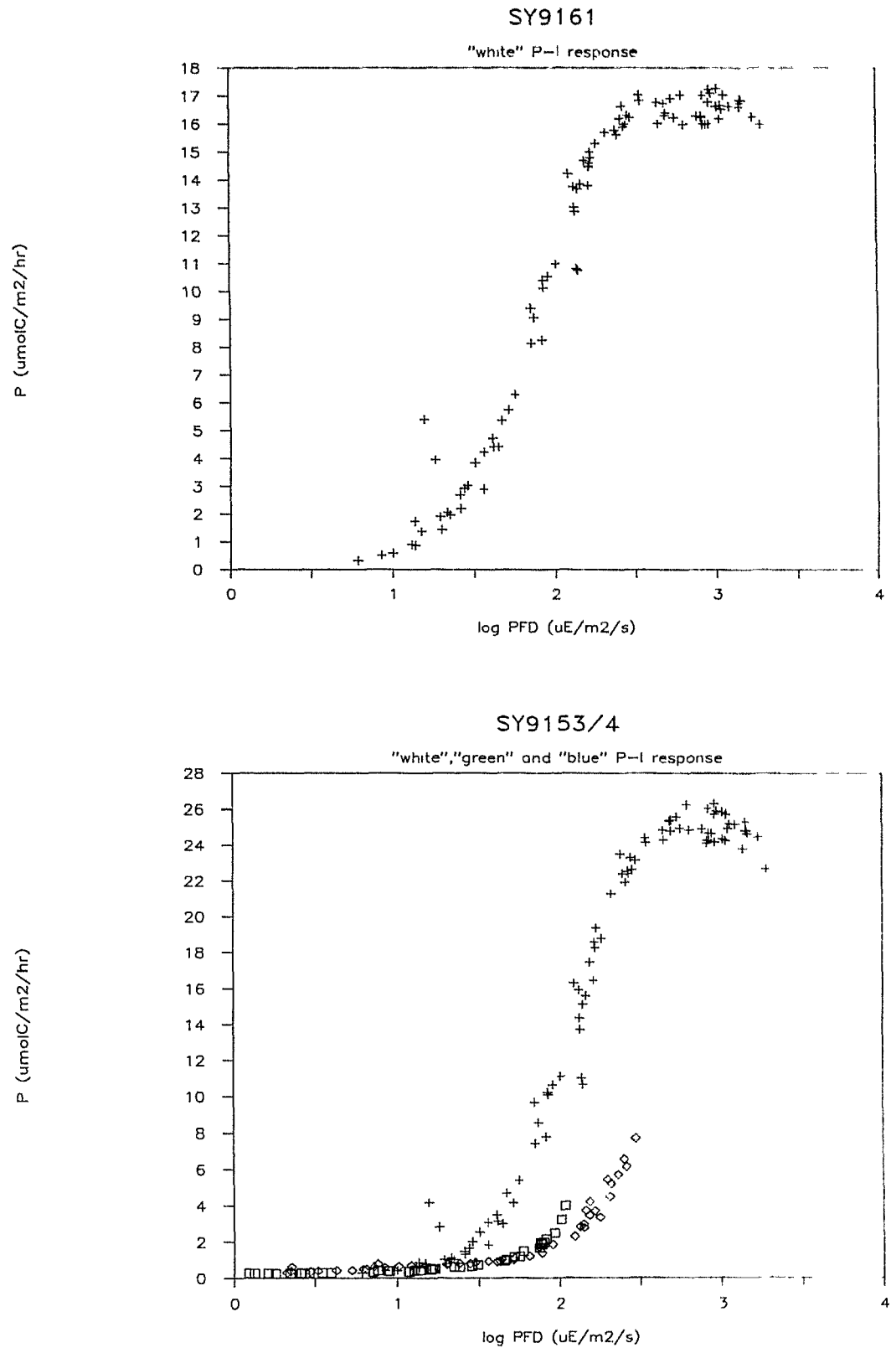

Figure 5. 22 (contd.)

Figure 5. 23. Proportionality between the P-I responses of *Synechococcus* sp. WH 7803 in green (□), blue (◇) and white (+) polychromatic light. Growth PFDs for the different cultures were 7 μmol m^{-2} s^{-1} (DC 9130), 15 μmol m^{-2} s^{-1} (DC 9126/7), 35 μmol m^{-2} s^{-1} (DC 9117/8) and 70 μmol m^{-2} s^{-1} (DC 9121/2).

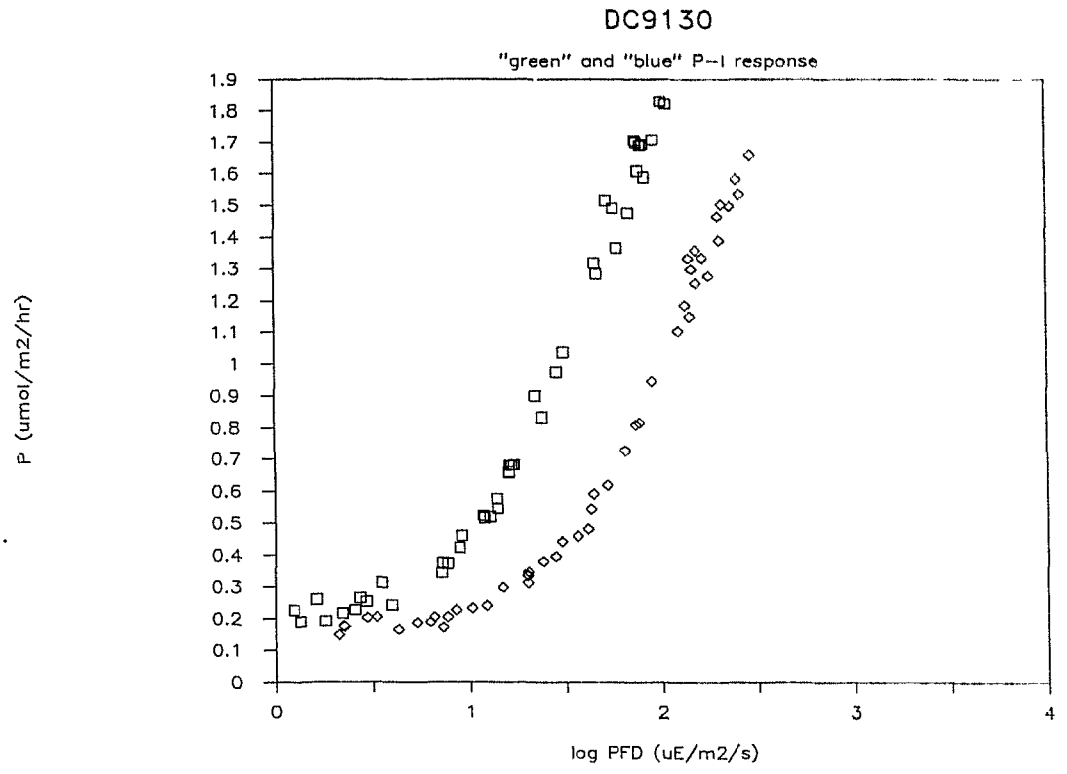
DC9130
"green" and "blue" P--I response
P (umol/m2/hr)
log PFD (uE/m2/s)

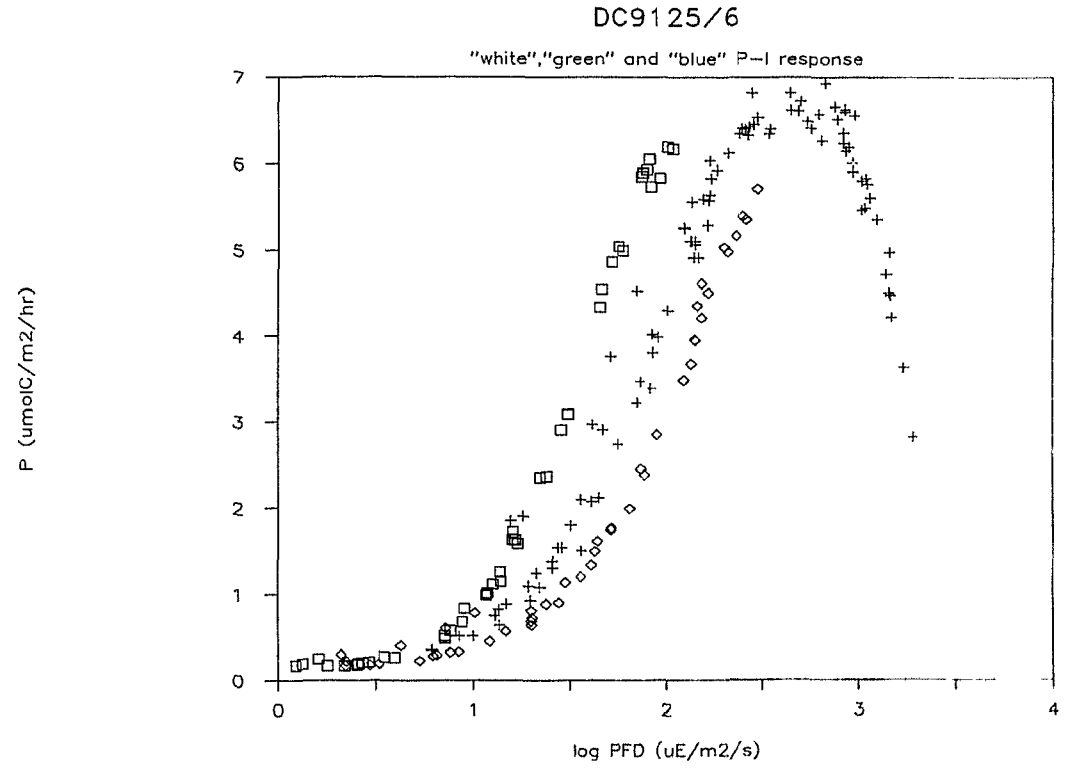
DC9125/6
"white","green" and "blue" P--I response
P (umolC/m2/hr)
log PFD (uE/m2/s)

Figure 5.23

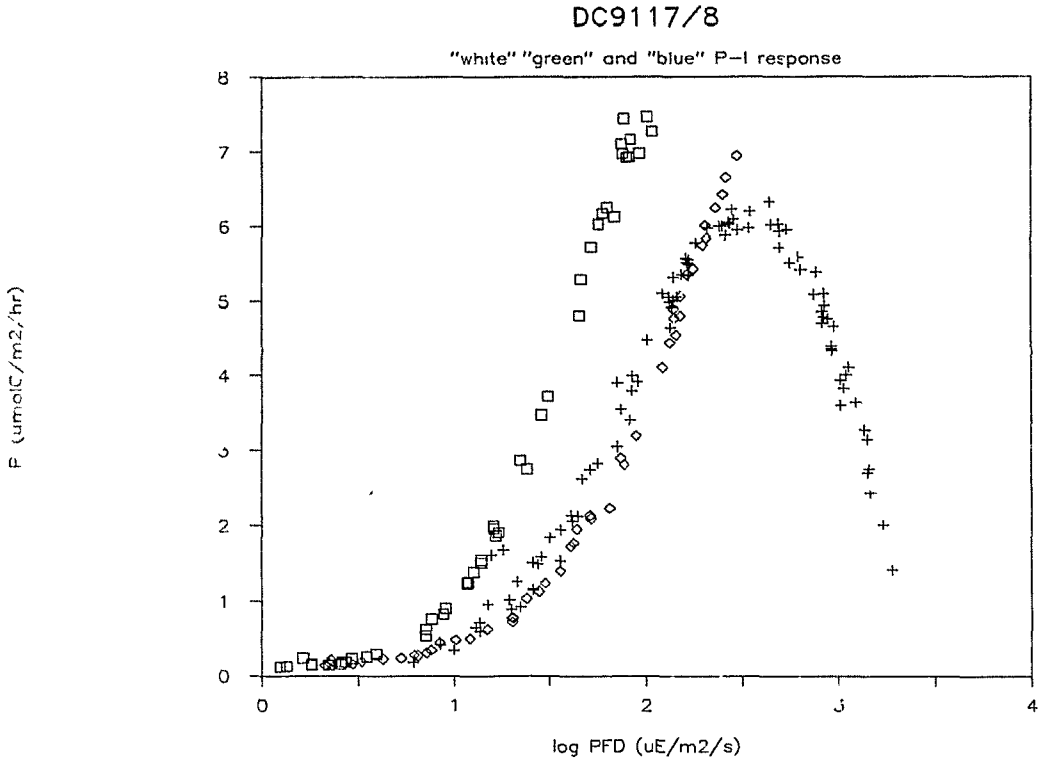

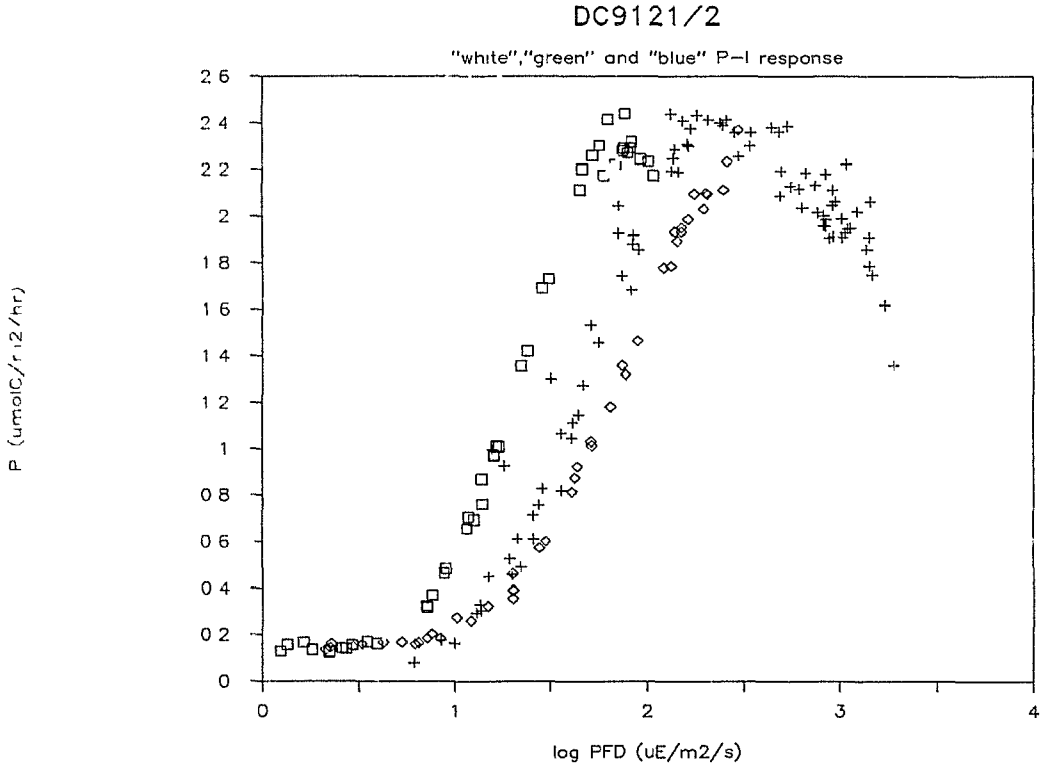

Figure 5. 23 (contd.)

Figure 5. 24. Proportionality between the P-I responses of *Pavlova* sp. (clone NEP) in green (□), blue (◇) and white (+) polychromatic light. Growth PFDs for the different cultures were 8 μmol m^{-2} s^{-1} (PA 9133/4), 12 μmol m^{-2} s^{-1} (PA 9137/8) and 45 μmol m^{-2} s^{-1} (PA 9141/2).

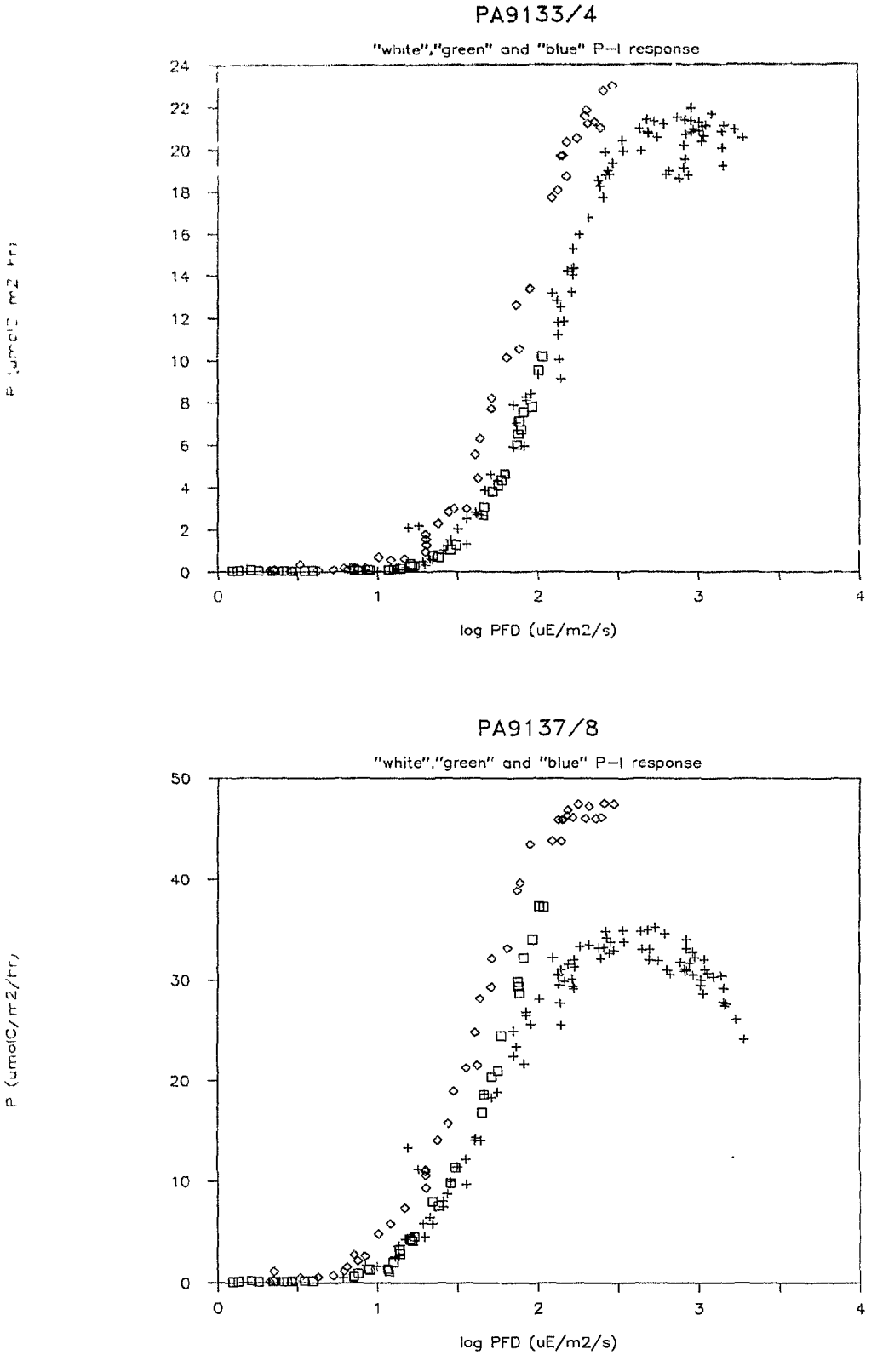
PA9133/4
"white","green" and "blue" P-I response
P (umolC/m2/hr)
log PFD (uE/m2/s)
PA9137/8
"white","green" and "blue" P-I response
P (umolC/m2/hr)
log PFD (uE/m2/s)

Figure 5.24

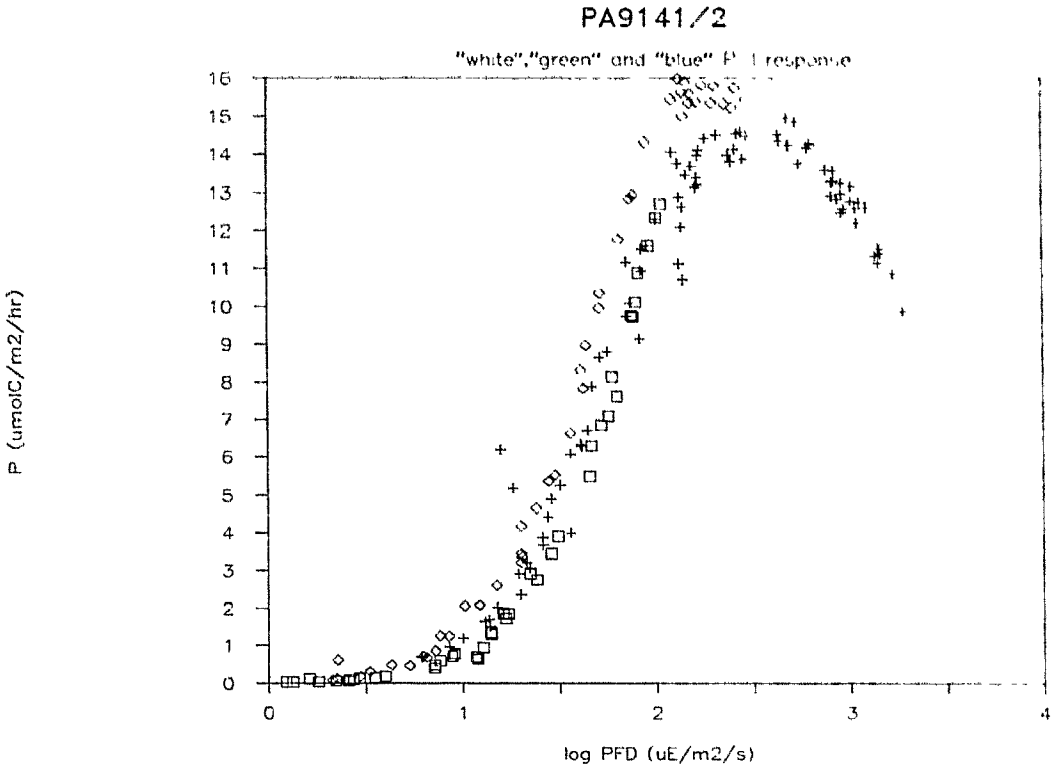

Figure 5. 24 (contd.)

Figure 5. 25. P-I parameters of *Synechococcus* sp. WH 5701 in white polychromatic light as a function of growth PFD.

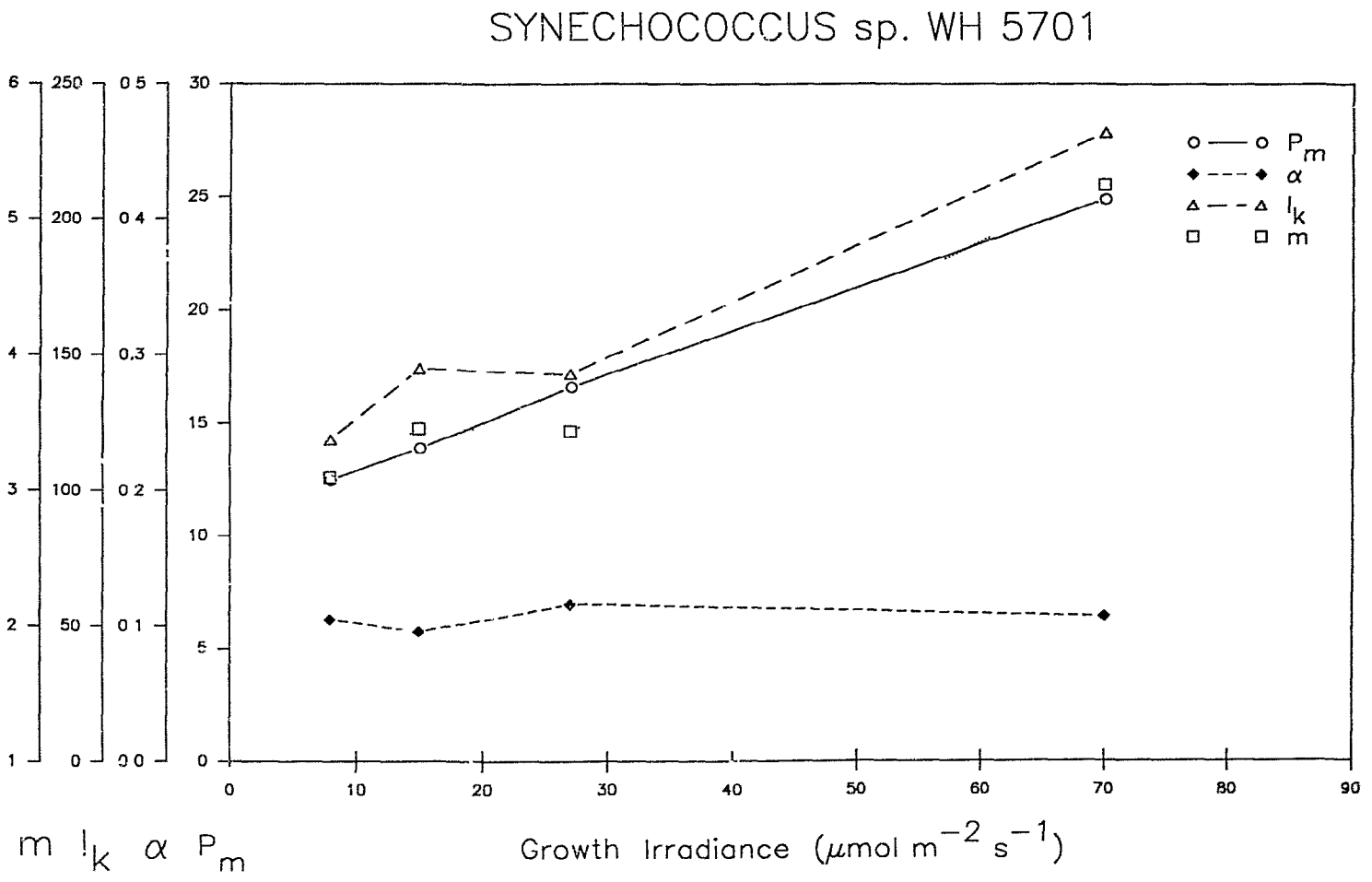
SYNECHOCOCCUS sp. WH 5701
m
I_k
α
P_m
Growth Irradiance (μmol m^{-2} s^{-1})
P_m
α
I_k
m

Figure 5.25

Figure 5. 26. P-I parameters of *Synechococcus* sp. WH 7803 in white polychromatic light as a function of growth PFD.

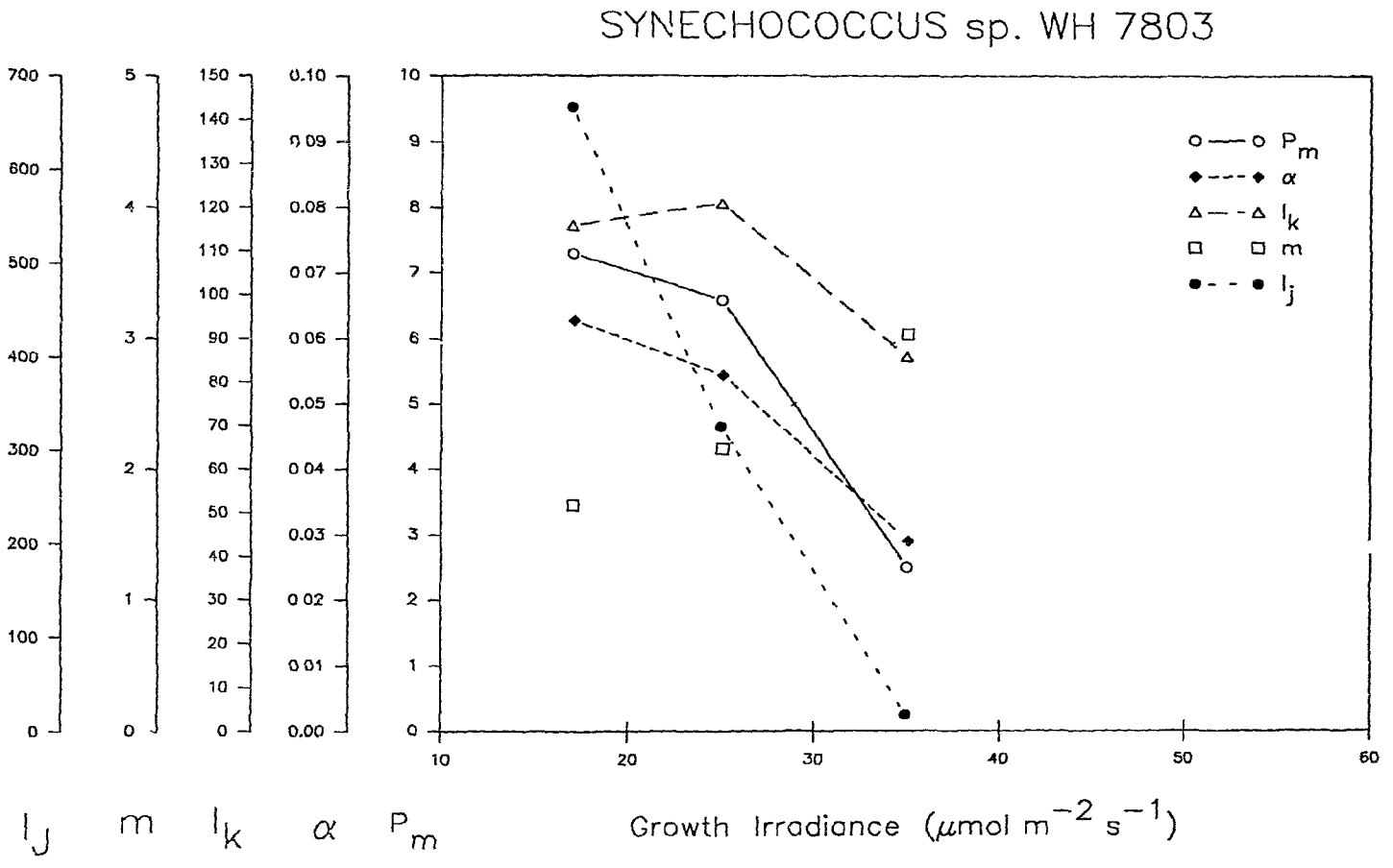
SYNECHOCOCCUS sp. WH 7803
P_m
α
I_k
m
I_j
I_J
m
I_k
α
P_m
Growth Irradiance (μmol m^{-2} s^{-1})

Figure 5.26

Figure 5. 27. P-I parameters of *Pavlova* sp. (clone NEP) in white polychromatic light as a function of growth PFD.

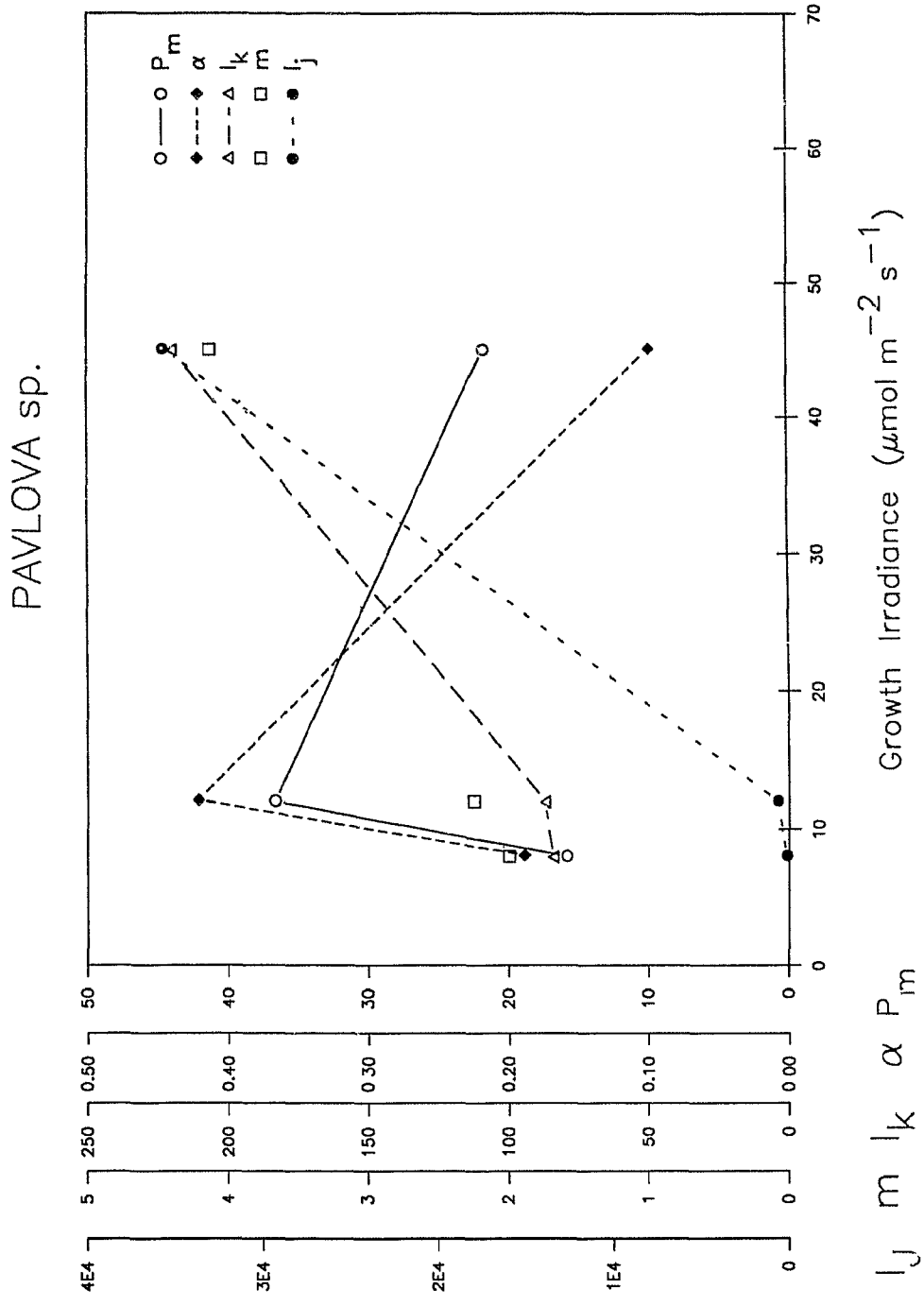
PAVLOVA sp.
P_m
α
I_k
m
I_j
Growth Irradiance (μmol m^{-2} s^{-1})
I_j m I_k α P_m

Figure 5. 27

Figure 5. 28. Correlation between the initial slope (α^B) and the slope describing photoinhibition (β^B) of the P-I response in *Synechococcus* sp. WH 7803 and *Pavlova* sp. (clone NEP). Each pair of parameter values represents a culture grown under a different growth PFD.

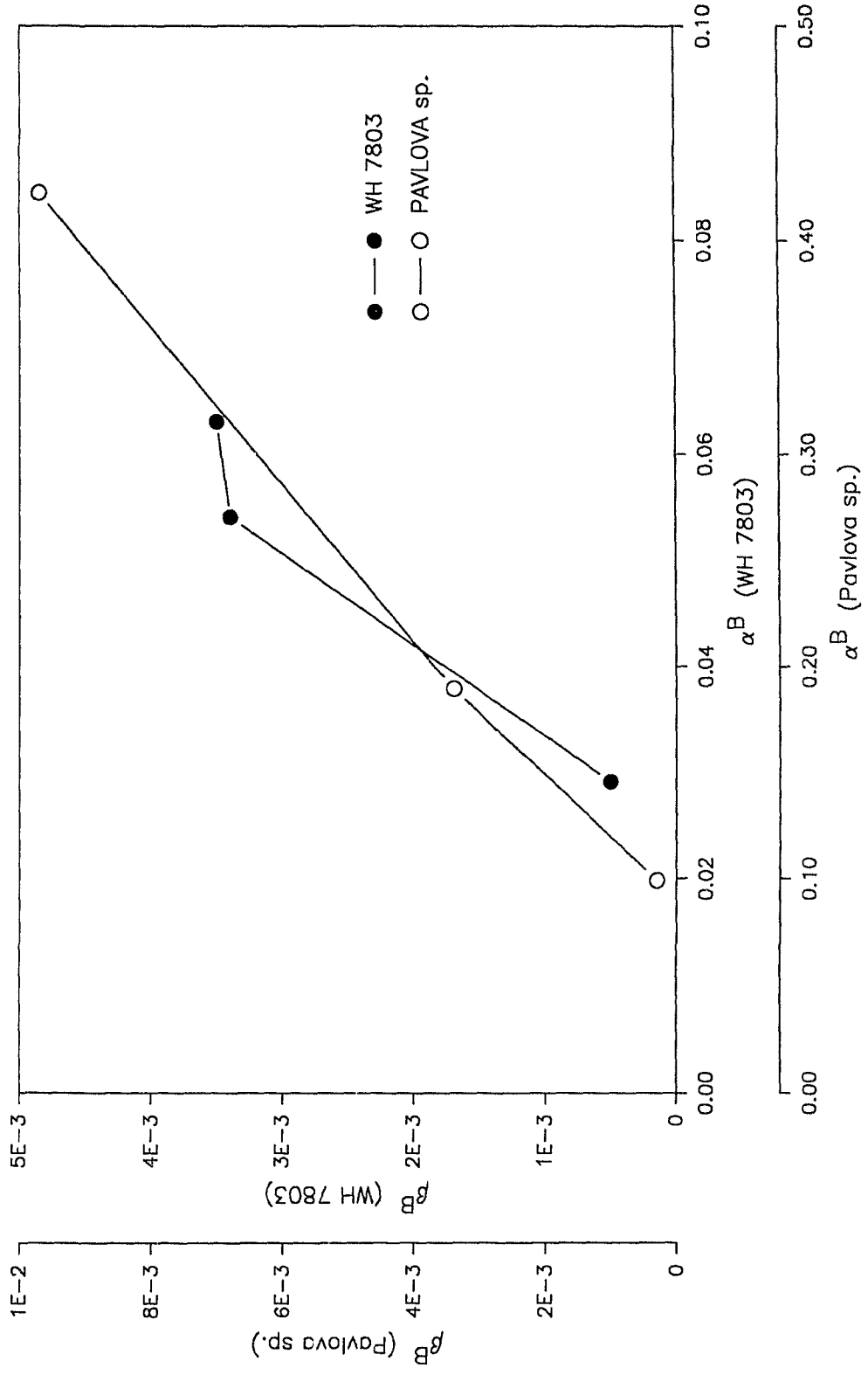
WH 7803
PAVLOVA sp.
β^B (WH 7803)
β^B (Pavlova sp.)
α^B (WH 7803)
α^B (Pavlova sp.)
0
1E-3
2E-3
3E-3
4E-3
5E-3
0
2E-3
4E-3
6E-3
8E-3
1E-2
0.00
0.02
0.04
0.06
0.08
0.10
0.00
0.10
0.20
0.30
0.40
0.50

Figure 5.28

Figure 6. 1. Estimates of the diffuse attenuation coefficient a^*_p as a function of particle concentration in the diatom *Chaetoceros gracilis*. Aliquants of a stock culture of *Chaetoceros gracilis* were diluted with GF/F filtered seawater and made up to a volume of one liter. Each liter was filtered onto a GF/F filter and the the diffuse attenuation coefficient (m^{-1}) estimated as described in the methods. The upper panel shows the entire range of chlorophyll concentrations examined (0 - 10 mg Chl m^{-3}), the lower panel shows the lower part of this range (0 - 1 mg Chl m^{-3}) where curvature is most significant.

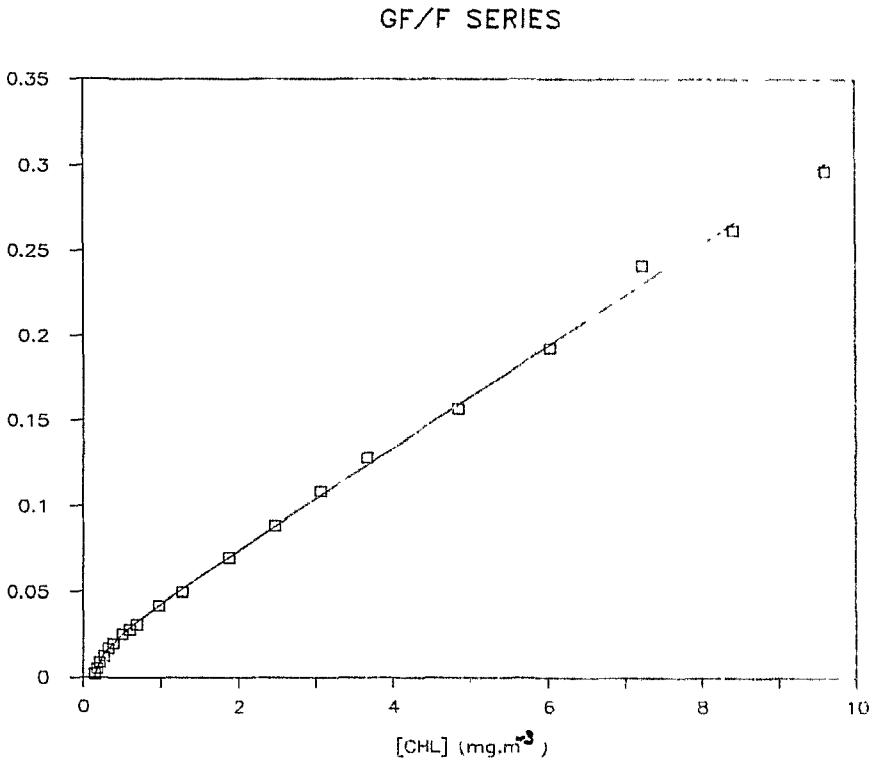
GF/F SERIES
0.35
0.3
0.25
0.2
0.15
0.1
0.05
0
0
2
4
6
8
10
[CHL] (mg.m-3)

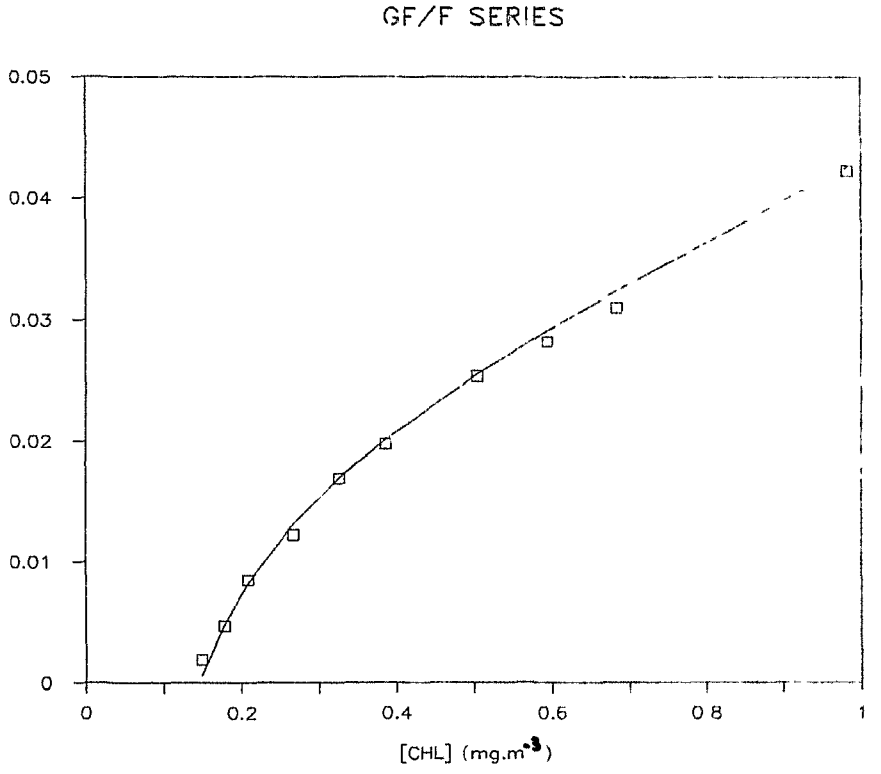
GF/F SERIES
0.05
0.04
0.03
0.02
0.01
0
0
0.2
0.4
0.6
0.8
1
[CHL] (mg.m-3)

Figure 6. 1

Figure 6. 2. *In vivo* absorption spectra of *Synechococcus* sp. WH 7803 cultured at different growth PFDs.

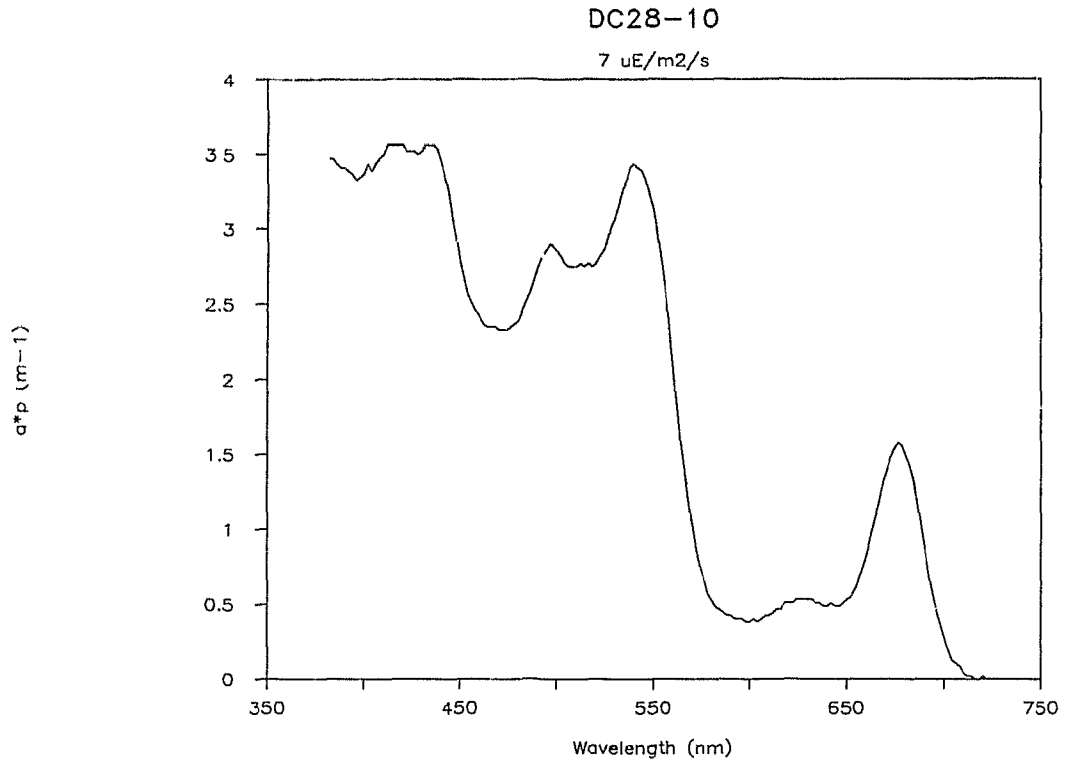
DC28-10
7 uE/m2/s
a*p (m-1)
4
3.5
3
2.5
2
1.5
1
0.5
0
350
450
550
650
750
Wavelength (nm)

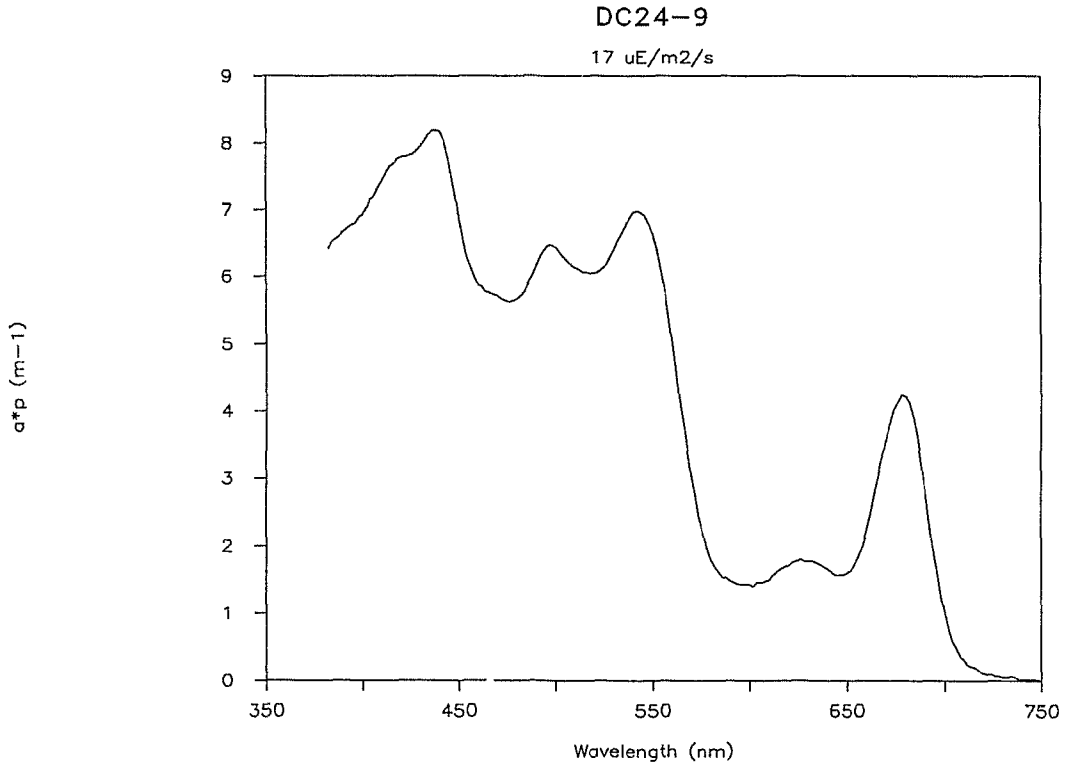
DC24-9
17 uE/m2/s
a*p (m-1)
9
8
7
6
5
4
3
2
1
0
350
450
550
650
750
Wavelength (nm)

Figure 6.2

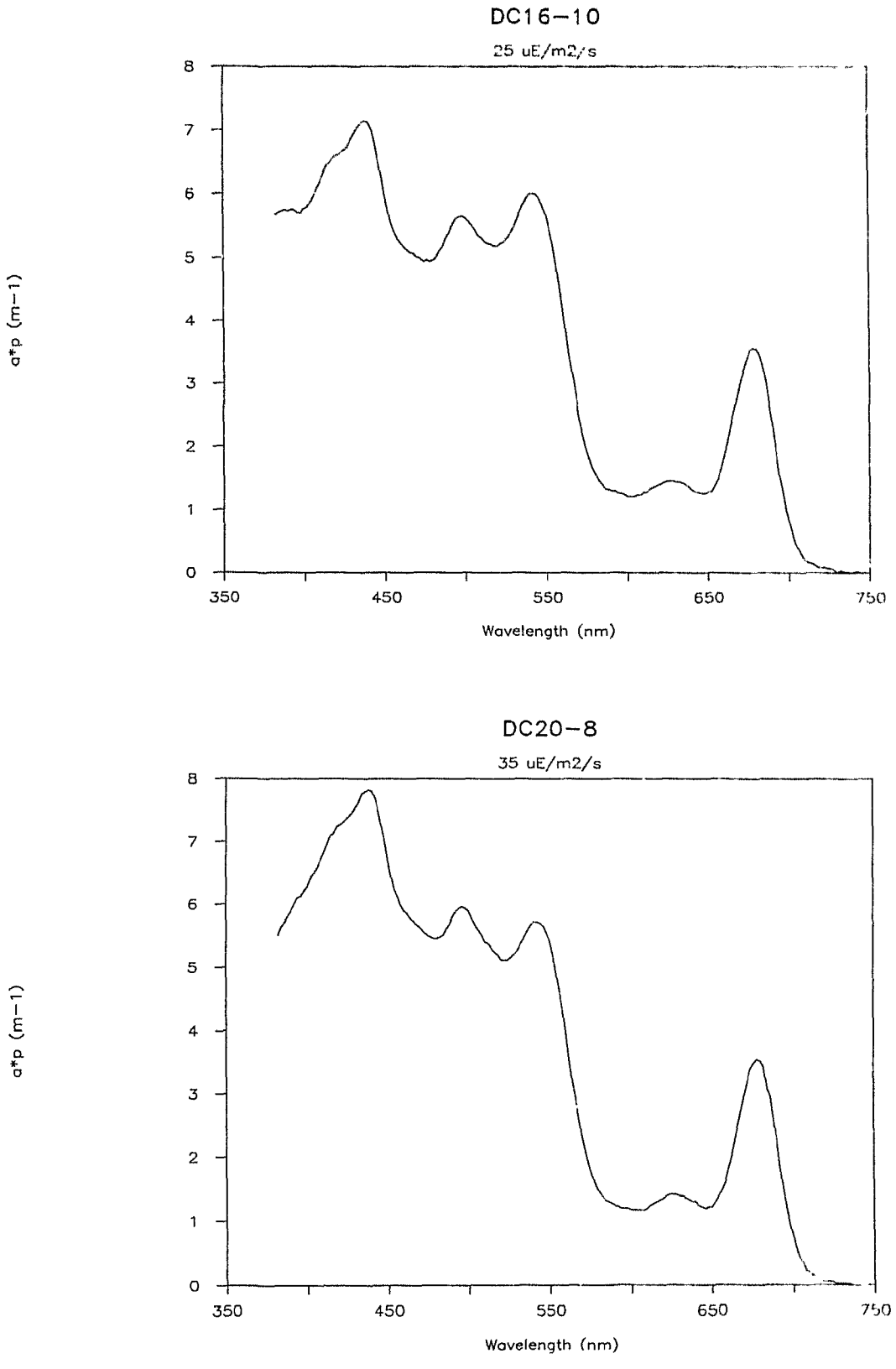

Figure 6. 2 (contd.)

Figure 6. 3. *In vivo* absorption spectra of *Synechococcus* sp. WH 5701 cultured at different growth PFDs.

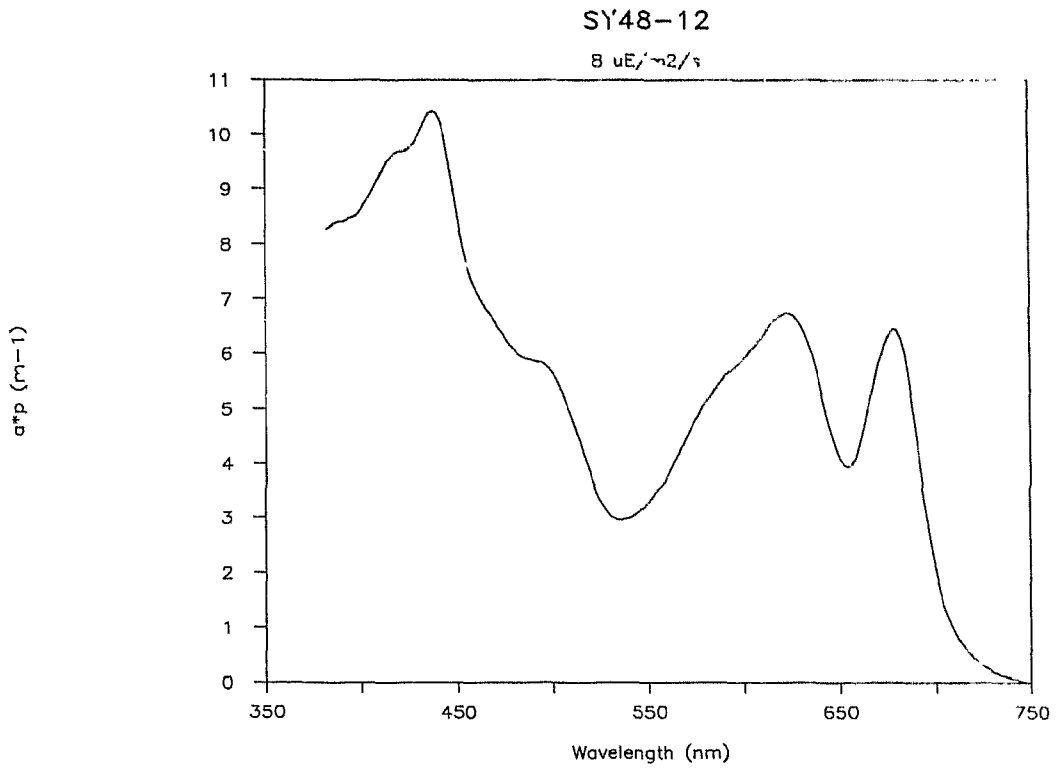
SY48-12
8 uE/m2/s
a*p (m-1)
Wavelength (nm)
0
1
2
3
4
5
6
7
8
9
10
11
350
450
550
650
750

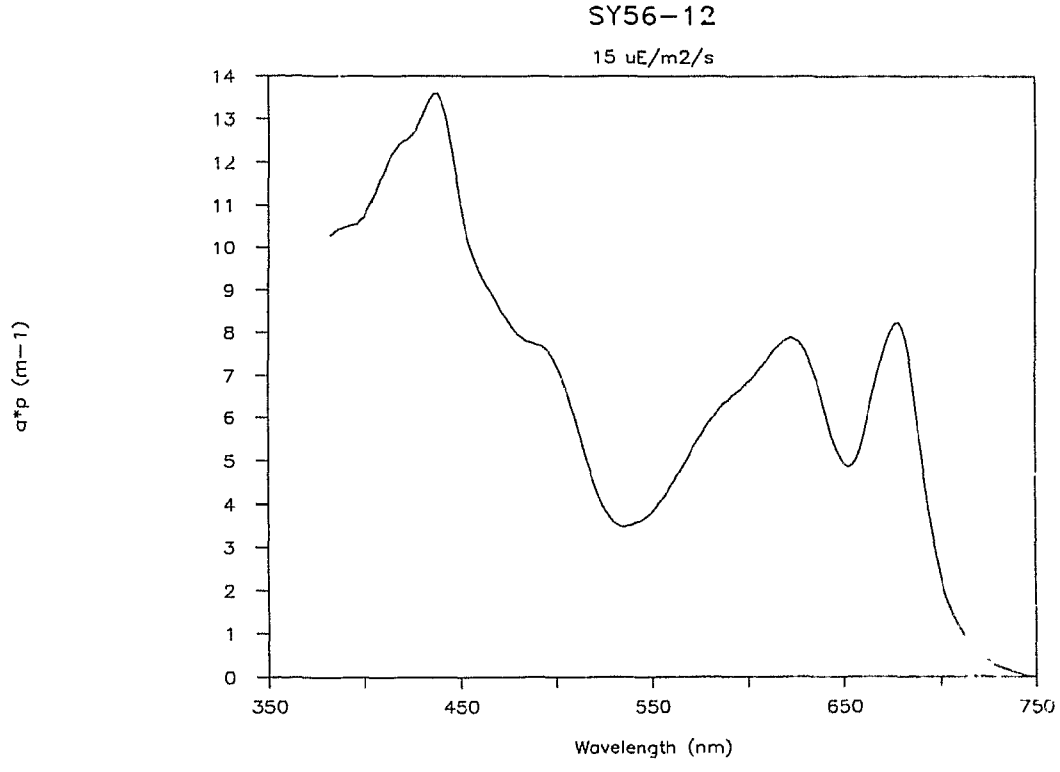
SY56-12
15 uE/m2/s
a*p (m-1)
Wavelength (nm)
0
1
2
3
4
5
6
7
8
9
10
11
12
13
14
350
450
550
650
750

Figure 6.3

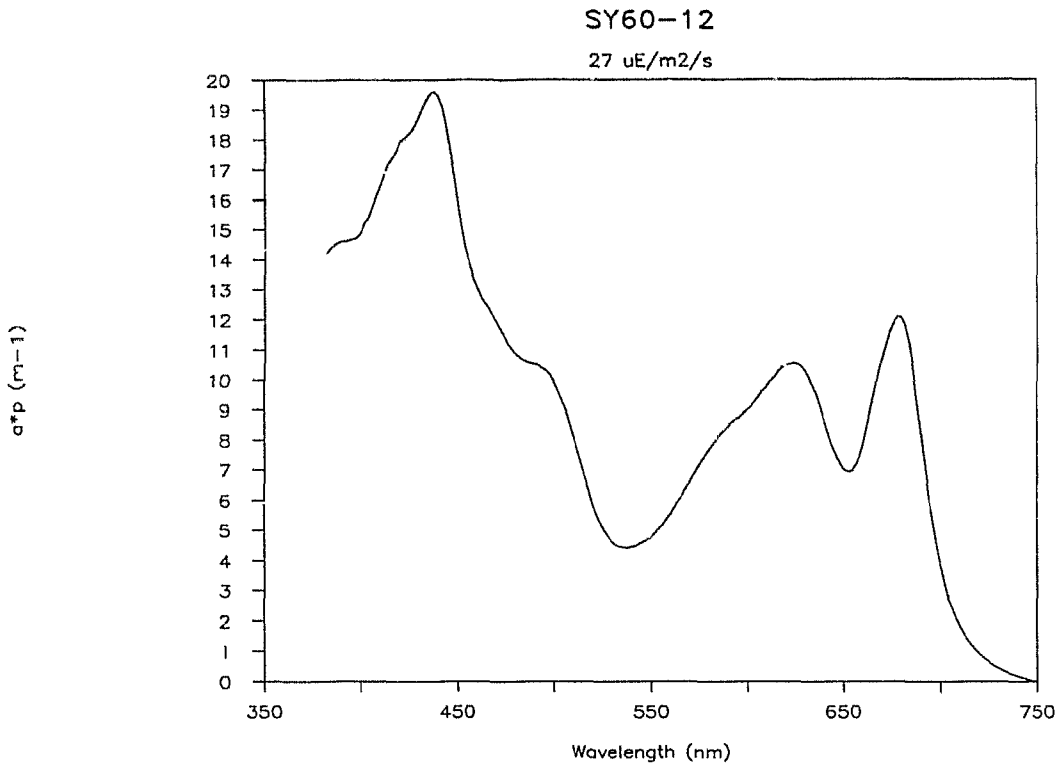

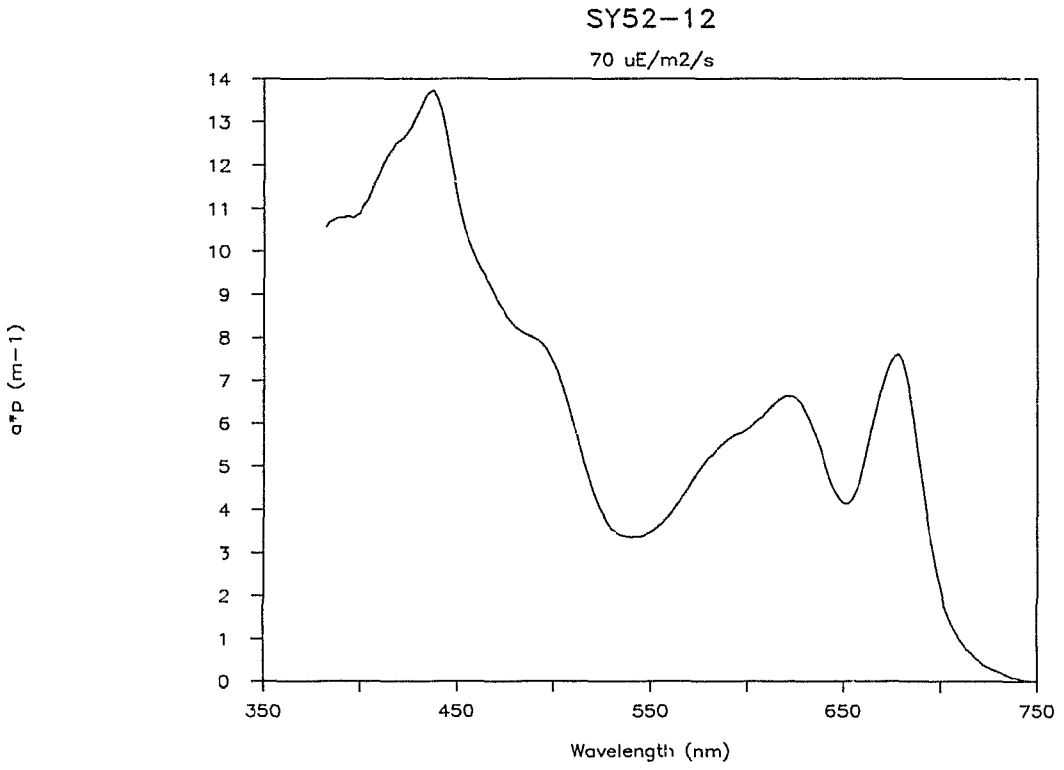

Figure 6. 3 (contd.)

Figure 6. 4. *In vivo* absorption spectra of *Pavlova* sp. (clone NEP) cultured at different growth PFDs.

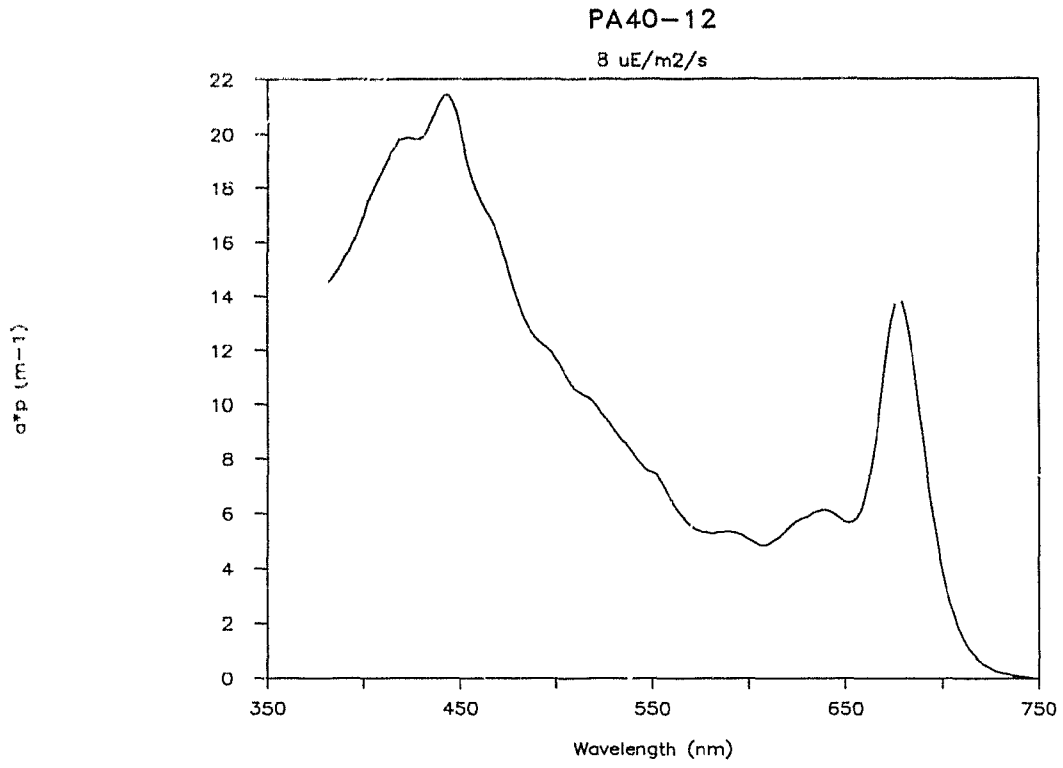
PA40–12
8 uE/m2/s
a*p (m–1)
22
20
18
16
14
12
10
8
6
4
2
0
350
450
550
650
750
Wavelength (nm)

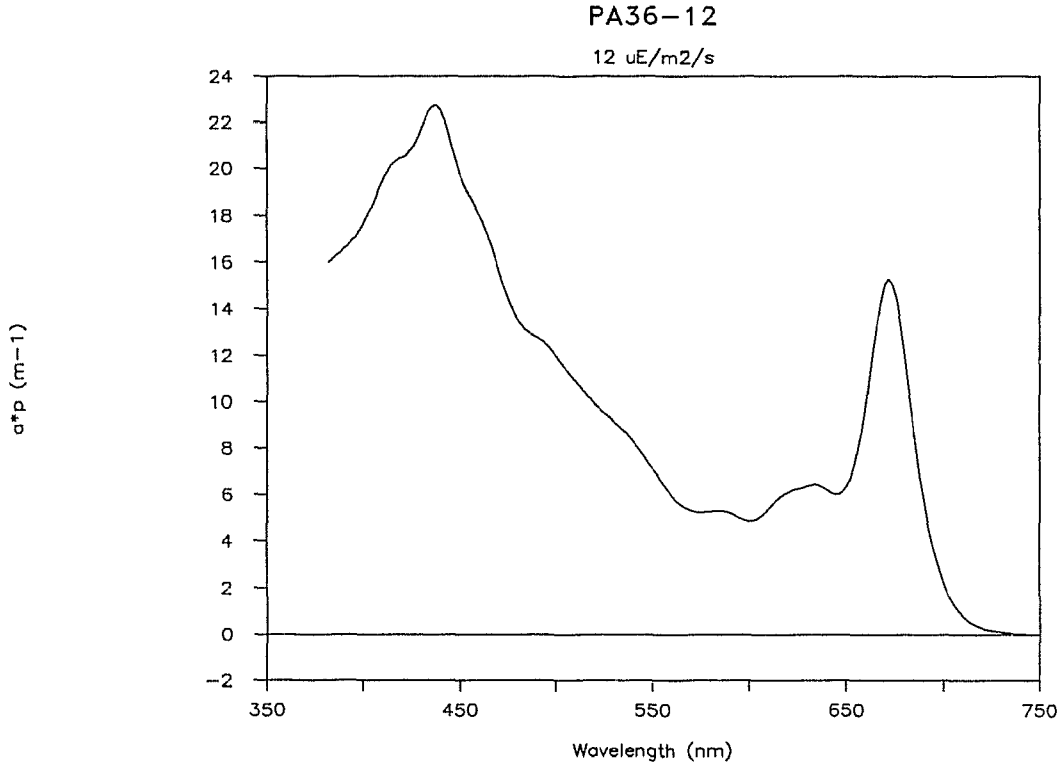
PA36–12
12 uE/m2/s
a*p (m–1)
24
22
20
18
16
14
12
10
8
6
4
2
0
–2
350
450
550
650
750
Wavelength (nm)

Figure 6.4

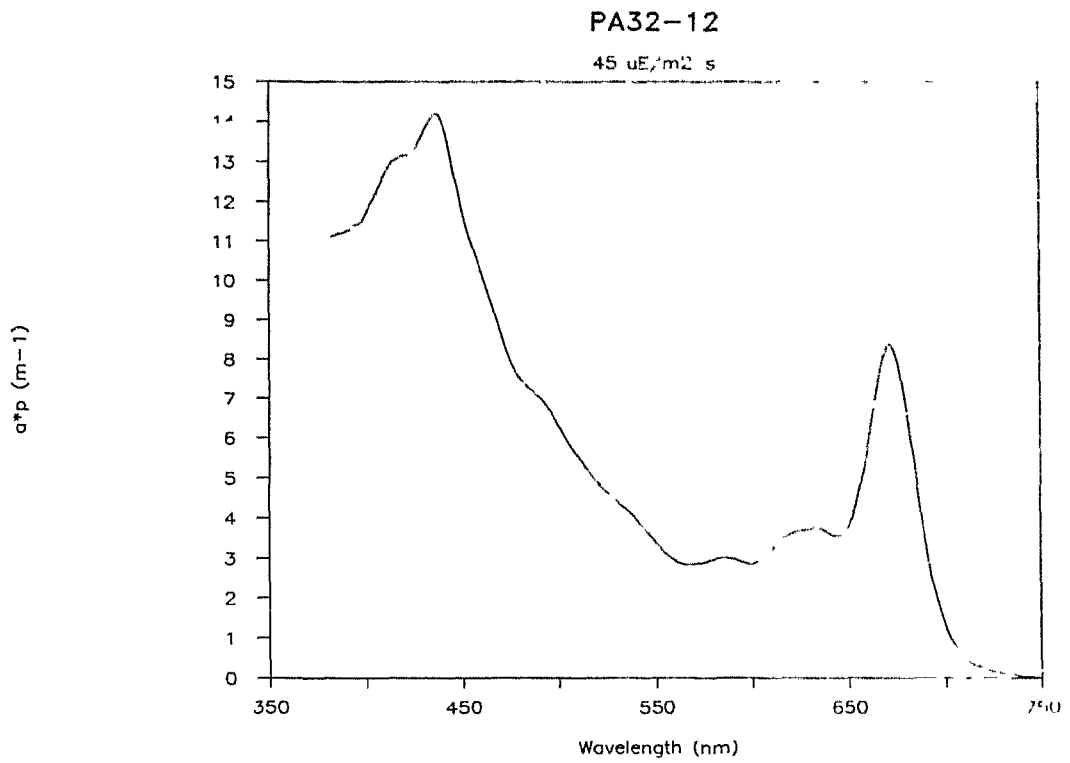

Figure 6. 4 (contd.)

Figure 6. 5. Estimates of $a^*_p(\lambda)$ in *Synechococcus* sp. WH 7803 as a function of the volume of culture filtered onto the GF/F filter. Wavelengths represented are 438 nm (□), 498 nm (+), 542 nm (◇), 604 nm (△), 626 nm (×) and 678 nm (▽). Cultures were grown at PFDs of 17 μmol m^{-2} s^{-1} (DC 24), 25 μmol m^{-2} s^{-1} (DC 16) and 35 μmol m^{-2} s^{-1} (DC 20).

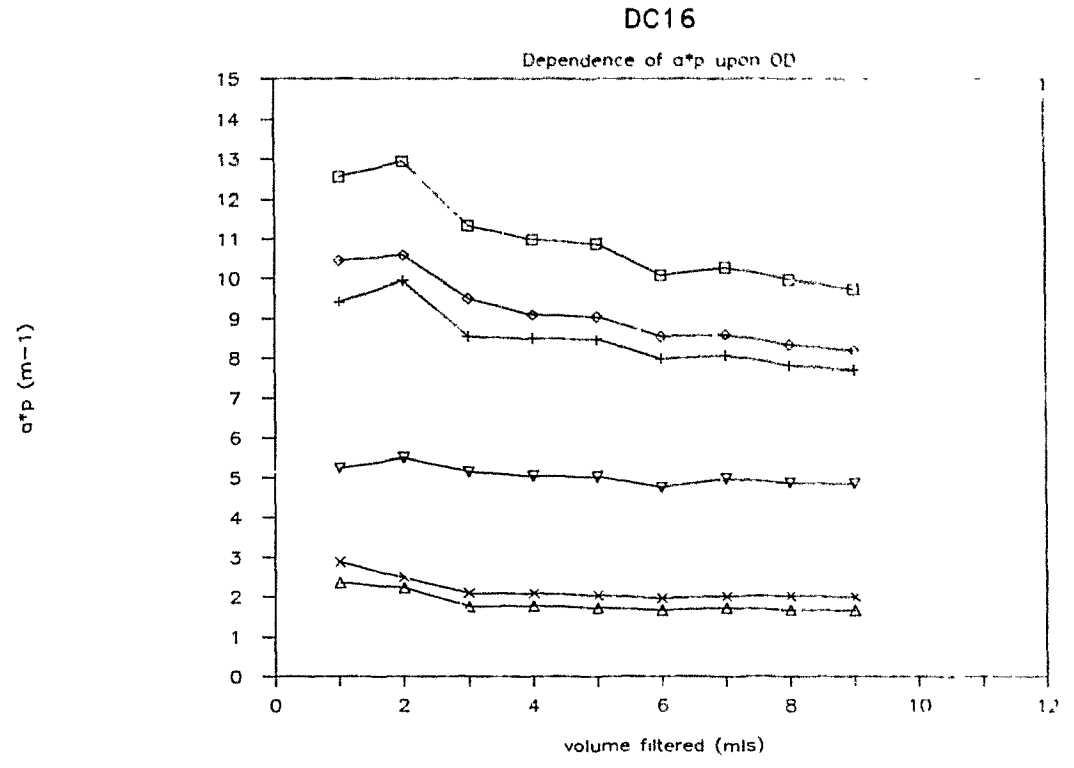
DC16
Dependence of a*p upon OD
a*p (m-1)
volume filtered (mls)

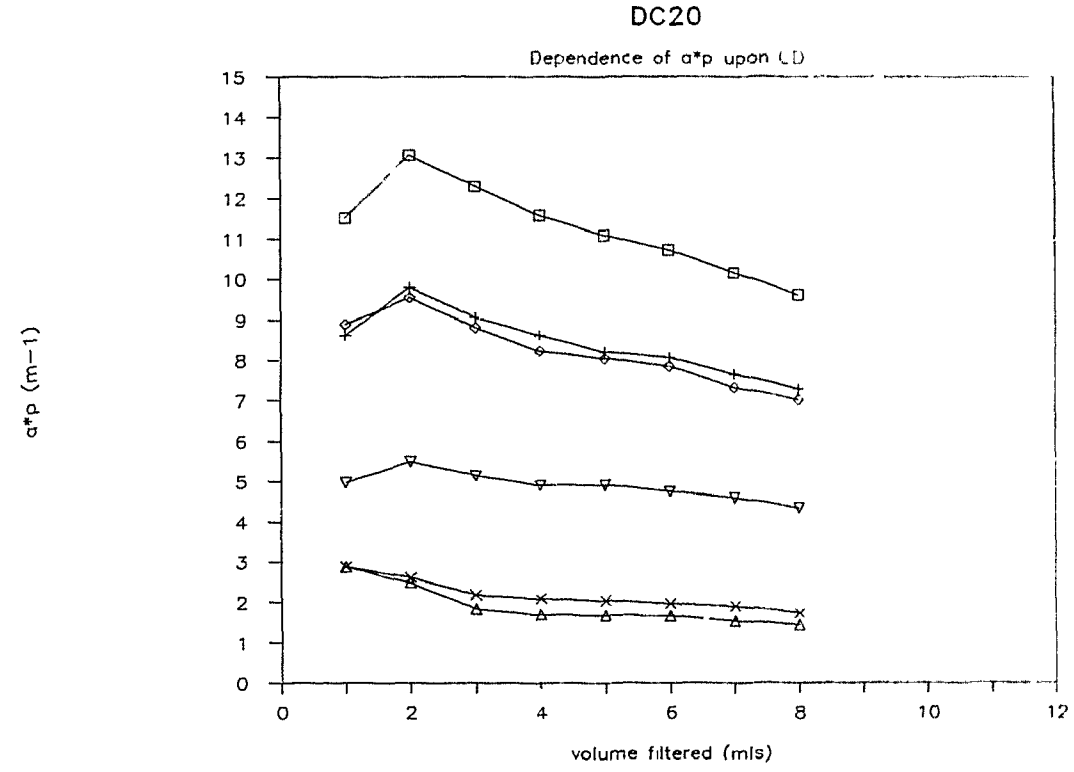
DC20
Dependence of a*p upon OD
a*p (m-1)
volume filtered (mls)

Figure 6.5

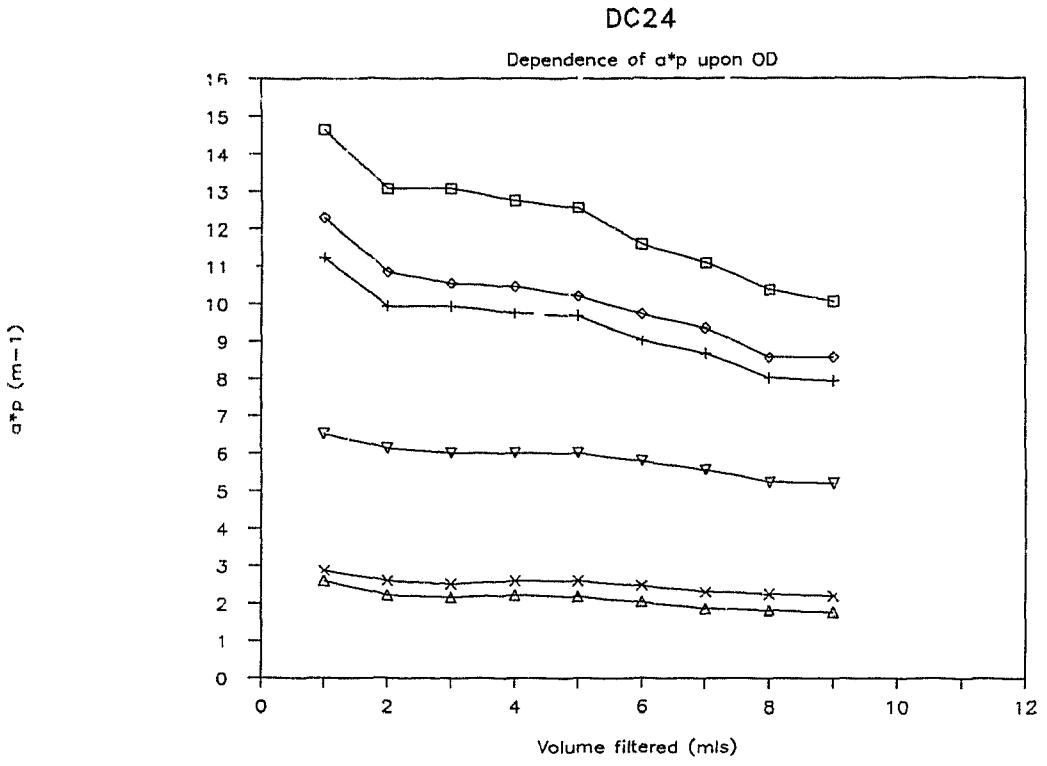

Figure 6. 5 (contd.)

Figure 6. 6. Estimates of $a^*_p(\lambda)$ in *Synechococcus* sp. WH 5701 as a function of the volume of culture filtered onto the GF/F filter. Wavelengths represented are 438 nm (□), 492 nm (+), 542 nm (◇), 622 nm (△), 654 nm (×) and 675 nm (▽). Cultures were grown at PFDs of 8 μmol m^{-2} s^{-1} (SY 48), 15 μmol m^{-2} s^{-1} (SY 56), 27 μmol m^{-2} s^{-1} (SY 60) and 70 μmol m^{-2} s^{-1} (SY 52).

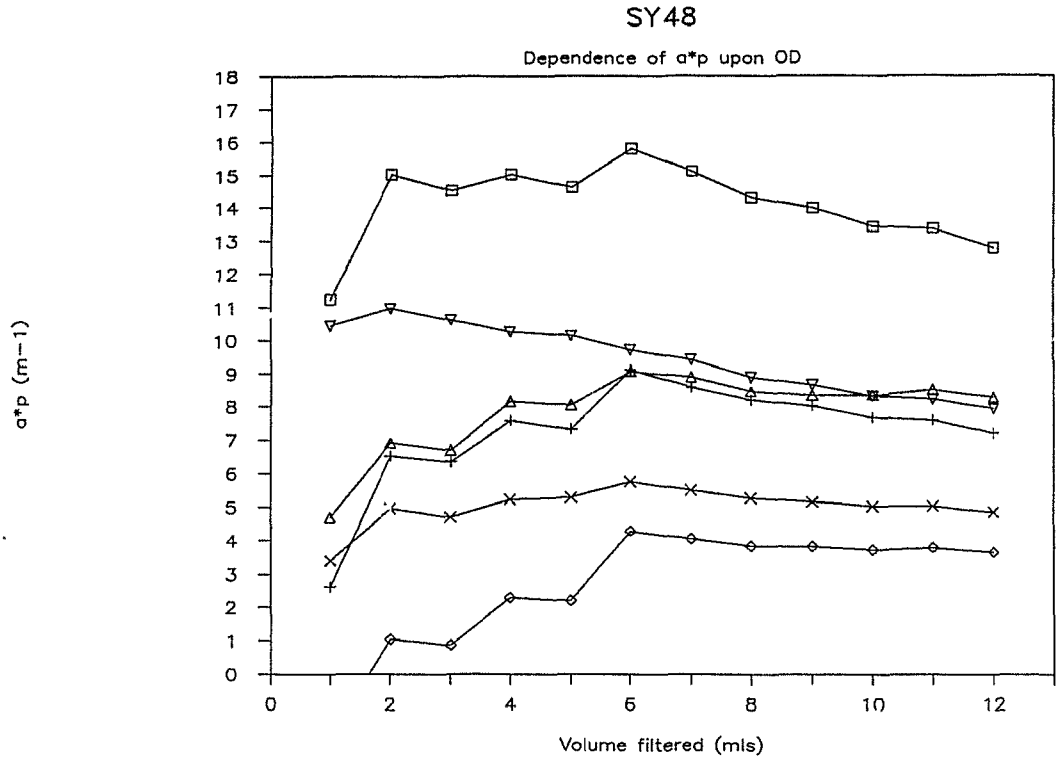
SY48
Dependence of a*p upon OD
a*p (m-1)
Volume filtered (mls)

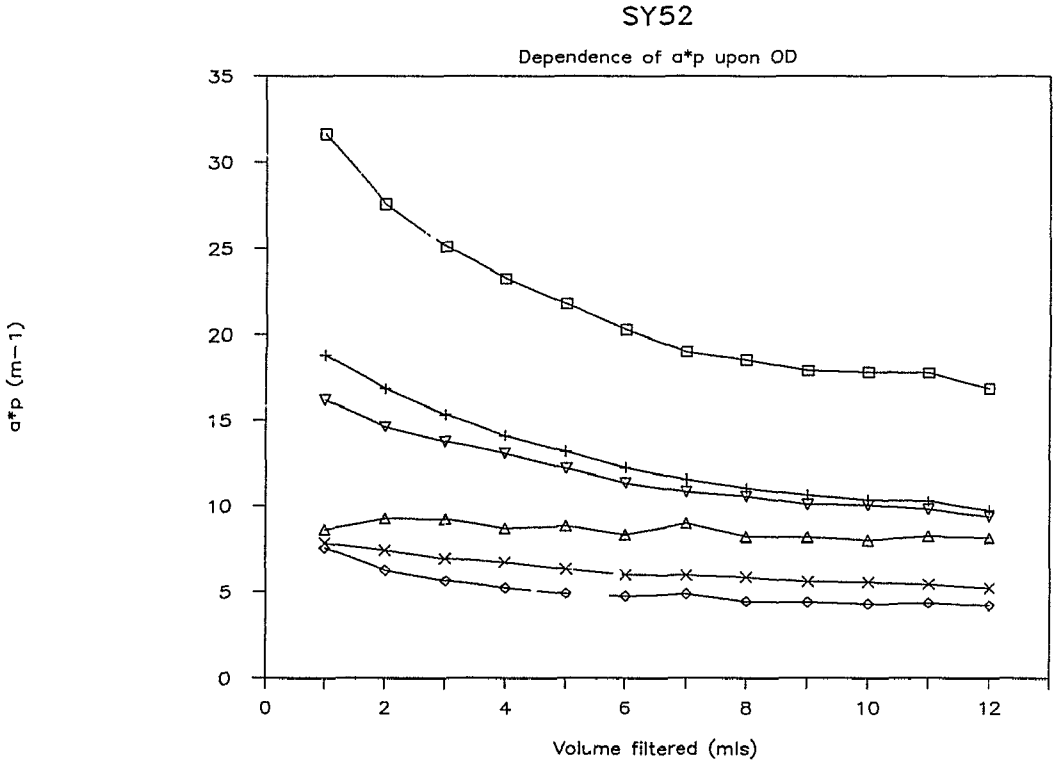
SY52
Dependence of a*p upon OD
a*p (m-1)
Volume filtered (mls)

Figure 6.6

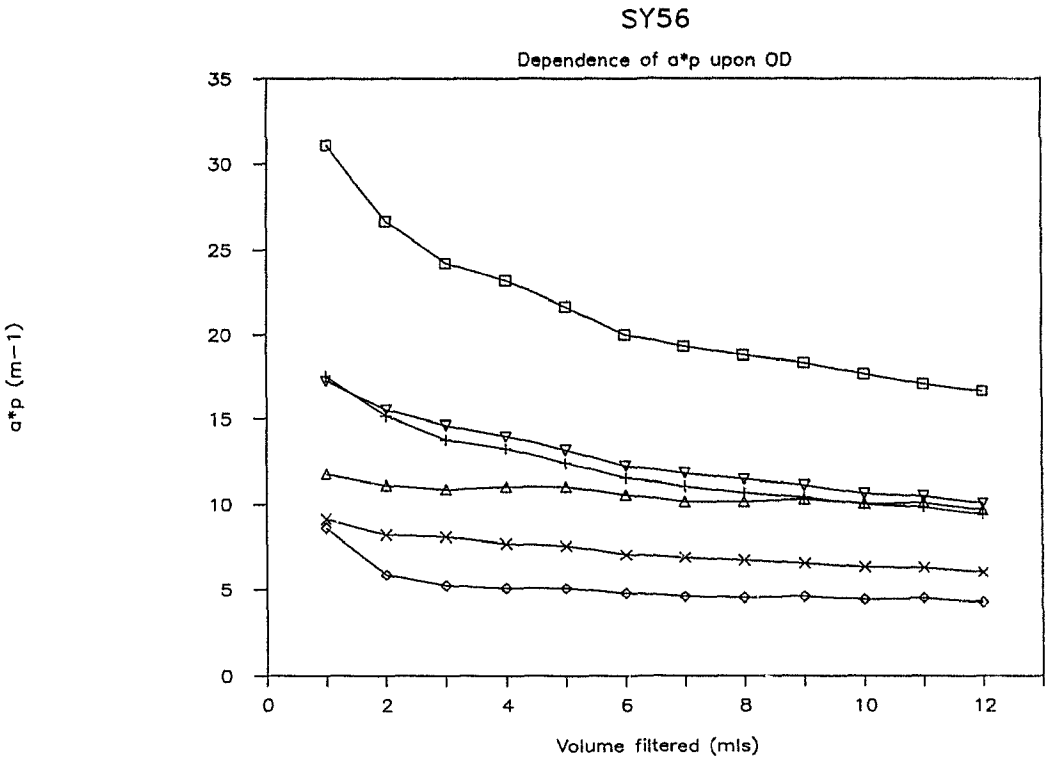

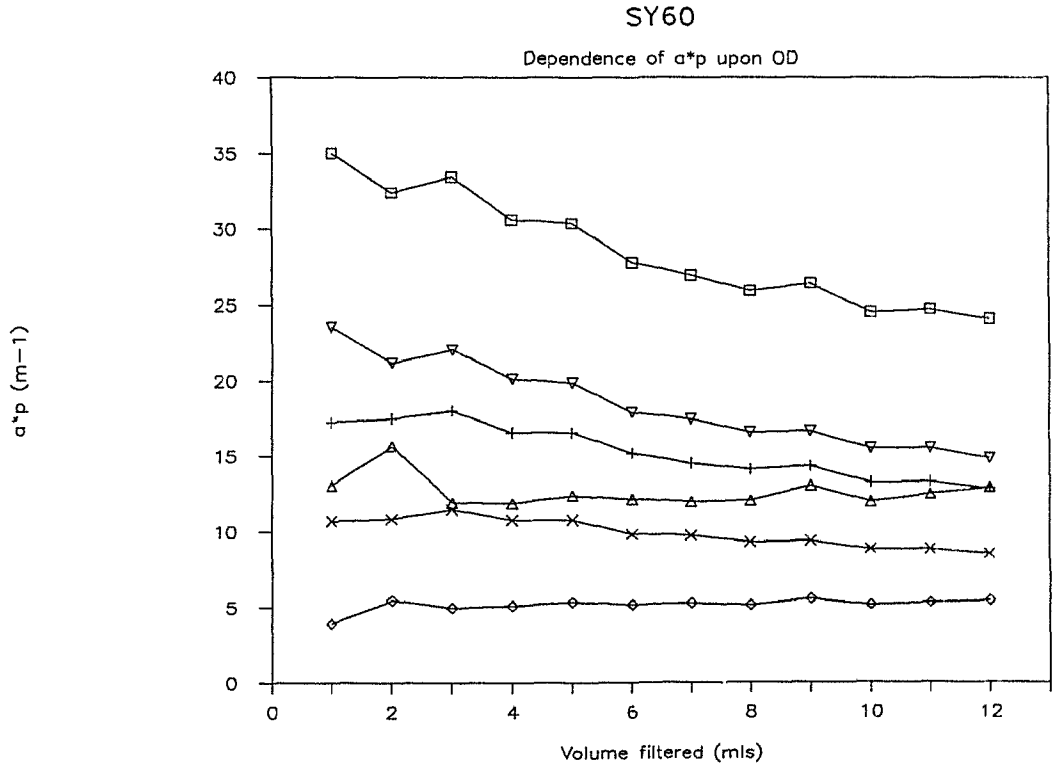

Figure 6. 6 (contd.)

Figure 6.7. Estimates of $a^*_p(\lambda)$ in *Pavlova* sp. (clone NEP) as a function of the volume of culture filtered onto the GF/F filter. Wavelengths represented are 436 nm (□), 598 nm (+), 632 nm (◇) and 678 nm (△). Cultures were grown at PFDs of 8 μmol m^{-2} s^{-1} (PA 40), 12 μmol m^{-2} s^{-1} (PA 36) and 45 μmol m^{-2} s^{-1} (PA 32).

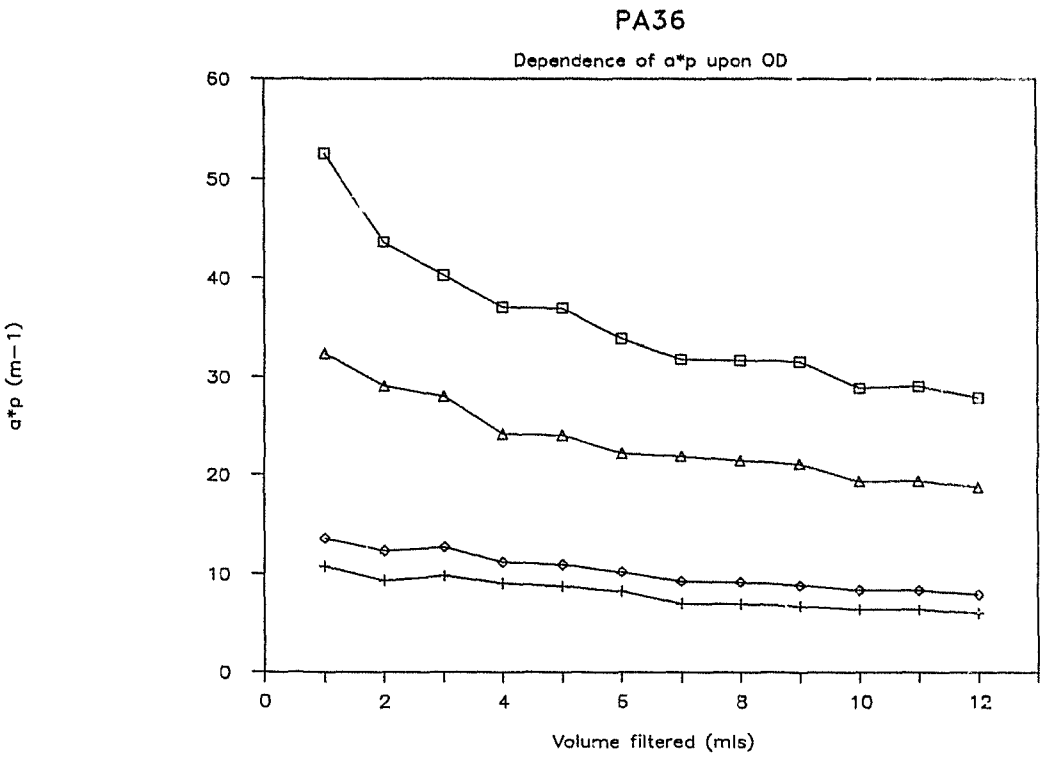
PA36
Dependence of a*p upon OD
a*p (m-1)
60
50
40
30
20
10
0
0
2
4
6
8
10
12
Volume filtered (mls)

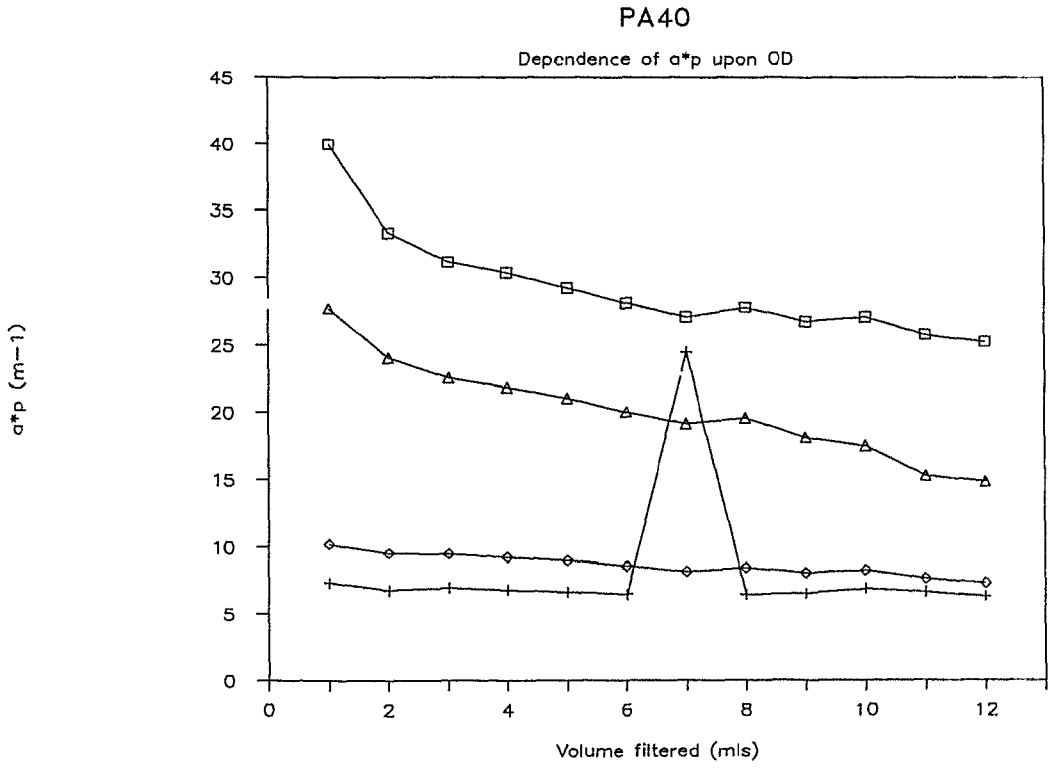
PA40
Dependence of a*p upon OD
a*p (m-1)
45
40
35
30
25
20
15
10
5
0
0
2
4
6
8
10
12
Volume filtered (mls)

Figure 6.7

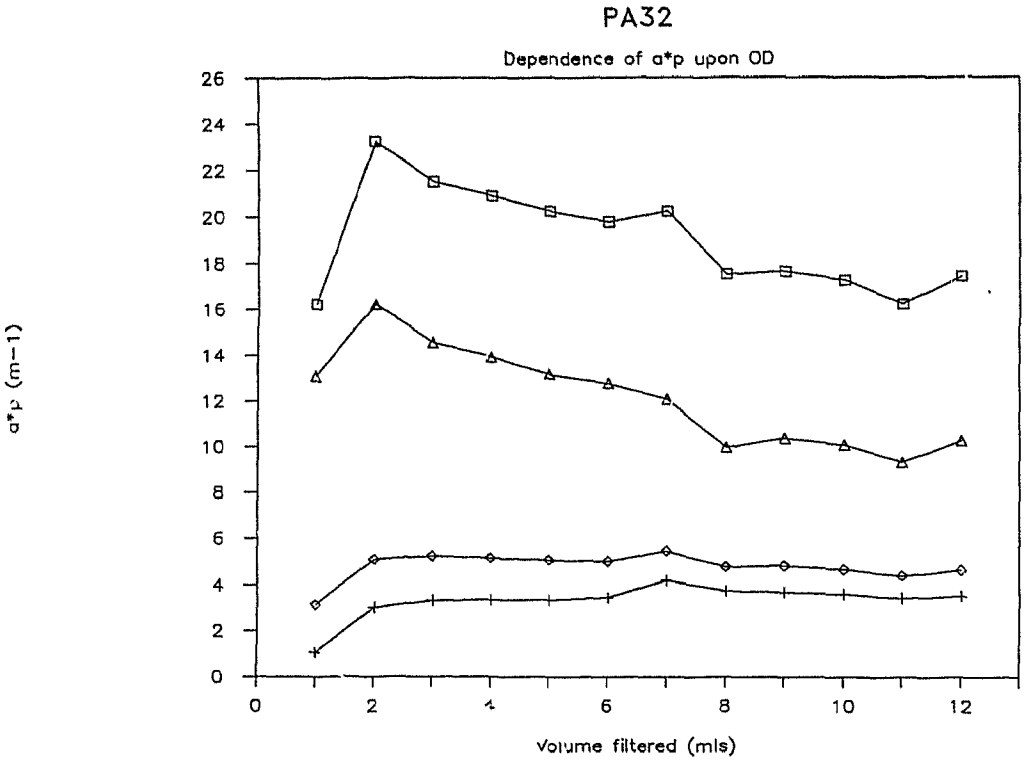

Figure 6.7 (contd.)

Figure 6. 8. Ratios of the principal *in vivo* absorbance peaks in *Synechococcus* sp. WH 7803 as a function of growth PFD. Peak ratios represented are 438/678 nm (□), 542/678 nm (◇), 542/498 nm (×) and 542/438 nm (▽). Absorbance at 438 and 678 nm may be attributed to chlorophyll *a*, absorbance at 542 nm and 498 nm may be attributed to the PEB and PUB chromophores of phycoerythrin respectively.

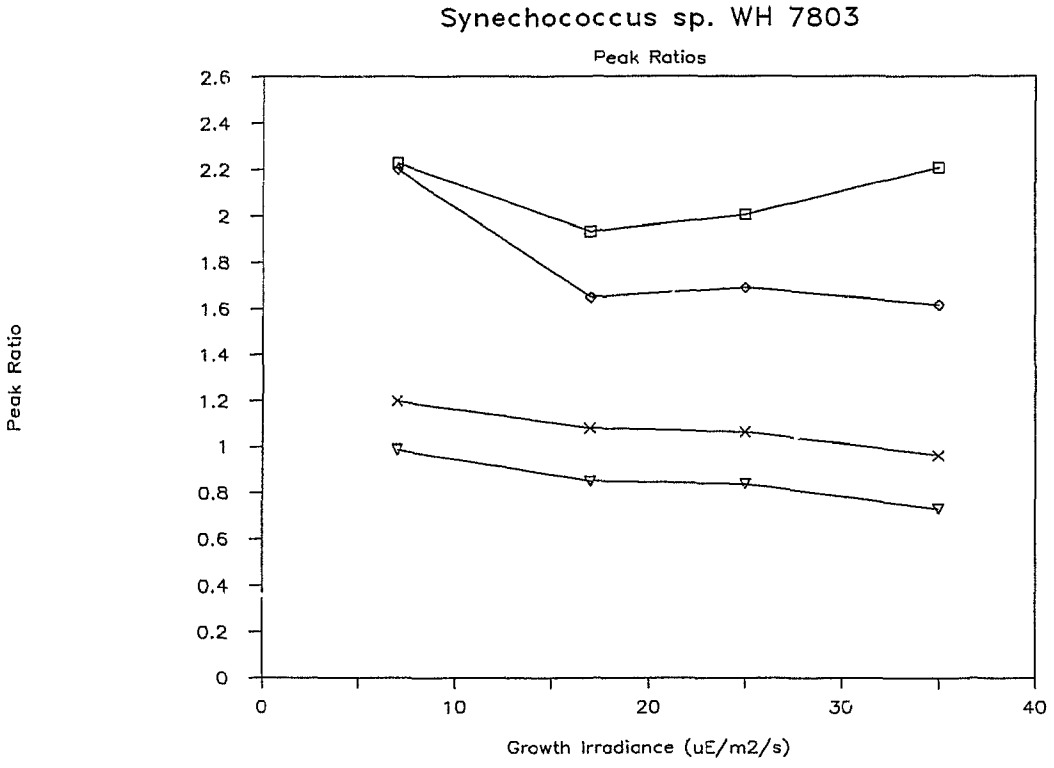
Synechococcus sp. WH 7803
Peak Ratios
Peak Ratio
2.6
2.4
2.2
2
1.8
1.6
1.4
1.2
1
0.8
0.6
0.4
0.2
0
0
10
20
30
40
Growth Irradiance (uE/m2/s)

Figure 6.8

Figure 6. 9. Ratios of the principal *in vivo* absorbance peaks in *Synechococcus* sp. WH 5701 as a function of growth PFD. Peak ratios represented are 438/678 nm (□), 492/678 nm (+), 622/678 nm (◇), 492/438 nm (△) and 622/438 nm (×). Absorbance at 438 and 678 nm may be attributed to chlorophyll *a*, absorbance at 622 nm may be attributed to the PCB chromophore of phycocyanin.

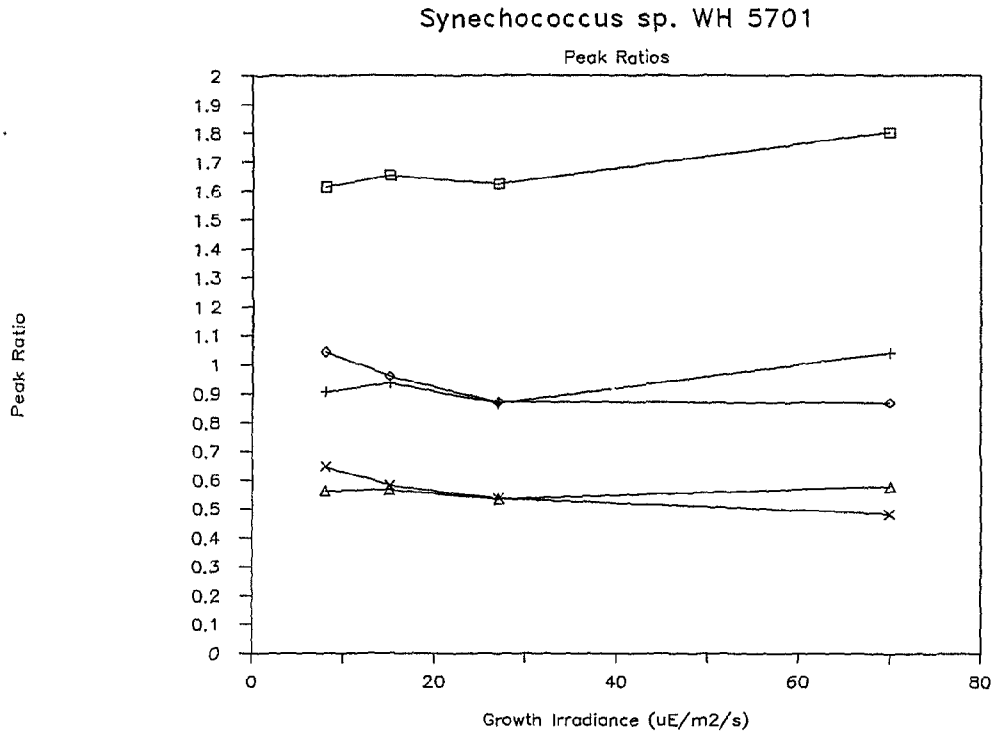
Synechococcus sp. WH 5701
Peak Ratios
Peak Ratio
2
1.9
1.8
1.7
1.6
1.5
1.4
1.3
1.2
1.1
1
0.9
0.8
0.7
0.6
0.5
0.4
0.3
0.2
0.1
0
0
20
40
60
80
Growth Irradiance (uE/m2/s)

Figure 6.9

Figure 6. 10. Ratios of the principal *in vivo* absorbance peaks in *Pavlova* sp. (clone NEP) as a function of growth PFD. Peak ratios represented are 436/672 nm (□), 598/672 nm (+) and 632/672 nm (◇). Absorbance at 436 and 672 nm may be attributed to chlorophyll *a*. Absorbance is at a minimum at 598 nm.

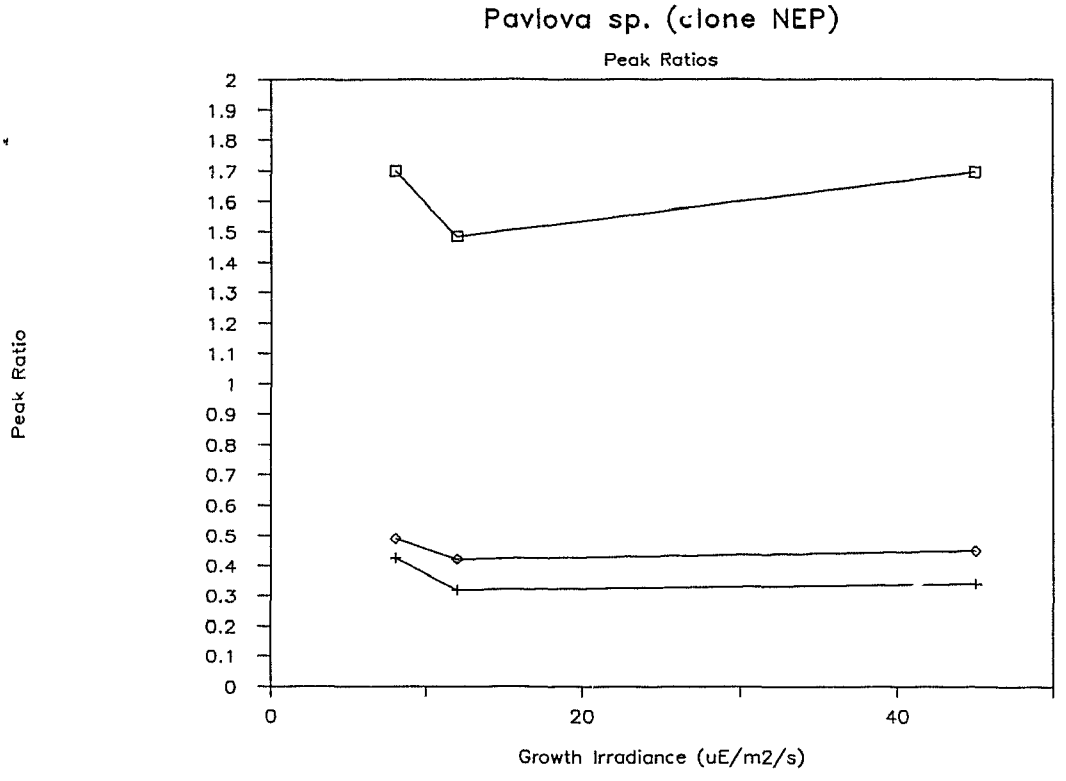
Pavlova sp. (clone NEP)
Peak Ratios
Peak Ratio
2
1.9
1.8
1.7
1.6
1.5
1.4
1.3
1.2
1.1
1
0.9
0.8
0.7
0.6
0.5
0.4
0.3
0.2
0.1
0
0
20
40
Growth Irradiance (uE/m2/s)

Figure 6. 10

Figure 6. 11. *In vivo* absorption spectra of particulate material collected on GF/F filters from waters of the eastern Canadian Arctic. In each panel the upper trace is the absorption by the total particulates and the lower trace corresponds to absorption by the particulates passing a 1 μm Nuclepore® filter. The intermediate trace represents the absorption spectra of particulates > 1 μm nominal diameter calculated by subtraction. The series illustrates the change in spectral shape with decreasing chlorophyll concentration. Geographical location (Station No.), depth and chlorophyll concentration (mg Chl m^{-3}) were:

(a) #4053: Stn. 116, 30 m, 11.2 mg Chl m^{-3},

(b) #8730: Stn. 73, 10 m, 8.3 mg Chl m^{-3},

(c) #4025, Stn. 113, 20 m, 2.94 mg Chl m^{-3},

(d) #4071, Stn. 124, 15 m, 3.0 mg Chl m^{-3},

(e) #4059, Stn. 116, 40 m, 0.53 mg Chl m^{-3},

(f) #4052, Stn. 116, 10 m, 0.16 mg Chl m^{-3}.

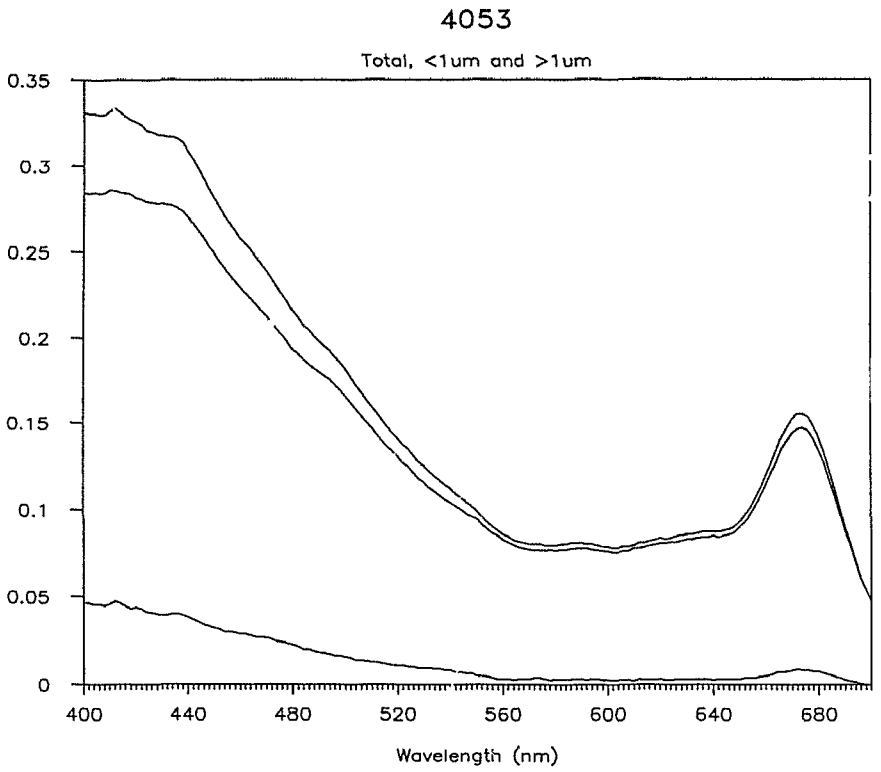
4053
Total, <1um and >1um
0.35
0.3
0.25
0.2
0.15
0.1
0.05
0
400
440
480
520
560
600
640
680
Wavelength (nm)

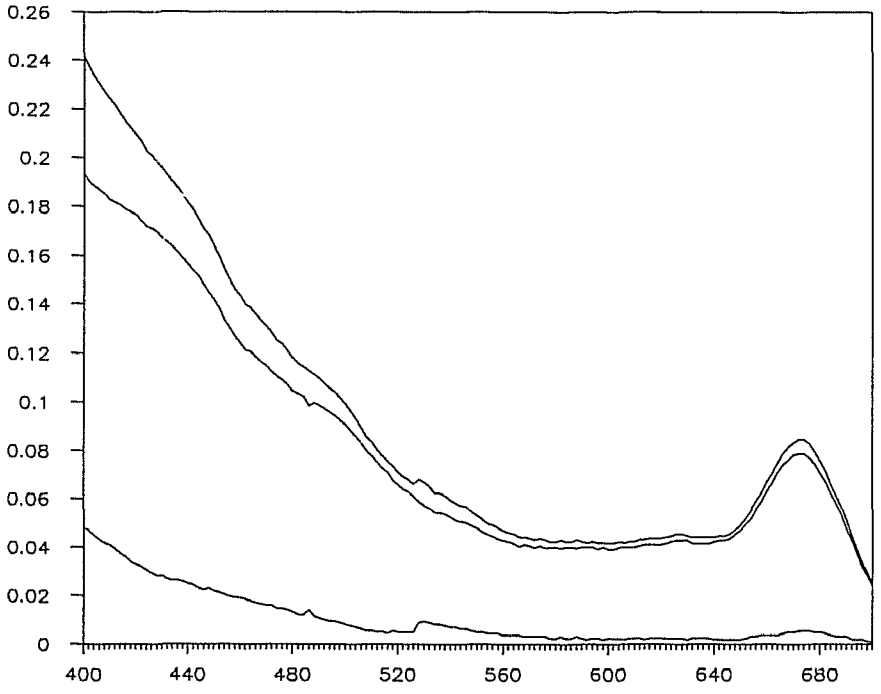
0.26
0.24
0.22
0.2
0.18
0.16
0.14
0.12
0.1
0.08
0.06
0.04
0.02
0
400
440
480
520
560
600
640
680

Figure 6. 11

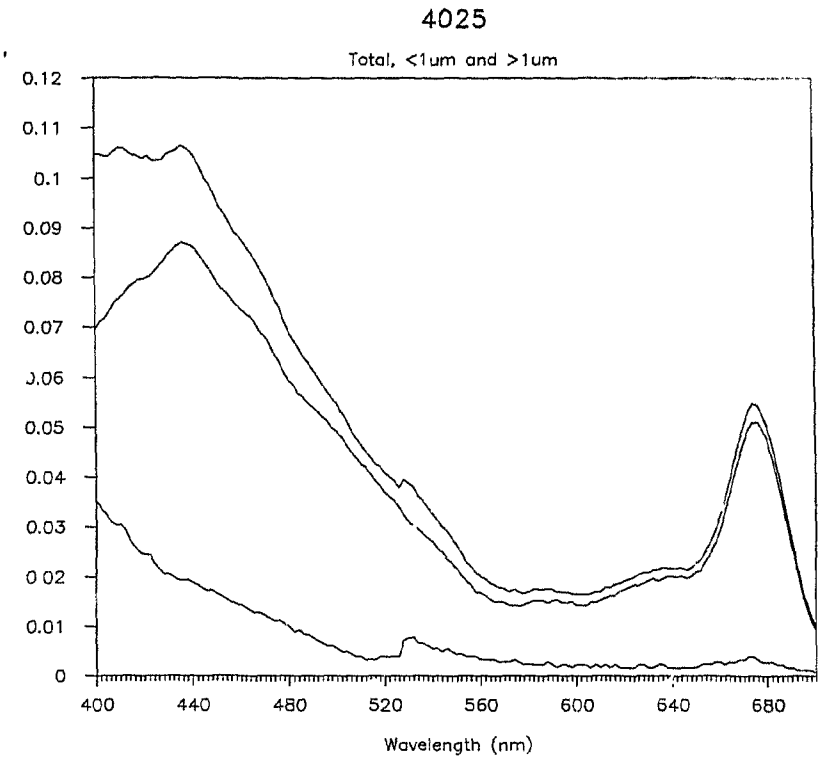

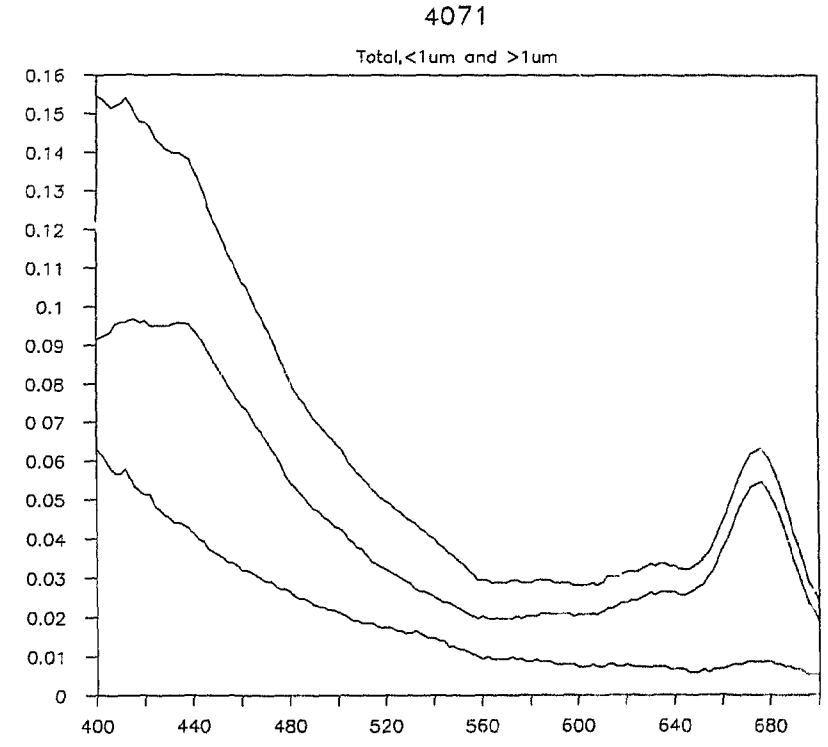

Figure 6. 11 (contd.)

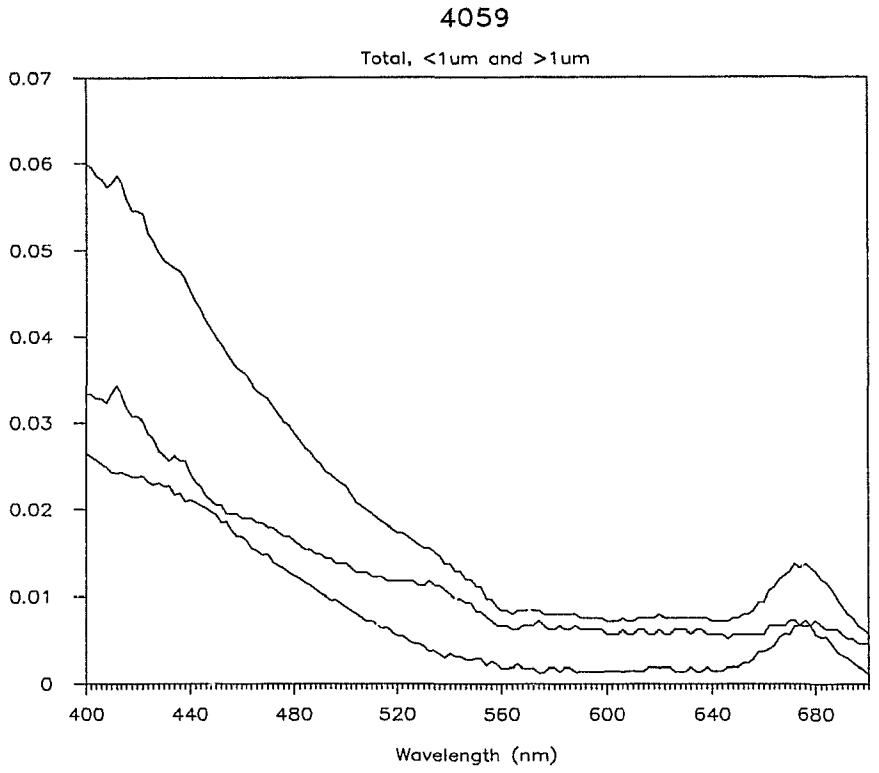

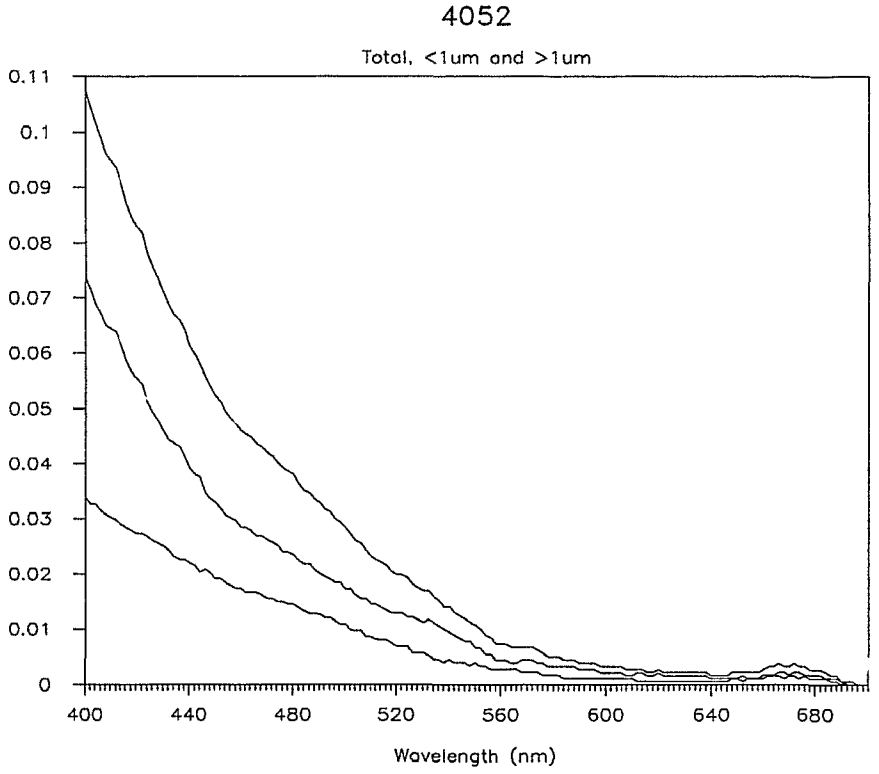

Figure 6. 11 (contd.)

Figure 6. 12. *In vivo* absorption spectra of particulate material collected on GF/F filters from the chlorophyll maximum at Stations 17 and 23 in the eastern North Atlantic Ocean (see Figure 4.3. for geographical location).

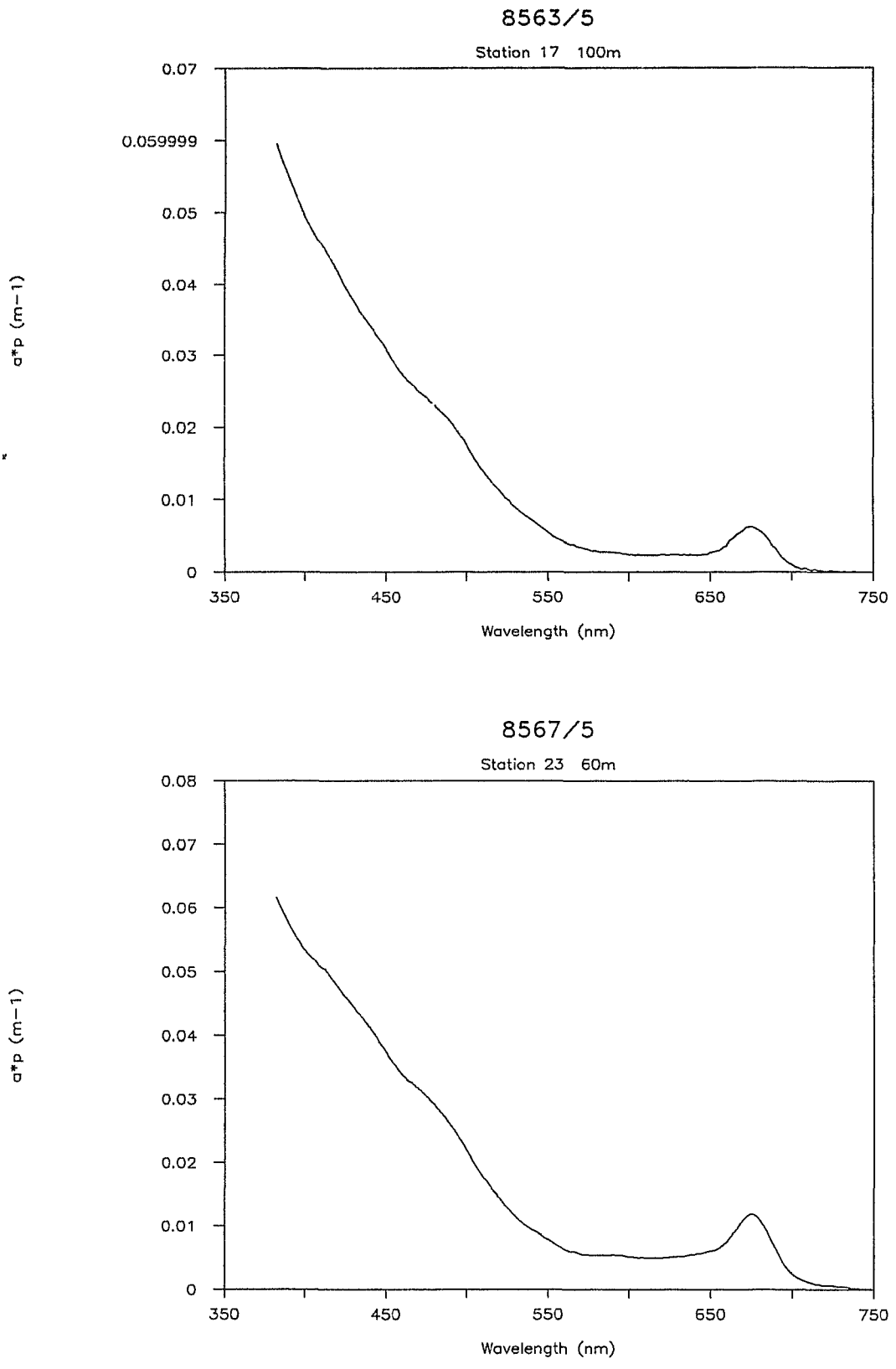
8563/5
Station 17 100m
0.07
0.059999
0.05
0.04
0.03
0.02
0.01
0
a*p (m-1)
350
450
550
650
750
Wavelength (nm)
8567/5
Station 23 60m
0.08
0.07
0.06
0.05
0.04
0.03
0.02
0.01
0
a*p (m-1)
350
450
550
650
750
Wavelength (nm)

Figure 6. 12

Figure 6. 13. *In vivo* absorption spectra of particulate material collected on GF/F filters from two depths (80 m and 5 m) at Station 21 in the eastern North Atlantic Ocean.

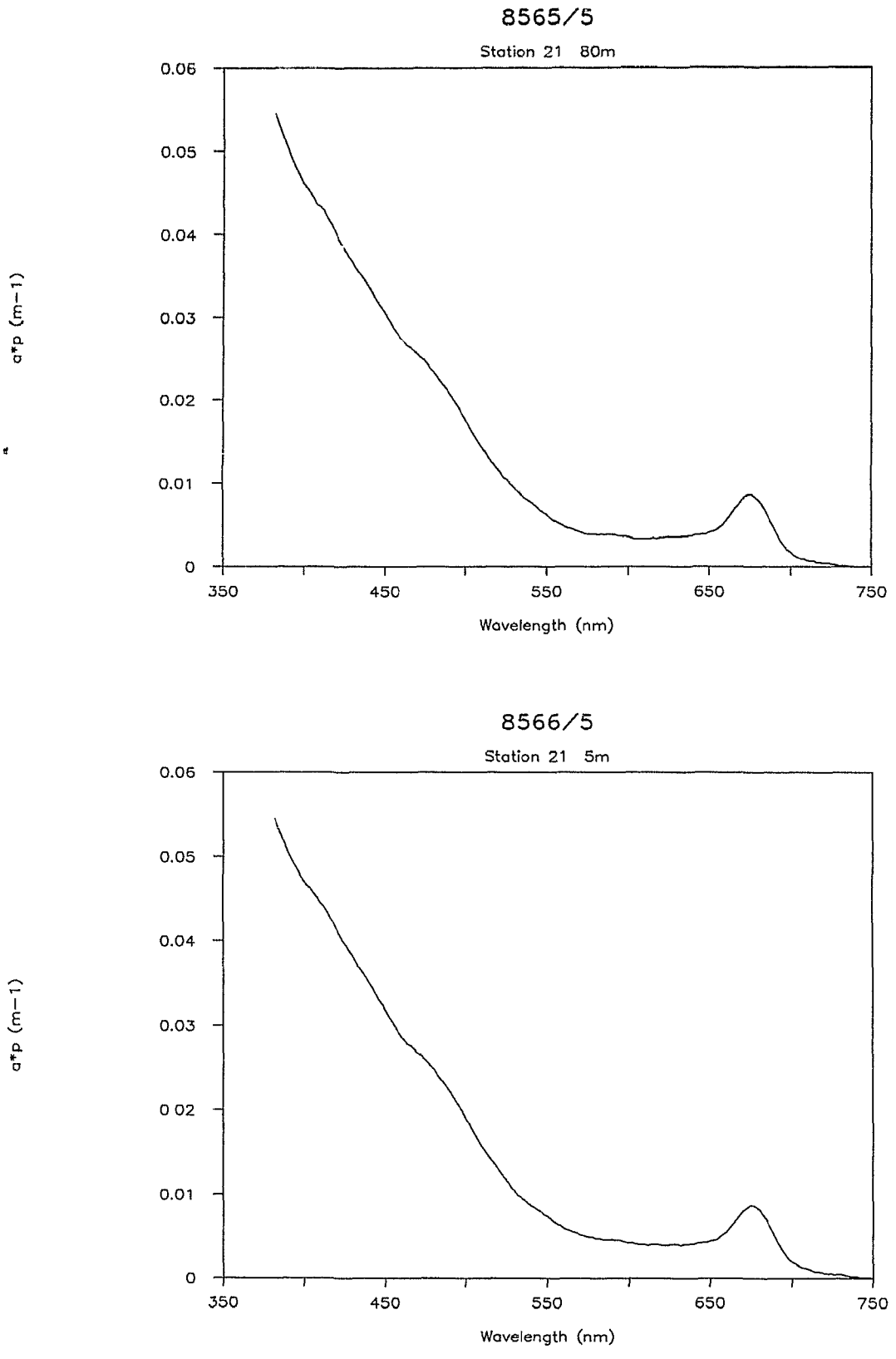
8565/5
Station 21 80m
0.06
0.05
0.04
0.03
0.02
0.01
0
a*p (m-1)
350
450
550
650
750
Wavelength (nm)
8566/5
Station 21 5m
0.06
0.05
0.04
0.03
0 02
0.01
0
a*p (m-1)
350
450
550
650
750
Wavelength (nm)

Figure 6. 13

Figure 6. 14. *In vivo* absorption spectra of total particulate material and particulate material passing a 3 μm Nuclepore® filter at Station 15 (100 m depth) in the eastern North Atlantic Ocean.

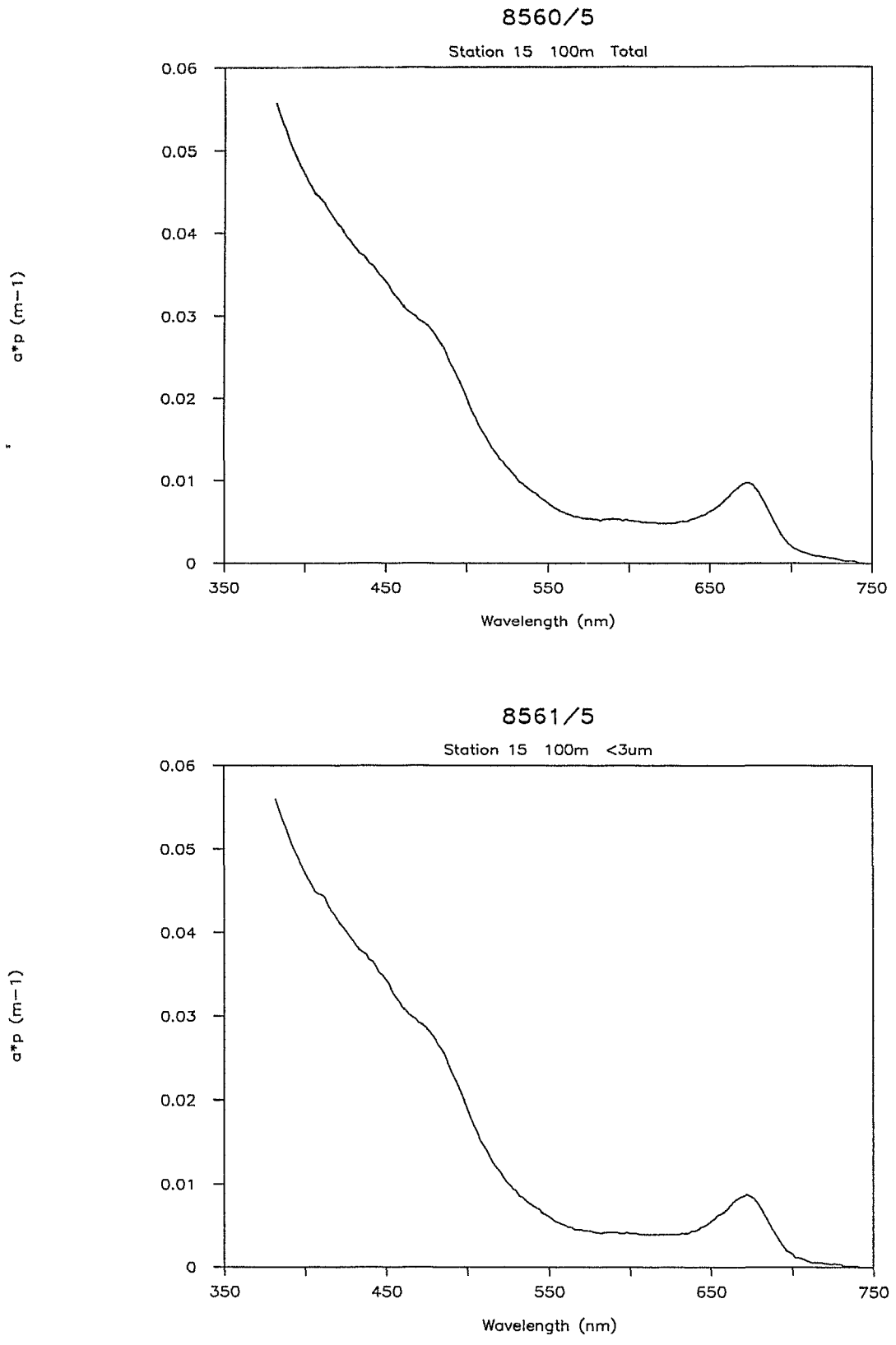
8560/5
Station 15 100m Total
a*p (m-1)
0.06
0.05
0.04
0.03
0.02
0.01
0
350
450
550
650
750
Wavelength (nm)
8561/5
Station 15 100m <3um
a*p (m-1)
0.06
0.05
0.04
0.03
0.02
0.01
0
350
450
550
650
750
Wavelength (nm)

Figure 6. 14

Figure 6. 15. Estimates of the diffuse attenuation coefficient (a^*_p; m^{-1}) and the chlorophyll-specific attenuation cross-section (a^*_{chl}; m^2 mg Chl^{-1}) as a function of the chlorophyll concentration (mg Chl m^{-3}) in samples collected from the eastern Canadian Arctic. Since a constant volume of seawater was filtered for each sample, the chlorophyll concentration is a measure of the optical density of the filter.

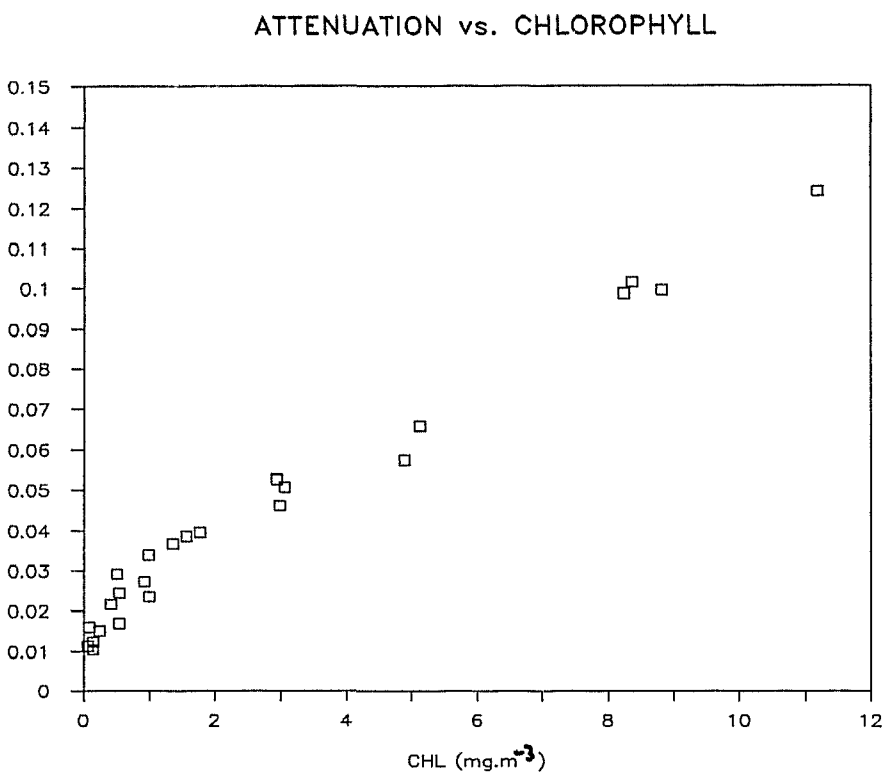
ATTENUATION vs. CHLOROPHYLL
0.15
0.14
0.13
0.12
0.11
0.1
0.09
0.08
0.07
0.06
0.05
0.04
0.03
0.02
0.01
0
0
2
4
6
8
10
12
CHL (mg.m-3)

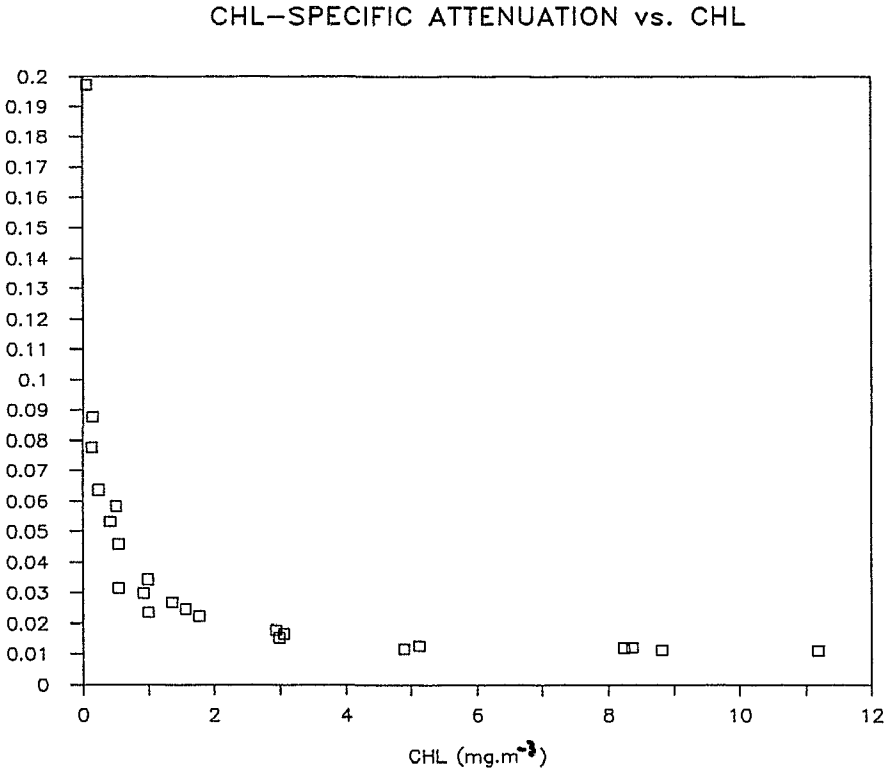
CHL–SPECIFIC ATTENUATION vs. CHL
0.2
0.19
0.18
0.17
0.16
0.15
0.14
0.13
0.12
0.11
0.1
0.09
0.08
0.07
0.06
0.05
0.04
0.03
0.02
0.01
0
0
2
4
6
8
10
12
CHL (mg.m-3)

Figure 6. 15

Figure 6. 16. Computed estimates of the chlorophyll-specific attenuation cross-section ($a^*_{chl}(\lambda)$; m^2 (mg Chl)$^{-1}$) for each 25 nm waveband from 400 nm to 675 nm. Values were obtained by non-linear fitting of the hyperbolic function [Eq. 6.1] to the relationship between $a^*_p(\lambda)$ and chlorophyll concentration for all samples collected from waters of the eastern Canadian Arctic. Error bars represent ± 1 standard deviation.

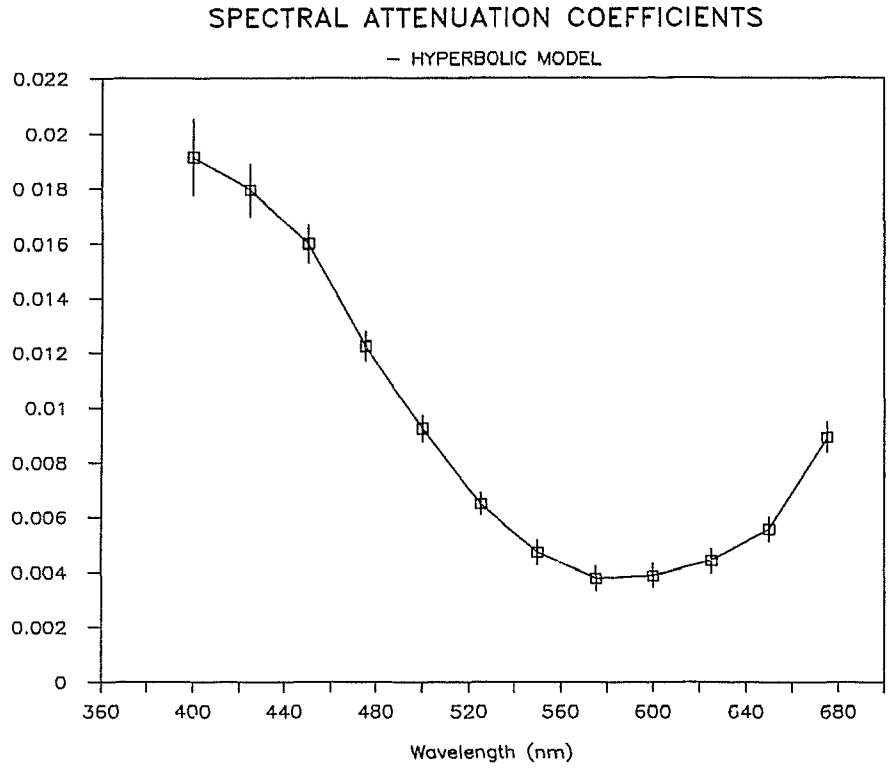
SPECTRAL ATTENUATION COEFFICIENTS
– HYPERBOLIC MODEL
0.022
0.02
0 018
0.016
0.014
0.012
0.01
0.008
0.006
0.004
0.002
0
360
400
440
480
520
560
600
640
680
Wavelength (nm)

Figure 6. 16

Figure 6. 17. The effect of filtration volume upon the estimates of the attenuation coefficient ($a^*_p(\lambda)$; m^{-1}) and the chlorophyll-specific attenuation cross-section ($a^*_{chl}(\lambda)$; m^2 mg Chl^{-1}) in two samples from the eastern North Atlantic Ocean. The upper panels are for $\lambda = 676$ nm, the lower panels are for $\lambda = 476$ nm. Samples are from Stations 17 (# 8563) and 23 (# 8567).

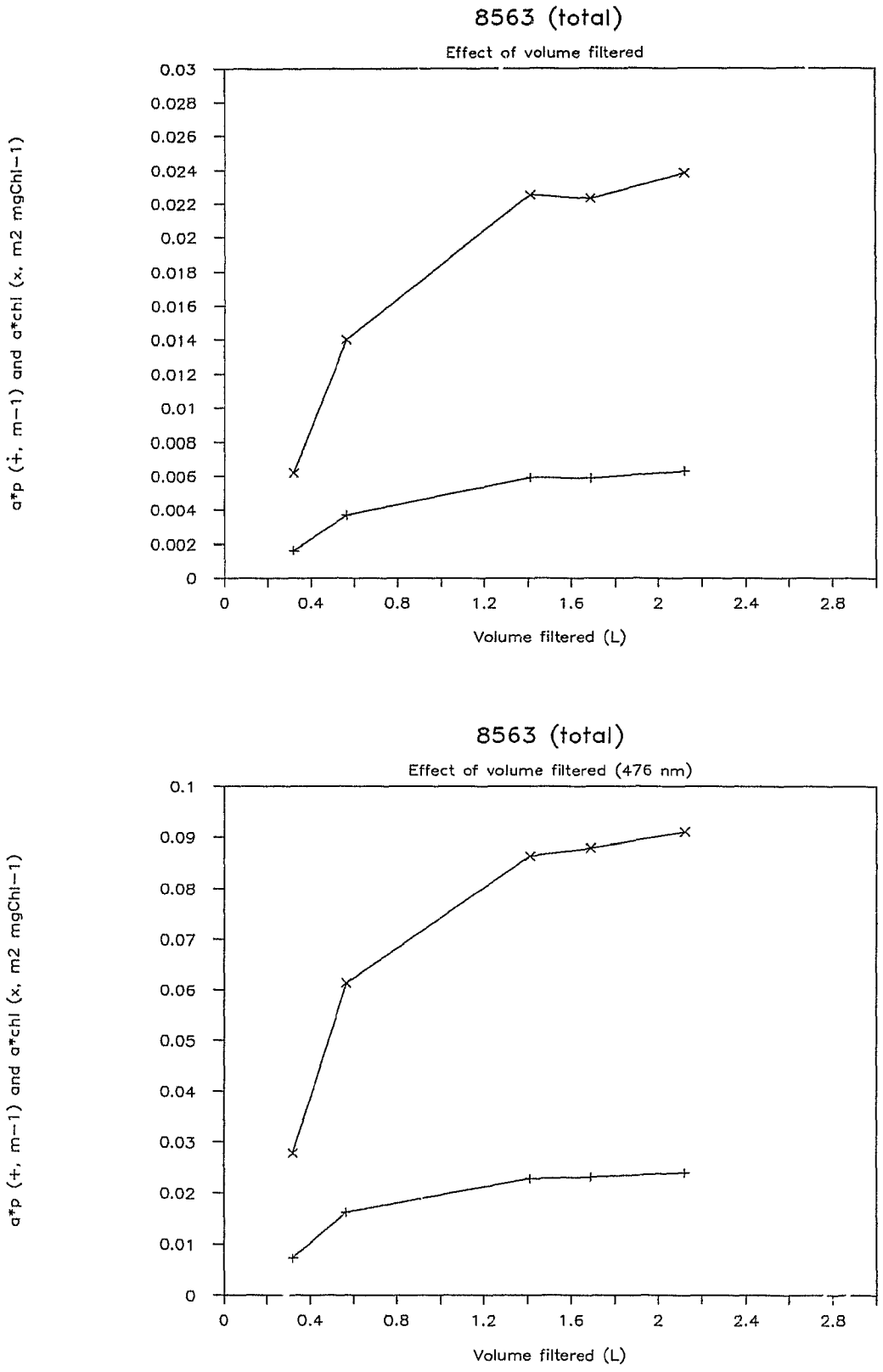
8563 (total)
Effect of volume filtered
a*p (+, m-1) and a*chl (x, m2 mgChl-1)
0.03
0.028
0.026
0.024
0.022
0.02
0.018
0.016
0.014
0.012
0.01
0.008
0.006
0.004
0.002
0
0
0.4
0.8
1.2
1.6
2
2.4
2.8
Volume filtered (L)
8563 (total)
Effect of volume filtered (476 nm)
a*p (+, m-1) and a*chl (x, m2 mgChl-1)
0.1
0.09
0.08
0.07
0.06
0.05
0.04
0.03
0.02
0.01
0
0
0.4
0.8
1.2
1.6
2
2.4
2.8
Volume filtered (L)

Figure 6. 17

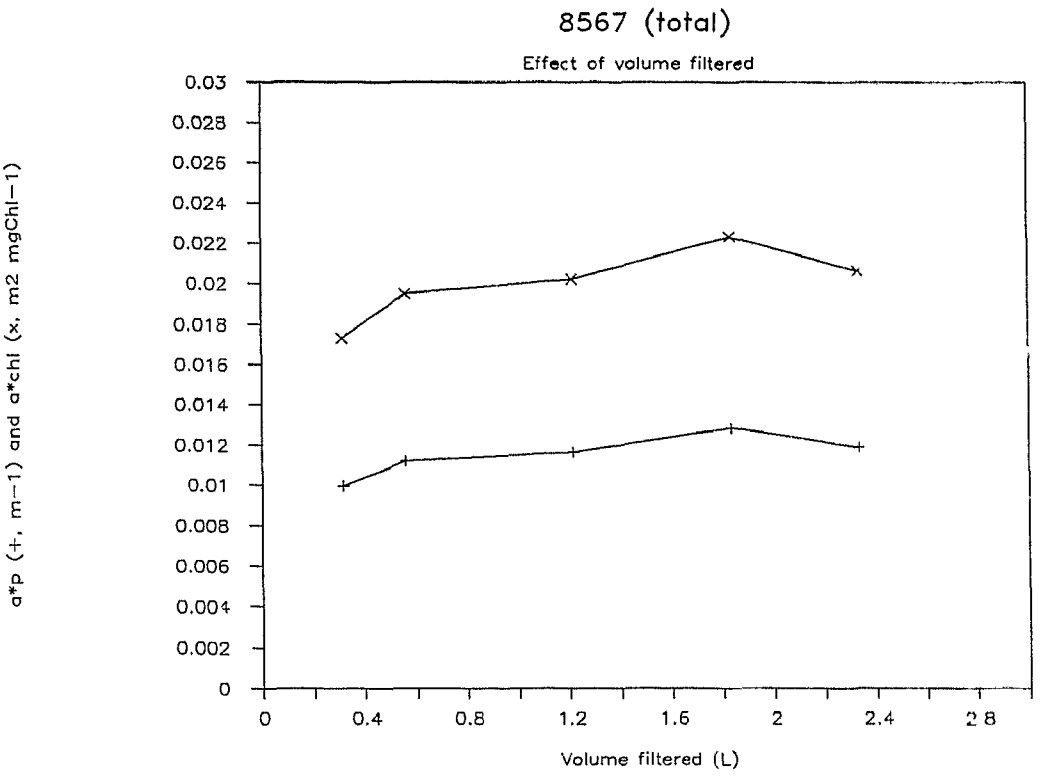

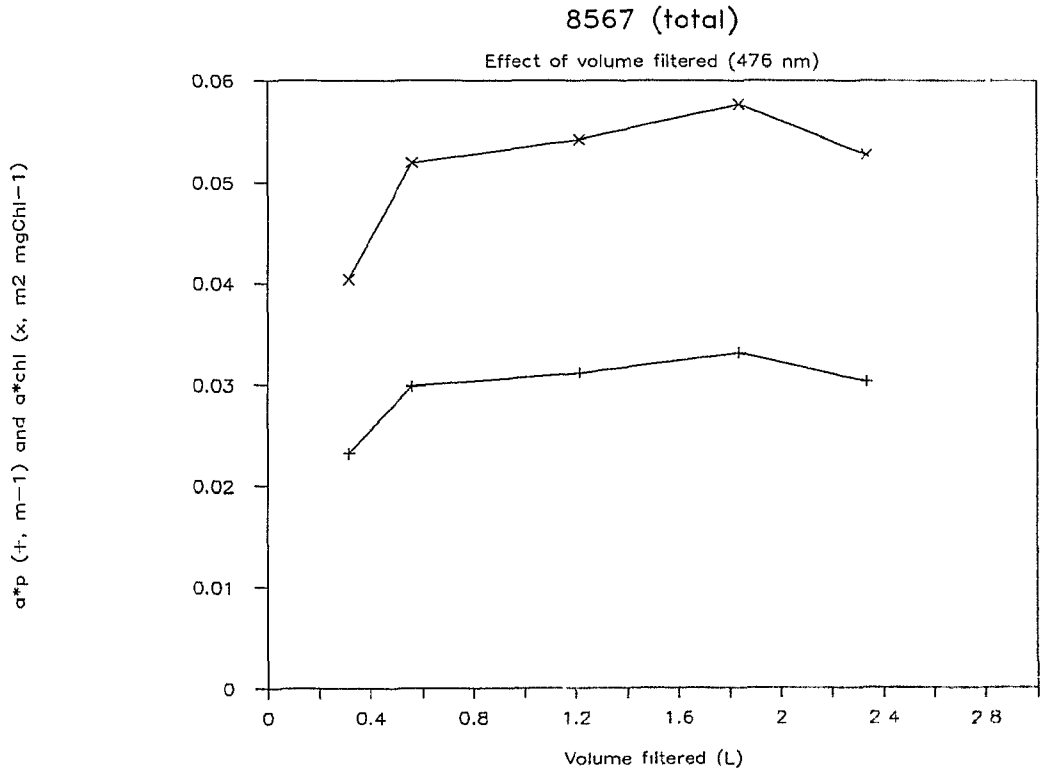

Figure 6. 17 (contd.)

Figure 6. 18. The effect of filtration volume upon the estimates of the attenuation coefficient ($a^*_p(\lambda)$; m^{-1}) and the chlorophyll-specific attenuation cross-section ($a^*_{chl}(\lambda)$; m^2 (mg Chl)$^{-1}$) in samples two depths at the same location (Stn. 21) in the eastern North Atlantic Ocean. The upper panels are for λ = 676 nm, the lower panels are for λ = 476 nm. Samples were collected from depths of 5 m (# 8566) and 80 m (# 8565).

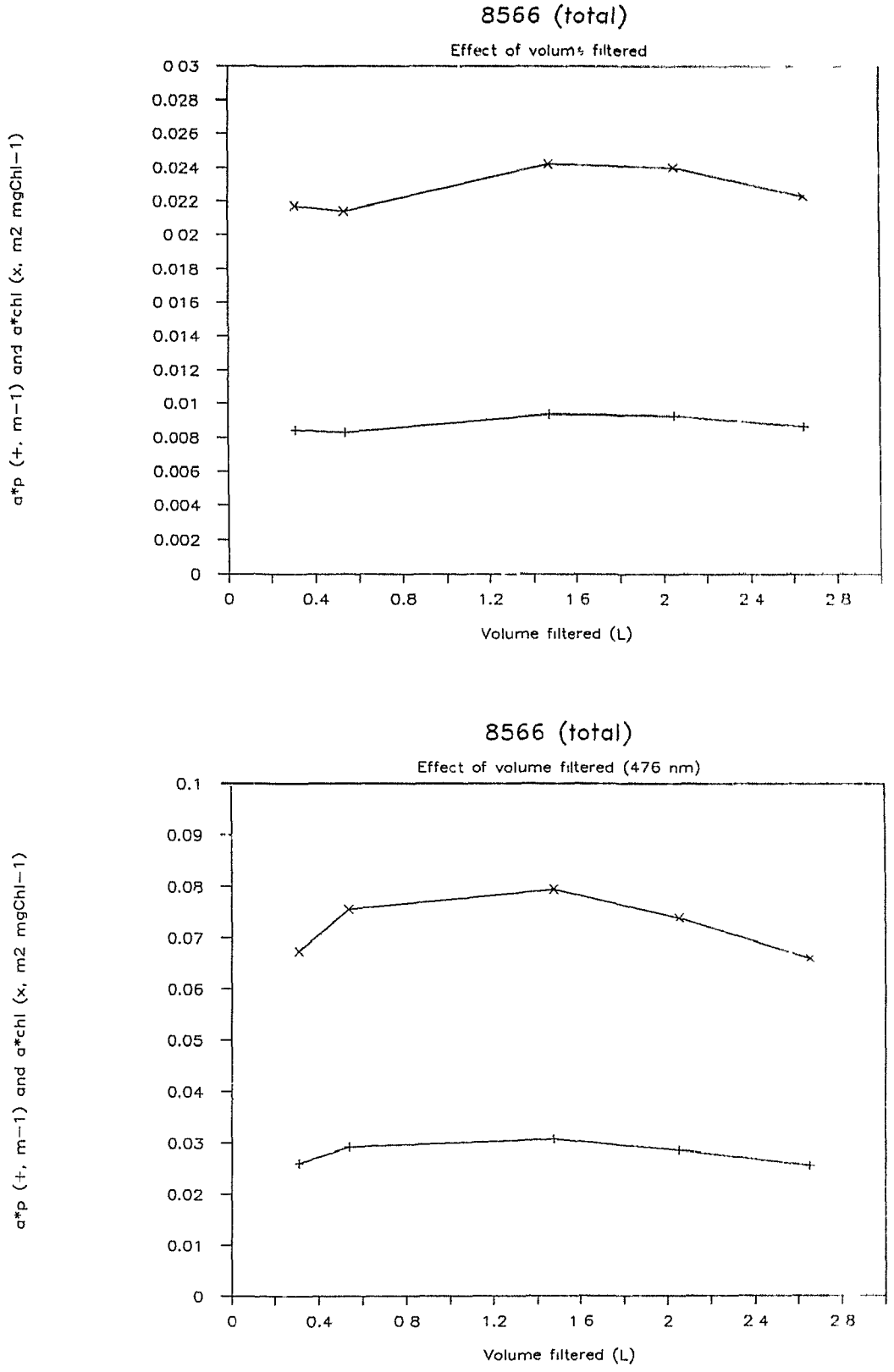
8566 (total)
Effect of volume filtered
a*p (+, m−1) and a*chl (x, m2 mgChl−1)
0.03
0.028
0.026
0.024
0.022
0.02
0.018
0.016
0.014
0.012
0.01
0.008
0.006
0.004
0.002
0
0
0.4
0.8
1.2
1.6
2
2.4
2.8
Volume filtered (L)
8566 (total)
Effect of volume filtered (476 nm)
a*p (+, m−1) and a*chl (x, m2 mgChl−1)
0.1
0.09
0.08
0.07
0.06
0.05
0.04
0.03
0.02
0.01
0
0
0.4
0.8
1.2
1.6
2
2.4
2.8
Volume filtered (L)

Figure 6. 18

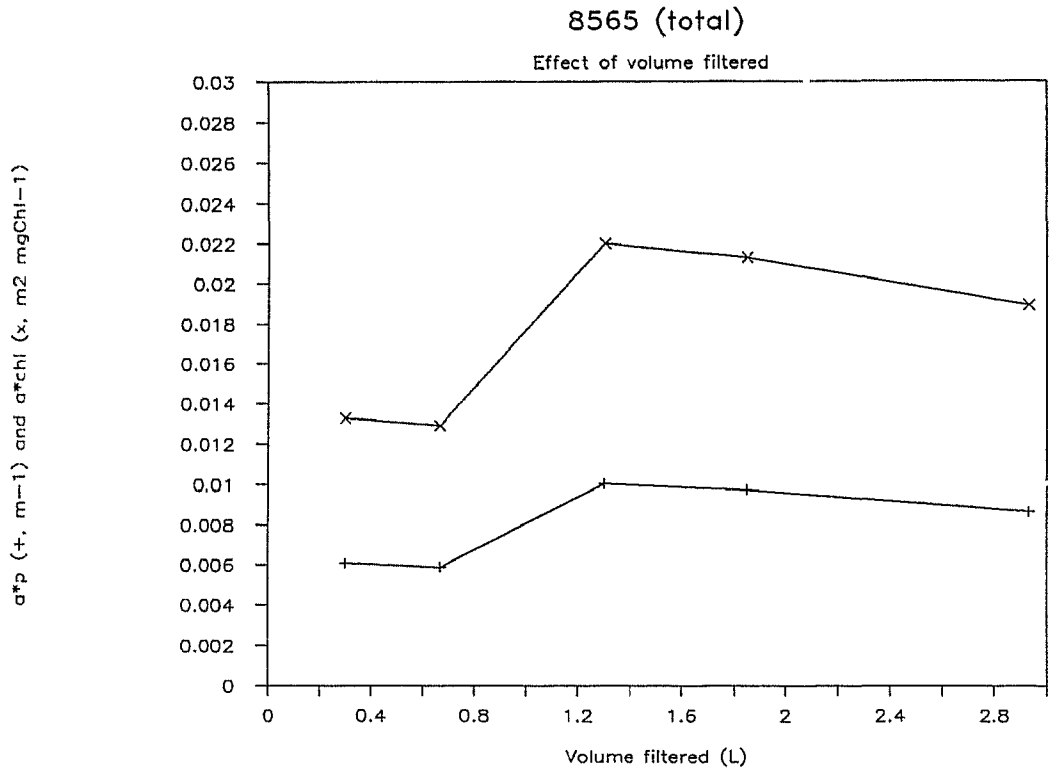

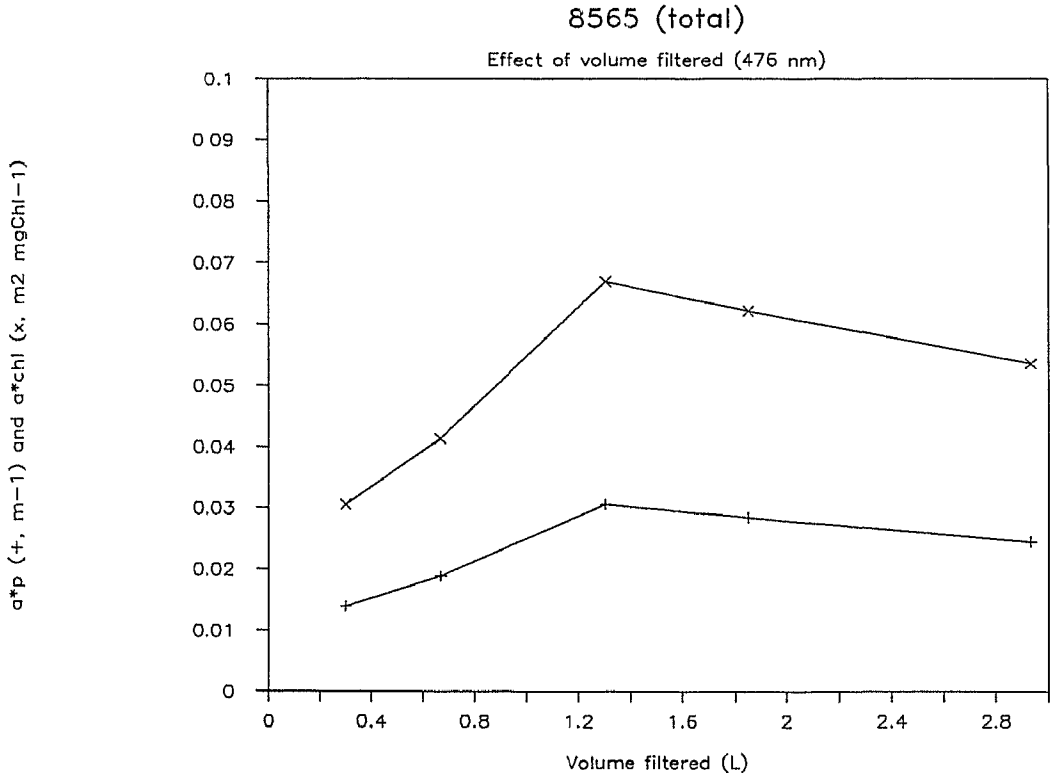

Figure 6. 18 (contd.)

Figure 6. 19. The effect of filtration volume upon the estimates of the attenuation coefficient ($a^*_p(\lambda)$; m^{-1}) and the chlorophyll-specific attenuation cross-section ($a^*_{chl}(\lambda)$; m^2 (mg Chl)$^{-1}$) of total particulates (# 8560) and particulates < 3 μm (# 8561) at Stn. 15 (100 m depth) in the eastern North Atlantic Ocean. The upper panels are for λ = 676 nm, the lower panels are for λ = 476 nm.

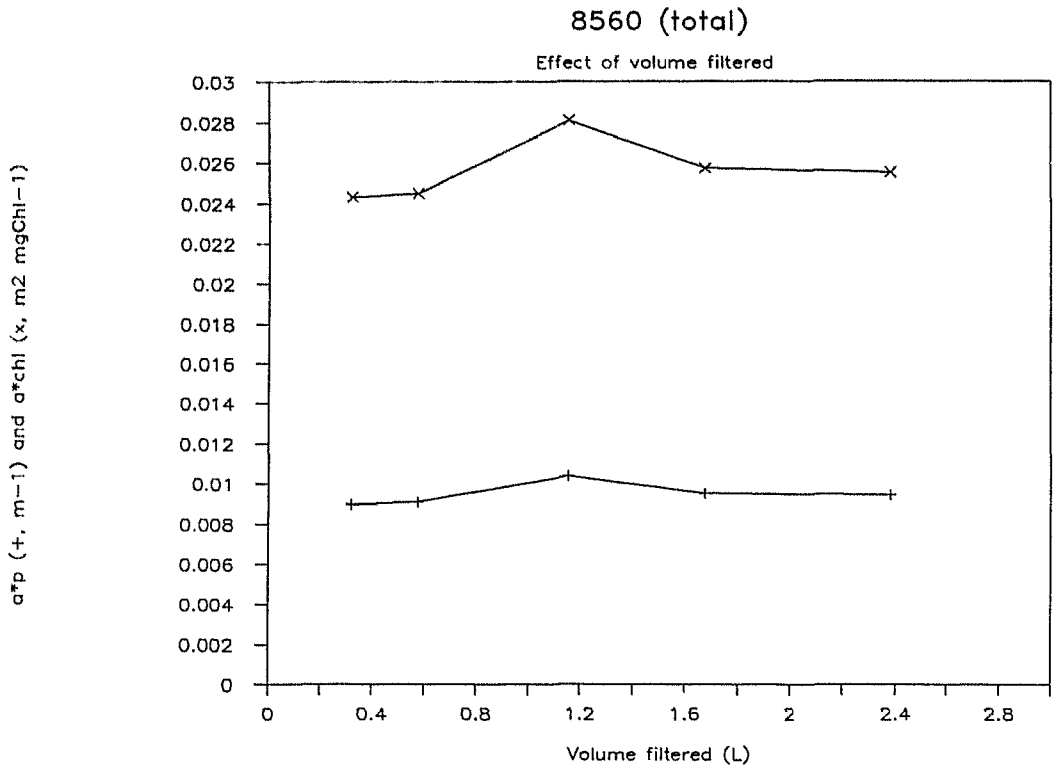
8560 (total)
Effect of volume filtered
a*p (+, m-1) and a*chl (x, m2 mgChl-1)
0.03
0.028
0.026
0.024
0.022
0.02
0.018
0.016
0.014
0.012
0.01
0.008
0.006
0.004
0.002
0
0
0.4
0.8
1.2
1.6
2
2.4
2.8
Volume filtered (L)

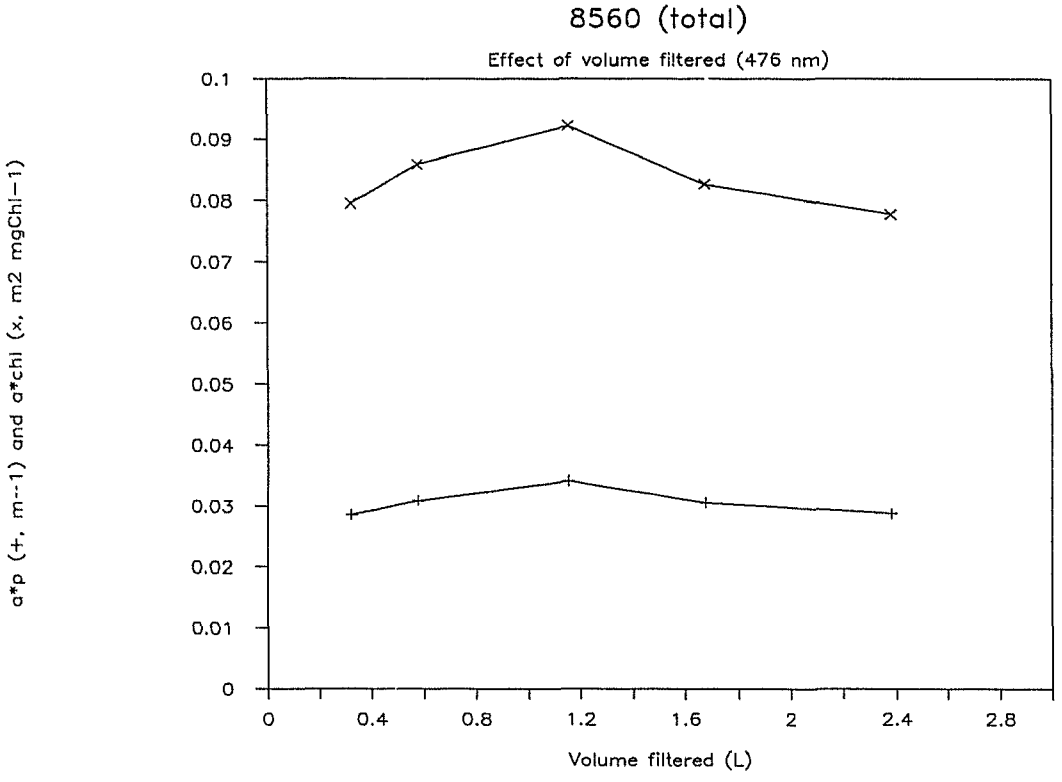
8560 (total)
Effect of volume filtered (476 nm)
a*p (+, m-1) and a*chl (x, m2 mgChl-1)
0.1
0.09
0.08
0.07
0.06
0.05
0.04
0.03
0.02
0.01
0
0
0.4
0.8
1.2
1.6
2
2.4
2.8
Volume filtered (L)

Figure 6. 19

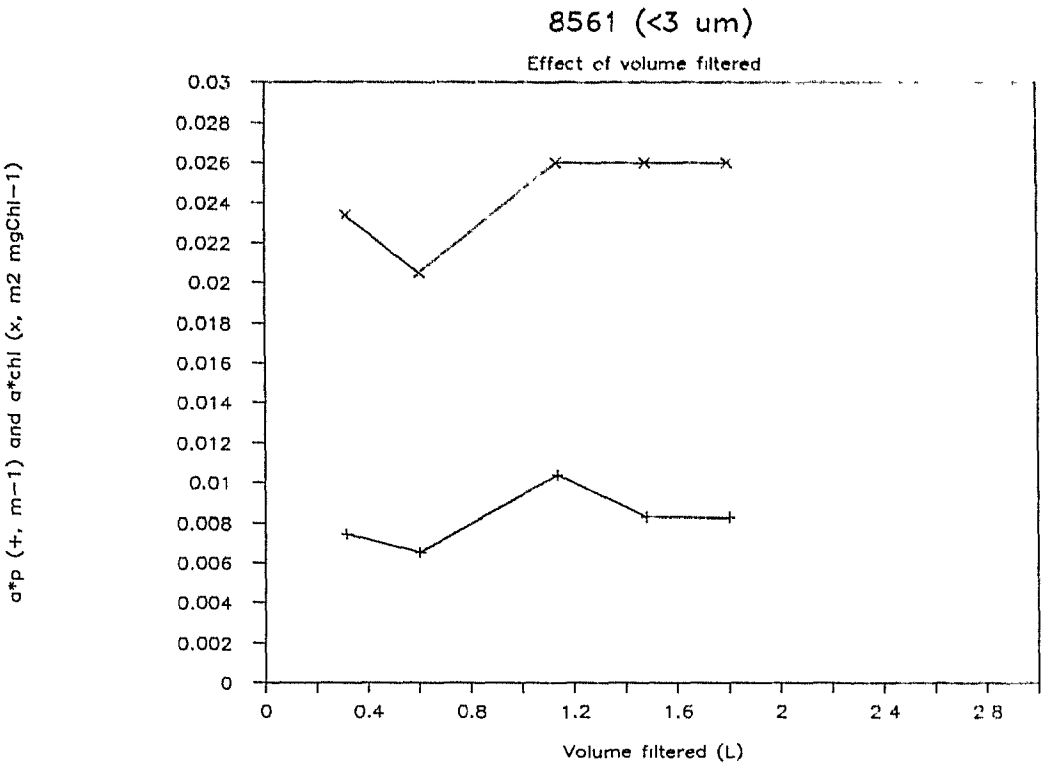

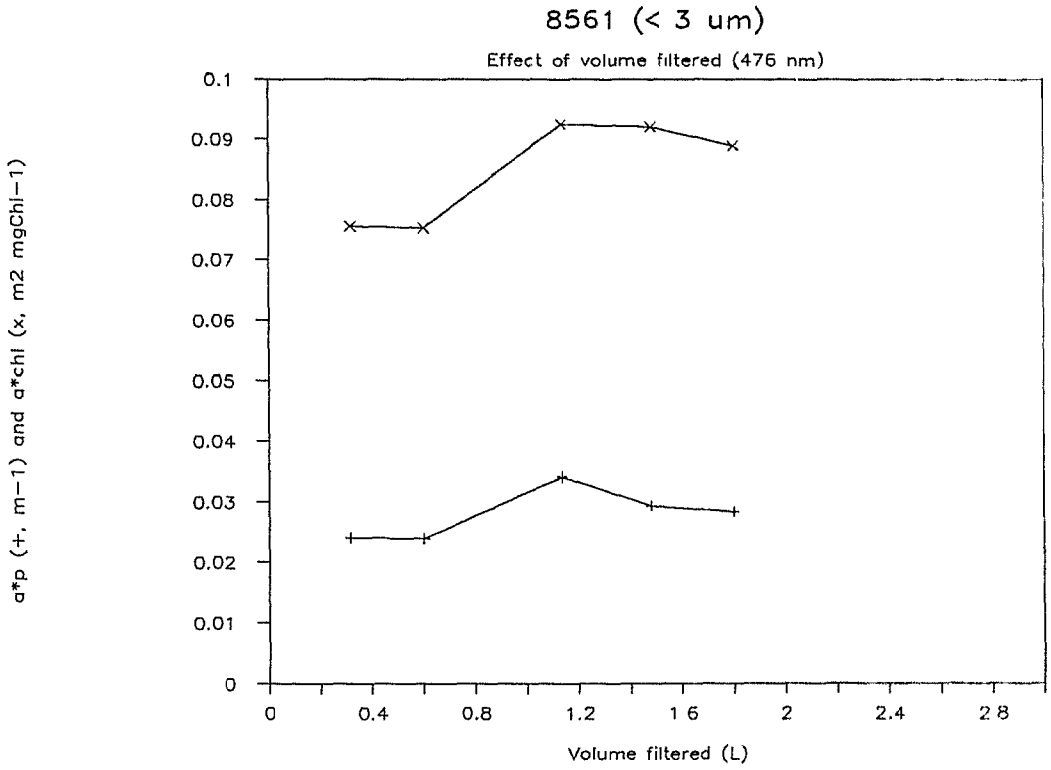

Figure 6. 19 (contd.)

Figure 7. 1. Photosynthetic action spectra ($\alpha^B(\lambda)$) of *Synechococcus* sp. WH 5701 grown at different PFDs. Growth PFDs were 8 μmol m^{-2} s^{-1} (SY 9148), 15 μmol m^{-2} s^{-1} (SY 9156), 27 μmol m^{-2} s^{-1} (SY 9160) and 70 μmol m^{-2} s^{-1} (SY 9152). Values of $\alpha^B(\lambda)$ were calculated from the initial slope of the P-I curve by linear regression, error bars correspond to ± the 95% confidence interval associated with the estimate of the initial slope.

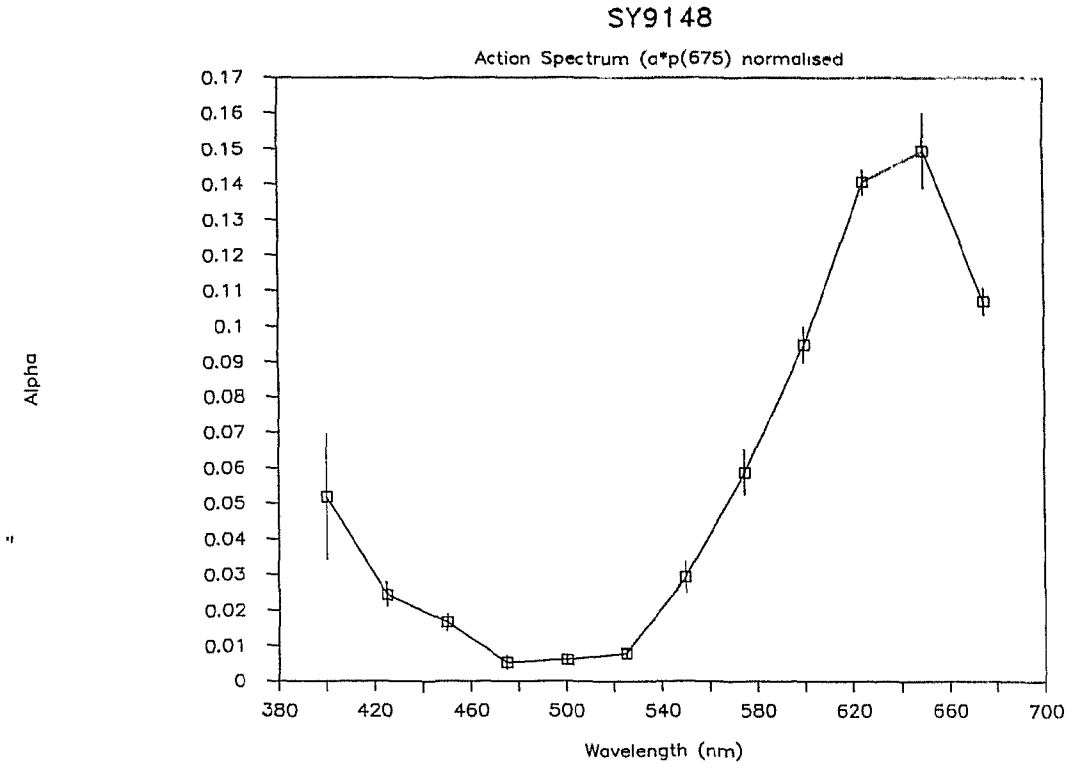
SY9148
Action Spectrum (a*p(675) normalised
Alpha
0.17
0.16
0.15
0.14
0.13
0.12
0.11
0.1
0.09
0.08
0.07
0.06
0.05
0.04
0.03
0.02
0.01
0
380
420
460
500
540
580
620
660
700
Wavelength (nm)

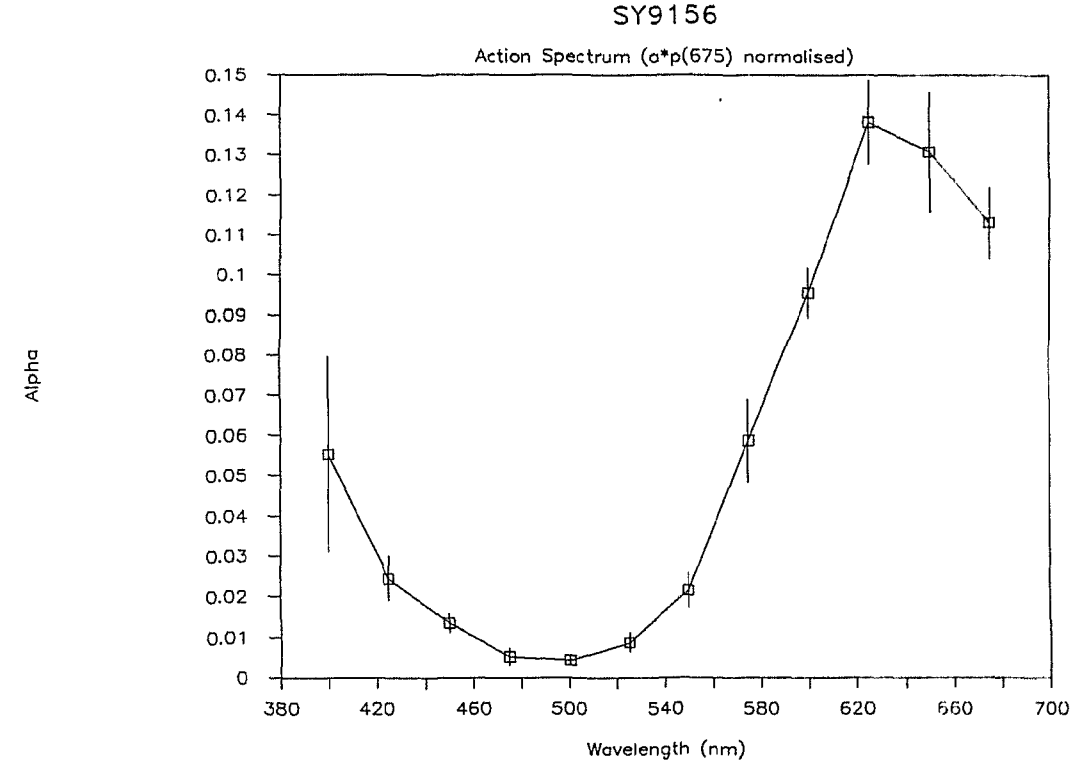
SY9156
Action Spectrum (a*p(675) normalised)
Alpha
0.15
0.14
0.13
0.12
0.11
0.1
0.09
0.08
0.07
0.06
0.05
0.04
0.03
0.02
0.01
0
380
420
460
500
540
580
620
660
700
Wavelength (nm)

Figure 7.1

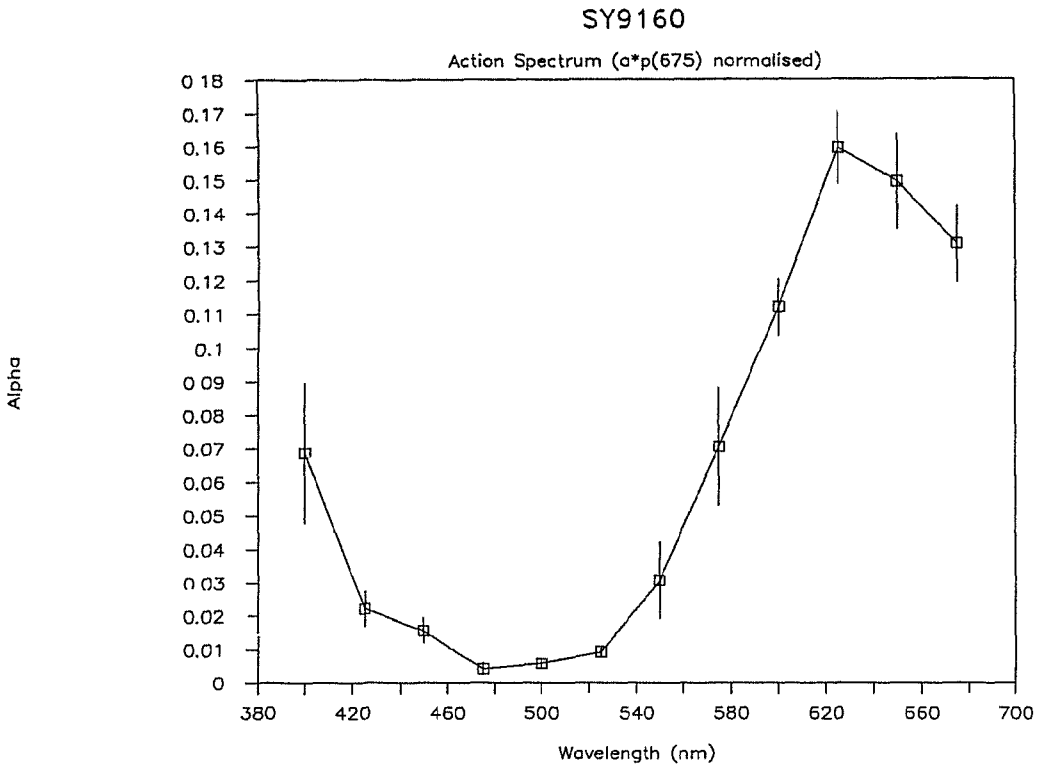

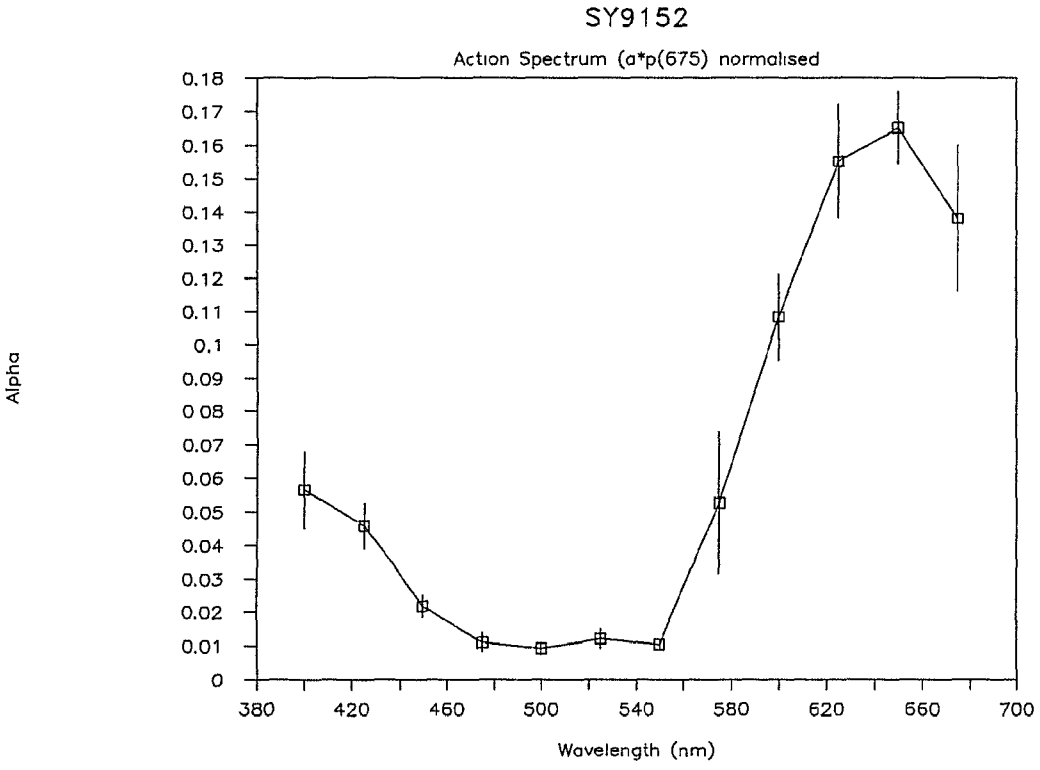

Figure 7. 1 (contd.)

Figure 7. 2. Photosynthetic action spectra ($\alpha^B(\lambda)$) of *Synechococcus* sp. WH 7803 grown at different PFDs. Growth PFDs were 17 μmol m^{-2} s^{-1} (DC 9124), 25 μmol m^{-2} s^{-1} (DC 9116) and 35 μmol m^{-2} s^{-1} (DC 9120). Values of $\alpha^B(\lambda)$ were calculated from the initial slope of the P-I curve by linear regression, error bars correspond to ± 95% confidence intervals associated with the estimate of the initial slope.

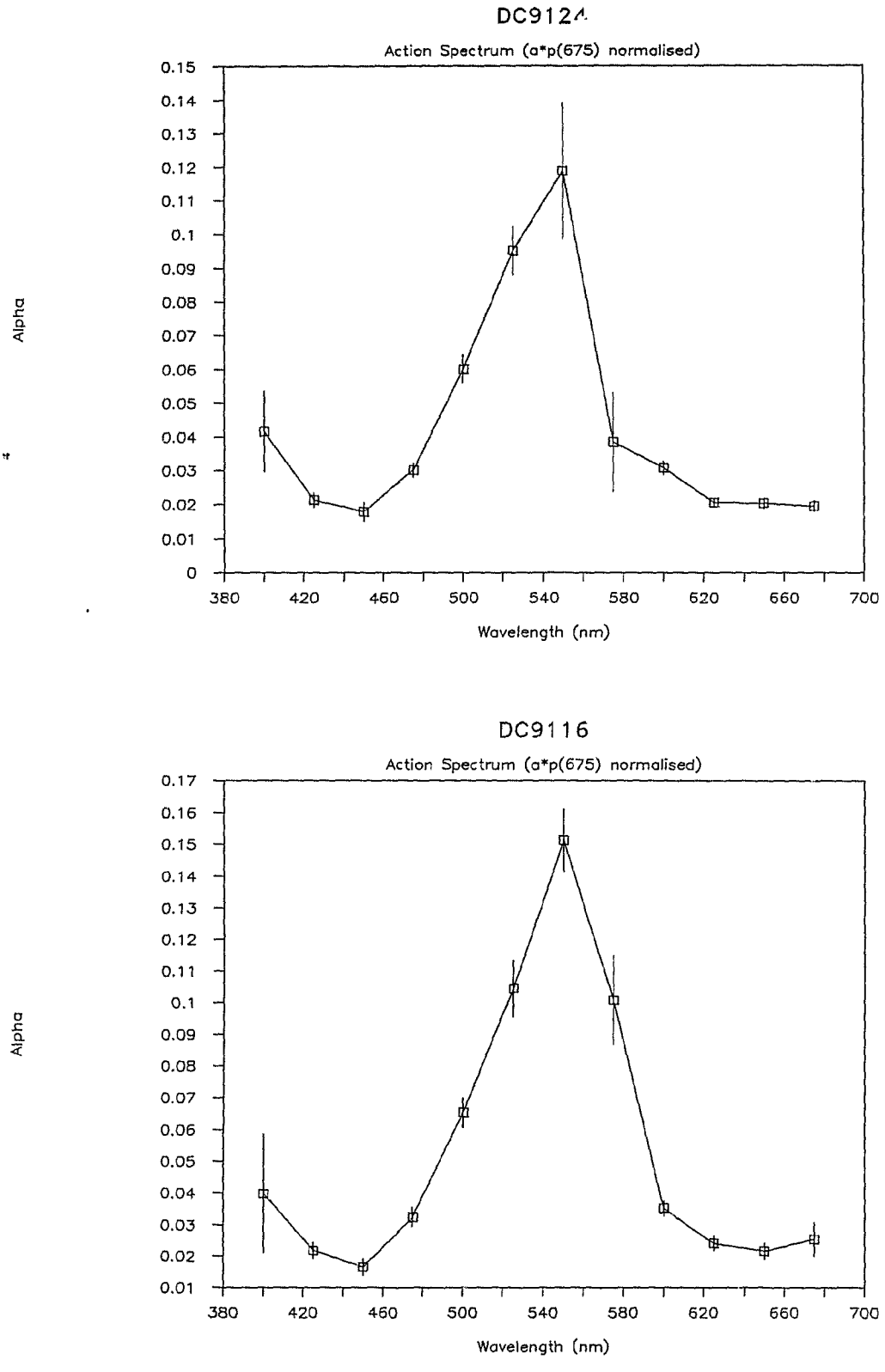
DC9124
Action Spectrum (a*p(675) normalised)
Alpha
0.15
0.14
0.13
0.12
0.11
0.1
0.09
0.08
0.07
0.06
0.05
0.04
0.03
0.02
0.01
0
380
420
460
500
540
580
620
660
700
Wavelength (nm)
DC9116
Action Spectrum (a*p(675) normalised)
Alpha
0.17
0.16
0.15
0.14
0.13
0.12
0.11
0.1
0.09
0.08
0.07
0.06
0.05
0.04
0.03
0.02
0.01
380
420
460
500
540
580
620
660
700
Wavelength (nm)

Figure 7.2

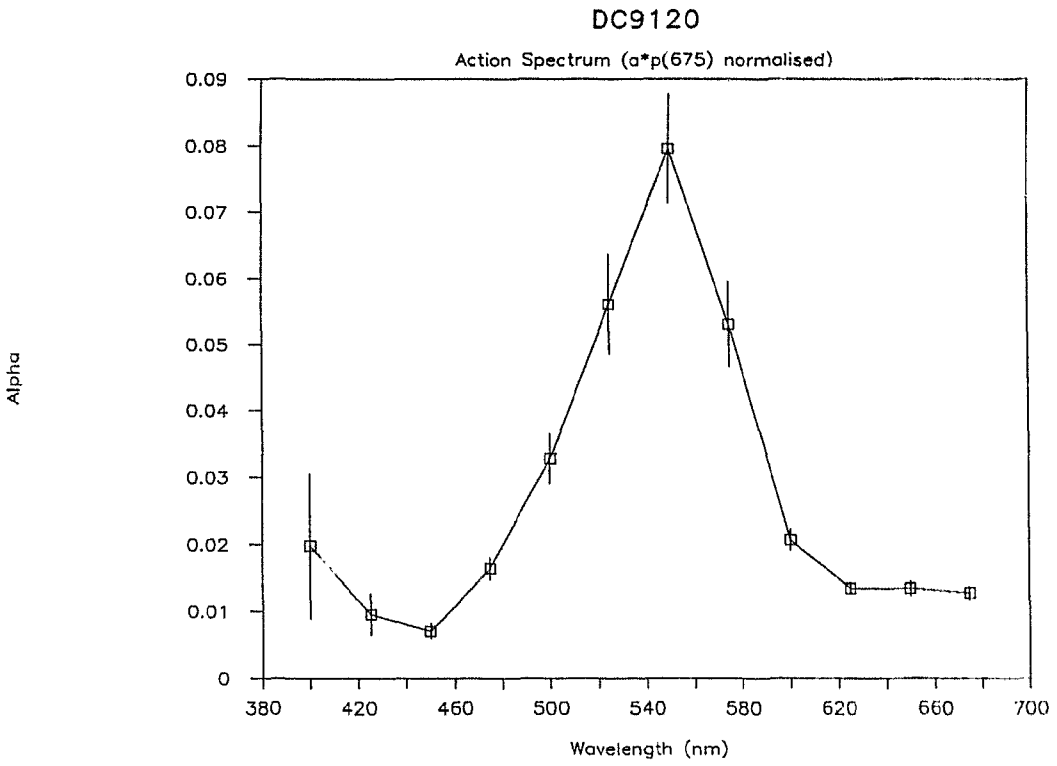

Figure 7. 2 (contd.)

Figure 7. 3. Photosynthetic action spectra ($\alpha^B(\lambda)$) of *Pavlova* sp. (clone NEP) grown at different PFDs. Growth PFDs were 8 μmol m^{-2} s^{-1} (PA 9140), 12 μmol m^{-2} s^{-1} (PA 9136) and 45 μmol m^{-2} s^{-1} (PA 9132). Values of $\alpha^B(\lambda)$ were calculated from the initial slope of the P-I curve by linear regression, error bars correspond to ± the 95% confidence interval associated with the estimate of the initial slope.

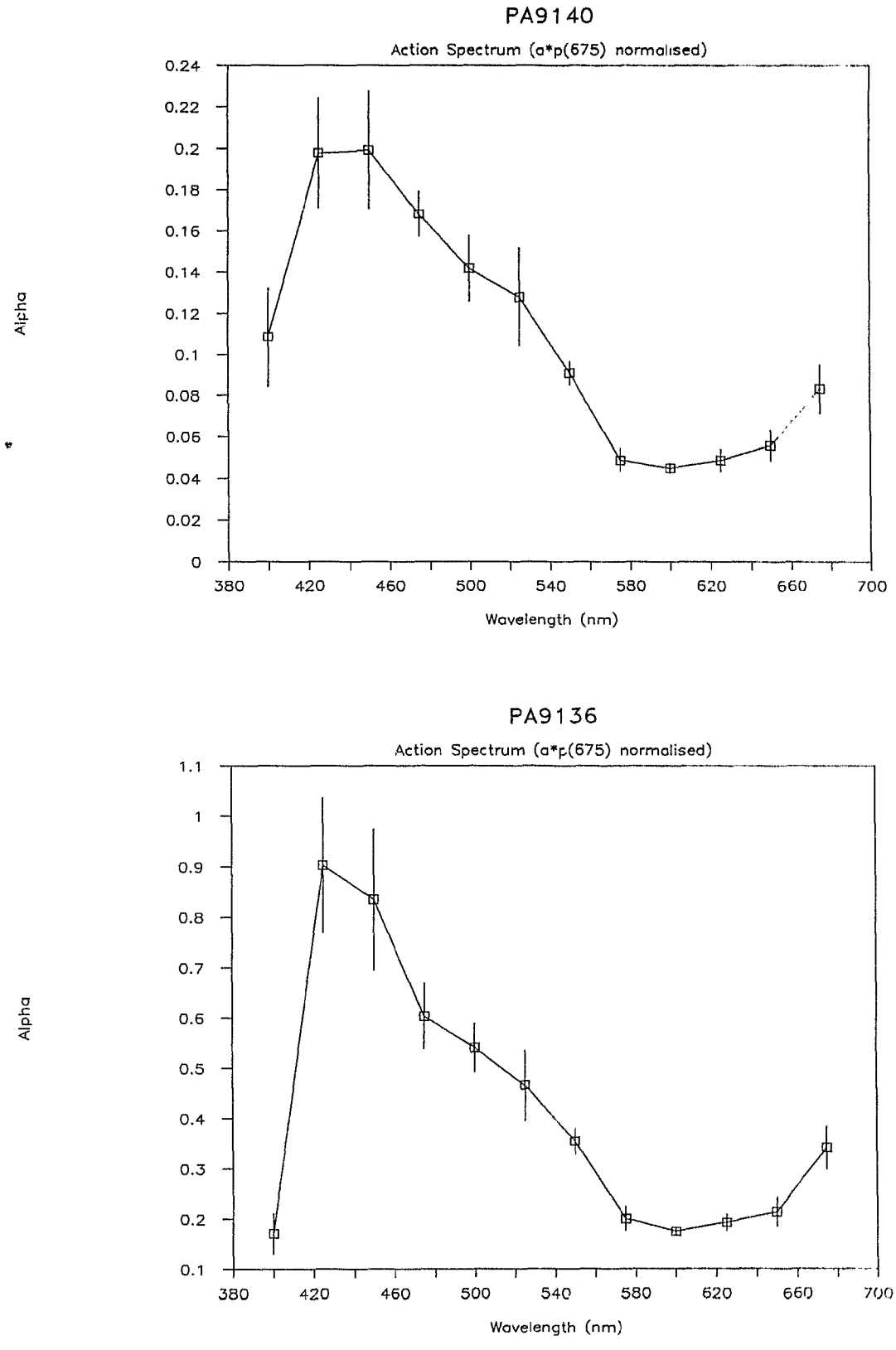
PA9140
Action Spectrum (a*p(675) normalised)
Alpha
0.24
0.22
0.2
0.18
0.16
0.14
0.12
0.1
0.08
0.06
0.04
0.02
0
380
420
460
500
540
580
620
660
700
Wavelength (nm)
PA9136
Action Spectrum (a*p(675) normalised)
Alpha
1.1
1
0.9
0.8
0.7
0.6
0.5
0.4
0.3
0.2
0.1
380
420
460
500
540
580
620
660
700
Wavelength (nm)

Figure 7.3

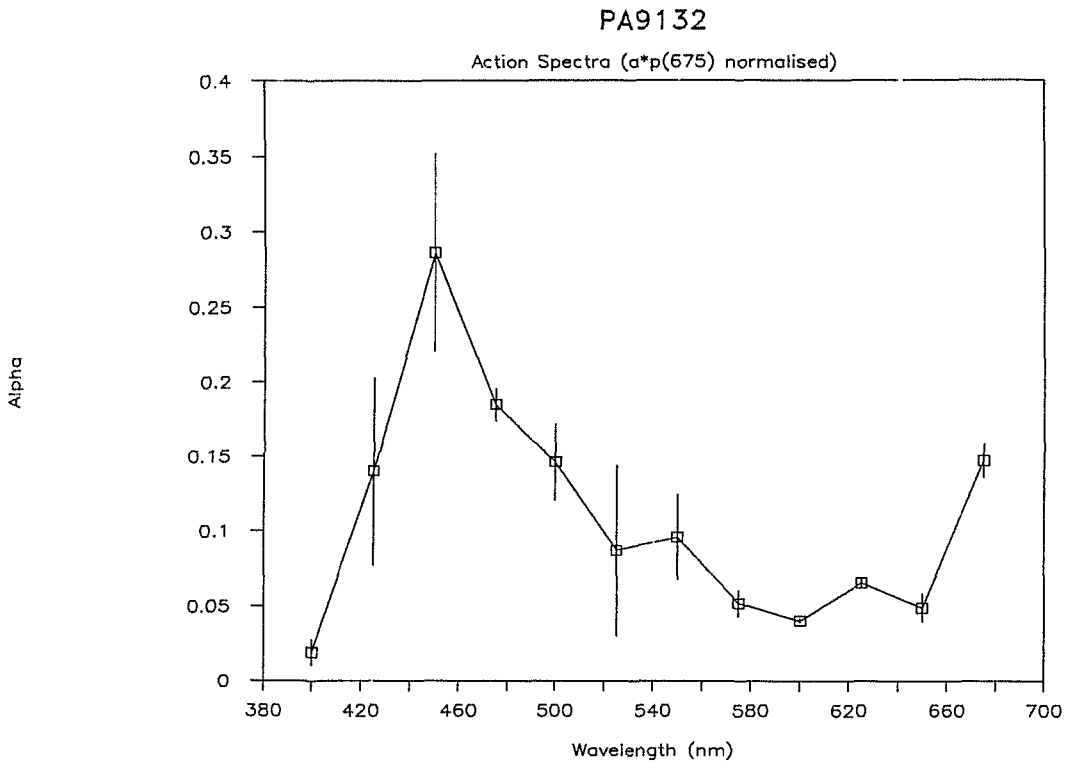

Figure 7. 3 (contd.)

Figure 7. 4. Depth profile of the sampling location in the Sargasso Sea. Chlorophyll concentrations were relatively uniform throughout the upper 60 m as a result of wind-generated mixing.

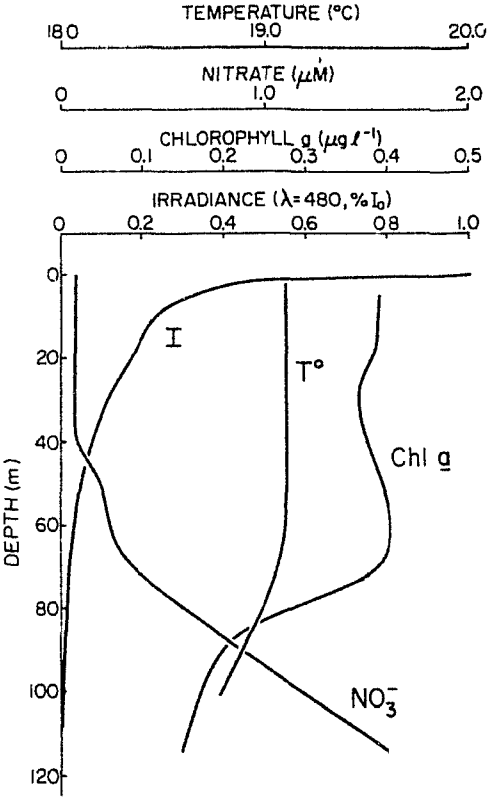
TEMPERATURE (°C)
18.0
19.0
20.0
NITRATE (μM)
0
1.0
2.0
CHLOROPHYLL a (μg ℓ⁻¹)
0
0.1
0.2
0.3
0.4
0.5
IRRADIANCE (λ=480, %I₀)
0
0.2
0.4
0.6
0.8
1.0
DEPTH (m)
0
20
40
60
80
100
120
I
T°
Chl a
NO₃⁻

Figure 7.4

Figure 7. 5. Photosynthetic action spectra ($\alpha^B(\lambda)$) of the natural phytoplankton assemblages collected from depths of 10 m, 20 m, 40 m, 50 m 70 m and 100 m at the Sargasso Sea station NE of Bermuda. Values of $\alpha^B(\lambda)$ were calculated from the initial slope of the P-I curve by linear regression, error bars correspond to ± the 95% confidence interval associated with the estimate of the initial slope.

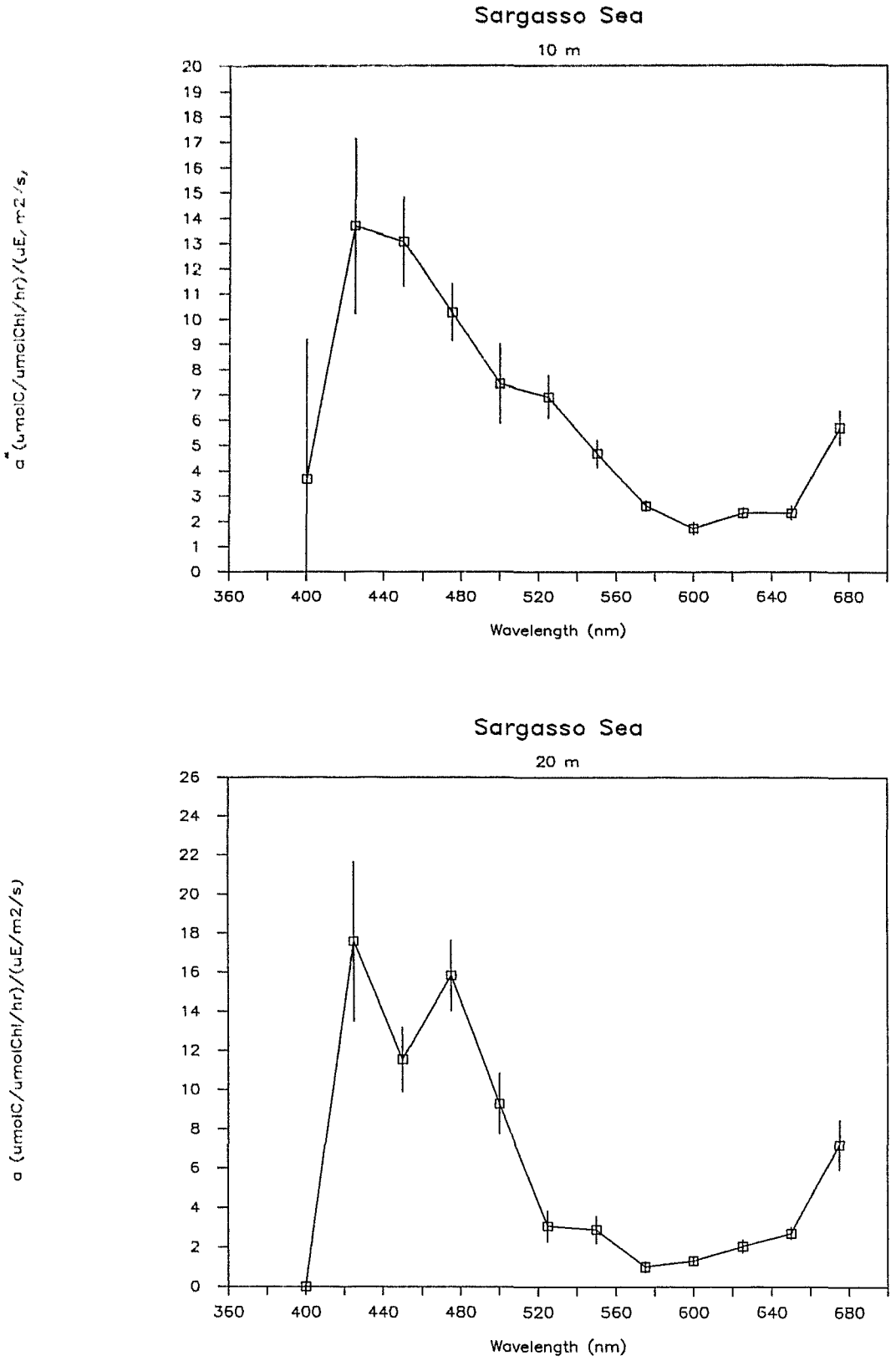
Sargasso Sea
10 m
a* (umolC/umolChl/hr)/(uE/m2/s)
Wavelength (nm)
Sargasso Sea
20 m
a (umolC/umolChl/hr)/(uE/m2/s)
Wavelength (nm)

Figure 7.5

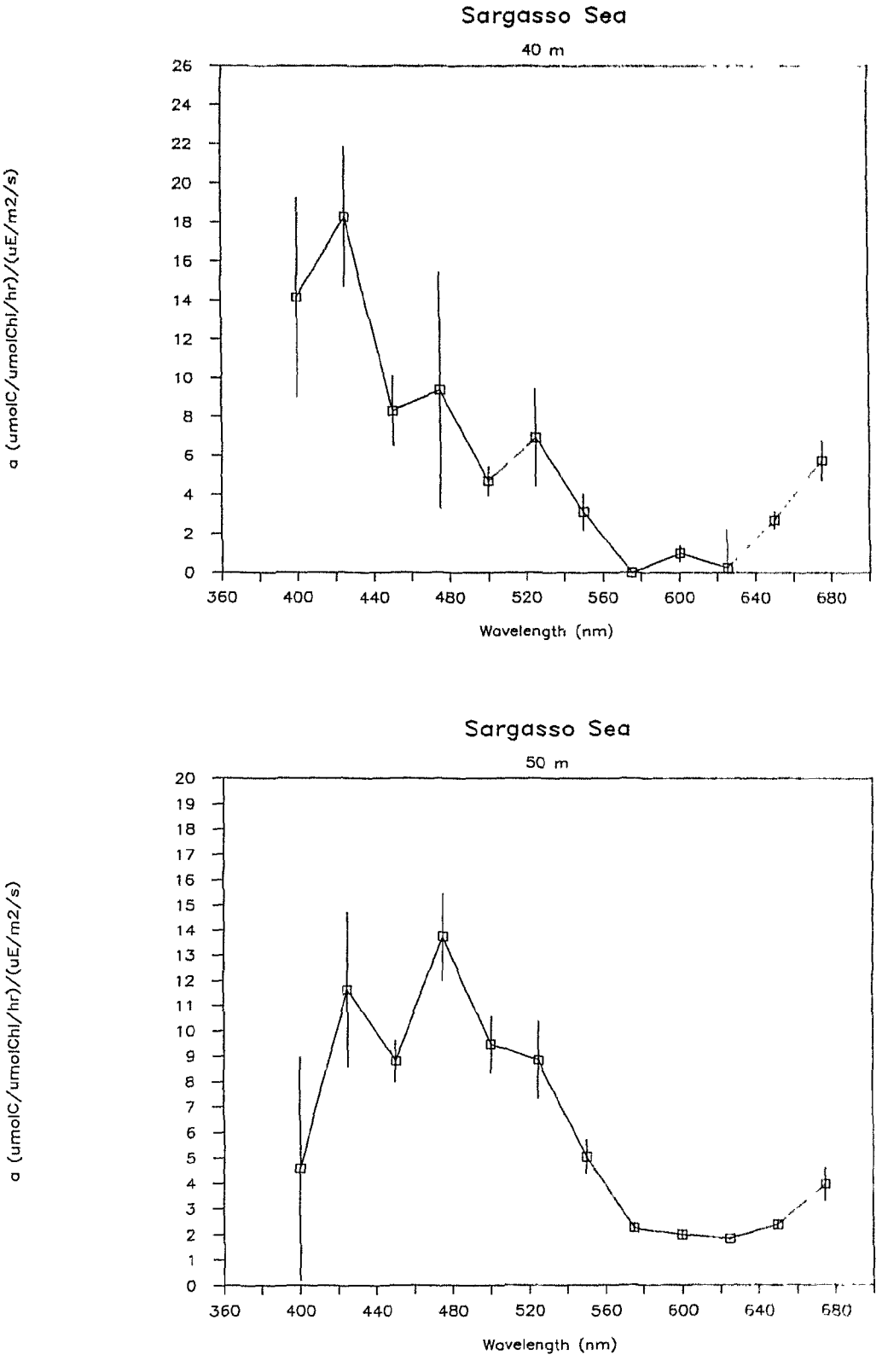

Figure 7.5 (contd.)

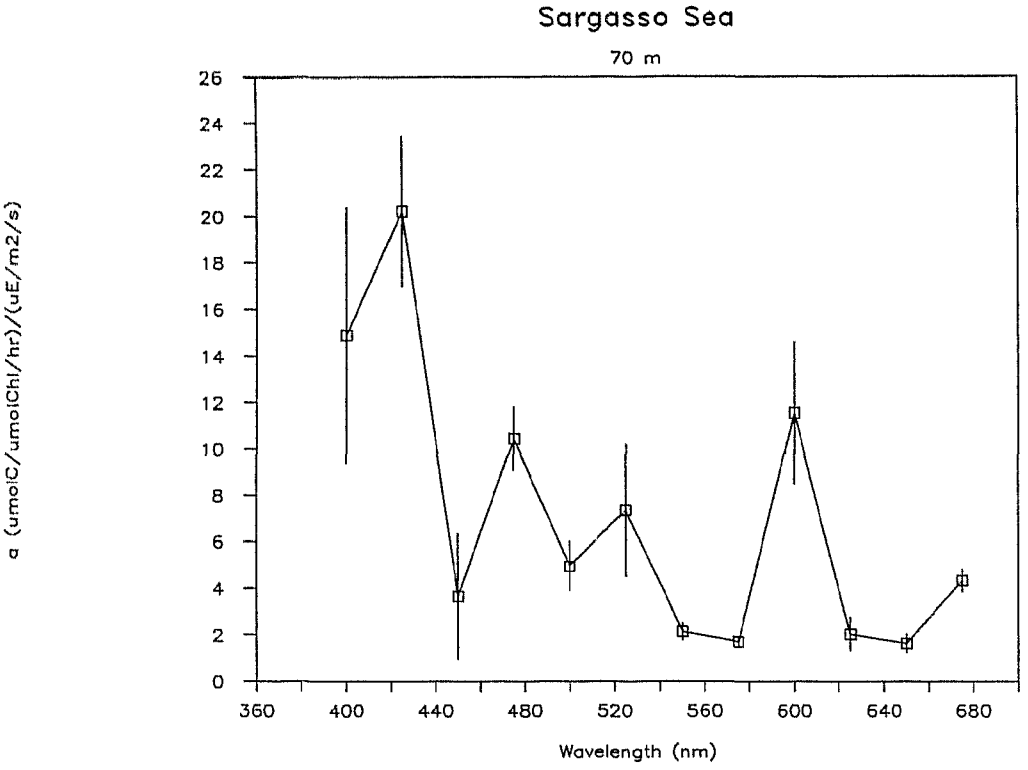

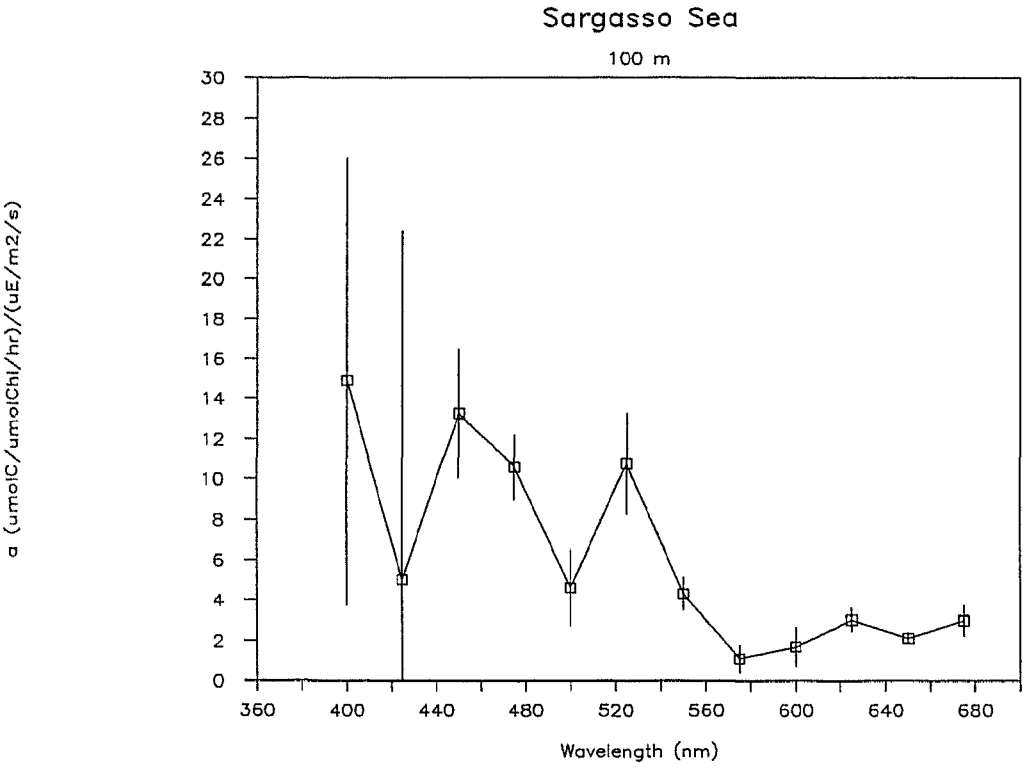

Figure 7. 5 (contd.)

Figure 7. 6. Photosynthetic action spectra ($\alpha^B(\lambda)$) of the natural phytoplankton assemblages collected from the sub-surface chlorophyll maximum along a latitudinal transect in the eastern Canadian Arctic. Values of $\alpha^B(\lambda)$ were calculated from the initial slope of the P-I curve by linear regression. Sampling locations included Labrador Sea (◊, Stn. 39, 43 m; ×, Stn. 40, 10 m; +, Stn. 43, 10 m), Davis Strait (◊, Stn. 45, 40 m), north Baffin Bay (▽, Stn. 50, 31 m), Lancaster Sound (△, Stn 90, 20 m; ◇, Stn. 93, 40 m) and Jones Sound (▲, Stn. 53, 18 m; X, Stn. 54, 15 m).

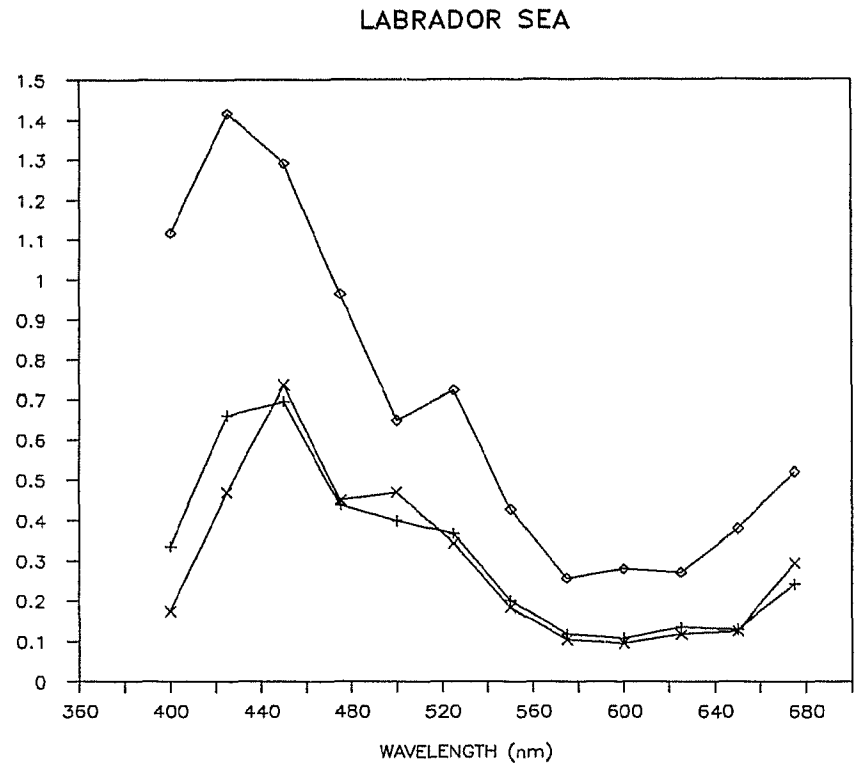
LABRADOR SEA
1.5
1.4
1.3
1.2
1.1
1
0.9
0.8
0.7
0.6
0.5
0.4
0.3
0.2
0.1
0
360
400
440
480
520
560
600
640
680
WAVELENGTH (nm)

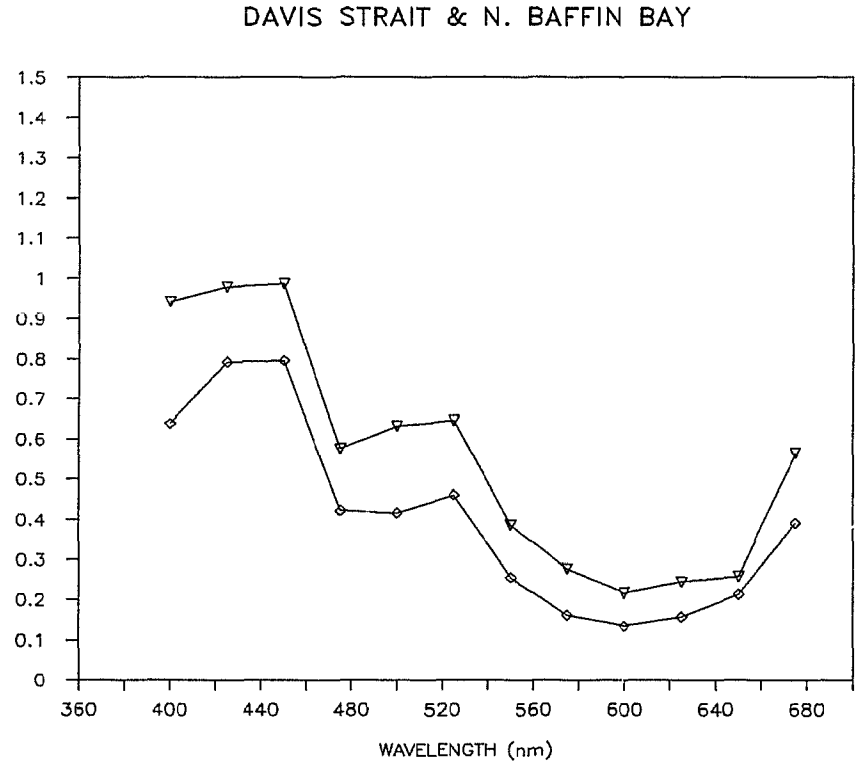
DAVIS STRAIT & N. BAFFIN BAY
1.5
1.4
1.3
1.2
1.1
1
0.9
0.8
0.7
0.6
0.5
0.4
0.3
0.2
0.1
0
360
400
440
480
520
560
600
640
680
WAVELENGTH (nm)

Figure 7.6

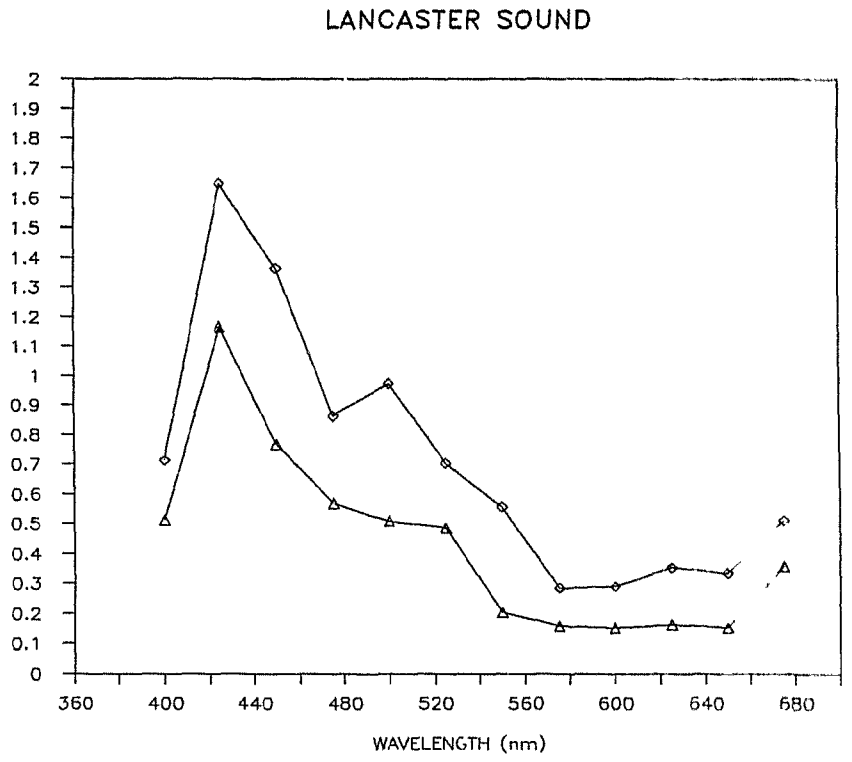

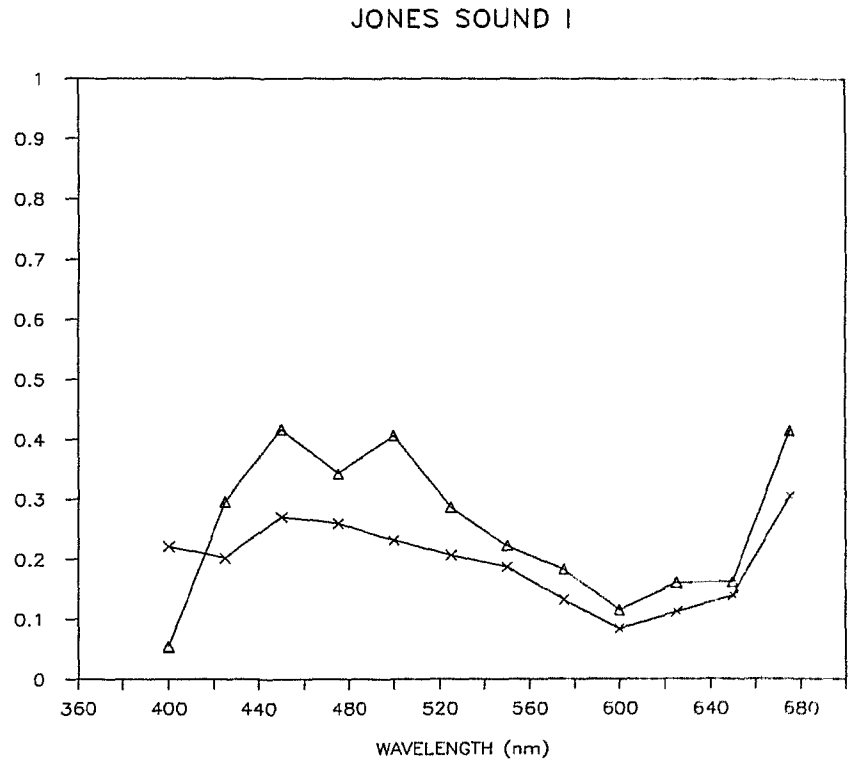

Figure 7. 6 (contd.)

Figure 7. 7. Photosynthetic action spectra ($\alpha^B(\lambda)$) of the natural phytoplankton assemblages collected from the sub-surface chlorophyll maximum at two promimate stations in Jones Sound. Values of $\alpha^B(\lambda)$ were calculated from the initial slope of the P-I curve by linear regression. Sampling locations were Stn. 73 (10 m (×)) and Stn. 75 (12.5 m (△)).

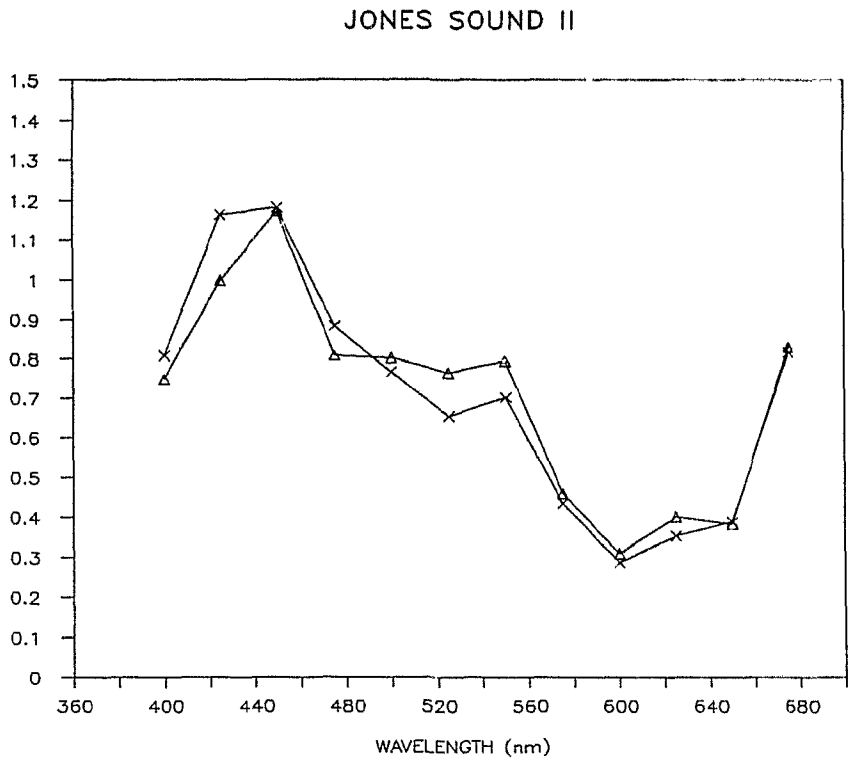
JONES SOUND II
1.5
1.4
1.3
1.2
1.1
1
0.9
0.8
0.7
0.6
0.5
0.4
0.3
0.2
0.1
0
360
400
440
480
520
560
600
640
680
WAVELENGTH (nm)

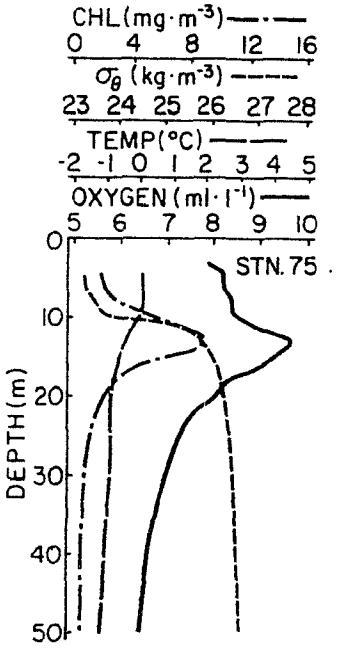
CHL (mg·m-3)
0 4 8 12 16
σθ (kg·m-3)
23 24 25 26 27 28
TEMP(°C)
-2 -1 0 1 2 3 4 5
OXYGEN (ml·l-1)
5 6 7 8 9 10
STN. 75
DEPTH (m)
0
10
20
30
40
50

Figure 7.7

Figure 7. 8. Photosynthetic action spectra ($\alpha^B(\lambda)$) of the natural phytoplankton assemblages collected from different depths in central Baffin Bay (Stn. 113) and coastal Baffin Bay (Stn. 116). Values of $\alpha^B(\lambda)$ were calculated from the initial slope of the P-I curve by linear regression. The water column at the coastal Baffin Bay station (Stn. 116) was more strongly stratified, with a well-developed chlorophyll maximum, compared to the central Baffin Bay station (Stn. 113). Sampling depths at Stn. 113 were 2 m (+), 10 m (×), 20 m (△), 30 m (▽) and 40 m (◇). Sampling depths at Stn. 116 were 10 m (×), 20 m (△), 30 m (▽), 40 m (◇) and 50 m (□).

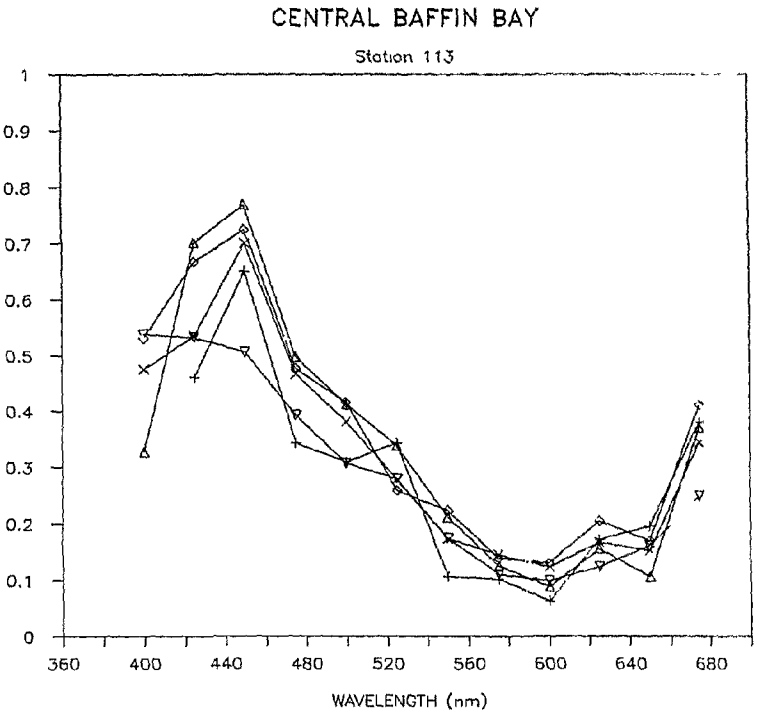
CENTRAL BAFFIN BAY
Station 113
1
0.9
0.8
0.7
0.6
0.5
0.4
0.3
0.2
0.1
0
360
400
440
480
520
560
600
640
680
WAVELENGTH (nm)

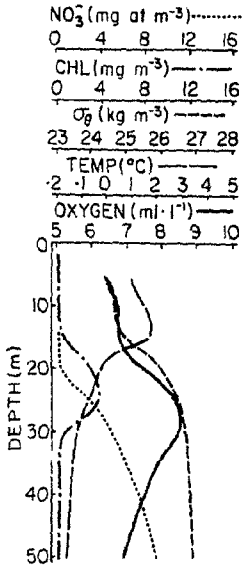
NO3 (mg at m-3)
0 4 8 12 16
CHL (mg m-3)
0 4 8 12 16
σθ (kg m-3)
23 24 25 26 27 28
TEMP(°C)
-2 -1 0 1 2 3 4 5
OXYGEN (ml·l-1)
5 6 7 8 9 10
0
10
20
30
40
50
DEPTH (m)

Figure 7.8

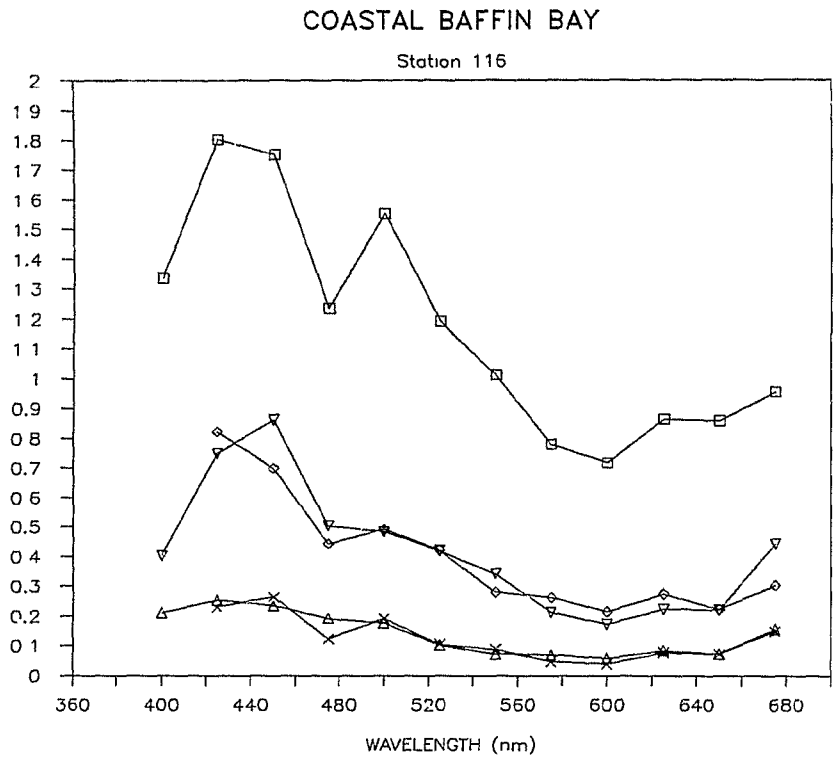

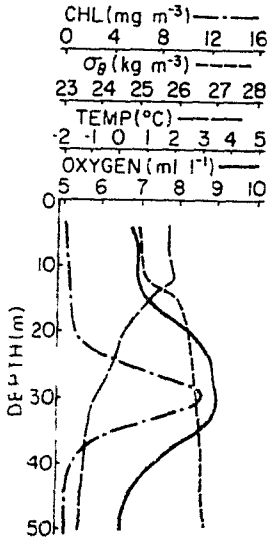

Figure 7. 8 (contd.)

Figure 7. 9. Photosynthetic action spectra ($\alpha^B(\lambda)$) of the natural phytoplankton assemblages collected from different depths in Jones Sound under conditions where the water column was well-stratified. Values of $\alpha^B(\lambda)$ were calculated from the initial slope of the P-I curve by linear regression. Samples were collected from Stn. 94 (X , 9 m), Stn. 95 (+, 5 m; Δ, 20 m) and Stn. 98 (◇ , 10 m; □, 20 m).

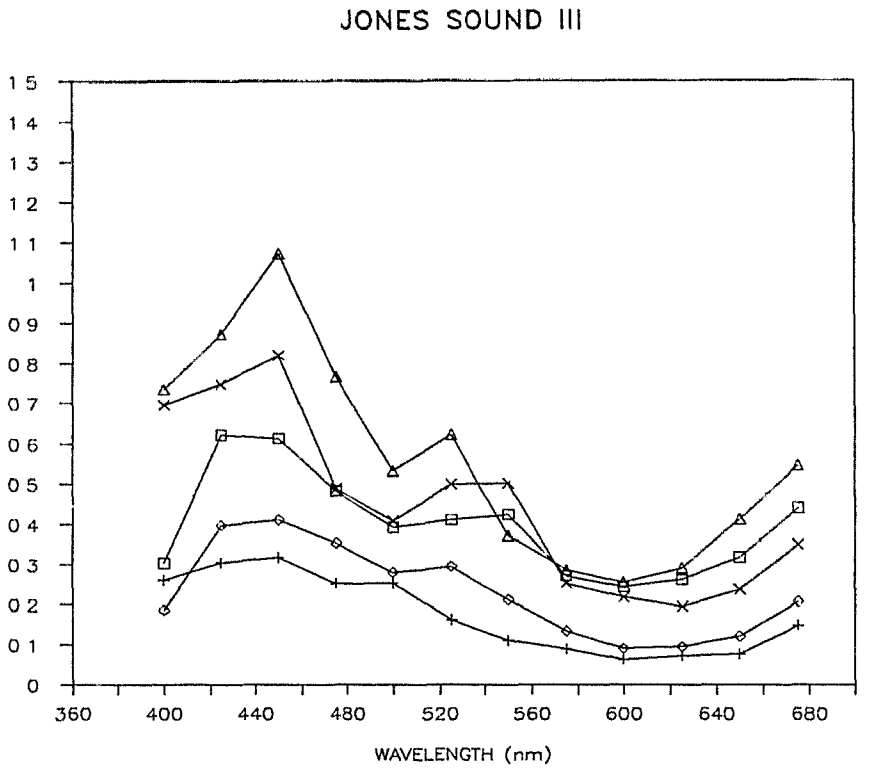
JONES SOUND III
15
14
13
12
11
1
09
08
07
06
05
04
03
02
01
0
360
400
440
480
520
560
600
640
680
WAVELENGTH (nm)

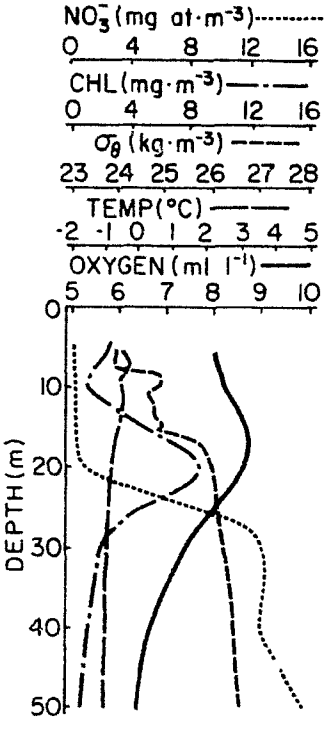
NO3- (mg at·m-3)
0 4 8 12 16
CHL (mg·m-3)
0 4 8 12 16
σθ (kg·m-3)
23 24 25 26 27 28
TEMP (°C)
-2 -1 0 1 2 3 4 5
OXYGEN (ml l-1)
5 6 7 8 9 10
0
10
20
30
40
50
DEPTH (m)

Figure 7.9

Figure 7. 10. Photosynthetic action spectra ($\alpha^B(\lambda)$) of the natural phytoplankton assemblages collected from different depths in Jones Sound following a wind-generated mixing event. Values of $\alpha^B(\lambda)$ were calculated from the initial slope of the P-I curve by linear regression. Samples were collected from Stn. 124 (+ , 5 m; ×, 10 m; △, 15 m; ▽, 20 m) and Stn. 125 (◇, 5 m).

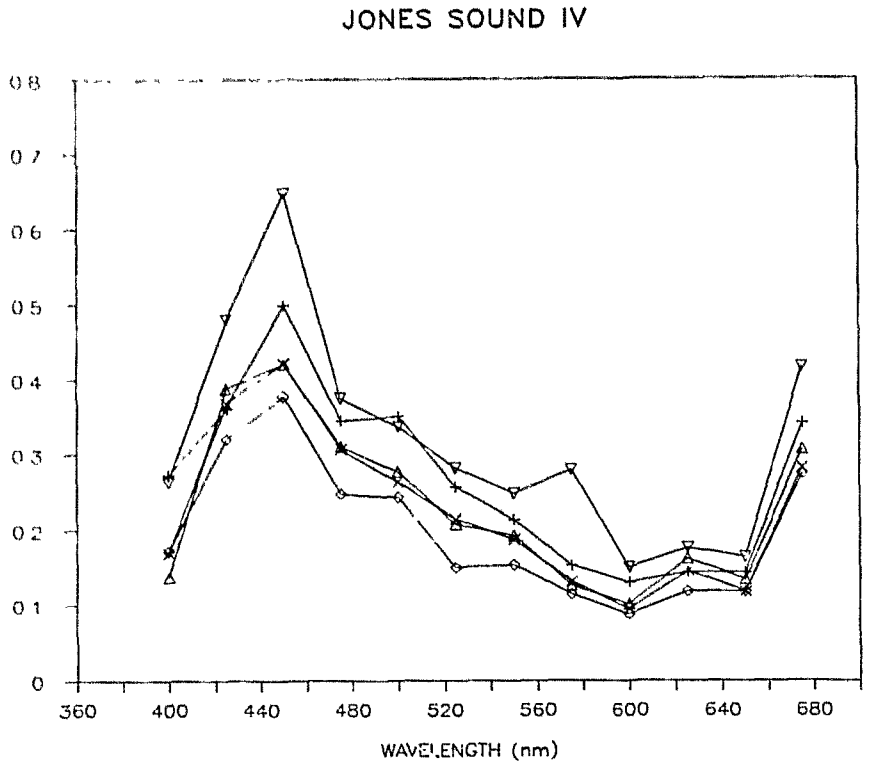
JONES SOUND IV
0.8
0.7
0.6
0.5
0.4
0.3
0.2
0.1
0
360
400
440
480
520
560
600
640
680
WAVELENGTH (nm)

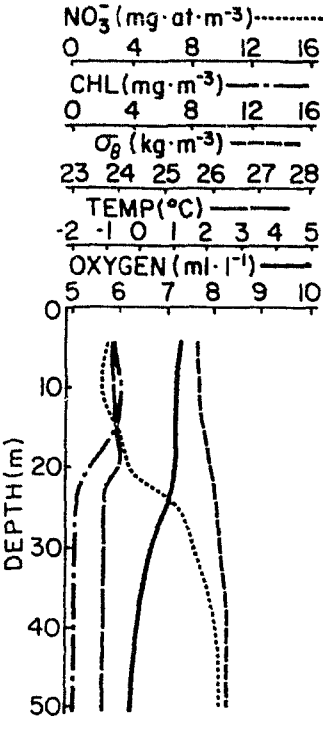
NO3- (mg·at·m-3)
0 4 8 12 16
CHL(mg·m-3)
0 4 8 12 16
σθ (kg·m-3)
23 24 25 26 27 28
TEMP(°C)
-2 -1 0 1 2 3 4 5
OXYGEN (ml·l-1)
5 6 7 8 9 10
0
10
20
30
40
50
DEPTH(m)

Figure 7. 10

Figure 7. 11. Sample-averaged relative photosynthetic action spectra ($\alpha^B(\lambda)$) for all the natural phytoplankton assemblages collected from locations in the eastern Canadian Arctic. The relative action spectra ($\alpha^B(\lambda)_{rel}$) of each sample was first calculated by normalizing the action in each 25 nm waveband to the mean action found in all twelve wavebands ($\alpha^B(\lambda)_{rel} = \alpha^B(\lambda) / (\Sigma\, \alpha^B(\lambda)/12)$). The "sample-averaged" relative action spectrum ($\alpha^B(\lambda)_{rel}$) shown is the average of all such relative action spectra obtained for the different samples. The error bars represent the 95% confidence interval of this "sample-averaged" relative action ($\alpha^B(\lambda)_{rel}$) within each waveband.

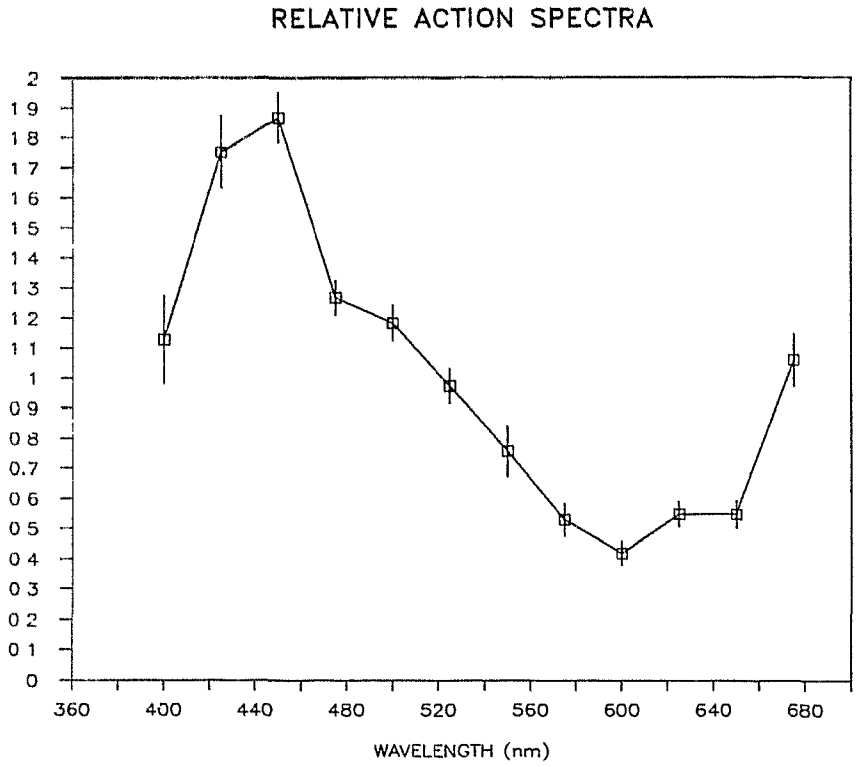
RELATIVE ACTION SPECTRA
2
1 9
1 8
1 7
1 6
1 5
1 4
1 3
1 2
1 1
1
0 9
0 8
0.7
0 6
0 5
0 4
0 3
0 2
0 1
0
360
400
440
480
520
560
600
640
680
WAVELENGTH (nm)

Figure 7. 11

Figure 7. 12. Photosynthetic action spectra ($\alpha^B(\lambda)$) of the natural phytoplankton assemblage collected from the chlorophyll maximum (70 m) over the Yakutat seamount. The upper panel represents the action spectra of particulates retained by a 3 μm Nuclepore® filter, the lower panel corresponds to particulates that passed a 3 μm Nuclepore® filter but were retained by a 0.2 μm Nuclepore® filter. The CTD profile of an adjacent station indicates the chlorophyll maximum at 80 m and elevated oxygen concentrations in the upper mixed layer (above 100 m).

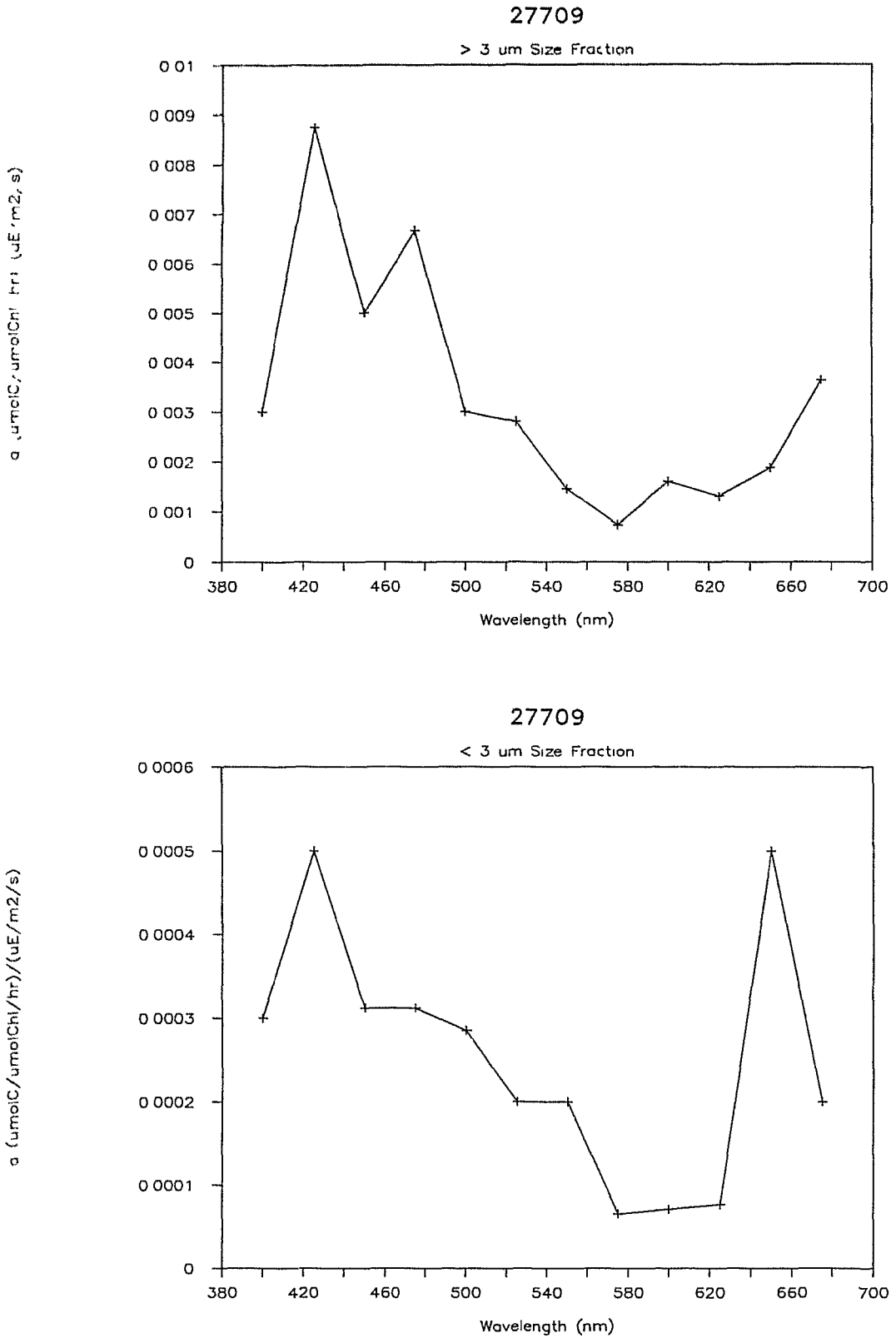
27709
> 3 um Size Fraction
0 01
0 009
0 008
0 007
0 006
0 005
0 004
0 003
0 002
0 001
0
380
420
460
500
540
580
620
660
700
Wavelength (nm)
27709
< 3 um Size Fraction
0 0006
0 0005
0 0004
0 0003
0 0002
0 0001
0
380
420
460
500
540
580
620
660
700
Wavelength (nm)

Figure 7. 12

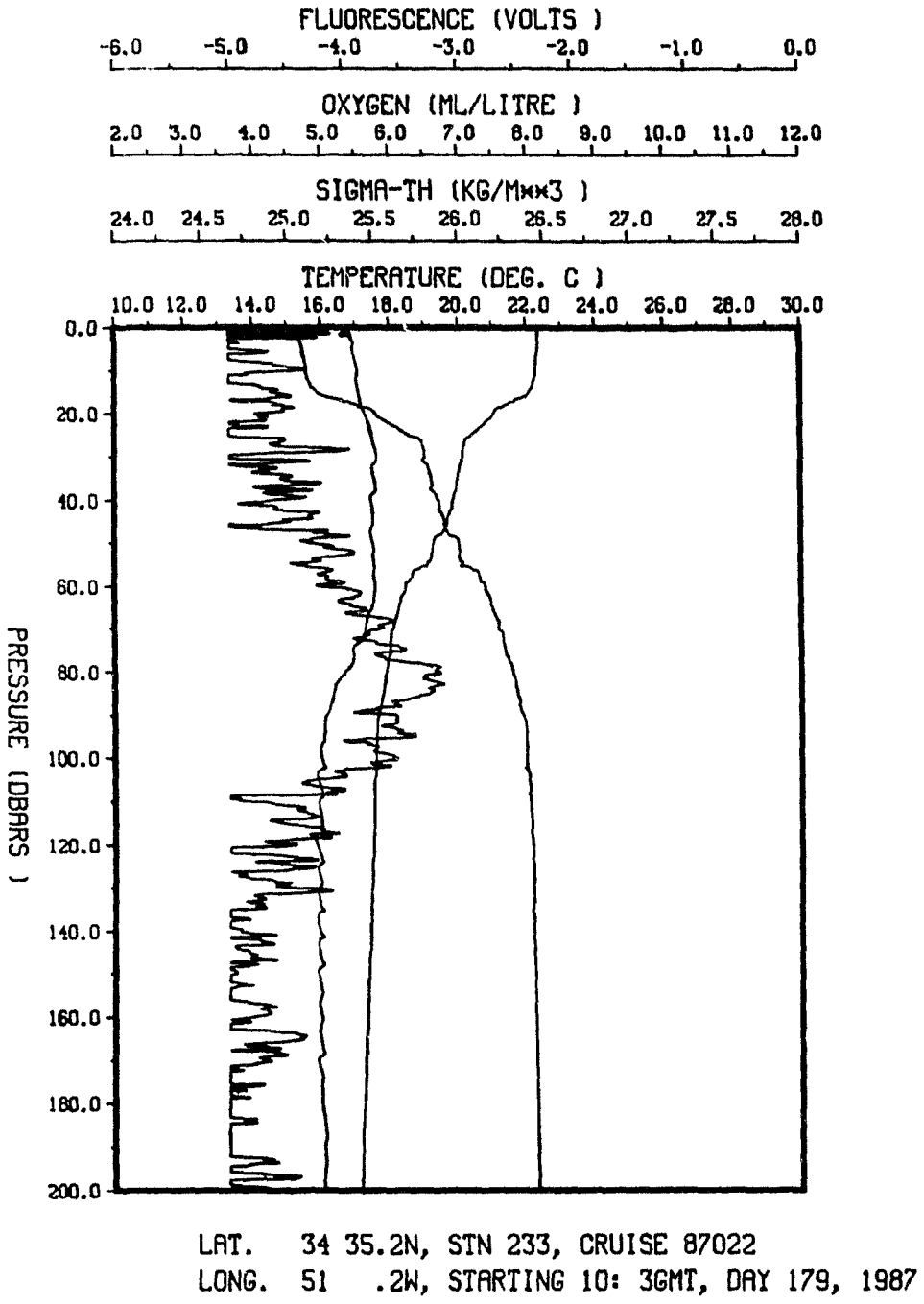

Figure 7. 12 (contd.)

Figure 7. 13. Photosynthetic action spectra ($\alpha^B(\lambda)$) of the natural phytoplankton assemblage collected from the chlorophyll maximum (70 m) over the Nashville seamount. The upper panel represents the action spectra of particulates retained by a 3 μm Nuclepore® filter, the lower panel corresponds to particulates that passed a 3 μm Nuclepore® filter but were retained by a 0.2 μm Nuclepore® filter. Note the peak at 550 nm in the < 3 μm size fraction. The CTD profile of an adjacent station illustrates the structure of the water column. A well defined chlorophyll maxima occurs at 70 m, a depth corresponding to the base of the mixed layer.

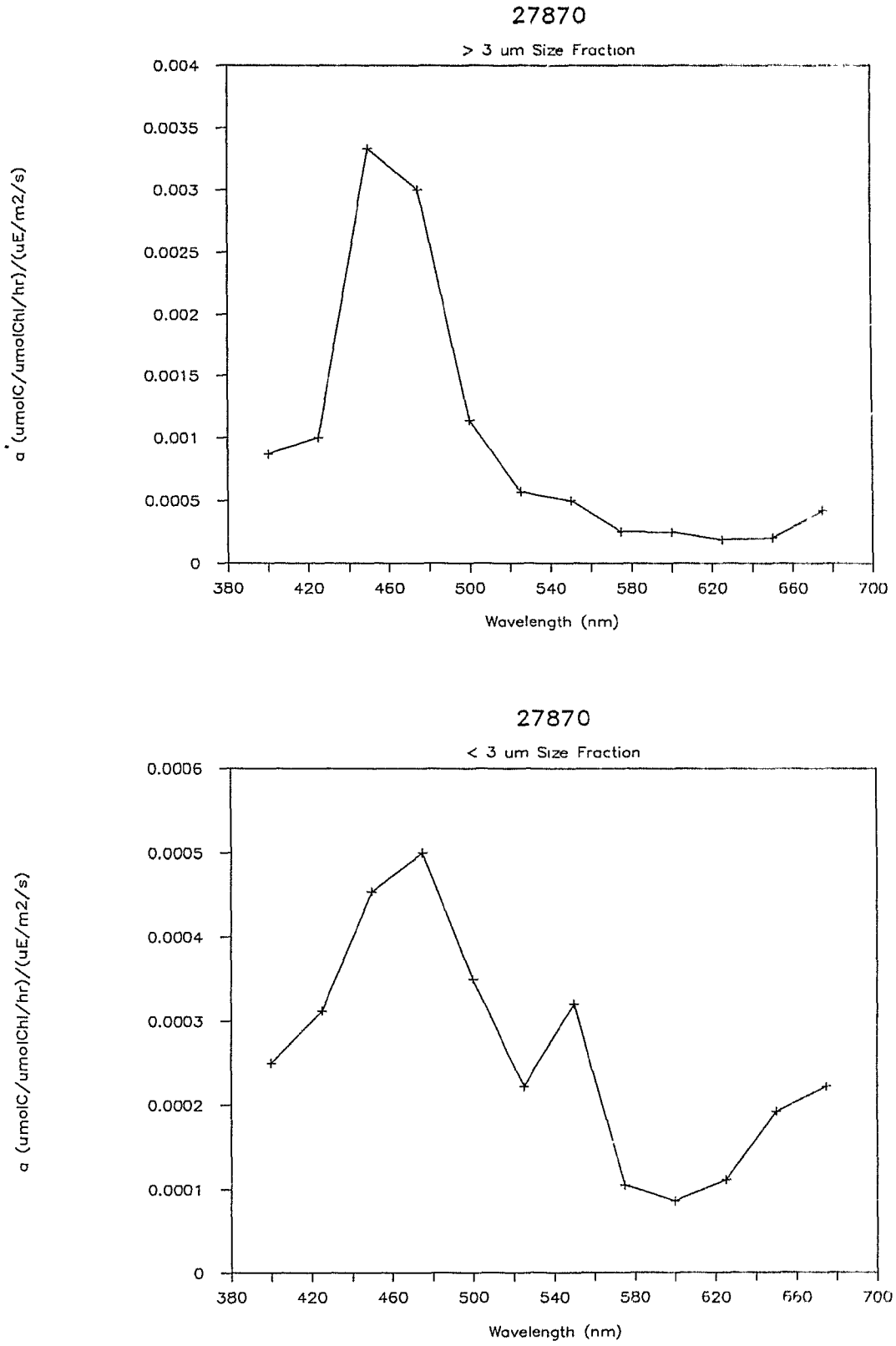
27870
> 3 um Size Fraction
a (umolC/umolChl/hr)/(uE/m2/s)
0.004
0.0035
0.003
0.0025
0.002
0.0015
0.001
0.0005
0
380
420
460
500
540
580
620
660
700
Wavelength (nm)
27870
< 3 um Size Fraction
a (umolC/umolChl/hr)/(uE/m2/s)
0.0006
0.0005
0.0004
0.0003
0.0002
0.0001
0
380
420
460
500
540
580
620
660
700
Wavelength (nm)

Figure 7. 13

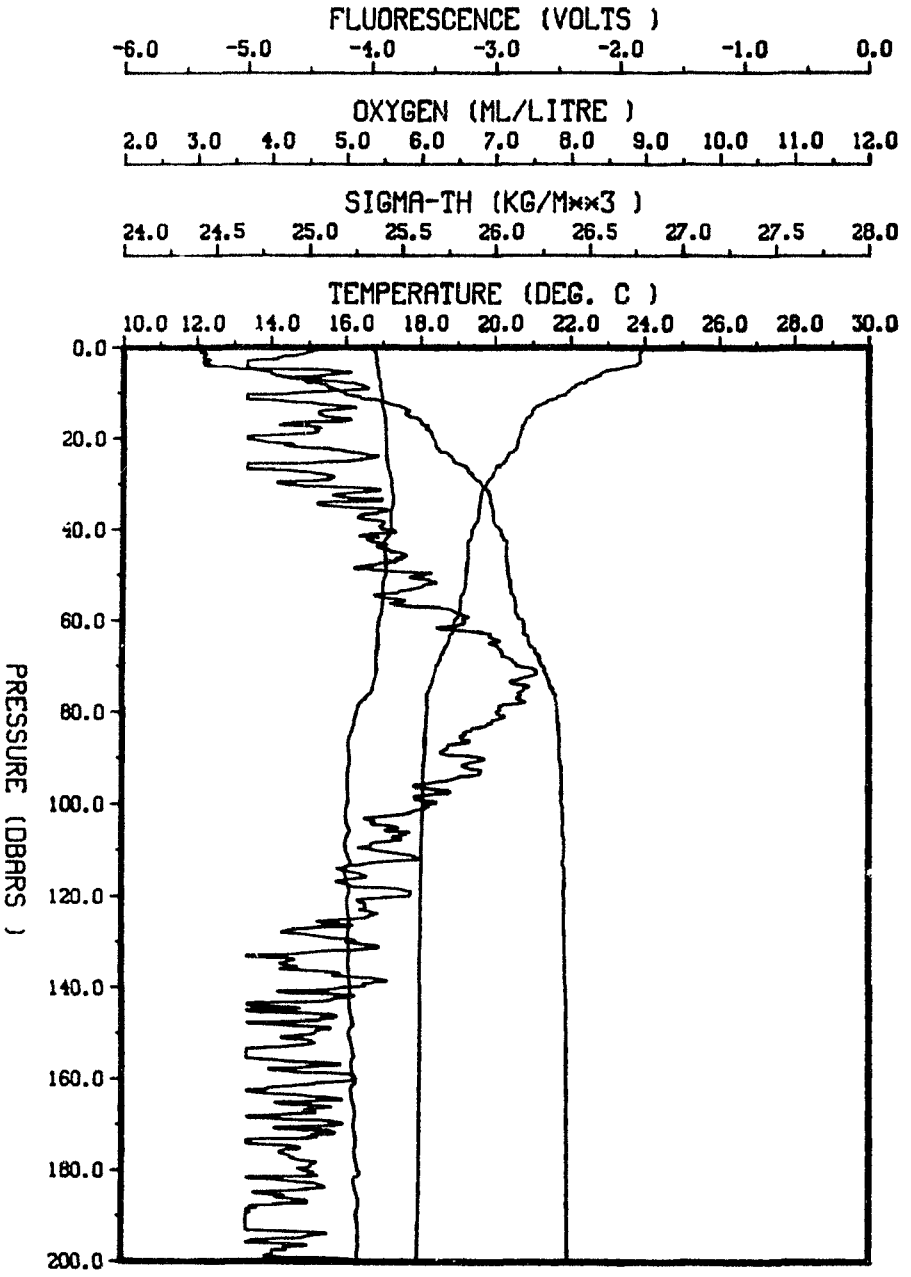

Figure 7. 13 (contd.)

Figure 7. 14. Photosynthetic action spectra ($\alpha^B(\lambda)$) of the natural phytoplankton assemblage collected from the chlorophyll maximum (110 m) at the oligotrophic Station Purple. The action spectra is for particulates retained by a 3 μm Nuclepore® filter. No discernable signal was obtained for particulates that passed a 3 μm Nuclepore® filter but were retained by a 0.2 μm Nuclepore® filter. The CTD profile of an adjacent station illustrates the lack of a well-defined chlorophyll maximum. A small increase in chlorophyll is present at 110 m corresponding to the depth sampled.

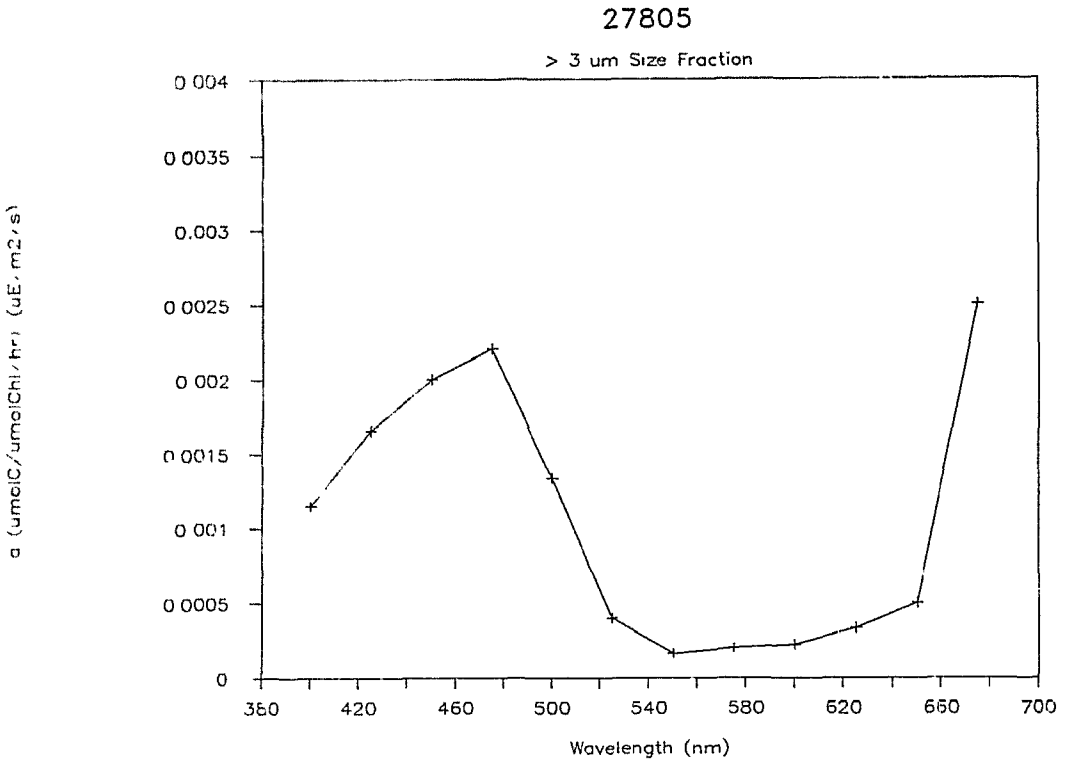
27805
> 3 um Size Fraction
a (umolC/umolChl/hr) (uE/m2/s)
0.004
0.0035
0.003
0.0025
0.002
0.0015
0.001
0.0005
0
360
420
460
500
540
580
620
660
700
Wavelength (nm)

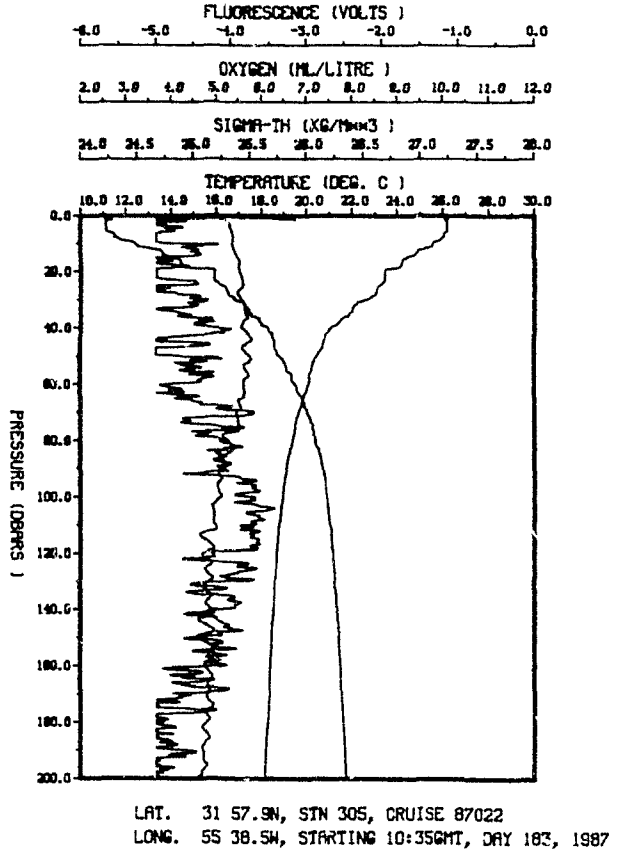
FLUORESCENCE (VOLTS)
OXYGEN (ML/LITRE)
SIGMA-TH (XG/MXX3)
TEMPERATURE (DEG. C)
PRESSURE (DBARS)
LAT. 31 57.9N, STN 305, CRUISE 87022
LONG. 55 38.5W, STARTING 10:35GMT, DAY 183, 1987

Figure 7.14

Figure 7. 15. Apparent quantum yield spectra ($\phi_a(\lambda)$) of *Synechococcus* sp. WH 5701 cultured at different growth PFDs. Growth PFDs were 8 μmol m^{-2} s^{-1} (SY 9148), 15 μmol m^{-2} s^{-1} (SY 9156), 27 μmol m^{-2} s^{-1} (SY 9160) and 70 μmol m^{-2} s^{-1} (SY 9152).

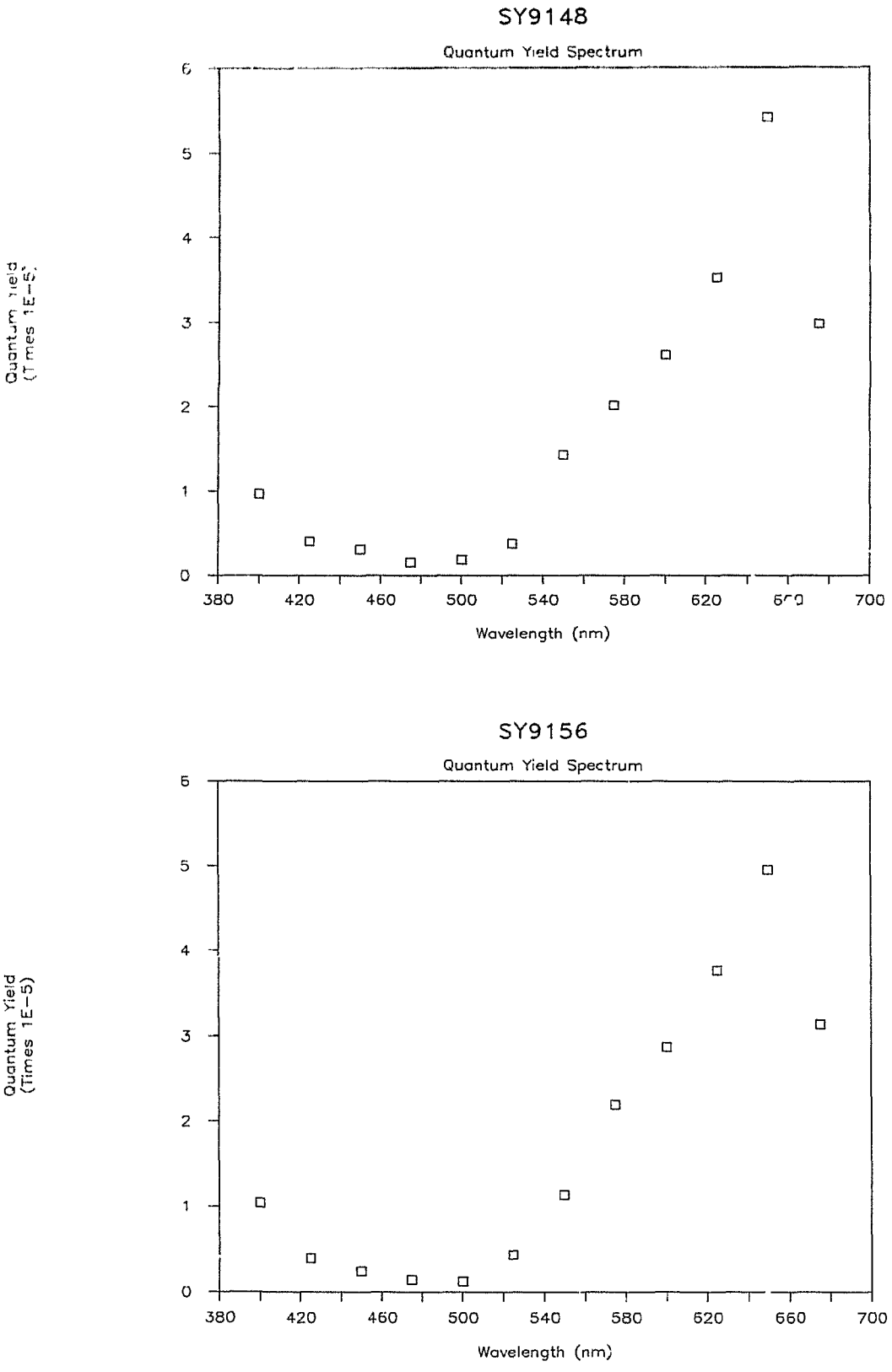
SY9148
Quantum Yield Spectrum
Quantum Yield
(Times 1E-5)
0
1
2
3
4
5
6
380
420
460
500
540
580
620
700
Wavelength (nm)
SY9156
Quantum Yield Spectrum
Quantum Yield
(Times 1E-5)
0
1
2
3
4
5
6
380
420
460
500
540
580
620
660
700
Wavelength (nm)

Figure 7. 15

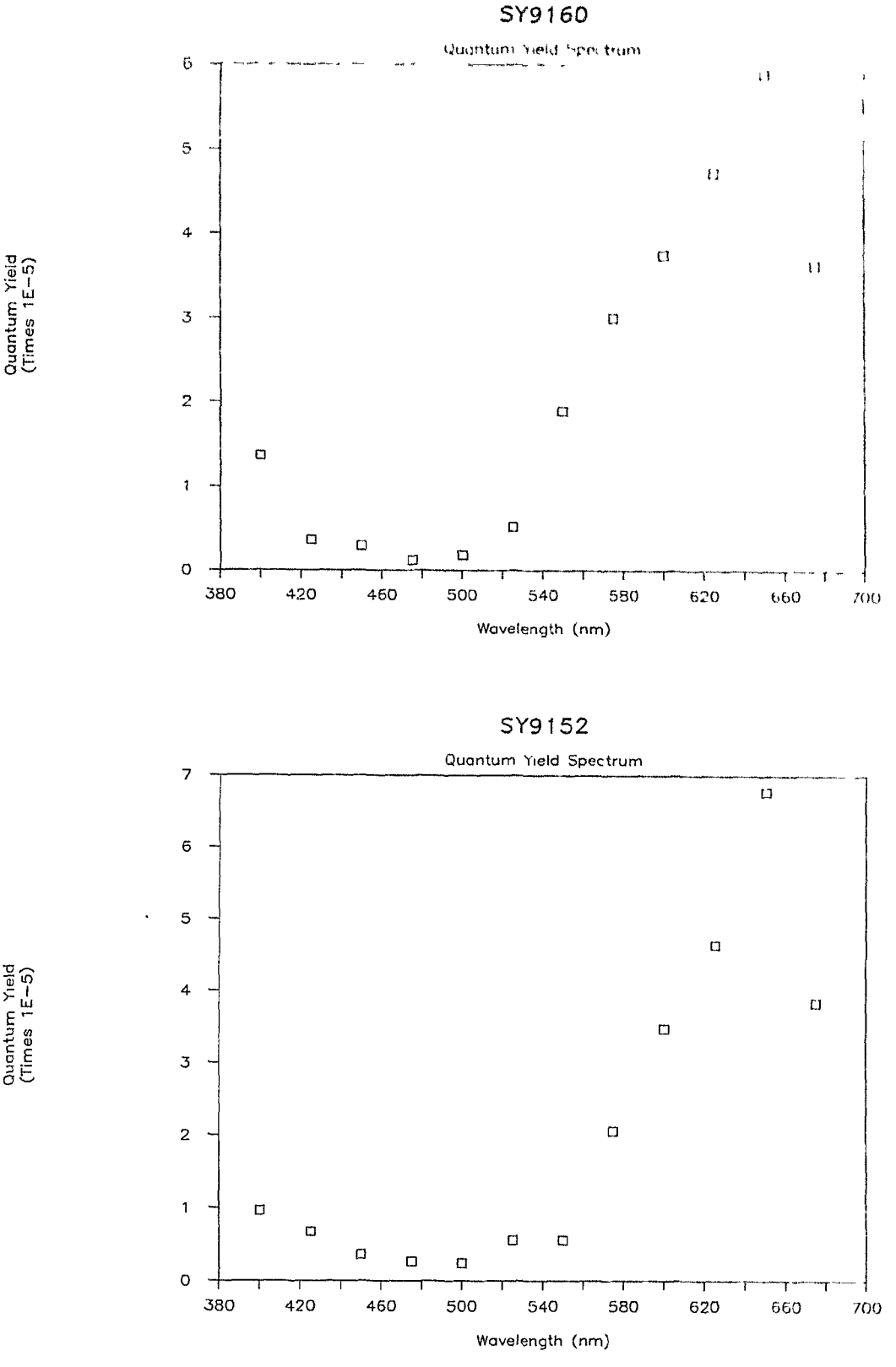

Figure 7. 15 (contd.)

Figure 7. 16. Apparent quantum yield spectra ($\phi_a(\lambda)$) of *Synechococcus* sp. WH 7803 cultured at different growth PFDs. Growth PFDs were 17 μmol m^{-2} s^{-1} (DC 9124), 25 μmol m^{-2} s^{-1} (DC 9116) and 70 μmol m^{-2} s^{-1} (DC 9120).

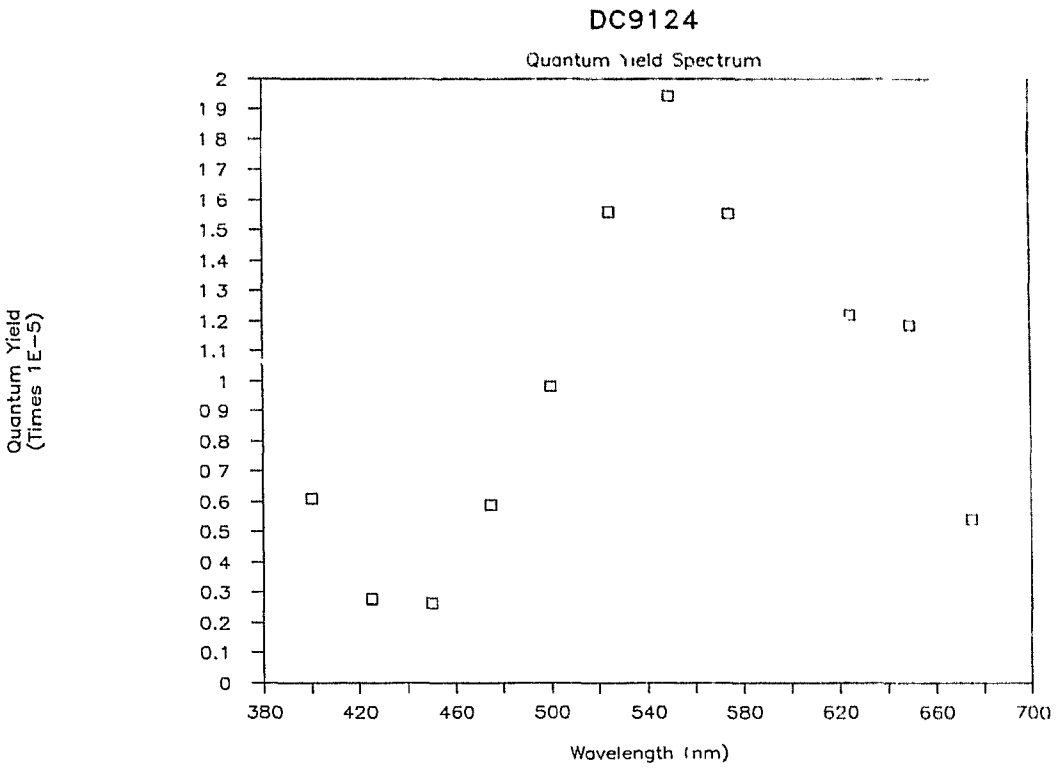
DC9124
Quantum Yield Spectrum
Quantum Yield (Times 1E-5)
2
1.9
1.8
1.7
1.6
1.5
1.4
1.3
1.2
1.1
1
0.9
0.8
0.7
0.6
0.5
0.4
0.3
0.2
0.1
0
380
420
460
500
540
580
620
660
700
Wavelength (nm)

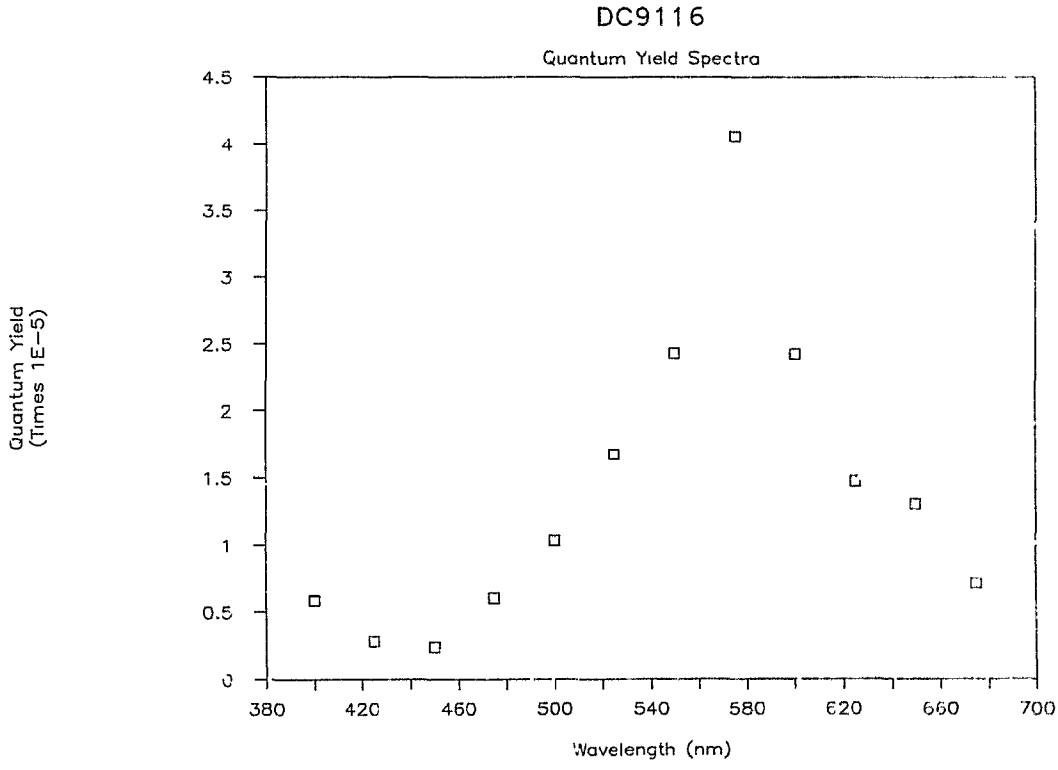
DC9116
Quantum Yield Spectra
Quantum Yield (Times 1E-5)
4.5
4
3.5
3
2.5
2
1.5
1
0.5
0
380
420
460
500
540
580
620
660
700
Wavelength (nm)

Figure 7.16

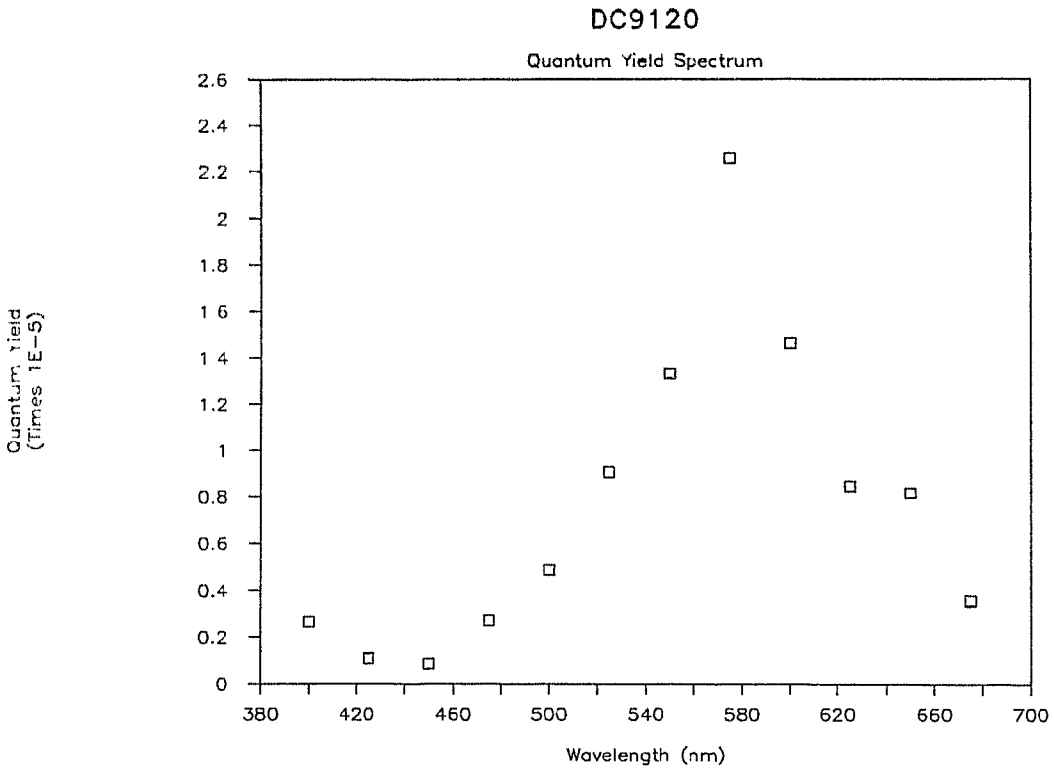

Figure 7. 16 (contd.)

Figure 7. 17. Apparent quantum yield spectra ($\phi_a(\lambda)$) of *Pavlova* sp. (clone NEP) cultured at different growth PFDs. Growth PFDs were 8 µmol m^{-2} s^{-1} (PA 9140), 12 µmol m^{-2} s^{-1} (PA 9136) and 45 µmol m^{-2} s^{-1} (PA 9132).

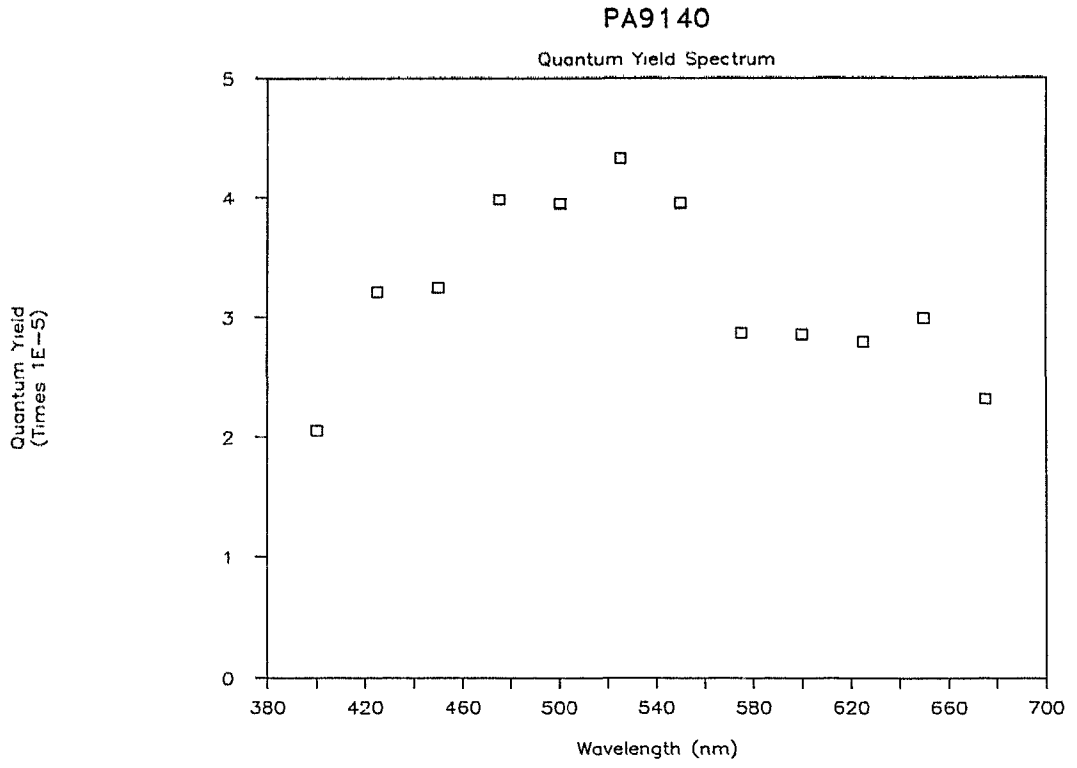
PA9140
Quantum Yield Spectrum
Quantum Yield (Times 1E-5)
5
4
3
2
1
0
380
420
460
500
540
580
620
660
700
Wavelength (nm)

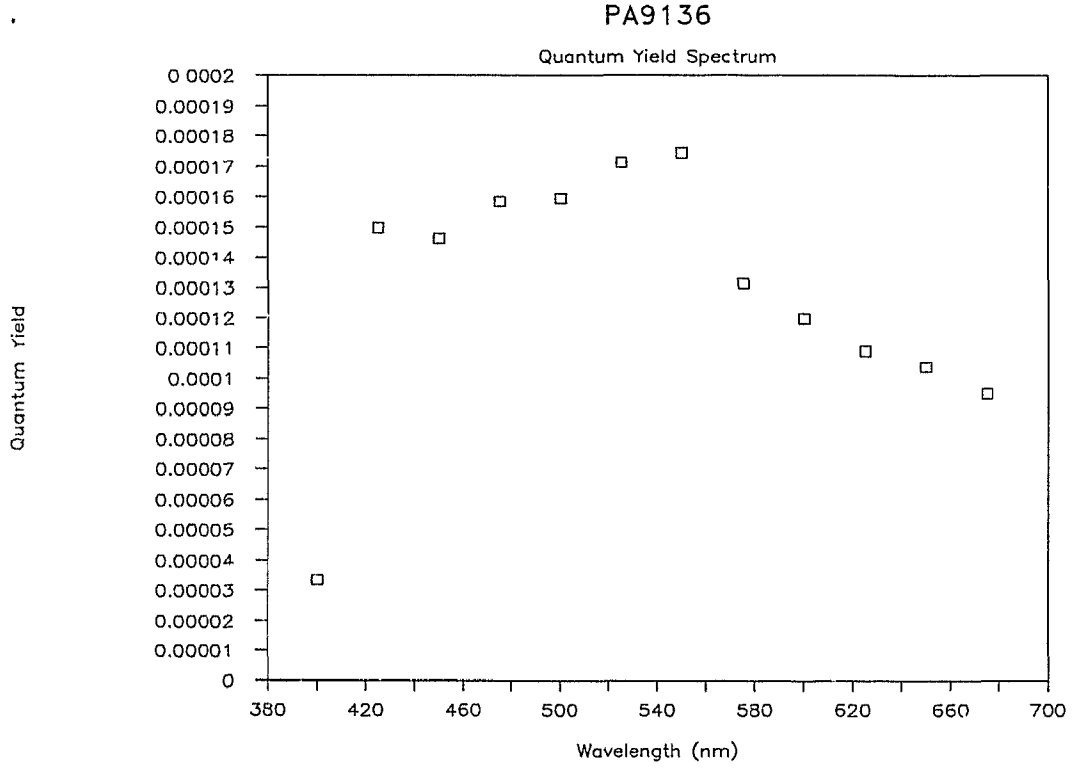
PA9136
Quantum Yield Spectrum
Quantum Yield
0.0002
0.00019
0.00018
0.00017
0.00016
0.00015
0.00014
0.00013
0.00012
0.00011
0.0001
0.00009
0.00008
0.00007
0.00006
0.00005
0.00004
0.00003
0.00002
0.00001
0
380
420
460
500
540
580
620
660
700
Wavelength (nm)

Figure 7. 17

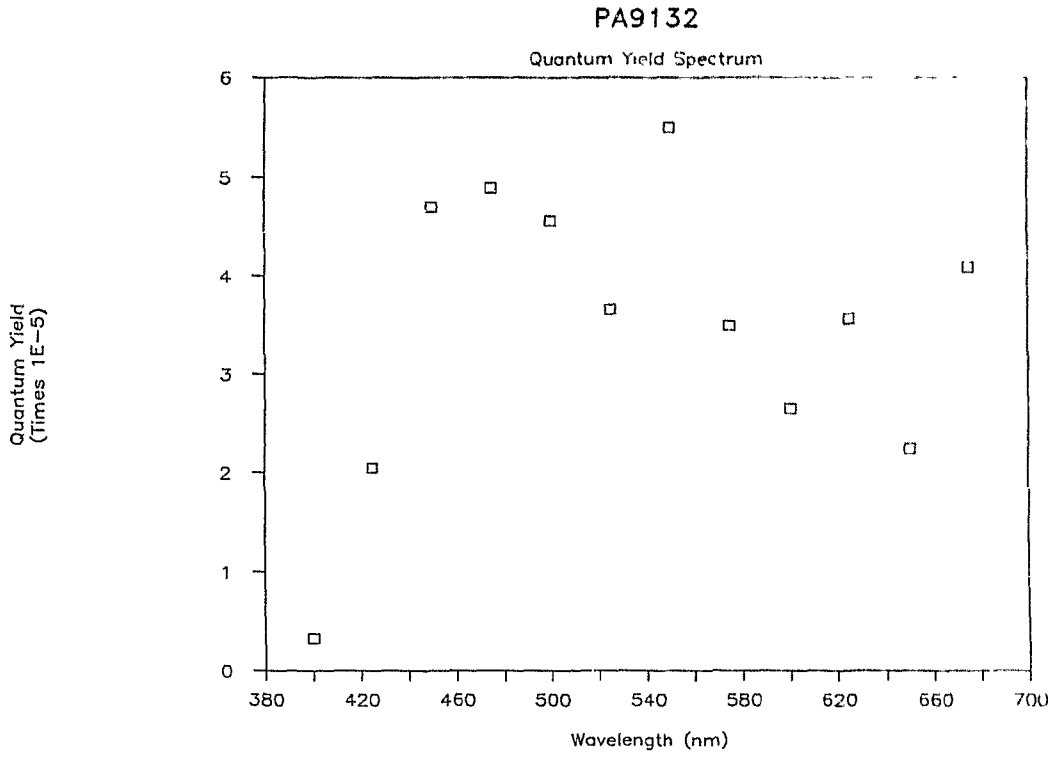

Figure 7. 17 (contd.)

Figure 7. 18. Relative apparent quantum yield spectra ($\phi_a(\lambda)_{rel}$) of natural phytoplankton assemblages from the eastern Canadian Arctic. Apparent quantum yield spectra ($\phi_a(\lambda)$) of individual samples were first calculated by dividing the chlorophyll-normalized action spectra ($\alpha^B(\lambda)$) by estimates of the chlorophyll-specific attenuation cross-sections ($a^*_{chl}(\lambda)$) obtained from the hyperbolic model [Eq. 6.1]. The relative apparent quantum yield ($\phi_a(\lambda)_{rel}$) was then calculated by dividing the apparent quantum yield at each waveband by the mean apparent quantum yield over all twelve wavebands ($\phi_a(\lambda)_{rel} = \phi_a(\lambda) / (\Sigma \phi_a(\lambda)/12)$). The "sample-averaged" relative quantum yields shown were then calculated as the average of the relative apparent quantum yields of all samples from the eastern Canadian Arctic. Error bars represent the 95% confidence intervals of these averages.

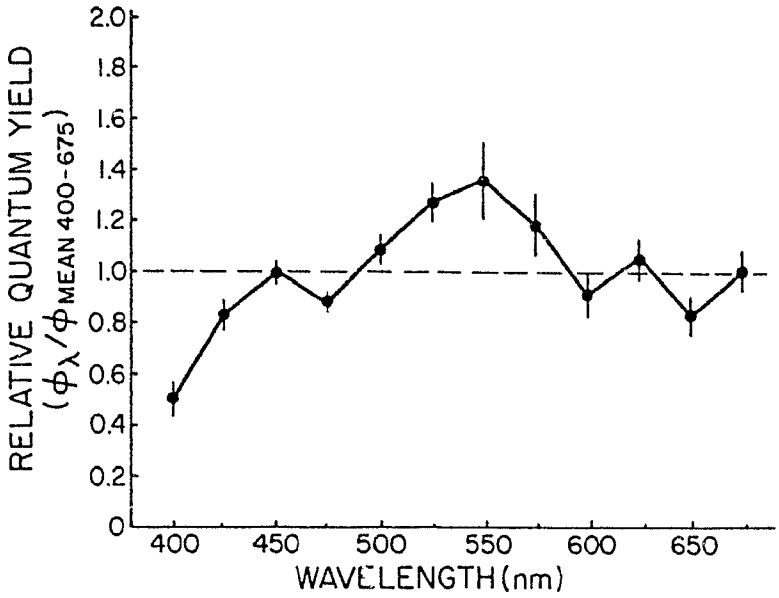
RELATIVE QUANTUM YIELD
$(\phi_\lambda/\phi_{MEAN\ 400-675})$
2.0
1.8
1.6
1.4
1.2
1.0
0.8
0.6
0.4
0.2
0
400
450
500
550
600
650
WAVELENGTH (nm)

Figure 7. 18

Figure 7. 19. Wavelength dependence of curvature in the P-I response at low PFDs in *Synechococcus* sp. WH 5701 and *Synechococcus* sp. WH 7803. Plot shows the magnitude of the parameter $R_m^B(\lambda)$ as a function of wavelength.

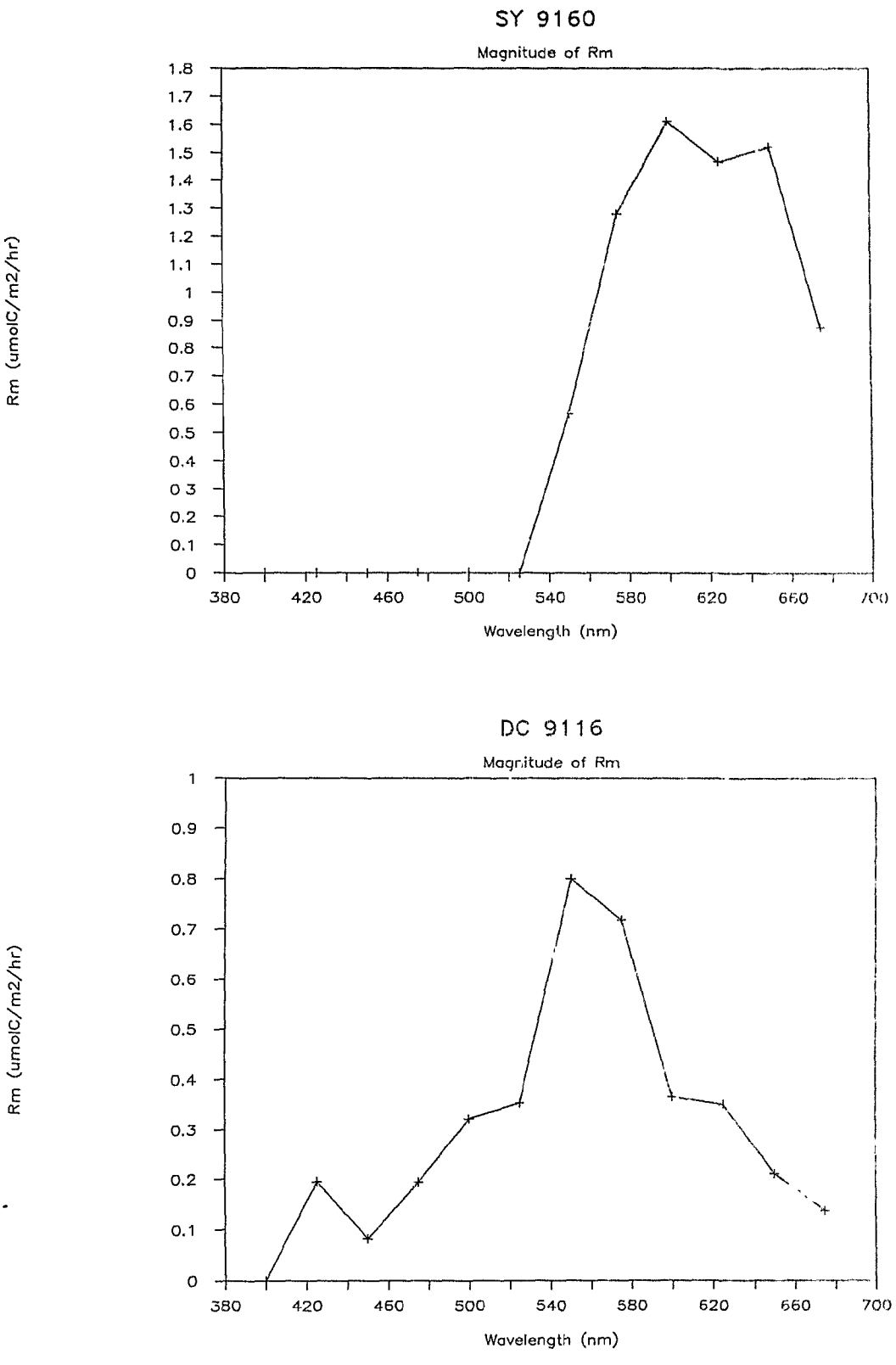
SY 9160
Magnitude of Rm
Rm (umolC/m2/hr)
1.8
1.7
1.6
1.5
1.4
1.3
1.2
1.1
1
0.9
0.8
0.7
0.6
0.5
0.4
0 3
0.2
0.1
0
380
420
460
500
540
580
620
660
Wavelength (nm)
DC 9116
Magnitude of Rm
Rm (umolC/m2/hr)
1
0.9
0.8
0.7
0.6
0.5
0.4
0.3
0.2
0.1
0
380
420
460
500
540
580
620
660
700
Wavelength (nm)

Figure 7. 19

Figure 8. 1. Hypothetical interaction between photosynthetic and respiratory electronm transport in cyanobacteria.

(a) The basic electron transfer reactions.

(b) The pattern of electron flow in the dark.

(c) The pattern of electron flow under Light 2 when PS II is preferentially excited.

(d) The pattern of electron flow under Light 1 when PS I is preferentially excited.

(a) Interaction of photosynthetic and respiratory electron transport pathways.

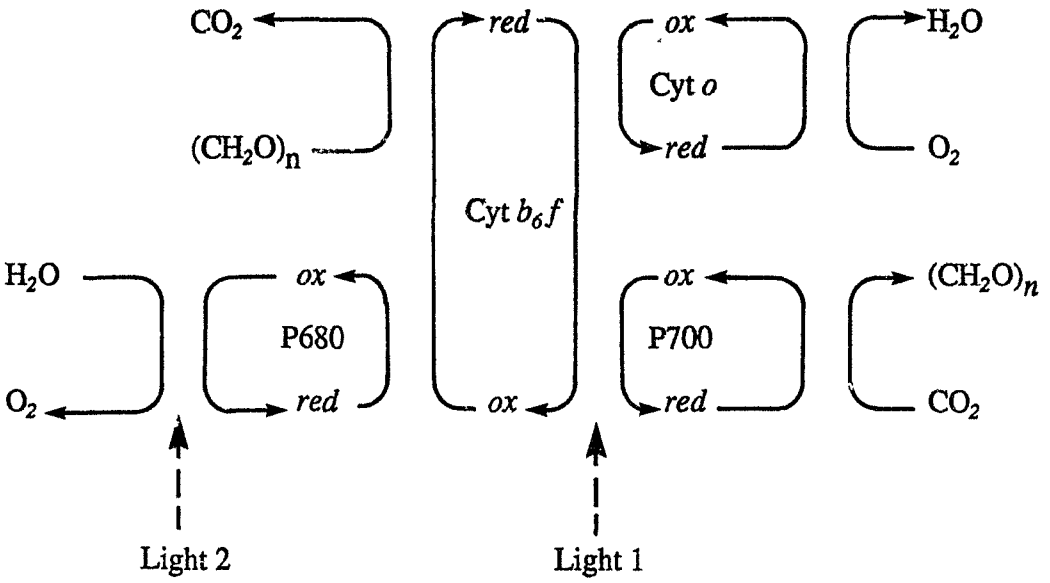

(b) Pattern of electron flow in the DARK.

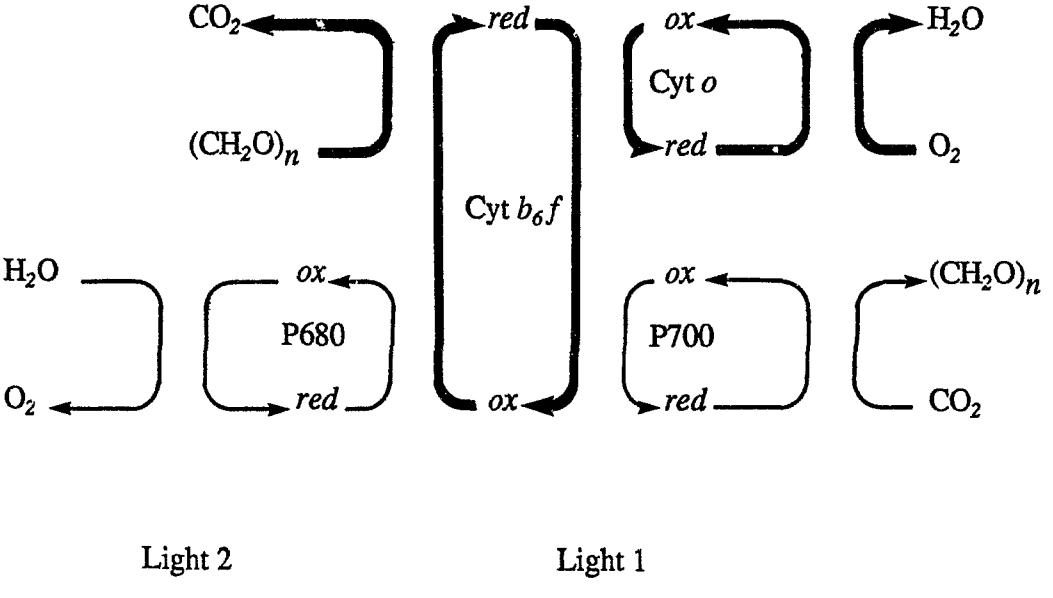

Figure 8. 1

(c) Pattern of electron flow under LIGHT 2.

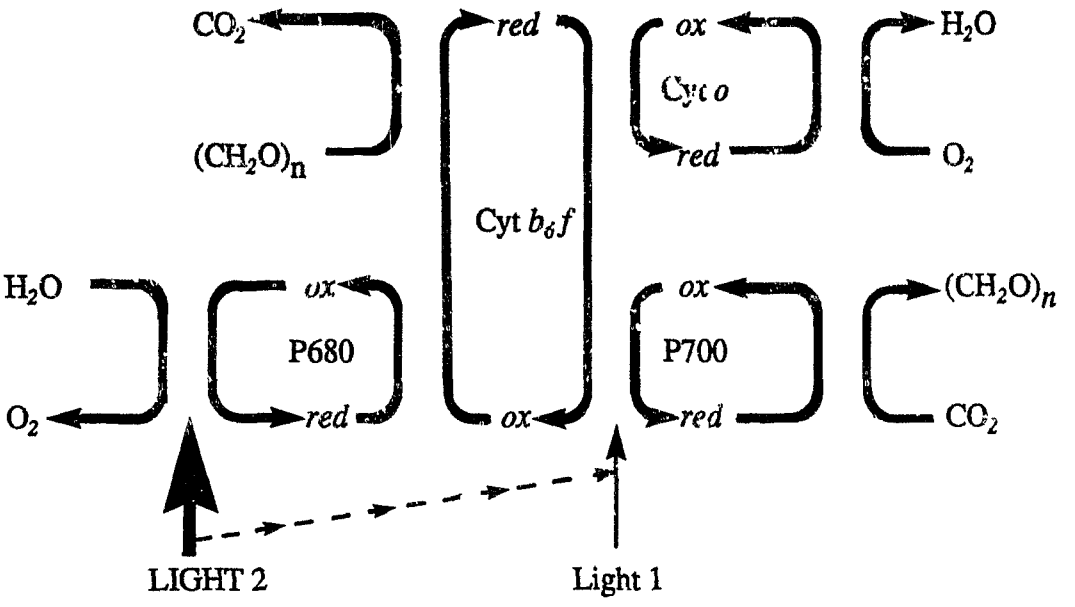

(d) Pattern of electron flow under LIGHT 1.

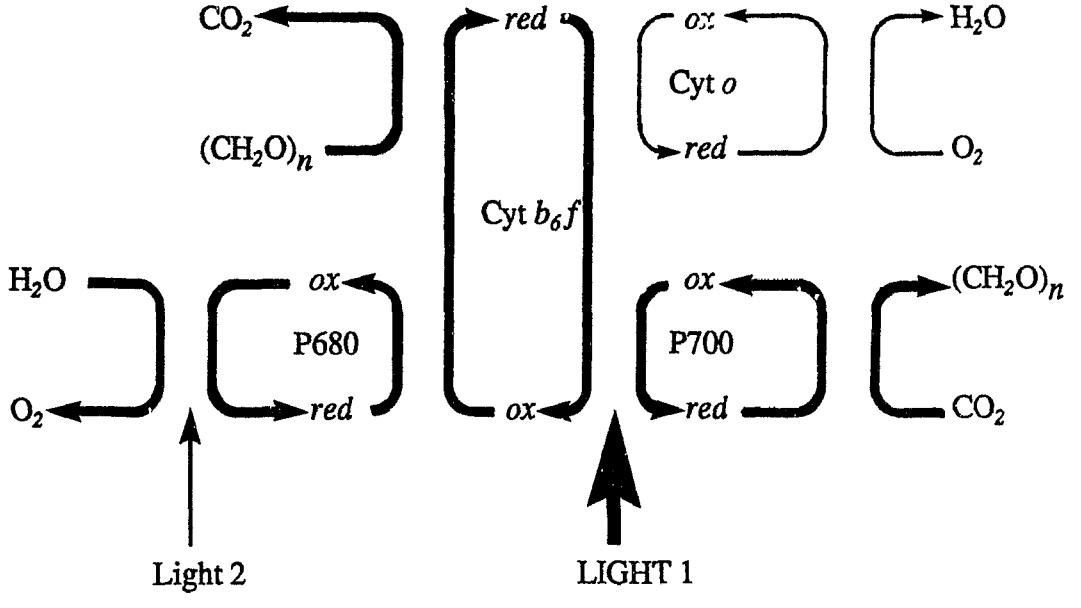

Figure 8. 1 (contd.)

Figure 8. 2. Relative spectral response ($\alpha(\lambda)$) of different phytoplankton and fractional spectral composition ($I(\lambda)$) of different light sources used in simulation model.

(a) Relative photosynthetic action spectra of natural phytoplankton assemblages from the eastern Canadian Arctic (□), the prymnesiophyte *Pavlova* sp. (clone NEP) (+), and the cyanobacteria *Synechococcus* sp. WH 5701 (◇) and *Synechococcus* sp. WH 7803 (△).

(b) Fractional spectral composition of natural sunlight at the sea surface (□), "white" tungsten light (+), blue polychromatic light (◇) and green polychromatic light (△).

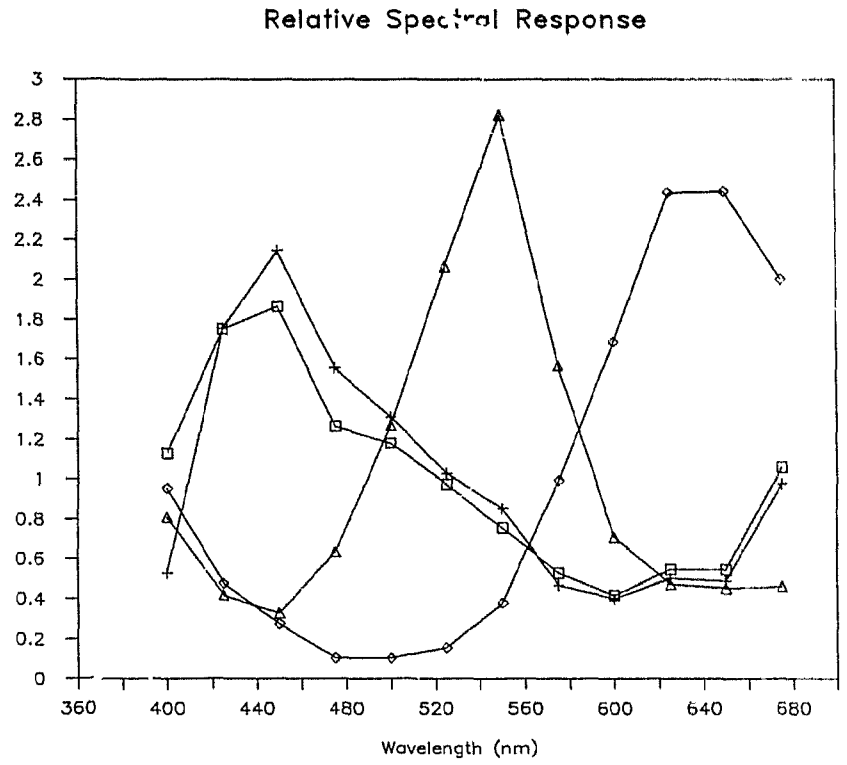
Relative Spectral Response
3
2.8
2.6
2.4
2.2
2
1.8
1.6
1.4
1.2
1
0.8
0.6
0.4
0.2
0
360
400
440
480
520
560
600
640
680
Wavelength (nm)

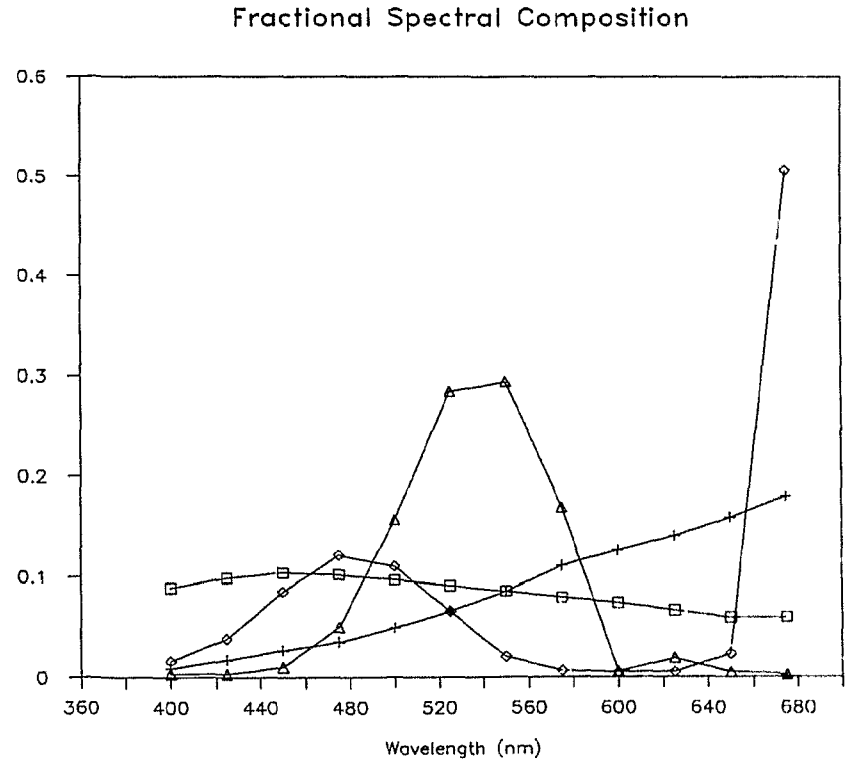
Fractional Spectral Composition
0.6
0.5
0.4
0.3
0.2
0.1
0
360
400
440
480
520
560
600
640
680
Wavelength (nm)

Figure 8.2

Figure 8. 3. Spectral attenuation coefficients ($k(\lambda)$; m^{-1}) for different wavelengths in different water types. Values calculated from Jerlov (1976; Table XXVI). The upper panel is for oceanic water types I (□), IA (+), IB (◇), II (△) and III (×). The lower panel is for coastal waters types 1 (□), 3 (+), 5 (◇), 7 (△) and 9 (×).

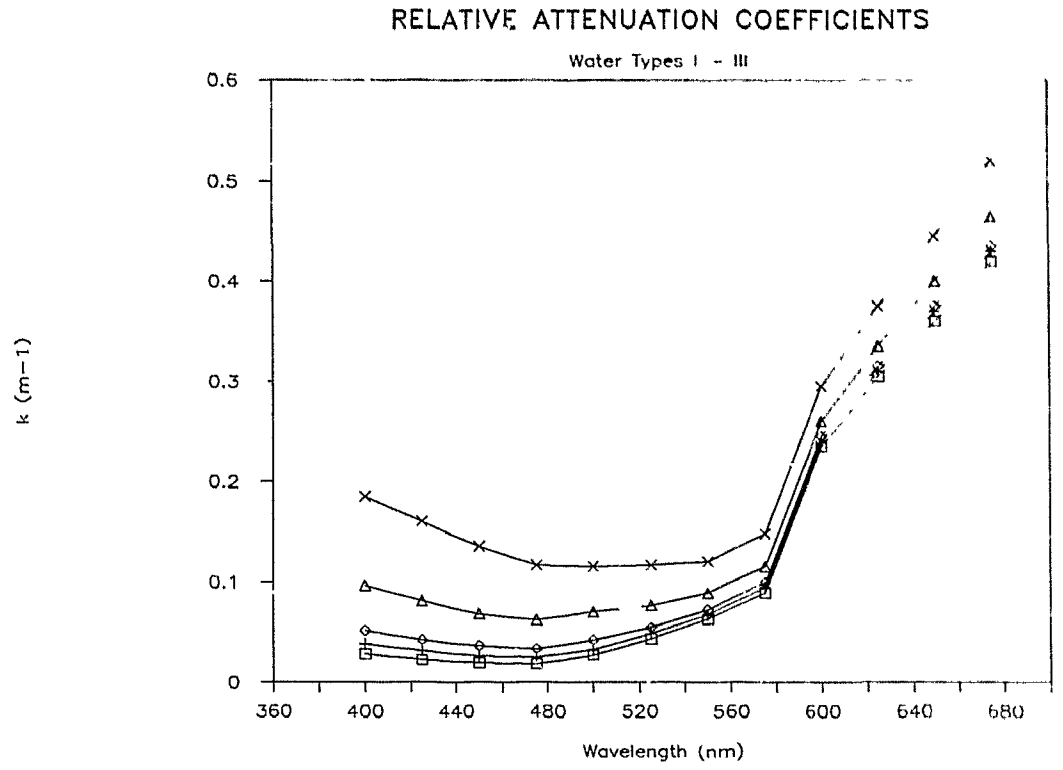
RELATIVE ATTENUATION COEFFICIENTS
Water Types I - III
k (m-1)
0.6
0.5
0.4
0.3
0.2
0.1
0
360
400
440
480
520
560
600
640
680
Wavelength (nm)

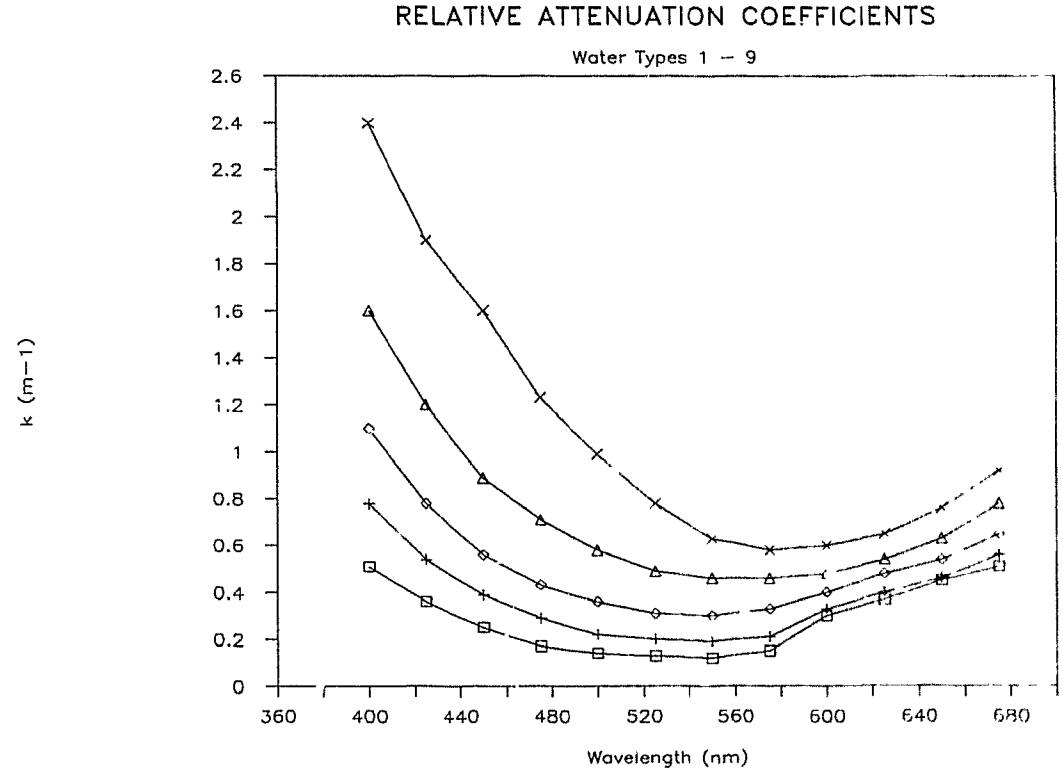
RELATIVE ATTENUATION COEFFICIENTS
Water Types 1 — 9
k (m-1)
2.6
2.4
2.2
2
1.8
1.6
1.4
1.2
1
0.8
0.6
0.4
0.2
0
360
400
440
480
520
560
600
640
680
Wavelength (nm)

Figure 8.3

Figure 8. 4. The quasi-exponential decrease in PAR with depth in oceanic waters. Curves are based upon the spectral composition of sunlight at the sea surface and the spectral attenuation of the component wavelengths with depth (assuming uniform attenuation of each wavelength with depth). The upper panel shows the decrease in PAR relative to the surface (I_z/I_o) in water types I (□), IA (+), IB (◇), II (△) and III (×) as a function of depth. The lower panel shows a logarithmic transformation of the same data (*ie.* $\log_{10}(I_z/I_o)$ versus depth) to illustrate that the decrease in PAR with depth is almost exponential, particularly at depths where $I_z/I_o < 0.5$. The lower limit of I_z/I_o is set to 0.001 corresponding to the 0.1% light level.

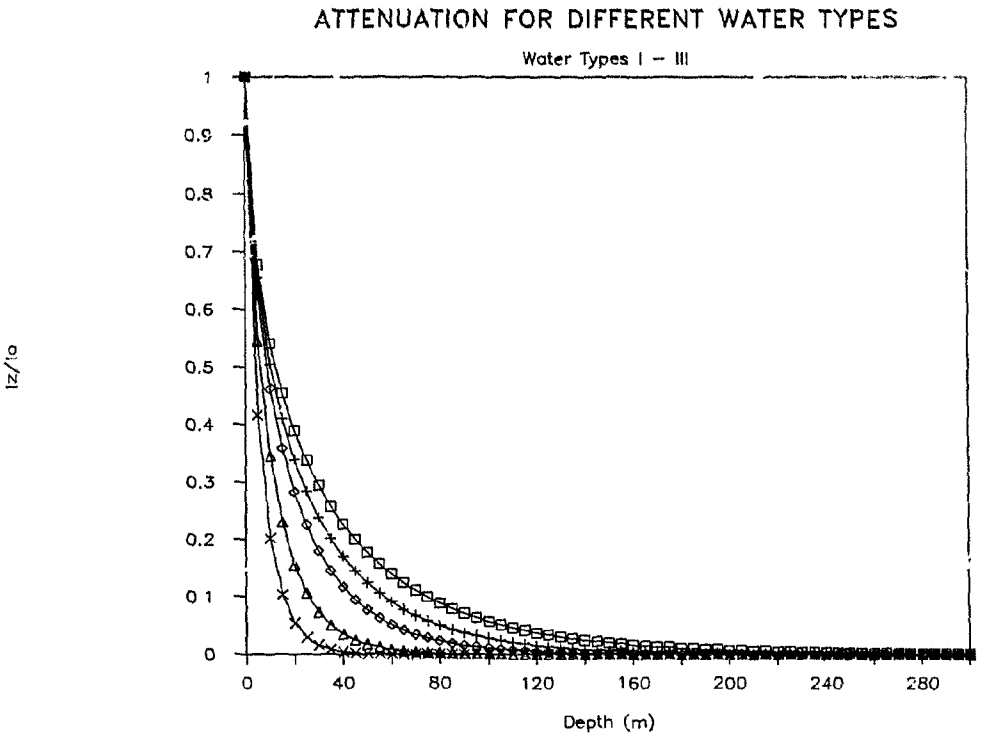
ATTENUATION FOR DIFFERENT WATER TYPES
Water Types I – III
1
0.9
0.8
0.7
0.6
0.5
0.4
0.3
0.2
0.1
0
0
40
80
120
160
200
240
280
Depth (m)
I1/I0

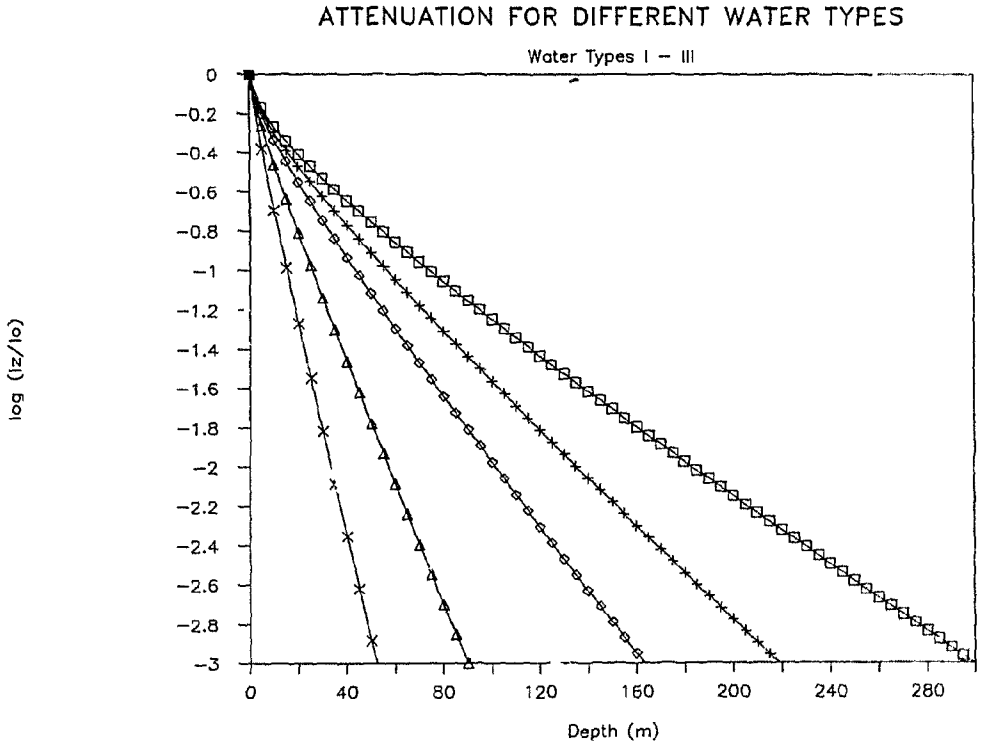
ATTENUATION FOR DIFFERENT WATER TYPES
Water Types I – III
0
-0.2
-0.4
-0.6
-0.8
-1
-1.2
-1.4
-1.6
-1.8
-2
-2.2
-2.4
-2.6
-2.8
-3
0
40
80
120
160
200
240
280
Depth (m)
log (I1/I0)

Figure 8.4

Figure 8. 5. The depth dependence of the light utilization index ($\alpha^{B\prime}$) if the relative action spectrum for photosynthesis ($\alpha^{B}(\lambda)'$) is that of natural phytoplankton assemblages isolated from the eastern Canadian Arctic. The light utilization index is computed for both oceanic (I (□), IA (+), IB (◇), II (△) and III (×)) and coastal water types (1 (□), 3 (+), 5 (◇), 7 (△) and 9 (×)). The upper panel plots the light utilization index as a function of depth. The lower panel plots the light utilization index as a function of the dimensionless PFD I_z/I_o. Light utilization indices were computed for all depths for $1 \leq I_z/I_o \leq 0.001$, a depth maximum corresponding to the 0.1% light level.

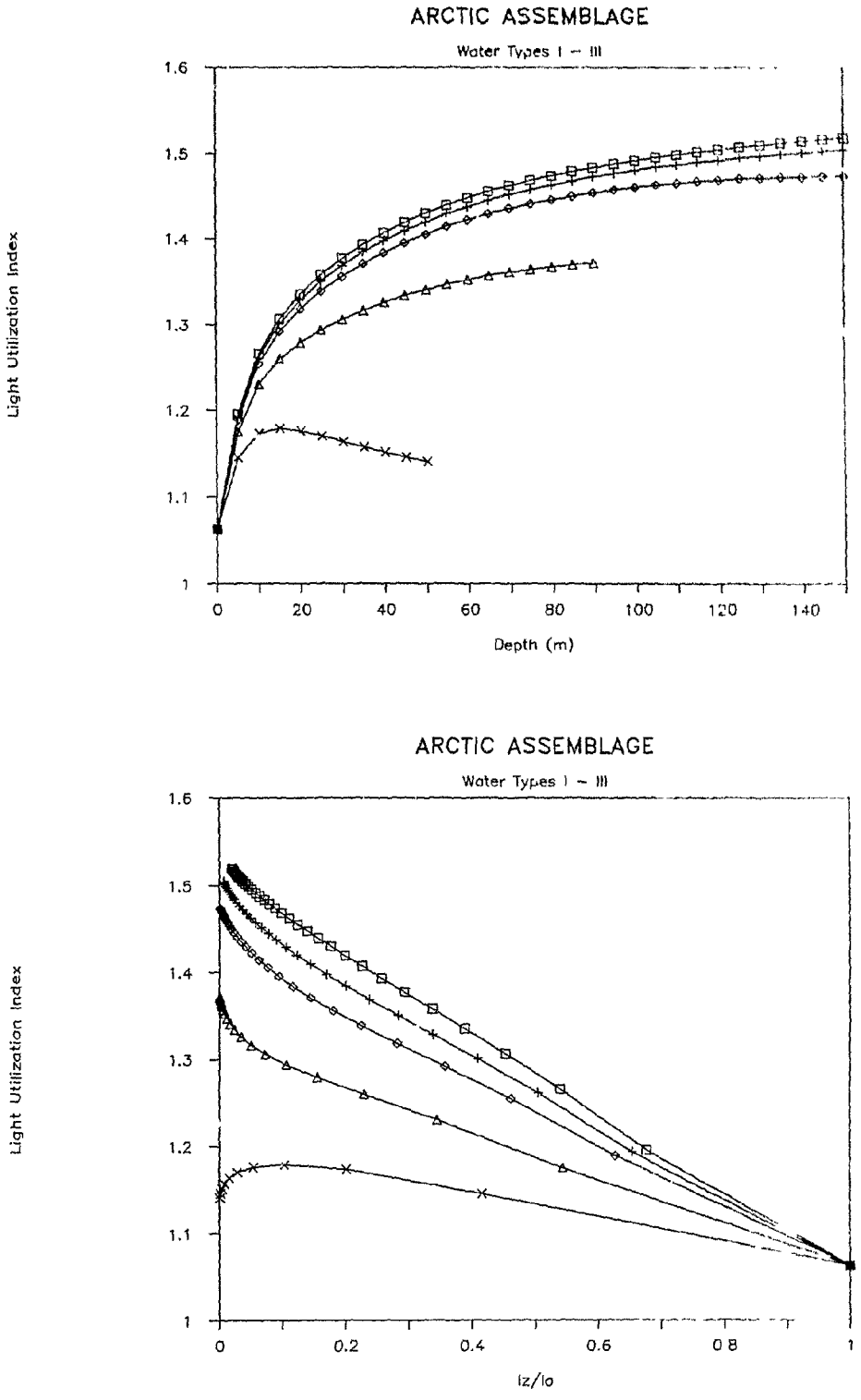
ARCTIC ASSEMBLAGE
Water Types I – III
Light Utilization Index
1.6
1.5
1.4
1.3
1.2
1.1
1
0
20
40
60
80
100
120
140
Depth (m)
ARCTIC ASSEMBLAGE
Water Types I – III
Light Utilization Index
1.6
1.5
1.4
1.3
1.2
1.1
1
0
0.2
0.4
0.6
0 8
1
Iz/Io

Figure 8.5

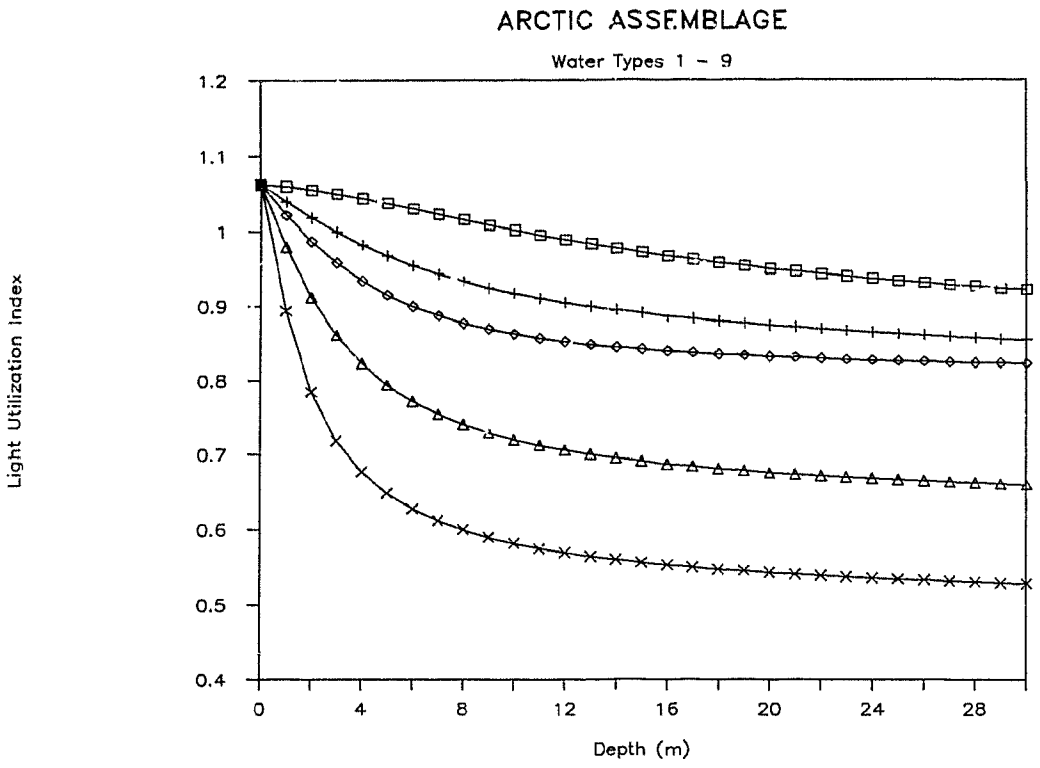

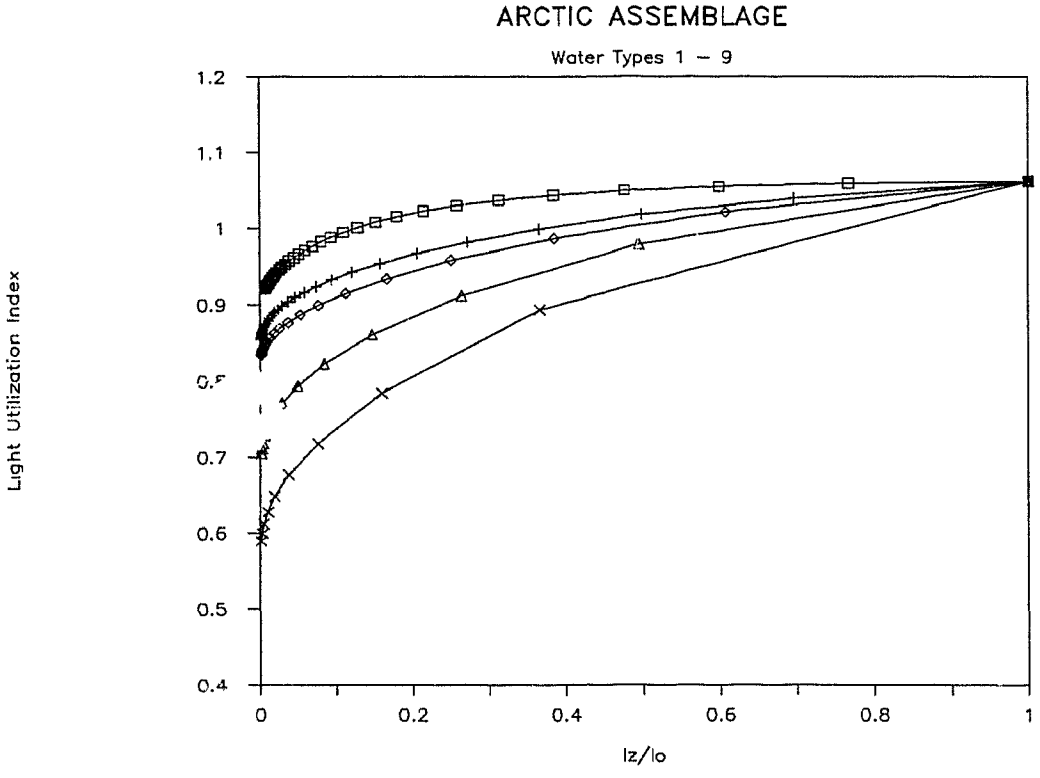

Figure 8. 5 (contd.)

Figure 8. 6. The depth dependence of the light utilization index ($\alpha^{B\prime}$) if the relative action spectrum for photosynthesis ($\alpha^{B}(\lambda)'$) is that of the prymnesiophyte *Pavlova* sp. (clone NEP). The light utilization index is computed for both oceanic (I (□), IA (+), IB (◇), II (△) and III (×)) and coastal water types (1 (□), 3 (+), 5 (◇), 7 (△) and 9 (×)). The upper panel plots the light utilization index as a function of depth. The lower panel plots the light utilization index as a function of the dimensionless PFD I_z/I_o. Light utilization indices were computed for all depths for $1 \leq I_z/I_o \leq 0.001$, a depth maximum corresponding to the 0.1% light level.

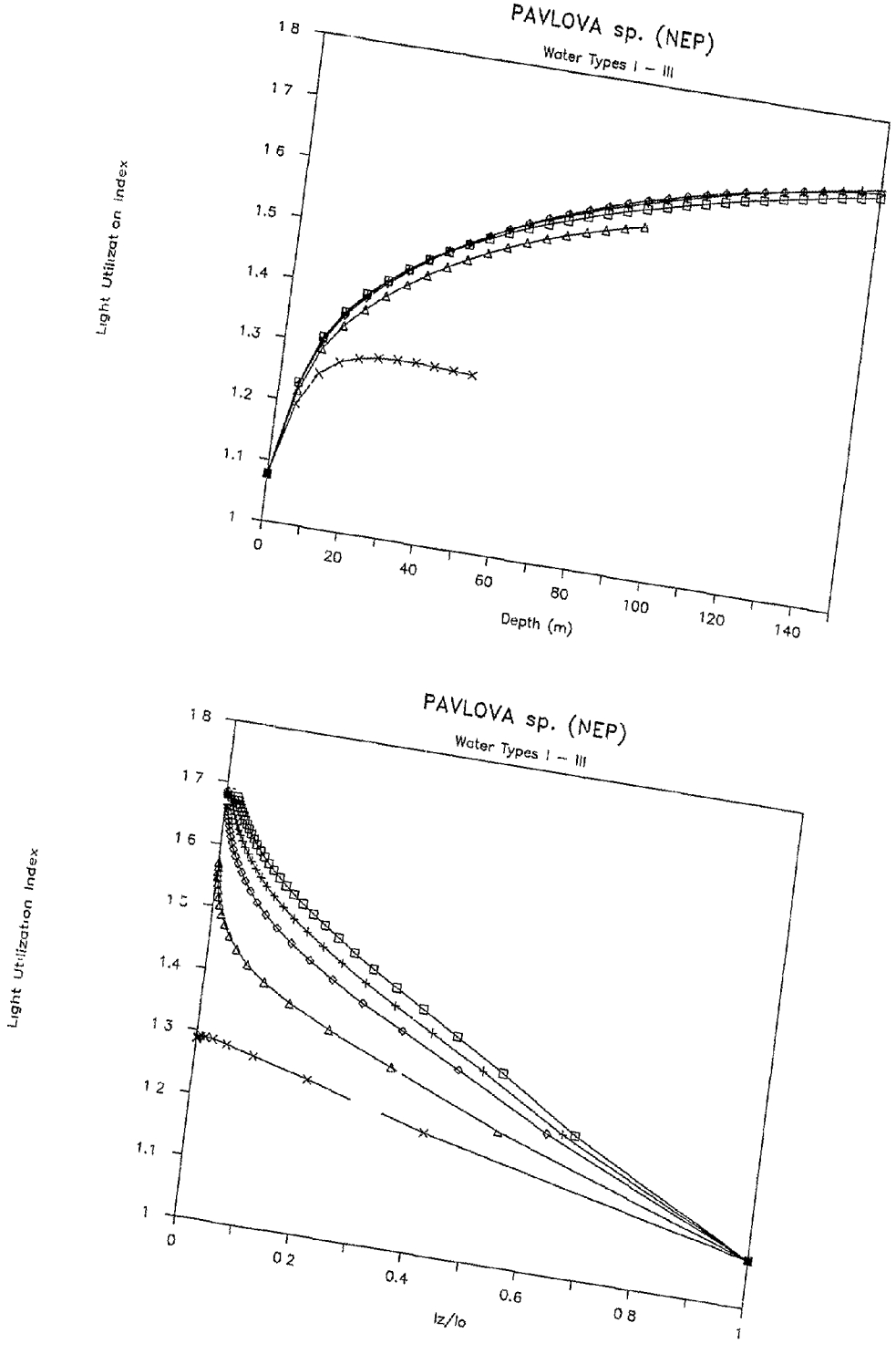
PAVLOVA sp. (NEP)
Water Types I – III
Light Utilization Index
Depth (m)
Iz/Io

Figure 8.6

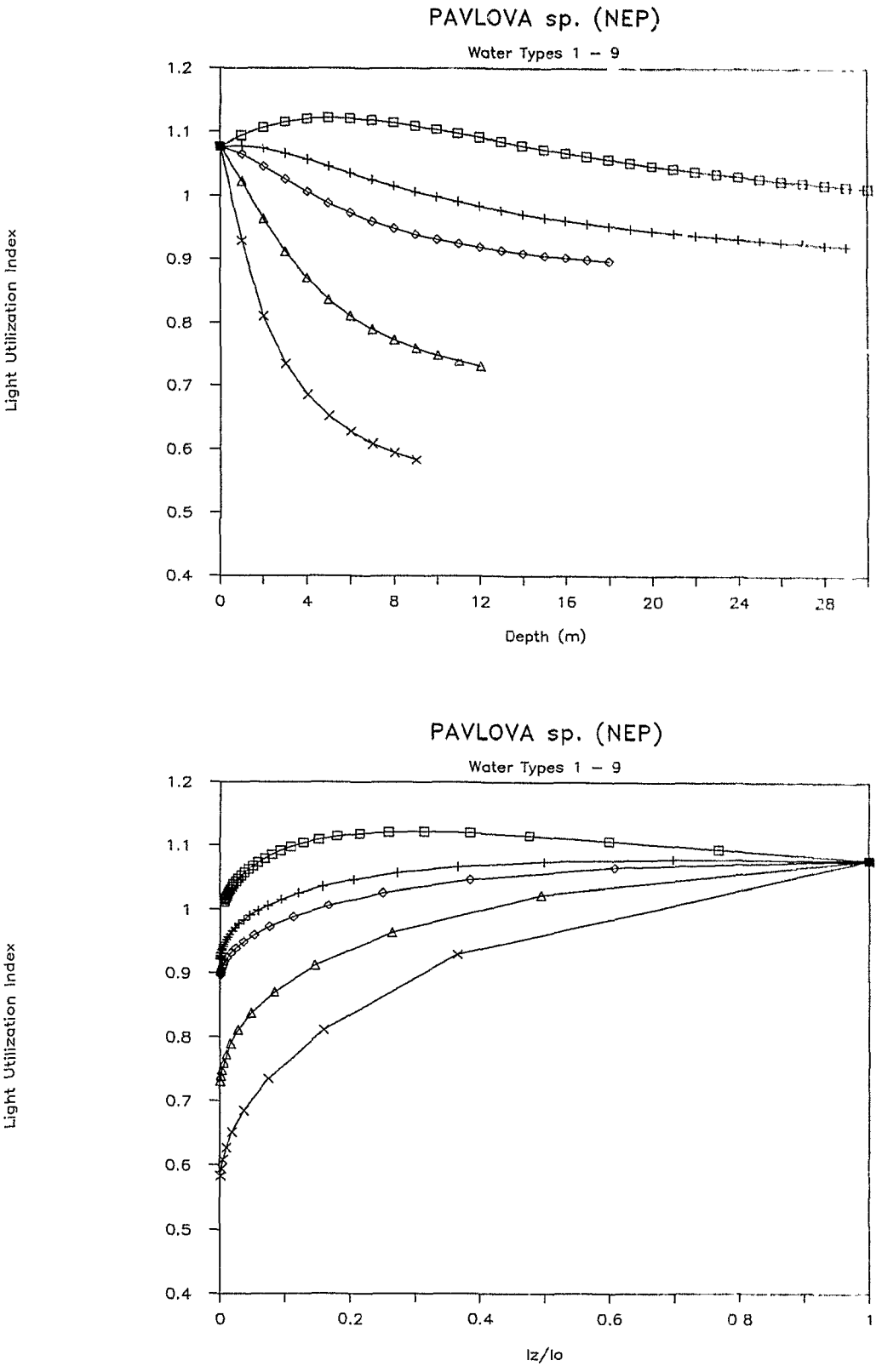

Figure 8. 6 (contd.)

Figure 8. 7. The depth dependence of the light utilization index ($\alpha^{B\prime}$) if the relative action spectrum for photosynthesis ($\alpha^{B}(\lambda)'$) is that of the cyanobacteria *Synechococcus* sp. WH 7803. The light utilization index is computed for both oceanic (I (□), IA (+), IB (◇), II (△) and III (×) and coastal water types (1 (□), 3 (+), 5 (◇), 7 (△) and 9 (×)). The upper panel plots the light utilization index as a function of depth. The lower panel plots the light utilization index as a function of the dimensionless PFD I_z/I_o. Light utilization indices were computed for all depths for $1 \leq I_z/I_o \leq 0.001$, a depth maximum corresponding to the 0.1% light level.

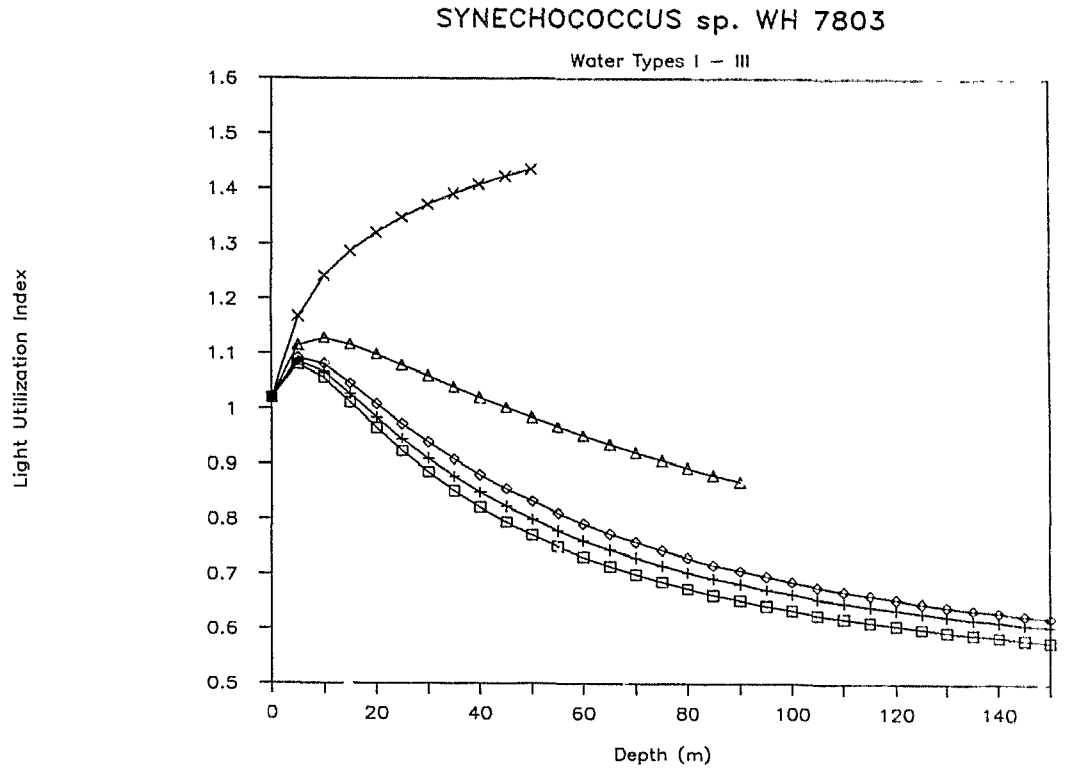
SYNECHOCOCCUS sp. WH 7803
Water Types I – III
Light Utilization Index
1.6
1.5
1.4
1.3
1.2
1.1
1
0.9
0.8
0.7
0.6
0.5
0
20
40
60
80
100
120
140
Depth (m)

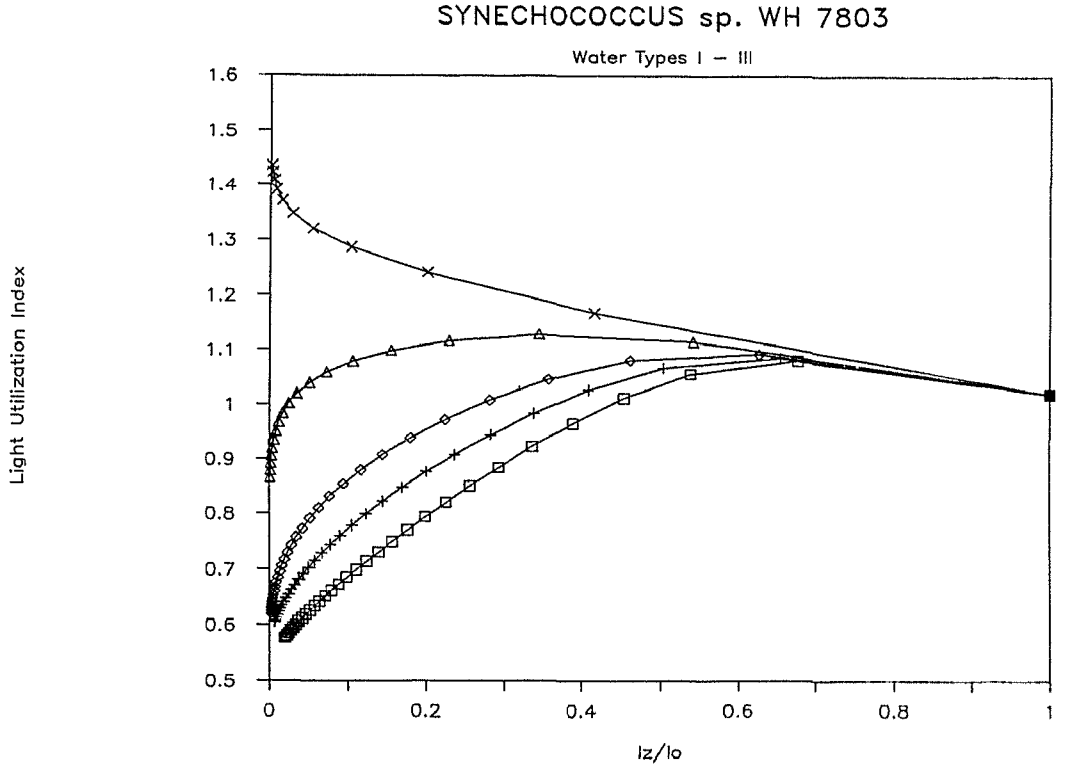
SYNECHOCOCCUS sp. WH 7803
Water Types I – III
Light Utilization Index
1.6
1.5
1.4
1.3
1.2
1.1
1
0.9
0.8
0.7
0.6
0.5
0
0.2
0.4
0.6
0.8
1
Iz/Io

Figure 8.7

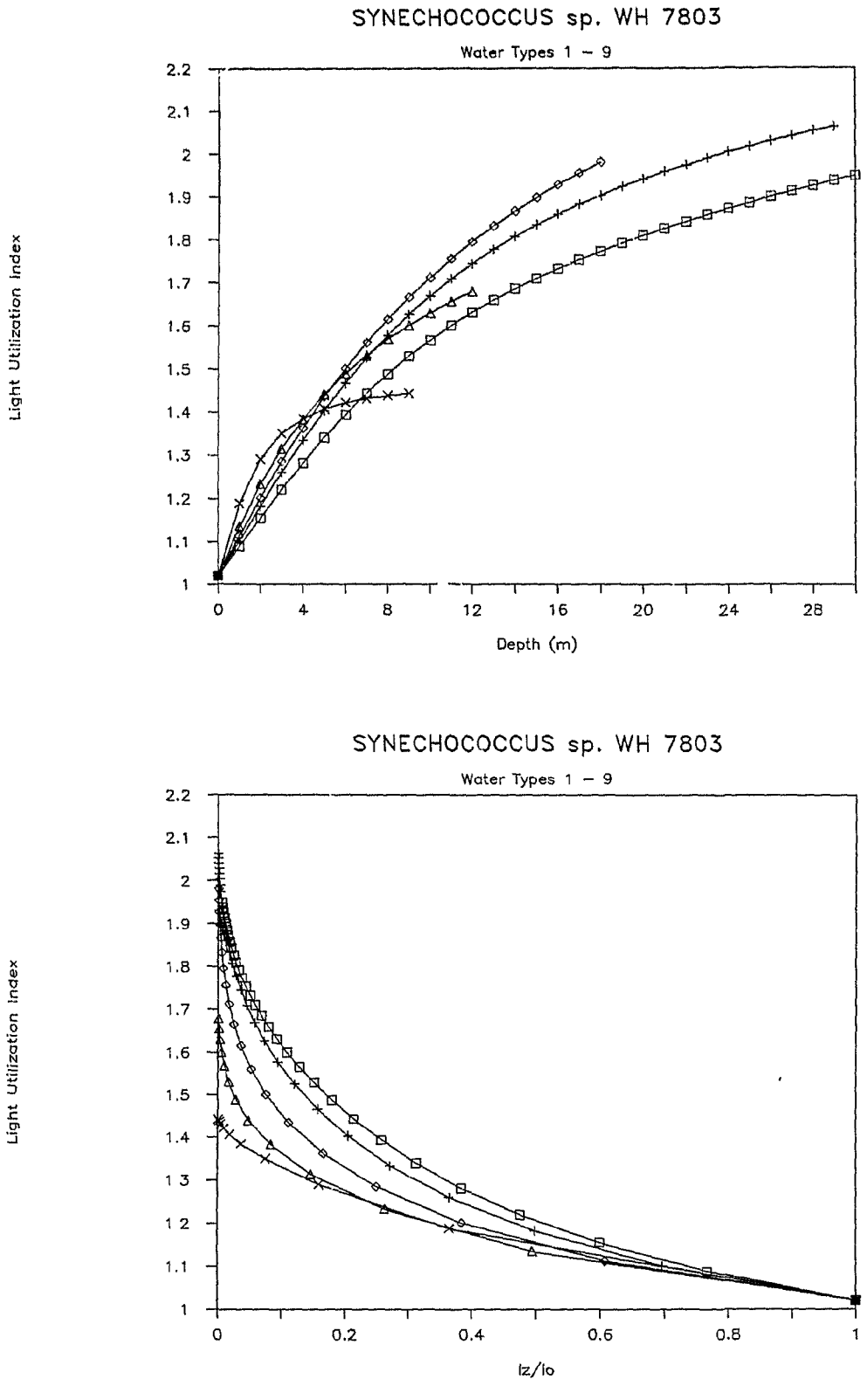

Figure 8.7 (contd.)

Figure 8. 8. The depth dependence of the light utilization index ($\alpha^{B\prime}$) if the relative action spectrum for photosynthesis ($\alpha^{B}(\lambda)'$) is that of the cyanobacteria *Synechococcus* sp. WH 5701. The light utilization index is computed for both oceanic (I (□), IA (+), IB (◇), II (△) and III (×)) and coastal water types (1 (□), 3 (+), 5 (◇), 7 (△) and 9 (×)). The upper panel plots the light utilization index as a function of depth. The lower panel plots the light utilization index as a function of the dimensionless PFD I_z/I_o. Light utilization indices were computed for all depths for $1 \leq I_z/I_o \leq 0.001$, a depth maximum corresponding to the 0.1% light level.

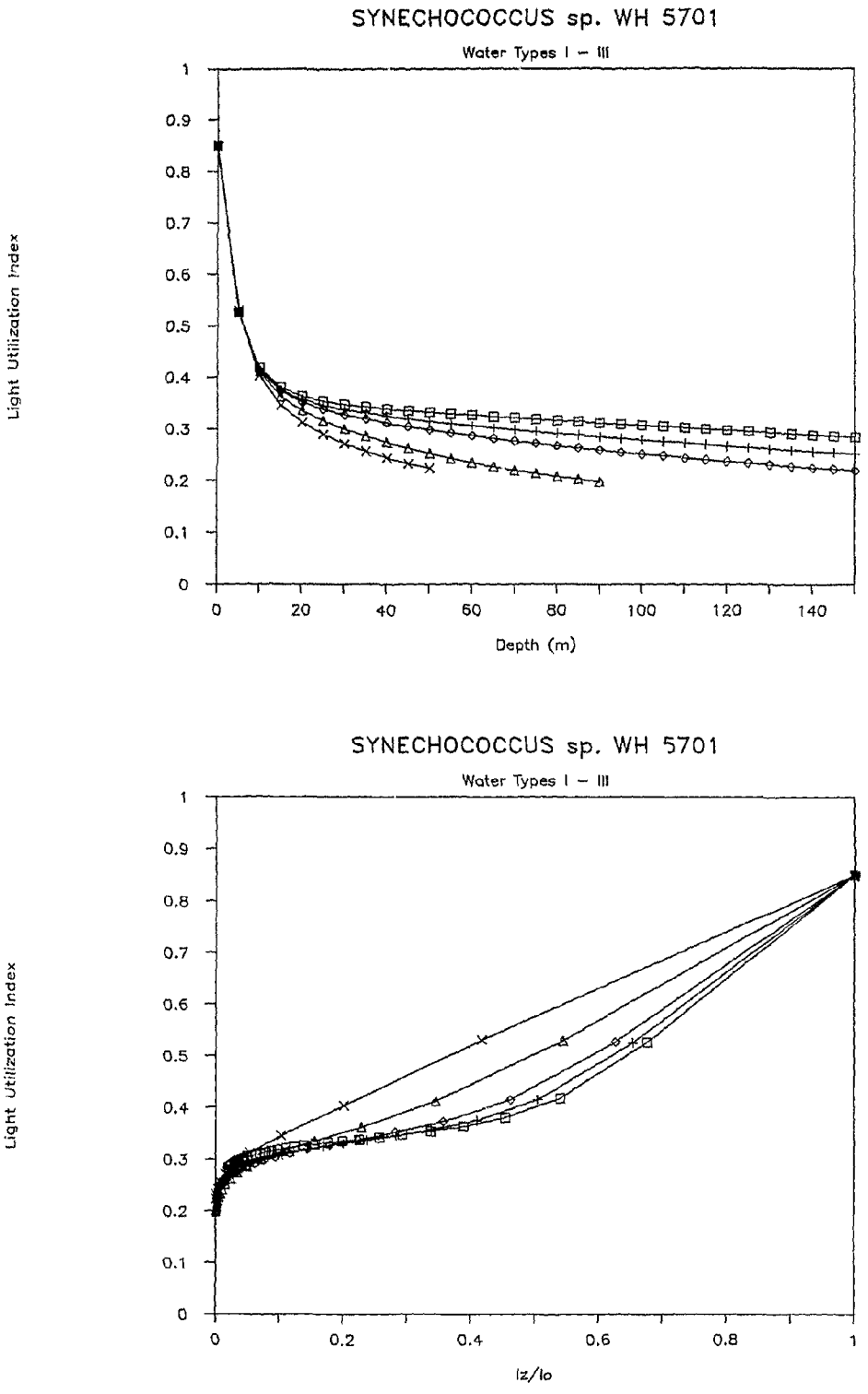
SYNECHOCOCCUS sp. WH 5701
Water Types I – III
Light Utilization Index
Depth (m)
SYNECHOCOCCUS sp. WH 5701
Water Types I – III
Light Utilization Index
Iz/Io

Figure 8.8

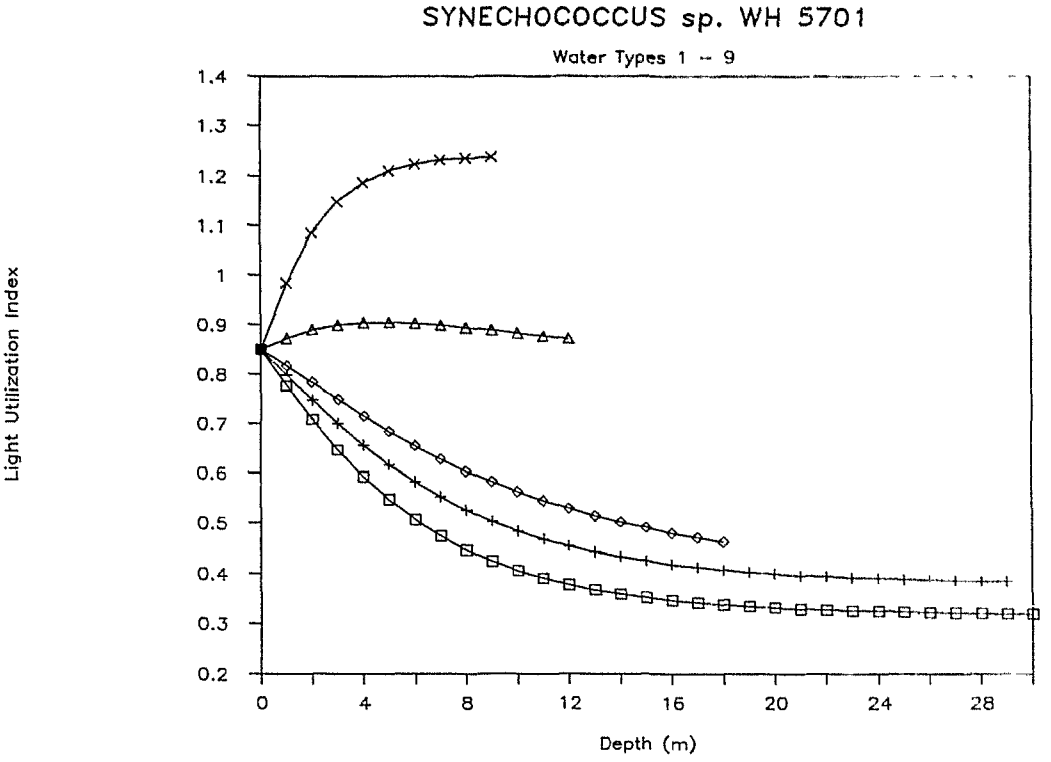

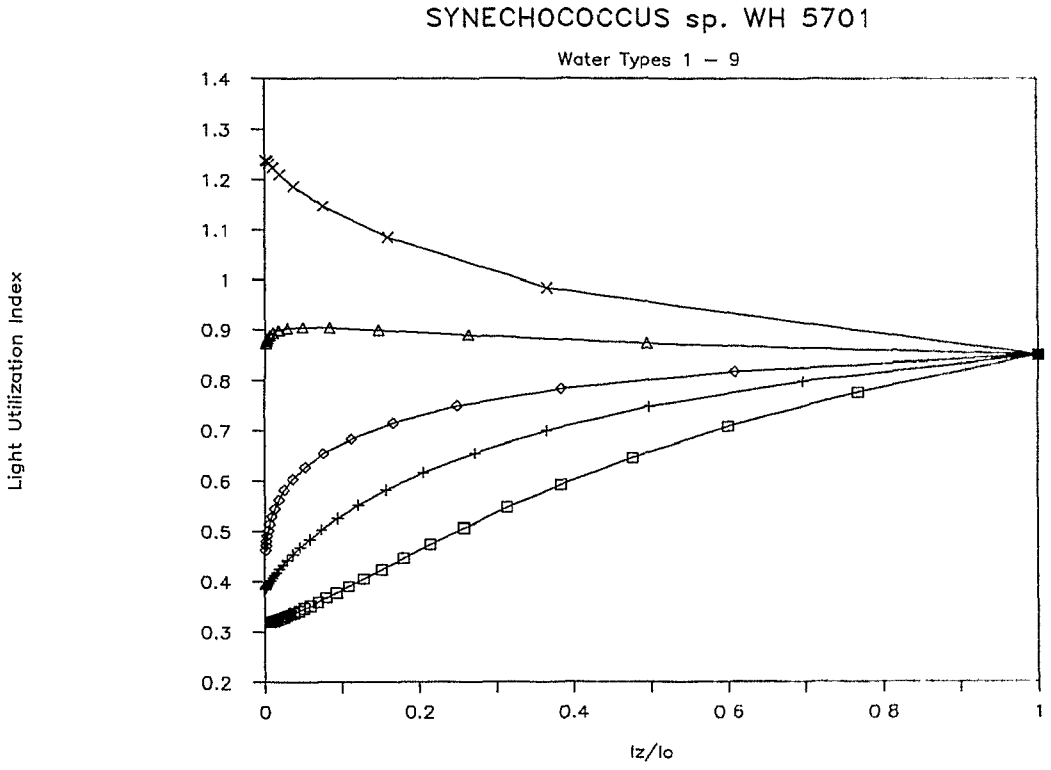

Figure 8. 8 (contd.)

Figure 8. 9. The light utilization index for tungsten light ($\alpha^{B\prime}{}_{T}$) relative to that expected at depth ($\alpha^{B\prime}{}_{Z}$) in water types I (□), III (+), 1 (◇), 5 (△) and 9 (×). The upper panel is case where the relative action spectrum for photosynthesis ($\alpha^{B}(\lambda)'$) resembles that of the natural phytoplankton assemblages of the eastern Canadian Arctic. The lower panel is the case where the relative action spectrum for photosynthesis ($\alpha^{B}(\lambda)'$) resembles that of the prymnesiophyte *Pavlova* sp. (clone NEP).

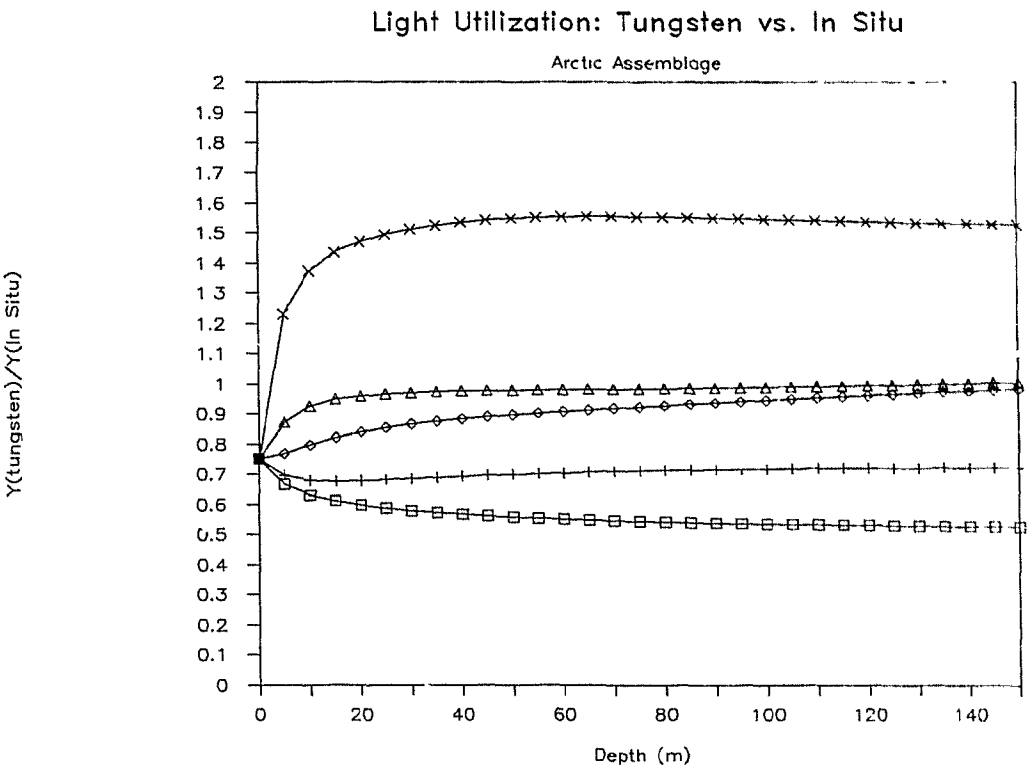
Light Utilization: Tungsten vs. In Situ
Arctic Assemblage
Y(tungsten)/Y(In Situ)
2
1.9
1.8
1.7
1.6
1.5
1.4
1.3
1.2
1.1
1
0.9
0.8
0.7
0.6
0.5
0.4
0.3
0.2
0.1
0
0
20
40
60
80
100
120
140
Depth (m)

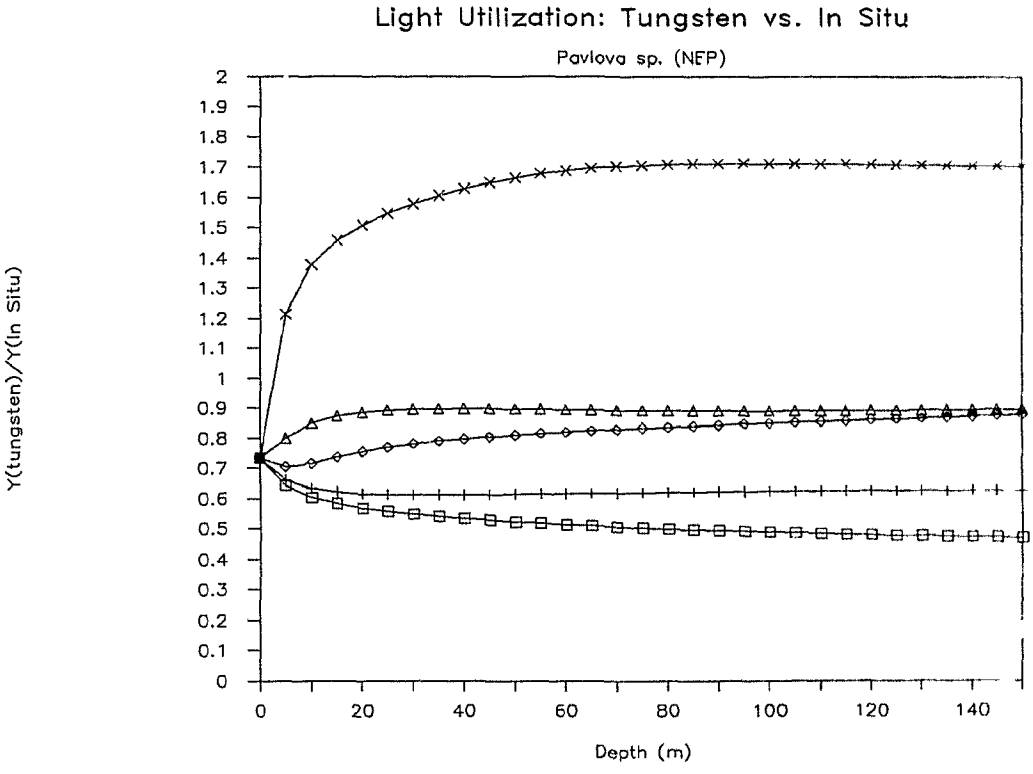
Light Utilization: Tungsten vs. In Situ
Pavlova sp. (NEP)
Y(tungsten)/Y(In Situ)
2
1.9
1.8
1.7
1.6
1.5
1.4
1.3
1.2
1.1
1
0.9
0.8
0.7
0.6
0.5
0.4
0.3
0.2
0.1
0
0
20
40
60
80
100
120
140
Depth (m)

Figure 8.9

Figure 8. 10. The light utilization index in tungsten light ($\alpha^{B'}{}_{T}$) relative to that expected at depth ($\alpha^{B'}{}_{Z}$) in water types I (□), III (+), 1 (◇), 5 (△) and 9 (×). The upper panel is case where the relative action spectrum for photosynthesis ($\alpha^{B}(\lambda)'$) resembles that of the cyanobacterium *Synechococcus* sp. WH 5701. The lower panel is the case where the relative action spectrum for photosynthesis ($\alpha^{B}(\lambda)'$) resembles that of the cyanobacterium *Synechococcus* sp. WH 7803.

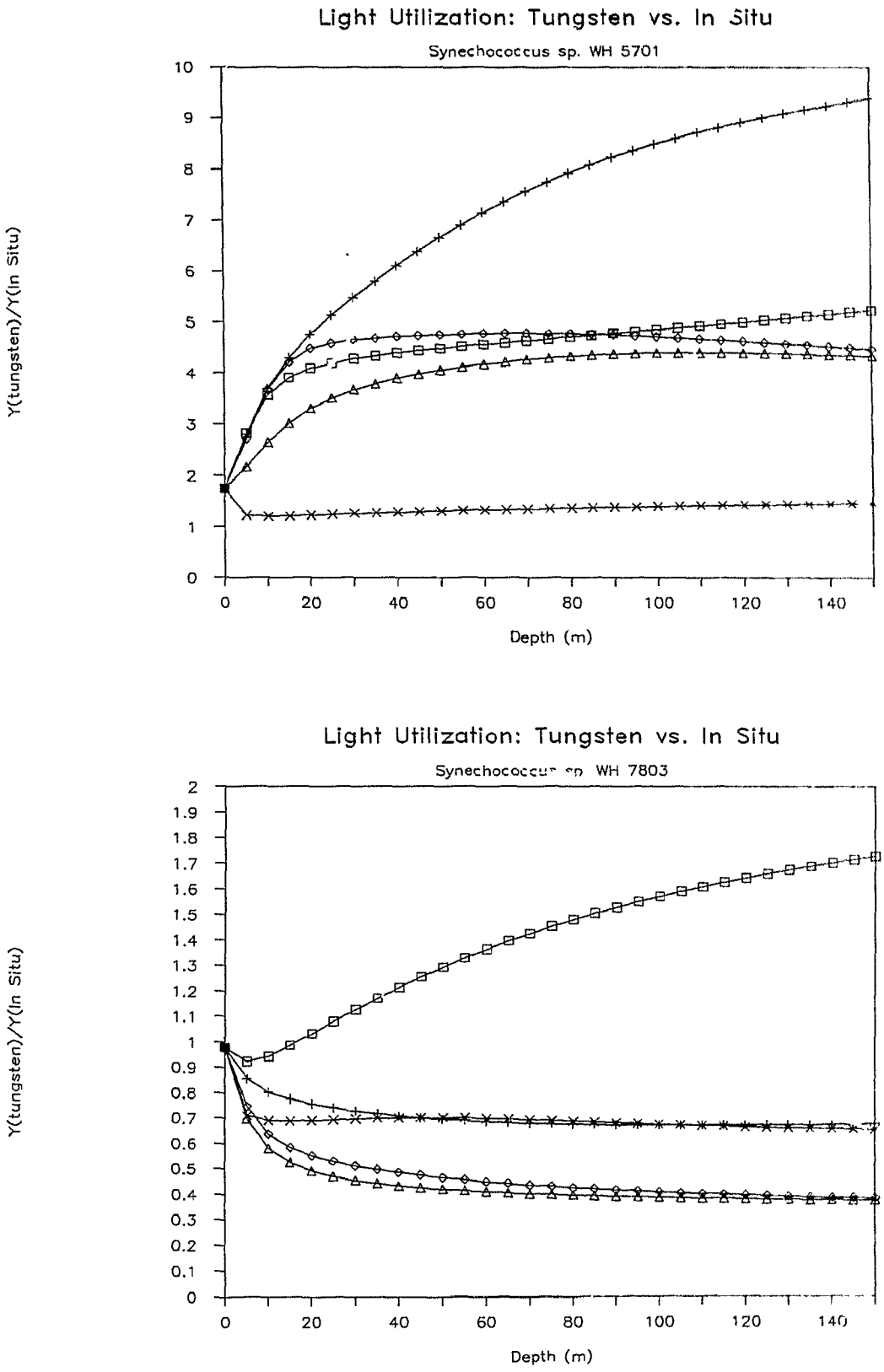
Light Utilization: Tungsten vs. In Situ
Synechococcus sp. WH 5701
Y(tungsten)/Y(In Situ)
Depth (m)
Light Utilization: Tungsten vs. In Situ
Synechococcus sp. WH 7803
Y(tungsten)/Y(In Situ)
Depth (m)

Figure 8. 10

APPENDIX A

Equivalence between the formulation of Fasham and Platt (1983) in the absence of photoinhibition and the generalized non-rectangular formulation of Thornley (1976).

Fasham and Platt (1983) expression:

$$P^2 - (\mu + (\chi + \alpha)I)P + \alpha \mu I = 0 \qquad ...(1)$$

As $I \rightarrow \infty$ then

$$P = P_m = \frac{\mu}{1 + \chi/\alpha} \qquad ...(2)$$

so that

$$\mu = P_m(1 + (\chi/\alpha)) \qquad ...(3)$$

Substituting (3) into (1) yields:

$$P^2 - [P_m(1 + \chi/\alpha) + (\chi + \alpha)I]P + \alpha[P_m(1 + \chi/\alpha)]I = 0$$

or

$$P^2 - [\alpha + \chi(P_m/\alpha + I)]P + (\alpha + \chi)P_m I = 0 \qquad ...(4)$$

Multiplying across by $\alpha/(\alpha + \chi)$ yields:

$$[\alpha/(\alpha + \chi)]P^2 - (P_m + \alpha I)P + \alpha P_m I = 0 \qquad ...(5)$$

which equals the expression of Thornley (1976):

$$\Theta P^2 - (P_m + \alpha I)P + \alpha P_m I = 0 \qquad ...(6)$$

where $\Theta = \alpha/(\alpha + \chi)$.

APPENDIX B

Incubation apparatus used in ^{14}C uptake experiments. Phytoplankton cultures and natural seawater samples were incubated in scintillation vials (V) held in a temperature-controlled aluminum block (B). Irradiance from the tungsten-halogen lamp (L) passed through a cooling cuvette of running water (C) and a series of optical filters before striking the base of the scintillation vial. Both interference filters (IF) and neutral density filters (NDF) were used when determining the monochromatic action spectrum. Only neutral density filters were used when determining the P-I response in "white" tungsten light. Blue or green acetate filters (AF) and neutral density filters were used for measuring the P-I response in blue and green polychromatic light.

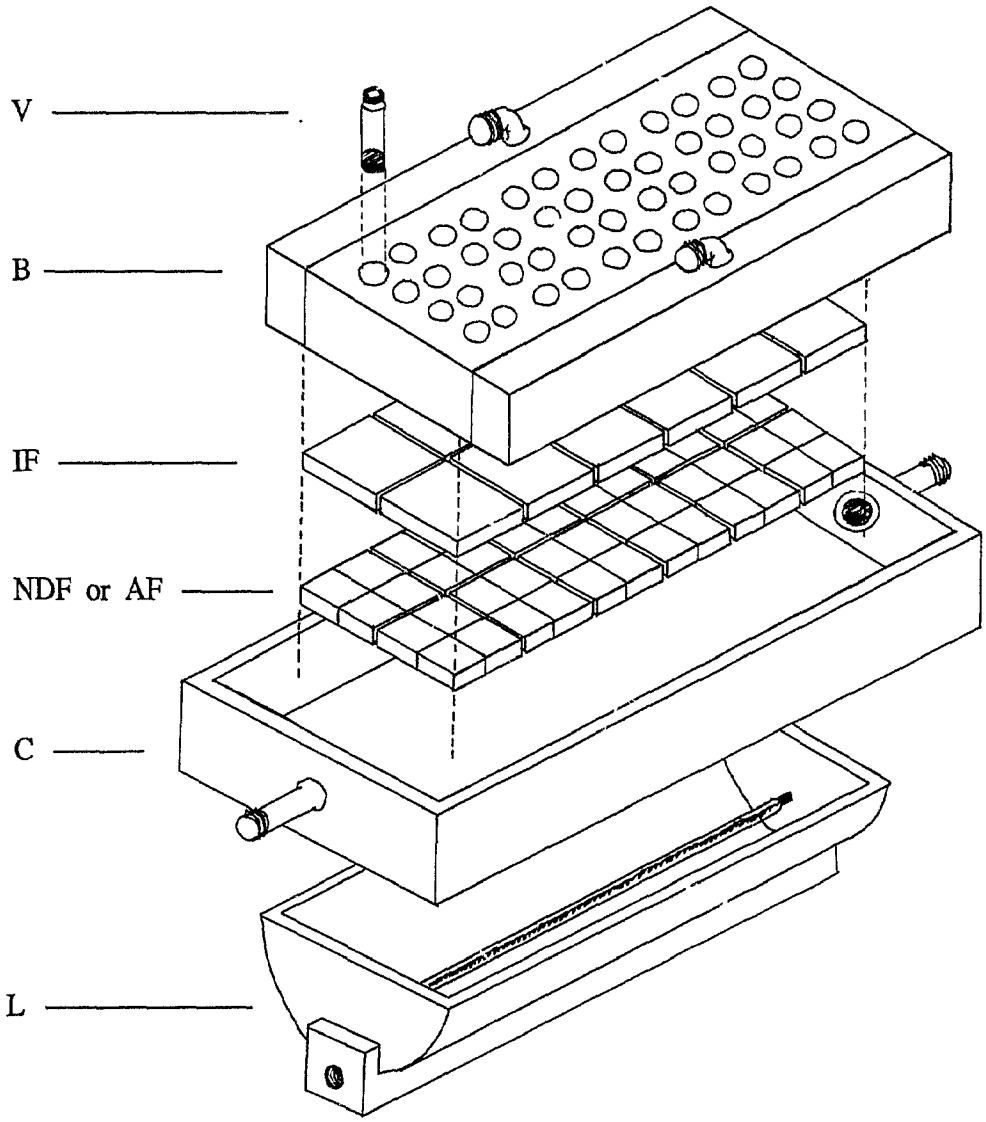

BIBLIOGRAPHY.

Alberte R.S., Wood A.M., Kursar T.A. and Guillard R.R.L. (1984) Novel phycoerythrins in marine *Synechococcus* spp.: Characterization and evolutionary and ecological implications. Plant Physiol. 75: 732-739.

Amesz J. and Duysens L.N.M. (1962) Action spectrum, kinetics and quantum requirement of phosphopyridine nucleotide reduction and cytochrome oxidation in the blue-green alga *Anacystis nidulans*. Biochim. Biophys. Acta 64: 261-278.

Anderson L.K., Rayner N.C., Sweet R.M. and Eiserling F.A. (1983) Regulation of *Nostoc* sp. phycobilisome structure by light and temperature. J. Bacteriol. 155: 1407-1416.

Arnold W. (1935) Kinetics of photosynthesis in *Chlorella*. Cold Spring Harbour Symposia on Quantitative Biology 3: 124-127.

Arnold W. and Kohn H.I. (1934) The chlorophyll unit in photosynthesis. J. Gen. Physiol. 18: 109-112.

Arpin N., Svec W.A. and Liaaen-Jensen S. (1976) New fucoxanthin-related carotenoids from *Coccolithus huxleyi*. Phytochem. 15: 529-532.

Atlas D. and Bannister T.T. (1980) Dependence of mean spectral extinction coefficient of phytoplankton on depth, water color and species. Limnol. Oceanogr. 25: 157-159.

Azam F., Fenchel T., Field J.G., Gray J.S., Meyer-Reil L.A. and Thingstad F. (1983) The ecological role of water-column microbes in the sea. Mar. Ecol. Prog. Ser. 10: 257-263.

Baly E.C. (1935) The kinetics of photosynthesis. Proc. Roy. Soc. Lond. B 117: 218-237.

Bannister T.T. (1974) Production equations in terms of chlorophyll concentration, quantum yield, and the upper limit to production. Limnol. Oceanogr. 19: 1-12.

Bannister T.T. (1979) Quantitative description of steady state, nutrient-saturated algal growth, including adaptation. Limnol. Oceanogr. 24: 76-96.

Bannister T.T. and Vrooman M.J. (1964) Enhancement of the photosynthesis of *Chlorella pyrenoidosa* as a function of far-red and short-wave illuminations. Plant Physiol. 39: 622-629.

Bannister T.T. and Weidemann A.D. (1984) The maximum quantum efficiency of phytoplankton photosynthesis *in situ*. J. Plankton Res. 6: 275-294.

Banse K. (1976) Rates of growth, respiration and photosynthesis of unicellular algae as related to cell size - a review. J. Phycol. 12: 135-140.

Bard Y. (1974) Non-linear parameter estimation. Academic Press, New York, NY., 332 pp.

Barlow R.G. and Alberte R.S. (1985) Photosynthetic characteristics of phycoerythrin-containing marine *Synechococcus* spp. I. Responses to growth photon flux density. Mar. Biol. 86: 63-74.

Barlow R.G. and Alberte R.S. (1987) Photosynthetic characteristics of phycoerythrin-containing marine *Synechococcus* spp. II. Time course responses of photosynthesis to photoinhibition. Mar. Ecol. Prog. Ser. 39: 191-196.

Baule B. (1917) Zu Mitscherlichs Gesetz der physiologischen Beziehungen. Landw. Jahrbuch 51: 363-385.

Baumert H. and Uhlmann D. (1983) Theory of the upper limit to phytoplankton production per unit area in natural waters. Int. Rev. Ges. Hydrobiol. 68: 753-783.

Beers J.R., Reid F.M.H. and Stewart G.L. (1975) Microplankton of the North Pacific central gyre. Population structure and abundance, June 1973. Int. Revue Ges. Hydrobiol. 60: 607-638.

Beers J.R., Reid F.M.H. and Stewart G.L. (1982) Seasonal abundance of the microplankton population in the North Pacific central gyre. Deep-Sea Res. 29: 227-245.

Bender M., Grande K., Johnson K., Marra J., Williams P.J.LeB., Sieburth J., Pilson M., Langdon C., Hitchcock G., Orchardo J., Hunt C., Donaghay P. and Heinemann K. (1987) A comparison of four methods for determining planktonic community production. Limnol. Oceanogr. 32: 1085-1097.

Bevington P.R. (1969) Data redeuction and error analysis for the physical sciences. McGraw Hill, New York, NY. 336 pp.

Bidwell R.G.S. (1977) Photosynthesis and light and dark respiration in freshwater algae. Can. J. Bot. 55: 802-818.

Bidigare R.R., Kennicutt M.C.II. and Brooks J.M. (1985) Rapid determination of chlorophylls and their degradation products by high-performance liquid chromatography. Limnol. Oceanogr. 30: 432-435.

Bienfang P.K. and Szyper J.P. (1981) Phytoplankton dynamics in the subtropical Pacific Ocean off Hawaii. Deep-Sea Res. 28: 981-1000.

Bienfang P.K. and Takahashi M. (1983) Ultraplankton growth rates in a subtropical ecosystem. Mar. Biol. 76: 213-218.

Blackman F.F. (1905) Optima and limiting factors. Ann. Bot. 19: 281.

Blasco D., Packard T.T. and Garfield P.C. (1982) Size dependence of growth rate, respiratory electron transport system activity and chemical composition in marine diatoms in the laboratory. J. Phycol. 18: 58-63.

Blum J.J. (1977) On the geometry of four-dimensions and the relationship between metabolism and body size. J. Theor. Biol. 64: 599-601.

Bricaud A. (1989) Ph.D thesis, Université de P. et M. Curie, Paris VI.

Bricaud A. and Morel A. (1986) Light attenuation and scattering by phytoplanktonic cells: a theoretical modelling. Appl. Opt. 25: 571-580.

Bricaud A., Morel A. and Prieur L. (1981) Absorption by dissolved organic matter of the sea (yellow substance) in the UV and visible domains. Limnol. Oceanogr. 26: 43-53.

Bricaud A., Morel A. and Prieur L. (1983) Optical efficiency factors of some phytoplankters. Limnol. Oceanogr. 28: 816-832.

Brody M. and Emerson R. (1959a) The effect of wavelength and intensity of light on the proportion of pigments in *Porphyridium cruentum*. Am. J. Bot. 46: 433-440.

Brody M. and Emerson R. (1959b) The quantum yield of photosynthesis in *Porphyridium cruentum* and the role of chlorophyll *a* in the photosynthesis of red algae. J. Gen. Physiol. 43: 251-264.

Brown P.C. (1982) Phytoplankton production measured *in situ* and under simulated *in situ* conditions in the Southern Benguala upwelling region. Fish. Bull. S. Afr. 16: 31-37.

Bryant D.A. (1986) The cyanobacterial photosynthetic apparatus: Comparisons to those of higher plants and photosynthetic bacteria. In: Platt T. and Li W.K.W. (eds.) Photosynthetic Picoplankton. Can. Bull. Fish. Aquat. Sci. 214: 423-500.

Bullerjahn G.S., Mathijs H.C.P., Mur L.R. and Sherman L.A. (1987) Chlorophyll-protein composition of the thylakoid membrane from *Prochlorothrix hollandica*, a prokaryote containing chlorophyll *b*. Eur. J. Biochem. 168: 295-300.

Burger-Wiesma T., Veenhuis M., Korthals H.J., Van de Wiel C.C.M. and Mur L.R. (1986) A new prokaryote containing chlorophylls *a* and *b*. Nature 320: 262-264.

Burk D. and Lineweaver H. (1935) The kinetic mechanism of photosynthesis. Cold Spring Harbour Symposia on Quantitative Biology 3: 165-183.

Butler W. (1962) Absorption of light by turbid materials. J. Opt. Soc. Am. 52: 292-299.

Calder W.A. (1985) Size and metabolism in natural systems. In: Ecosystem theory for biological oceanography. Ulanowicz R.E. and Platt T. (eds.). Can. Bull. Fish. Aquat. Sci. 213: 65-75.

Campbell L. and Carpenter E.J. (1986) Diel patterns of cell division in marine *Synechococcus* spp. (Cyanobacteria): use of the frequency of dividing cells technique to measure growth rate. Mar. Ecol. Prog. Ser. 32: 139-148.

Campbell L. and Carpenter E.J. (1988) Characterization of phycoerythrin-containing *Synechococcus* spp. populations by immunofluorescence. J. Plankton Res. 10: 1167-1181.

Caron D.A., Pick F.R. and Lean D.R.S. (1985) Chroococcoid cyanobacteria in Lake Ontario: vertical and seasonal distributions during 1982. J. Phycol. 21: 171-175.

Caron D.A., Davis P.G., Madin L.P. and Sieburth J.McN. (1986) Enrichment of microbial populations in macroaggregates (marine snow) from surface waters of the North Atlantic. J. Mar. Res. 44: 543-565.

Carpenter E.J. and Campbell L. (1988) Diel patterns of cell division and growth rates of *Synechococcus* spp. in Long Island Sound. Mar. Ecol. Prog. Ser. 47: 179-183.

Chalker B.E. (1981) Simulating light-saturation curves for photosynthesis and calcification by reef-building corals. Mar. Biol. 63: 135-141.

Chartier P. (1966) Etude theorique de l'assimilation brute de la feuille. Ann. Physiol. Veg. 8: 167.

Chartier P. (1970) A model of CO_2 assimilation in the leaf. In: Prediction and Measurement of Photosynthetic Productivity. Setlik I. (Ed.), p.307, PUDOC, Wageningen, The Netherlands,

Chartier P. and Prioul J. (1976) The effects of irradiance, carbon dioxide and oxygen on the net photosynthetic rate of the leaf: a mechanistic model. Photosynthetica 10: 20.

Chisholm S.W., Olson R.J., Zettler E.R., Goericke R., Waterbury J.B. and Welschmeyer N. (1988) A novel free-living prochlorophyte abundant in the oceanic euphotic zone. Nature 334: 340-343.

Clayton R.K. (1980) Photosynthesis: Physical Mechanisms and Chemical Patterns. Cambridge University Press, Cambridge.

Cleland R.E., Melis A. and Neale P.J. (1986) Mechanism of photoinhibition: photochemical reaction center inactivation in system II of chloroplasts. Photosyn. Res. 9: 79-88.

Conway G.R., Glass N.R. and Wilcox J.C. (1970) Fitting non-linear models to biological data by Marquart's algorithm. Ecology 51: 503-507.

Craig S.R. (1986) Picoplankton size distributions in marine and fresh waters: Problems with filter fractionation studies. FEMS Microbiol. Ecol. 38: 171-177.

Crill P.A. (1977) The photosynthesis-light curve: A simple analog model. J. Theor. Biol. 64: 503-516.

Davies J.M. and Williams P.J.LeB. (1984) Verification of ^{14}C and O_2 derived primary production using an enclosed ecosystem. J. Plankton Res. 6: 457-474.

Davis P.G., Caron D.A., Johnson P.W. and Sieburth J.McN. (1985) Phototrophic and apochlorotic components of picoplankton and nanoplankton in the North Atlantic: geographic, vertical, seasonal and diel distributions. Mar. Ecol. 21: 15-26.

Douglas D.J. (1984) Microautoradiography-based enumeration of photosynthetic picoplankton with estimates of carbon-specific growth rates. Mar. Ecol. Prog. Ser. 14: 223-228.

Doukas A.G., Stefanic V., Buchert J., Alfano R.R. and Zilinskas B.A. (1981) Exciton annihilation in the isolated phycobiliprotein from the blue-green alga *Nostoc* sp. using picosecond absorption spectroscopy. Photochem. Photobiol. 34: 505-510.

Dring M.J. (1981) Chromatic adaptation of photosynthesis in benthic marine algae: An examination of its ecological significance using a theoretical model. Limnol. Oceanogr. 26: 271-284.

Dring M.J. and Jewson D.H. (1982) What does ^{14}C uptake by phytoplankton really measure? A theoretical modelling approach. Proc. Roy. Soc. Lond. B 214: 351-368.

Dubinsky Z. (1980) Light utilization efficiency in natural phytoplankton communities. In: Falkowski P.G. (ed.) Primary Productivity in the Sea. Plenum Press, New York, pp. 83-97.

Dubinsky Z. and Berman T. (1981) Light utilization by phytoplankton in Lake Kinneret (Israel). Limnol. Oceanogr. 26: 660-670.

Dubinsky Z., Falkowski P.G. and Wyman K. (1986) Light harvesting and utilization by phytoplankton. Plant Cell Physiol. 27: 1335-1349.

Duysens L.N.M. (1952) Ph.D Thesis, University of Utrecht.

Duysens L.N.M. and Amesz J. (1962) Function and identification of two photochemical systems in photosynthesis. Biochim. Biophys. Acta 64: 243-260.

Eilers P. and Peeters J.C.H. (1988) A model for the relationship between light intensity and the rate of photosynthesis in phytoplankton. Ecological Modelling 42: 199-215.

El Hag A.G.D. and Fogg G.E. (1986) The distribution of coccoid blue-green algae (Cyanobacteria) in the Menai Straits and the Irish Sea. Br. Phycol. J. 21: 45-54.

Eley J.H.Jr. and Myers J. (1967) Enhancement of photosynthesis by alternated light beams and a kinetic model. Plant Physiol. 42: 598-607.

Emerson R. (1958) The quantum yield of photosynthesis. Ann. Rev. Plant Physiol. 9: 1-24.

Emerson R. and Arnold W. (1932) A separation of the reactions in photosynthesis by means of intermittant light. J. Gen. Physiol. 15: 391-420.

Emerson R. and Arnold W. (1933) The photochemical reaction in photosynthesis. J. Gen. Physiol. 16: 191-205.

Emerson R. and Lewis C.M. (1942) The photosynthetic efficiency of phycocyanin in *Chroococcus*, and the problem of carotenoid participation in photosynthesis. J. Gen. Physiol. 25: 579-595.

Emerson R. and Lewis C.M. (1943) The dependence of the quantum yield of *Chlorella* photosynthesis on the wavelength of light. Am. J. Bot. 30: 165-178.

Emerson R., Chalmers R. and Cederstrand C. (1957) Some factors influencing the long-wave limit of photosynthesis. Proc. Natl. Acad. Sci. U.S.A. 43: 133-143.

Eppley R. W. (1980) Estimating phytoplankton growth rates in oligotrophic oceans. In: Falkowski P.G. (ed.) Primary Productivity in the Sea. Plenum Press, New York, pp. 231-242.

Eppley R.W. and Peterson B.W. (1979) Particulate organic matter flux and planktonic new production in the deep ocean. Nature, Lond. 282: 677-680.

Eppley R.W. and Sloan P.R. (1966) Growth rates of marine phytoplankton: correlation with light absorption by chlorophyll *a*. Physiol. Plant. 19: 47-59.

Eppley R.W., Rodgers J.N. and McCarthy J.J. (1969) Half-saturation constants for uptake of nitrate and ammonium by marine phytoplankton. Limnol. Oceanogr. 14: 912-920.

Estep K.W., Davis P.G., Hargraves P.E. and Sieburth J. McN. (1984) Chloroplast containing microflagellates in natural populations of North Atlantic nanoplankton, their identification and distribution; including a description of five new species of *Chrysochromulina* (Prymnesiophyceae). Protistologica 20: 613-634.

Exton R.J., Houghton W.M., Esaias W., Haas L.W. and Hayward D. (1983) Spectral differences and temporal stability of phycoerythrin fluorescence in estuarine and coastal waters due to the domination of labile cryptophytes and stabile cyanobacteria. Limnol. Oceanogr. 28: 1225-1231.

Fahnenstiel G.L., Sicko-Goad L., Scavia D. and Stoermer E.F. (1986) Importance of picoplankton in Lake Superior. Can. J. Fish. Aquat. Sci. 43: 235-240.

Falkowski P.G., Fujita Y., Ley A. and Mauzerall D. (1986a) Evidence for cyclic electron flow around Photosystem II in *Chlorella pyrenoidosa*. Plant Physiol. 81: 310-312.

Falkowski P.G., Wyman K., Ley A.C. and Mauzerall D.D. (1986b) Relationship of steady-state photosynthesis to fluorescence in eucaryotic algae. Biochim. Biophys. Acta 849: 183-192.

Farquhar G.D. and von Caemmerer S. (1983) Modelling of photosynthetic response to environmental conditions. In: Physiological Plant Ecology II: Water Relations and Carbon Assimilation. Lange O., Nobel P.S., Osmond C.B. and Ziegler H. (eds.), pp. 549-587, Encyclopedia of Plant Physiology New Series, Volume 12B, Pirson A. and Zimmermann H.H. (eds.), Springer Verlag, Berlin.

Fasham M.J.R. and Platt T. (1983) Photosynthetic response of phytoplankton to light: a physiological model. Proc. R. Soc. Lond. B 219: 355-370.

Fee E.J. (1969) A numerical model for the estimation of photosynthetic production, integrated over time and depth, in natural waters. Limnol. Oceanogr. 14: 906-911.

Fee E.J. (1973) A numerical model for determining integral primary production and its application to Lake Michigan. J. Fish. Res. Bd. Can. 30: 1447-1468.

Fenchel T. (1974) Intrinsic rate of natural increase: the relationship with body size. Oecologia 14: 317-326.

Fenchel T. (1988) Marine plankton food chains. Ann. Rev. Ecol. Syst. 19: 19-38.

Flik B.J.G., Bos M., Royackers K. and Ringelberg J. (1987) Underestimation of primary production as indicated by measurements with size-fractionated phytoplankton in Lake Maarsseveen I (The Netherlands). Hydrobiol. Bull. 21: 39-47.

Fogg G.E. (1986) Picoplankton. Proc. R. Soc. Lond. B 228: 1-30.

Foss P., Guillard R.R.L. and Liaaen-Jensen S. (1984) Prasinoxanthin - a chemosystematic marker for algae. Phytochem. 23: 1629-1633.

Förster T. (1948) Zwischenmolekulare Energiewanderung und Fluoreszenz. Annalen der Physik (6th Ser) 2: 55-75.

Förster T. (1959) Transfer mechanisms of electronic excitation. Discuss. Faraday Soc. 27: 7-17.

Förster T. (1965) Delocalized excitation and excitation transfer. In: Modern Quantum Chemistry, Part III, Sinanoglu O. (ed.), Academic Press, New York.

Fujita Y., Ohki K. and Murakami A. (1985) Chromatic regulation of photosystem composition in the photosynthetic system of red and blue-green algae. Plant Cell Physiol. 26: 1541-1548.

Fujita Y., Murakami A. and Ohki K. (1987) Regulation of photosystem composition in the cyanobacterial photosynthetic system: the regulation occurs in response to the redox state of the electron pool located between the two photosystems. Plant Cell Physiol. 28: 283-292.

Furnas M.J. and Mitchell A.W. (1988) Photosynthetic characteristics of Coral Sea picoplankton (<2 μm size fraction). Biol. Oceanogr. 5: 163-182.

Furuya K. and Marumo R. (1983) The structure of the phytoplankton community in the subsurface chlorophyll maxima in the western North Pacific Ocean. J. Plankton Res. 5: 393-406.

Gaffron H. and Wohl W. (1934) Zur theorie der assimilation. Naturwiss. 24: 81-90.

Gallegos C.L. and Platt T. (1981) Photosynthesis measurements on natural populations of phytoplankton: numerical analysis. In: Platt T. (ed.) Physiological bases of phytoplankton ecology. Can. Bull. Fish. Aquat. Sci. 210: 103-112.

Gautier C. (1982) Mesoscale insolation variability derived from satellite data. J. Appl. Meteorol. 21: 51-58.

Gautier C., Diak G. and Masse S. (1980) A simple physical model to estimate incident solar radiation at the surface from GOES satellite data. J. Appl. Meteorol. 19: 1005-1012.

Geider R.J. and Osborne B.A. (1987) Light absorption by a marine diatom: experimental observations and theoretical calculations of the package effect in a small *Thalassiosira* species. Mar. Biol. 96: 299-308.

Geider R.J., Platt T. and Raven J.A. (1986) Size dependence of growth and photosynthesis in diatoms: a synthesis. Mar. Ecol. Prog. Ser. 30: 93-104.

Gieskes W.W.C. and Kraay G.W. (1983) Unknown chlorophyll a derivatives in the North Sea and tropical Atlantic Ocean by HPLC analyses. Limnol. Oceanogr. 28: 757-766.

Gieskes W.W.C. and Kraay G.W. (1986) Floristic and physiological differences between the shallow and the deep nanophytoplankton community in the euphotic zone of the open tropical Atlantic revealed by HPLC analysis of pigments. Mar. Biol. 91: 567-576.

Gieskes W.W.C., Kraay G.W. and Baars M.A. (1979) Current ^{14}C methods for measuring primary production: gross under-estimates in oceanic waters. Neth. J. Sea Res. 13: 58.

Glazer A.N. (1982) Phycobilisomes: structure and dynamics. Ann. Rev. Microbiol. 36: 173-198.

Glazer A.N. (1983) Comparative biochemistry of photosynthetic light-harvesting systems. Ann. Rev. Biochem. 52: 125-157.

Glazer A.N. (1984) Phycobilisome. A macromolecular complex optimized for light energy transfer. Biochim. Biophys. Acta 768: 29-51.

Glazer A.N. (1985) Light harvesting by phycobilisomes. Ann. Rev. Biophys. Biophys. Chem. 14: 47-77.

Glover H.E. (1986) The physiology and ecology of marine Cyanobacteria, *Synechococcus* spp. Adv. Aquat. Microbiol. 3: 49-107.

Glover H. and Morris I. (1981) Photosynthetic characteristics of coccoid marine cyanobacteria. Arch. Microbiol. 129: 42-46.

Glover H.E., Phinney D.A. and Yentsch C.S. (1985) Photosynthetic characteristics of picoplankton compared to those of larger populations, in various water masses in the Gulf of Maine. Biol. Oceanogr. 3: 223-248.

Glover H.E., Campbell L. and Prezelin B.B. (1986a) Contribution of *Synechococcus* spp. to size-fractionated primary productivity in three water masses in the Northwest Atlantic Ocean. Mar. Biol. 91: 193-203.

Glover H.E., Keller M.D. and Guillard R.R.L. (1986b) Light quality and oceanic ultraplankters. Nature 319: 142-143.

Glover H.E., Keller M.D. and Spinrad R.W. (1987) The effects of light quality and intensity on photosynthesis and growth of marine eukaryotic and prokaryotic phytoplankton clones. J. Exp. Mar. Biol. Ecol. 105: 137-159.

Glover H.E., Prezelin B.B., Campbell L., Wyman M. and Garside C. (1988) A nitrate-dependent *Synechococcus* bloom in surface Sargasso Sea water. Nature 331: 161-163.

Goedheer J.C. (1970) On the pigment systems of brown algae. Photosynthetica 4: 97-106.

Gordon H.R. and Morel A.Y. (1983) Remote Assessment of Ocean Color for Interpretation of Satellite Visible Imagery. Springer-Verlag, New York.

Govindjee and Whitmarsh J. (1982) Introduction to photosynthesis: Energy conversion by plants and bacteria. In: Photosynthesis Volume I, Energy conversion by Plants and Bacteria. Govindjee (ed.), Academic Press, New York, NY.

Gradinger R. and Lenz J. (1989) Picocyanobacteria in the high Arctic. Mar. Ecol. Prog. Ser. 52: 99-101.

Grande K.D., Williams P.J.LeB., Marra J., Purdie D.A., Heinemann K., Eppley R.W. and Bender M.L. (1989) Primary production in the North Pacific gyre: a comparison of rates determined by the ^{14}C, O_2 concentration and ^{18}O methods. Deep-Sea Res. 36: 1621-1634.

Gross F. (1937) Notes on the culture of some marine plankton organisms. J. Mar. Biol. Assoc. U.K. 21: 753-768.

Guillard R.R.L. and Ryther J.H. (1962) Studies on marine planktonic diatoms. I. *Cyclotella nana* Hustedt and *Detonula confervaceae* (Cleve) Gran. Can. J. Microbiol. 8: 229-239.

Hallegraeff G.M. (1981) Seasonal study of phytoplankton pigments and species at a coastal station off Sydney: Importance of diatoms and the nanoplankton. Mar. Biol. 61: 107-118.

Hallegraeff G.M. (1983) Scale-bearing and loricate nanoplankton from the East Australian Current. Bot. Mar. 26: 493-515.

Hameedi M.J. (1978) Aspects of water column primary productivity in the Chukchi Sea during summer. Mar. Biol. 48: 37-46.

Hardy F.J., Shortreed K.S. and Stockner J.G. (1986) Bacterioplankton, phytoplankton, and zooplankton communities in a British Columbia coastal lake before and after nutrient reduction. Can. J. Fish. Aquat. Sci. 43: 1504-1514.

Harnschfeger G. and Herold B. (1981) Aspects of energy-transfer between phycobilins and chlorophyll in *Chroomonas* species (Cryptophyceae). Ber. Deutsch. Bot. 94: 65-73.

Harris G.P. (1978) Photosynthesis, productivity and growth: the physiological ecology of phytoplankton. Ergeb. Limnol. 10: 1-171.

Harris G.P. (1980) The measurement of photosynthesis in natural populations of phytoplankton. In: The Physiological Ecology of Phytoplankton. Morris I. (ed.), pp. 129-187, Blackwell, Oxford.

Hartmann K.M. (1977) Aktionsspektroskopie. In: Biophysik. Hoppe W., Lohmann W., Markl H. and Ziegler H. (eds.), pp. 197-222, Springer Verlag, Berlin.

Hartmann K.M. and Unser C. (1972) Analytical action spectroscopy with living systems: Photochemical aspects and attenuance. Ber. Deutsch. Bot. Ges. Bd. 85: 481-551.

Haxo F.T. (1960) Wavelength dependence of photosynthesis and the role of accessory pigments. In: Comparative Biochemistry of Photoreactive Pigments. Allen M.B. (ed.), PP. 330-360, Academic Press, London.

Haxo F.T. and Blinks L.R. (1950) Photosynthetic action spectra of marine algae. J. Gen. Physiol. 33: 389-422.

Haxo F.T. and Fork D.C. (1959) Photosynthetically active accessory pigments in Cryptomonads. Nature 184: 1051-1052.

Herman A.W., Mitchell M.R. and Young S.W. (1984) A continuous pump sampler for profiling copepods and chlorophyll in the upper oceanic layers. Deep-Sea Res. 31: 439-450.

Herron H.A. and Mauzerall D. (1972) The development of photosynthesis in a greening mutant of *Chlorella* and an analysis of the light saturation curve. Plant Physiol. 50: 141-148.

Hertzberg S., Mortensen T., Borch G., Siegelman H.W. and Liaaen-Jensen S. (1977) On the absolute configuration of 19'-hexanoyloxyfucoxanthin. Phytochem. 16: 587-590.

Hill R. and Bendall F. (1960) Function of two cytochrome components in chloroplasts: a working hypothesis. Nature 186: 136-137.

Hiller R.G. and Larkum A.W.D. (1985) The chlorophyll-protein complexes of *Prochloron* sp. (Prochlorophyta). Biochim. Biophys. Acta 806: 107-115.

Hiller R.G., Larkum A.W.D. and Wrench P.M. (1988) Chlorophyll proteins of the prymnesiophyte *Pavlova lutherii* (Droop) comb. nov.: identification of the major light-harvesting complex. Biochim. Biophys. Acta 932: 223-231.

Hirano M., Satoh K. and Katoh S. (1980) Plastoquinone as a common link between photosynthesis and respiration in a blue-green alga. Photosynthesis Res. 1: 149-162.

Hoge F.E. and Swift R.N. (1983) Airborne dual laser excitation and mapping of phytoplankton photopigments in a Gulf Stream Warm Core Ring. Appl. Optics 22: 2272-2281.

Holm-Hansen O., Lorenzen C.J. Holmes R.W. and Strickland J.D.H. (1965) Fluorometric determination of chlorophyll. J. Cons. Cons. Int. Explor. Mer 30: 3-15.

Ingraham K. and Hiller R.G. (1983) Isolation and characterization of a major chlorophyll *a*/c_2 light-harvesting protein from *Chroomonas* species (Cryptophyceae). Biochim. Biophys. Acta 772: 310-319.

Iturriaga R. and Marra J. (1988) Temporal and spatial variability of chroococcoid cyanobacteria *Synechococcus* spp. specific growth rates and their contribution to primary production in the Sargasso Sea. Mar. Ecol. Prog. Ser. 44: 175-181.

Iturriaga R. and Mitchell B.G. (1986) Chroococcoid cyanobacteria: a significant component in the food web dynamics of the open ocean. Mar. Ecol. Prog. Ser. 28: 291-297.

Iwakuma T. and Yasuno M. (1983) A comparison of several mathematical equations describing photosynthesis-light curve for natural phytoplankton populations. Arch. Hydrobiol. 97: 208-226.

Jassby A.D. and Platt T. (1976) Mathematical formulation of the relationship between photosynthesis and light for phytoplankton. Limnol. Oceanogr. 21: 540-547.

Jeffrey S.W. (1974) Profiles of photosynthetic pigments in the ocean using thin-layer chromatography. Mar. Biol. 26: 101-110.

Jeffrey S.W. (1976) A report of green algal pigments in the Central North Pacific. Mar. Biol. 37: 33-37.

Jeffrey S.W. (1980) Algal pigment systems. In: Primary Productivity in the Sea. Falkowski P.G. (ed.), Plenum Press, New York, NY., pp. 33-58.

Jeffrey S.W. (1984) Responses of unicellular marine plants to natural blue-green light environments. In: Blue Light Effects in Biological Systems. Senger H. (ed.), PP. 497-508, Springer Verlag, Berlin.

Jeffrey S.W. and Hallegraeff G.M. (1980) Studies of phytoplankton species and photosynthetic pigments in a warm core eddy of the East Australian Current. II. A note on pigment methodology. Mar. Ecol. Prog. Ser. 3: 295-301.

Jenkins W.J. (1982) Oxygen utilization rates in the North Atlantic subtropical gyre and primary production in oligotrophic systems. Nature 300: 246-248.

Jerlov N.G. (1954) Color filters to simulate the extinction of daylight in the sea. J. Cons. Cons. Int. Explor. Mer. 20: 156-159.

Jerlov N.G. (1976) Marine Optics. Elsevier, New York, NY. 231pp.

Jitts H.R. (1963) The simulated *in situ* measurement of oceanic primary production. Aust. J. Mar. Freshwater Res. 14: 139-147.

Jochem F. (1988) On the distribution and importance of picocyanobacteria in a boreal inshore area (Kiel Bight, Western Baltic). J. Plankton Res. 10: 1009-1022.

Johnson P.W. and Sieburth J. McN. (1979) Chroococcoid cyanobacteria in the sea: a ubiquitous and diverse phototrophic biomass. Limnol. Oceanogr. 24: 928-935.

Johnson P.W. and Sieburth J.McN. (1982) *In situ* morphology and occurence of eucaryotic phototrophs of bacterial size in the picoplankton of estuarine and oceanic waters. J. Phycol. 18: 318-327.

Johnson K.M., Burney C.M. and Sieburth McN.J. (1981) Enigmatic marine ecosystem metabolism measured by direct diel ΣCO_2 and O_2 flux in conjunction with DOC release and uptake. Mar. Biol. 65: 49-60.

Joint I.R. (1986) Physiological ecology of picoplankton in various oceanographic provinces. In: Platt T. and Li W.K.W. (eds.) Photosynthetic Picoplankton. Can. Bull. Fish. Aquat. Sci. 214: 287-309.

Joint I.R. and Pomroy A.J. (1983) Production of picoplankton and small nanoplankton in the Celtic Sea. Mar. Biol. 77: 19-27.

Joint I.R. and Pomroy A.J. (1986) Photosynthetic characteristics of nanoplankton and picoplankton from the surface mixed layer. Mar. Biol. 92: 465-474.

Joint I.R., Owens N.J.P. and Pomroy A.J. (1986) The seasonal production of picoplankton and nanoplankton in the Celtic Sea. Mar. Ecol. Prog. Ser. 28: 251-258.

Jones H.G. and Slayter R.O. (1972) Estimation of transport and carboxylation components of intracellular limitation to leaf photosynthesis. Plant Physiol. 50: 283-288.

Jones L.W. and Myers J. (1963) A common link between photosynthesis and respiration in a blue-green alga. Nature (Lond.) 199: 670-672.

Jones L.W. and Myers J. (1964) Enhancement in the blue green alga, *Anacystis nidulans*. Plant Physiol. 39: 938-946.

Jones L.W. and Myers J. (1965) Pigment variation in *Anacystis nidulans*. J. Phycol. 1: 7-13.

Kana T.M. and Glibert P.M. (1987a) Effect of irradiances up to 2000 μE m^{-2} s^{-1} on marine *Synechococcus* WH7803. I. Growth, pigmentation, and cell composition. Deep-Sea Res. 34: 479-495.

Kana T.M. and Glibert P.M. (1987b) Effect of irradiances up to 2000 μE m^{-2} s^{-1} on marine *Synechococcus* WH7803. II. Photosynthetic responses and mechanisms. Deep-Sea Res. 34: 497-516.

Kana T.M., Glibert P.M., Goericke R. and Welschmeyer N. (1988) Zeaxanthin and β-carotene in *Synechococcus* WH 7803 respond differently to irradiance. Limnol. Oceanogr. 33: 1623-1627.

Kawamura M., Mimuro M. and Fujita Y. (1979) Quantitative relationship between two reaction centers in the photosynthetic system of blue-green algae. Plant Cell Physiol. 20: 697-705.

Kerr R.A. (1983) Are the oceans deserts blooming. Science 220: 397-398.

Kiefer D.A. and SooHoo J.B. (1982) Spectral absorption by marine particles of coastal waters of Baja California. Limnol. Oceanogr. 27: 492-499.

Kiefer D.A. and Strickland J.D. (1970) A comparative study of photosynthesis in seawater samples incubated under two types of light attenuator. Limnol. Oceanogr. 15: 408-412.

Kishino M., Takahashi M., Okami N. and Ichimura S. (1985) Estimation of the spectral absorption coefficients of phytoplankton in the sea. Bull. Mar. Sci. 37: 634-642.

Kirk J.T.O. (1975a) A theoretical analysis of the contribution of algal cells to the attenuation of light within natural waters. I. General treatment of suspensions of pigmented cells. New Phytol. 75: 11-20.

Kirk J.T.O. (1975b) A theoretical analysis of the contribution of algal cells to the attenuation of light within natural waters. II. Spherical cells. New Phytol. 75: 21-36.

Kirk J.T.O. (1976) A theoretical analysis of the contribution of algal cells to the attenuation of light within natural waters. III. Cylidrical and spheroidal cells. New Phytol. 77: 341-358.

Kirk J.T.O. (1980) Spectral absorption properties of natural waters: contribution of the soluble and particulate fractions to light absorption in some inland waters of southeastern Australia. Aust. J. Mar. Freshwater Res. 31: 287-296.

Kirk J.T.O. (1983) Light and photosynthesis in aquatic ecosystems. Cambridge University Press, Cambridge.

Kirk J.T.O. (1986) Optical properties of picoplankton suspensions. In: Platt T. and Li W.K.W. (eds.) Photosynthetic Picoplankton. Can. Bull. Fish. Aquat. Sci. 214: 501-520.

Kishino M., Takahashi M., Okami N. and Ichimura S. (1985) Estimation of the spectral absorption coefficients of phytoplankton in the sea. Bull. Mar. Sci. 37: 634-642.

Kishino M., Okami N., Takahashi M. and Ichimura S. (1986) Light utilization efficiency and quantum yield of phytoplankton in a thermally stratified sea. Limnol. Oceanogr. 31: 557-566.

Kok B. (1949) On the interrelation of respiration and photosynthesis in green plants. Biochim. Biophys. Acta 3: 625-631.

Kolber Z., Zehr J. and Falkowski P. (1988) Effects of growth irradiance and nitrogen limitation on photosynthetic energy conversion in photosystem II. Plant Physiol. 88: 923-929.

Kopelevich O.V. and Burenkov V.I. (1977) Relation between the spectral values of the light absorption coefficients of seawater, phytoplankton pigments, and the yellow substances. Oceanology 17: 278-282.

Krempin D.W and Sullivan C.W. (1981) The seasonal abundance, vertical distribution, and relative microbial biomass of chroococcoid cyanobacteria at a station in southern Californian coastal waters. Can. J. Microbiol. 27: 1341-1344.

Krogmann D.W., Butalla R. and Sprinkle J. (1986) Blooms of cyanobacteria on the Potomac River. Plant Physiol. 80: 667-671.

Kursar T.A., Swift H. and Alberte R.S. (1981) Morphology of a novel cyanobacterium and characterizations of light-harvesting complexes from it: Implications for phycobiliprotein evolution. Proc. Natl. Acad. Sci. USA 78: 1-5.

Kyle D.J. (1985) The 32000 dalton-QB protein of photosystem II. Photochem. Photobiol. 41: 107-116.

Kyle D.J. (1987) The biochemical basis for photoinhibition of photosystem II. In: Photoinhibition. Kyle D.J, Osmond C.B. and Arntzen C.J. (eds.), Elsevier Science Publishers, New York, NY.

Kyle D.J., Ohad I. and Arntzen C.J. (1984) Membrane-protein damage and repair - selective loss of a quinone protein function in chloroplast membranes. Proc. Natl. Acad. Sci. USA 81: 4070-4074.

Kyle D.J., Ohad I. and Arntzen C.J. (1985) In: Cellular and Molecular Biology of Plant Stress. Key J.L anf Kosuge T. (eds.), pp. 51-70, UCLA Symposium Series, No. 22, A.R. Liss, New York, NY.

Landry M.R., Haas L.W. and Fagerness V.L. (1984) Dynamics of microbial plankton communities: experiments in Kaneohe Bay Hawaii. Mar. Ecol. Prog. Ser. 16: 127-133.

Lederman T.C. and Tett P. (1981) Problems in modelling the photosynthesis-light relationship for phytoplankton. Bot. Mar. 24: 125-134.

Legendre L., Demers S., Delesalle B. and Harnois C. (1988) Biomass and photosynthetic activity of phototrophic picoplankton in coral reef waters (Moorea Island, French Polynesia). Mar. Ecol. Prog. Ser. 47: 153-160.

Lewin J., Norris R.E., Jeffrey S.W. and Pearson B.E. (1977) An aberrant chrysophycean alga *Pelagococcus subviridus* gen. nov. et sp. nov. from the North Pacific Ocean. J. Phycol. 13: 259-266.

Lewin R.A. (1975) A marine *Synechocystis* (Cyanophyta, Chroococcales) epizoic on ascidians. Phycologia 14: 153-160.

Lewis M.R. and Smith J.C. (1983) A small-volume, short incubation-time method for the measurement of photosynthesis as a function of incident irradiance. Mar. Ecol. Prog. Ser. 13: 99-102.

Lewis M.R., Warnock R.E. and Platt T. (1985) Absorption and photosynthetic action spectra for natural phytoplankton populations: implications for production in the open ocean. Limnol. Oceanogr. 30: 794-806.

Lewis M.R., Warnock R.E. and Platt T. (1986) Photosynthetic response of marine picoplankton at low photon flux. In: Platt T. and Li W.K.W. (eds.) Photosynthetic Picoplankton. Can. Bull. Fish. Aquat. Sci. 214: 235-250.

Ley A.C. and Mauzerall D.D. (1982) Absolute absorption cross-sections for Photosystem II and the minimum quantum requirement for photosynthesis in *Chlorella vulgaris*. Biochim. Biophys. Acta 680: 95-106.

Ley A.C. and Mauzerall D.D. (1986) The extent of energy transfer among photosystem II reaction centers in *Chlorella*. Biochim. Biophys. Acta 850: 234-248.

Li W.K.W. (1986) Experimental approaches to field measurements: Methods and interpretation. In: Platt T. and Li W.K.W. (eds.) Photosynthetic Picoplankton. Can. Bull. Fish. Aquat. Sci. 214: 251-286.

Li W.K.W. and Platt T. (1987) Photosynthetic picoplankton in the ocean. Science Progress, Oxford 71: 117-132.

Li W.K.W. and Wood A.M. (1988) Vertical distribution of North Atlantic ultraplankton: Analysis by flow cytometry and epifluorescence microscopy. Deep-Sea Res. 35: 1615-1638.

Li W.K.W., Subba Rao D.V., Harrison W.G., Smith J.C., Cullen J.J., Irwin B. and Platt T. (1983) Autotrphic picoplankton in the tropical ocean. Science 219: 292-295.

Lichtle C., Jupin H. and Duval J.C. (1980) Energy transfers from photosystem II to photosystem I in *Cryptomonas rufescens* (Cryptophyceae). Biochim. Biophys. Acta 591: 104-112.

Liebig J. (1840) Die orgaische Chemie in ihrer Anwendung auf Agricultur und Physiologie. First Ed., Vieweg, Braunschweig, 1840.

Liebig J. (1843) Die Wechselwirthscaft. Ann. Chem. (Liebig's) 46: 58-97.

Lochte K. and Turley C.M. (1988) Bacteria and cyanobacteria associated with phytodetritus in the deep sea. Nature 333: 67-69.

Lohmann H. (1911) Uber das Nannoplankton und die Zentrifugierung kleinster Wasserproben zur Gewinnung desselben in lebendem Zustand. Int. Rev. Gesamten. Hydrobiol. Hydrog. 4: 1-38.

Lucas H.L. (1964) Stochastic elements in biological models; their sources and significance. In: Stochastic Models in Medicine and Biology. Gurland J. (ed.) Publ. No. 10, Mathematics Center, U.S. Army, pp. 355-383, The University of Wisconsin, Madison.

Maguzzu G., Bruni V., Piccione A., Platt T., Irwin B. and Subba Rao D.V. (1987) Picoplankton: Contribution to phytoplankton production in the Strait of Messina. P.S.Z.N. I:Marine Ecology 8: 21-31.

Malkin S. (1967) Theoretical analysis of the enhancement effect in photosynthesis - evidence for the "spill-over" model. Biophys. J. 7: 629-649.

Mann J.E. and Myers J. (1968) Photosynthetic enhancement in the diatom *Phaeodactylum tricornutum*. Plant Physiol. 43: 1991-1995.

Manodori A. and Melis A. (1986a) Light quality regulates photosystem stoichiometry in cyanobacteria. In: Regulation of Chloroplast Differentiation. Akoyunoglou G. and Senger H. (eds.). pp. 653-662. Plant Biology Series, Alan R. Liss Inc., New York.

Manodori A. and Melis A. (1986b) Cyanobacterial acclimation to photosystem I or photosystem II light. Plant Physiol. 82: 185-189.

Marchant H.J., Davidson A.T. and Wright S.W. (1987) The distribution and abundance of chroococcoid cyanobacteria in the Southern Ocean. Proc. Nat. Inst. Polar Res. (NIPR) Symp. Polar Biol. 1: 1-9.

Marshall B. and Biscoe P.V. (1980) A model for C_3 leaves describing the dependence of net photosynthesis on irradiance. J. Exp. Bot. 31: 29-39.

Marquardt D.W. (1963) An algorithm for least-squares estimation of non-linear parameters. J. Soc. Ind. Appl. Math. 11: 431-441.

Matsuura K. and Fujita Y. (1986) Chromatic regulation of cytochrome composition and electron transfer from cytochrome b_6f complex to photosystem I in *Anacystis nidulans* (Tx20). Plant Cell Physiol. 27: 685-691.

Mauzerall D. (1986) The optical cross-section and absolute size of a photosynthetic unit. Photosyn. Res. 10: 163-170.

Megard R.O., Tonkyn D.W. and Senft W.H. II. (1984) Kinetics of oxygenic photosynthesis in planktonic algae. J. Plankton Res. 6: 325-337.

Melis A. (1989) Spectroscopic methods in photosynthesis: photosystem stoichiometry and chlorophyll antenna size. Phil. Trans. R. Soc. Lond. B 323: 397-409.

Mimuro M. and Fujita Y. (1977) Estimation of chlorophyll *a* distribution in the photosynthetic pigment systems I and II of the blue-green alga *Anabaena variabilis*. Biochim. Biophys. Acta 459: 376-389.

Mitchell B.G. and Kiefer D.A. (1984) Determination of absorption and fluorescence excitation spectra for phytoplankton. In: Marine Phytoplankton and Productivity. Holm-Hansen O. *et al.* (eds.), pp. 157-169. Springer Verlag, Berlin.

Mitchell B.G., Iturriaga R. and Kiefer D.A. (1984) Variability of particulate spectral absorption coefficients in the Eastern Pacific Ocean. Proc. Soc. Photo-opt. Instr. Engin. 489: 113-118.

Morel A. (1978) Available, usable, and stored radiant energy in relation to marine photosynthesis. Deep-Sea Res. 25: 673-688.

Morel A. and Bricaud A. (1981a) Theoretical results concerning light absorption in a discrete medium, and application to specific absorption of phytoplankton. Deep-Sea Res. 28A: 1375-1393.

Morel A. and Bricaud A. (1981b) Theoretical results concerning the optics of phytoplankton, with special reference to remote sensing applications. In: Oceanography from Space. Plenum Press, New York, NY. pp. 313-327.

Morel A. and Bricaud A. (1986) Inherent optical properties of algal cells including picoplankton: theoretical and experimental results. In: Platt T. and Li W.K.W. (eds.) Photosynthetic Picoplankton. Can. Bull. Fish. Aquat. Sci. 214: 521-559.

Morel A. and Prieur L. (1977) Analysis of variations in ocean colour. Limnol. Oceanogr. 22: 709-722.

Morel A. and Prieur L. (1978) Mesures par teledetection de la teneur de la mer en chlorophylle. Possibilites et limitations des methodes. Publ. Sci. Techn. CNEXO, Actes Colloq., NÁ 5: 67-92.

Moriarty D.J.W., Pollard P.C. and Hunt W.G. (1985) Temporal and spatial variation in bacterial production in the water column over a coral reef. Mar. Biol. 85: 285-292.

Morris I. and Glover H. (1981) Physiology of photosynthesis by marine chroococcoid cyanobacteria - some ecological implications. Limnol. Oceanogr. 26: 957-961.

Murphy L.S. and Haugen E.M. (1985) The distribution and abundance of phototrophic ultraplankton in the North Atlantic. Limnol. Oceanogr. 30: 47-58.

Myers J. (1971) Enhancement studies in photosynthesis. Ann. Rev. Plant Physiol. 22: 289-312.

Myers J. (1986) Photosynthetic and respiratory electron transport in a cyanobacterium. Photosynthesis Res. 9: 135-147.

Myers J. and French C.S. (1960) Evidences from action spectra for a specific participation of chlorophyll *b* in photosynthesis. J. Gen. Physiol. 43: 723-736.

Myers J. and Graham J.-R. (1963) Enhancement in *Chlorella*. Plant Physiol. 38: 105-116.

Myers J., Graham J.-R. and Wang R.T. (1978) On spectral control of pigmentation in *Anacystis nidulans* (Cyanophyceae). J. Phycol. 14: 513-518.

Myers J., Graham J.-R. and Wang R.T. (1980) Light harvesting in *Anacystis nidulans* studied in pigment mutants. Plant Physiol. 66: 1144-1149.

Nelson D.M., Ducklow H.W., Hitchcock G.L., Brzezinski M.A., Cowles T.J., Garside C., Gould R.W., Joyce T.M., Langdon C., McCarthy J.J. and Yentsch C.S. (1985) Distribution and composition of biogenic particulate matter in a Gulf Stream warm-core ring. Deep-Sea Res. 32: 1347-1369.

Neori A., Vernet M., Holm-Hansen O. and Haxo F.T. (1986) Relationship between action spectra for chlorophyll *a* fluorescence and photosynthetic O_2 evolution in algae. J. Plankton Res. 8: 537-548.

Neori A., Vernet M., Holm-Hansen O. and Haxo F.T. (1988) Comparison of chlorophyll far-red and red fluorescence excitation spectra with photosynthetic oxygen action spectra for photosystem II in algae. Mar. Ecol. Prog. Ser. 44: 297-302.

Nelson S.G. and Siegrist A.W. (1987) Comparison of mathematical expressions describing light-saturation curves for photosynthesis by tropical marine macroalgae. Bull. Mar. Sci. 41: 617-622.

O'hEocha C. and Raftery R. (1959) Phycoerythrins and phycocyanins of cryptomonads. Nature 184: 1049-1054.

Oquist G. (1974a) Iron deficiency in the blue-green alga, *Anacystis nidulans*: changes in pigmentation and photosynthesis. Physiol. Plant. 30: 30-37.

Oquist G. (1974b) Iron deficiency in the blue-green alga, *Anacystis nidulans*: fluorescence and absorption spectra recorded at 77 K. Physiol. Plant. 33: 55-58.

Olson R.J., Chislolm S.W., Zettler E.R. and Armbrust E.V. (1988) Analysis of *Synechococcus* pigment types in the sea using single and dual beam flow cytometry. Deep-Sea Res. 35: 425-440.

Ong L.J., Glazer A.N. and Waterbury J.B. (1984) An unusual phycoerythrin from a marine cyanobacterium. Science 224: 80-83.

Parker R.A. (1973) Some problems associated with computer simulation of an ecological system. In: The Mathematical Theory of the Dynamics of Biological Populations. Barlett M.S. and Hiorns R.W. (eds.), pp. 269-288, Academic Press, London.

Patten B.C. (1968) Mathematical models of plankton production. Int. Rev. Gesamten Hydrobiol. 53: 357-408.

Peeters J.C.H. and Eilers P. (1978) The relationship between light intensity and photosynthesis - a simple mathematical model. Hydrobiol. Bull. 12: 134-136.

Pelevin V.N. (1978) Estimation of the concentration of suspension and chlorophyll in the sea from the spectrum of the outgoing radiation measured from a helicopter. Oceanology 18: 278-282.

Pellegrino F., Wong D., Alfano R.R. and Zilinskas B.A. (1981) Fluorescence relaxation kinetics and quantum yield from isolated phycobiliproteins of the blue-green alga *Nostoc* sp. measured as a function of single picosecond pulse intensity. II. Photochem. Photobiol. 33: 691-696.

Peters R.H. (1983) The Ecological Implications of Body Size. Cambridge University Press, Cambridge.

Peterson B.J. (1980) Aquatic primary productivity and the $^{14}CO_2$ method: a history of the productivity problem. Ann. Rev. Ecol. Syst. 11: 369-385.

Peterson D.H., Perry M.J., Bencala K.E. and Talbot M.C. (1987) Phytoplankton productivity in relation to light intensity: A simple equation. Estuar. Coast. Shelf Sci. 24: 813-832.

Pickett J.M. and Myers J. (1966) Monochromatic light saturation curves for photosynthesis in *Chlorella*. Plant Physiology 41: 90-98.

Platt T. (1969) The concept of energy efficiency in primary production. Limnol. Oceanogr. 14: 653-659.

Platt T. (1984) Primary productivity in the central North Pacific: comparison of oxygen and carbon fluxes. Deep-Sea Res. 31: 1311-1319.

Platt T. (1985) Structure of the marine ecosystem: its allometric basis. In: Ulanowicz R.E. and Platt T. (eds.) Ecosystem theory for biological oceanography. Can. Bull. Fish. Aquat. Sci. 213: 55-64.

Platt T. (1986) Primary production of the ocean water column as a function of surface light intensity: algorithms for remote sensing. Deep-Sea Res. 33: 149-163.

Platt T. and Denman K. (1977) Organization in the pelagic ecosystem. Helgolander wiss. Meeresunters. 30: 575-581.

Platt T. and Denman K. (1978) The structure of the pelagic marine ecosystem. Rapp. P.-v. Reun. Cons. int. Explor. Mer 173: 60-65.

Platt T. and Gallegos C.L. (1980) Modelling primary production. In: Falkowski P.G. (ed.) Primary Productivity of the Sea. pp. 339-361. Plenum Publ. Corp.

Platt T. and Harrison W.G. (1985) Biogenic fluxes of carbon and oxygen in the ocean. Nature 318: 55-58.

Platt T. and Harrison W.G. (1986) Reconciliation of oxygen and carbon fluxes in the upper ocean. Deep-Sea Res. 33: 273-276.

Platt T. and Jassby A.D. (1976) The relationship between photosynthesis and light for natural assemblages of coastal marine phytoplankton. J. Phycol. 12: 421-430.

Platt T. and Li W.K.W. (eds.) (1986) Photosyntheic Picoplankton. Can. Bull. Fish. Aquat. Sci. 214: 583 pp.

Platt T. and Lewis M.R. (1987) Estimation of phytoplankton production by remote sensing. Adv. Space Res. 7: 131-135.

Platt T. and Sathyendranath S. (1988) Oceanic primary production: Estimation by remote sensing at local and regional scales. Science 241: 1613-1620.

Platt T. and Silvert W. (1981) Ecology, physiology, allometry and dimensionality. J. Theor. Biol. 93: 855-860.

Platt T., Denman K. and Jassby A.D. (1977) Modelling the productivity of phytoplankton. In: Goldberg E.D. (ed.) The Sea: Ideas and observations on Progress in the Study of the Seas. pp. 807-856. J. Wiley, New York.

Platt T., Gallegos C.L. and Harrison W.G. (1980) Photoinhibition of photosynthesis in natural assemblages of marine plankton. J. Mar. Res. 38: 687-701.

Platt T., Subba Rao D.V. and Irwin B. (1983) Photosynthesis of picoplankton in the oligotrophic ocean. Nature 300: 702-704.

Platt T., Lewis M. and Geider R. (1984) Thermodynamics of the pelagic ecosystem: elementary closure conditions for biological production in the open ocean. In: Fasham M.J.R. (ed.) Flows of Energy and Materials in Marine Ecosysytems. Plenum Publishing Corp. pp. 49-84.

Platt T., Harrison W.G., Lewis M.L., Li W.K.W., Sathyendranath S., Smith R.E.H. and Vezina A.F. (1988a) Biological production of the oceans: the case for a consensus. Mar. Ecol. Prog. Ser. 52: 77-88.

Platt T., Sathyendranath S., Caverhill C. and Lewis M.R. (1988b) Ocean primary production and available light: further algorithms for remote sensing. Deep-Sea Res. 35: 855-879.

Powles S.B. (1984) Photoinhibition of photosynthesis induced by visible light. Ann. Rev. Plant Physiol. 35: 15-44.

Preisendorfer R.W. (1961) Application of radiative transfer theory to light measurements in the sea. Int. Geophys. Geod. Monogr. 10: 11-29.

Press W.H., Flannery B.P., Teukolsky S.A. and Vetterling W.T. (1986) Numerical Recipes: The Art of Scientific Computing. Cambridge University Press, Cambridge.

Prezelin B.B., Ley A.C. and Haxo F.T. (1976) Effect of growth irradiance on the photosynthetic action spectra of the marine dinoflagellate *Glenodinium* sp. Planta 130: 251-256.

Prezelin B.B., Putt M. and Glover H.E. (1986) Diurnal patterns in photosynthetic capacity and depth-dependent photosynthesis-irradiance relationships in *Synechococcus* spp. and larger phytoplankton in three water masses in the Northwest Atlantic Ocean. Mar. Biol. 91: 205-217.

Prieur L. and Sathyendranath S. (1981) An optical classification of coastal and oceanic waters based upon the specific spectral absorption curves of phytoplankton pigments, dissolved organic matter, and other particulate materials. Limnol. Oceanogr. 26: 671-689.

Prioul J.L. and Chartier P. (1977) Partitioning of transfer and carboxylation components of intracellular resistance to photosynthetic CO_2 fixation: A critical analysis of the methods used. Ann. Bot. 41: 789-800.

Priscu J.C. (1984) *In situ* quantum yield of phytoplankton in a subalpine lake. J. Plankton Res. 4: 531-542.

Probyn T.A. (1985) Nitrogen uptake by size-fractionated phytoplankton populations in the southern Benguela upwelling system. Mar. Ecol. Prog. Ser. 22: 249-258.

Putt M. and Prezelin B.B. (1985) Observations of diel patterns of photosynthesis in cyanobacteria and nanoplankton in the Santa Barbara Channel during 'el Nino'. J. Plankton Res. 7: 779-790.

Rabinowitch E.I. (1951) Photosynthesis and Related Processes. Vol. II, Part 1, pp. 964-1047.

Radmer R.J. and Kok B. (1977a) Light conversion efficiency in photosynthesis. In: A. Trebst and M. Avron (eds.), Photosynthesis I: Photosynthetic Electron Transport and Photophosphorylation. Springer-Verlag, New York, NY.

Radmer R.J. and Kok B. (1977b) Photosynthesis: limited yields, unlimited dreams. Bioscience 27: 599-605.

Raps S., Wyman K., Siegelman H.W. and Falkowski P.G. (1983) Adaptation of the cyanobacterium *Microcystis aeroginosa* to light intensity. Plant Physiol. 72: 829-832.

Raven J.A. (1986) Physiological consequences of extremely small size for autotrophic organisms in the sea. In: Platt T. and Li W.K.W. (eds.) Photosynthetic Picoplankton. Can. Bull. Fish. Aquat. Sci. 214: 1-70.

Raven J.A. and Beardall J. (1981) The intrinsic permeability of biological membranes to H^+: significance for low rates of energy transformation. F.E.M.S. Microbiol. Lett. 10: 1-5.

Raven J.A. and Beardall J. (1982) The lower limit of photon fluence rate for phototrophic growth: the significance of 'slippage' reactions. Plant Cell Environ. 5: 117-124.

Reed R.K. (1977) On estimating insolation over the ocean. J. Phys. Oceanogr. 7: 482-485.

Reid J.L. and Shulenberger E. (1986) Oxygen saturation and carbon uptake near 28°N, 155°W. Deep-Sea Res. 33: 267-271.

Revelle R. (1985) Oceanography from Space. Science 228: 133.

Ried A. and Reinhardt B. (1977) Distribution of excitation energy between photosystem I and photosystem II in red algae. II. Kinetics of the transition between state 1 and state 2. Biochim. Biophys. Acta 460: 25-35.

Ried A., Hessenberg B., Metzler H. and Ziegler R. (1977) Distribution of excitation energy among photosystem I and photosystem II in red algae. I. Action spectra of light reactions I and II. Biochim. Biophys. Acta 459: 175-186.

Riley G.A. (1946) Factors controlling phytoplankton populations on Georges Bank. J. Mar. Res. 6: 54-73.

Rippka R., Dereulles J., Waterbury J.B., Herdman M. and Stanier R.Y. (1979) Generic assignments, strain histories and properties of pure cultures of cyanobacteria. J. Gen. Microbiol. 111: 1-61.

Rodriguez J. and Mullin M.M. (1986a) Diel and interannual variation of size-distribution of oceanic zooplanktonic biomass. Ecology 67: 215-222.

Rodriguez J. and Mullin M.M. (1986b) Relation between biomass and body weight of plankton in steady state oceanic ecosystem. Limnol. Oceanogr. 31: 361-370.

Ryther J.H. (1956) Photosynthesis in the ocean as a function of light intensity. Limnol. Oceanogr. 1: 61-70.

Sandmann G. and Malkin R. (1983) NADH and NADPH as electron donors to respiratory and photosynthetic electron transport in the blue-green alga, *Aphanocapsa*. Biochim. Biophys. Acta 725: 221-224.

Sarmiento J.L. and Toggweiler J.R. (1984) A new model for the role of the oceans in determining pCO_2. Nature 308: 621-624.

Sathyendranath S. (1986) Remote sensing of phytoplankton: A review, with special reference to picoplankton. In: Platt T. and Li W.K.W. (eds.) Photosynthetic Picoplankton. Can. Bull. Fish. Aquat. Sci. 214: 561-583.

Sathyendranath S. and Morel A. (1983) Light emerging from the sea - interpretation and uses in remote sensing. In: Remote Sensing Applications in Marine Science and Technology. Cracknell A.P. (ed.), D. Reidel Publishing Company, Dordrecht, Holland, pp. 323-357.

Sathyendranath S., Prieur L. and Morel A. (1982) Interpretation of ocean color data with special reference to OCM. Mid term report Contract ESA 4726-81-F-DD-SC, 61 pp.

Sathyendranath S., Prieur L. and Morel A. (1983) Rapport complementaire. Contrat ESA 4726-81-F-DD-SC. 29 pp.

Schafer E., Fukshansky L. and Shropshire W. Jr. (1983) Action spectroscopy of photoreversible pigment systems. In: Photomorphogenesis. Shropshire W.Jr. and Mohr H. (eds.), Encyclopedia of Plant Physiology New Series, Volume 16A, Pirson A. and Zimmermann M.H. (eds.), Springer Verlag, Berlin.

Scherer S. and Boger P. (1982) Respiration of blue-green algae in the light. Arch. Microbiol. 132: 329-332.

Schuster G., Owens G.C., Cohen Y. and Ohad I. (1984) Thylakoid polypeptide composition and light-independent phosphorylation of the chlorophyll *a*,*b*-protein in *Prochloron*, a prokaryote exhibiting oxygenic photosynthesis. Biochim. Biophys. Acta 767: 596-605.

Shapiro L.P. and Guillard R.R.L. (1986) Physiology and ecology of the marine eukaryotic ultraplankton. In: Platt T. and Li W.K.W. (eds.) Photosynthetic Picoplankton. Can. Bull. Fish. Aquat. Sci. 214: 371-389.

Shapiro L.P. and Haugen E.M. (1988) Seasonal distribution and temperature tolerance of *Synechococcus* in Boothbay Harbor, Maine. Est. Coast. Shelf Sci. 26: 517-525.

Sheldon R.W. and Sutcliffe W.H. (1978) Generation times of 3h for Sargasso Sea microplankton determined by ATP analysis. Limnol. Oceanogr. 23: 1051.

Shibata K. (1958) Spectrophotometry of intact biological materials. Absolute and relative measurements of their transmission, reflection and absorption spectra. J. Biochem. 45: 599-623.

Shimura S. and Fujita Y. (1973) Some properties of the chlorophyll fluorescence of the diatom *Phaeodactylum tricornutum*. Plant Cell Physiol. 14: 341-352.

Shimura S. and Ichimura S. (1973) Selective transmission of light in the ocean waters and its relation to phytoplankton photosynthesis. J. Oceanogr. Soc. Jap. 29: 257-266.

Shulenberger E.L. and Reid J.L. (1981) The Pacific shallow oxygen maximum, deep chlorophyll maximum, and primary productivity, reconsidered. Deep-Sea Res. 28A: 901-919.

Shuter B.J. (1978) Size dependence of phosphorus and nitrogen subsistence quotas in unicellular microorganisms. Limnol. Oceanogr. 23: 1248-1255.

Sieburth J.McN., Smetacek V. and Lenz J. (1978) Pelagic ecosystem structure: heterotrophic compartments of the plankton and their relationship to plankton size. Limnol. Oceanogr. 23: 1256-1263.

Siefermann-Harms D. (1985) Carotenoids in photosynthesis. I. Location in photosynthetic membranes and light-harvesting function. Biochim. Biophys. Acta 811: 325-355.

Siefermann-Harms D. (1987) The light-harvesting and protective functions of carotenoids in photosynthetic membranes. Physiol. Plant 69: 561-568.

Silvert W. (1979) Practical curve fitting. Limnol. Oceanogr. 24: 767-773.

Silvert W. and Platt T. (1978) Energy flux in the pelagic ecosystem: a time-dependent equation. Limnol. Oceanogr. 23: 813-816.

Silvert W. and Platt T. (1980) Dynamic energy-flow model of the particle size distribution in pelagic ecosystems. In: Kerfoot W.C. (ed.) Evolution and Ecology of Zooplankton Commumities. pp. 754-763. The University Press of New England, Hanover, New Hampshire.

Smith E.L. (1936) Photosynthesis in relation to light and carbon dioxide. Proc. Natl. Acad. Sci. U.S.A. 22: 504.

Smith J.C., Platt T., Li W.K.W., Horne E.P.W., Harrison W.G., Subba Rao D.V. and Irwin B.D. (1985) Arctic marine photoautotrophic picoplankton. Mar. Ecol. Prog. Ser. 20: 207-220.

Smith R.C. and Baker K. (1978a) The bio-optical state of ocean waters and remote sensing. Limnol. Oceanogr. 23: 247-259.

Smith R.C. and Baker K. (1978b) Optical classification of natural waters. Limnol. Oceanogr. 23: 250-267.

Smith R.E.H. and Platt T. (1984) Carbon-exchange and ^{14}C tracer methods in a nitrogen-limited diatom, *Thalassiosira pseudonana*. Mar. Ecol. Prog. Ser. 16: 75-87.

Smith W.R. (1979) Parameter estimation in non-linear models of biological systems. Fish. Mar. Tech. Rep. 889, 90 pp.

Spitzer D. (1980) Efficiency of primary production in the upper layer of the euphotic zone of the tropical North Atlantic. Neth. J. Sea Res. 14: 220-228.

Sondergaard M. (1988) Comparison of $^{14}CO_2$ and $^{12}CO_2$ uptake in marine macroalgae. Bot. Mar. 31: 417-422.

Staehelin L.A. and Arntzen C.J. (1986) (Eds.) Photosynthesis III: Photosynthetic Membranes and Light Harvesting Systems. Encyclopedia of Plant Physiology, New Series, Volume 19, Springer Verlag, Berlin.

Stanier R.Y. and Cohen-Bazire G. (1977) Phototrophic prokaryotes: The cyanobacteria. Ann. Rev. Microbiol. 31: 225-274.

Stauber J.L. and Jeffrey S.W. (1988) Photosynthetic pigments in fifty-one species of marine diatoms. J. Phycol. 24: 158-172.

Steel J.A. (1973) Reservoir algal productivity. The use of mathematical models in water pollution. University of Newcastle-upon-Tyne Symposium, James A. (Ed.), Newcastle-upon-Tyne.

Steele J.H. (1962) Environmental control of photosynthesis in the sea. Limnol. Oceanogr. 7: 137-150.

Steele J.H. (1965) Notes on some theoretical problems in production ecology. In: Primary Production in Aquatic Environments. Goldman C.R. (Ed.), pp. 385-398. Mem. Inst. Idrobiol., 18 Suppl., Univ. California Press, Berkeley, California.

Stockner J.G. (1988) Phototropic picoplankton: an overview from marine and freshwater ecosystems. Limnol. Oceanogr. 33: 765-775.

Stockner J.G. and Antia N.J. (1986) Algal picoplankton from marine and freshwater ecosystems: A multidisciplinary perspective. Can. J. Fish. Aquat. Sci. 43: 2472-2503.

Straskraba von M. (1974) Development of an analytical phytoplankton model with parameters empirically related to dominant controlling variables. Abr. Akad. Wiss. DDR 33-66. Academie Verlag, Berlin 1976.

Strickland J.D.H. (1958) Solar radiation penetrating the ocean. A review of requirements, data, and methods of measurement, with particular reference to photosynthetic productivity. J. Fish. Res. Bd. Can. 15: 453-493.

Suttle C.A. and Harrison P.J. (1988) Ammonium and phosphate uptake kinetics of size-fractionated plankton from an oligotrophic freshwater lake. J. Plankton Res. 10: 133-149.

Sverdrup H.U. (1953) On conditions for the vernal blooming of phytoplankton. J. Cons. Perm. Int. explor. Mer 18: 287-295.

Sverdrup H.U., Johnson M.W. and Fleming R.H. (1942) The Oceans: Their Physics, Chemistry and General Biology. Prentice-Hall Inc., Englewood Cliffs, NJ.

Taguchi S. and Laws E.A. (1987) Patterns and causes of temporal variability in the physiological condition of the phytoplankton community in Kaneohe Bay, Hawaii. J. Plankton Res. 9: 1143-1157.

Takahashi M. and Bienfang P.K. (1983) Size structure of phytoplankton biomass and photosynthesis in subtropical Hawaiian waters. Mar. Biol. 76: 203-211.

Takahashi M. and Hori T. (1984) Abundance of picoplankton in the subsurface chlorophyll maximum layer in subtropical and tropical waters. Mar. Biol. 79: 177-186.

Takahashi M., Kikuchi K. and Hara Y. (1985) Importance of picocyanobacteria biomass (unicellular, blue-green algae) in the phytoplankton population of the coastal waters off Japan. Mar. Biol. 89: 63-69.

Talling J.F. (1957) Photosynthetic characteristics of some fresh-water plankton diatoms in relation to underwater radiation. New Phytol. 56: 29-50.

Tamiya H. (1951) Some theoretical notes on the kinetics of algal growth. Bot. Mag., Tokyo, 64: 167-173.

Tanada T. (1951) The photosynthetic efficiency of carotenoid pigments in *Navicula minima*. Am. J. Bot. 38: 276-283.

Tandeau de Marsac N. (1977) Occurence and nature of chromatic adaptation in cyanobacteria. J. Bacteriol. 130: 82-91.

Tandeau de Marsac N. (1983) Phycobilisomes and complementary chromatic adaptation in cyanobacteria. Bull. Inst. Pasteur 81: 201-254.

Tenhunen J.D., Hesketh J.D. and Gates D.M. (1980) Leaf photosynthesis models. In: Predicting Photosynthesis for Ecosystem Models. Volume I. pp.123-181. CRC Press Inc., Boca Raton, Florida.

Thomsen H.A. (1986) A survey of the smallest eucaryotic organisms of the marine phytoplankton. In: Platt T. and Li W.K.W. (eds.) Photosynthetic Picoplankton. Can. Bull. Fish. Aquat. Sci. 214: 121-158.

Thornley J.H.M. (1976) Mathematical Models in Plant Physiology. Academic Press, London.

Tilzer M.M. (1984) The quantum yield as a fundamental parameter controlling photosynthetic profiles of phytoplankton in Lake Constance. Arch. Hydrobiol. 2: 169-198.

Truper H.G. and Yentsch C.S. (1967) Use of glass-fiber filters for the rapid preparation of *in vivo* absorption spectra of photosynthetic bacteria. J. Bact. 94: 1255-1256.

Tyler J.E. and Smith R.C. (1970) Measurements of spectral irradiance underwater. Gorden and Breach, New York, NY.

Vesk M. and Jeffrey S.W. (1977) Effect of blue-green light on photosynthetic pigments and chloroplast structure in unicellular marine algae from six classes. J. Phycol. 13: 280-288.

Vezina A.F. and Platt T. (1987) Small-scale variability of new production and particulate fluxes in the ocean. Can. J. Fish. Aquat. Sci. 44: 198-205.

Vollenweider R.A. (1965) Calculation models of photosynthesis-depth curves and some implications regarding day rate estimates in primary production measurements. In: Goldman C.R. (ed.) Primary Productivity in Aquatic Environments. pp. 425-457. Mem. Ist Ital. Idrobiol. 18(suppl.).

Vollenweider R.A. (1970) Models for calculating integral photosynthesis and some implications regarding structural properties of the community metabolism of aquatic systems. In: Prediction and Measurement of Photosynthetic Productivity. Setlik I. (ed.), pp. 455-472, Purdoc, Wageningen.

Wang R.T. and Myers J. (1976a) On the distribution of excitation energy to two photoreactions of photosynthesis. Photochem. Photobiol. 23: 405-410.

Wang R.T. and Myers J. (1976b) Simultaneous measurement of action spectra for photoreactions I and II of photosynthesis. Photochem. Photobiol. 23: 411-414.

Wang R.T., Stephens C.L.R. and Myers J. (1977) Action spectra for photoreactions I and II of photosynthesis in the blue-green alga *Anacystis nidulans*. Photochem. Photobiol. 25: 103-108.

Wasielewski M.R., Liddell P.A., Barrett D., Moore T.A. and Gust D. (1986) Ultrafast carotenoid to pheophorbide energy transfer in a biomimetic model for antenna function in photosynthesis. Nature 322: 570-572.

Waterbury J.B., Watson S.W., Guillard R.R.L. and Brand L.E. (1979) Widespread occurence of a unicellular, marine, planktonic, cyanobacterium. Nature 277: 293-294.

Waterbury J.B., Watson S.W. and Valois F.W. (1980) Preliminary assessment of the importance of *Synechococcus* spp. as oceanic primary producers. In: Falkowski P.G. (ed.) Primary Production in the Sea. Plenum Press, New York. pp. 516-517.

Waterbury J.B., Watson S.W., Valois F.W. and Franks D.G. (1986) Biological and ecological characterization of the marine unicellular cyanobacterium *Synechococcus*. In: Platt T. and Li W.K.W. (eds.) Photosynthetic Picoplankton. Can. Bull. Fish. Aquat. Sci. 214: 71-120.

Webb W.L., Newton M. and Starr D. (1974) Carbon dioxide exchange of *Alnus rubra*: A mathematical model. Oecologia 17: 281-291.

Wheeler P.A. and Kirchman D.L. (1986) Utilization of inorganic and organic nitrogen by bacteria in marine systems. Limnol. Oceanogr. 31: 998-1009.

Williams N. (1978) Annual variation of photosynthetic parameters in Lake Tahoe. Verh. Internat. Verein. Limnol. 20: 419-425.

Williams P.J.leB. (1981) Incorporation of microheterotrophic processes into the classical paradigm of the planktonic food web. Kiel. Meeresforsch. 5: 1-28.

Williams P.J.leB., Heinemann K.R., Marra J. and Purdie D.A. (1983) Comparison of ^{14}C and O_2 measurements of phytoplankton production in oligotrophic waters. Nature 305: 49-50.

Winokur M. (1948) Photosynthesis relationship of *Chlorella* species. Am. J. Bot. 35: 207-214.

Withers N.M., Alberte R.S., Lewin R.A., Thornber J.P., Britton G. and Goodwin T.W. (1978) Photosynthetic unit size, carotenoids, and chlorophyll-protein composition of *Prochloron* sp., a prokaryotic green alga. Proc. Natl. Acad. Sci. USA 75: 2301-2305.

Wong D., Pellegrino F., Alfano R.R. and Zilinskas B.A. (1981) Fluorescence relaxation kinetics and quantum yield from isolated phycobiliproteins of the blue-green alga

Nostoc sp. measured as a function of single picosecond pulse intensity. I. Photochem. Photobiol. 33: 651-662.

Wood A.M. (1979) Chlorophyll *a*:*b* ratios in marine phytoplankton. J. Phycol. 15: 330-332.

Wood A.M. (1985) Adaptation of photosynthetic apparatus of marine ultraphytoplankton to natural light fields. Nature 316: 253-255.

Wood A.M., Horan P.K., Muirhead K., Phinney D.A., Yentsch C.M. and Waterbury J.B. (1985) Discrimination between types of pigments in marine *Synechococcus* spp. by scanning spectroscopy, epifluorescence microscopy, and flow cytometry. Limnol. Oceanogr. 30: 1303-1315.

Wyman M. and Fay P. (1986a) Underwater light climate and the growth and pigmentation of planktonic blue-green algae (Cyanobacteria). I. The influence of light quantity. Proc. R. Soc. Lond. B 227: 367-380.

Wyman M. and Fay P. (1986b) Underwater light climate and the growth and pigmentation of planktonic blue-green algae (Cyanobacteria). I. The influence of light quality. Proc. R. Soc. Lond. B 227: 381-393.

Wyman M., Gregory R.P.F. and Carr N.G. (1985) Novel role for phycoerythrin in a marine cyanobacterium *Synechococcus* strain DC-2. Science 230: 818-820.

Yeh S.W., Ong L.J. and Glazer A.N. (1986) Role of phycoerythrin in marine picoplankton *Synechococcus* spp. Science 234: 1422-1423.

Yentsch C.S. (1957) A non-extractive method for the quantitative estimation of chlorophyll in algal cultures. Nature 179: 1302-1304.

Yentsch C.S. (1962) Measurement of visible light absorption by particulate matter in the ocean. Limnol. Oceanogr. 7: 207-217.

Yentsch C.S. (1980) Light attenuation and phytoplankton photosynthesis. In: The Physiological Ecology of Phytoplankton. Morris I. (ed.), Univ. California Press, California.

Yentsch C.S. (1983) A note on the fluorescence characteristics of the particles that pass through glass-fiber filters. Limnol. Oceanogr. 28: 597-599.

Yentsch C.S. and Yentsch C.M. (1979) Fluorescence spectral signatures: the characterization of phytoplankton populations by the use of excitation and emission spectra. J. Mar. Res. 37: 471-483.

Yocum C.S. and Blinks L.R. (1954) Photosynthetic efficiency of marine plants. J. Gen. Physiol. 38: 1-16.

Yocum C.S. and Blinks L.R. (1958) Light-induced efficiency and pigment alterations in red algae. J. Gen. Physiol. 41: 1113-1117.

Zaika V.Ye (1986) Vertical distribution of autotrophic picoplankton in the Indian Ocean and the Mediterranean Sea. Oceanol. Acad. Sci. USSR 26: 209-212.

Zevenbo n W. (1986) Tracing red-pigmented marine cyanobacteria using *in vivo* absorption maxima. FEMS Microbiol. Ecol. 38: 267-275.

Zvalinskii V.I. and Litvin F.F. (1982) Analysis of the light curve of photosynthesis on continuous illumination. Biophysics 27: 204-210.

Zvalinskii V.I. and Litvin F.F. (1983) Photosynthetic light curves for different organization of photosynthetic units. Soviet Plant Physiology 30: 881-892.

Zvalinskii V.I. and Litvin F.F. (1984a) Coupling of photochemical and dark cycle reactions during photosynthesis. Biophysics 29: 379-382.

Zvalinskii V.I. and Litvin F.F. (1984b) Light dependence of photosynthesis in a model with two photochemical reactions. Biophysics 29: 590-596.

Zvalinskii V.I. and Litvin F.F. (1986) Steady-state kinetics of chains of coupled reactions. Biokhimiya 51: 1741-1755.